THE JOURNAL
OF
CHEMICAL PHYSICS

VOLUME 20, NUMBER 12 DECEMBER, 1952

Nonequilibrium Thermodynamics of the Sedimentation Potential and Electrophoresis

S. R. DE GROOT, *Institute for Theoretical Physics, The University, Utrecht, Netherlands,*
P. MAZUR, *Faculté des Sciences, Université Libre, Brussels, Belgium,*
AND
J. TH. G. OVERBEEK, *Van 't Hoff Laboratory, The University, Utrecht, Netherlands*
(Received May 29, 1952)

The thermodynamics of irreversible processes is developed for a system placed in a centrifugal field and consisting of a number of components, some of which carry electrical charges. It is found that an Onsager reciprocal relation connects the sedimentation potential with a quantity which we call barycentric electrophoresis (i.e., the quotient of the total mass flow and the electrical field at zero centrifugal field). The latter quantity turns out to be ordinary electrophoresis in a colloid (i.e., in a system of one neutral and a number of charged components, one of which consists of colloidal particles) under certain limiting, but frequently realized, circumstances. If conduction relaxation exists, it appears in both connected phenomena described here.

I. INTRODUCTION

THE problem of the connection between sedimentation potential and electrophoresis in arbitrary systems has not heretofore been studied in a systematic manner. It was therefore thought useful to employ the thermodynamical theory of irreversible processes[1,2] to discuss this problem for a system composed of charged and neutral components. In this paper it is proved (Secs. II–V) that a relationship can be established between the sedimentation potential and a phenomenon which we call barycentric electrophoresis. This latter quantity is defined as the quotient of the total mass flow and electrical field in the absence of a centrifugal (gravitation) field. From the general formulas, the conditions are derived (Sec. 6) under which the relation mentioned above transforms into a connection between sedimentation potential and ordinary electrophoresis (defined as the quotient of a flow of one kind of charged particles and the electrical field at zero centrifugal field). It turns out that these conditions are usually fulfilled when one charged component consists of colloid particles. It is proved that, if relaxation exists, its influence appears in both coupled phenomena.

(It may be noted here that other electrokinetic effects, *viz.*, electro-osmosis and streaming potentials in diaphragms, have been treated[3] by means of the thermodynamics of irreversible processes previously.)

[1] I. Prigogine, *Etude Thermodynamique des Processus Irréversibles* (Thesis, Brussels, 1947), pp. 76, 100.
[2] S. R. de Groot, *Thermodynamics of Irreversible Processes* (North Holland Publishing Company, Amsterdam, and Interscience Publishers, Inc., New York, 1951), pp. 94, 106.

II. THE ENTROPY BALANCE

Let us consider a system composed of n components ($k=1, 2, \cdots, n$), of which m carry electrical charges e_k ($k=1, 2, \cdots, m$) per unit mass, and of which $n-m$ are neutral ($e_{m+1}=e_{m+2}=\cdots=e_n=0$). This system is brought into a centrifugal (gravitation) field $\mathbf{g}$. The temperature is assumed to be uniform. In this paper we limit ourselves to the study of the behavior of the system in the homogeneous region between the electrodes, and we do not consider the problem of possible electrode reactions here. In the thermodynamics of irreversible processes,[1,2] "the entropy balance equation," which we shall need further on, is derived from a set of fundamental equations. Those equations have the following forms in our case of a so-called "continuous system," i.e., where the state variables are continuous functions of the space coordinates.

A. Law of Conservation of Mass

For the change of the concentration c_k of component k,

$$\rho dc_k/dt = -\operatorname{div}\mathbf{J}_k \quad (k=1, 2, \cdots, n). \tag{1}$$

[3] P. Mazur and J. Th. G. Overbeek, Rec. Trav. Chim. Pays-Bas **70**, 83 (1951).

Here $c_k=\rho_k/\rho$, where ρ_k is the density of k, and ρ is the total density; the flow $\mathbf{J}_k$ of substance k is defined* with respect to the center-of-mass movement $\mathbf{v}$

$$\mathbf{J}_k=\rho_k(\mathbf{v}_k-\mathbf{v}) \quad (k=1, 2, \cdots, n), \tag{2}$$

where $\mathbf{v}_k$ is the velocity of k. The left-hand side of (1) contains the (barycentric) substantial time derivative

$$d/dt=\partial/\partial t+\mathbf{v}\cdot\text{grad}. \tag{3}$$

B. Law of Conservation of Momentum (Force Law)

$$\rho d\mathbf{v}/dt=-\text{grad}P+\sum_{k=1}^{n}\mathbf{F}_k\rho_k. \tag{4}$$

Here P is the pressure and $\mathbf{F}_k$ is the external force per unit mass on substance k. We have, in our case,

$$\mathbf{F}_k=e_k\mathbf{E}+\mathbf{g} \quad (k=1, 2, \cdots, n), \tag{5}$$

where e_k is the charge of k per unit mass, $\mathbf{E}$ the electric field strength, and $\mathbf{g}$ the centrifugal (gravitational) force per unit mass. Coriolis forces do not need to be taken into account when $\mathbf{g}$ is sufficiently uniform, i.e., when the dimensions of the vessel are fairly small compared with its distance from the rotation axis. (Coriolis forces would anyway not contribute to the entropy production, but the Onsager relations might be impaired, and new cross-effects arise.)

C. Law of Conservation of Energy

In the absence of heat flow, this law has the form

$$0=du/dt+Pd\rho^{-1}/dt-\rho^{-1}\sum_{k=1}^{n}\mathbf{F}_k\cdot\mathbf{J}_k, \tag{6}$$

where u is the (internal) energy per unit mass (specific energy).

D. The Second Law (Gibbs' Relation)

The second law is

$$Tds/dt=du/dt+Pd\rho^{-1}/dt-\sum_{k=1}^{n}\mu_k dc_k/dt, \tag{7}$$

where T is the temperature, s the specific entropy, and μ_k the chemical potential (partial specific Gibbs function) of substance k.

The entropy balance equation follows when c_k from (1) and u from (6) are introduced into (7):

$$\rho ds/dt=-\text{div}\,\mathbf{J}_s+\sigma. \tag{8}$$

The change of entropy is seen to be the result of an entropy flow

$$\mathbf{J}_s\equiv-\sum_{k=1}^{n}\mu_k\mathbf{J}_k/T, \tag{9}$$

and an entropy production of source strength σ,

$$T\sigma\equiv\sum_{k=1}^{n}\mathbf{J}_k\cdot\mathbf{X}_k, \tag{10}$$

where

$$\mathbf{X}_k\equiv\mathbf{F}_k-\text{grad}\mu_k \quad (k=1, 2, \cdots, n). \tag{11}$$

The entropy production σ (10), which is essentially positive, measures the irreversibility of the process. It is the starting point of further considerations.

III. THE ENTROPY PRODUCTION AT MECHANICAL EQUILIBRIUM AND VANISHING VOLUME FLOW

Equation (10) for the entropy source strength σ may be modified for the following two reasons. In the first place, we can assume that the system is in mechanical equilibrium. Then, according to a theorem of Prigogine,[1,2] Eq. (10) for the entropy production remains invariant when we choose in (2), instead of $\mathbf{v}$, any arbitrary reference velocity. For our purpose zero is the best choice, or, in other words, we employ absolute flows

$$\mathbf{J}_k^0=\rho_k\mathbf{v}_k \quad (k=1, 2, \cdots, n) \tag{12}$$

in the entropy production σ from

$$T\sigma=\sum_{k=1}^{n}\mathbf{J}_k^0\cdot\mathbf{X}_k. \tag{13}$$

(It may be noted, incidentally, that at mechanical equilibrium, i.e., the left-hand side of (4) vanishing, it follows from (4) and (5) that

$$\text{grad}P=\mathbf{g}\rho, \tag{14}$$

because electroneutrality,

$$\sum_{k=1}^{m}\rho_k e_k=0, \tag{15}$$

can be assumed.)

In the second place, we can further modify the entropy production σ by introducing the boundary conditions for a liquid contained in a vessel, which may be stated as the vanishing of the total volume flow through a section (*cf.* appendix)

$$\sum_{k=1}^{n}v_k\mathbf{J}_k^0=0. \tag{16}$$

We shall from now on restrict ourselves to the region in the vessel where concentration gradients are negligible. We have then, because we have also assumed uniform temperature, for (11),

$$\mathbf{X}_k=\mathbf{F}_k-v_k\,\text{grad}P, \quad (k=1, 2, \cdots, n), \tag{17}$$

where v_k is the partial specific volume of k.

With (16) $\mathbf{J}_n^0$ can be eliminated from (13). This

* Flows and electrical currents will be understood as flow densities and current densities (i.e., they are counted per unit area) throughout this paper.

gives, on introducing (17) and (5),

$$T\sigma=\sum_{k=1}^{n-1}\mathbf{J}_k^0\cdot\{e_k\mathbf{E}+(1-v_k/v_n)\mathbf{g}\},\tag{18}$$

an expression which can be rewritten in the alternative form

$$T\sigma=\mathbf{I}\cdot\mathbf{E}+\mathbf{J}\cdot\mathbf{g},\tag{19}$$

with the electrical current

$$\mathbf{I}=\sum_{k=1}^{m}e_k\mathbf{J}_k^0,\tag{20}$$

and the total mass flow

$$\mathbf{J}=\sum_{k=1}^{n-1}(1-v_k/v_n)\mathbf{J}_k^0=\rho\mathbf{v}.\tag{21}$$

The last form follows from (16) and the definition of center-of-gravity velocity

$$\mathbf{v}=(\sum_{k=1}^{n}\rho_k\mathbf{v}_k)/\rho.$$

The fact that this velocity occurs now in σ is a result of the specializations in this section. This is not in contradiction with the fact that in general $\mathbf{v}$ gives no contribution to σ (see Eq. (10)).

IV. THE PHENOMENOLOGICAL LAWS

The expressions for the entropy production (18) and (19) have the form of a sum of products of so-called "fluxes" and "forces." In the thermodynamics of irreverisble processes, linear relationships are assumed between these fluxes and forces, which are called phenomenological laws. From (18) we obtain

$$\mathbf{J}_k^0=\sum_{j=1}^{n-1}a_{kj}\{e_j\mathbf{E}+(1-v_j/v_n)\mathbf{g}\}\qquad(k=1,2,\cdots,n-1)\tag{22}$$

with, between the phenomenological coefficients, the Onsager relations[4]

$$a_{kj}=a_{jk},\quad(k,j=1,2,\cdots,n-1),\tag{23}$$

which follows from the time reversal invariance of the equations of motion of individual constituent particles ("microscopic reversibility"). With the fluxes and forces of (19), the phenomenological laws are

$$\mathbf{I}=b_{11}\mathbf{E}+b_{12}\mathbf{g},\tag{24}$$

$$\mathbf{J}=b_{21}\mathbf{E}+b_{22}\mathbf{g},\tag{25}$$

with the Onsager relation

$$b_{12}=b_{21}.\tag{26}$$

[4] L. Onsager, Phys. Rev. **37**, 405 (1931); **38**, 2265 (1931); H. B. G. Casimir, Revs. Modern Phys. **17**, 343 (1945), or, Philips Research Rept. **1**, 185 (1945).

The following relations exist between the phenomenological coefficients:

$$b_{11}=\sum_{k,j=1}^{m}a_{kj}e_ke_j,\tag{27}$$

$$b_{12}=\sum_{j=1}^{n-1}(1-v_j/v_n)\sum_{k=1}^{m}a_{kj}e_k,\tag{28}$$

$$b_{22}=\sum_{k,j=1}^{n-1}(1-v_k/v_n)(1-v_j/v_n)a_{kj}.\tag{29}$$

The Onsager relations have been used in these expressions. Since σ is positive definite, we have inequalities

$$\left.\begin{aligned}&a_{kk}\geqslant 0,\quad|a_{kj}|=|a_{jk}|\leqslant(a_{kk}a_{jj})^{\frac{1}{2}},\\&\qquad\qquad(k,j=1,2,\cdots,n-1)\\&b_{11}\geqslant 0,\quad b_{22}\geqslant 0,\quad|b_{12}|=|b_{21}|\leqslant(b_{11}b_{22})^{\frac{1}{2}},\end{aligned}\right\}\tag{30}$$

etc., between the phenomenological coefficients.

V. THE PHYSICAL MEANING OF THE PHENOMENOLOGICAL COEFFICIENTS AND OF THE ONSAGER RELATIONS

We shall now consider the physical meaning of the coefficients in (24) and (25), and of the relation (26).

The diagonal coefficients b_{11} and b_{22} are the specific electric conductivity and the sedimentation rate in a short-circuited vessel, because from (24) and (25) it follows that

$$(\mathbf{I}/\mathbf{E})_{g=0}=b_{11},\tag{31}$$

$$(\mathbf{J}/\mathbf{g})_{E=0}=b_{22}.\tag{32}$$

The cross-coefficient b_{12} is connected with the sedimentation phenomena, *viz.*, the sedimentation potential and current. For both effects two definitions can be given. The sedimentation potential is defined as the electrical field per unit centrifugal force (or sometimes per unit total mass flow) in the stationary state of zero electrical current. From (24) and (25) the effect follows immediately:

$$(\mathbf{E}/\mathbf{g})_{I=0}=-b_{12}/b_{11},\tag{33}$$

$$(\mathbf{E}/\mathbf{J})_{I=0}=-b_{12}/(b_{11}b_{22}-b_{12}b_{21}).\tag{34}$$

The sedimentation current is the electrical current per unit centrifugal force (or per unit total mass flow) in the absence of an electrical field (i.e., in a short-circuited vessel). In formulas

$$(\mathbf{I}/\mathbf{g})_{E=0}=b_{12},\tag{35}$$

$$(\mathbf{I}/\mathbf{J})_{E=0}=b_{12}/b_{22}.\tag{36}$$

The other cross-coefficient, b_{21}, is connected with the electrophoretic phenomena. We define the barycentric electrophoresis coefficient as the mass flow per unit electrical current (or per unit electrical field) in the

absence of centrifugal forces. This gives from (24) and (25)

$$(\mathbf{J}/\mathbf{I})_{g=0}=b_{21}/b_{11}, \tag{37}$$

$$(\mathbf{J}/\mathbf{E})_{g=0}=b_{21}. \tag{38}$$

The other electrophoretic phenomenon has no conventional name. It is the gravitational field per unit electrical field (or per unit electrical current) in the stationary state of zero mass flow. Its magnitude is

$$(\mathbf{g}/\mathbf{E})_{J=0}=-b_{21}/b_{22}, \tag{39}$$

$$(\mathbf{g}/\mathbf{I})_{J=0}=-b_{21}/(b_{11}b_{22}-b_{12}b_{21}). \tag{40}$$

It is clear that the Onsager relation (26) connects a sedimentation with an electrophoretic phenomenon. We have, for instance, from (33), (37), and (26),

$$(\mathbf{E}/\mathbf{g})_{I=0}=-(\mathbf{J}/\mathbf{I})_{g=0}, \tag{41}$$

the connection between sedimentation potential and barycentric electrophoresis. Similar Onsager connections exist between (34) and (40), between (35) and (38), and between (36) and (39). In practice, usually the sedimentation potential (33) and the barycentric electrophoresis coefficient (38) are measured. When the Onsager relation (26) is employed one finds the following connection between these two effects and the electrical conductivity coefficient (31):

$$(\mathbf{J}/\mathbf{E})_{g=0}=-(\mathbf{I}/\mathbf{E})_{g=0}(\mathbf{E}/\mathbf{g})_{I=0}. \tag{42}$$

Besides the ordinary electrical and material conductivities (31) and (32), one could measure these conductivities in the stationary states of zero mass flow and zero electrical current. The electrical conductivity in the stationary state of zero mass flow follows from (24) and (25)

$$(\mathbf{I}/\mathbf{E})_{J=0}=b_{11}-(b_{12}b_{21}/b_{22}). \tag{43}$$

The sedimentation rate in the stationary state of zero electrical current is

$$(\mathbf{J}/\mathbf{g})_{I=0}=b_{22}-(b_{12}b_{21}/b_{11}). \tag{44}$$

In practice, not all the coefficients defined in this section are measured. The usual ones are the ordinary electrical conductivity (31), the sedimentation potential (33), the sedimentation current (35), the electrophoresis usually in the form of (38) but less frequently also as (37), and finally the sedimentation rate at zero electrical current (44), because the condition of zero electrical field would rather complicate the sedimentation experiment.

From (31) and (33) or from (38) the coefficient $b_{12}(=b_{21})$ can be calculated. The coefficient b_{22} should be determined from (44) in combination with (31) and (38) or directly from (32) if the experiment with zero electrical field can be done.

VI. THE CASE OF A COLLOID

We can apply the general formalism of the preceding sections to special cases. Let us consider a mixture of four components ($n=4$), of which three ($m=3$) carry electrical charges. We shall assume that the particles of the first charged component (the colloid) are very much larger than those of the other three. The second and third components are ions of opposite charge. The fourth component is a neutral solvent.

All relations derived in the previous section apply to this system. We shall prove, however, that in some limiting cases these formulas may be reduced to a new form. For the system considered here, Eqs. (27)–(29) can be written in the following way, if (12) and (22) are taken into account:

$$b_{11}=\sum_{j=1}^{3} e_j\rho_j(\mathbf{v}_j/\mathbf{E})_{g=0}, \tag{45}$$

$$b_{12}=\sum_{j=1}^{3} (1-v_j/v_4)\rho_j(\mathbf{v}_j/\mathbf{E})_{g=0}, \tag{46}$$

$$b_{22}=\sum_{j=1}^{3} (1-v_j/v_4)\rho_j(\mathbf{v}_j/\mathbf{g})_{E=0}. \tag{47}$$

As a rule $(1-v_j/v_4)$ is of the order 1, and $(\mathbf{v}_1/\mathbf{E})_{g=0}$ is not very much smaller than $(\mathbf{v}_2/\mathbf{E})_{g=0}$ and $(\mathbf{v}_3/\mathbf{E})_{g=0}$. Consequently the second and third terms on the right-hand side of (46) may be neglected provided that

$$\rho_1\gg\rho_2 \quad \text{and} \quad \rho_1\gg\rho_3, \tag{48}$$

conditions which are frequently fulfilled in colloidal systems. If these conditions are satisfied, the second and the third term of (47) may be neglected *a fortiori*. This is not possible with (45), where the terms contain factors e_j (the specific charges), which, on account of the condition of electroneutrality (15), compensate the effect of conditions (48).

It therefore follows that the expressions (46) and (47), or the equivalent (28) and (29), can be simplified, with the aid of conditions (48), to

$$b_{12}=(1-v_1/v_4)\sum_{k=1}^{3} a_{1k}e_k, \tag{49}$$

$$b_{22}=(1-v_1/v_4)\sum_{k=1}^{3} (1-v_k/v_4)a_{1k}. \tag{50}$$

From (22) and (25), one obtains, employing these relations and only the a_{kj} occurring in them, the following formula for our limiting case:

$$\mathbf{J}=(1-v_1/v_4)\mathbf{J}_1^0, \tag{51}$$

which connects the total mass flow $\mathbf{J}$ with the flow $\mathbf{J}_1^0$ of the colloid particles alone. This is a very important special case for colloidal systems, and we shall give a

few results which can be derived from the general formalism of the preceding section, employing the approximation (51).

Equation (42), for instance, becomes then,

$$(\mathbf{J}_1^0/\mathbf{E})_{g=0} = -(\mathbf{I}/\mathbf{E})_{g=0}\{\mathbf{E}/\mathbf{g}(1-v_1/v_4)\}_{I=0}. \quad (52)$$

At the left-hand side we have now the ordinary electrophoresis coefficient, instead of the barycentric electrophoresis coefficient. At the right-hand side the sedimentation potential is now expressed with respect to a modified centrifugal field instead of the centrifugal field $\mathbf{g}$.

Similar formulas for colloidal systems could be derived from the other results of Sec. 5, employing the approximation (51). The first members of (32) and (44), for instance, take, on employing (51), the form

$$\{\mathbf{J}_1^0/\mathbf{g}(1-v_1/v_4)\}_{I=0} \quad (53)$$

of the quotient of the flow of colloid particles and the reduced centrifugal field.

An important conclusion can be drawn from the formula (49), because it shows the influence of conduction relaxation on sedimentation and electrophoresis phenomena. If relaxation exists, it manifests itself in the coefficients a_{12}, a_{13} and in contributions to the coefficients a_{11}, a_{22}, a_{33}, and a_{23}. All relations such as (52), which connect a sedimentation phenomenon (depending on b_{12}) with an electrophoresis phenomenon (depending on b_{21}) are ultimately Onsager relations (26). The value of the coefficients b_{12} and b_{21} is given by (49). We can draw the conclusion that relaxation phenomena contribute always to both the sedimentation and the electrophoresis phenomena in exactly the same way.

Furthermore, even when the approximation (49) is not valid, this conclusion holds. To show this, we may remark that, in the first place, our conclusion is correct for barycentric instead of ordinary electrophoresis, as can be seen, for instance, from the Onsager relation (42) (of which (52) was the approximation considered above). In the second place it is clear that if, in the general case, ordinary electrophoresis is affected by relaxation phenomena, this will also be the case for barycentric electrophoresis, and consequently (e.g., (42)) for sedimentation phenomena. Thus, if relaxation exists, its influence should be taken into account in the interpretation of sedimentation experiments.

VII. APPENDIX

The condition (16) of zero total volume flow can be connected with other physical characteristics of the system in the following way.

For the densities and the partial specific volumes, one has the identity

$$\sum_k \rho_k v_k = \rho v = 1. \quad (54)$$

From this follows

$$\sum_k v_k \partial\rho_k/\partial t + \sum_k \rho_k \partial v_k/\partial t = 0. \quad (55)$$

From this relation and the conservation of mass

$$\partial\rho_k/\partial t = -\operatorname{div}\mathbf{J}_k^0 \equiv -\operatorname{div}\rho_k\mathbf{v}_k \quad (56)$$

the following expression is obtained:

$$\operatorname{div}\sum_k v_k\mathbf{J}_k^0 = \sum_k \rho_k(\partial v_k/\partial t + \mathbf{v}_k\cdot\operatorname{grad}v_k). \quad (57)$$

At the right-hand side between the parentheses one recognizes a substantial derivative of the partial specific volume v_k with respect to the velocity $\mathbf{v}_k$. It vanishes if we assume that v_k does not appreciably depend on pressure and concentrations. Then the divergence of (16) turns out to be zero, and therefore also (16) itself.

One of us (P.M.) wishes to acknowledge the financial assistance received from the Centre de Chimie physique moléculaire Belge, which enabled him to pursue this research.

The Raman Spectrum, Structure, Force Constants, and Thermodynamic Properties of Bromine Pentafluoride*

C. V. STEPHENSON† AND E. A. JONES
Department of Physics, Vanderbilt University, Nashville, Tennessee

(Received June 3, 1952)

Using a Raman tube made of the plastic polychlorotrifluoroethylene, the Raman spectrum of bromine pentafluoride has been obtained. A method has been developed for making polarization measurements when Raman tubes constructed of this plastic are used. The spectrum of bromine pentafluoride has been correlated with a tetragonal pyramid configuration with symmetry C_{4v}. Force constants were calculated using the Wilson FG Matrix method. The thermodynamic functions for BrF_5 were calculated for temperatures ranging from 313.7°K to 1500°K, using the rigid rotator, harmonic oscillator approximation.

I. INTRODUCTION

THE published literature contains very little information about bromine pentafluoride, consisting mostly of methods of preparation and observed chemical reactions. Bromine pentafluoride was first prepared by Ruff and Menzel[1] in 1931, by mixing fluorine with vapor from heated bromine trifluoride and heating the mixture to 200°C. Bromine pentafluoride is one of the most chemically active compounds known. It reacts with almost all known materials, and in many cases, it reacts violently. It reacts to some extent with all metals, but in some cases at low and intermediate temperatures, a protective fluoride film is formed on the metal surface which halts further action. BrF_5 can be handled in some steels up to 250°C, in copper up to 400°C, and in nickel up to 750°C.

This extreme chemical activity has prevented all but the simplest physical measurements on this molecule. Recent nuclear magnetic shielding experiments[2] have given indications that BrF_5 has a C_{4v} structure. The recent development of the plastic polychlorotrifluoroethylene, known commercially as Fluorothene or Kel-F, has made the spectroscopic study of this compound possible. This report presents the results of a vibrational analysis of BrF_5.

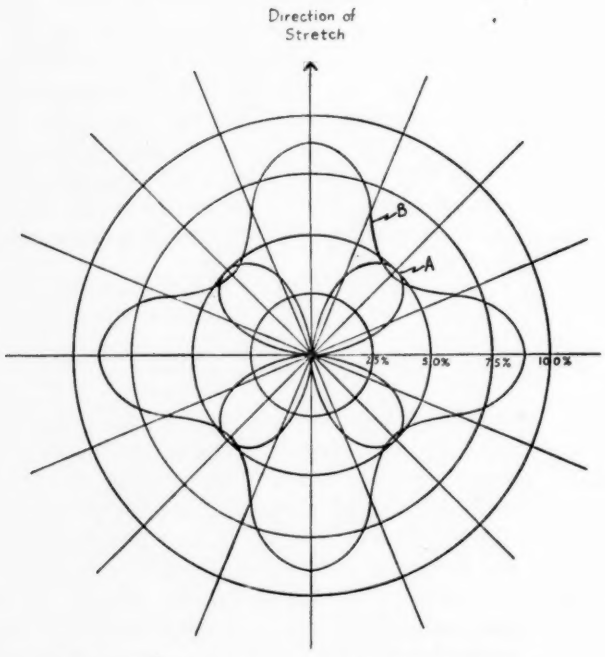

FIG. 1. Transmission curve for stretched fluorothene.

II. EXPERIMENTAL

The use of a Raman tube made of Fluorothene was first reported by Kirby-Smith and Jones.[3] The construction of the Raman tube in this investigation is essentially the same as described by them, with one important exception regarding the window on the tube. It was found that Fluorothene in its ordinary state was depolarizing, a fact easily demonstrated by holding a piece of the plastic between two crossed polaroids. It was also found that stretching the plastic had some effect on this property of the plastic. Thus an investigation was made into the properties of the stretched plastic with the result that a method of treatment has been developed whereby the material can be used for Raman tubes when polarization measurements are desired.

A strip of the plastic was mounted in a tensile strength machine and at room temperature stretched over a period of five days to a length equal to twice the original length. Two windows were cut from the center of the sheet and studied in the following way: Two polaroids were crossed and a window was mounted between them. The percent transmission of a beam of light through this system was obtained as the window was rotated through various angles. The two polaroids were then uncrossed and the percent transmission at various angles again noted. These curves are shown in Fig. 1. Curve *A* is the transmission curve when the polaroids

* This document is based on work performed under contract No. AT(40-1)-1087 for the A.E.C.

† Present address: Sandia Corporation, Albuquerque, New Mexico.

[1] O. Ruff and W. Menzel, Z. anorg. Chem. **202**, 49 (1931).

[2] H. S. Gutowsky and C. J. Hoffman, J. Chem. Phys. **19**, 1259 (1951).

[3] J. S. Kirby-Smith and E. A. Jones, J. Opt. Soc. Am. **39**, 780 (1949).

were crossed and curve B is the transmission curve when the polaroids were uncrossed. No correction has been made for reflection at the surface.

From these transmission curves it is seen that the stretched plastic seems to act as a uniaxial crystal which does not separate the two perpendicularly polarized beams. The curves also show that there are two directions—one perpendicular and one parallel to the direction of stretch—in which the plastic does not affect polarized light. These two directions then must be perpendicular and parallel to the direction of propagation of the incident light on the Raman tube in order to make polarization measurements.

Using a Raman tube with a window made of the stretched plastic and properly oriented with respect to the incident exciting light, a spectrogram was made of benzene as a test of the stretched window material. The spectrogram showed marked polarization of the 992 cm^{-1} line and considerable polarization of the 3062 cm^{-1} line.

The high reactivity of bromine pentafluoride presented a considerable problem in transferring a relatively pure sample into the Raman tube. To accomplish this a transfer system made of Fluorothene and copper was used. The sample was purified by distillation.

TABLE I. Vibrational spectra of BrF_5.

Raman spectrum (liquid)			Infrared spectrum (gas)	
$\Delta\nu$ (cm^{-1})	I[a]	Assignment	ν (cm^{-1})	Assignment
683	10 pol	$\nu_1(A_1)$	690	$\nu_1(A_1)$
626	1 dep	$\nu_7(E)$	645	$\nu_7(E)$
572	10 pol	$\nu_2(A_1)$	583	$\nu_2(A_1)$
536	10 dep	$\nu_4(B_1)$		
481	1 dep	$\nu_6(B_2)$		
415	5 dep	$\nu_8(E)$	418	$\nu_8(E)$
365	4 pol	$\nu_3(A_1)$		
315	4 dep	$\nu_5(B_1)$		
244	4 dep	$\nu_9(E)$		

[a] Pol = polarized; dep = depolarized.

The Raman spectrum of BrF_5 was obtained on a Hilger E 612 spectrograph using the 4358 A and 4047 A lines of mercury as the exciting radiation. The irradiation unit consisted of eight G. E. AH-2 mercury arcs. Eastman 103a-0 spectrographic plates were used to record the spectrum of liquid BrF_5.

III. DISCUSSION OF BrF_5 SPECTRUM

The Raman spectrum of bromine pentafluoride is summarized in Table I. This table includes the Raman shifts, the estimated intensity, whether polarized or depolarized, and the vibrational type assigned. The table also includes the infrared spectrum reported recently by Burke and Jones.[4] The infrared spectrum was obtained only to 400 cm^{-1}.

Using the 4358 A line of mercury as the parent, it seemed possible that the two weak shifts at 626 cm^{-1} and 481 cm^{-1} were just the 683 cm^{-1} and 536 cm^{-1} shifts having the 4348 A line of mercury as the parent. To verify that these two weak lines belonged in the spectrum, the Raman spectrum was obtained having the 4047 A line of mercury as the parent. This spectrogram contained Raman shifts at 480 cm^{-1} and 625 cm^{-1} so that the weak lines were shown to be part of the Raman spectrum.

[4] T. G. Burke and E. A. Jones, J. Chem. Phys. **19**, 1611 (1951).

TABLE II. Possible structures of bromine pentafluoride and a summary of their vibrational selection rules.

Symmetry group	Total frequencies	Raman spectrum Total	Raman spectrum Polarized	Infrared spectrum	Coincidences Total	Coincidences Polarized
D_{5h}	6	3	1	3	0	0
D_{3h}	8	6	2	5	3	0
C_{5v}	7	7	2	4	4	2
C_{4v}	9	9	3	6	6	3
C_{3v}	8	8	4	8	8	4
C_{2v}	12	12	5	11	11	5
C_s	12	12	9	12	12	9
Observed:	9	9	3	4	4	2

The polarization measurements showed definite polarization of the 683, 572, and 365 cm^{-1} lines. No accurate quantitative measurements of the depolarization factor could be made.

In Table II are summarized the vibrational selection rules for various possible structures of bromine pentafluoride. In the selection of the symmetry group which is most likely for this molecule, we may eliminate the symmetry groups D_{5h}, D_{3h}, and C_{5v}, since it has been shown that there are at least three polarized Raman lines and these symmetry groups predict less than three. Also D_{5h} and D_{3h} may be eliminated since there are polarized coincidences. The symmetry groups C_{2v} and C_s have a predicted Raman spectrum of twelve lines whereas only nine have been found. It is not likely that as many as three frequencies have been overlooked. The symmetry group C_{3v} has a predicted Raman spectrum of only eight lines. If this is the symmetry of the molecule then one of the Raman lines found must be an overtone of one of the fundamental frequencies or a combination line of two or more of the fundamental frequencies. However, none of the lines seem to be overtones or combinations of any other lines. Furthermore, two lines found in the Raman spectrum above 400 cm^{-1} are not found in the infrared spectrum. The C_{3v} and C_s symmetry groups predict coincidences of all lines and C_{2v} predicts coincidences for all but one frequency. There are no discrepancies between the spectra predicted by a C_{4v} symmetry group and the observed spectra. C_{4v} predicts a total of nine Raman lines with three being polarized. This is in agreement with the observed Raman spectrum. It also predicts six infrared frequencies, all of which coincide with Raman frequencies and three of which coincide with the polarized Raman frequencies. The observed infrared spectrum contains four frequencies above 400 cm^{-1}, all of which

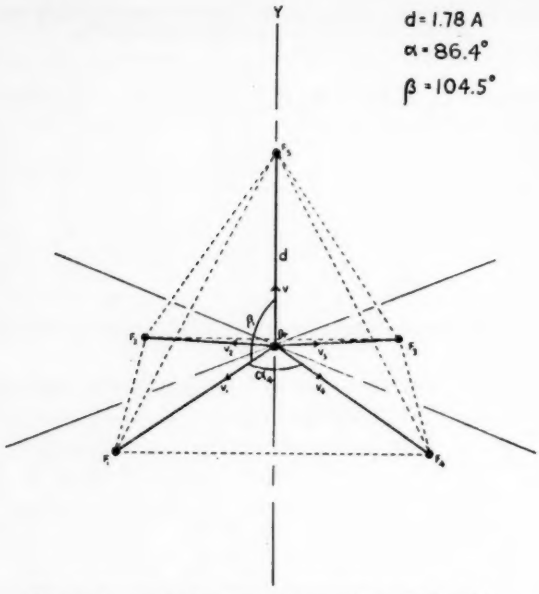

FIG. 2. Assumed structure of bromine pentafluoride.

coincide with Raman frequencies and two of which coincide with polarized Raman frequencies. Three Raman frequencies including one polarized frequency lie beyond the region included in the infrared spectrum. Thus it was concluded that the C_{4v} symmetry group was the most likely structure for bromine pentafluoride. This agrees with the structure predicted by Gutowsky and Hoffman.[2] The C_{4v} model is also in accord with the predictions of directed valence theory for d^2p^3 bonds.

Frequency assignments are made rather easily. The polarized lines at 683, 572, and 365 cm^{-1} are classified A_1. The two remaining frequencies in the infrared spectrum are assigned to the E type. The two remaining frequencies above 400 cm^{-1} are either B_1 or B_2. The higher of these is assigned to B_1 since one of the B_1 vibrations is a bond stretching vibration. The remaining frequencies are angle deformations. The B_2 should be the stronger of these and is assigned to the 481 cm^{-1} frequency. The second B_1 is assigned at 315 cm^{-1} leaving 244 cm^{-1} as the third E frequency.

IV. CALCULATIONS

The calculation of force constants and thermodynamic properties of a molecule requires a more detailed knowledge of the structure of the molecule than is available. In the absence of any data on interbond distances and angles, the following assumptions have been made: (1) The bromine atom is located at the center of mass of the molecule; (2) The five interbond distances are equal to the sum of the single covalent bond radii as given by Pauling.[5] No attempt is made to justify these assumptions other than that they seem fairly reasonable. With these assumptions the molecule has the dimensions show in Fig. 2.

[5] L. Pauling, *The Nature of the Chemical Bond* (Cornell University Press, Ithaca, New York, 1944).

A. Force Constants

Force constants were calculated using the Wilson FG matrix method.[6] The internal coordinates used in the construction of symmetry coordinates were the changes in the five Br−F bond lengths, the four angles α between bonds of the fluorine atoms at the base of the pyramid, and the four angles β between bonds at the base of the pyramid and the bond to the apex of the pyramid. This made thirteen internal coordinates, whereas only twelve were needed. Thus, in order to preserve symmetry, one redundant symmetry coordinate was constructed. Denoting the change in the bond lengths by Δd and the change in the angles by $\Delta\alpha$ and $\Delta\beta$ the symmetry coordinates were the following:

$$A_1\begin{cases} R_1=\Delta d_5 \\ R_2=\frac{1}{2}(\Delta d_1+\Delta d_2+\Delta d_3+\Delta d_4) \\ R_3=\dfrac{1}{2\sqrt{2}}(\Delta\alpha_1+\Delta\alpha_2+\Delta\alpha_3+\Delta\alpha_4 \\ \qquad -\Delta\beta_1-\Delta\beta_2-\Delta\beta_3-\Delta\beta_4) \\ R_3'=\dfrac{1}{2\sqrt{2}}(\Delta\alpha_1+\Delta\alpha_2+\Delta\alpha_3+\Delta\alpha_4+\Delta\beta_1+\Delta\beta_2 \\ \qquad +\Delta\beta_3+\Delta\beta_4)\equiv 0 \text{ (redundant)} \end{cases}$$

$$B_1\begin{cases} R_4=\frac{1}{2}(\Delta d_1-\Delta d_2+\Delta d_3-\Delta d_4) \\ R_5=\frac{1}{2}(\Delta\beta_1-\Delta\beta_2+\Delta\beta_3-\Delta\beta_4) \end{cases}$$

$$B_2\{\ R_6=\tfrac{1}{2}(\Delta\alpha_1-\Delta\alpha_2+\Delta\alpha_3-\Delta\alpha_4)$$

$$E\begin{cases} R_{7a}=\frac{1}{2}(\Delta d_1+\Delta d_2-\Delta d_3-\Delta d_4) \\ R_{7b}=\frac{1}{2}(\Delta d_1-\Delta d_2-\Delta d_3+\Delta d_4) \\ R_{8a}=\frac{1}{2}(\Delta\beta_1+\Delta\beta_2-\Delta\beta_3-\Delta\beta_4) \\ R_{8b}=\frac{1}{2}(\Delta\beta_1-\Delta\beta_2-\Delta\beta_3+\Delta\beta_4) \\ R_{9a}=\frac{1}{2}(\Delta\alpha_1+\Delta\alpha_2-\Delta\alpha_3-\Delta\alpha_4) \\ R_{9b}=\frac{1}{2}(\Delta\alpha_1-\Delta\alpha_2-\Delta\alpha_3+\Delta\alpha_4). \end{cases}$$

The G matrix elements are as follows: For the A_1 vibrations,

$$G_{11}=\mu_F+\mu_{Br}$$

$$G_{12}=2\mu_{Br}\cos\beta$$

$$G_{13}=\mu_{Br}\left[\frac{\sqrt{2}\sin\beta}{d}-\frac{2\sqrt{2}(1-\cos\alpha)\cos\beta}{d\sin\alpha}\right]$$

$$G_{22}=\mu_F+\mu_{Br}(1+2\cos\alpha+\cos 2\beta)$$

[6] E. B. Wilson, Jr., J. Chem. Phys. **7**, 1047 (1939); **9**, 76 (1941).

$$G_{23}=-\mu_{Br}\left[\frac{\sqrt{2}(1-\cos\alpha)(1+2\cos\alpha+\cos2\beta)}{d\sin\alpha}-\frac{(1-\cos\beta)(4\cos\beta+1+2\cos\alpha+\cos2\beta)}{2d\sin\beta}\right]$$

$$G_{33}=\mu_F\left[\frac{1+\cos2\beta-2\cos^2\alpha}{d^2\sin^2\alpha}+\frac{1}{2d^2}-\frac{2\cos\beta(1-\cos\alpha)}{d^2\sin\alpha\sin\beta}+\frac{(1+2\cos\alpha+\cos2\beta-4\cos^2\beta)}{2d^2\sin^2\beta}\right]$$

$$+\mu_{Br}\left[\frac{2(1-\cos\alpha)^2(1+2\cos\alpha+\cos2\beta)}{d^2\sin^2\alpha}+\frac{(1-\cos\beta)^2(5+8\cos\beta+2\cos\alpha+\cos2\beta)}{2d^2\sin^2\beta}-\frac{2(1-\cos\alpha)(1-\cos\beta)\times(1+2\cos\alpha+\cos2\beta+4\cos\beta)}{d^2\sin\alpha\sin\beta}\right].$$

For the B_1 vibrations,

$$G_{11}=\mu_F+\mu_{Br}(1-2\cos\alpha+\cos2\beta)$$

$$G_{12}=-\mu_{Br}\frac{(1-\cos\beta)(1-2\cos\alpha+\cos2\beta)}{d\sin\beta}$$

$$G_{22}=\frac{\mu_F}{d^2}+\frac{\mu_F(1-2\cos\alpha+\cos2\beta)}{d^2\sin^2\beta}+\frac{\mu_{Br}(1-\cos\beta)^2(1-2\cos\alpha+\cos2\beta)}{d^2\sin^2\beta}.$$

For the B_2 vibration,

$$G_{11}=\frac{2\mu_F(1-\cos2\beta)}{d^2\sin^2\alpha}.$$

TABLE III. Force constants for bromine pentafluoride.

f_D	3.9635×10^5 dynes/cm
f_d	3.1114
f_{dd}	0.0636
$f_{dd'}$	0.2314
f_α	0.7524
$f_{\alpha\alpha}$	0.0323
f_β	0.6521
$f_{\beta\beta}$	0.4596
$f_{\alpha\beta}$	0.0526

TABLE IV. Thermodynamic properties of BrF_5 cal $mole^{-1}$ deg^{-1}.

T (°K)	C_p^0	$H^0-H_0^0/T$	$-(F^0-E_0^0)/T$	S^0
313.7	24.49	15.45	62.51	77.96
400.0	26.80	17.68	66.55	84.23
500.0	28.41	19.68	70.71	90.39
600.0	29.36	21.24	74.47	95.71
700.0	29.96	22.42	77.78	100.20
800.0	30.37	23.39	80.87	104.26
900.0	30.66	24.20	83.67	107.87
1000.0	30.86	24.85	86.48	111.33
1100.0	31.02	25.40	88.64	114.04
1200.0	31.14	25.87	90.88	116.75
1300.0	31.23	26.29	92.97	119.26
1400.0	31.31	26.64	94.94	121.58
1500.0	31.37	26.95	96.78	123.73

For the E vibrations,

$$G_{11}=\mu_F+\mu_{Br}(1-\cos2\beta)$$

$$G_{12}=-\mu_{Br}\frac{(1-\cos\beta)(1-\cos2\beta)}{d\sin\beta}$$

$$G_{13}=-\mu_{Br}\frac{(1-\cos\alpha)(1-\cos2\beta)}{d\sin\alpha}$$

$$G_{22}=\frac{\mu_F}{d^2}+\frac{\mu_F(1-\cos2\beta)}{d^2\sin^2\beta}+\frac{\mu_{Br}(1-\cos\beta)^2(1-\cos2\beta)}{d^2\sin^2\beta}$$

$$G_{23}=\frac{\mu_F\cos\beta(1-\cos\alpha)}{d^2\sin\alpha\sin\beta}+\frac{\mu_{Br}(1-\cos\beta)(1-\cos\alpha)(1-\cos2\beta)}{d^2\sin\alpha\sin\beta}$$

$$G_{33}=\frac{2\mu_F}{d^2}+\frac{2\mu_{Br}(1-\cos\alpha)^2(1-\cos2\beta)}{d^2\sin^2\alpha}.$$

The most general quadratic potential function for BrF_5 contained nineteen force constants. However, it was possible to solve for only nine. Therefore, selecting the nine force constants which were thought to make the greatest contributions, the potential function used was the following:

$$\begin{aligned}2V=&f_D(\Delta d_5)^2+f_d[(\Delta d_1)^2+(\Delta d_2)^2+(\Delta d_3)^2+(\Delta d_4)^2]\\&+f_\alpha d^2[(\Delta\alpha_1)^2+(\Delta\alpha_2)^2+(\Delta\alpha_3)^2+(\Delta\alpha_4)^2]\\&+f_\beta d^2[(\Delta\beta_1)^2+(\Delta\beta_2)^2+(\Delta\beta_3)^2+(\Delta\beta_4)^2]\\&+2f_{dd}[(\Delta d_1+\Delta d_3)(\Delta d_2+\Delta d_4)]\\&+2f_{dd'}d(\Delta d_1\Delta d_3+\Delta d_2\Delta d_4)+2f_{\beta\beta}d^2(\Delta\beta_1\Delta\beta_3+\Delta\beta_2\Delta\beta_4)\\&+2f_{\alpha\alpha}d^2[(\Delta\alpha_1+\Delta\alpha_3)(\Delta\alpha_2+\Delta\alpha_4)]\\&+2f_{\alpha\beta}d^2[\Delta\alpha_1(\Delta\beta_1+\Delta\beta_2)+\Delta\alpha_2(\Delta\beta_2+\Delta\beta_3)\\&+\Delta\alpha_3(\Delta\beta_3+\Delta\beta_4)+\Delta\alpha_4(\Delta\beta_4+\Delta\beta_1)].\end{aligned}$$

The calculated values of the force constants in the potential energy function are given in Table III.

B. Thermodynamic Properties

The heat content, free energy, entropy, and heat capacity at constant pressure were calculated at 313.7°K and at 100° intervals from 400°K to 1500°K, assuming the usual rigid rotator, harmonic oscillator approximations. Using the previously assumed structure for bromine pentafluoride, the principal moments of inertia are $I_x = I_z = 31.227 \times 10^{-39}$ g cm² and $I_y = 37.472 \times 10^{-39}$ g cm². The symmetry number is 4 and the pressure was assumed to be one atmosphere. The values of the physical constants were those of Birge.[7] The values obtained for the thermodynamic properties are given in Table IV.

[7] R. T. Birge, Revs. Modern Phys. **13**, 233 (1941).

THE JOURNAL OF CHEMICAL PHYSICS VOLUME 20, NUMBER 12 DECEMBER, 1952

Physical Properties of Liquid Fluorine*

GERARD W. ELVERUM, JR., AND RUSSELL N. DOESCHER
California Institute of Technology, Jet Propulsion Laboratory, Pasadena, California

(Received July 28, 1952)

The viscosity, density, and surface tension of liquid fluorine and their dependence on temperature have been measured. The change in viscosity with temperature indicates that fluorine behaves as a normal liquid in the region studied. The results of the measurement of the density confirm a new much larger value for this property than previously accepted. Measurements of the surface tension given in this paper are in substantial agreement with values reported earlier in the literature if these early values are adjusted by means of the density determinations made by the authors.

INTRODUCTION

As part of a program at the Jet Propulsion Laboratory for the study of the physical properties of some pure substances, the measurement of the viscosity of liquid fluorine was undertaken since this property had not been reported previously in the literature for any temperature. In connection with this work, the density and surface tension were also redetermined. The first value of the density of liquid fluorine was obtained by Moissan and Dewar[1] in 1897. This single value of 1.14 g/cc at −200°C was quantitatively supported by Kanda,[2] who measured the density and surface tension in the temperature region 57 to 85°K. Recently a much larger value of 1.54±0.02 g/cc at −196°C was reported by Kilner, Randolph, and Gillespie.[3] The results of the density measurements from 65 to 85°K given in the present paper confirm this larger value almost within the reported experimental errors.

If the values of the surface tension given by Kanda are modified by the use of the density results reported in the present paper, they are in good agreement with the values determined by the authors.

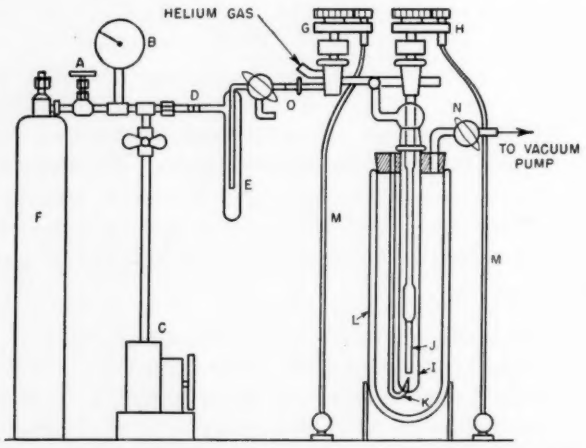

FIG. 1. Apparatus used for the determination of viscosity and surface tension of liquid fluorine.

EQUIPMENT AND PROCEDURE

A diagram of the apparatus used in the present study is shown in Fig. 1. The fluorine was contained under

TABLE I. Density of liquid fluorine.

Temperature (°K)	Density (g/cc)
65.4	1.639±0.002
67.1	1.630±0.002
70.0	1.613±0.002
74.1	1.587±0.002
75.4	1.578±0.002
77.8	1.562±0.002
80.0	1.547±0.002
81.0	1.539±0.002
82.1	1.531±0.002
83.4	1.522±0.002
84.3	1.516±0.002
85.2	1.509±0.002

* This paper presents the results of one phase of research carried out at the Jet Propulsion Laboratory under Contract No. DA-04-495-ORD 18, sponsored by the Department of the Army, Ordnance Corps.

[1] H. Moissan and J. Dewar, Bull. soc. chim. Paris **XVII**, 931 (1897).

[2] E. Kanda, Bull. Chem. Soc. Japan **12**, 469 (1937).

[3] Kilner, Randolph, and Gillespie, J. Am. Chem. Soc. **74**, 1086 (1952).

pressure in cylinder F. A represents a Monel needle valve packed with Teflon, and B represents a Monel Bourdon vacuum gauge for measuring the pressure in the system approximately. A graded seal of Kovar to Pyrex glass connected the metal parts to the glass apparatus at D. The trap at E was filled with sodium fluoride in order to eliminate as much as possible of the hydrogen fluoride present in the gas coming from the cylinder. The Duo Seal Vacuum Pump at C was filled with Fluorolube Standard,† and the system was flushed with helium and evacuated several times before the introduction of fluorine. The stopcocks at G and H and all other ground-glass joints were lubricated with a mixture of Fluorolube Heavy Grease† and Fluorolube Standard; this lubricant made possible the maintenance of a given vacuum for periods of over 24 hours, even during manipulation of the stopcocks. In order to prevent dislodging of a stopcock during operation by pressures greater than atmospheric, a remote stopcock turner was devised which could be operated outside the fume hood containing the apparatus by means of a flexible cable M. The container L was filled with mixtures of liquid nitrogen and liquid oxygen and had two unsilvered strips to allow a view of the interior. The fluorine was condensed in tube I (3.6-cm inside diameter) which contained a thin glass well K, into which a calibrated copper-constantan thermocouple was inserted. The position of the capillary tube used in the measurements is shown at J.

TABLE II. Surface tension of liquid fluorine.

Temp. T (°K)	h (cm)	ρ_l (g/cm)	ρ_v (g/cm)	γ (dynes/cm)
69.2	0.895	1.618	0.70×10^{-3}	17.9
71.2	0.875	1.606	0.95×10^{-3}	17.4
73.2	0.850	1.593	1.30×10^{-3}	16.7
75.3	0.830	1.580	1.75×10^{-3}	16.2
76.4	0.820	1.571	2.05×10^{-3}	15.9
78.2	0.800	1.559	2.50×10^{-3}	15.4
81.0	0.770	1.539	3.45×10^{-3}	14.6

The temperature of the system was lowered and maintained by pumping off nitrogen vapor through various settings of stopcock N. Temperatures could be held within 0.1° for periods of 15 to 20 minutes by this method.

The capillary tube was selected for shape and uniformity of bore and was determined to have a radius of 0.0252_3 cm at 73.2°K. The measurements of viscosity were made by condensing fluorine in tube I to a height of 4 cm above the lower end of the capillary tube and then closing off the upper reservoir by means of stopcock H. Stopcock G was then opened to admit helium gas to I, fluorine thus being forced into the upper bulb. The liquid height in I was measured when the meniscus in the upper reservoir was at each of two etched marks of previously determined heights. Stopcock H was then turned so that the pressure in the two parts of the system was equalized, and the time of flow between the two marks was recorded. This procedure was repeated at each temperature until the difference in time of flow did not exceed 0.6 second. Temperature equilibrium was assumed at this point. The effective length and volume of flow were determined by the use of water and several alcohols.

For the measurement of the density, a small float possessing a thin stem 7 cm long was made and cali-

† Product of Hooker Electrochemical Company, Niagara Falls, New York.

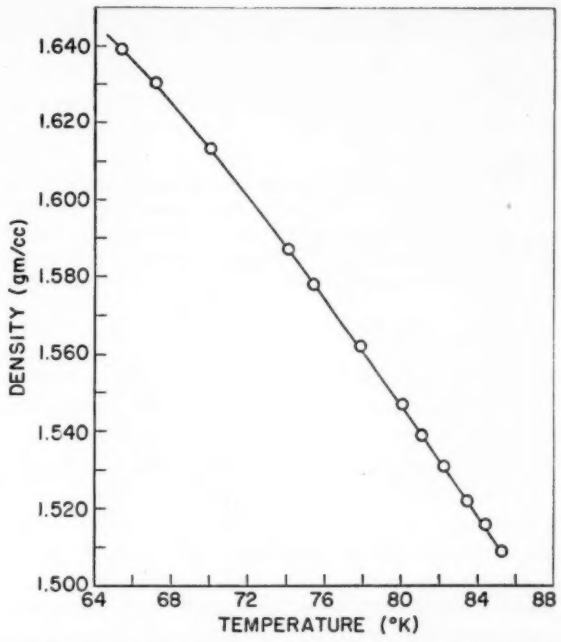

FIG. 2. Temperature dependence of the density of liquid fluorine.

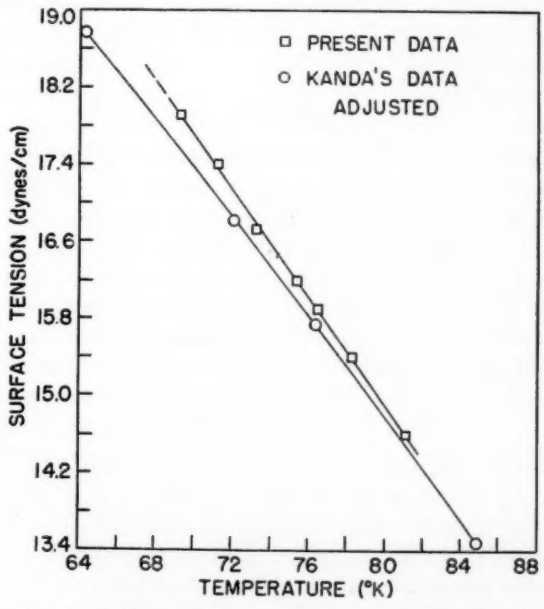

FIG. 3. Comparison of the modified surface-tension results of Kanda with the data presented in this paper.

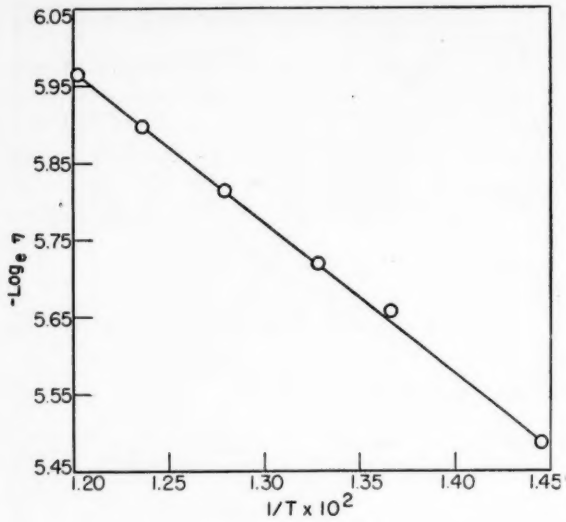

FIG. 4. Log$_e\eta$ *versus* $1/T$.

brated by means of a cathetometer and mixtures of carbon tetrachloride, methyl alcohol, and bromoform of known densities. The float was finally adjusted to have a 6-cm rise over the density range 1.500 to 1.650 g/cc. This float was enclosed in a tube of the same diameter as that used for its calibration, and the tube was inserted in place of the viscosity apparatus at 0 in Fig. 1. When the thermal contraction of the float and the differences in surface tension between fluorine and the calibrating liquids were taken into account, the density of liquid fluorine could be determined by direct observation with a cathetometer.

The two cylinders of fluorine used in this study were obtained from the Pennsylvania Salt Manufacturing Company and were found by chemical analysis to contain 98.66 and 98.68 mole percent F_2. The remaining constituents were O_2, 0.67 and 0.58 percent; N_2, 0.40 and 0.61 percent; and HF, 0.27 and 0.13 percent, respectively.

RESULTS

A summary of the experimental results for the density of liquid fluorine is presented in Table I. The boiling point at atmospheric pressure in these experiments was 85.2°K, and the density at this temperature was found to be 1.509 with an accuracy of ±0.002 g/cc (estimate of the authors). The change of density with temperature over the range 65.0 to 85.2°K is shown in Fig. 2.

The surface tension γ was found by using the equation

$$\gamma=\tfrac{1}{2}rhg(\rho_l-\rho_v), \tag{1}$$

where r is the radius of the capillary, h is the capillary rise, g is the acceleration due to gravity, and ρ_l and ρ_v are the densities of the liquid and vapor, respectively. The angle of contact for fluorine was taken to be zero, and the meniscus was assumed to be spherical in shape. The error caused by capillary rise in tube I was found to be negligible in comparison with an estimated error of 1 percent in these data. The experimental data for the surface tension is given in Table II, and Fig. 3 shows a comparison of these results with those of Kanda, his results having been adjusted by means of the density values presented in this paper.

The viscosity η was calculated from the equation

$$\eta=\frac{\pi r^4 gt}{8lV}(\rho_l-\rho_v)\frac{h_1-h_2}{\log_e(h_1/h_2)}-\frac{\rho_l V}{8\pi lt}, \tag{2}$$

where l is the length of the capillary tube, V is the volume of flow in the time t, and h_1 and h_2 are the differences in height between the liquid levels in the upper and lower reservoirs at the beginning and end of the time interval, respectively. When the data obtained from calibration were used, Eq. (2) could be expressed as

$$\eta=8.379\times10^{-7}t(\rho_l-\rho_v)\frac{h_1-h_2}{\log_e(h_1/h_2)}-\frac{0.0370\rho_l}{t}, \tag{2a}$$

where η is in poises when cgs units are used for all of the other quantities. The values obtained are given in Table III, and Fig. 4 shows the straight line obtained when a plot is made of log$_e\eta$ *versus* $1/T$. The effect of the differences in surface tension between fluorine and the liquids used for calibration was found to be negligible in comparison with an average accuracy of 1 percent estimated by the authors for these results. The Reynolds number for the highest velocity of flow through the capillary tube is 1350, which is below the critical value by an amount sufficient to prevent the initiation of turbulent flow.

TABLE III. Viscosity of liquid fluorine.

Temp, T (°K)	$\frac{h_1-h_2}{\log_e(h_1/h_2)}$ cm	t (sec)	η (centipoises)
69.2	16.38	200.0	0.414
73.2	16.27	176.2	0.349
75.3	16.23	169.0	0.328
78.2	16.17	159.0	0.299
80.9	16.12	150.6	0.275
83.2	16.08	144.5	0.257

The viscosity in poises can be calculated from the equation

$$\eta=2.43\times10^{-4}\exp^{196/T}, \tag{3}$$

where T is the temperature in degrees Kelvin. The measured value of η at $T=73.2$°K deviates from the value calculated by means of Eq. (3) by −1 percent; all other measured values agree within 0.5 percent of those calculated.

ACKNOWLEDGMENT

The authors wish to thank H. F. Keller, Jr. and Lois L. Taylor, who made the analysis of the fluorine used in these experiments, and Dr. L. G. Cole for a number of helpful suggestions during the course of the work.

The Influence of Temperature and State on Infrared Absorption Spectra: Methyl Iodide*

IRVING L. MADOR AND RUTH S. QUINN†
Applied Physics Laboratory, The Johns Hopkins University, Silver Spring, Maryland
(Received July 7, 1952)

The spectra of methyl iodide were determined in the range 2 to 15 microns for the vapor at 25°C, the liquid at 25° and −50°C, and the solid at −78°, −196°, and −269°C. Differences were observed in frequencies, intensities, and band shapes resulting from changes in state and temperature. There is band narrowing with reduction in temperature even in the solid. At the lowest temperatures, band splitting could be resolved in the degenerate bands as well as in the 1252 cm^{-1} nondegenerate fundamental. Several additional assignments are offered.

SINCE the marked sharpening of infrared absorption bands of substances in the condensed phase at low temperatures was first demonstrated by Avery and Ellis,[1] a number of workers have examined low temperature spectra of simple molecules.[2] In many cases where there was band overlapping at ordinary temperatures, the low temperature spectra have made apparent considerably more structure. Low temperature spectra have also been examined and interpreted from the point of view of rotational isomerism and of crystal structure.[3]

An investigation of the temperature dependence of infrared absorption bands is of importance in providing information in regard to the existence of free or restricted rotation in the liquid and solid states. Infrared absorption bands of liquids and solids do not exhibit rotational fine structure because perturbations produced by the force fields of closely packed neighboring molecules broaden the rotational energy levels so that they overlap. However, if infrared band envelopes reflect the thermal distribution of rotational levels, they should narrow markedly as the temperature is lowered, since higher rotational energy levels will be depopulated.

The distinct narrowing of infrared bands of several liquids and solids observed by Avery[1,4] and his coworkers and by Rank and Axford[5] was considered by these workers as being in agreement with the expected behavior of band envelopes ascribed to rotational-vibrational transitions. Crawford, Welsh, and Harrold[6] have investigated the wings of Raman bands of liquid oxygen, nitrogen, and liquid and solid methane and have interpreted the extent and intensity distribution of these wings as a direct reflection of the presence of free rotation. They further predicted that all similar molecules which have sufficiently high symmetry and low interaction energies should have free rotation in the liquid and even in the solid state.

Based on an investigation of several polymers, King Hainer, and McMahon[7] state that the lack of marked band narrowing with decrease in temperature provides evidence for the absence of rotation in the solid state. These authors propose that at low temperatures "the band widths are directly related to the statistical distribution of the absorbing group in a variety of environments." Walsh and Willis[8,9] measured the temperature dependence of infrared absorption of several substances and found that there was little effect on band width. They interpreted Avery's observations on band narrowing as a result of change of phase only.

It should be noted that most of the negative conclusions as to band narrowing are based on studies of high molecular weight or associated compounds (e.g., rubber, polystyrene, Nujol, 1,4,5,8 tetrahydroxyanthraquinone, and methanol). It has also been pointed out[10] that the observance of narrowing, especially at low temperatures, may be limited by the resolving power of the spectrometer.

Except for benzene,[11,12] no effort has been made to study systematically the effect on the infrared spectra of change of temperature and phase. It seemed worth while to conduct such a study with a substance whose spectrum was readily subject to analysis and to extend the observations down to liquid helium temperature. Because of its geometric simplicity (simple symmetric top) and because the infrared spectrum of the vapor is well understood, methyl iodide was chosen for this investigation.

EXPERIMENTAL METHODS

The methyl iodide used in these experiments was Eimer and Amend cp grade. Purification of the methyl iodide was accomplished by passage through a silica gel adsorption column, followed by fractional distillation. The middle fraction had a boiling point of 42.1°C and a refractive index (n_D^{25}) equal to 1.5270. The infrared absorption spectra of the purified and unpurified samples were identical.

* This work supported by the Bureau of Ordnance, U. S. Navy, under Contract NOrd 7386.
† Present address: Spectroscopy Laboratory, Massachusetts Institute of Technology, Cambridge, Massachusetts.
[1] W. H. Avery and C. F. Ellis, J. Chem. Phys. **10**, 10 (1942).
[2] For review, see D. F. Hornig, Disc. Faraday Soc. **9**, 115 (1950).
[3] J. K. Brown and N. Sheppard, Disc. Faraday Soc. **9**, 144 (1950).
[4] W. H. Avery and J. R. Morrison, J. Appl. Phys. **18**, 960 (1947).
[5] D. H. Rank and D. W. E. Axford, J. Chem. Phys. **17**, 1339 (1949).
[6] Crawford, Welsh, and Harrold, Canadian J. Phys. **30**, 81 (1952).
[7] King, Hainer, and McMahon, J. Appl. Phys. **20**, 559 (1949).
[8] A. Walsh and J. B. Willis, J. Chem. Phys. **17**, 838 (1949).
[9] A. Walsh and J. B. Willis, J. Chem. Phys. **18**, 552 (1950).
[10] R. M. Hainer and G. W. King, Nature **166**, 1029 (1950).
[11] R. S. Halford and O. A. Schaeffer, J. Chem. Phys. **14**, 141 (1946).
[12] R. D. Mair and D. F. Hornig, J. Chem. Phys. **17**, 1236 (1949).

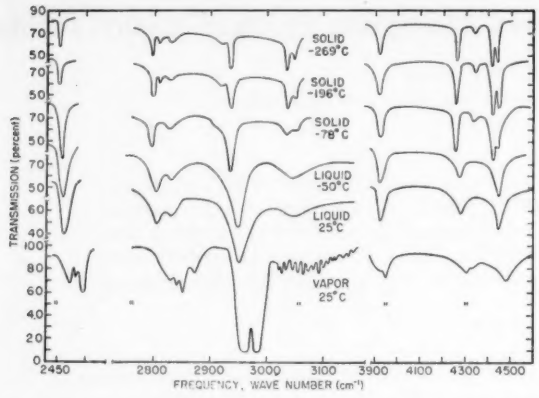

FIG. 1. The infrared spectra of methyl iodide between 2430 cm^{-1} and 4600 cm^{-1}. Spectral slit widths used in each region are indicated.

A Perkin-Elmer Model 12B infrared spectrometer employing a Golay detector-amplifier system was used to determine the infrared spectra. A lithium fluoride prism was employed for the spectral region 2 to 6μ and a sodium chloride prism from 6 to 15μ.

(A) Preparation of Samples

The low temperature absorption cell suitable for use with liquid helium refrigerant has been described.[13] Methyl iodide from an external reservoir was transferred as a vapor into the cell, where it was frozen out on a sodium chloride support window refrigerated with liquid nitrogen or helium. The rate of transfer of sample was controlled by a stopcock and by refrigerating the sample reservoir. The best films, approaching 90 percent transparency and quite uniform, were obtained with a very slow transfer rate. The cell had to be refrigerated far below the freezing point of methyl iodide (−66°C) or else deposition took place elsewhere than on the sample window.

To obtain the spectrum of a single methyl iodide sample over the range 25° to −269°C, it was necessary to use a sealed sample cell. Liquid methyl iodide was confined between two polished sodium chloride plates which were separated by a polyethylene spacer, and this assembly was clamped in the sample holder. The infrared spectrum of the liquid sample was measured at 25° and −50°C and that of the solid at −78°, −196°, and −269°C. The solid samples prepared in this manner scattered incident radiation more strongly than the crystalline films of small grain size prepared by the sublimation process. Nevertheless, in regions where it could be assumed that methyl iodide did not absorb, the solid samples transmitted approximately 85 percent of the incident radiation.

Malherbe and Bernstein[14] have found that some organic materials when rapidly deposited from the

[13] W. H. Duerig and I. L. Mador, Rev. Sci. Instr. **23**, 421 (1952).
[14] F. E. Malherbe and H. J. Bernstein, J. Chem. Phys. **19**, 1607 (1951).

TABLE I. Absorption maxima and assignments of methyl iodide vapor.

Assignment	Frequencies (cm^{-1}) This research	Bennet and Meyer[a]	Other	Assignment	Frequencies (cm^{-1}) This research	Bennet and Meyer	Other
$\nu_4+\nu_5$	4481		4478[b]	$\nu_2+\nu_6$	2184		
	[illegible]				2158		
$\nu_2+\nu_4$	4307		4302[b]		2150		
					2142		
$\nu_4+\nu_6$	3943		3949[c]		2134		
			3925		2125		
					2118		
ν_4	3155	3151.4	3153.6		2111		
	3147	3143.8	3144.9		2102		
	3136	3134.5	3136.5		2096		
	3127	3127.3	3127.8		2089		
	3119	3118.8	3119.5				
	3111	3109.9	3111.0				
	3101	3100.9	3102.1	ν_5	1522		1527.5[d]
	3094	3092.4	3093.1			1515.9	1517.8
	3084	3083.6	3084.1			1505.6	1504.8
	3075	3074.2	3075.1		1488	1494.0	1493.1
	3065	3065.2	3065.9		1473	1480.5	1481.3
	3056	3056.2	3056.8			1470.1	1470.0
	3048	3046.8	3047.7		1452		1457.8
	3034	3037.5	3038.5		1437	1445.5	1446.0
	3027	3027.5	3029.3		1426	1434.8	1433.9
	3020	3019.3	3020.2		1412	1422.9	1422.1
	3008	3009.3	3010.7		1404	1410.6	1409.9
					1390	1398.3	1398.9
ν_1			2984.2[d]			1385.5	1387
	2981	2981	2979.4			1378.2	
			2974.6		1370	1367.6	
			2969.8		1358	1356.9	
			2964.9		1348	1346.7	
	2960	2960	2960.1				
			2955.4	ν_2	1261	1263	
					1252	1251.8	1251.8[d]
$2\nu_5$	2874	2872	2855[e]		1238	1240	
	2852	2851					
	2841			ν_6	968		
	2830				960		
					951	949.0	
$2\nu_2$	2494				942	940.6	
	2483				934	932.6	
	2472				925	924.4	
					916	916.4	
$\nu_5+\nu_6$	2293				908	908.6	909.2[d]
	2284				900	900.7	901.0
	2274				893	892.8	893.1
	2263				885	885.1	885.4
	2253				877	877.5	877.7
	2234				869	869.7	
					862	862.4	
					855	854.9	
					848	847.6	
					841	840.0	
					834	833.5	
					827		
					819		

[a] See reference 15.
[b] From Herzberg and Herzberg, see reference 16.
[c] From Moorhead, see reference 17.
[d] From Lagemann and Nielsen, see reference 18.
[e] From Verleger, see reference 19.

[15] W. H. Bennet and C. F. Meyer, Phys. Rev. **32**, 888 (1928).
[16] G. Herzberg and L. Herzberg, Canadian J. Research **27B**, 332 (1949).
[17] J. G. Moorhead, Phys. Rev. **39**, 788 (1932).
[18] R. T. Lagemann and H. H. Nielsen, J. Chem. Phys. **10**, 668 (1942).
[19] H. Verleger, Z. Physik **98**, 342 (1935).

TABLE II. Absorption maxima and assignments for vapor, liquid, and solid methyl iodide.

Frequency (cm^{-1})						
25°C (vapor)	25°C (liquid)	−50°C (liquid)	−78°C (solid)	−196°C (solid)	−269°C (solid)	Assignment
4481	4447	4447	4442 4422	4442 4422	4442 4422	$\nu_4+\nu_5(A_1+A_2+E)$
			4331	4331	4331	$\nu_1+\nu_5(E)$
4307	4275	4275	4255	4255	4255	$\nu_2+\nu_4(E)$
3943	3923[a]	3923[a]	3923[a]	3923[a]	3923[a]	$\nu_4+\nu_6(A_1+A_2+E)$
3061[b]	3046	3046	3056 3037	3052 3037	3050 3037	$\nu_4(e)$
2970	2951	2951	2938	2938	2938	$\nu_1(a_1)$
	2832	2832	2830	2830 2809	2830 2809	$2\nu_5(A_1+E)$
	2804	2804	2798	2798	2798	
2483	2462	2462	2457	2453	2453	$2\nu_2(A_1)$
	[c]	[c]	[c]	2280	2280	$\nu_5+\nu_6(A_1+E)$
	2121	2121	2121	2128 2120	2128 2120	$\nu_2+\nu_6(E)$
1440[b]	1427	1427	1422 1399	1422 1399	1422 1399	$\nu_5(e)$
1252[b]	1239	1239	1239	1241 1236	1241 1236	$\nu_2(a_1)$
882[b]	885	885	892	895 888	895 888	$\nu_6(e)$

[a] Frequency values unreliable because of interference from atmospheric water vapor absorption.
[b] Band centers taken from Lagemann and Nielsen (see reference 18). Other values for the vapor taken from Table I.
[c] Probably obscured by atmospheric CO_2 absorption.

vapor in a manner similar to the method of deposition described here were deposited as glasses. Similar glass formation has been observed with several other substances in this laboratory. Because the sealed samples of methyl iodide which were cooled slowly through the freezing point exhibited an infrared spectrum which was identical in all respects to the spectrum of samples deposited from the vapor, and also because the latter could be seen to be composed of very tiny crystals, it was concluded that the solid methyl iodide in all cases was in a true crystalline state.

(B) Thermometry

A thermocouple junction was soldered with indium into a small depression drilled in the front surface of the sample window. The measured temperatures were 2 to 3° higher than the liquid nitrogen or liquid helium refrigerants.[13] The temperature differential was somewhat greater at −50° and −78°C because of the poorer thermal conductivity of the alkali halide sample windows at these higher temperatures. All sample temperatures referred to in this paper are those of the refrigerant.

EXPERIMENTAL RESULTS

The spectra of methyl iodide vapor, liquid, and solid are shown in Figs. 1 and 2. The spectral slit widths used in each region are indicated on the figures. Identical spectral conditions were employed at all temperatures.

The vapor spectrum was taken with a gas cell of 10-cm path length at a methyl iodide pressure of 250 mm in the lithium fluoride region and at a 100-mm pressure in the region scanned with a sodium chloride prism. The frequencies of the major absorption maxima in the vapor spectrum together with their assignments are given in Table I. Some assignments have been made for bands not previously reported by other investigators.

The spectra of liquid and solid methyl iodide were obtained with a sample confined in a sealed cell. The sample thickness used for the spectral region examined with a lithium fluoride prism was 75μ, and that used in the sodium chloride region was 30μ. The frequencies of the major absorption bands of liquid[20] and solid methyl iodide are given in Table II.

Figure 3 shows three fundamentals of methyl iodide at liquid nitrogen and liquid helium temperatures. This methyl iodide sample was prepared by deposition from the vapor. Its thickness was particularly suitable for an investigation of these bands at the lowest temperatures. The exact thickness was not determined.

The frequency values given for this research are not corrected to vacuum. The uncertainties in the frequency values are estimated as ± 7 cm^{-1} at 2.2μ, ± 2 cm^{-1} at 3μ, ± 3 cm^{-1} at 5μ, ± 2 cm^{-1} at 8μ, and ± 1 cm^{-1} at 11μ. In regions where there is interference by atmospheric absorption, the uncertainties are somewhat higher.

DISCUSSION

(A) Frequency Shifts with Change of Phase and Temperature

Comparison of frequencies of absorption bands of liquid and solid methyl iodide from Table II with the

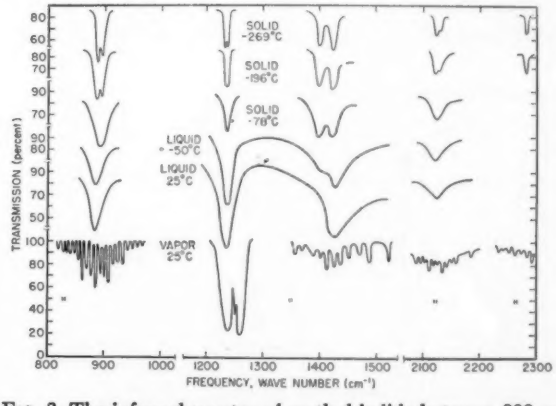

FIG. 2. The infrared spectra of methyl iodide between 800 cm^{-1} and 2300 cm^{-1}. Spectral slit widths used in each region are indicated.

[20] The values for the fundamentals of liquid methyl iodide at room temperature are in agreement with those reported by Fenlon, Cleveland, and Meister, J. Chem. Phys. **19**, 1561 (1951).

corresponding values for the vapor given in Table I shows that there is generally a shift of absorption maxima towards the longer wavelength on condensation and on solidification. The direction and magnitude of frequency changes of overtone and combination bands show poor correlation with changes of their fundamentals. In most cases there is no frequency shift with change in temperature for a given phase. The data do not lend themselves to analysis on the basis of band type (e.g., bending, stretching vibrations), and no explanation can be offered for the seemingly inconsistent pattern of frequency changes with changes in temperature and phase.

(B) Band Splitting

An examination of the spectra shows that all degenerate fundamentals are split in the crystal. The intensities of the two components of these vibrations are comparable except in the case of ν_4, where the high frequency band is less intense. It is likely that ν_6 is split at $-78°C$ as well as at $-196°$ and $-269°C$, but, because of band narrowing with decrease in temperature, this splitting becomes obvious at only the lower temperatures.

Degenerate bands do not appear to be split in the liquid state with the exception of ν_5 which exhibits a shoulder at $-50°C$. The splitting of this fundamental may indicate that a quasi-crystalline structure exists in the liquid at this temperature, while there is a lesser degree of molecular orientation at 25°C. The possibility that splitting of other degenerate fundamental and combination bands in the liquid state is masked by overlapping of broad bands cannot be excluded.

The nondegenerate fundamental ν_2 shows two branches which are separated by 5 cm^{-1}. The splitting of this nondegenerate fundamental may be a result of the presence of more than one molecule per unit cell in crystalline methyl iodide. The splitting observed in degenerate bands might also be the result of space group coupling, rather than removal of degeneracy in the crystalline field. There was some suggestion that each of the branches of ν_5 and ν_6 were split at the lowest temperature, but the resolving power of the spectrometer was insufficient to show that there were definitely four components associated with these fundamentals.

The nondegenerate fundamental ν_1 exhibits a shoulder on the low frequency side at the lowest temperatures. Because this band is very weak, it is probably not a component of ν_1, but it may be the combination $2\nu_5+\nu_3(A_1+E)$.

The degenerate combination band $\nu_4+\nu_5$ is split into two components in the solid state spectra at all three temperatures. The band which appears at 4331 cm^{-1} in all the solid spectra is so weak and is separated by such a large frequency interval, i.e., 76 cm^{-1}, from the degenerate combination $\nu_2+\nu_4$ that it cannot be ascribed to a degeneracy splitting of this band. The band at 4331 cm^{-1} may be the combination $\nu_1+\nu_5$ which is not resolved at the higher temperatures because of overlapping by adjacent bands, or, which may only be active in the solid state. Because there is a question of assignments for discrete bands within the envelope ascribed to $2\nu_5$ in the vapor state,‡ no explanation can be offered for the behavior of this band at low temperatures.

Although the nondegenerate fundamental ν_2 was found to be split at the lowest temperatures, its overtone $2\nu_2$ does not mirror the behavior of this fundamental. The degeneracy of the combination $\nu_2+\nu_6$ is removed in the solid state since this band is split into two components of comparable intensities at the lowest temperatures.

(C) Intensity Alterations with Change of State and Temperature

The series of spectra in Figs. 1 and 2 show that there is a considerable diminution in intensity of most of the absorption bands as the temperature is lowered. This change of intensity cannot be due to a cracking and uneven distribution of the sample upon solidification since all absorption bands would be affected to approximately the same degree and in contrast to the general diminution in intensity, some of the bands, particularly in the short wavelength region, actually show an increase in intensity of absorption.

The integrated intensity of three of the fundamentals ν_1, ν_2, and ν_6 at five temperatures was measured. Two of these fundamental, ν_2 and ν_6, were split at the lowest

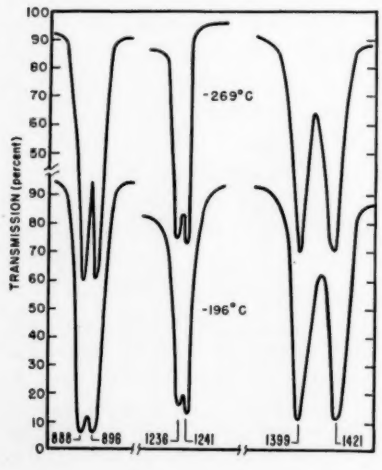

FIG. 3. The fundamentals ν_6, ν_2, and ν_5 of solid methyl iodide. Frequencies of components are indicated.

‡ The bands in the vapor spectrum at 2852 and 2874 cm^{-1} reported by Bennet and Meyer (see reference 15) have been assigned as P and R branches of the A_1 component of $2\nu_5(A_1+E)$. Adel and Barker (J. Chem. Phys. 2, 627 (1934)) have concluded that there is a Fermi resonance between ν_1 and the A_1 component of $2\nu_5$ which causes the mutual displacement of the two bands and explains the unexpected intensity of $2\nu_5$, the perpendicular component of $2\nu_5$ not partaking in the interaction. In addition to the two maxima tabulated by Bennet and Meyer, their experimental curve indicates a strong shoulder at approximately 2835 cm^{-1} to which no assignment has been given. The vapor spectrum determined in this research showed this shoulder resolved into two maxima at 2841 and 2830 cm^{-1}. Until this band is examined with an instrument of higher resolving power, no assignment can be given for the two components.

temperatures and both components were integrated and compared to the single band obtained at the higher temperature. The comparison of the two branches present at liquid nitrogen and liquid helium with the single band obtained at the higher temperatures appears to be valid because this degeneracy, which is either unresolved or unremoved in the liquid and solid samples at the higher temperatures, must contribute to the overall intensity of the single band. The data obtained from these measurements, corrected for differences in scattering between liquid and solid samples, are given in Table III.

In most cases the integrated intensities of bands at various temperatures cannot be used as an indication of the degree of band narrowing. For such a comparison to be valid the percent absorption at the maxima must be the same. For those bands where the percent absorption at the maxima were comparable, the integrated intensity was chosen as a measure of the degree of band narrowing instead of the observed half-width of the absorption band. There may be considerable error in the observed half-width when the true band width approaches or is smaller than the spectral slit width of the spectrometer.§ The experimentally measured integrated intensity should be influenced to a lesser extent by the spectral conditions, although some error may be introduced by incomplete delineation of the wings of the absorption band.[21]

The fundamental ν_1 shows the same value of percent transmission at the maximum in both liquid samples; therefore, the decrease in integrated intensity of approximately 30 percent between 25° and −50°C must be a reflection of band narrowing. The decrease in integrated intensities and the improved characterization of ν_4, $\nu_4+\nu_5$, and $\nu_2+\nu_4$ in the solid must be a result of band narrowing with decrease in temperature since the intensities of the absorption maxima are comparable. There seems to be no general formula which may be applied to estimate quantitatively the amount of band narrowing with temperature.

SUMMARY

The infrared spectra of methyl iodide in three states and at five temperatures have been determined. Samples of solid methyl iodide crystallized from the liquid were identical to those deposited from the vapor. The spectra show that in addition to a general diminution of intensity of absorption with decrease in temperature, there is band narrowing even down to the lowest temperature. This narrowing results in improved characterization of all bands so that degeneracy splitting of fundamentals and combination bands is revealed.

Several additional assignments of overtone and combination bands are made on the basis of the low temperature spectra. From the splitting of a nondegenerate fundamental, it is probable that crystalline methyl iodide has more than one molecule per unit cell.‖ There is usually a frequency shift of the maxima of absorption bands with change of phase, but in most cases there is no frequency shift with change of temperature within a given phase. Most bands are shifted towards the longer wavelengths with increase in state of aggregation.

TABLE III. Integrated intensities at various temperatures relative to the liquid at 25°C.

Temp. °C	State	Band ν_1	ν_2	ν_6
25	liquid	1.00	1.00	1.00
−50	liquid	0.72	0.73	0.76
−78	solid	0.43	0.35	0.72
−196	solid	0.18	0.27	0.56
−269	solid	0.12	0.23	0.25

Conclusion

Any interpretation of the multiple changes manifest in the infrared spectrum of methyl iodide with change of phase and temperature would be extremely complex because of the many factors which must be taken into consideration. These include density changes with accompanying changes in intermolecular force fields, degree of order in closely packed molecules, presence or absence of rotation in either or both liquid and solid, and coupling of molecular vibrations with those of the lattice in the crystal. These factors will influence the frequency, intensity, shape, and width of infrared absorption bands. Any interpretations made at the present time are of necessity speculative because of the lack of adequate foundation on theory and on experimental data.

The narrowing observed in the liquid with decrease in temperature must be due, at least in part, to the depopulation of higher rotational levels. Some contribution to the band width in the liquid state may be made by the absorbing group in a variety of different environments. If the degree of randomness of molecular orientations in the liquid changes with temperature, there should be an attendant change in the band shape.

In the transition liquid to solid, intermolecular force fields must be changed resulting in increased perturbations of molecular vibrations as reflected in frequency shifts of band centers. Since only a few of the random molecular orientations permitted in the liquid will be retained in the crystal, band shapes should change on

§ An attempt was made to determine the true width of the absorption bands at low temperature using the quantitative expressions derived by Willis [Australian J. Sci. 4A, 172 (1951)] which should enable one to calculate the influence of slit width on infrared absorption bands. It was found that this expression was of little use in this application because small errors in experimentally determined quantities such as spectral slit width, which must be employed in the calculations, were reflected as relatively large errors in the evaluation of the "true" band width.

[21] D. A. Ramsay, J. Am. Chem. Soc. 74, 72 (1952).

‖ Neither the crystal structure of methyl iodide nor that of any other methyl halide has been reported in the literature.

solidification. In the solid the frequencies of band centers and the frequency interval between components of degenerate bands are for the most part temperature independent. Assuming there are no crystalline transitions, the narrowing of bands with decreasing temperature in the solid is most probably a manifestation of rotational freedom.

The authors wish to express their appreciation to Dr. W. H. Avery for suggesting the problem and for many helpful discussions.

THE JOURNAL OF CHEMICAL PHYSICS VOLUME 20, NUMBER 12 DECEMBER, 1952

Ion Exchange Mechanism and Isotherms from Deep Bed Performance*

C. Neale Merriam, Jr., Raymond W. Southworth, and Henry C. Thomas
Sterling Chemistry Laboratory, New Haven, Connecticut

(Received August 7, 1952)

The rate laws for diffusion controlled chromatographic ion-exchange are discussed in connection with their application to deep beds of exchanger. Results of experiments with a carboxylic acid resin indicate that solid diffusion is the rate-determining step under the conditions of the experiments. An estimate is found for the value of the diffusion constant. The information is applied to the computation, from a chromatographic elution, of a cesium-sodium isotherm for the exchanger. This result is compared with a direct determination of the isotherm.

THE deduction of exchange isotherms from the performance of chromatographic columns is frequently the most expeditious means of obtaining these data. In favorable cases the disturbances in the columns have little effect upon the form of the boundary of an elution chromatogram, and a fairly accurate isotherm can be deduced on the assumption of true equilibrium.[1,2] However, in order to estimate the effects of the disturbances, one likes to have first-hand information as to the mechanism of the interaction between solution and exchanger in the column. The fact that the differential equations for column performance become linear for isotopic exchanges makes possible a direct test of the mechanism on the column set up for the isotherm determination.

For synthetic cation exchange resins it now appears that the rate determining laws for column performance depend on diffusion either in the solid or in the solution. We will suppose that we are dealing with uniformly packed columns of sufficiently large diameter to make edge effects negligible. We have to deal with three possible extreme cases: slow diffusion in the solid particles; slow diffusion in a liquid film surrounding the solid particles; and, possibly, diffusion downstream in the liquid. Undoubtedly, any real case will be made up of the combined effects of all three, together with other accidental disturbances much more difficult to take into account, which are usually lumped together under the term "channeling."

It will be convenient to summarize the present status of the mathematical descriptions of the three extreme cases. The case of diffusion in the solid has been discussed by several writers.[3–5] The recent work of Rosen[5] is by far the most complete and takes both film diffusion and solid diffusion simultaneously into account. At best, even for the pure solid diffusion case, the numerical treatment for the usual step input is a rather formidable job, and detailed calculations would be worthwhile only under special circumstances. This situation is considerably alleviated by the existence of a very good first approximation to the solid diffusion case. This approximation has long been known, but we will develop it anew in such a way as to evaluate the constant involved and to make reasonable the conditions under which it is applicable. We confine ourselves to spheres of exchanger of uniform radius r_0. If a column contains n of these spheres per unit length, if $q(r)$ is the volume concentration in the solid of the isotopic species of interest, and if Q is the total amount of adsorbed material per unit length of column, then

$$Q=n\int_0^{r_0}4\pi r^2q(r)dr=(4/3)\pi nr_0^3q(r_0)$$
$$-4\pi nr_0^2\frac{r_0^2}{12}\frac{\partial q(r_0)}{\partial r}+\frac{n\pi}{3}\int_0^{r_0}r^4\frac{\partial^2 q}{\partial r^2}dr.$$

When we can neglect the last integral, we have

$$4\pi nr_0^2\frac{\partial q(r_0)}{\partial r}=\frac{12}{r_0^2}\left\{\frac{4\pi nr_0^3}{3}q(r_0)-Q\right\}$$

or

$$\frac{\partial Q}{\partial y}=\frac{12D}{r_0^2\dot{V}}\{ac-Q\}, \tag{1}$$

---

* Contribution No. 1111 from the Sterling Chemistry Laboratory, New Haven, Connecticut.

[1] Don de Vault, J. Am. Chem. Soc. **65**, 532 (1943).

[2] E. Glückauf, J. Chem. Soc. **1949**, 3280.

[3] E. Wicke, Kolloid-Z. **86**, 295 (1939).

[4] H. C. Thomas, J. Chem. Phys. **19**, 1213 (1951).

[5] J. B. Rosen, J. Chem. Phys. **20**, 387 (1952).

in which y is the volume downstream and $\dot{V}$ the (constant) rate of flow, since the rate of exchange is the rate of transfer across the total boundary of the particles and since $(4/3)\pi n r_0^3 q(r_0)$ is the total amount of exchanged material when equilibrium is reached at concentration c. We suppose, since we are deliberately neglecting film diffusion, that we have instantaneous equilibrium at the surface of the particles. Equation (1), of course, presupposes a linear isothermal relation between q and c.

The approximation involved in neglecting the integral containing $\partial^2 q/\partial r^2$ corresponds to replacing the q *vs* r contours within the particles by straight lines. The approximation will be most accurate for high $D/r_0^2\dot{V}$; i.e., under conditions of near approach to equilibrium. It is thus most useful when the rate law is needed to estimate differences from equilibrium behavior. For computational purposes this is a fortunate circumstance; the necessary tables are available.[6]

The validity of the assumption that diffusion in the solid is the factor of principal importance in a particular case is subject to direct test.[4] If two columns are prepared, one of definite capacity with uniform spheres of radius r_0 and the second with spheres of radius θr_0 and capacity θ^2 times that of the first, then the abscissas of the elution curve of the second column should be given by θ^2 times the abscissas of the elution curve of the first column. This test avoids all computational difficulties but, of course, necessitates considerably more experimental work.

If the performance of the column is determined solely by the rate of diffusion through a static liquid film of thickness Δr_0 surrounding the particles, the first approximation to the rate law has the same form[7] as (1). In this case the constant has the form $3D_l/\kappa r_0 \Delta r_0 \dot{V}$, in which the diffusion constant now refers to the value for the liquid solution and κ is the distribution coefficient of concentrations (solid/solution). The different dependence on r_0 is most significant.

Although it is unlikely that downstream diffusion could have any large effect on the shape of an elution chromatogram when high concentration gradients are "washed out" by other slow processes, it is of some interest to test the possibility for a case in which all the data are available and no adjustable constants remain in the formula. On the assumption of instantaneous equilibrium the effect of downstream diffusion is given by

$$c/c_0 = (1/2)\,\mathrm{erfc}\left\{\frac{x(m+a)-V}{2\sqrt{V}}\left(\frac{\dot{V}}{D_l(m+a)}\right)^{\frac{1}{2}}\right\}$$

$$+(1/2)\exp(\dot{V}x/D_l)\,\mathrm{erfc}\left\{\frac{x(m+a)+V}{2\sqrt{V}}\left(\frac{\dot{V}}{D_l(m+a)}\right)^{\frac{1}{2}}\right\},$$

in which V is the elution volume and m is the free space per unit length of column. This expression, or its equivalent, was apparently first given by Wicke.[3]

In order to assess the applicability of the above formulas in a well-defined case, experiments have been carried out with specially prepared samples of Amberlite XE-79[8] (Lot No. 2136). This material is a carboxylic acid resin in the form of nearly spherical beads. Approximately 800 grams of the resin was stirred for 2–3 days in five liters of water with 928 g of sodium chloride and about 250 g of sodium hydroxide. After decantation the resin was washed somewhat with water, packed in a two-inch glass tube, and washed continuously for five days with a stream of 0.1970M sodium chloride solution. A total of about 110 liters was passed through the column. The pH of the effluent dropped from 11.2 to 9.8 after four days of elution. The pH of the influent was raised to 9.2, then to 9.8, by addition of small amounts of sodium hydroxide. The pH of the final 10–20 liters of effluent remained constant at 9.8. The resin was then separated into six fractions by wet-sieving through Tyler screens Nos. 14, 20, 28, 40, and 60, using the same sodium chloride solution. The various fractions were preserved under this solution.

Two of the fractions were used in the experiments reported here: the 14–20 fraction with average particle radius 0.050 cm and the 28–40 fraction with average radius 0.025 cm. These figures are merely the average sieve openings. No attempt was made to measure the particles more exactly or to determine the distribution of sizes in a given fraction.

Three columns were constructed in glass tubing of 1.5-cm inside diameter: column AD of length 9.1 cm containing the smaller particles; column AF, 18.1 cm long containing the larger particles; and column AE, 37.9 cm long, also with the larger particles. The AE column was shortened twice during the course of the experiments in order to obtain data which could be interpolated to represent a column of just four times the capacity of the AD column.

Numerous isotopic exchanges at room temperature were carried out, using always the 0.1970M NaCl solution adjusted to pH 9.8, with and without Na^{22} as tracer. The flow rate was regulated manually and was maintained as closely as possible to an average value of 5.3×10^{-3} ml/sec. Slow variations in rate amounting to as much as twenty percent did occur. The rate, however, was readjusted at frequent intervals, except during the night hours of some of the longer runs. Samples were collected automatically. A drop counter actuated the sampling mechanism so that samples of nearly the same size were taken. The exact sizes of the samples were determined by weighing, the volumes being calculated from a measured value of the density (1.006). The isotopic concentrations were determined by standard techniques using Geiger-Müller counters.

[6] In this connection, see Faucher, Southworth, and Thomas, J. Chem. Phys. **20**, 159 (1952).

[7] Boyd, Adamson, and Myers, J. Am. Chem. Soc. **69**, 2836 (1947).

[8] Rohm and Haas Company, Philadelphia, Pennsylvania.

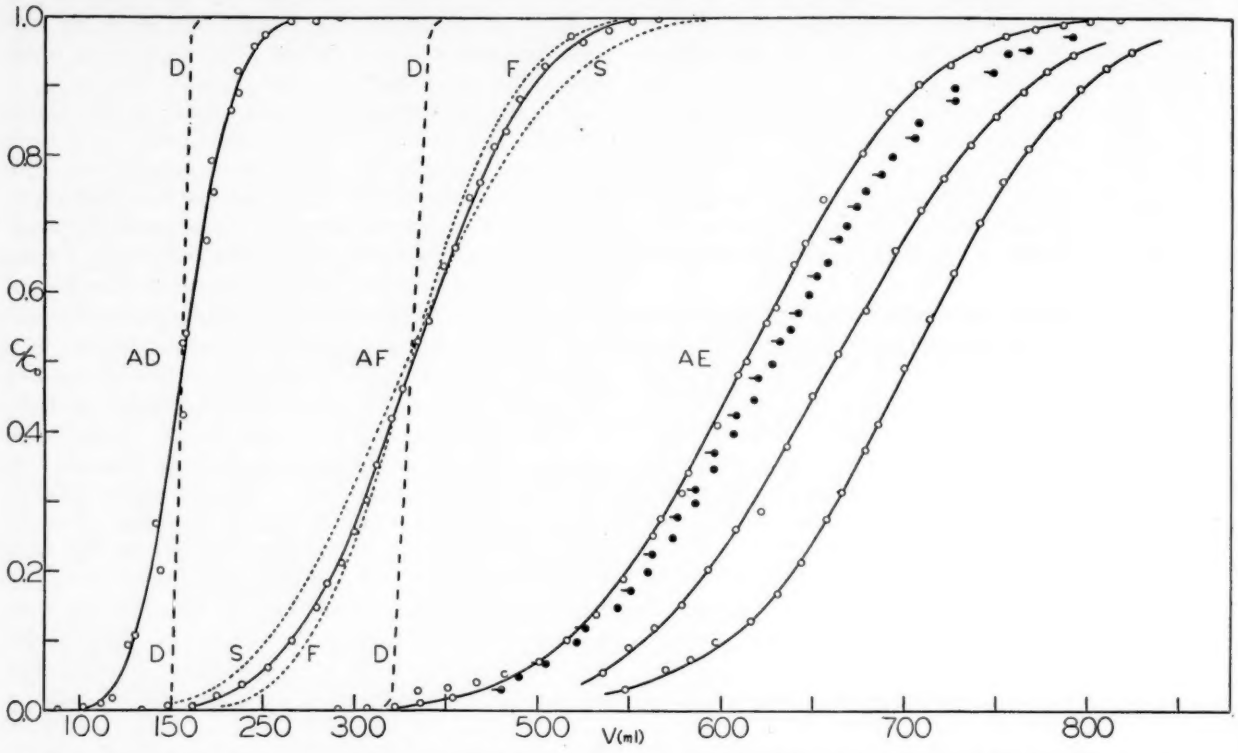

FIG. 1. Isotopic exchanges, observed and calculated, on deep beds of a carboxylic acid exchanger. (For explanation see text.)

We did not succeed in devising a scheme for measuring the hold-up volumes of the columns without changing the characteristics of the resin. These volumes were estimated for the three columns as 7, 14, and 28 ml. (Using a hypodermic syringe connected to the bottom of the *AD* column, we did succeed in withdrawing 5 ml of solution from the full column.)

The data for the isotopic exchanges are summarized in the curves of Fig. 1. The concentration ratios, from the count determinations, are plotted against the midpoints of the sample volumes taken. The capacities of the columns were determined either by direct summation of the samples or by reading points from the curves at equally spaced intervals and using the Simpson formula. As to precision there was nothing to choose between the two procedures. The solid line for the *AD* column represents the curve given by

$$c/c_0 = \exp(-98-0.654y)\times\varphi(98, 0.654y), \qquad (2)$$

in which the constants correspond to a total column capacity of $98\times0.1970/0.654=29.5$ meq. (The definition and properties of the φ-function are given in the appendix.) The constants in (2) were determined by purely empirical curve fitting, the only fixed guide being the necessity of preserving the agreement between the ratio of the parameters and the known capacity of the column. As is apparent, the calculated curve agrees with the data to well within the reproducibility. (A more or less random selection of points from three runs is shown in conjunction with the *AD* curve.) This agreement, of course, proves little or nothing as to the mechanism of the exchange process.

Several isotopic exchanges were carried out on column *AE* with intervening removal of resin in attempts to obtain a column of just four times the capacity of the *AD* column. From the three sets of data, for two columns too long and one slightly short, points at round concentrations were interpolated for the desired column. These are shown in Fig. 1 as solid circles without tails. The corresponding points obtained by multiplying the abscissas of the *AD* column by four are shown as solid circles with tails. The agreement here is certainly within the experimental error.

For changes only in particle size and capacity the parameters in formula (2) for column *AD* can immediately be converted to the appropriate parameters for the longer columns if we assume one or the other of the simple rate laws. The appropriate sets of parameters follow:

	Approximate Solid diffusion		Film Diffusion	
	Bx	*A*	*Bx*	*A*
AF	51.8	0.1635	103.6	0.327
AE	98	0.1635	196	0.327

(In the case of the *AF* column the capacity was 2.114 times that of the *AD* column. For the *AE* column the calculation is for the "fourfold" interpolated data.) To avoid confusion in the figure, the calculated curves are given, as dashed lines, only for the *AF* column (*S* signifies solid diffusion; *F*, film diffusion).

The film diffusion curves in all cases predict somewhat too sharp a breakthrough. The discrepancy is well outside the experimental error. The approximate rate law for solid diffusion predicts too gentle a breakthrough. A little consideration shows that this is just what is to be expected. If the development of the approximate rate law is carried out by parts integration of rq, the neglected integral then contains $\partial^2(rq)/\partial r^2 = (1/D)\partial(rq)/\partial t > 0$ and is certainly positive. Thus when we compute as above for the larger particles, where the neglected integral is larger, we are using too low a rate and obtain too gentle a breakthrough.

Also in Fig. 1, in conjunction with the curves for the AD and AF columns, are given the curves calculated for downstream diffusion as the only disturbance. Here we have used the value $D_l = 1.32\times10^{-5}$ cm^2/sec for the self-diffusion constant of sodium in 0.1970M NaCl solution.[9] It is quite apparent that the effect cannot explain the results. It is of interest to notice that as such a front progresses down the column it becomes but slightly more diffuse; once the high concentration gradients are lost, downstream diffusion produces little further effect.

TABLE I. Cesium-sodium isotherm for carboxylic acid exchanger from chromatographic data.

$q/q_0 = (c_0/q_0x)\{F/c_0 + y(c/c_0) + \Delta[y\partial(c/c_0)/\partial y - c/c_0]\}$
$q_0 = 28.63$ meq.; $y = (V-7)$ ml; $\Delta = 1/0.654$

V	F/c	c/c_0	$\partial(c/c_0)/\partial y \times 10^4$	q/q_0
70	82.35	1.000	0.00	1.000
80	72.79	0.978	31.25	0.979
90	62.99	0.930	60.24	0.950
100	53.98	0.842	106.9	0.891
110	46.12	0.730	107.5	0.815
120	39.35	0.630	101.0	0.742
130	33.56	0.528	94.33	0.660
140	28.68	0.444	81.63	0.589
150	24.62	0.372	65.15	0.522
170	18.28	0.268	43.57	0.416
190	13.65	0.198	29.96	0.335
210	11.23	0.148	19.05	0.278
230	7.58	0.118	13.21	0.229
250	5.48	0.092	12.08	0.189
270	3.87	0.070	9.20	0.150
290	2.65	0.054	7.84	0.120
310	1.73	0.039	6.47	0.091

Having established fairly satisfactorily that solid diffusion is the most important effect in the case under consideration, we may calculate the value of the diffusion constant necessary to explain the results: $12D/r_0^2\dot{V} = 0.654$, giving $D = 1.8\times10^{-7}$ for the carboxylic acid exchanger. (For the case in which the neglected integral is definitely positive, we find $D < 3.6\times10^{-7}$.) Because of variation in the size of the particles as well as because of the uncertain magnitude of the neglected integral, the value $D = 1.8\times10^{-7}$ can be considered only as an estimate. It is about one-hundredfold lower than the corresponding constant for the solution, as might be expected. Confirmation as to order of magnitude is to be found in the unpublished experiments of C. Raseman and R. H. Bretton,[10] who obtained in a different type of experiment $D = 5\times10^{-7}$ for the phenolic exchanger Dowex 50.

[9] Jui Hsin Wang and Sara Miller, J. Am. Chem. Soc. **74**, 1611 (1952).

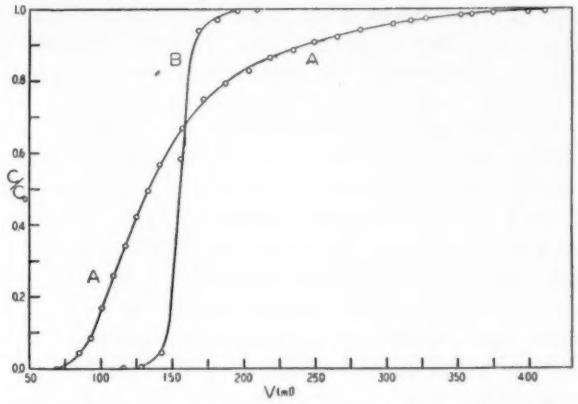

FIG. 2. Cesium-sodium exchanges on a carboxylic acid exchanger. *A*. Displacement of sodium by cesium. *B*. Displacement of cesium by sodium.

As an illustration of the use of the information obtained, we have carried out experiments in which the AD column was eluted with a solution 0.1970M in cesium chloride. The elution curve is shown in Fig. 2 as curve A. Curve B in this figure shows the displacement of cesium from this column by sodium. Using the method given by Faucher, Southworth, and Thomas,[6] the exchange isotherm has been calculated. The essential parts of the calculation are given in Table I, and the resulting isotherm is shown as the solid line in Fig. 3.

The sodium-cesium isotherm was investigated independently of the chromatographic work in several

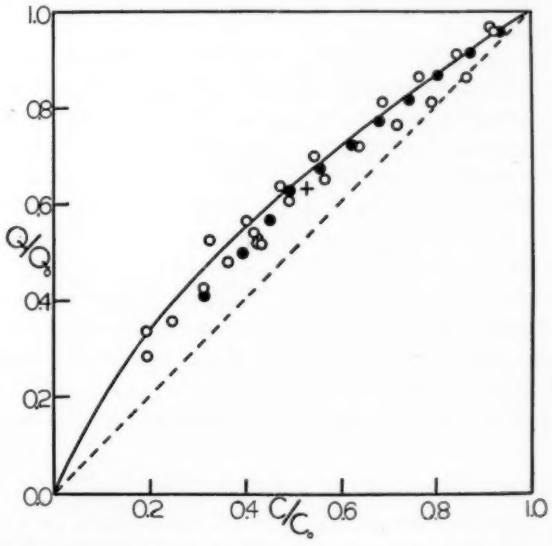

FIG. 3. Sodium-cesium isotherm on a carboxylic acid exchanger. Solid curve from chromatographic elution. Circles from direct determinations.

[10] R. H. Bretton (private communication).

series of experiments. These experiments were designed to produce the exchange data without introducing large uncertainties in the character of the solid phase. In the first series a portion of the 28–40 mesh resin was equilibrated anew with 0.1970*M* NaCl at *p*H 9.8. The material was merely drained free of liquid, and twelve five-gram samples of the moist resin were weighed out. To each portion in a glass-stoppered flask was added 100 ml of 0.1970*M* NaCl carrying Na^{22} tracer. The flasks were shaken at room temperature for 48 hours, and carefully measured samples of solution were withdrawn and replaced with equal volumes of 0.1970*M* CsCl. The flasks were again shaken for at least 48 hours; samples were again removed and replaced by cesium solution. The process was repeated twice more. The sizes of the samples taken were adjusted so that the isotherm was covered from $c/c_0=0.2$ to $c/c_0=1$. The concentration ratios were determined with the aid of the Geiger counter. Using only the fact of uniform distribution of activity at equilibrium, sufficient data were available to calculate the total capacity of the resin and its sodium content after each stage of the experiment.

The experiment just described has the disadvantage that as it progresses the counting errors have a progressively larger effect on the results; the computations necessarily depend on differences of the counting rates. To eliminate some of these errors eight of the samples of resin were quantitatively removed to small columns and re-equilibrated with dead NaCl. The resins were returned to the shaking flasks, and various mixtures of NaCl solution and $CsCl+Cs^{137}$ were added. After a 48-hour period of equilibration samples were withdrawn for counting. No successive withdrawals and additions were employed. The computations do depend, however, on the previously determined capacities of the resin samples.

Still dissatisfied with the results, we carried out a third series of experiments with fresh portions of freshly equilibrated resin. This resin was drained, rinsed quickly with acetone, and dried in a stream of air in order to obtain more uniform and more easily weighable samples. Fourteen samples of 5.000 g each were taken. With three of these the capacity was determined by the addition of 100 ml of 0.1970*M* $NaCl+Na^{22}$. Isotherm points were obtained with the remaining samples in the fashion indicated for the second series above. The flasks were shaken for four days before sampling. The capacity determinations gave 3.20, 3.04, and 3.10 meq./g for the acetone-air dried material. The average of these figures was used in the computations. The results of all the experiments are shown in Fig. 3. The large cross in the figure gives a somewhat pessimistic estimate of the effect of the experimental errors on a single point, the largest error being that of the counting.

We are inclined to give most weight to the results of the last series of determinations, which are indicated as solid circles in the figure. These results are quite adequately described by the expression

$$K=q(c_0-c)/(q_0-q)c=1.55,$$

in which all concentrations refer to sodium. The results of the chromatographic experiments cannot be reproduced by the simple equilibrium constant expression. The empirical equation

$$q/(q_0-q)=1.61c/(c_0-c)+0.19[c/(c_0-c)]^{\frac{1}{2}}$$

will, however, reproduce the data. It is apparent, unfortunately, that our experiments do not admit of a decision as to the adequacy of the correction procedure applied to the chromatographic data.

This work was done as a part of an investigation supported by a contract between Brookhaven National Laboratory and Yale University. We are much indebted to Brookhaven Laboratory for its continued interest.

APPENDIX

The φ-function is defined by either of the following relations:

$$\varphi(u,v)=e^u\int_0^u e^{-t}I_0[2(vt)^{\frac{1}{2}}]dt$$

$$=\sum_{0\le n<m}^{\infty}\frac{u^m v^n}{m!n!}.$$

The function is the solution of the hyperbolic equation $\partial^2\varphi/\partial u\partial v=\varphi$, which has the boundary values

$$\varphi(0,v)=0,$$
$$\varphi(u,0)=e^u-1.$$

In using the φ-function the following relations are essential:

$$\varphi(u,v)+\varphi(v,u)=e^{u+v}-I_0(2uv),$$
$$\partial\varphi(u,v)/\partial u=\varphi(u,v)+I_0[2(uv)^{\frac{1}{2}}],$$
$$\partial\varphi(u,v)/\partial v=\varphi(u,v)-\partial I_0[2(uv)^{\frac{1}{2}}]/\partial v.$$

(In the above formulas I_0 is the Bessel function for purely imaginary argument.)

Absorption Studies of the Vapors of the Three Isomeric Picolines in the Near Ultraviolet*,†

J. H. RUSH‡ AND H. SPONER
Department of Physics, Duke University, Durham, North Carolina
(Received July 7, 1952)

Studies of the near ultraviolet absorption spectra of α-, β-, and γ-picoline vapor have been made in low and medium dispersion. Conclusive evidence is found for two electronic transitions in the vicinities of 35500 and 38500 cm^{-1}. The former transition is interpreted as an allowed A_1-B_2 transition resulting from the excitation of an sp^2 nonbonding electron of the nitrogen atom into the first unfilled π-orbital of the ring. The latter transition is considered an allowed A_1-B_1 transition resulting from the excitation of a π ring electron. The A_1-B_2 system exhibits narrow headless bands similar to the first absorption bands in pyridine. It is of weak intensity comparable to that of the forbidden $A_{1g}-B_{2u}$ transition in benzene. The A_1-B_1 system, which is much stronger, consists of broad diffuse bands. There is evidence that this system may be overlapped by another transition in β-picoline.

INTRODUCTION

In recent years a number of spectroscopic studies in the near ultraviolet have been published for the vapor phase of simple aromatic molecules consisting of a benzene ring with single and multiple substitutions of atoms or simple groups for an H atom in the ring. A logical further step has been to study spectroscopically the effect of a substituent in the carbon ring itself, as in pyridine (C_5H_5N), and also to compare the effects of a given substituent replacing an H atom in benzene and in pyridine.

The analysis of the near ultraviolet absorption spectrum of pyridine was undertaken by Henri and Angenot in 1935,[1] and later by Sponer and Stücklen.[2,3] In the latter publications it was assumed that the excitation in pyridine is caused by the $2p\pi$ electrons of the ring as in benzene. The treatment leads to an electronic level of symmetry type B_1 as first excited singlet in pyridine. The molecule itself belongs to symmetry group C_{2v}. These analyses were not entirely satisfactory. It was hoped that a study of simple pyridine derivatives would yield information which would also be of significance in the analysis of pyridine. The picolines (methyl-pyridines $C_5H_4N\cdot CH_3$) were chosen for the present study. Apparently no data on their ultraviolet absorption spectra in the vapor phase had been published since some early exploratory studies,[4,5] when this research was carried out. A preliminary report on our experimental findings was published.[6] It was learned that at the same time the near ultraviolet absorption spectrum of pyridine was being reinvestigated at M.I.T. with large dispersion together with a study of the corresponding absorption in completely deuterated pyridine.[7] Recently Herington,[8] in a paper on the use of the electronic spectra of pyridine homologues for quantitative analysis, has reported a number of absorption bands in the vapors of all three picolines. He has also taken the spectra in nonpolar and polar solutions. Similar measurements had been carried out in this laboratory.[9] Absorption curves of α-picoline in isooctane may also be found in the Catalog of Ultraviolet Spectrograms.[10] Raman and infrared frequency values for α- and β-picolines have been well established by Jatkar,[11] Manzoni-Ansidei,[12] Kohlrausch and associates,[13] Lecomte,[14] and others. On the spectrum of γ-picoline, apparently the only published information[15] in this region, is a curve of absorption in the region 800–2000 cm^{-1}.

EXPERIMENTAL PROCEDURES

Samples of α-picoline 99.85 percent pure (bp 129.44°C) and β-picoline 99 percent pure (bp of fraction 143.0 to 143.5°C) were supplied by Dr. J. J. McGovern of the Mellon Institute of Pittsburgh. The γ-picoline was from a lot purified (bp of fraction 144.5 to 145.0°C) by

* This work was supported by the ONR under contract N6ori-107, T.O.I. with Duke University.

† Based in part on a dissertation by J. H. Rush submitted in partial fulfillment of the requirements for the degree of Doctor of Philosophy at Duke University, 1950.

‡ Present address: High Altitude Observatory, University of of Colorado, Boulder, Colorado.

[1] V. Henri and P. Angenot, Compt. rend. **200**, 1032 (1935); Compt. rend. **201**, 895 (1935); J. chim. phys. **33**, 641 (1936).

[2] H. Sponer, Revs. Modern Phys. **16**, 224 (1944).

[3] H. Sponer and H. Stücklen, J. Chem. Phys. **14**, 101 (1946).

[4] F. Baker and E. C. C. Baly, J. Chem. Soc. **91**, 1122 (1907); J. E. Purvis, J. Chem. Soc. **95**, 294 (1909); **97**, 692 (1910); E. Herrmann, Z. wiss. Phot. **18**, 253 (1919).

[5] We are indebted to Drs. J. Duchesne and L. d'Or for such data for α-picoline, from the Ph.D. dissertation of P. Angenot at Liège in 1936.

[6] H. Sponer and J. H. Rush, J. Chem. Phys. **17**, 587 (1949).

[7] Betty Jane Fax, Ph.D. thesis, M.I.T. (1950).

[8] E. F. G. Herington, Disc. Faraday Soc. **9**, 26 (1950).

[9] Harold P. Stephenson, Phys. Rev. **76**, 199A (1949); **83**, 246A (1951).

[10] Am. Petroleum Institute Research Project 44 at the National Bureau of Standards. Catalog of Ultraviolet Spectrograms, Serial No. 213, 2-methyl-pyridine, contributed by Mellon Institute.

[11] S. K. K. Jatkar, Indian J. Phys. **10**, 23 (1936).

[12] R. Manzoni-Ansidei, Boll. Sci. facolta chim. ind. Bologna **1**, **137**, 184 (1940).

[13] Herz, Kahovec and Kohlrausch, Z. physik. Chem. **B53**, 124 (1943).

[14] J. Lecomte, Compt. rend. **207**, 395 (1938); J. phys. radium **9**, 512 (1938).

[15] Barnes, Gore, Liddell and Williams, *Infrared Spectroscopy* (Reinhold Publishing Corporation, New York, 1944), p. 96.

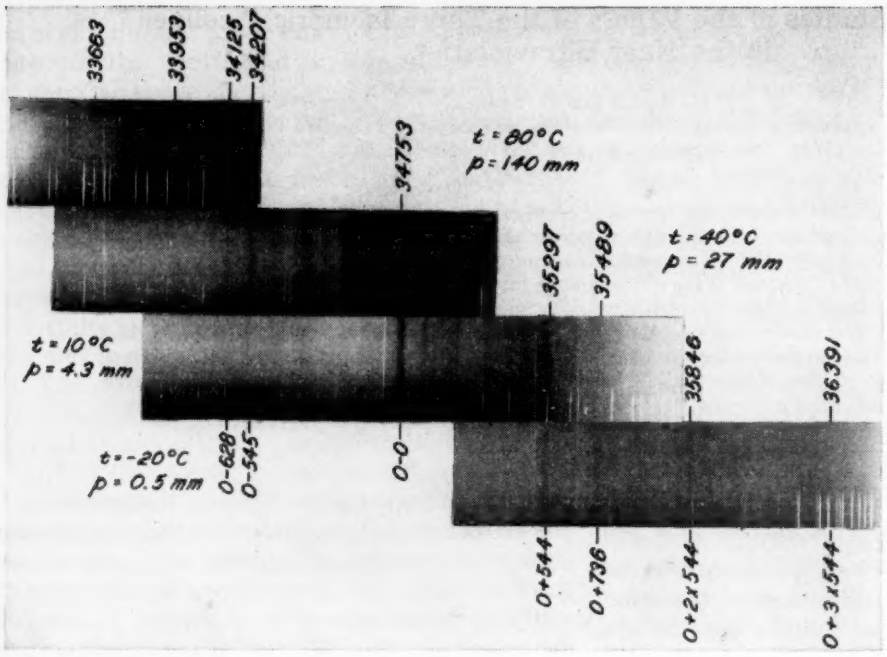

FIG. 1. Spectrum of transition I in α-picoline taken in 75-cm cell.

Dr. J. C. Shivers of the Department of Chemistry of Duke University, and redistilled by us.

Some preliminary studies on the medium Hilger quartz prism spectrograph were made using three short fused quartz cells. Most of the final measurements of the long-wavelength portion of each spectrum were made from plates taken in the first order of a 3-m grating spectrograph. In this latter series a single 75-cm quartz cell was used. Each cell was provided with a reservoir tube for taking the substance.

The spectra were obtained in dependence of the vapor pressures of the substances by varying the temperature of the substance in the cell reservoir. This procedure, of course, has the disadvantage that changes in concentration necessarily involve changes in the degree of thermal excitation of vibrational levels in the ground state of the molecule, since the cell temperature must equal or exceed that of the reservoir to prevent condensation in the cell. But the effects of pressure changes and excitation changes can usually be disentangled to

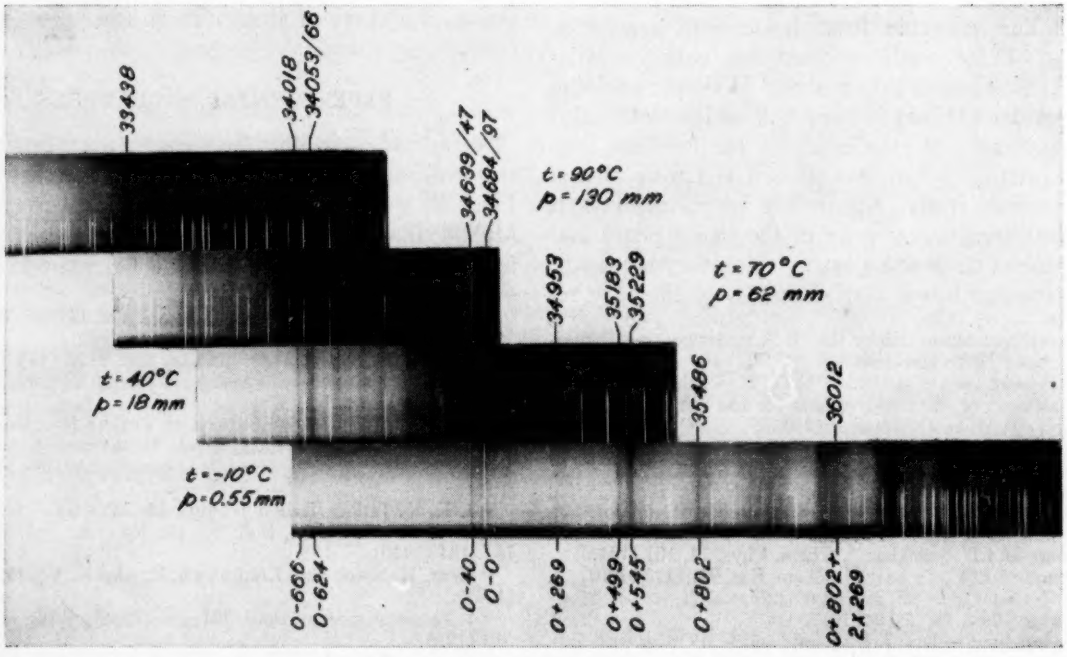

FIG. 2. Spectrum of transition I in β-picoline taken in 75-cm cell.

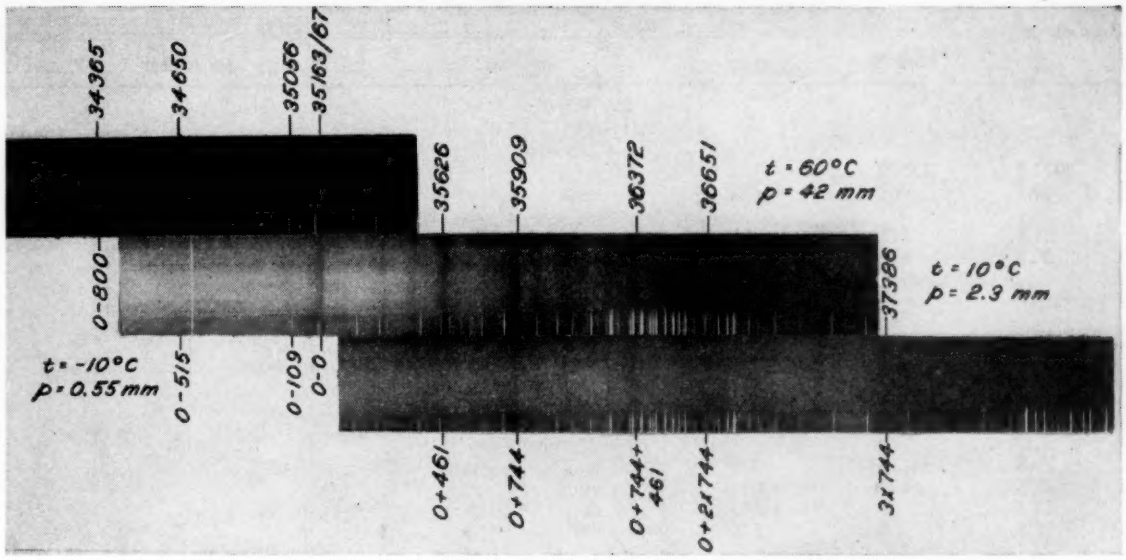

FIG. 3. Spectrum of transition I in γ-picoline taken in 75-cm cell.

some extent, particularly when plates taken with cells of different lengths are compared. Temperature control was effected by using two separate electrical ovens for the absorption tube and the reservoir arm, the latter always being 2 to 5 degrees cooler than any other part of the cell. In working below room temperature, the cell was customarily left at room temperature while the reservoir was immersed in suitable coolants in a small Dewar flask.

The pressures corresponding to the various cell temperatures were evaluated from the data on pyridine and picoline vapor pressures already in the literature. The vapor pressures of α-picoline were obtained from a plot of Riley and Bailey's[16] values, which extended down

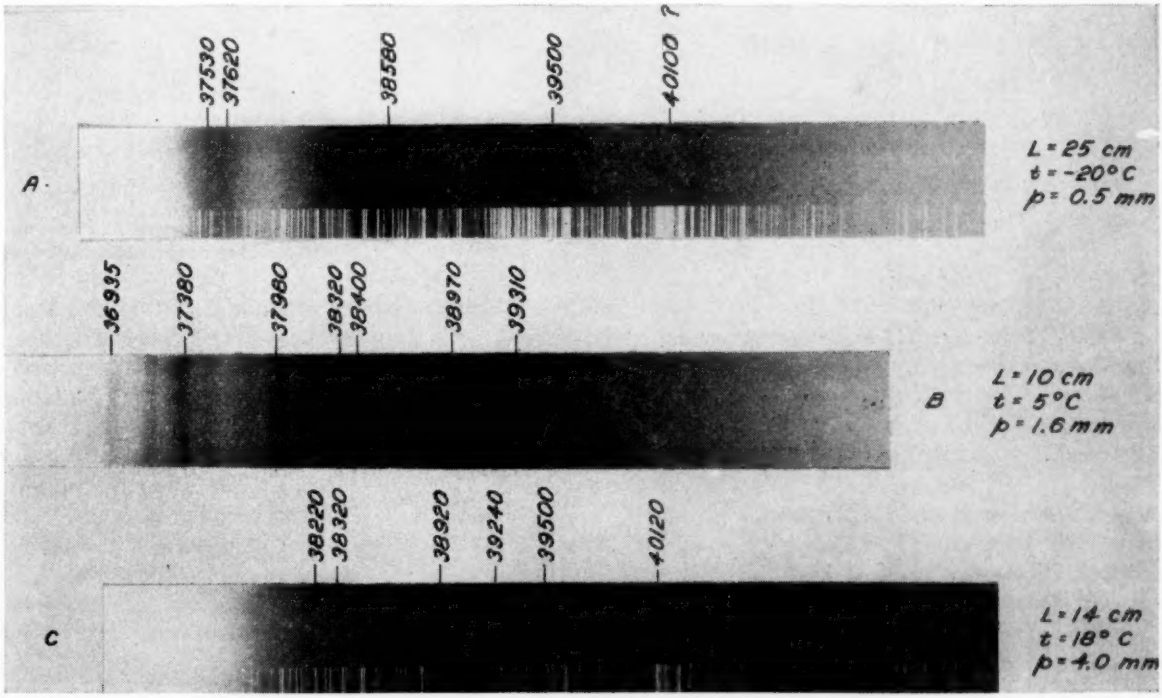

FIG. 4. Spectra of transition II. A: α-picoline, B: β-picoline, C: γ-picoline.

[16] F. T. Riley and K. C. Bailey, Proc. Roy. Irish Acad. **38B**, 450 (1929).

TABLE I. Absorption bands in transition I of α-picoline.

λ(A)	ν (cm⁻¹)	ν−ν₀₋₀	Intensity		Assignment
			L=75 cm t=80°C p=140 mm		
2977.2	33579	−1174	wd		
69.7	663	−1090	vwd		0−2×545 0−1100
51.4	872[a]	−881			0−887
50.8	879	−874	vwd		
				t=60°C p=66 mm	
45.6	939	−814	vwd	vwd	0−813
44.4	953[a]	−800			0−800
			t=40°C p=27 mm		
29.5	34125	−628	w	mwr	0−628
28.8	134	−619	vw		
22.5	207	−546	m	s	0−545
21.8	215	−538	vw	w	
19.3	245	−508		vw	0+120−628 0+207−2×358
18.2	258	−495		vw	
15.5	289	−464	wd	msd	
06.1	400	−353	wd		
05.5	407	−346	wd		0−358
04.4	420	−333	vwd		0+207−545?
				L=25 cm t=60°C p=66 mm	
2899.2	482	−271	wd	vw	0+355−628 0+544−813
96.3	517	−236	vwd		0+120−358
94.7	536	−217	vwd	vw	
93.4	552	−201	wd		0−204
92.3	565	−188	wd	vw	0−188?
88.2	613	−140	mwr	w	
86.4	635	−118	vwd	vw	
83.6	669	−84	wd	vw	0−84; 0−2×42? 0+544−628; 0+120−204
80.1	711	−42	vwd	vw	0−42
			L=75 cm t=20°C p=8.0 mm		
76.6	753	0	vsr	sr	0−0
76.0	760	7	m		
72.4	804[a]	51			
70.1	832	79	mw	mw	
69.5	839	86	w		
69.1	844	91	wd		
66.7	873	120	mr	w	0+120
64.3	903[a]	150			0+355−204
				L=75 cm t=10°C p=4.3 mm	
62.9	920	167		vw	
61.4	938	185	w	vw	0+544−358
59.6	960	207	ms		0+207
56.5	998[a]	245			0+2×120
55.8	35006	253	wr		
55.0	016	263	vwd		
54.0	028	275	vwd		0+355−84
51.0	065	312	md		0+355−42
50.0	078	325	mwd		0+120+207
49.1	089	336	wd	vwd	0+544−204
47.8	105	352	md		0+355

TABLE I—*Continued.*

λ(A)	ν (cm⁻¹)	ν − ν₀₋₀	Intensity		Assignment
			t=0°C p=2.1 mm		
44.5	146	393	vwd		0+207+544−358
40.9	190	437		vwd	
39.3	210	457		wd	0+544−84
36.1	250	497		vwd	0+582−84
32.3	297	544	sr	vs	0+544
31.7	304	551		w	
29.2	335	582	w	vw	0+582
26.8	365	612	vwd	vw	0+355+544−84−204?
24.4	395	642	wr	w	
17.0	489	736	mdr	msdr	0+736
				L=25 cm t=20°C p=8 mm	
12.9	540	787		vwd	0+582+207
10.7	568	815		vwd	0+355+544−84
07.1	614	861	w	w	0+861? 0+736+120 0+355+544−42
03.8	656	903	w	vw	0+355+544 0+952−42
2799.9	705	952	w	vw	0+952?
95.7	758	1005	vw	vwd	0+2×544−84
92.0	805	1052		vwd	0+2×544−42
88.8	846	1093	msr	ms	0+736+355 0+2×544
83.7	912[a]	1159			
82.8	924	1171		mwd	0+1052+120?
78.8	975	1222		wd	
74.8	36027	1274		md	0+3×544−358? 0+736+544
71.0	077	1324		vwd	0+582+736
67.6	122	1369		vwd	
64.4	163	1410		wd	0+355+2×544−42?
61.7	199	1446		wd	0+355+2×544
57.0	260	1507		wd	
			L=25 cm t=10°C p=4.3 mm		
54.3	296	1543	wd	wd	
51.6	332	1579	vwd	vwd	
49.9	354	1601	vwd	vwd	0+3×544−42
47.1	391	1638	mwd	mwd	0+3×544
41.8	461	1706	mwd	mwd	
37.2	522	1769	mwd	mwd	

[a] Unpublished data of Henri and Angenot.

only to 6 mm (16°C). The vapor pressure of β-picoline and γ-picoline was determined at 0° and 20°C by Brown and Barbaras.[17] Extension to lower and higher values was obtained by Dühring's rule from the normal boiling points of these compounds and from the vapor pressure data on pyridine given by van der Meulen and Mann.[18] For low pressures below 1 mm new data were used, obtained[19] on all three picolines in this laboratory.

The optical arrangement was of the conventional type. A low voltage dc hydrogen discharge lamp, watercooled, was used with the Hilger instrument, and a high voltage lamp (0.7 amp at 2200 volts) with the grating spectrograph. A Corning "red purple Corex A" No. 9863 filter, passing the region 2400 to 4000A, was put in front of the source in most exposures. Iron lines were used as the comparison spectrum. Exposure times on the Hilger instrument were about one minute while they ranged on the grating spectrograph from 20 minutes to 2 hours.

It was found that the spectra consist of a long-wavelength portion of low intensity exhibiting narrow, headless bands, and a short-wavelength portion of higher intensity with broad, diffuse bands and with a steep absorption gradient in the region where the portions overlap. Eastman III-O emulsion was found to be best suited for most of the picoline research.

The narrow bands of the long-wavelength region exhibit no clear-cut band heads, but are like the narrow, diffuse-edged bands of pyridine. It seemed, therefore,

[17] H. C. Brown and G. K. Barbaras, J. Am. Chem. Soc. **69**, 1137 (1947).

[18] P. A. van der Meulen and R. F. Mann, J. Am. Chem. Soc. **53**, 451 (1931).

[19] E. R. Hopke and G. W. Sears, J. Chem. Phys. **19**, 1345 (1951).

TABLE II. Absorption bands in transition I of β-picoline.

λ(A)	ν (cm⁻¹)	ν−ν₀₋₀	Intensity		Assignment
			L=75 cm t=100°C p=190 mm		
3030.7	32986	−1698	vw		
26.0	33037	−1647	vwd		
2994.2	388	−1296	m		
91.2	421	−1263	vw		0−1263
89.7	438	−1246	mw		0−2×624
				L=75 cm t=80°C p=90 mm	
88.3	454	−1230	vw	vw	
85.8	482	−1202	vw	vw	
84.4	498	−1186		vw	
81.3	532	−1152	w	vw	0−1154?
79.3	555	−1129		vwd	
77.6	574	−1110		vwd	0−1099? 0−1034−2×40?
			t=70°C p=60 mm		
73.8	617	−1067	w	mw	0−1034−40 0−2×535
73.0	626	−1058		vw	
70.8	651	−1033		vw	0−1034
70.4	656	−1028	vw	vw	
69.5	666	−1018	vw	mw	
68.8	674	−1010		vw	0−2×490−40
65.2	715	−969		vw	0−2×490?
63.6	733	−951		vw	
61.3	759	−925		vwd	
60.2	772	−912		vwd	
59.0	785	−899		vwd	
53.9	844	−840	vw	vw	0−800−40
52.8	856	−828		vw	
51.7	869	−815		vw	
50.8	879	−805	vw	vw	0−800 0−714−2×40
47.0	923	−761	vwd	vw	0−714−40?
43.1	968	−716	vw		0−714
39.4	34010	−674	vw		0−2×338
				t=40°C p=16 mm	
38.8	018	−666	sr	m	0−666 0−624−40
37.9	028	−656	vw		0−535−3×40
35.7	053	−631	md	vw	0−624
34.6	066	−618	msr	mw	
34.0	073	−611	vw	vw	0−535−2×40
33.2	082	−602	vw	vw	
30.7	112	−572	mwr	w	0−535−40 0−490−2×40
27.6	147	−537	mwd	vw	0−535
26.4	161	−523	md	mwd	0−490−40
24.3	186	−498	vwd	vw	0−490
23.0	201	−483	mw	w	
20.0	237	−447		vwd	
18.5	254	−430		wd	0−2×215
13.2	316	−368		w	
12.4	326	−358		w	
10.1	353	−331		vwd	0−338
04.6	418	−266		mwd	
03.1	436	−248		vwd	0−215−40
01.5	455	−229		vwd	
			t=20°C p=4.6 mm		
2899.9	474	−210	wr	m	0−215
98.7	488	−196		vw	0−198
98.1	495	−189	vw	mw	
97.2	506	−178	w	m	
93.5	550	−134	vwd	w	
92.5	562	−122	vwd	mwr	

TABLE II—*Continued.*

λ(A)	ν (cm⁻¹)	ν−ν₀₋₀	Intensity		Assignment
90.8	583	−101		vwd	
89.3	600	−84	vwd	mwd	0−84; 0+131−215
87.5	622	−62		mw	
86.1	639	−45	vw	vw	0−40; 0+158−198
85.4	647	−37	vsr	vsr	
84.8	655	−29	vw		
82.3	684	0	vs		0−0
81.3	697	13	ms		
80.8	702	18	mw		0+269−3×84
80.4	708	24	w		
79.8	714	30	vw		
77.4	743	59	vwr		
75.1	771	87	vwd		
				t=0°C	
				p=1.1 mm	
73.7	788	104	mwr	w	0+269−2×84?
71.5	815	131	vwd		0+131
69.3	842	158	vwd		0+158
67.5	864	180	wd	vwd	0+269−84
61.1	941	257	mwd	vw	
60.2	953	269	sr	ms	0+269
57.6	984	300	md	mwd	
54.8	35019	335	vwd	vwd	
52.1	052	368	vwd	vwd	
50.0	078	394	vwd	vwd	
42.3	093	409	vwd	vwd	
46.7	128	444	vwd	vwd	
43.1	163	479		vwd	0+545−65?
42.1	175	491			
			t=−10°C		
			p=0.6mm		
41.5	183	499	w	m	0+499
40.8	191	507	w	mw	0+545−40
40.2	199	515		w	
38.6	219	535		mw	0+2×269
37.8	229	545	mwr	sr	0+545; 0+580−40
36.7	242	558		mw	
34.9	264	580	vwd	w	0+580
34.1	275	591		w	
33.2	286	602		vw	
30.9	314	630		vwd	
28.6	343	659		w	
26.4	371	687		vw	
23.7	405	721		w	
22.5	420	736		w	
18.3	472	788		w	0+802
17.2	486	802	mr	vs	0+3×269?
14.2	524	840	vwd	w	
10.9	566	882		w	
09.1	588	904		w	0+2×180+545
04.7	644	960	vwd	mw	0+960?
01.3	688	1004	vw	mw	0+2×499; 0+1004
2799.8	706	1012		vw	0+2×545−84
98.7	720	1036	w	mw	
96.7	754	1070	mwd	ms	0+802+269
96.0	765	1081		vw	0+545+2×269
95.2	776	1092	vwd	vw	0+2×545
92.9	794	1110	vwd	mw	
90.7	822	1138	vwd	w	
85.2	893	1209		vw	
80.9	949	1265	mwd	ms	0+802+545−84?
79.2	971	1287	vwd		
76.0	36012	1328	wd	wd	0+802+2×269
72.7	055	1371	vwd	vw	
68.2	114	1430	vwd	w	
63.1	180	1496	wd	w	0+3×499
59.7	225	1537	wdr		0+802+545+269−84?
55.6	279	1595	vwd		0+2×802
51.0	340	1656	vwd		
46.0	405	1721			0+802+2×545−2×84?
40.9	473	1789	vwd		Transition II?
32.5	586	1902	vwd		
28.0	646	1962	vwd		

TABLE III. Absorption bands in transition I of γ-picoline.

λ(A)	ν (cm⁻¹)	ν − ν₀₋₀	Intensity		Assignment
			L=75 cm t=80°C p=85 mm		
2913.8	34310	−855		vw	
11.9	332	−833		vw	
18.7	352	−813		vw	
			t=60°C p=42 mm		
09.1	365	−800	w	mw	0−800
07.9	379	−786	vw		
06.1	400	−765	vw		
2897.8	499	−666	vw		
86.2	638	−527	vw		
			t=40°C p=15 mm		
85.2	650	−515	mw	wdr	0−513
84.8	654	−511	w		
76.7	752	−413	vw		0−413?
75.1	771	−394	vw		
73.1	806	−359	vw		0−359?
69.6	838	−327	vw		
67.2	867	−298		vw	
65.2	892	−273	w	w	0−273? 0+245−513?
63.2	916	−249		vw	
60.3	951	−214		vw	0−214
57.0	992	−173		vw	
			t=30°C p=8 mm		
51.8	35056	−109	vw	wr	0−109
45.8	129	−36	w		
45.0	140	−25	vw		
44.1	151	−14	mw	vw	
43.1	163	0	s	mw	0−0
42.8	167		s	mw	
41.1	188	23	vwd		
38.8	216	51	vwd		
			t=20°C p=4.6 mm		
36.7	242	77	vw	vw	
35.9	252	87	vw	vw	
31.4	308	143		vw	0+143?
24.4	395	230	vw		0+744−513?
23.7	404	239	w	mwr	0+239
17.5	482	317	vwd		0+744−2×214?
16.7	492	327		vw	
15.8	504	339	vwd		
			t=20°C p=4.6 mm		
15.1	513	348	wd	w	0+461−109
14.1	535	370	vw	vw	
08.4	598	433		vw	0+943−513?
06.2	626	461	mwd	ms	0+461
03.1	665	500	vwd	w	
			t=0°C p=1.1 mm		
00.6	696	531	vw	w	0+744−214? 0+531?
2798.2	726	561		vwd	0+744−182?
92.9	794	629		vw	0+744−109
84.0	909	744	wdr	sr	0+744
78.3	982	817		w	
68.6	36108	943	vwd		0+943
65.2	153	988	vwd		0+744+239 0+988?
56.6	265	1100	vwd		0+744+461−109 0+1100

TABLE III—*Continued.*

λ(A)	ν (cm⁻¹)	ν−ν₀₋₀	Intensity		Assignment
				t=−10°C p=0.6 mm	
48.5	372	1207	wdr	vwd	0+744+461
41.2	470	1305	vwd		0+2×744−182
35.4	546	1381	vwd		0+2×744−109 0+3×461
27.6	651	1486	vwd	vwd	0+2×744
21.0	740	1574	vwd		
14.0	835	1669	wd	wd	
			L=14 cm t=10°C p=2.2 mm		
09.6	917	1752	vwd	vwd	
02.6	37012	1847	vwd	wd	0+2×744+461−109 0+4×461?
2695.9	105	1940	wd	wd	0+2×744+461
88.3	209	2044	vwd	vwd	0+3×744−182
82.3	293	2128	wd	vwd	0+3×744−109
74.0	386	2221	wd	vwd	0+3×744
67.9	472	2307	wd	vwd	0+5×461?
62.0	554	2389	wd		
50.4	719	2554	vwd		
40.8	856	2691	wd		0+3×744+461
34.6	946	2781	wd		

most practicable to measure to the most intense region of the band, recognizing that the relation of this setting to the true rotationless frequency of the band must be uncertain and probably variable. Uncertainties in the resulting values range up to 10 wave numbers.

The bands of the short-wavelength region are so diffuse that it was found best to measure them on photographic prints of the Hilger prism spectrograms, enlarged about 5 times. Since the frequency dispersion of the prism is nearly linear in the region concerned, uncertainties in locating the diffuse bands were within 10 to 100 cm^{-1}.

EXPERIMENTAL RESULTS

As mentioned before, the relative intensities in the long-wavelength and short-wavelength parts of the spectrum, which we call regions I and II, differ markedly. Region I with its narrow pyridine-like bands occurs at about 2900–2700A. Region II occurs at about 2700–2400A, and its diffuse broad bands resemble the spectra of some substituted benzenes. No attempt was made to determine intensities quantitatively. It is possible, however, to obtain a rough estimate of the relative intensities of the two regions by observing at what temperature each spectrum first appears in a cell of given length. For this purpose the expression for the extinction coefficient was combined with the approximately valid assumption that the ideal gas law holds for the vapor. Adjusting then the conditions of pressure, temperature, and length of light path for the two absorption regions, so that they exhibit the same absorption intensity, an expression was obtained from which their relative absorption may be roughly estimated. The intensity relations so obtained showed that the I spectra of the picolines are of the same order of intensity and that the II spectra diminish in intensity going from α- over to γ-picoline. This is in agreement with recent research[20] in which separate f values for the two regions were obtained from solution spectra.

The appearance of the I spectra may be seen from Figs. 1–3 which are assembled from sections of the respective spectra taken under various conditions. Spectrograms of the II spectra are reproduced in Fig. 4. The diffuse bands of the II spectra occur in three major groups of bands, of which the middle group is strongest. These groups have nearly the same position in the spectra of α- and β-picoline, with their maxima at about 38600 and 38400 cm^{-1}, respectively. The band groups are not clearly differentiated in the vapor of γ-picoline; but the maximum is shifted to about 39300 cm^{-1}, and in solution three distinct peaks appear at nearly the same positions as those in pyridine solution.

The observational data for the picoline spectra are listed in Tables I–VI. Each table includes in the first column the wavelength, measured to the most intense part of the band, in the second column the wave number, and in the third column the separation of each band from the assumed 0, 0 band. Column four contains visual estimates of relative intensities. It is divided into two sub-columns giving intensity estimates under conditions stated in these columns. Notations used are vw—very weak, w—weak, mw—medium weak, ms—medium strong, s—strong, vs—very strong, d—diffuse, r—apparently degraded to the red. The last column gives assignments of component vibrational frequencies of each band, by means of analysis to be detailed later; ( ) indicates a frequency which is itself unassigned; ? indicates a doubtful assignment.

[20] H. P. Stephenson, Ph.D. thesis (Duke University, 1952).

TABLE IV. Absorption bands in transition II of α-picoline.

λ(A)	ν (cm⁻¹)	ν−ν₀₋₀	Intensity	Assignment
			L=25 cm t=−15°C p=0.7 mm	
2669	37450	−170	vw	
64	530	−90	w	
57	620	0	mw	0−0
14	38250?	630	m	
2601	430?	810	s	0+180
91	580	960	vs	0+960
50	39200	1580	s	0+2×810
2531	500	1880	s	0+2×960
2493	40100?	2480	mw	0+2×810+960?

This column arrangement is modified slightly to allow for only one column of intensity estimates in Tables IV–VI and for alternate assignments in Table V.

In Table I, certain wave numbers are taken from the results obtained for α-picoline by Henri and Angenot.[5] Only those values are included which do not appear to be duplicated by any values derived from the present research.

DISCUSSION AND ANALYSIS OF THE SPECTRA

General Remarks on the Electronic Levels

In discussing the picoline spectra it is logical to compare them with the spectrum of pyridine, just as the spectra of substituted benzenes have been compared to that of benzene. The first electronic transition in benzene, of type $^1A_{1g}-{}^1B_{2u}$ and forbidden, becomes an A_1-B_1 and allowed in simple monosubstituted benzenes, when the D_{6h} symmetry of benzene is reduced to the group C_{2v} upon substitution. The same type transition, A_1-B_1, would apply to pyridine if the first excitation were caused by the $2p\pi$ electrons of the ring as in benzene, as mentioned in the Introduction. Now, the pyridine spectrum with its narrow, line-like bands distributed rather evenly in the spectrum and not in groups, does not resemble the benzene spectrum nor that of a substituted benzene as has been remarked previously (for example, reference 3). While the line-like bands which become diffuse toward shorter wavelengths are finally submerged in a strong continuous background, the picolines exhibit two separate band systems of distinctly different patterns and of different intensities as described earlier. The picoline spectra taken in iso-octane solution by Stephenson[9] in a Beckmann spectrophotometer in this laboratory do not show the two absorption regions separated as in the vapor. He found however, that the tail-end of the absorption on the long wavelength side "disappears" in ethanol solutions of the picolines and also of pyridine (see also reference 8). These observations in solution spectra

TABLE V. Absorption bands of transition II in β-picoline.

λ(A)	ν (cm⁻¹)	Intensity	ν−ν₀₋₀	Assignment	ν−ν₀₋₀′	Assignment
		L=10 cm t=5°C p=1.6 mm				
2741	36475	w	−905		0′	0−0′
32	585	vw	−795	Transition I?	110	
28	645	vw	−735	Transition I?	170	0′+170
21	745	mw	−635	Transition I?	270	0′+460−190
16	800	mw	−580	Transition I? 0−3×190	325	
07	935	ms	−445	0−445?	460	0′+460
02	995	w	−385	0−2×190	520	
2695	37100	w	−280		625	0+170+460
88	190	ms	−190	0−190	715	
74	380	s	0	0−0	905	0′+2×460
63	540	ms	160	0+160 0+600−445	1065	
47	770	m	390	0+(390)	1295	0′+460+1020−190
32	980	ms	600	0+600	1505	0′+460+1020
25	38090	mw	710	0+710	1615	
18	180	s	800	0+800 0+1020−190	1705	
09	320	vs	940	0+940	1845	
03	400	vs	1020	0+1020	1925	
2594	540	m	1160	0+160+1020 0+160+940	2065	
79	760	mw	1380	0+(390)+940 0+(390)+1020	2285	0′+460+2×1020−190
65	970	m	1590	0+600+940 0+600+1020	2495	0′+460+2×1020
51	39190	ms	1810	0+800+1020 0+2×1020−190	2715	
43	310	s	1930	0+2×940? 0+940+1020	2835	
28	540	m	2160	0+160+2×1020	3065	
14	760	m	2380	0+(390)+2×940 0+(390)+2×1020	3285	0′+460+3×1020−190
02	960	m	2580	0+600+2×940 0+600+2×1020	3485	0′+460+3×1020

and the fact that two absorption regions of different character occur in the picoline vapor spectra suggest the existence of two close-lying levels also in pyridine. Kasha,[21] from research on halogenated pyridines and on pyridine in condensed systems has also come to this conclusion. A re-examination of Sponer and Stücklen's plates confirms the possibility of two levels and a rough estimate would place the beginning of the second transition around 38350 cm^{-1}.

It is obvious from these findings that the interpretation of the picoline spectra must follow, in general, the same pattern as that of the pyridine spectra. This necessitates reconsidering the previous interpretation of sharp pyridine bands as A_1-B_1 transition. It has been suggested by Kasha[21] that excitation of a nonbonding sp^2 electron of the nitrogen atom into the first unfilled π-orbital of the pyridine ring causes the occurrence of system I, ($n-\pi$ transition). It is then logical to assign the diffuse bands of type II in the picolines to the A_1-B_1 transition ($\pi-\pi$ transition), resulting from the $2p\pi$ electrons of the ring. Since the nonbonding $sp^2\sigma$ orbitals are symmetric to the molecular plane, the corresponding single electron levels are of type a_1. Excitation of an a_1 electron into the two lowest empty π orbitals of symmetry types b_2 and a_2 gives molecular levels B_2 and A_2 as lowest excited singlet states. This order is obtained by using the simplest molecular orbital calculation for the π-electron orbitals, neglecting overlap and electronic repulsion.[22] In Kasha's scheme of levels the A_2 is the lowest excited singlet state of pyridine; then follow the B_2 and the B_1 which is the upper state of the II spectra. An A_1-B_2 transition is allowed with a transition moment perpendicular to the molecular plane. We shall see later that the analysis suggests an order of the A_2 and B_2 levels in agreement with the simple calculations. This may be taken as an indication that inclusion of refinements in the calculation of the π-orbitals will not reverse the order given by the crude treatment.

It should be added that the level notation used here applies strictly to pyridine only, and to γ-picoline if the CH_3 group is regarded as one atom. α-Picoline and β-picoline belong, even if the CH_3 groups are taken as one-atom substitutions, to group C_s. The symmetry classes A_1 and B_1 of group C_{2v} go over into the class A' for C_s, and the two transitions involving the sp^2 electrons become $A'-A''$ transitions with the moment perpendicular to the molecular plane. The appearance of the electronic spectra and a comparison of the different Raman spectra indicate that α-picoline and β-picoline also conform spectroscopically to C_{2v} symmetry to a rather fair approximation.

[21] M. Kasha, Disc. Far. Soc. **9**, 14 (1950).
[22] Gertrud P. Nordheim and H. Sponer, J. Chem. Phys. **20**, 285 (1952).

TABLE VI. Absorption bands of transition II in γ-picoline.

λ(A)	ν (cm^{-1})	$\nu-\nu_{0-0}$	I	Assignment
			L=14 cm t=10°C p=2.25 mm	
2616	38220	−100	mw	
2609	320	0	m	0−0?
92	570	250	m	
69	920	600	ms	0+600
48	39240	920	s	0+920
31	500	1180	s	0+1180; 0+2×600
2512	800	1480	ms	0+600+920
92	40120	1800	ms	0+2×920
74	410	2090	m	0+920+1180; 0+2×600+920
30	41140?	2820	m	
2417	360?	3040	mw	0+2×920+1180?

TRANSITION II IN THE REGION 2600A

From the description (diffuseness and position) given before, the II spectra of the four compounds appear to fall into two groups corresponding to their different symmetries: pyridine and γ-picoline (C_{2v}), and α- and β-picoline (C_s).

α-Picoline

Estimated band positions in spectrum II of α-picoline are listed in Table IV. This spectrum is so diffuse (Fig. 4) that no individual bands can be distinguished clearly except the three in the first group. The separation of the order of 1000 cm^{-1} between the maxima of successive groups corresponds presumably to progressions of the analog of the totally symmetric carbon ring vibration in benzene. The strongest band of the first group, at 37620 cm^{-1}, is taken as the 0−0 band. Another symmetric ring vibration is probably represented in the separation 810. The bands on the long-wavelength side of the 0−0 band must correspond to 1−1 transitions of low-lying vibrations.

β-Picoline

The only transition II spectrum whose band structure is sufficiently discrete to permit of any detailed analysis is that of β-picoline (Fig. 4, Table V). Even in this case the interpretation is not satisfactory. If the strongest band in the first group, at 37380 cm^{-1}, be designated 0−0, most of the strong bands can be accounted for by progressions of frequencies of about 940 and 1020 cm^{-1} superimposed upon the 0−0 transition and upon the following vibrational frequencies in the excited state: 160, 390, 600, 800 cm^{-1}. The 940 and 1020 probably correspond to the strongly polarized Raman frequencies 993 and 1034 cm^{-1} in the ground state which quite likely represent symmetric carbon ring vibrations. If the first band on the long-wavelength side of the 0−0 band at 37190 cm^{-1}, is interpreted as arising from the vibration of approximately 190 cm^{-1} (Raman value 198), then the 160 cm^{-1} difference may correspond to the same vibration in the excited state.

This would place the 1−1 transition of this vibration about 30 cm^{-1} to the red from the main bands. Since the widths of most bands are of the order 30–60 cm^{-1}, it is quite possible that these 1−1 transitions contribute at least partially to the broadness of the bands.

The 0+600 cm^{-1} difference (band 37980) has about the same intensity as the 0−0 band, and has a breadth and uniformity of intensity which suggests that it may consist of two close-lying bands. The band may correspond in the upper state to the 624 cm^{-1} level observed in the Raman spectrum, but this possibility must be regarded as uncertain. It is very probable that the Raman lines 624 and 535 cm^{-1} correspond to the degenerate ϵ^+_g 606 carbon vibration in benzene, and one would expect that, if one component appeared in the excited state of β-picoline, the other would appear also. But the 390 cm^{-1} difference seems too low to be correlated with 535 in the ground state.

The 800 cm^{-1} difference (band 38180) may be attributed to a ring vibration in the upper state in which the substituent is strongly participating. An alternative explanation is possible as a superposition and given in Table V.

Perhaps the greatest objection to the foregoing interpretation is that it offers no explanation of the prominent bands at 36475 and 36935 cm^{-1}. If instead of 37380 the band at 36935 cm^{-1} is itself taken as the 0−0 band, most of the system can be accounted for by progressions of about 940 and 1020 cm^{-1} superimposed upon the frequencies: 445, 605, 835, 1045 cm^{-1}. The band at 37380 becomes 0+445. This frequency may then represent the vibration which has the Raman value 535 cm^{-1}. The fact that its intensity is markedly greater than that of the 0−0 band may result from the Franck-Condon principle. In that case, however, a progression of one, two, and possibly three times 445 would be expected, whereas only the single 445 cm^{-1} difference appears. In the lower state, 605 cm^{-1} may be reasonably identified with the 624 vibration in the same manner as before. The 255 cm^{-1} difference agrees with 445–190. The analog of the 190 cm^{-1} vibration in the upper state is possibly represented by the 165 cm^{-1} difference (band 37100). It is very difficult to account for the differences of 835 (band 37770) and 1045 (band 37980). Altogether, the first interpretation—taking the 0−0 band at 37380 cm^{-1}—seems preferable.

Still another interesting possibility remains. According to Kasha,[21] two overlapping electronic transitions occur in pyridine and its monohalogenated derivatives very close together in the region of 2600A. This view is based on the assumption that the A_1-B_2 transition (Kasha's scheme) occurs only slightly below the benzene-like A_1-B_1 transition discussed here. No evidence of a second transition in this region was found in the spectrum of α-picoline. Its occurrence cannot be ruled out, however, in β-picoline. Careful examination of this spectrum in plates and enlarged prints reveals that the band at 36475 cm^{-1} does not look like the bands of transition I, while certain weak bands at shorter wavelengths—e.g., those at 36585, 36745, and 36800 cm^{-1}—do resemble the bands of spectrum I. The band at 36475 actually resembles that at 36935 cm^{-1}, except that it is weaker.

If it is assumed that 36475 is the 0−0′ band of a second electronic transition, the prominent band at 36935 cm^{-1} then becomes 0′+460 cm^{-1} and may be correlated with the 535 cm^{-1} vibration in the lower state. This vibration, with the lower-state vibration of 190 cm^{-1} and an upper-state vibration of about 1020 cm^{-1}, accounts for several bands which are not included in the scheme based on a 0−0 band at 37380 cm^{-1}, and duplicates some which are (Table V). Because of accidental near coincidence between the two proposed systems and the diffuseness of the bands, it is not possible to propose the existence of two transitions in the II region with entire confidence, although it is considered quite likely.

It should perhaps be mentioned that the band at 36475 can be related to the 0−0 band at 37380 by the assignment 0−190−714 cm^{-1}. No weight is placed on this interpretation, however, and no similar interpretation of the band at 36935 is possible.

It seems desirable to emphasize again that the analysis of the bands in region II in β-picoline suggested here is necessarily tentative. It has been mentioned in some detail because it is important to establish definite proof whether two superimposed transitions occur in region II or not. We shall come back to this question after the analysis of transition I has been taken up.

γ-Picoline

The bands of transition II in γ-picoline are so few and so diffuse that a systematic analysis of them does not carry much weight. It is believed that probably the band at 38320 cm^{-1} is the 0−0 band. With this assumption the assignment scheme in Table VI may be obtained as a possible one. This interpretation, like the intensity considerations mentioned earlier in this section, indicates a marked shift of the γ-picoline II spectrum to the violet as compared with α- and β-picoline. This shift and the lower intensity of the γ-picoline II spectrum are contrary to the usual characteristics of *para*-substituted benzenes. We shall come back to it in a later section.

Because of the diffuseness of the γ-picoline spectrum in both transitions I and II, it is impossible to judge whether a second electronic transition occurs in the short-wavelength II region.

TRANSITION I IN THE REGION 2800A

In considering the analyses of the I spectra it will be recalled that these spectra are expected to arise from the excitation of an sp^2 electron localized on the nitrogen into the first nonbonding π-ring orbital. On the basis of this theory the I spectra represent either a

forbidden A_1-A_2 transition or an allowed A_1-B_2 transition with a moment perpendicular to the molecular plane. Consequently, the analyses of the spectra should lead to a decision between these possibilities.

Before going into details, it will be mentioned that nothing could be found in the structure of these spectra that would suggest a forbidden transition. The detailed analyses will be found rather to provide support for the assumption of an A_1-B_2 transition. The fact that the I spectra are allowed, and yet are of markedly lower intensity than the II spectra, is noteworthy. A transition depending upon a perpendicular moment will be weak because the overlapping of the π-ring orbital and the localized σ-orbital is small.

The characteristic narrowness of the bands in the I spectra may also be related to an A_1-B_2 transition. In benzene, whose rotational levels may be treated as those of a symmetric top, all strong bands should be perpendicular bands[23] (change of electric moment $\perp$ to the figure axis). In pyridine and in γ-picoline the figure axis lies in the molecular plane and goes through the N atom and the para carbon atom. The transition moment, being perpendicular to the molecular plane, is perpendicular to the figure axis as in benzene. Bands involving symmetric vibrations should then be perpendicular bands. However, if one considers, in good approximation, pyridine as a symmetric top like benzene,[3] the z axis may be taken as the figure axis, and the principal moment of inertia is the one about this axis. Bands involving symmetric vibrations become parallel bands in this treatment, whereas they are perpendicular bands in benzene. The difference stems, of course, from the different origins of the two spectra, one having a transition moment perpendicular and the other parallel to the molecular plane. The parallel bands of a symmetric top molecule in the infrared have a simpler appearance than the perpendicular bands. They have extremely narrow intense qQ branches. Little is known about their structure in electronic bands of polyatomic molecules, but in the case of the strong benzene bands (theoretically perpendicular), it was noted[24] that the relation between the variation in spacing of the rotational lines and the change in moments of inertia would be the same if the bands were interpreted as parallel bands. In the discussion of the pyridine spectrum[3] it was pointed out that if the moments of inertia stay very nearly the same in the upper and lower states of the transition, the qQ branch will be intense and narrow, while the P and R branches may extend so far to each side that their intensities decline to negligible values before a head is reached. This latter effect, occurring in suitable degrees, could account for the shading and fuzziness at the edges of most bands. If the transition moment is perpendicular to the molecular plane, as is required in an A_1-B_2 transition, the charge distribution in the plane will not have changed, although the electronic wave function of the excited state will be somewhat extended. Nearly equal moments of inertia in the two electronic states will require that the potential minima of bands involving symmetrical vibrations are approximately above one another. Equal equilibrium positions in the combining states are always most probable for non-totally symmetric vibrations.

Assuming an A_1-B_2 transition as a working hypothesis, one might expect in the I spectra few and relatively short progressions of totally symmetric vibrations. Furthermore, singly excited α_2 and β_2 vibrations in pyridine and γ-picoline, which produce vibrational moments in the plane of the ring, should appear with intensities comparable to those of the α_1 allowed vibrations which accompany the weak pure electronic transition in the z direction. But singly excited β_1 vibrations, prominent in A_1-B_1 transitions, should be excluded. In α- and β-picoline, however, the reduction of C_{2v} symmetry to C_s produces allowed electronic transitions only.

It will be noted as the analyses are developed that the I spectra of α- and β-picoline, particularly the former, resemble that of pyridine, while the spectrum of γ-picoline is similar in some respects to that of toluene.[25]

γ-Picoline

The analysis of the γ-picoline I spectrum is taken up first, because it is the least complex and offers a better opportunity for unambiguous interpretation than do the less symmetric α- and β-picolines. It is unfortunate that no Raman data are available for γ-picoline. The observed spectrum is, however, sufficiently simple that it is relatively easy to isolate a few fundamental frequencies upon which an internally consistent analysis can be developed.

The strong doublet at 35165 cm^{-1} is taken as the 0—0 band. The basic pattern of the γ-picoline I spectrum is a series of dispersed groups; each of these consists of three prominent frequencies superimposed upon a progression of 744 cm^{-1}. The lower state of this vibration appears in the band at -800 cm^{-1}. The corresponding frequencies in toluene are 751 and 785, and in paraxylene they are 775 in the upper state[26] and 829 in the lower state. Although the precise nature of these frequencies is not certain, they do involve a strong participation of the substituent in the motion by either lowering the value of the benzene "breathing" vibration[27] or by actually representing the $-C-C-(H_3)$

[23] Sponer, Nordheim, Sklar, and Teller, J. Chem. Phys. **7**, 207 (1939).
[24] A. Turkevich and M. Fred, Revs. Modern Phys. **14**, 246 (1942).
[25] Ginsburg, Robertson and Matsen, J. Chem. Phys. **14**, 511 (1946).
[26] C. D. Cooper and M. L. N. Sastri, J. Chem. Phys. **20**, 607 (1952).
[27] K. S. Pitzer and D. W. Scott, J. Am. Chem. Soc. **65**, 803 (1943).

valence vibration.[28] A slight preference is given here to the first alternative. The three observed bands of the 744 progression are strong and diffuse, and are degraded to the red, similarly to the bands in the spectra of substituted benzenes. Observation of higher members is rendered impossible because of the increasing intensity of the continuous background. The 744 bands form the only progression that could be established with certainty. This fact and the diffuse quality of the bands indicate that during the transition a slight change takes place of the internuclear distances involved in this vibrational mode.

The 239 cm^{-1} frequency is ascribed tentatively to either an α_2 or β_2 carbon vibration. The corresponding frequency in the lower state is uncertain.

The 461–513 cm^{-1} pair is considered as the α_1 component resulting from the ϵ^+_g 606 carbon vibration in benzene. Both values agree closely with those in toluene as might be expected for the vibrational mode concerned. The 461 frequency occurs superimposed upon the 0−0 frequency and upon each member of the 744 progression; but it is not certain that it forms itself a progression.

The β_1 component derived from the ϵ^+_g 606 benzene vibration is missing from the I spectrum of γ-picoline. A weak band at 0+531 cm^{-1} may possibly represent it in the upper state, but the low intensity of this band and the absence of the corresponding vibration from the lower state indicate that, if any representation of the β_1 vibration is present at all, it must arise from a very weak moment. This finding is in accord with the hypothesis of an A_1-B_2 transition. The presence of the CH_3 group may cause a sufficient deviation from C_{2v} symmetry to permit such a weak transition of an otherwise forbidden vibration.

The third frequency which is found superimposed upon the 744 cm^{-1} terms is a difference of 109 cm^{-1} which is taken to be a 1−1 transition of a vibration which is not identified explicitly. The 109 difference frequency is also found in combination with the 0−0 transition and with the 461 frequency.

The frequencies which have been mentioned account for nearly all of the more prominent features of the spectrum. Of the numerous weak bands remaining, several probably represent fundamental frequencies; but the assignments are made chiefly by analogy, and lack supporting combinations.

The band at −214 cm^{-1} probably corresponds to the 204 and 198–208 cm^{-1} Raman frequencies in α- and β-picoline, and should appear in the Raman spectrum of γ-picoline. The band at 143 cm^{-1} is a likely upper-state analog.

Weak bands at 0+943 and 0+988 cm^{-1} probably represent α_1 carbon vibrations. The band at 0+1100 cm^{-1} possibly includes the 0−1 term of a fundamental frequency superimposed upon the known combination 744+461−109 cm^{-1}. The 1100 frequency agrees closely with similar frequencies in α- and β-picoline.

Several more uncertain assignments have a question mark in Table III.

It should be mentioned that the 0−0 and the 0−513 cm^{-1} bands are very sharp doublets of 4 cm^{-1} separation. No other bands appear to have this doublet structure, and no explanation of the doubling is apparent.

α- and β-Picoline

It is convenient to treat the I spectra of α- and β-picoline in a single discussion, because of their marked similarities. Because of the low symmetry of these molecules, all their spectra will actually represent allowed transitions $A'-A''$ with a moment perpendicular to the molecular plane, (see previous discussion). Single excitation of α'' vibrations will produce bands in which the transition moment is in the ring plane. The symmetry of these vibrations corresponds to the α_2 and β_2 vibrations of point group C_{2v}, and these are the vibrations that were believed to account for some of the weaker bands in the γ-picoline spectrum. Hence the I spectrum of α- and β-picoline will be richer in bands than that of the γ-isomer, just as the ortho and meta spectra of disubstituted benzenes have more bands than the corresponding *para* spectra. Although the vibrations fall, in the strict sense, into two classes only, one would expect from what has been said before that those will occur with more prominence that were recognized in the γ-spectrum. In spite of this aid, it was found that the number of numerical coincidences of interpretation was so great that many assignments must be considered as tentative.

In α-picoline the sharp band at 34753 cm^{-1} was taken as 0−0 band. In β-picoline the close pair 34684/97 contains in all probability the 0−0 transition. Here the lower value was chosen for the calculation because of a rather consistent fit with Raman values. As may be seen from Table II, there appear in the spectrum several other "doublets" with a separation of 12–14 cm^{-1}. The 544 cm^{-1} frequency in the upper state, which is the outstanding feature of the pyridine spectrum, is similarly prominent in α-picoline but forms a less clearly defined progression in the β-spectrum. If it is associated in each case with a vibration of 628 cm^{-1} in the ground state (depolarized Raman line), then the 544, 628 cm^{-1} pair would represent the β_1 component derived from the ϵ^+_g 606 cm^{-1} carbon vibration in benzene. The fact that it is depolarized in Raman spectra of α- and β-picoline, even though the class β_1 of group C_{2v} goes into the totally symmetric class α' in C_s, indicates that the effect of the CH_3 substitution in destroying the C_2 axial symmetry of pyridine is incomplete. Nevertheless, it may be sufficient to make allowed the transition of the β_1 vibration which is forbidden in γ-picoline if this is treated as a C_{2v} molecule. The association of the 544

[28] K. W. F. Kohlrausch and associates, Monatsh. Chem. **72**, 268 (1939); **74**, 175 (1942); **76**, 200 (1947).

and 628 cm^{-1} frequencies is supported by the occurrence of 84 cm^{-1} differences in both spectra. Although all symmetry requirements are formally met, the β_1 vibrational bands should occur with low intensity because of the "remembrance" of being originally forbidden transitions. This is not the case. It is therefore of interest that another assignment is possible. The 544 may namely correspond to the vibrations of 545 and 551/35 in the lower states of α- and β-picoline, respectively. Raman data indicate that these vibrations are totally symmetric; they are believed to arise from the α_1 component of the ϵ^+_g 606 cm^{-1} vibration in benzene. In fact, this interpretation, which is preferred here, fits in better than the first one with results in the spectrum of pyridine, where a long progression of 542 steps has been found and assigned to the α_1 component. The difficulty that in β-picoline there is definite evidence of an upper state 499 cm^{-1} vibration may be met by pairing it with the 515 in the lower state. Both α- and β-picoline have an upper-state vibration of about 580 cm^{-1}, occurring weakly, which then might be paired with the 628 cm^{-1}.

Polarized Raman lines have been reported at 801 and 813 in α-, and at 714 and 800 cm^{-1} in β-picoline.[11–13] The same frequencies were found in the ultraviolet absorption spectra. One of these frequencies will correspond to the analog of the benzene "breathing" vibration as discussed for γ-picoline. In α-picoline, it is possibly represented in the upper state by the band at $0+736$ cm^{-1}, and in β-picoline by a strong band at $0+802$ cm^{-1}. A short progression of 269 cm^{-1} is superimposed upon this transition. The 802 band consists of a closely spaced sharp doublet from which diffuse wings are degraded unequally to either side; they appear to end abruptly at a low intensity and do not form a head.

Several low-lying fundamental frequencies are found which are difficult to interpret definitely. In α-picoline some almost identical separations which probably represent fundamental frequencies are observed to either wavelength side from the 0–0 band. These pairs have been noted: 207, 204; 355, 358; 544, 545 cm^{-1}. Yet there remains a 120 cm^{-1} frequency which, if paired with 204 cm^{-1} in the lower state, would account for the 1–1 difference of 84 cm^{-1}. This difference could possibly be interpreted as the twofold excitation of a 42 cm^{-1} difference occurring a few times in α-picoline; but the predominance of the 84 over the 42 difference, its likely origin in the 120–204 difference, and other internal evidence argue for two distinct frequency differences. In β-picoline no such closely-matched pairs occur. Here, 158 and 198 cm^{-1} are paired, and their difference may account for the prominent 1–1 difference of 40 cm^{-1} which is observed singly and in progressions to the red from many strong bands. The 84 cm^{-1} difference may result from pairing the lower state frequency of 215 with the upper-state frequency of 131 cm^{-1}. The 207 and 269 cm^{-1} upper-state vibrations of α- and β-picoline, respectively, are quite likely of type α_2 or $\beta_2(\alpha'')$, and hence their single excitation would produce a moment in the molecular plane. This fact may account for the prominence of the respective bands.

Frequencies of 900–1000 cm^{-1}, which produce strong bands in the II transitions and in benzene and its monoderivatives, give rise to weak inconspicuous bands only in the I transitions under discussion. Their assignment to particular modes of vibration is uncertain and will therefore not be discussed in detail.

A few words may be added on the origin of the bands in the II region of β-picoline, which were tentatively assigned to another transition besides the A_1-B_1 (or $A'-A'$) containing the main groups. As mentioned, this other transition may belong to the second excitation of a nonbonding sp^2 electron from the nitrogen. And as such, it should be of type $A'-A''$, but should resemble a forbidden transition A_1-A_2. The very tentative and incomplete analysis is not in contradiction to this assignment, but it would be more interesting and important if corresponding bands could be identified in pyridine and γ-picoline where the systems would be more of type A_1-A_2. They could appear through interaction of β_1 and β_2 vibrations. Excitation of β_2 vibrations should be more effective because it would produce a transition moment in the molecular plane in the same direction as in the overlapping A_1-B_1 π-electron transition. In fact, because of the proximity of the two transitions, they should be of comparable intensities,[29] as is the case in β-picoline.

SUMMARY AND CONCLUSIONS

The evidence summarized in the last section indicates that the question of symmetry of the electronic I transitions cannot be considered settled on the basis of the analyses alone. Among these, the more definite findings in the study of the γ-picoline spectrum carry more weight than do the less definite results in the cases of α- and β-picoline. It is evident, however, that the observations as to narrowness of bands, shortness of progressions, and the operation of symmetry selection rules upon various classes of vibrations, together with the low intensity and allowed character of the transition, all constitute a strong argument for B_2 symmetry in the electronic excited state.

Another argument in favor of the interpretation may be raised from a comparison of the intensities of the I transitions of pyridine and the picolines with those of the diazines which have been studied by Halverson and Hirt.[30] If the I spectra are allowed transitions due to the excitation of a nonbonding electron from the nitrogen, then the corresponding spectra in the diazines should be about twice as intense as the I transition in pyridine or the picolines. Comparison of the f values of the I transitions in the latter substances with those

[29] G. Herzberg and Teller, Z. physik Chem. **B21**, 410 (1933); H. Sponer and E. Teller, Revs. Modern Phys. **13**, 75 (1941).
[30] F. Halverson and R. C. Hirt, J. Chem. Phys. **19**, 711 (1951).

TABLE VII. Electronic transitions (in cm^{-1}) in pyridine and the picolines in the near ultraviolet.

Molecule	$^1A_1-{}^1B_2$ / $^1A'-{}^1A''$ $n-\pi$	$^1A_1-{}^1B_1$ / $^1A'-{}^1A'$ $\pi-\pi$	Difference $^1B_1-{}^1B_2$ / $^1A'-{}^1A''$	$^1A_1-{}^1A_2$ / $^1A'-{}^1A''$ $n-\pi$	$^3A_1-{}^3B_2$ $n-\pi$	$^3A_1-{}^3B_1$ $\pi-\pi$
Pyridine	34769	(38350)	(3581)		30876	25500
α-Picoline	34753	37620	2867			
β-Picoline	34684	37380	2696	(36475?)		
γ-Picoline	35165	38320	3155			

derived from the published diazine absorption curves shows that this is indeed the case.

The electronic transitions in pyridine and the picolines discussed here have been summarized in Table VII. As has become apparent from the text, the values for transitions II are considered more liable to possible future changes than those for transitions I. Still more uncertain is the analysis of the A_1-A_2 system of β-picoline. The steep absorption gradient between the I and II spectra makes it very difficult to establish with certainty another electronic transition in this region. On the other hand, the very existence of this gradient and the diffuseness of transitions II make overlapping of another and possibly more transitions in this region likely.

It may be seen from the last table that the red shift of the $^1A_1-{}^1B_2(n-\pi)$ transition is smaller than that of the $^1A_1-{}^1B_1(\pi-\pi)$ transition for all molecules except for γ-picoline. Accordingly, the difference between the excited levels $^1B_1-{}^1B_2$ decreases from pyridine to β-picoline. Of course, it should be remembered that the location of the $^1A_1-{}^1B_1$ transition in pyridine is a rough estimate only. In γ-picoline both spectra shift to the violet, the II transition twice as much as the I transition, so that the difference $^1B_1-{}^1B_2$ increases again and comes close to that in pyridine. In regard to intensities, the A_1-B_1 transition is the weakest in γ-picoline and the A_1-B_2 is just a little stronger in γ-picoline than in the other two isomers.

For completeness, the two singlet-triplet transitions of pyridine have been added which were recently studied by Reid.[31] However, the assignments of the system to symmetry types are reversed here. The 31000 cm^{-1} intercombination system, which resembles the $^1A_1-{}^1B_2$ transition, is connected here with the unpaired nonbonding electrons on the nitrogen. It is at least 10^3 times weaker than the corresponding singlet system. The second intercombination system at 25500 is still weaker by another factor 10^2–10^3. It resembles transition II in its diffuseness and may be regarded as a $\pi-\pi$ transition. This means that, while the singlet and triplet B_2 levels lie only about 4000 cm^{-1} apart and actually overlap a little, the singlet and triplet B_1 levels are more than 12000 cm^{-1} apart and lie in different spectral regions. It is hoped to treat later the energy and intensity relations in these molecules.

We would like to thank Dr. J. J. McGovern of the Mellon Institute, Pittsburgh, for the samples of α- and β-picoline, and Dr. J. C. Shivers of the Chemistry Department, Duke University, for the sample of γ-picoline.

[31] C. Reid, J. Chem. Phys. 18, 1673 (1950).

THE JOURNAL OF CHEMICAL PHYSICS VOLUME 20, NUMBER 12 DECEMBER, 1952

An Analytical Method for the Approximate Determination of the Eigenfunctions and Energies of Electrons in Atoms

R. GÁSPÁR
Physical Institute of the University for Technical Sciences, Budapest, Hungary
(Received July 1, 1952)

The first part of this paper shows that the reduced effective nuclear charges Z_p/Z, determined without exchange by the "self-consistent field" method, can be approximated by a universal function, if the distance from the nucleus is measured in the unit of length $\mu=0.8853a_0/Z^{\frac{1}{3}}$, which changes from atom to atom. This universal function can also be approximated by a simple analytical expression. One of the possible applications of the above result is to use it to determine good starting potentials for calculations to be carried out by the "self-consistent field" method. The universal effective nuclear charge, especially in its analytical form, also allows the determination of important atomic constants for each element of the periodic system. The second part of the paper solves the one-electron Schrödinger equation by Rasetti's method, developing it to determine analytically the eigenfunctions and energies of electrons in the deepest *s*, *p*, *d*, and *f* energy states. The x-ray terms obtained by this method and the experimental ones are in good agreement with each other and with those calculated by the "self-consistent field" method.

RECENTLY several authors have called attention to the possibilities of utilizing the theoretical results of statistical atomic theory in wave mechanics.[1] In what follows we shall show a simple but easily applied example of how the analogy between statistical atomic theory and wave mechanics can be utilized for the calculation of atomic eigenfunctions and energy terms.

The well-known Thomas-Fermi equation of statistical atomic theory is

$$d^2\varphi/dx^2=\varphi^{\frac{3}{2}}/x^{\frac{1}{2}}, \tag{1}$$

where $x=r/\mu$, $\mu=0.8853a_0/Z^{\frac{1}{3}}$, and r denotes the distance from the nucleus. a_0 is the radius of the first Bohr electron orbit in the hydrogen atom and Z the atomic number. For neutral atoms the solution of Eq. (1) satisfying the boundary conditions

$$\varphi(0)=1, \quad \varphi(x_0)=0, \quad \text{and} \quad \varphi'(x_0)=0 \tag{2}$$

is a universal function of x; i.e., it is independent of the atomic number Z. x_0 in (2) corresponds to the boundary radius, which, for neutral atoms, is ∞.

In the "self-consistent field" theory of wave mechanics it is the approximation without exchange, the so-called Hartree approximation, that corresponds to the Thomas-Fermi approximation of statistical theory. From the possible interaction energies between the electrons—Coulomb, exchange, and correlation interaction energies—only the Coulomb energy is taken into account in both theories. According to the usual notation of the "self-consistent field" theory the effective nuclear charge determining the potential is Z_pe, where $-e$ is the charge of the electron. In the Thomas-Fermi theory there can also be defined an effective nuclear charge $Z_p'e$. The relation between Z_p' and $\varphi_0(x)$ is the following:

$$Z_p'/Z=\varphi_0(x). \tag{3}$$

Thus $\varphi_0(x)$ denotes the reduced effective nuclear charge of the atom.

Now it can be examined how, in calculations made for neutral atoms by the "self-consistent field" method, the function Z_p/Z changes with the distance from the nucleus, if the coordinate x is introduced instead of r. It can clearly be seen in Fig. 1 that in the coordinate system chosen, the function Z_p/Z calculated by the "self-consistent field" method can be regarded in good approximation as independent of the atomic number. Only such neutral atoms are taken into account for which calculations without exchange are known, and for simplicity only a few points are exhibited in Fig. 1. The dotted curve represents the function $\varphi_0(x)$ of the Thomas-Fermi theory and the continuous one the approximate analytical function. It is worth noting that the function

$$(Z_p/Z)=(e^{-\lambda_0 x})/(1+A_0x), \tag{4}$$

if

$$\lambda_0=0.1837 \quad \text{and} \quad A_0=1.05, \tag{5}$$

well approximates the reduced nuclear charges obtained by the "self-consistent field" method for neutral atoms of larger atomic numbers and also gives a good approximate value for atoms of smaller atomic numbers. The ideas outlined here can be used in various ways—one being to transform the effective nuclear charges, determined by the "self-consistent field" method into those of atoms of different atomic numbers. Thus, good starting potentials can be obtained.

Another possible application is to insert the analytical potential of (4) into the Schrödinger equation and to use it as a universal potential function. Thus calculations can be carried out for all the elements of the periodic system. Assuming the dependence of the one-electron eigenfunction on the angle in the usual form of $Y_{lm}=P_l^{|m|}(\cos\vartheta)e^{im\varphi}$, the Schrödinger equation to be

[1] E. H. Kerner, Phys. Rev. **83**, 71 (1951); L. L. Foldy, Phys. Rev. 83, 397 (1951); P. Gombás, Acta Phys. Hung. I.3 (1952). Concerning the older literature, see P. Gombás, *Die statistische Theorie des Atoms und ihre Anwendungen* (Springer-Verlag, Wien, 1949).

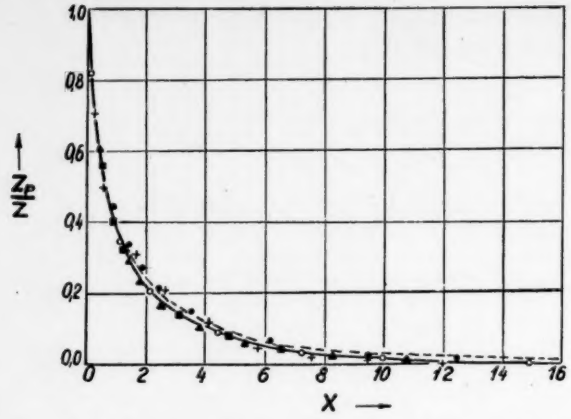

FIG. 1. The reduced effective nuclear charges of neutral atoms in a universal coordinate system. Points calculated by the "self-consistent field" method: ○Hg, ■W, ▲Kr, ●Ca, +Be. – – – – – $\varphi_0(x)$, curve of the Thomas-Fermi theory. ———— $e^{-\lambda_0 x}/(1+A_0 x)$, with (5).

solved is

$$\frac{d^2f}{dr^2}+\left[\frac{8\pi^2 m_0}{h^2}\left(\epsilon+\frac{Z_p e^2}{r}\right)-\frac{l(l+1)}{r^2}\right]f=0, \qquad (6)$$

where $R(r)=f(r)/r$ is the radial part of the eigenfunction and m_0 is the mass of the electron. l and m denote the quantum numbers of the electron treated. Equation (4) must be substituted into Eq. (6) for Z_p/Z. Using the effective nuclear charge in Eq. (4) the Schrödinger equation [Eq. (6)] can only be solved by approximate methods. The following procedure is chosen.[2] Equation (6) can be solved immediately by the approximate potential

$$\frac{Z_p''e}{r}=\frac{Z^*e}{r}+\frac{1}{2}\frac{\lambda e a_0}{r^2}+\frac{\chi_0}{e}. \qquad (7)$$

The solution can be written in the form

$$f=Ar^{n^*}e^{-\gamma r}. \qquad (8)$$

The parameters defining Eq. (8) are

$$n^*=\tfrac{1}{2}\{[1-4\lambda+4l(l+1)]^{\frac{1}{2}}+1\}, \qquad (9)$$

$$\gamma=(Z^*/n^*a_0), \qquad (10)$$

and the energy is

$$\epsilon=-\tfrac{1}{2}\gamma^2e^2a_0-\chi_0, \qquad (11)$$

A being a normalization constant.

The arbitrary parameters in the potential (7), Z^*, λ, and χ_0, are chosen so that the value of the potential (7) and that of Z_pe/r, which can be determined by Eq. (4), and their first and second derivatives should be equal at the maximum of the function (8). From the last two conditions it follows that

$$\lambda=\frac{Z\mu}{a_0}f_\lambda(x_m)$$

$$=\frac{Z\mu}{a_0}\frac{x_m^3e^{-\lambda_0x_m}}{(1+A_0x_m)^3}[2\lambda_0A_0+2A_0^2+\lambda_0^2+2(\lambda_0A_0^2+\lambda_0^2A_0)x_m+\lambda_0^2A_0^2x_m^2], \qquad (12)$$

$$Z^*r_m=Z\mu f_{Z^*}(x_m)$$

$$=Z\mu\frac{x_me^{-\lambda_0x_m}}{(1+A_0x_m)^3}[1+(\lambda_0+3A_0)x_m-\lambda_0^2x_m^2-(\lambda_0A_0^2+2\lambda_0^2A_0)x_m^3-\lambda_0^2A_0^2x_m^4]. \qquad (13)$$

The function (8) reaches its maximum at r_m. $x_m=r_m/\mu$ in Eqs. (12) and (13). Inserting Eqs. (12) and (13) into the equation determining r_m, found by differentiating

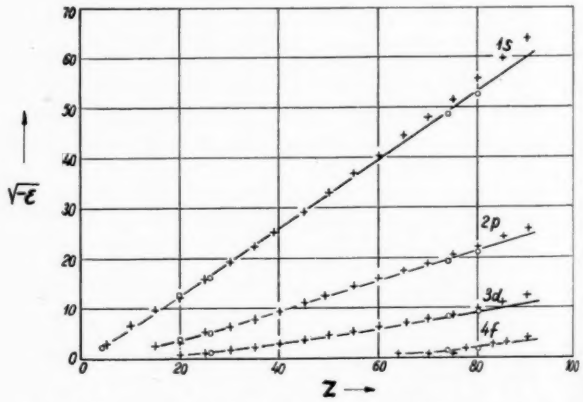

FIG. 2. The energy of the $1s$, $2p$, $3d$ and $4f$ electrons as a function of the atomic number. +++++ experimental x-ray terms. ———— calculated here. ○○○○○ calculated by the "self-consistent field" method without exchange.

Eq. (8), the following relation between $\xi=(Z\mu/a_0)^{\frac{1}{2}}=0.8853^{\frac{1}{2}}Z^{\frac{1}{2}}$ and x_m is obtained:

$$\xi^2(f_{Z^*}+f_\lambda)-\xi f_{Z^*}^{\frac{1}{2}}-l(l+1)=0. \qquad (14)$$

By means of Eqs. (12), (13) and (14) and the use of $x_m=r_m/\mu$, the relations $Z=Z(x_m)$ and $Z=Z(r_m)$ respectively, can be tabulated easily. By means of Eqs. (8), (9), (10), (11), (12), and (13), the eigenfunction and the energy of the electron in question can be obtained. No difficulty arises in carrying out calculations for all the elements of the periodic system. The energy terms of the $1s$, $2p$, $3d$, and $4f$ electrons of all the elements have been determined by this method, namely, that the eigenfunction of these electrons can be approximated by the eigenfunction (8). The continuous line in Fig. 2 represents the function resulting from these calculations. The crosses indicate the experimental x-ray energy terms K_I. In the case of spin doublets L_{II}, L_{III}; M_{IV}, M_V; and N_{VI}, N_{VII}, a cross indicates the algebraic mean of each

[2] F. Rasetti, Rend. Lincei (6) 7, 915 (1928); Z. Phys. 49, 546 (1928).

doublet term value.[3] For comparison's sake the energy terms calculated by the "self-consistent field" method are marked by circles. It can be seen in Fig. 2 that the results of the calculations are in very good agreement with those obtained by the "self-consistent field" method and the experiment.

The method developed here contains two approximations: 1. The Schrödinger equation [Eq. (6)] has been solved by the universal potential function of the neutral atom, instead of taking into account the potential of the ion corresponding to the electron in question. 2. The potential obtained in this way has been replaced by the approximate potential (7). The error of each approximation can be estimated by perturbation methods; these estimations show that these errors are negligible in the cases considered above.

The energy terms of the s, p, d, and f electrons with larger principal quantum numbers are now being calculated by a method similar to that above. This will be the subject of a future paper.

[3] Landolt-Börnstein, *Zahlenwerte und Funktionen* (Springer-Verlag, Wien, 1950), Vol. I, Part 1.

THE JOURNAL OF CHEMICAL PHYSICS VOLUME 20, NUMBER 12 DECEMBER, 1952

A Free-Electron Model for π-Molecular Complexes*

KURT E. SHULER
Applied Physics Laboratory, The Johns Hopkins University, Silver Spring, Maryland
(Received May 26, 1952)

The free-electron model for conjugated molecules is extended to a discussion of molecular complexes formed from conjugated molecules (π-molecular complexes). The forces responsible for complex formation are identified as "π-delocalization" forces. The stability and the absorption spectra of these complexes are discussed for a linear, one-dimensional model. The influence of hydrostatic pressure on the position of the complex absorption spectrum is considered, and some predictions are made regarding the resulting shifts of various absorption peaks. The free-electron model is compared with the models suggested by other workers, and good agreement is found in regard to the factors governing the formation and spectra of molecular complexes.

INTRODUCTION

MULLIKEN[1] has recently published a quantum mechanical investigation of the structure and spectra of molecular complexes using the MO-LCAO approximation. It is the purpose of this paper to call attention to the possibility of using the free-electron model for the study of certain types of molecular complexes, i.e., those complexes formed between π-electron acceptors and π-electron donors where both partners are linear or planar conjugated systems. These complexes, following the nomenclature introduced by Dewar,[2] will be termed "π-molecular complexes". The free-electron model would appear to be particularly well suited for the study of the position and intensity of the π-complex absorption spectrum, and for the analysis of the effects of pressure on the position of the absorption maxima.[3]

APPLICATION OF THE FREE-ELECTRON MODEL

The free-electron model as developed by Kuhn,[4] Bayliss,[5] and others[6] treats the π-electrons of conjugated molecules as a free-electron gas moving in the (simplified) potential field of the molecule. This model, when applied to the study of various organic dyes, has lead to promising results in the calculation of the wavelengths of absorption bands and their relative intensities. While these calculations were made initially for one-dimensional models, they have been extended recently[4,7] to three-dimensional cases with good results. In the application of the free-electron model to π-molecular complexes, it will however suffice for purposes of demonstration to limit oneself initially to the one-dimensional case using linear conjugated molecules.[8]

* The work described in this paper was supported by the Bureau of Ordnance under Contract NOrd-7386.

[1] R. S. Mulliken, J. Am. Chem. Soc. **72**, 600 (1950); **74**, 811 (1952).

[2] M. J. S. Dewar, *The Electronic Theory of Organic Chemistry* (Oxford University Press, London, 1949), p. 18.

[3] R. E. Gibson and O. H. Loeffler, J. Am. Chem. Soc. **62**, 1324 (1940).

[4] H. Kuhn, J. Chem. Phys. **16**, 840 (1948); **17**, 1198 (1949); and later papers in the Helv. Chim. Acta and Z. Elektrochem.

[5] N. S. Bayliss, (a) J. Chem. Phys. **16**, 287 (1948); (b) **17**, 1353 (1949), (c) Australian J. Sci. **3A**, 109 (1950).

[6] For further references, particularly to the work of Simpson, Platt, and Nikitine, see "Annual reviews of physical chemistry" (Annual Revs., Inc., Stanford, 1951), Vol. 2, Secs. 8 and 10.

[7] K. Rudenberg and R. G. Parr, J. Chem. Phys. **19**, 1268 (1951).

[8] This one-dimensional application could also readily be made for aromatic molecules for which the pertinent formulae have been given by W. T. Simpson, J. Chem. Phys. **16**, 1124 (1948); and J. R. Platt, J. Chem. Phys. **17**, 484 (1949). Although the use of the aro-

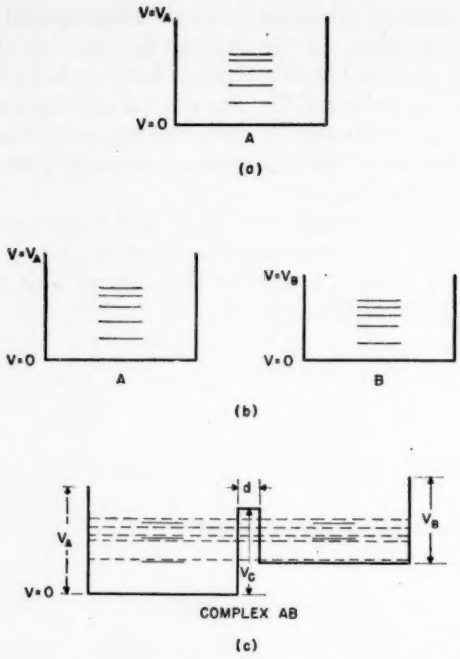

FIG. 1. (a) One-dimensional potential model for a linear conjugated molecule. (b) Two linear conjugated molecules at a separation too large for interaction. (c) A π-molecular complex AB formed from the two linear conjugated molecules of (1b) on closer approach. The potential barrier for the π-electrons corresponds to the non-conjugated "linkage" of the complex. The dotted lines show the resulting splitting of the one minimum potential energy levels.

Let Fig. 1(a) represent the (simplified) potential energy field in which a π-electron moves in a linear conjugated molecule. The energy levels are indicated schematically by the horizontal lines. For brevity, such a potential box will be referred to hereafter as the molecule. The height of the potential wall V_A can be determined as outlined by Bayliss[5c]; it corresponds to the ionization energy of the K electron plus the zero-point energy. Figure 1(b) shows two conjugated linear molecules which are still too far apart to have undergone any interaction. Figure 1(c) shows the complex which is formed from the two molecules as they approach sufficiently close for interaction. The potential barrier ($V=V_C$, width$=d$) to the mobility of the π-electrons is due to the nonconjugated "linkage" of the complex; the penetration of this barrier by the π-electrons produces a splitting of energy levels in the resulting two minimum potential. This has been indicated schematically by the dotted lines in Fig. 1(c).

In formulating the complex as shown in Fig. 1(c), only the case $V_C \gg 0$ will be considered, i.e., this discussion is not concerned with the formation of stable *compounds*, conjugated throughout, formed by rearrangement of the σ-electrons into new covalent bonds between the two molecular partners. It is assumed, instead, that in the formation of the molecular *complex* of Fig. 1(c) there is no rearrangement of the σ-electrons and that whatever stability the complex may have can be ascribed to the delocalization of the π-electrons as they tunnel through the potential barrier and move more or less freely through the whole complex. The relationship between this delocalization and the forces postulated by other authors to account for complex formation will be discussed in more detail in the last section.

The height and width of the potential barrier in a complex are functions of the intermolecular distance between the molecular components. Thus, for instance, there will be a decrease in barrier width as the molecular partners approach one another; if this approach leads to the formation of a molecular complex there will also be a concomitant decrease in the barrier height. At some equilibrium intermolecular separation corresponding to the minimum potential energy of the complex, the barrier attains its equilibrium dimensions with height V_C and width d (Fig. 1(c)). A knowledge of this variation of barrier dimension with intermolecular separation is essential if the equilibrium height V_C and width d of the complex barriers are to be calculated from the molecular constants of the component molecules. Such an "absolute" approach, however, would appear to be rather difficult. For an initial attack on the problem, it would be preferable to consider V_C and d as parameters which are to be determined by fitting the experimental data on the position of the absorption peaks in the complex spectrum. This procedure is analogous to that used by Bayliss in his recent study[5c] and would seem to be quite feasible.

For the purpose of a qualitative discussion, it is, however, possible to make some general statements in regard to the equilibrium barrier dimensions and their relation to the stability of the molecular complex without performing any detailed calculation. The decrease of the barrier height from V_A to V_C in complex formation can be attributed to the electron affinity of molecule B for the mobile π-electrons of A; for a given ionization potential I_A of molecule A the lowering of the potential barrier in the complex from V_A to V_C will thus be greater for larger values of the electron affinity E_B of B. The barrier height V_C for a given complex AB is thus roughly proportional to the difference between the ionization energy of one of the molecular partners and the electron affinity of the other one.[9] The stability of the complex increases with increasing delocalization of the π-electrons and since this delocalization increases, for a given fixed barrier width, with decreasing barrier height V_C it follows that the most stable complexes are formed when one of the molecular partners has a low ionization

matic model would have been more realistic in view of the discussion to follow, the linear model was chosen as it is more familiar in terms of the particle in a box.

[9] It would be incorrect to say that V_C is approximately *equal* to $I_A - E_B$ since the barrier height is reckoned with respect to the K electrons whereas the experimentally determined ionization energies and electron affinities refer to the energetically highest π-electrons.

energy and the other one has a high electron affinity. This condition for complex stability is fulfilled when one of the molecules is a π-electron donor and the other one a π-electron acceptor. Substitutents in the molecules or functional groups attached to the molecules which affect the formation and stability of the complex[1,3] would seem to do so by changing the ionization potentials and electron affinities of the molecular components of the complex.†,[10]

The equilibrium width of the potential barrier corresponds roughly to the equilibrium "intermolecular" distance in the complex; a reasonable value of this barrier width could probably be obtained by summing the van der Waals diameters of the atoms forming the nonconjugated "bridge" between the conjugated molecular components of the complex. According to this picture, atoms or groups of atoms attached to the conjugated components but not conjugated with them constitute part of the potential barrier if the complex is formed across these groups. The width of the barrier will thus increase if long nonconjugated side chains are involved in complex formation. The consequent decrease of the delocalization energy, brought about by the decreased penetration of the mobile π-electrons through these wider barriers, would then make for only very slightly stable complexes or no complex formation at all. This is illustrated by the observation of Gibson and Loeffler[3] that α-phenylethylamine apparently does not form a complex with nitrobenzene. The lowering of the potential barrier brought about by the greater basicity of α-phenylthylamine as compared to aniline is apparently outweighted by the increase in barrier width due to the nonconjugated side chain. The efficacy of the direct attachment, or conjugated attachment, of the electron donor and/or acceptor group to the conjugate ring (or chain) for complex formation had already been commented upon by Gibson and Loeffler on the basis of their observations with various aromatic amines and nitro compounds.

† *Note added in proof:*—Recent work by Dr. C. V. Mace in our laboratory has furnished some evidence in regard to the complexing of benzene with itself (see reference 10). A dilute solution of benzene in (inert) isooctane (mole fraction $C_6H_6=0.001$) subjected to a hydrostatic pressure of 1000 atmos showed a shift in the absorption maxima of about 5A toward longer wavelengths (2545A→2550A; 2606A→2610A). Similar red shifts were also obtained for dilute solutions of naphthalene in isooctane at 1000 atmos (2550A→2555A; 2650A→2665A; 2750A→2750A; 2855A→2860A). As is to be expected, no such shifts were obtained for cyclohexane under the same conditions. A detailed account of this work will be published shortly by Dr. Mace.

[10] In the case of two identical conjugated molecules ($A=B$) such as benzene and benzene, there is no lowering of the potential barrier between the molecules and $V_C=V_A=V_B$. Nevertheless, there may be a small but finite probability for π-electron tunneling through the potential barrier between the molecules so that a weakly stable complex could be formed. In the case of liquid benzene there is evidence from x-ray diffraction that such a complex formation may take palce [W. C. Pierce, J. Chem. Phys. **5**, 717 (1937); P. H. Bell and W. P. Davey, J. Chem. Phys. **9**, 441 (1941)]. There is found to be a definite structure in the liquid with each Bz molecule surrounded by 6 neighbors in a plane. This coplanarity would be predicted by the free-electron model. See also the discussion on this point in reference 1(b), Sec. VIII.

The energy levels of the free molecules A and B will be "split" during the formation of the complex as shown in Fig. 1(c), each level of the free molecular partner splitting into two for the complex corresponding to the change from a one-minimum potential (Fig. 1(a)) to a two-minimum potential (Fig. 1(c)). The amount of splitting will depend in a complicated, but readily calculable manner on the height and width of the potential barrier and on the energy of the particular level (see Appendix). The splitting will increase with decreasing barrier height and width and with increasing height of the energy levels. In the one-dimensional case each energy level of the free molecules is occupied, for molecules with no unpaired electrons, by two π-electrons (+ and − spin). In the complex, where the number of energy levels is double that of the free molecule, each occupied level has still two electrons because two molecules now contribute their π-electrons to the complex. Since a conjugated molecule with n carbon atoms has n mobile π-electrons the number of occupied energy levels in the complex will be $(n_A+n_B)/2$.[11]

The electronic transitions giving rise to the characteristic absorption spectrum of the complex will take place (a) between a filled energy level of the complex and an empty level above it and (b) from filled complex levels into half-filled levels after transitions of type (a) have taken place. The selection rules governing these transitions can readily be determined for symmetrical complexes, i.e., complexes with a centrally located potential barrier. In this case the wave functions for consecutive energy levels are alternately symmetrical and antisymmetrical in the midpoint of the barrier.[12] For dipole transitions one then has the well-known $s\leftrightarrow a$ selection rule which gives $\Delta N=$ odd as the selection rule for the symmetrical complex, where N is the quantum number of the complex level. For nonsymmetrical complexes, i.e., complexes with noncentrally located barriers, where the wave functions cannot be classified simply as symmetrical or antisymmetrical, these selection rules will no longer hold. One would expect, however, that for a complex which does not depart too much from the symmetrical model described above, the transitions with $\Delta N=$ odd would still be the strongest ones. This is a point which would seem to merit further investigation. Some of the permitted transitions (for a symmetrical complex) of both type (a) and (b) are shown in Fig. 2; the numbering of the transitions and the designation of the energy levels on the right-hand side of the figure refer to the discussion in the next section. The wavelength λ_C of the absorption peaks

[11] The situation will be somewhat more complicated in conjugated systems with hetero atoms such as N and/or O since they can contribute 2 π-electrons each.

[12] See e.g., J. C. Slater, *Quantum Theory of Matter* (McGraw-Hill Book Company, Inc., New York, 1951), p. 51. This can readily be seen if one considers the centrally placed potential barrier as a perturbation which splits each degenerate level of the two single minimum potentials into two levels with a symmetrical and an antisymmetrical wave function, respectively.

corresponding to these transitions is given by $\lambda_C = hc/\Delta E$ where ΔE is the energy difference of the levels involved in the transition.

Since the wave functions of the π-electrons for the free-electron model of the complex can readily be obtained in analytical form by the usual method of matching ψ and $d\psi/dx$ at the potential discontinuities, the intensities of the transition, i.e., the dipole moment Q and the f values, can be calculated by the methods discussed by Kuhn[4] and Bayliss.[5,13] Experience has shown that the actual calculations for the complex are quite laborious owing to the difficulty encountered in normalizing the wave functions. It is, however, possible to show in a rather general way that the f values of the transitions in a π-molecular complex are comparable to those of the molecular partners which form the complex and that they may thus be quite strong. If one considers a symmetrical complex of the type discussed above as a perturbation problem with the origin at the center of the system, one can write

$$\Psi_{\text{sym}}{}^{N+1} = \frac{1}{\sqrt{2}}(\psi_A{}^{N+1} + \psi_B{}^{N+1}), \tag{1}$$

$$\Psi_{\text{anti}}{}^{N} = \frac{1}{\sqrt{2}}(\psi_A{}^{N} - \psi_B{}^{N}), \tag{2}$$

where the Ψ's are the wave functions for the complex levels and the ψ's are the wave functions for the unperturbed one-minimum potentials A and B.[14] The dipole moment Q_C is then given by

$$Q_C = \int_{-\infty}^{\infty} \Psi_s{}^{N+1} x \Psi_a{}^{N} dx = \tfrac{1}{2}\left[\int_{-\infty}^{\infty} \psi_A{}^{N} x \psi_A{}^{N+1} dx - \int_{-\infty}^{\infty} \psi_B{}^{N} x \psi_B{}^{N+1} dx + \int_{-\infty}^{\infty} \psi_A{}^{N} x \psi_B{}^{N+1} dx - \int_{-\infty}^{\infty} \psi_A{}^{N+1} x \psi_B{}^{N} dx\right]. \tag{3}$$

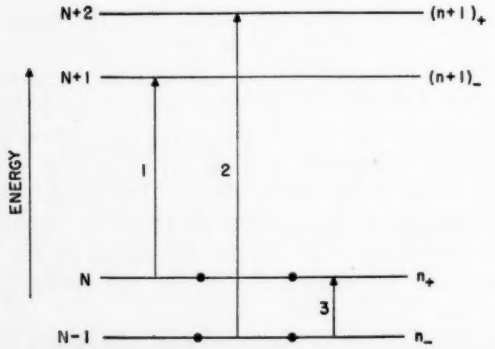

FIG. 2. Schematic energy levels and some possible optical transitions for π-molecular complexes. Transition 3 could take place subsequent to transition 1.

[13] The statement of Bayliss in reference 5c in regard to the necessity of choosing the origin at the center of the system is not correct. See H. Shull and F. O. Ellison, J. Chem. Phys. **19**, 1610 (1951).

[14] See reference 12, Fig. 4.2.1.

The consecutive levels ($\Delta n = 1$) in the one-minimum potential are alternately symmetrical and antisymmetrical so that all of the integrals of Eq. (3) have nonzero values. However, the "mixed" integrals $\int \psi_A x \psi_B\, dx$ may be neglected, in first approximation, in comparison with the first two terms of Eq. (3) since for potential barriers of any size the overlap of ψ_A and ψ_B will be quite small. Since

$$\int_{-\infty}^{\infty} \psi_A{}^{N} x \psi_A{}^{N+1} dx \quad \text{and} \quad \int_{-\infty}^{\infty} \psi_B{}^{N} x \psi_B{}^{N+1} dx$$

are equal and of opposite sign for the above model (symmetrical complex with origin at center of barrier), the square of the dipole moment will be given approximately by

$$Q_C{}^2 \approx \left[\int_{-\infty}^{\infty} \psi_A{}^{N} x \psi_A{}^{N+1} dx\right]^2. \tag{4}$$

The f values for the complex absorption thus should be, as stated above, approximately comparable to that of the molecular components. This should hold true to a certain degree even if the π-molecular complex is no longer strictly symmetrical in the midpoint of the barrier.

The simplified linear one-dimensional model presented above, while bringing out the salient points in regard to the application of the free-electron model to the study of π-molecular complexes, would probably have to be refined considerably before quantitative calculations could be expected to give satisfactory agreement with experimental data. These refinements would be analogous to those introduced[4-6] in the study of conjugated molecules, i.e., the oscillation of the potential energy (instead of a flat well), potential sinks and humps to take account of hetero atoms, two- and three-dimensional treatments, and consideration of the ring structure of aromatic molecules. Since the π-complexes for which data are at hand mostly involve aromatic molecules, the introduction of the last mentioned factor would seem to be a good starting point for quantitative calculations.

THE EFFECTS OF PRESSURE ON THE ABSORPTION SPECTRUM

The free electron model for π-molecular complexes lends itself well to an analysis of the effect of pressure (or temperature at constant volume) on the position of the complex absorption bands. If one takes for simplicity of argument the symmetrical one-dimensional complex considered above, one has the simple relationship $E_A{}^n = E_B{}^n$ for all the energy levels of the conjugated molecular partners. The energy levels E_C of the complex AB which correspond to the energy levels $E_A{}^n$ and $E_B{}^n$

of A and B can be written to a good approximation[15] as

$$E_C{}^{n+} = E_A{}^n + \epsilon^n, \tag{5}$$

$$E_C{}^{n-} = E_A{}^n - \epsilon^n, \tag{6}$$

where $2\epsilon^n$ is the delocalization energy for the nth level. If $E_A{}^n$ and $E_B{}^n$ are the highest filled levels of A and B, then $E_C{}^{n+}$ is the highest filled energy level of the complex. The main absorption band is then due to the transition

$$E_C{}^{n+} \longrightarrow E_C{}^{(n+1)-},$$

where

$$E_C{}^{(n+1)-} = E_A{}^{(n+1)} - \epsilon^{(n+1)}, \tag{7}$$

and the wavelength λ_C of this absorption peak is given by

$$\lambda_C = \frac{hc}{\Delta E} = \frac{hc}{[E_A{}^{(n+1)} - E_A{}^n] - [\epsilon^{(n+1)} + \epsilon^n]}. \tag{8}$$

Owing to the rather small compressibility of molecules, an increase in hydrostatic pressure on a solution of molecules A and B will bring about primarily *inter*-molecular changes rather than *intra*-molecular ones. The main effect of the increased pressure on the solution of A and B will thus be a reduction of the equilibrium inter-molecular distance in the complex. According to the discussion given previously, this is equivalent to a decrease of the barrier width in the complex to a new equilibrium value $d' < d$. There will also be a concomitant decrease of barrier height in the complex to a new equilibrium value $V_C' < V_C$, owing to the stronger interaction of the π-electron acceptor B with the π-electron donor A at the smaller inter-molecular separation. This reduction of barrier height and barrier width with increasing pressure is accompanied by an increase in the delocalization energy ϵ since the mobile π-electrons can now tunnel more easily through the smaller potential barrier in the complex. As may be seen from Eq. (8), this increase in ϵ produces an increase in λ_C so that the main absorption peak of the complex will shift toward longer wavelength at higher pressure.[16] This is in accord with the findings of Gibson and Loeffler[3] regarding the effects of pressure on the absorption of the complexes formed by aromatic amines and aromatic nitro and nitroso compounds to which the above model of a symmetrical complex would apply to a good approximation.

The above analysis will also serve to explain the observed shift in the complex absorption peak to longer wavelength with increased temperature at constant volume[3] since such a change of experimental conditions

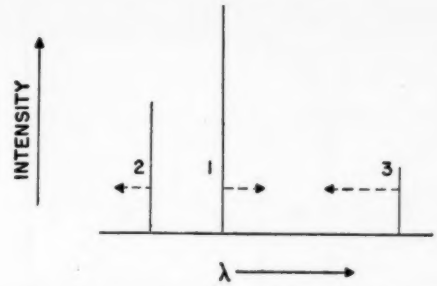

FIG. 3. Schematic diagram of the wavelengths of the transitions of Fig. 2. The extensions of the vertical lines indicate the relative intensities of the absorption bands. The arrows indicate the direction and magnitude of the shifts of the absorption bands of the complex with increasing pressure.

is equivalent to the increase of pressure discussed above. Considered from a kinetic-molecular point of view, the increased temperature at constant volume will being about more violent collisions between the molecules A and B so that the average inter-molecular separation in the collision complex AB will be reduced below its former low temperature value. Averaging over all the collision complexes then leads to the result that the equilibrium inter-molecular separation of the complex AB decreases with increasing temperature at constant volume. This analysis again presupposes that the intra-molecular changes can be neglected, to a first approximation, in comparison with the inter-molecular ones.

The above discussion can readily be extended to other allowed transitions of the (symmetrical) complex. Figure 2 shows some of these transitions; those labeled 1 and 2 are of type (*a*), the one labeled 3 is of type (*b*). Figure 3 which is only schematic and qualitative, indicates the effects of increasing pressure on these transitions. If transition 1, which has been analyzed above, is in the visible region, as it appears to be in the system investigated by Gibson and Loeffler, then transition 2 will be at a shorter wavelength and transition 3 would be at a much longer wavelength (probably in the infrared). The relative intensities of these transitions are given schematically by the height of the vertical lines. The arrows show the shift of the complex absorption peaks with increasing pressure; their lengths are roughly proportional to the relative magnitude of the shift.[17] It is interesting to note that these wavelength shifts are in different directions for different transitions. The shift to the red noted so far[3] corresponds to the (most intense) main absorption band [transition 1 of type (*a*)]; the shift of an absorption band toward the ultraviolet with increasing pressure does not appear to have been observed as yet. It would seem to be worthwhile to make some further pressure studies to see if the above predic-

[15] This is not quite correct since the splitting is not symmetrical about the one-minimum energy level but is slightly larger for the upper level. This, however, is a minor factor in the above considerations.

[16] The small change in E brought about by the intra-molecular effects of pressure (compression of molecules A and B) can be neglected in comparison with the much greater change in ϵ so that E_A can be taken as a pressure independent quantity in Eqs. (5) to (8).

[17] It can readily be verified by the methods outlined above [Eqs. (5)–(8)] that for a given pressure the shifts in wavelength of transitions 1 and 2 are equal in magnitude, but that the absorption peak corresponding to transition 3 will undergo a much more pronounced shift at the same pressure.

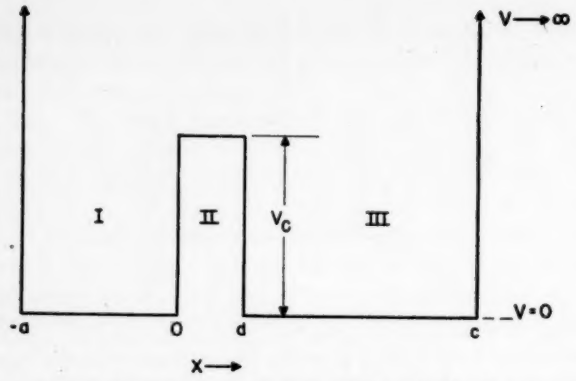

FIG. 4. Simplified one-dimensional potential for linear π-molecular complex.

tions in regard to the different wavelength shifts are borne out experimentally.

The pressure imposed on these complex forming solutions affects not only the position of the complex absorption bands but also the strength of the absorption. This is due to the pressure dependence of the equilibrium $A+B \rightleftarrows A \cdot B$ which has been discussed in some detail by Weiss.[18] The strength of the complex absorption will also be affected by changes in temperature since the above equilibrium is temperature-dependent for nonzero values of the heat of complex formation.[18] The analysis of these effects is, however, outside the scope of this paper.

DISCUSSION

The free-electron model may be considered as a molecular orbital treatment using non-atomic orbitals. As such, it should lead to concordant results with the MO-LCAO treatment used by Mulliken[1] in as far as the two methods are valid for the problem investigated. The differences should be primarily in the language used to describe the quantum mechanical results. Such an agreement on the salient points of complex formation, properties, and spectra indeed appears in the two formulations.

Both methods are in accord that the forces responsible for complex formation are not the usual chemical bonding forces in the sense that they do not involve the rearrangement of electrons to form covalent bonds between the two molecules. In this respect the free-electron model for π-molecular complexes is also in accord with the conclusions reached by Gibson and Loeffler.[3,19] The resonance leading to "charge-transfer forces" in Mulliken's model is equivalent to the delocalization of π-electrons in the free-electron model. This gives rise to what has been termed here the "delocalization forces" for π-molecular complexes. The free-electron model, similar to the charge transfer model, has orientational properties (the complex will be formed with the molecules oriented in such a manner that the potential barrier will be as small as possible) and additivity in that the formation of a 1:1 complex would not prevent the addition of other suitable molecules to the complex (see e.g., reference 10). The decrease in barrier width with increasing pressure leads to an increased stability of the complex under compression, a feature which is also predicted by the charge transfer model. Both models further predict strong absorption for the complex.

Another point brought out clearly by the free-electron model is that the characteristic absorption spectrum of the complex must be attributed to the whole complex rather than to any of the functional groups or to one of the molecular partners. This is in accord with the views of Brackmann[20] and also agrees with Mulliken's conclusions.[21] Since the stability of the complex depends to a large extent upon the height V_C of the potential barrier (see Fig. 1(c)), it follows that a low ionization potential of the π-donor and a high electron affinity of the π-acceptor, which have the effect of lowering the potential barrier, will bring about a more stable complex. Substituents and functional groups in both π-donors and acceptors which respectively lower I and increase E will enhance the probability of complex formation. These results, too, are in agreement with the conclusions of Weiss[18] and Mulliken.[1]

The importance of the symmetry of the combining wave functions on the geometrical configuration of the molecular complex has been emphasized by Mulliken.[1] This factor does not enter very prominently into the *one-dimensional* free-electron model discussed above, since all the wave functions must either be $C_{\infty v}$ or $D_{\infty h}$. It is, however, a question which would have to be considered in some detail in any two- or three-dimensional free-electron treatment in order for the geometrical configuration of the complex to be established. It appears from a very cursory examination of this question for the three-dimensional model that the molecular components would have to be coplanar for π-molecular complex formation.[22]

ACKNOWLEDGMENTS

The author is very much indebted to Dr. R. E. Gibson and Dr. F. T. McClure for calling his attention to

[18] J. Weiss, J. Chem. Soc., 245 (1942).

[19] Gibson and Loeffler suggest that the term "compound formation in solution" be confined to entities formed with covalent bonds between the atoms of the two original components. If this suggestion is accepted, the entities formed by "charge-transfer forces" or "delocalization forces" may then be termed molecular *complexes*, as has been done in the body of this paper.

[20] W. Brackmann, Rec. trav. chim. 68, 147 (1949).

[21] The suggestion of Gibson and Loeffler that in complexes involving nitro compounds the N:O group is the most probable seat of absorption does not seem to be a valid one.

[22] After this manuscript was completed, a paper of J. Landauer and H. McConnel on molecular complexes of aniline and aromatic nitro compounds appeared [J. Am. Chem. Soc. 74, 1221 (1952)]. Since these authors apply the theory developed by Mulliken[1] to interpret their results, there is general agreement between their conclusions and the ones reached in this paper. Their discussion of the three-dimensional configuration of these complexes is of particular interest in connection with the concluding remarks above. There seems to be good evidence for the off-axis packing they suggest in the writings listed in reference 10 of this paper.

this problem and for several stimulating discussions during the course of this work. He is also indebted to Dr. C. V. Mace for many interesting discussions on experimental points bearing on this investigation.

APPENDIX

Energy Levels for the One-Dimensional Two Minimum Potential

It is desired to obtain an expression which relates the energy levels of the (linear, one-dimensional) complex to the dimensions of the potential barrier and the potential minima. From such a relationship it will then be possible to calculate the wavelengths $\lambda_C = hc/\Delta E$ of the complex absorption peaks as a function of the potential parameters.

We shall use the simplified potential shown in Fig. 4 where V_C is the height of the potential barrier and d is its width. The energy levels $E_C < V_C$ for this potential are given by the eigenvalues of the wave equations

$$\begin{aligned} d^2\psi_I/dx^2 + \kappa E_C \psi_I &= 0, \\ d^2\psi_{II}/dx^2 + \kappa(E_C - V_C)\psi_{II} &= 0, \\ d^2\psi_{III}/dx^2 + \kappa E_C \psi_{III} &= 0, \end{aligned} \tag{9}$$

with $\kappa = 8\pi^2 m/h^2$ and boundary conditions $\psi_I = 0$ at $x = -a$ and $\psi_{III} = 0$ at $x = c$. The solution of Eqs. (9) subject to the condition[23] that ψ and $d\psi/dx$ be continuous throughout the regions *I*, *II*, and *III* is

$$\begin{aligned} [(\beta^2 - \alpha^2)/2\alpha\beta]\cos\alpha(c-d+a) - [(\beta^2+\alpha^2)/2\alpha\beta] \\ \times \cos\alpha(c-d-a) = \sin\alpha(c-d+a)\coth\beta d, \end{aligned} \tag{10}$$

where

$$\alpha = (\kappa E_C)^{\frac{1}{2}}, \tag{11}$$

$$\beta = [\kappa(V_C - E_C)]^{\frac{1}{2}}. \tag{12}$$

Equation (10) relates the complex energy levels $E_C = \alpha^2/\kappa$ of the potential of Fig. 4 to the various parameters of this potential.

For the *symmetrical* linear two minimum potential with $a = c - d$, Eq. (10) reduces to

$$(\beta/\alpha)\tan\alpha a + (\alpha/\beta)\cot\alpha a + 2\coth\beta d = 0. \tag{13}$$

In the case that $\beta d \geq 2$ so that $\coth\beta d \sim 1$, Eq. (13) can be further reduced to

$$\pm 1/a(\kappa V_C)^{\frac{1}{2}} = \sin\alpha a/\alpha a, \tag{14}$$

which permits a ready graphical solution for the energy levels E_C of the symmetrical complex as a function of a and V_C.[24] Figure 5, which is a plot of $a(\kappa E_C)^{\frac{1}{2}}$ *vs* $1/a(\kappa V_C)^{\frac{1}{2}}$, shows the position, the spacing, and the splitting of the energy levels in the symmetrical complex

In the approximation $\beta d \geq 2$, $\coth\beta d \sim 1$, there is no longer any dependence of E_C on d for the symmetrical complex (Eq. (14)). For the more general, nonsymmetrical potential of Fig. 4, however, this dependence of E_C on d remains since d in general cannot be neglected in the factors $(c-d+a)$ and $(c-d-a)$ of Eq. (10).

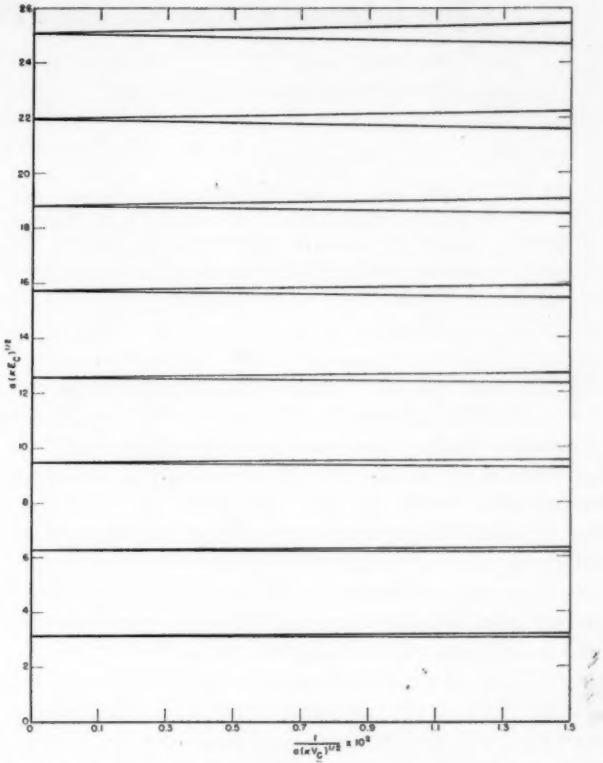

FIG. 5. Plot of $a(\kappa E_C)^{\frac{1}{2}}$ *vs* $1/a(\kappa V_C)^{\frac{1}{2}}$ for a symmetrical complex ($a = c - d$) showing the position, spacing, and splitting of the complex energy levels as a function of a and V_C.

[23] See V. Rojansky, *Introductory Quantum Mechanics* (Prentice-Hall, Inc., New York, 1946), Chaps. IV and VI.

[24] The assumption $\beta d \geq 2$ is a physically reasonable one. For $V_C \sim 15$ ev (see references 9 and 5c) and for the lower energy levels, $\beta \sim 10^8$ cm^{-1}. The barrier width d which is approximately equal to the "inter-molecular" separation of the complex components is probably of the order of 10^{-7} cm. The above condition should thus be fulfilled for most cases of interest.

THE JOURNAL OF CHEMICAL PHYSICS VOLUME 20, NUMBER 12 DECEMBER, 1952

The Intensity of Spectral Lines Produced in Nonhomogeneous Flames

ALAN C. KOLB* AND E. R. STREED
Basic Sciences Research Department, U. S. Naval Civil Engineering Research and Evaluation Laboratory, Port Hueneme, California

(Received October 15, 1951)

The emission and absorption of radiant energy in a nonhomogeneous flame is discussed. Multiple scattering is neglected and the solution of the basic one-dimensional equation of transfer is obtained in series form. The series is rapidly convergent and a first term approximation yields a simple formula for a flame source having a plane of symmetry which gives satisfactory agreement with experimentally determined nonlinear spectrochemical calibration curves.

THE techniques of flame spectrophotometry have received increased attention as a rapid analytical procedure during the past decade. Empirically determined spectrochemical calibration curves are usually employed to relate spectral line intensities to the number of atoms introduced into a flame. Because of the relatively low excitation temperature in flames as compared to arcs and sparks, it is found that a scarcity of strong lines sometimes necessitates the use of lines for which self-absorption is severe. This complicates the preparation of a spectrochemical calibration curve since a large number of comparison standards are normally required to establish these nonlinear curves. It is the primary objective of this paper to develop analytical equations which may be used to describe the functional relationship between line intensities and the concentration of atoms introduced into a flame source. It is hoped that this will result in a procedure for constructing a spectrochemical calibration curve through the use of a minimum number of comparison standards.

In a recent study of the effect of self-absorption on the intensity of spectral lines, Cowan and Dieke[1] demonstrated that a relatively simple model in which the emitting and absorbing atoms are spatially separated may be used successfully as a basis for the calculation of line shapes for arc and spark excitation. This model will be discussed in the light of our results, and it will be shown that the equations which are obtained through the use of this special model are of more general validity than is implied by the rather restricting assumptions upon which it is based.

I. EQUATION OF TRANSFER

In formulating the equations for radiative transfer in a steady-state nonhomogeneous flame consider a small cylindrical element of volume of cross section $d\sigma$ and height dx oriented along a suitably chosen x axis in the flame source. The x axis is taken to be coincident with the optic axis of the spectrograph used to obtain intensity measurements. According to Chandrasekhar,[2] the formal solution of the equation of transfer may be written in the form

$$I_\nu(l')=\int_{-l_0'}^{l'} \mathfrak{J}_\nu(x)\kappa_\nu(x)\rho(x)\exp-\tau_\nu(x,l')dx, \quad (1)$$

where $I_\nu(l')$ is the intensity of radiation at $x=l'$ in the direction of the positive x axis. The points $x=l'$, $-l_0'$ are positions along the x axis where the vapors which comprise the flame become sufficiently dilute so that a negligible amount of incident radiation is absorbed $[\rho(l')=\rho(-l_0')=0]$. The function $\kappa_\nu(x)$ is the mass absorption coefficient for radiation of frequency ν and $\rho(x)$ is the density of material in the element of volume $d\sigma\cdot dx$ at the point x. The quantity $\tau_\nu(x,l')$ is the optical density (thickness) of the flame between x and l' and is given by

$$\tau_\nu(x,l')=\int_x^{l'} \kappa_\nu(x)\rho(x)dx. \quad (2)$$

The source function $\mathfrak{J}_\nu(x)$ may be written in terms of an emission coefficient $j_\nu(x)$ which is defined as the amount of energy radiated along the x axis through the element of area $d\sigma$ per unit of mass per unit time per unit frequency interval by atoms (or molecules) present in the element of volume $d\sigma\cdot dx$. Hence, it follows from the formulation of Chandrasekhar that

$$\mathfrak{J}_\nu(x)=\frac{j_\nu(x)}{\kappa_\nu(x)}. \quad (3)$$

For a flame in local thermodynamic equilibrium, it is assumed that a local population temperature $T(x)$ can be defined such that

$$\mathfrak{J}_\nu(x)=B_\nu(T(x)), \quad (4)$$

where $B_\nu(T(x))$ is the Planck function by Kirchoff's law.

It is of fundamental importance to note that if $x=\pm l$ are taken to be limits between which the emitting atoms are confined by choosing the origin of the x axis midway between these limits, then it is not necessarily true that the limits of emission $(x=\pm l)$ coincide with the limits of absorption $(x=l', -l_0')$ for a flame surrounded by a cooler atmosphere. This is a consequence of the fact that

* Present address: Randall Laboratory of Physics, University of Michigan, Ann Arbor, Michigan.

[1] R. D. Cowan and G. H. Dieke, Revs. Modern Phys. **20**, 418–455 (1948).

[2] S. Chandrasekhar, *Radiative Transfer* (Oxford University Press, London, 1950). See also reference 1.

the flame temperature $T(x)$ approaches atmospheric temperature at its periphery, and the number of emitters may be negligibly small as compared to the number of absorbers on the outer edges of the flame. For this problem, therefore, one can replace the limits of integration l', $-l_0'$ which appear in Eq. (1) by $\pm l$ without loss of generality since the possibility that $l=l'=l_0'$ is not excluded by this substitution. Hence,

$$I_\nu(l')=\int_{-l}^{+l} j_\nu(x)\rho(x)\exp-\tau_\nu(x,l')dx. \tag{5}$$

If multiple scattering within the flame source is neglected, then this equation can be integrated at once by the method of partial integration to yield an infinite series which may be assymptotic, so that if one uses only a small number of terms one has a physically satisfactory solution. This integration gives

$$I_\nu(l')=\exp-\tau_\nu(x,l')\sum_{n=1}^{\infty}(-1)^{n-1}R_n(x)\times\{[\kappa_\nu(x)\rho(x)]^{n-1}+F_n(x)\}\Big|_{x=-l}^{x=+l}, \tag{6}$$

where the following abbreviations have been introduced: the indefinite integrals

$$R_n(x)=\int\int\cdots n\cdots\int j_\nu(x)\rho(x)(dx)^n,$$

$$F_1(x)=F_2(x)=0, \tag{7}$$

and

$$F_3(x)=\frac{d}{dx}[\kappa_\nu(x)\rho(x)];$$

and the general term $F_n(x)$ may be calculated from the differential recurrence formula

$$F_n(x)=F_{n-1}(x)\kappa_\nu(x)\rho(x)+\frac{d}{dx}\{F_{n-1}(x)+[\kappa_\nu(x)\rho(x)]^{n-1}\},\quad \text{for } n=4,5,6\cdots. \tag{8}$$

In order to use Eq. (6) to completely describe the radiation from an actual light source, the boundary conditions and symmetry properties of the source must be specified. $\kappa_\nu(x)$, $j_\nu(x)$, and $\rho(x)$ must be known functions, the intensity of scattered radiation must be small relative to the total radiation observed, and the experimental conditions must be such that the solid angle subtended at the source by a collimating mirror or lens is small so that a relatively small portion of the flame is observed at any one time. This latter assumption justifies the evaluation of a one-dimensional integral.

II. DISCUSSION OF THE SERIES (6)

Superficially, Eq. (6) does not seem very much simpler than the basic one-dimensional equation for radiative transfer as given by Chandrasekhar in Eq. (1). It will be instructive to first discuss some specializations of Eq. (6).

In all of the following applications, it will be assumed that we are dealing with a flame source whose geometry is defined only by the condition that there be a plane of symmetry perpendicular to the direction in which the flame is viewed. Let the x axis be perpendicular to the plane of symmetry with $x=0$ at the plane. With this assumption one can put $l_0'=l'$ in the equations to follow.

1. Homogeneous Flame Source

For a homogeneous flame with constant temperature throughout,

$$\left.\begin{aligned} l&=l'\\ \kappa_\nu(x)&=\kappa_\nu\\ j_\nu(x)&=j_\nu\\ \rho(x)&=\rho\end{aligned}\right\}\quad \text{for } -l\leqslant x\leqslant l$$

and

$$\kappa_\nu(x)=j_\nu(x)=\rho(x)=0\quad \text{for}\quad l<x<-l.$$

Therefore, it follows that

$$F_n(\pm l)=0,$$

$$R_n(\pm l)=\frac{(\pm l)^n}{n!}j_\nu\cdot\rho,$$

$$-\tau_\nu(x,l')=(x-l)\kappa_\nu\rho.$$

Substitution into Eq. (6) yields

$$I_\nu(l)=\frac{j_\nu}{\kappa_\nu}\sum_{n=1}^{\infty}\frac{(-1)^{n-1}}{n!}(l\kappa_\nu\rho)^n-(\exp-2l\kappa_\nu\rho)\cdot\sum_{n=1}^{\infty}\frac{(-1)^{2n-1}}{n!}(l\kappa_\nu\rho)^n.$$

Remembering that

$$\sum_{n=1}^{\infty}\frac{(-1)^{n-1}a^n}{n!}=1-e^{-a},$$

one obtains the well-known expression for a homogeneous light source in thermodynamic equilibrium at the temperature T,

$$I_\nu(l)=B_\nu(T)(1-\exp-2l\kappa_\nu\rho). \tag{9}$$

It is evident from this equation that the self-reversal of spectral lines is not possible in a homogeneous light source since $I_\nu(l)$ is a monotonic increasing function of the density of material ρ. For this reason, this model is generally found to be unsatisfactory for flames in which self-reversal can occur.

2. Source with Emitting and Absorbing Atoms Spatially Separated

For this model it is assumed that the excitation temperature in the central portion of the light source is very high and therefore contains relatively few atoms in lower states of excitation. The absorbers are assumed to lie outside of this region in a cooler layer of gas which contains a negligible number of emitters. Thus,

$$l'>l,$$
$$\kappa_\nu(x)=0 \quad \text{for} \quad -l\leq x\leqslant l,$$

and, therefore, the derivatives of $\kappa_\nu(x)$ with respect to the variable x, evaluated at $x=\pm l$, are also zero. Hence,

$$F_n(\pm l)=0;$$

also,

$$\tau_\nu(-l, l)\equiv\int_{-l}^{l}\kappa_\nu(x)\rho(x)dx=0.$$

For purposes of simplification we define a term $2P_\nu'(l)$ which represents the intensity of radiation that would be observed if there were no self-absorption in the light source:

$$2P_\nu'(l)=\int_{-l}^{+l}j_\nu(x)\rho(x)dx. \tag{10}$$

It is easily demonstrated that Eq. (6) reduces to

$$I_\nu(l')=2P_\nu'(l)\exp-\tau_\nu(l, l')=2P_\nu'(l)\exp-\tau_\nu(0, l') \tag{11}$$

for a model in which the emitting and absorbing atoms are spatially separated [$\tau_\nu(0, l')=\tau_\nu(l, l')$ for this model].

Various other models have been suggested on which to base the calculation of line intensities.[3] Generally, it is assumed that flame sources are composed of one or more homogeneous isothermal regions and calculations are then made upon this basis.

3. Flame Sources for Which $l\to l'$ and $\kappa_\nu(l)\rho(l)\cong 0$

A more realistic model than those discussed previously would not be based upon the simplifying assumption that the flame is composed of one or more sharply defined zones. For the models of Sec. II (1, 2), it was necessary to assume that discontinuities exist in the coefficients of emission and absorption in passing across plane parallel boundaries which separate the hypothetical zones. To improve upon these models, consider first a source in which emitting and absorbing atoms are present at all points within the flame source (i.e., $l=l'$). Corresponding to the physical situation which one might expect, the coefficients of emission and absorption are continuous functions which *gradually* approach zero on the periphery of the flame as the flame temperature approaches atmospheric temperature and the surrounding vapors become sufficiently dilute. It follows from this description that as $l\to l'$ one can assume also that

$$\left(\frac{d^n}{dx^n}[\kappa_\nu(x)\rho(x)]\right)_{x=\pm l}\to 0 \tag{12}$$

and

$$\kappa_\nu(\pm l)\rho(\pm l)\to 0.$$

It can be verified from the symmetry conditions that

$$\begin{aligned} P_\nu'(l)&=-P'_\nu(-l),\\ \tau_\nu(-l, l)&=-\tau_\nu(l, -l),\\ 2\tau_\nu(0, l)&=\tau_\nu(-l, l), \end{aligned} \tag{13}$$

and

$$2\tau_\nu(0, l')=\tau_\nu(-l', l').$$

Substitution of (12) and (13) into Eq. (6) yields

$$I_\nu(l)=2P_\nu'(l)\exp-\tau_\nu(0, l)\cosh\tau_\nu(0, l). \tag{14}$$

If it is assumed that $\rho(x)$ is proportional to the concentration C of atoms introduced[4] (atomized) into the base of the flame, one can use this theory to obtain an analytical equation which describes the dependence of $I_\nu(l')$ upon the concentration C. On the basis of this assumption, two quantities, $P_\nu(x)$ and $\mathrm{K}_\nu(x)$, are defined such that

$$\begin{aligned} P_\nu'(x)&=P_\nu(x)C,\\ \tau_\nu(0, x)&=\mathrm{K}_\nu(x)C. \end{aligned} \tag{15}$$

These relations follow directly from the definitions of $P_\nu'(x)$ and $\tau_\nu(0, x)$ and allow us to write Eq. (14) as

$$I_\nu(l)=(2P_\nu(l)C)\cdot(\exp-\mathrm{K}_\nu(l)C)\cdot\cosh\mathrm{K}_\nu(l)C. \tag{16}$$

The following two relations can be obtained from this expression: For small values of C,

$$\ln\frac{I_\nu(l)}{C}=-\mathrm{K}_\nu(l)C+\ln 2P_\nu(l); \tag{16a}$$

and for large values of C,

$$\ln\frac{I_\nu(l)}{C}=\ln P_\nu(l). \tag{16b}$$

Consequently, if Eq. (16) is valid for a specified light source, a plot of $\ln[I_\nu(l)/C]$ *vs* C should yield two straight line sections with a constant slope of $-\mathrm{K}_\nu(l)$ at low values of the concentration C and a slope of zero at high values of the concentration C. Experimentally, two linear sections have been observed for the spectral lines studied. However, for high concentrations the slopes of these curves are not found to be zero. Furthermore, Eq. (16) does not provide for the self-reversal of spectral lines since $I_\nu(l)$ is a monotonic increasing function of the

[3] See, for example, W. Bleeker, Z. Physik **52**, 808–814 (1929).

[4] Solutions containing dissolved salts are atomized into the flame at a constant rate. Intensities corresponding to various concentrations of the element of interest are then measured, and a spectrochemical calibration curve is drawn from these data.

concentration C. It is necessary, therefore, to investigate sources for which $l'>l$ in an attempt to resolve these difficulties.

4. Sources for Which $l'>l$: Approximate Formula

For the range of concentrations employed by us during the course of this investigation[5] it was found that the first term in the series (6) was sufficient to account for the data (e.g., Ag 3383 was studied at concentrations ranging from 0–750 ppm; Cu 3248 from 0–1800 ppm; CaO 5540 from 0–72,000 ppm; BaO 7450 from 0–1000 ppm, etc.) with a very satisfactory agreement between theory and experiment. It can be readily shown that a first term approximation to Eq. (6) yields

$$I_\nu(l')=2P_\nu'(l)\cdot(\exp-\tau_\nu(0,l'))\cdot\cosh\tau_\nu(0,l); \quad (17)$$

or, for spectrochemical applications,

$$I_\nu(l')=2P_\nu(l)C\cdot(\exp-\mathrm{K}_\nu(l')C)\cdot\cosh\mathrm{K}_\nu(l)C. \quad (18)$$

For small values of C, Eqs. (17) and (18) reduce to

$$I_\nu(l')=2P_\nu'(l)\exp-\tau_\nu(0,l') \quad (17a)$$

or

$$I_\nu(l')=2P_\nu(l)C\exp-\mathrm{K}_\nu(l')C; \quad (18a)$$

and for large values of C,

$$I_\nu(l')=P_\nu'(l)\exp-\tau(l,l') \quad (17b)$$

or

$$I_\nu(l')=P_\nu(l)C\exp-[\mathrm{K}_\nu(l')-\mathrm{K}_\nu(l)]C. \quad (18b)$$

Equations (18a) and (18b) suggest that there should be a linear relationship between $\ln I_\nu(l')/C$ and C at both high and low values of the concentration C for a source with the symmetry properties and boundary conditions assumed in this section. As stated in Sec. II (3), this result is confirmed by experiment. These $\ln I_\nu(l')/C$ *vs* C plots afford a rapid and direct means of determining the validity of these equations for a particular light source. It is also evident from Eq. (18) that differentiation of $I_\nu(l')$ with respect to C shows that $I_\nu(l')$ reaches a maximum intensity, and therefore, self-reversal can occur for large C.

Equations (17a), (17b), and (11) obviously have the same functional form. Cowan and Dieke have observed that the general intensity distribution within a line depends very little on the particular assumption made concerning the excitation function for an arc and is never far from that of a model in which the emitting and absorbing atoms are spatially separated. The results of this section are clearly in accord with these conclusions. The fact that good agreement with experiment was obtained by Cowan and Dieke through the use of this model indicates that the 2nd, 3rd,$\cdots n$th terms in the series (6) were indeed negligible for the concentration ranges in which their experimental data were taken. It is more reasonable to assume that this is the case rather than to assume that an arc consists of spatially separated emitters and absorbers. (Cowan and Dieke agree that their model is far from the actual state of affairs in an actual light source.) It should be noted, however, that there is an intermediate range of concentrations for which an equation with the form of (17a), (17b), or (11) fails to describe the intensity-concentration relationship. Fortunately, it has been found experimentally that this intermediate range is usually quite small relative to the total concentration range in which Eq. (17) may be utilized, and therefore, the calculations of Cowan and Dieke are probably valid for many flames.

[5] Concentrations were measured on a weight per volume basis (parts per million; ppm).

5. Total Line Intensities as a Function of the Concentration C

The equations derived previously were developed on the assumption that essentially monochromatic spectral intensities are to be observed. The spectrophotometer used in the course of this investigation,[6] however, passed a finite wavelength band which necessitated the measurement of total line intensities I as a function of the concentration C of metallic ions introduced into the flame.

A plot of $\ln I/C$ *vs* C for various lines was found to yield two straight line sections as is predicted by the equations for spectral intensities $I_\nu(l')$. This indicates that an equation with the *form* of (18) may be used to represent the functional relationship between I and C. The coefficients of emission and absorption will represent average coefficients which refer to the line as a whole when total line intensities are measured. Although it is difficult to show theoretically that these average coefficients remain very nearly constant over appreciable ranges of concentration, it was found experimentally that this is the case. In estimating the radiant heat transfer from gaseous emitters, Penner[7] also employs an average absorption coefficient for an effective width of an entire vibration-rotation band. This simple assumption was found to yield satisfactory results for diatomic absorbers even at relatively low total pressures.

III. SPECTROCHEMICAL APPLICATIONS

1. Background Intensity $I_B\neq 0$

For brevity we will omit to write the dependence of the various functions upon the suffix ν, and we will also put $I_\nu(l')=I$. It will be understood from the context whether spectral intensities or total line intensities are under consideration.

If more than one chemical species present in the flame source radiates at the frequency ν, then it is a simple matter to generalize Eq. (18). Since the background intensity of a flame source may be different from zero,[8]

[6] The Beckman Model DU spectrophotometer, together with the No. 10300 Beckman flame excitation accessory, was used to obtain experimental data.

[7] S. S. Penner, J. Appl. Mech. **18**, 53 (1951).

[8] K. J. Laidler and K. E. Shuler, Ind. and Eng. Chem. **43**, 2758–2761 (1951).

it is necessary to write Eq. (18) in the form

$$I=2(P(l)C+P'_B(l))\cdot\exp-[\mathrm{K}(l')C+\tau_B(0,l')]\times\cosh[\mathrm{K}(l)C+\tau_B(0,l)], \quad (19)$$

where the subscript B refers to molecules characteristic of the flame which radiate energy at the frequency ν. For the various lines studied, using an oxygen-butane flame, it was found that $\tau_B(0,l)\lesssim 10^{-1}$; hence, $\cosh\tau_B(0,l)$ is very nearly unity in many instances. With this approximation Eq. (19) may be written as

$$I=(SC+I_B)(\exp-\mathrm{K}(l')C)\cosh[\mathrm{K}(l)C+\tau_B(0,l)], \quad (20)$$

where I_B is the background intensity when $C=0$ and

$$S=2P(l)\exp-\tau_B(0,l').$$

It is expedient to define a new function $F(C, I)$ such that for small values of C,

$$F(C,I)\equiv\ln\left[\frac{SC+I_B}{I}\right]=-\mathrm{K}(l')C; \quad (20a)$$

and for large values of C,

$$F(C,I)=-[\mathrm{K}(l')-\mathrm{K}(l)]C+\text{const.} \quad (20b)$$

This is the functional relation between I and C which was chosen to represent experimental data for copper and silver standard solutions in Fig. 1. The observed behavior of the function $F(C, I)$ is in complete agreement with the theory. In addition to these plots of $F(C, I)$, Fig. 1 includes a plot of

$$F(C,I)+\ln\cosh(\mathrm{K}(l)C+\tau_B(0,l))\ vs\ C,$$

which is linear over the concentration ranges in which Eqs. (20a) and (20b) are applicable.

2. Experimental Determination of the Various Constants

In order to determine S and $\mathrm{K}(l')$ in Eq. (20), two comparison standards $C_a{}^L$ and $C_b{}^L$ are chosen at low (L) concentrations such that $C_a{}^L=2C_b{}^L$. The following relations are easily obtained from Eq. (20a):

$$S=\frac{(I_b{}^2-I_BI_a)}{I_aC_b}\left[1+\frac{I_b}{(I_b{}^2-I_BI_a)^{\frac{1}{2}}}\right] \quad (21)$$

and

$$\mathrm{K}(l')=\frac{F(C_b{}^L,I_b)}{C_b{}^L}=\frac{F(C_a{}^L,I_a)}{C_a{}^L}, \quad (22)$$

where I_b and I_a are the intensities corresponding to $C_b{}^L$ and $C_a{}^L$. $\mathrm{K}(l)$ and $\tau_B(0,l)$ can then be calculated from two intensity measurements at high concentrations.

If the background intensity I_B is negligibly small then the three constants $P(l)$, $\mathrm{K}(l')$, and $\mathrm{K}(l)$ are readily evaluated by first plotting $\ln(I/C)$ *vs* C in order to determine the concentration ranges in which Eqs. (18a) and (18b) are valid and then choosing two standards for either low C or high C and carrying out the appropriate computations. These are simple calculations and will not be given here.

The data obtained for copper standards, 0–1760 ppm, were used to determine the four constants of Eq. (20) by a method of numerical approximation.[9] The computations were laborious, and since the results of these calculations gave about the same degree of accuracy as was yielded by the approximate computational method previously described in this section, it was not considered necessary to repeat the numerical calculations for the other metals investigated.

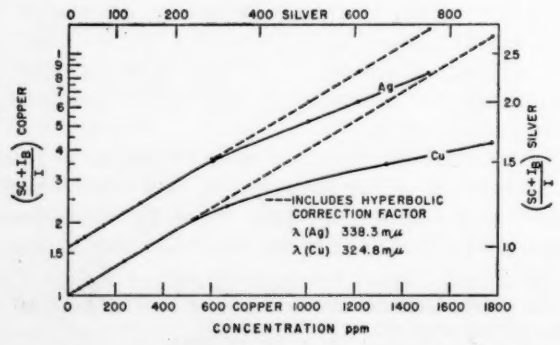

FIG. 1. A plot of $F(C, I)$ *vs* C for copper and silver standard solutions excited in an oxygen-butane flame.

3. Flame Sources for Which $l\cong l'$ and $I_B\neq 0$

Barium, when excited in either a butane-oxygen or acetylene-oxygen flame, exhibits a calibration curve for BaO−7450A with a steadily increasing slope if narrow slits are employed. This effect was also noticed by P. T. Gilbert.[10] The background intensity at 7450A is relatively intense for these flames. Our data for barium can be tentatively explained if we take $l'=l$, since these curves were nonlinear for small values of C and they were linear above 200-ppm Ba. This behavior is consistent with the model in which $l'=l$, but not for $l'>l$. It was found that cooler flames (excess oxygen) produced the maximum spectral intensity of the oxide band at 7450A which indicates that the so-called cooler barium vapors which surround the hot central portion of the flame may also contribute to the emission of radiant energy.

When $l=l'$ and $I_B\neq 0$, then Eq. (16) is of the form

$$I=(\alpha_1C+\alpha_2)(1+\alpha_3\exp-\alpha_4C). \quad (23)$$

The constants in this equation can be found from the

[9] The authors wish to thank Mr. Max Eaton and Mrs. Margaret E. Swanson, of the U. S. Naval Air Missil Test Center, Point Mugu, California, who solved these equations by a variation of the Newton-Raphson method.

[10] P. T. Gilbert, National Technical Laboratories, South Pasadena, California; private communication.

following relations:

$$I_B=\alpha_2(1+\alpha_3), \tag{24a}$$

$$(dI/dC)_{C=0}=\alpha_1(1+\alpha_3)-\alpha_2\alpha_3\alpha_4, \tag{24b}$$

and at high concentrations

$$I\rightarrow\alpha_1C+\alpha_2. \tag{24c}$$

Equation (23) may take two general forms in the neighborhood of $C=0$. When $(\alpha_2/\alpha_1)>(2/\alpha_4)$, then

$$(d^2I/dC^2)>0; \tag{25}$$

and if $(\alpha_2/\alpha_1)<(2/\alpha_4)$, then $(d^2I/dC^2)<0$. It was predicted from these inequalities that for low background intensities ($\alpha_2\rightarrow 0$) the calibration curve will be concave downward. Subsequently, this condition was realized experimentally by using an oxy-hydrogen flame in which the background intensity was negligibly small at 7450A, and a concave curve was observed. Equation (23) could be made to fit the experimental data almost exactly over a 1000-ppm range of concentrations using barium chloride standard solutions.

TABLE I. Typical values of K(l') and K(l) for various lines.

Line	K(l')	K(l)	Flame
Cu 3248 AU	1.41×10^{-2} ppm^{-1}	1.08×10^{-3} ppm^{-1}	Butane-Oxygen
Ag 3383	1.41×10^{-3}	0.993×10^{-3}	Butane-Oxygen
Ni 3524	1.36×10^{-3}	...	Butane-Oxygen
Fe 3726	7.04×10^{-4}	...	Butane-Oxygen
BaO 7450	2.86×10^{-4}	2.86×10^{-4}	Butane-Oxygen (Rich in O_2)
[a]CaO 5540	3.80×10^{-5}	$(4.7\pm1)\times10^{-5}$	Oxy-Hydrogen

[a] We wish to express our appreciation to P. T. Gilbert, South Pasadena, California, for supplying us with data on calcium solutions from 0–72,000 ppm. The Beckman burner No. 9200 was used as a flame source.

IV. NUMERICAL RESULTS

1. Flame Sources

Table I contains some typical values of K(l') and K(l) which are characteristic of the particular source and gas pressures used for a given set of measurements. In some cases clogging of the atomizer assembly prevented the measurement of intensities for solutions containing a high concentration of salt. For this reason, we were sometimes unable to calculate K(l). Gas pressures were adjusted to give maximum energy at the wavelength of interest. For this reason, flame conditions used in the study of each line were not necessarily identical. Standard solutions were prepared from reagent grade chemicals. Various desired concentrations were obtained by diluting aliquot portions of these standards in order to establish a proportionate relationship between the comparison standards. This procedure was employed in order to minimize any errors present in the relative concentrations.

In all cases, except for CaO 5540 and BaO 7450, K(l') was found to be slightly greater than K(l). This behavior is to be expected from the theory if the limits of emission and absorption are not the same (i.e., $l'>l$). For BaO 7450, K(l') = K(l) as was discussed in Sec. III (3). Intensity measurements corresponding to calcium concentrations of 11,500 ppm, 29,000 ppm, and 72,000 ppm showed K(l) to be slightly greater than K(l'). For very high salt concentrations some cooling of the flame is to be expected. This would result in larger absorption coefficients, and therefore, K(l) would be increased since it represents an integrated absorption coefficient which was necessarily calculated for relatively high concentrations of calcium.

TABLE II. Comparison between calculated and measured total line intensities.

	C	I_{exptl}	I_{calc} from Eq. (18a)
Fe 3736	414.8 ppm	22.2	21.6
	311.1	17.5	17.5
	207.4	12.5[a]	12.5
	103.7	6.7[a]	6.7
	51.9	3.5	3.5
	25.9	1.8	1.7
Ni 3524	334.3	31.1	31.5
	223.8	23.9	24.1
	172.2	19.9	19.9
	81.1	10.6[a]	10.6
	40.5	5.6[a]	5.6
	20.3	2.9	3.0
CaO 5540	4600	308.0	301.0
	1850	132.0	134.0
	740	56.1[a]	56.1
	296	22.8[a]	22.8
	118	9.1	9.1

[a] Intensities used in the calculation of $P(l)$ and K(l').

Table II gives representative data for some of the lines studied. The results for Cu 3248 and Ag 3383 are portrayed in Fig. 1. For the iron, nickel, and calcium standard solutions, only two measurements were needed to calculate $P(l)$ and K(l'), and to establish spectrochemical calibration curves over concentration ranges of about 420 ppm, 335 ppm, and 4600 ppm, respectively.

2. Spark Sources

Analytical data for the Ni 3414 I line has been obtained through the courtesy of J. H. Enns at the University of Michigan. The source parameters were 4 sparks—0.002 μf—15 μh—2.1 ohms—5 amps—15 kv, and an analytical gap of 120° cones—4-mm spacing. The background intensity at 3414A was nearly zero. The sample analyzed was a low alloy steel containing 0–5 percent Ni. Narrow slits were used so that the central portion of the line was under observation. Intensity ratios of Ni 3414 I/(2300–4000) band were obtained with standard multiplier tubes and recorded on a Leeds and Northrup recorder. There was evidence of considerable self-absorption.

$\ln I/C$ *vs* C was plotted as usual and the constants of Eq. (18) were calculated according to the methods outlined in Sec. III (2). The theoretical and experimental

TABLE III. Comparison of calculated and experimentally determined intensities for Ni 3414 I excited in a spark source.

C	I_{exptl}	$I_{calc}=45.7Ce^{-1.321C}\cdot\cosh 1.206C$
0.2 percent Ni	7.2±0.5	7.2
0.6	15.4	15.8
1.0	22.10[a]	22.10
1.5	29.9	29.4
2.0	36.8	36.3
2.5	42.7	42.5
3.0	48.2	48.0
3.5	52.7	52.7
4.0	56.77[a]	56.77
4.5	60.2	60.2
5.0	63.00[a]	63.00

[a] Intensities used in the calculation of $P(l)$, $K(l')$, and $K(l)$.

curves were in agreement within the limits of experimental error (Table III).

For these data, we obtained

$$K(l')=1.33\ (\text{percent Ni})^{-1},$$
$$K(l)=1.21\ (\text{percent Ni})^{-1},$$

when C is measured as percent nickel in the steel sample. Since $K(l')$ is very nearly equal to $K(l)$, it seems that most of the absorbing nickel atoms are actually contained in that portion of the spark where emission takes place. This is apparently in contradiction to the hypothesis that the source may consist of spatially separated emitters and absorbers.

The excitation processes which take place in a spark discharge are of an extremely complex nature. The emission and absorption coefficients which enter into the equations are to be considered as time averaged since the discharge is not a steady-state phenomena. In addition, the entire spark column was observed in obtaining data on the Ni 3414 I line. Because of these factors and the scarcity of data available to us for sources of this type, we refrain from drawing further conclusions concerning spark excitation at this time other than to note that Eq. (18) could be made to fit the data in this particular instance.

ACKNOWLEDGMENTS

The authors are grateful to Dr. Herbert McKennis, Head of the Basic Sciences Research Department, and Dr. F. E. Lowance, Technical Director, both of the U. S. Naval Civil Engineering Research and Evaluation Laboratory, who encouraged this work and offered many valuable suggestions.

THE JOURNAL OF CHEMICAL PHYSICS VOLUME 20, NUMBER 12 DECEMBER, 1952

The Infrared Spectrum of Chlorine Dioxide*

ALVIN H. NIELSEN† AND P. J. H. WOLTZ
K-25 Laboratories, Carbide and Carbon Chemicals Company, Oak Ridge, Tennessee and the University of Tennessee, Knoxville, Tennessee

(Received August 17, 1951)

The infrared spectrum of ClO_2 has been reinvestigated from 2–40μ. Several new bands have been discovered, among them the bending frequency ν_2 at 445 cm^{-1}. This band has the doublet character required if the molecular model is to be an obtuse triangle in accord with electron diffraction experiments. Three bands, ν_1, ν_2, and $2\nu_1$, were resolved with prism and grating methods, and the spacing of the Q lines was found to be about 3.0 cm^{-1}. An $A''-B''$ value of 1.413 cm^{-1} was obtained from the analysis of ν_2, and this value also is in excellent agreement with the electron diffraction measurements. Moments of inertia computed from the r (Cl—O)=1.49A and 2α (apex angle)=118.5° obtained from a combination of electron diffraction and infrared data are $I_A=16.09\times10^{-40}$ g cm^2, $I_B=86.34\times10^{-40}$ g cm^2, and $I_C=102.43\times10^{-40}$ g cm^2. A band which cannot be ascribed to an impurity was found at 290 cm^{-1}. The possibility that this band results from polymerization of ClO_2 is suggested.

INTRODUCTION

A NUMBER of investigations of the spectrum of ClO_2 have been made previously.[1] The earliest were some electronic band spectra taken by Goodeve and Stein,[2] Finkelnburg and Schumacher,[3] and Urey and Johnston.[4] The infrared spectrum was first observed by Bailey and Cassie,[5] who discovered absorption bands at 954, 1105, 1884, and 2034 cm^{-1}. The first two bands were, respectively, a doublet type and a Q branch type

* This document is based on work performed for the AEC by Carbide and Carbon Chemicals Company at Oak Ridge, Tennessee.

† Fulbright Research Scholar, Institut d'Astrophysique, University of Liège, Belgium, 1951–1952.

[1] Preliminary reports of the contents of this paper were made by P. J. H. Woltz and A. H. Nielsen at the Ohio State Symposium on Molecular Structure, June, 1951, and in the Phys. Rev. **83**, 485A (1951). In this issue will also be found a discussion of the vibration potential function of the ClO_2 molecule by J. Duchesne and A. H. Nielsen, J. Chem. Phys. **20**, 1968(L) (1952).

[2] C. F. Goodeve and C. P. Stein, Trans. Faraday Soc. **25**, 738 (1929).

[3] W. Finkelnburg and H. J. Schumacher, Z. physik. Chem. Bodenstein Festband, 704 (1931).

[4] H. Urey and H. Johnston, Phys. Rev. **38**, 2131 (1931).

[5] C. P. Bailey and A. B. D. Cassie, Proc. Roy. Soc. (London) **A137**, 622 (1932).

and were assigned as fundamental vibrations. The fundamentals as obtained by Urey and Johnston from electronic bands did not agree with these measurements. Z. W. Ku[6] observed the electronic band spectrum and also the infrared spectrum in the 4–11μ region. She verified Bailey and Cassie's observations and in addition predicted the third fundamental at 529 cm^{-1}. Her prediction that this band should have a Q branch and, thus, that the molecular model was an acute triangle was contradicted by the electron diffraction measurements of Pauling and Brockway,[7] who gave the (Cl—O) distance as 1.53±0.02A and the apex angle 2α as 137°±15°. Wu[8] suggested that the third fundamental should be a doublet type band to conform with the electron diffraction measurements. The only Raman work discovered in the literature concerns a line at 935±8 cm^{-1}, observed for ClO_2 in solution by Kujumzelis,[9] which confirms the infrared band observed by Bailey and Cassie and identifies it as the totally symmetric vibration ν_1. More recently Coon[10] has reported new observations of the electronic band spectrum in absorption. From this work he has given the fundamental frequencies in the ground state $\nu_1=945$, $\nu_2=447$, and $\nu_3=1109$ cm^{-1}. Also, from an analysis of the rotational structure of the bands together with the r(Cl—O) distance given by Pauling and Brockway[7] he determined the bond angle 2α as 109°±3°. This value is considerably smaller than the electron diffraction value given by Pauling and Brockway. Very recently, Coon and Ortiz[11] reported a new investigation of the electronic band spectrum. By using all previously available data they have computed the harmonic frequencies and anharmonic constants for the ground electronic state and the upper electronic state. The harmonic frequencies and anharmonic constants for the ground electronic state listed in their abstract are $\omega_2''=451.8$, $\omega_1''=964.8$, $\omega_3''=1127.3$, $x_{11}''=-4.0$, $x_{22}''=-0.8$, $x_{33}''=-4.6$, $x_{12}''=-2.2$, $x_{13}''=-21.0$, and $x_{23}''=-3.1$ cm^{-1}. The most recent infrared spectroscopic work on ClO_2 was a letter to the editor by Hedberg[12] listing the same infrared bands observed by the previous investigators[5,6] plus two new ones. A reference to new electron diffraction measurements by Dunitz and Hedberg[13] was also found. They give the apex angle 2α as 116.5°±2.5° and the (Cl—O) distance as 1.49_1 $\pm 0.01_4$A.

The investigation reported herein was undertaken during the past eighteen months in an effort to remeasure the infrared spectrum and, thus, to discover the location and band shape of the bending vibration of ClO_2 and to throw some light on the moments of inertia of the molecule.

EXPERIMENTAL DETAILS AND RESULTS

Chlorine dioxide samples for this investigation were prepared by W. B. Kenna and A. V. Faloon. Extreme caution is urged in its handling as one sample being prepared for a Raman experiment detonated at about −50°C resulting in the injury of Mr. Kenna. Quantities sufficiently large for Raman experiments were not again attempted.

The present paper concerns only measurements on gaseous ClO_2 in the infrared region from 2–40μ. Measurements were made on Perkin-Elmer spectrographs Model 12C and 21 equipped with NaCl, LiF, KBr, and KRS-5 prisms. Grating measurements were carried out on the University of Tennessee grating spectrograph utilizing a 3600 lines-per-inch replica grating.

The ClO_2 was contained at various pressures in fluorothene cells and a modified Perkin-Elmer meter cell fitted with suitable windows. Pressures ranged from 0.25 in. of mercury in a 10-cm long cell to 20 in. of mercury in the 1-meter long cell.

Figure 1 shows the complete infrared spectrum from 2–40μ observed prismatically. Bands were found with centers at 290, 445,‡ 943.2, 1110, 1888, 2040, 2215, 2473, 2967, and 3325 cm^{-1}.

It may be seen that an intense band is located at 445 cm^{-1} which is in good agreement with the frequency given by Coon[10,11] for the bending vibration. It may be further noted that this band exhibits doublet character and that rotation lines with a $\Delta\nu=3.5$ cm^{-1} are resolved in the R-side of the band. This is the proper band structure in order that the model be obtuse as predicted by electron diffraction experiments. It will also be observed that the three bands, ν_2 at 445 cm^{-1}, ν_1 at 943.2 cm^{-1}, and $2\nu_1$ at 1888 cm^{-1} all resolve into rotational structure with approximately the same spacing. A rotational analysis of the grating measurements on ν_1 at 943.2 cm^{-1}, shown in Fig. 2, was performed to obtain the band center and the $A''-B''$ value. The fundamental ν_3, shown in Fig. 3, was also examined with the grating, but no rotational structure could be discerned. An additional peak at 1099 cm^{-1} was, however, observed which is very likely the Q branch of ν_3 for $Cl^{37}O_2$. Such a displacement is very reasonable, and the band should, of course, occur with some intensity.§

The present investigation disclosed four new bands in the infrared which had not previously been reported at 290, 445, 2215, and 2473 cm^{-1}. With the exception of the

[6] Z. W. Ku, Phys. Rev. **44**, 376 (1933).
[7] L. Pauling and L. O. Brockway, J. Am. Chem. Soc. **57**, 2684 (1935).
[8] T. Y. Wu, *Vibrational Spectra and Structure of Polyatomic Molecules* (J. W. Edwards, Publisher, Ann Arbor, Michigan, 1946), p. 170.
[9] T. Kujumzelis, Physik Z. **39**, 665 (1938).
[10] J. B. Coon, Phys. Rev. **58**, 926 (1940); J. B. Coon, J. Chem. Phys. **11**, 665 (1946).
[11] J. B. Coon and E. Ortiz, Phys. Rev. **82**, 766(A) (1951).
[12] K. Hedberg, J. Chem. Phys. **19**, 509 (1951).
[13] J. D. Dunitz and K. Hedberg, J. Am. Chem. Soc. **72**, 3108 (1950).

‡ The band at 445 cm^{-1} was first observed in this laboratory by E. A. Jones and T. G. Burke in some preliminary studies.

§ In connection with the force constant calculations reported by Duchesne and Nielsen in reference 1, the isotopic shifts have been computed. For ν_3 the shift is 12 cm^{-1} in excellent agreement with the observed shift of 11.5 cm^{-1}. The shifts (unobserved) for ν_1 and ν_2 have been computed, respectively, as 2.3 and 4.8 cm^{-1}.

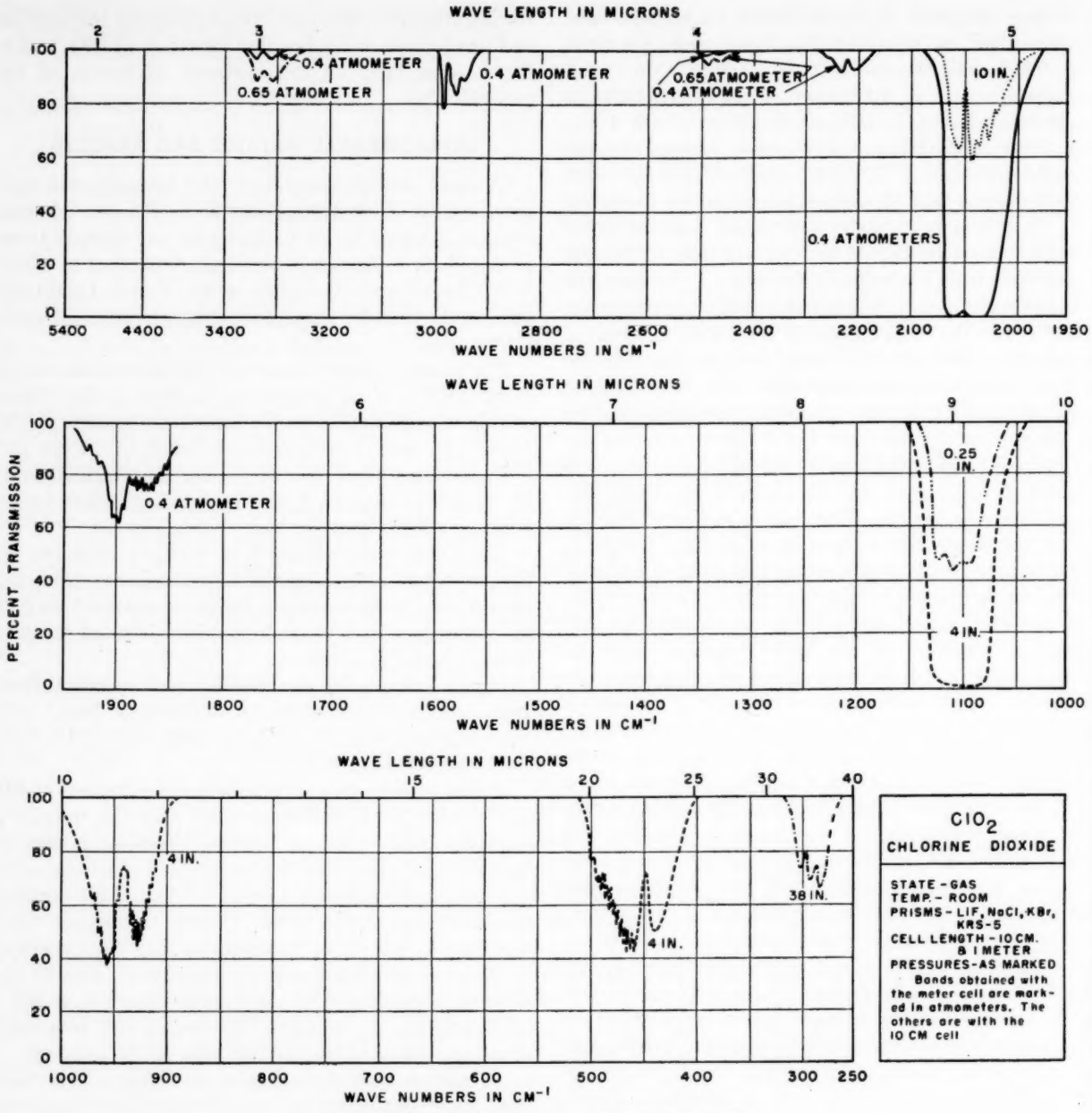

FIG. 1. Infrared prism spectrum of ClO_2 from 2–40μ.

one at 290 cm^{-1} they could be interpreted in terms of the three fundamentals as is shown in Table I.

Though the band at 290 cm^{-1} is less than half as intense as ν_2, the weakest of the fundamentals, it does appear to have a fairly large absorption coefficient at low pressures. As it appears to be impossible to fit this band into the ClO_2 system as an overtone, or as a sum or difference band, several other possibilities may be considered. The most obvious way to attempt to explain this band would be to ascribe it to an impurity in the sample. This way can immediately be eliminated for several reasons. The band appeared with about the same intensity in all the gas samples prepared. If it were an impurity, its intensity would imply that it either was

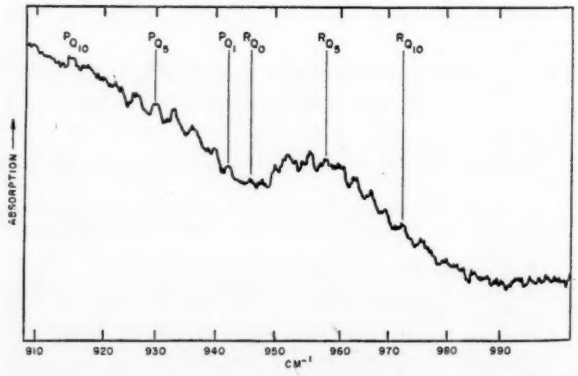

FIG. 2. Record of ν_1 obtained with a 3600 lines-per-inch grating.

TABLE I. Observed bands and assignments for ClO_2 (frequencies in cm^{-1}).

Assignments	Present work: Obs. ir freq.	Present work: Freq. calc. from const. of Coon and Ortiz[c]	Present work: Δ O−C	Freq. obs. by Ku[d] (ir and elect.)	Freq. obs. by Bailey and Cassie[e] ir	Freq. obs. by Hedberg[f] ir	Average of cols. 2, 5, 6, and 7	Δ col. 8−col. 3	Freq. calc. from present x_{ij} and ω_i	Δ col. 8−col. 10
Polymer	290									
ν_2	445	447.5	−2.5	529 calc.	···	···	445	−2.5	445	0.0
ν_1	943.2[b]	945.2	−2.0	954	954	945	943.2[b]	−2.0	943.2	0.0
ν_3	1110.5[b]	1106.1	+4.4	1106	1105	1108	1110.5[b]	+4.4	1110.5	0.0
$2\nu_1$	1888	1882.4	+5.6	1884	1884	1870	1882	−0.2	1882	0.0
$\nu_1+\nu_3$	2040	2030.2	+9.8	2034	2034	2031	2035	+4.8	2035	0.0
$2\nu_3$	2215	2203	+12.0	···	···	···	2215	+12.0	2215	0.0
$\nu_1+\nu_2+\nu_3$[a]	2473	2472.6	+0.4	···	···	···	2473	+0.4	2473	0.0
$2\nu_1+\nu_3$	2967	2946.4	+20.6	···	···	2954	2960	+13.6	2955.1	+4.9
$3\nu_3$[a]	3325	3280.5	+44.5	···	···	3333	3329	+48.5	3313.5	+15.5

[a] From the original records it is difficult to be certain of the envelope of these very weak bands. The interpretation given here demands that they be type *A* bands, whereas from Fig. 1 it would appear that they are type *B*. However, if the central branch of a type *A* band folds over into the low frequency side of the band, it may actually have the appearance of a doublet with the dispersion available here. It is, therefore, believed that they are actually type *A* because no other very reasonable combinations can be made to fit these observed frequencies.
[b] Grating measurements.
[c] Reference 11.
[d] Reference 6.
[e] Reference 5.
[f] Reference 12.

an intense absorber or was present in fairly high concentration. As no other impurity bands were found elsewhere in the spectrum the above explanation seems unlikely.

Many records over this region were made with various cells and pressures in an effort to obtain as reliable an envelope of the absorption as possible. The best effort is shown in Fig. 4 in which absorption maxima may be seen at 280, 290, 302, and 326 cm^{-1}. This record was obtained using a 10-cm cell closed with very thin polyethylene windows. The gas was mixed with dry air and admitted to the cell at atmospheric pressure because the cell could not be evacuated. The partial pressure of ClO_2 in the cell was, therefore, unknown. If it were supposed that the three strongest maxima formed three branches of a single band, the $P-R$ distance of 22 cm^{-1} is much too small for ClO_2, as ν_3 has a spacing of 30 cm^{-1}. The narrowness of the band is suggestive of a heavier molecule.

A possibility for interpreting the band at 290 cm^{-1} would then be to suppose that dimerization and perhaps higher polymerization takes place in ClO_2. Some evidence pointing to this possibility is found in Fig. 5, in which a series of plots of this region have been made showing percent absorption plotted *versus* waves/cm for pressures ranging between 2 inches and 38 inches of mercury. It may be seen that at 2 inches pressure the maximum at 290 cm^{-1} is the most intense and indeed there is no maximum at 280 cm^{-1}. At 5 inches pressure, the maximum at 280 cm^{-1} is almost as intense as the one at 290 cm^{-1}. As the pressure is increased, the maximum at 280 cm^{-1} overtakes and passes in intensity the 290 cm^{-1} peak. A further study of this absorption region to determine accurately how the intensity varies with pressure would, of course, be necessary in order to give support to the above suggestion.

In Table I the frequencies given by several investigators have been listed for comparison. It may be seen that differences exist between the frequencies given by Ku,[6] Bailey and Cassie,[5] Hedberg,[12] and the present authors. The differences are, however, in no case larger than 1.0 percent. As so many different values were available it was considered worth while to list in column 8 the average values as the best present values. By using

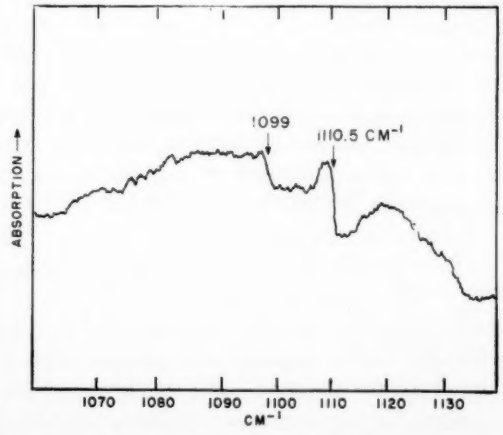

FIG. 3. Record of ν_3 obtained with a 3600 lines-per-inch grating.

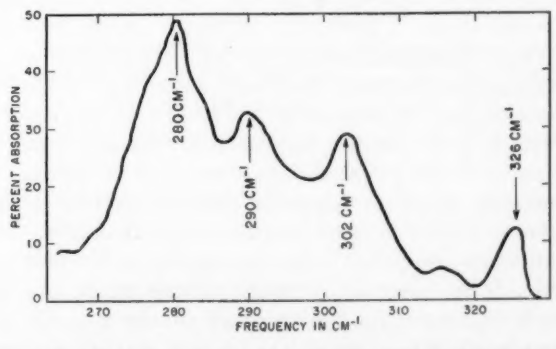

FIG. 4. Detailed plot of the absorption at 290 cm^{-1} showing the best resolution obtained.

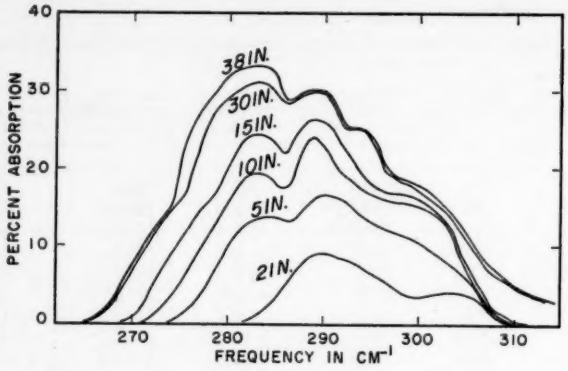

FIG. 5. Plot of the absorption in the region of 290 cm^{-1} showing the variation in envelope with pressure.

all the available electronic and previously available infrared data and by estimating x_{33} and x_{23}, Coon and Ortiz[11] calculated the harmonic frequencies ω_1, ω_2, and ω_3 along with the anharmonic constants x_{11}, x_{22}, x_{12}, and x_{13}. These values were used to compute the band centers of the observed infrared bands with the agreement shown in columns 4 and 9. For ν_1, ν_2, ν_3, $2\nu_1$, and $\nu_1+\nu_2+\nu_3$ the agreement is fairly satisfactory, but for $\nu_1+\nu_3$, $2\nu_3$, $2\nu_1+\nu_3$, and $3\nu_3$ the agreement is poor. For $2\nu_1+\nu_3$ and $3\nu_3$ it is indeed considerably worse than the dispersion between individual experimental values of the frequencies. It should be pointed out that the anharmonic constants are quite sensitive to inaccuracies in the observed frequencies, and if the x_{ij}s are not very well determined, their effect upon the calculated frequencies in general becomes greater with the higher order overtones and combination bands. The good agreement in the case of $\nu_1+\nu_2+\nu_3$ is, therefore, perhaps fortuitous. With the present number of observed infrared bands it is possible to compute $x_{11}^0=-2.2$, $x_{33}^0=-3.0$, $x_{13}^0=-18.7$, $x_{12}^0+x_{23}^0=-7.0$, $\omega_1^0=945.4$, $\omega_3^0=1113.5$ cm^{-1}. Though these x_{ij} values are of the same order as those given by Coon and Ortiz, they differ individually by amounts nearly as large as 100 percent. If, however, the above x_{ij}s are combined with $x_{12}^0=-2.2$ cm^{-1} and $x_{22}^0=-0.8$ cm^{-1} given by Coon and Ortiz, it is possible to compute the harmonic frequencies $\omega_1=958.1$ cm^{-1}, $\omega_2=449.3$ cm^{-1}, and $\omega_3=1128.3$ cm^{-1}. These frequencies do not differ from $\omega_1=964.8$ cm^{-1}, $\omega_2=451.8$ cm^{-1}, and $\omega_3=1127.3$ cm^{-1}, given by them, by more than 0.5 percent. The agreement of the calculated overtone and combination frequency positions with the average frequencies given in column 8, Table I is, of course, considerably better, as may be seen from columns 10 and 11. As most of the infrared data were used to obtain the constants, only $2\nu_1+\nu_3$ and $3\nu_3$ could be used for checks. Even so, these two agree much better with observations than when computed from the constants of Coon and Ortiz. It is, however, perhaps premature to put too much reliance upon the accuracy of the x_{ij}s. On the other hand, the ω_is appear to be quite well determined, because in spite of the discrepancies between the two sets of x_{ij}s the values of the ω_is do not differ very much. The accuracy of the x_{ij}s will doubtlessly be greatly improved when a larger number of infrared band centers have been determined by grating measurements, thus making it possible to derive all the constants from infrared data alone.

ROTATIONAL STRUCTURE

It was pointed out in the previous section that the rotational structure of ν_1, $2\nu_1$, and ν_2 was resolved making it possible to learn something about the moments of inertia and dimensions of the molecule. It was not possible with available gratings to record ν_2 in this manner, and thus only the R branch was resolved prismatically, giving an average spacing of 3.46 cm^{-1}. This is probably too large because the unresolved lines in the P branch were not included. $2\nu_1$ was resolved with the LiF prism and gave a spacing of 3.0 cm^{-1} average. However, ν_1 was resolved as shown in Fig. 2 with a 3600 lines-per-inch grating and exhibits an average spacing of 3.01 cm^{-1}. The positions of the Q lines were fairly well determined and a rotational analysis along conventional lines was carried out. ν_3 was also examined with the 3600 lines-per-inch grating, but no fine structure was observed. The band does, however, have a nicely defined Q branch, which makes the choice of band center fairly reliable. A second, but weaker absorption maximum at 1099 cm^{-1} is thought to be the ν_3 for $Cl^{37}O_2$.

Because ν_1, $2\nu_1$, and ν_2 exhibit rather well-resolved Q lines and ν_3 has a fairly sharp Q branch, it was reasonable to assume that ClO_2 was accidentally not far from a symmetric top. As the totally symmetric vibrations ν_1 and ν_2 have type B envelopes and the antisymmetric vibration ν_3 is of type A, the least axis of inertia I_A is perpendicular to the C_2 symmetry axis. The two nearly equal moments of inertia I_B and I_C then lie, respectively, parallel with the C_2 axis and perpendicular to the plane of the molecule.

A rotational analysis of the quite well-resolved Q lines of ν_1 (Fig. 2) was performed in order to obtain the quantity $(A''-B'')$, where $A''=h/8\pi^2 I_A''c$ and $B''=h/8\pi^2 I_B''c$. Two methods may be followed to determine these constants. In the first method the differences $({}^RQ_{K-1}-{}^PQ_{K+1})$ were plotted *versus* $4K$. A straight line results, the slope of which is $(A''-B'')$. In this treatment the centrifugal expansion term, which is very small, is neglected. A similar plot gives $(A'-B')=1.413$ cm^{-1}. The constants B'' and B', as used here, are the averages $(B''+C'')/2$ and $(B'+C')/2$.

In the second method the quantities $({}^RQ_{K-1}-{}^PQ_{K+1})/4K$ are plotted *versus* K^2. Such a plot gives a straight line of slope $-2D_K$ and intercept $(A''-B'')$ if additive terms involving D_{JK} and D_K are neglected in comparison with $(A''-B'')$. Actually, the present data give a fairly large scatter of points, and, as there are not very many points, the line is not very reliably located. However, it is the slope rather than the intercept, which is

most unreliable because the intercept is not very sensitive to fairly large changes of slope. One can, therefore, obtain virtually equivalent values of $A''-B''$ by either method of plotting the data. An estimate of $D_K=4\times10^{-5}$ cm^{-1} may be had from the slope of the best line through the points, while the $(A''-B'')$ intercept for this line is 1.425 cm^{-1}. The maximum value of $(A''-B'')$ would probably not be greater than 1.431 cm^{-1}, which is 1.3 percent larger than the value obtained from the first method.

Because it is difficult to decide just where the band center of ν_1 is from either the prism curve or grating curve, two alternate assignments are given in Table II. From choice 1 the band center is 943.2 cm^{-1} and from choice 2, it is 940.4 cm^{-1}. Choice 1 is favored because the scatter of the points in the $A''-B''$ plot is smaller than in choice 2. The difference $A''-B''$ is about the same in either choice.

TABLE II. Rotational lines and assignments in ν_1.

Assignment Choice 1	Assignment Choice 2	Frequency cm^{-1}	Assignment Choice 1	Assignment Choice 2	Frequency cm^{-1}
$^PQ_{12}$	$^PQ_{11}$	910.0	$^PQ_1$	$^RQ_0$	941.4
$^PQ_{11}$	$^PQ_{10}$	912.5	$^RQ_0$	$^RQ_1$	945.0
$^PQ_{10}$	$^PQ_9$	915.0	$^RQ_1$	$^RQ_2$	946.9
$^PQ_9$	$^PQ_8$	917.9	$^RQ_2$	$^RQ_3$	949.5
$^PQ_8$	$^PQ_7$	920.7	$^RQ_3$	$^RQ_4$	951.7
$^PQ_7$	$^PQ_6$	923.7	$^RQ_4$	$^RQ_5$	955.6
$^PQ_6$	$^PQ_5$	926.4	$^RQ_5$	$^RQ_6$	958.0
$^PQ_5$	$^PQ_4$	929.7	$^RQ_6$	$^RQ_7$	960.4
$^PQ_4$	$^PQ_3$	932.7	$^RQ_7$	$^RQ_8$	963.3
$^PQ_3$	$^PQ_2$	936.4	$^RQ_8$	$^RQ_9$	966.2
$^PQ_2$	$^PQ_1$	939.4	$^RQ_9$	$^RQ_{10}$	968.8

By utilizing the value $A''-B''=1.413$ cm^{-1} in a relation for r(Cl—O) as a function of α, the apex half-angle obtained from the geometry of the model, the graph shown in Fig. 6 was obtained. It is, of course, not possible to determine uniquely the r(Cl—O) and 2α from the infrared data alone, and any pair of values of r and 2α from the graph would be satisfactory. However, the recent electron diffraction measurements of r(Cl—O) and 2α given by Dunitz and Hedberg[13] should constitute a point of this graph if the results are to be consistent. A rectangle to represent the uncertainty in r and 2α quoted by them has been drawn into the figure, and it does indeed intersect the curve of r(Cl—O) *vs* α. Thus, within the experimental errors of both measurements, the internuclear distance r(Cl—O) and the apex angle can be made to agree. The values are taken from the

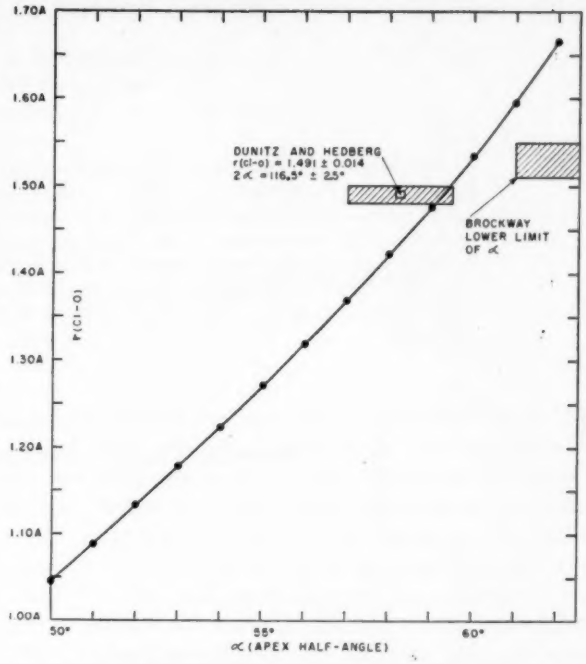

FIG. 6. Graph of r(Cl—O) *vs* α using $A''-B''=1.413$ cm^{-1}.

intersection of the curve with the rectangle of uncertainty and are r(Cl—O)=1.49A and $2\alpha=118.5°$.‖ According to Dunitz and Hedberg the values given for r and 2α by Pauling and Brockway are unreliable, and it may be seen that the lower limit values do not intersect the curve. The moments of inertia calculated from the r(Cl—O) and 2α taken from Fig. 6 are $I_A=16.09\times10^{-40}$ g cm^2, $I_B=86.34\times10^{-40}$ g cm^2, and $I_C=102.43\times10^{-40}$ g cm^2.

ACKNOWLEDGMENTS

The authors wish to express their gratitude to A. V. Faloon and W. B. Kenna for preparing the pure samples of ClO_2 for this work. Thanks are also due Dr. D. F. Smith and Mr. T. G. Burke of K-25 Laboratories for discussions throughout the work. Finally, one of the authors (AHN) acknowledges the support of the Frederick Gardner Cottrell Fund of the Research Corporation of New York for a grant which materially aided in completing the grating spectrograph used in some of this work.

‖ If the maximum value of $(A''-B'')=1.431$ cm^{-1} were used in the r (Cl—O) *versus* α relation instead of $(A''-B'')=1.413$ cm^{-1}, the value of 2α for r (Cl—O)=1.49A would be increased by 18 minutes of arc from 118.5° to 118.8°, which is an insignificant amount.

Infrared Spectra of H_2O and CO_2 at 500°C*

J. H. TAYLOR,† W. S. BENEDICT, AND J. STRONG
The Johns Hopkins University, Baltimore, Maryland

(Received July 7, 1952)

A porcelain-lined absorption cell of the Pfund type is described, in which 3 meters of gas may be heated to temperatures above 500°C. The spectra of air at atmospheric pressure containing varying amounts of H_2O and CO_2 have been obtained in this cell between 2.4–15μ with a prism spectrometer, and between 13–25μ with a grating spectrometer giving spectral resolution of about 2 cm^{-1}. A number of new lines in the pure rotation spectrum and the ν_2 vibration of H_2O, originating from levels of high energy, have been observed and classified. New CO_2 bands in the regions of 11–20μ and 5μ have also been observed, originating from levels as high as $5\nu_2$, and leading to improved values of higher-quanta levels of ν_2 and vibrational constants for this molecule.

IN order to obtain information concerning the higher energy levels of gaseous molecules, and infrared spectra in the vapor state of molecules that are condensed at room temperature, we have constructed an absorption cell in which an optical path of three meters length may be maintained at temperatures up to 500°C. A preliminary note on this work has been published,[1] and a more detailed presentation of the results has been issued as a report to the Office of Naval Research.[2] It is the purpose of the present paper to describe the absorption cell, and to present some of the results on the H_2O and CO_2 molecules in the region 4–25μ, as observed with spectrometers of moderate resolving power. These are, it is believed, sufficient to demonstrate the usefulness of the equipment in the analysis of the rotation-vibration spectra of those molecules, especially for the high energy levels of particular importance in the spectra of flames and combustion products. The ability to study gases as a function of temperature with long paths, avoids many complexities which are inherent in flame spectra.

These studies, especially if combined with really high resolving power, as is planned, should add to the detail of our knowledge of molecular structure.

DETAILS OF CONSTRUCTION OF HIGH TEMPERATURE ABSORPTION CELL

The cell (with a controlled optical path of about three meters) is of the Pfund type. In purpose and some details of construction this cell follows a cell described earlier.[3] A drawing of it appears in Fig. 1. The absorbing gas container consists of a steel tube of $\frac{3}{8}$-in. thickness, 12-in. inside diameter and $43\frac{3}{8}$-in. over-all length, flange to flange. It was lined on the inside with black porcelain enamel.‡ This liner restricts the interaction of gases with its inner walls and permits a thorough cleaning from time to time. The heavy black lines in Fig. 1 indicate the parts of the cell that are covered with porcelain.

The end plates of the cell are demountable, each being held in place by 24 stainless steel bolts placed 15 degrees apart. One insert in Fig. 1 shows the method provided for sealing the end plates with a fuse wire or copper gasket (this was not used in the studies on H_2O and CO_2). The other insert shows the water-cooled nozzle to which a rock salt or other infrared transparent window can be attached. Thus, the temperature of the window can be controlled independent of that of the rest of the absorption cell. The mountings for the two mirrors are depicted by Fig. 2. Once the mirrors are adjusted, there is no difficulty with optical alignment on heating and cooling the cell.

Elevated temperatures are attained by means of 36 strip heaters (Chromalox, 500 w, 110 v) attached symmetrically around the outside of the cell. These appear in Fig. 3. These heaters are arranged in three separate banks, those in each bank being connected in parallel. In addition, circular heaters (Chromalox, 450 w, 110 v) are mounted on the outside of each end plate. This arrangement of heaters permits easy control of temperature as well as elimination of temperature gradients throughout the cell. Nine thermocouples on the outside of the cell (chromel-alumel No. 14 wire), three on top, three on the bottom and three on one side of the cell, provide for monitoring of the temperature.

Figure 4 shows the cell surrounded by its insulation, four inches of magnesia blocks. Outside of the magnesia blocks a layer of $\frac{1}{2}$-in. transite serves both as additional insulation, and to hold the magnesia blocks in place. There is an air space of one to two inches between the outside of the cell and the magnesia blocks.

The small exit and entrance apertures ($\frac{3}{16}$-in. wide, 1-in. long) make it possible to heat more than 90 percent of the optical path of the tested gas uniformly to any temperature up to about 700°C. With the present

* This work was done under contract with the ONR Contract N-onr 248-01. Part of this work was done for a thesis presented by J. H. Taylor in partial fulfillment of the requirements for the Degree of Doctor of Philosophy at Johns Hopkins University.

† Now with the E. I. duPont de Nemours and Company, Inc., Wilmington, Delaware.

[1] Taylor, Benedict, and Strong, J. Chem. Phys. **20**, 528 (1952).

[2] Taylor, Benedict, and Strong, "Infrared Spectra of H_2O and CO_2 at 500°C," ONR Johns Hopkins University Report (March 1, 1952).

[3] J. Strong, Rev. Sci. Instr. **3**, 810 (1932).

‡ The cell was lined with porcelain by J. M. Seasholtz and Sons, Inc., Porcelain Enameled Metal Products, Reading, Pennsylvania.

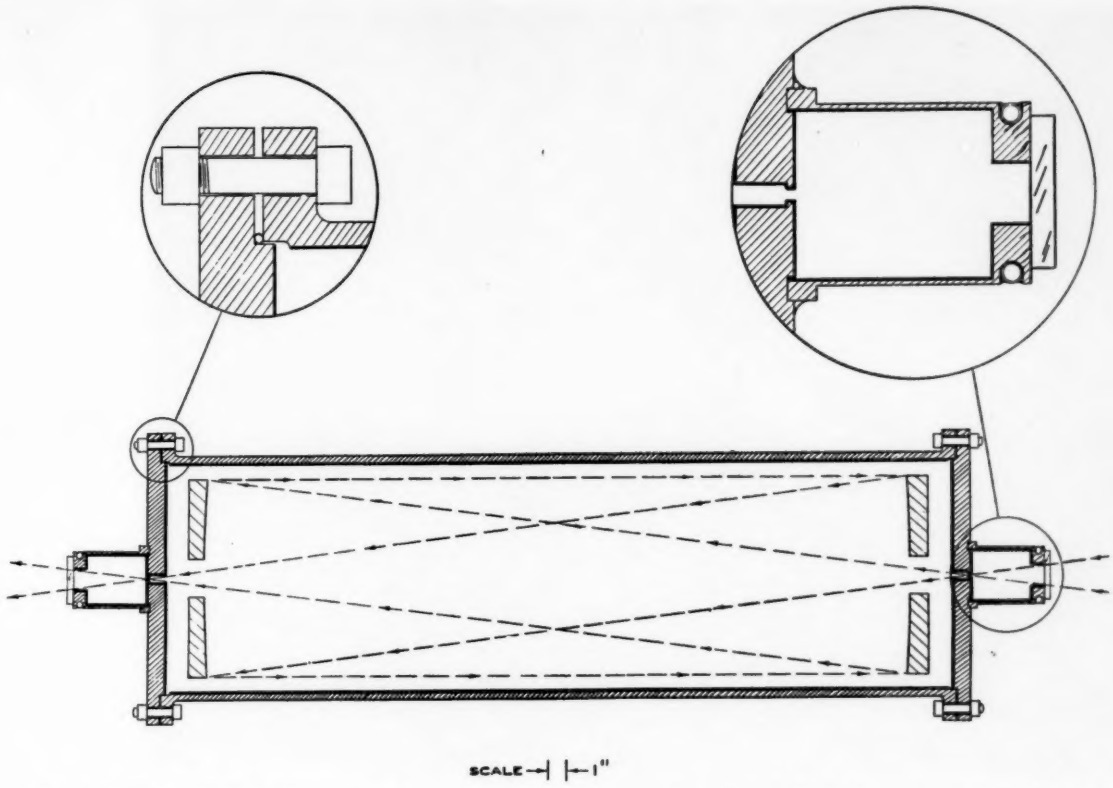

FIG. 1. Drawing of high temperature absorption cell. The heavy black lines indicate the parts of the cell that are covered with porcelain. Upper left insert shows the method provided for sealing the end plate with a fuse wire or copper gasket. Upper right insert shows the water-cooled nozzle to which a rock salt or other infrared transparent window can be attached.

arrangement of heaters, the limiting temperature is determined by the melting point of the porcelain liner in the cell, which is about 750°C. The absorbing gas, which lies in the short optical path (about eight inches) between these small apertures and the entrance and exit windows, varies in temperature from the cell temperature to the window temperature.

The specifications for the two mirrors inside such a high temperature cell are obviously severe.§ Soft glass or Pyrex would melt at these temperatures. Although solid metal mirrors might be employed, the two in the cell are of fused quartz, $10\frac{1}{2}$ in. in diameter, and 1-in. thick with a focal length of $41\frac{11}{16}$ in. Each mirror has a two-inch central hole which gives an axial "obscuration" of about 3.6 percent. Since aluminum melts around 660°C, it cannot be used for the reflecting surface. Because of its high melting point and chemical inertness, a platinum reflecting film was tried. The platinum was obtained from the Hanovia Chemical Company in the form of "Platinum Bright," a solution of organic platinum in volatile oils and other solvents. It contains certain base metal-organic compounds which serve as fluxes to fix the metal firmly on the fused quartz. This compound was applied to the surfaces of the mirrors by means of a camel's-hair brush. Then the mirror was fired at a temperature of about 650°C. The volatile oils are all

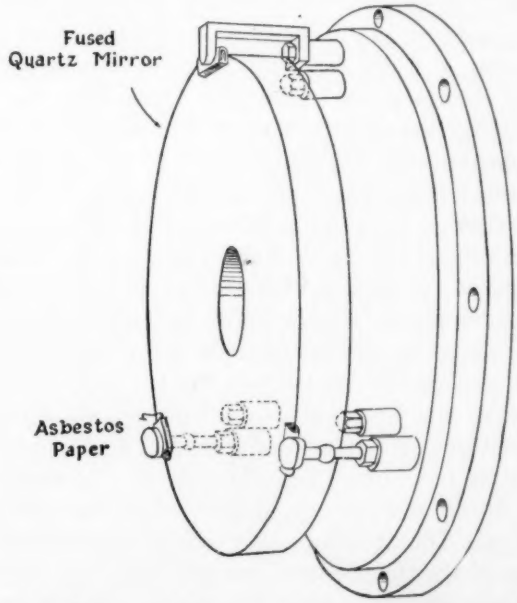

FIG. 2. Method used to mount the fused quartz mirrors to the end plates. Three stainless steel spacers separate the backs of the mirrors from the end plates.

§ Electrolytic stainless steel, nickel-plated copper, gold-plated copper, aluminum on fused quartz, zirconium and tantalum were tried—none of these combinations would stand up at these high temperatures.

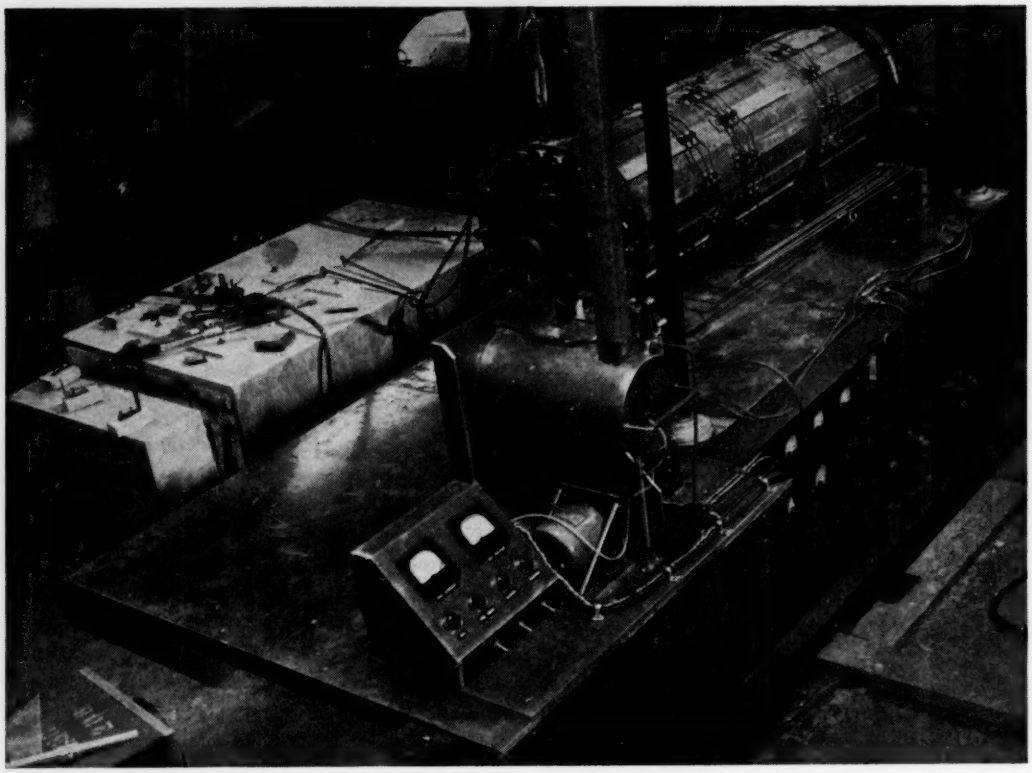

FIG. 3. High temperature absorption cell showing the arrangement of electrical strip heaters.

evaporated and the platinum is reduced at this temperature so that it becomes deposited as a reflecting film. Experience indicated that the best films were obtained when the mirror was fired in a highly oxidizing atmosphere. This was achieved by passing a small stream of air over its surface as the firing furnace was gradually brought up to about 650°C. The reflecting films obtained in this manner were excellent. A life test of one of these surfaces was made in an oven maintained continuously at 600°C for three weeks and resulted in no visual change in the appearance of the film, and the reflectivity throughout the rock salt region was later found to be greater than 90 percent. At this writing, the platinized fused quartz mirrors have been in use for more than six months, and but very little change in the reflectivity in the region under study can be detected.

Figure 2 shows the method used to mount the mirrors to the end plates. Three stainless steel spacers separate the backs of the mirrors from the end plates. By filing these spacers, the mirrors can be delicately and permanently aligned one at a time. Then the cell is bolted closed. Once the cell is closed there are no provisions for adjusting the mirrors from the outside. The weight of each mirror is supported from below by two stainless steel rods. The mirrors are kept from tipping forward by means of the stainless steel rod at the top. In order to maintain pressure against the mirror, asbestos paper was wedged between the front surface of the mirror and the lips of these three supporting rods.

THE SOURCE

The source of continuous infrared radiation was the positive crater of a low intensity water-cooled carbon arc, operated on direct current. For many applications this arc is the best possible source of infrared for absorption spectroscopy. There is no difficulty with instability, and the increase in scattered radiation attendant with its great "brightness" can be controlled by a plastic chopper and suitable filters (such as MgO reflectors).

Figures 3 and 4 show the carbon arc in its water-cooled housing.[4] An exhaust fan removes the fumes by means of the vertical pipe coming out of this water-cooled housing.

In addition to monitoring the current through the arc and the voltage across the arc with meters, a very small hole in the water-cooled housing is placed immediately below the ends of the two carbons. This hole serves as a pin-hole camera so that an image of the positive and negative rods shows when the arc is properly adjusted. After the arc has been struck and the carbons have been correctly positioned manually, they are then driven automatically by means of a synchronous motor. Both the positive and negative carbons are driven at the same rate. The carbons are cored projector carbons, the positive carbon being 12 mm in diameter and the negative 8 mm in diameter.

[4] C. S. Rupert and J. Strong, J. Opt. Soc. Am. 41, 867(A) (1951); a complete description of the source, with instructions for its duplication, has been issued as an ONR report, by C. S. Rupert (June 1, 1952).

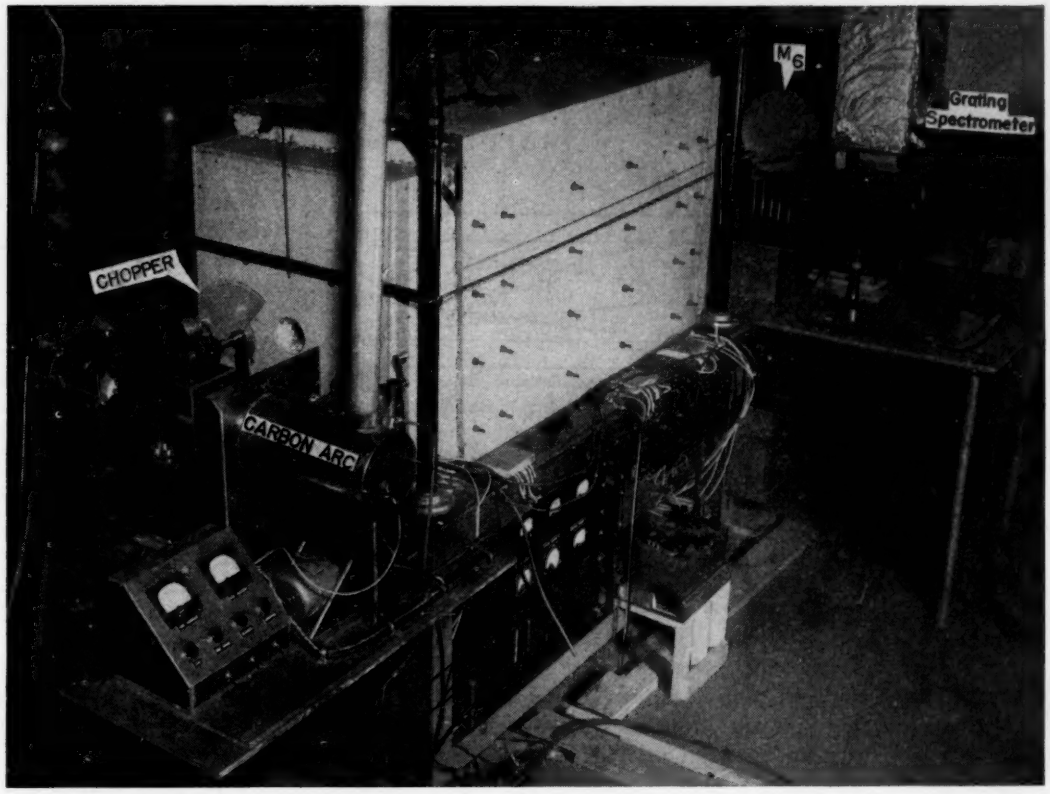

FIG. 4. High temperature absorption cell as now surrounded by its insulation.

Although the total radiation area of the positive crater of a carbon arc may vary, the radiation density from the crater does not vary. Hence, using the carbon arc it is necessary to avoid use of the perimeter of the image of the positive crater, so that the fluctuations in the arc will not appear on the slit of the spectrometer. This is accomplished by focusing the image of the positive crater (demagnified by a factor of about two) on a small diaphragm (4 mm×1 mm). Figure 5 shows a schematic diagram of the optical set-up. The condenser mirror M_1 and the illuminator mirror M_3 are both spherical mirrors of seven inches diameter and twelve inches radius of curvature. M_2 is a plane mirror (about 13 mm×13 mm). The diaphragm or baffle referred to above lies immediately in front of M_2, and it is represented by two dots in Fig. 5.

SPECTROMETERS AND OVER-ALL OPTICAL SYSTEM

Two spectrometers were used to study the spectral region from 2 to 25 microns.

For the region 2–15μ, a Perkin-Elmer Model 12 *C* infrared spectrometer was used with NaCl and LiF prisms. A thermocouple was used as the detector.

The 15–25μ spectral band was isolated for a grating spectrometer by means of four reflections from cleaved MgO crystals, as shown in Fig. 5. The grating spectrometer was constructed from the prism spectrometer described in an earlier paper.[3] Here the radiation is dispersed by means of a 1200 lines/inch grating which is blazed for 14 microns. A Golay cell was used with this grating for the detector.

With both spectrometers the radiation is chopped at 13 cycles per second by means of the Plexiglas chopper shown in Fig. 4. We are using Perkin-Elmer's chopping system and their Model 81 amplifier. The chopper is placed before the cell in order to avoid "seeing" the heated gases in the cell. Although their emission lines fall on the detector, they do not give a response after the synchronous rectifier, because their radiations are not synchronously chopped.

Figure 5 shows the arrangement of the two spectrometers. M_6 is a spherical mirror of 12 inches diameter and 48 inches radius of curvature. It is being used at its center of curvature. M_7 is a plane mirror. In order to change from the prism spectrometer to the grating spectrometer the mirror M_6 is rotated (as shown by dotted lines in Fig. 5) and M_7 is moved. M_8 and M_9 are spherical mirrors and are both used at the center of curvature. M_{10} is a plane mirror. M_4 and M_5 are the platinized fused quartz mirrors.

With the NaCl prism, the spectrometer slits were driven so that they opened at such a rate as to give approximately constant detector response‖ to the arc radiations. Fixed slits were used with the LiF prism and the grating. The effective slit widths (that give spectra with acceptable signal-to-noise characteristics) as calcu-

‖ This was achieved by a slit drive, designed and made available to us by Dr. E. K. Plyler, National Bureau of Standards, Washington, D. C., which we copied and adapted to our source.

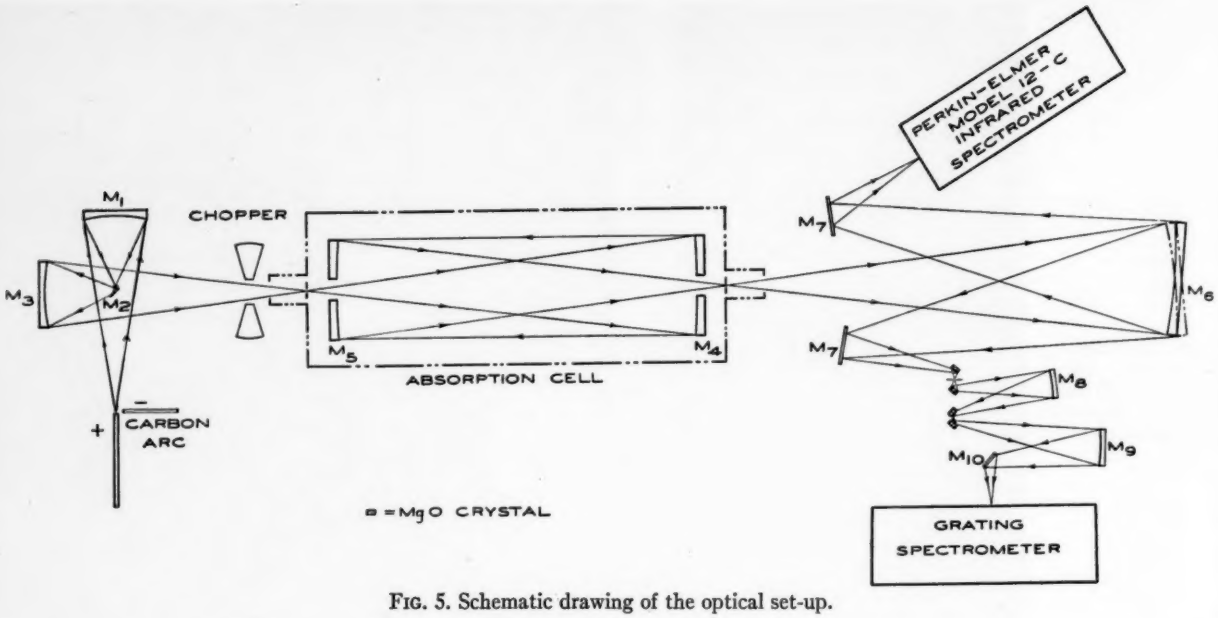

FIG. 5. Schematic drawing of the optical set-up.

lated from the optics of the instruments are graphed in Fig. 6. The actual effective slits, as judged by the resolution achieved and the intensities of single H_2O pure-rotation lines, may exceed the calculated values by 50 percent.

OBSERVATION OF SPECTRA

Spectra were obtained with the cell filled only with laboratory air, at atmospheric pressure, at various temperatures from 22°C to >500°C. The increase in temperature considerably increased the absorption due to the atmospheric H_2O and CO_2, especially in the frequency range 400–800 cm^{-1}. At elevated temperatures the actual number of absorbing molecules is lower than at room temperature, resulting from the decreased density, but the number in the high energy levels, which are the initial levels for most of the lines in this region, is greatly increased. In addition, to identify the H_2O lines from the CO_2 bands, and to bring out weaker lines, the concentration of H_2O and CO_2 in the hot cell was increased.

In all cases the gas under observation was at atmospheric pressure. Steam was flushed into the cell from a flask of boiling, distilled water by means of a small tube inserted in one end of the cell, and the steam was allowed to escape through the opposite end of the cell. A similar technique was used to add extra dry commercial-grade CO_2. After flushing with steam (or CO_2) until a suitable concentration was obtained, the pipe was removed and the spectra observed. During the course of a run the supply of steam (or CO_2) was not replenished.

The frequencies reported herein were obtained by fitting a number of standard absorption lines to the usual dispersion formulas. The standards were as follows: In the spectral region from 777 cm^{-1} to higher wave numbers, the LiF and NaCl prisms were calibrated in terms of the wave numbers of single H_2O lines as observed by Benedict, Claassen, and Shaw.[5] In the region from 555–770 cm^{-1}, frequencies are based on the CO_2 bands at 667.3, 618.3, and 721.0 cm^{-1}, and on single H_2O lines as calculated from known energy levels. In the region from about 400–550 cm^{-1}, our wavelengths are based on single water lines as observed by Randall, Dennison, Ginsburg, and Weber.[6]

RESULTS

In the region 405–600 cm^{-1} (25–17μ) the absorption due to water vapor at 500°C is intense, so that the hot cell filled with laboratory air reveals a number of new lines, which are either completely absent or quite weak at room temperature. The addition of a very small amount of superheated steam suffices to give complete opacity over most of this region. At shorter wavelengths, these lines, which are caused by high energy-level

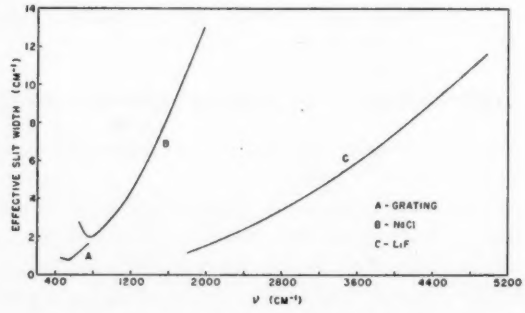

FIG. 6. Effective slit widths as calculated from the optics of the instruments.

[5] Benedict, Claassen, and Shaw, J. Research Natl. Bur. Standards **49**, 91 (1952).

[6] Randall, Dennison, Ginsburg, and Weber, Phys. Rev. **52**, 160 (1937).

transitions in the pure-rotation band, become weaker, but absorption resulting from addition of a small amount of H_2O occurs throughout the region to 1250 cm^{-1} (8μ). The 6-μ vibration-rotation band of H_2O, which at room temperature extends from about 1350–2000 cm^{-1} (7.5–5μ), is broadened upon heating; and with addition of superheated H_2O becomes opaque from about 1300–1900 cm^{-1}, with individual lines extending to long wavelengths overlapping the pure rotation band, and to short wavelengths as far as 2500 cm^{-1}, beyond the 4.3-μ band of CO_2. The 3.1-μ and 2.7-μ vibration-rotation bands of H_2O are also broadened at 500°C.

The absorption due to atmospheric CO_2 is also considerably enhanced upon heating in the wings of the 15-μ and 4.3-μ bands, and upon addition of hot CO_2 to the cell, a number of new bands appear, most strongly in the regions 540–870 cm^{-1} (upper-state transitions in ν_2), as well as in the region of the 10-μ "difference bands" ($\nu_3-\nu_1$), and in the region of 5μ ($\nu_1+\nu_2$).

These general remarks on the results are illustrated by Figs. 7–11.¶ Each figure includes a wave number scale at the top and bottom, for orientation purposes, and in addition wave number markers were drawn on each tracing. These latter should be more accurate, inasmuch as it is impossible to obtain tracings of the spectra, mount and photograph without introducing some distortion in the wavelength scale. The vertical deflections on each tracing of a given figure will not always be comparable, but the line of zero deflection is indicated for each tracing, and the deflection corresponding to no absorption may be inferred from the background.

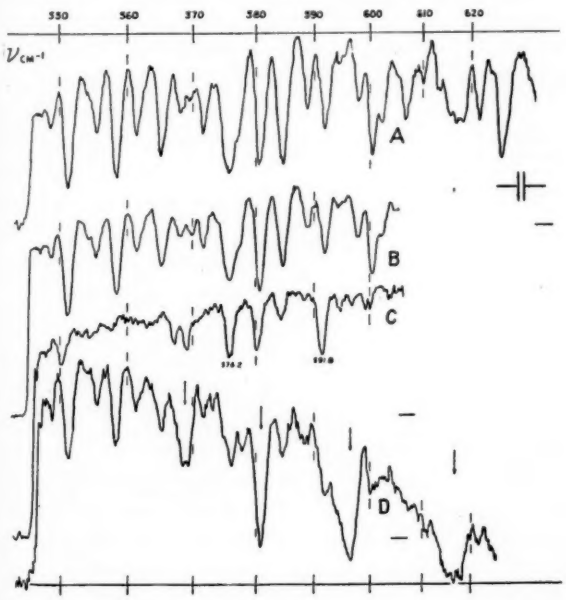

FIG. 7. Grating spectra, 547–630 cm^{-1} (18.3–15.9 microns). A; cell partially filled with small amount of additional water vapor at 486°C. B; cell heated to 539°C. C; ten meters of air at 23°C. D; cell partially filled with dry CO_2 at 510°C.

¶ Additional tracings of a similar nature, covering the entire spectral range 405–4200 cm^{-1}, have been reproduced in our detailed report to the ONR.

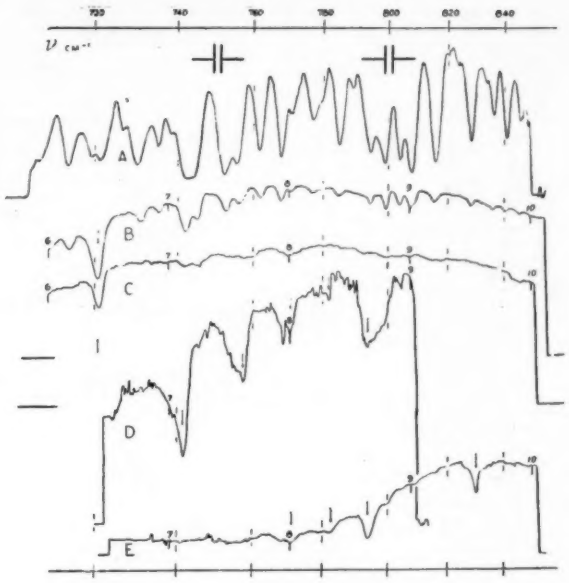

FIG. 8. NaCl prism spectra, 710–845 cm^{-1} (14.1–11.8 microns). A; cell filled with intermediate amount of water vapor at 511°C. B; cell heated to 480°C. C; ten meters of air at room temperature. D; cell partially filled with dry CO_2 at 511°C. E; cell nearly filled with dry CO_2 at 509°C.

Figure 7 shows the region from 547–630 cm^{-1} (18.3–15.9μ), as observed with the grating spectrometer. Tracing *C*, taken at room temperature, with an optical path of 10 meters of air at 23°C and 30 percent relative humidity, shows weak lines resulting from H_2O. In tracing *B*, taken with the cell heated to 539°C, the intensities of a few of the H_2O lines, e.g., those at 567.4 cm^{-1} (7_5-6_{-1}), 569.2 cm^{-1} (8_3-7_{-1}), and 591.8 cm^{-1} (9_1-8_{-5}) are weakened, because they originate on relatively low energy levels ($E''<900$ cm^{-1}). However, there are a number of new strong lines in *B*, the over-all absorption being greatly increased. Spectrum *A*, taken at 486°C, with a small amount of additional water vapor, confirms the fact that most of the new high-temperature lines are due to H_2O. A list of all the strongly temperature dependent H_2O lines, from 405–770 cm^{-1}, together with their probable identification, is given in Table I. This table will be discussed further at a later point.

Spectrum *D* of Fig. 7, taken with the cell partially filled with dry CO_2 at 510°C, shows a background of absorption caused by that molecule, increasing strongly at frequencies greater than 560 cm^{-1}, together with four *Q* branches (marked with arrows) also increasing in intensity at higher frequency. The two at highest frequency have been previously observed at room temperature,[7] being the transitions 02^0-01^1 and 03^1-02^2 ($V_1'\,V_2'^{l'}\leftarrow V_1''\,V_2''^{l''}$). The two new bands are assigned to higher members of the same sequence, 04^2-03^3 and 05^3-04^4.

Figure 8 shows the spectra from 710–845 cm^{-1} (14.1–

[7] P. E. Martin and E. F. Barker, Phys. Rev. 41, 291 (1932).

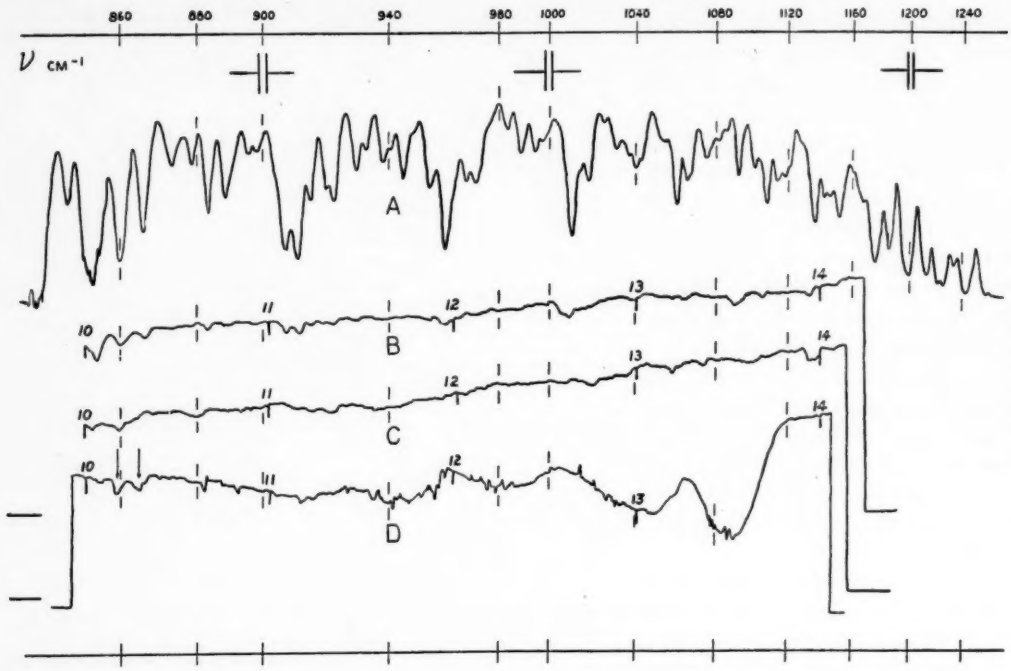

FIG. 9. NaCl prism spectra, 845–1160 cm^{-1} (11.8–8.6 microns). A; cell filled with large amount of water vapor at 511°C. B; cell heated to 480°C. C; ten meters of air at room temperature. D; cell nearly filled with dry CO_2 at 509°C.

11.8μ) as obtained with the NaCl prism spectrometer. Here the room-temperature tracing, *C*, shows very little absorption, except for the CO_2 band, 10^0-01^1 at 720.9 cm^{-1}. Upon heating to 480°C, tracing *B*, a number of relatively weak absorption lines appear. Tracing *A*, with the cell filled with a relatively small amount of steam at 511°C, shows that most of these are due to H_2O, the temperature-dependent wing of the rotation spectrum being intense throughout this region. Beyond 768 cm^{-1}, the spectrum of 8 meters of steam at 110°C has recently been mapped with much better resolution.[5] This work reveals that a number of the "lines" shown here consist of several components. The relative intensities at the higher temperatures observed here are quite different from those at 110°C, but the line assignments of the earlier work are in essential agreement with the new data.

Figure 8 also shows the strong CO_2 absorption on the short wavelength wing of the 15-μ band. Spectra *D* and *E* were both obtained at 510°C, with a larger quantity of gas in the latter case. The unresolved background decreases in intensity with decreasing wavelength, and

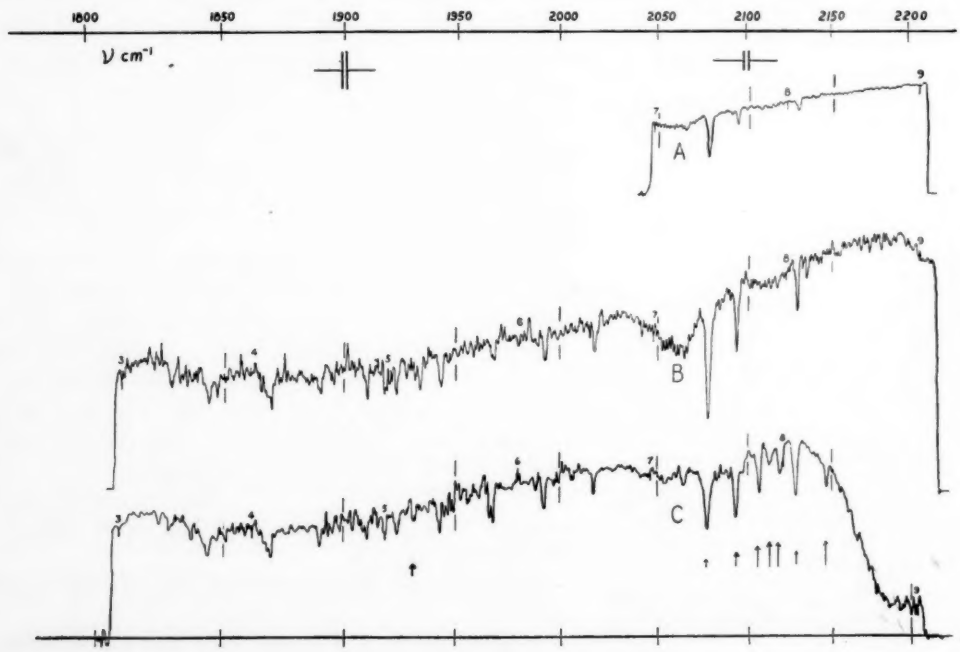

FIG. 10. LiF prism spectra, 1800–2210 cm^{-1} (5.55–4.52 microns). A; cell nearly filled with dry CO_2 at 42°C. B; same filling as A, higher amplification. C; cell nearly filled with dry CO_2 at 511°C.

a number of Q branches, marked by arrows, appear. Those at 741.8 cm^{-1} (11^1-02^2) and 791.8 cm^{-1} (11^1-02^0) have previously been observed in the laboratory,[7] and the one at 829.5 cm^{-1} (12^2-03^1) has been noted in the earth's atmosphere.[8] The three at 757.2 cm^{-1}, 769.5 cm^{-1}, and 780.9 cm^{-1} require the high temperatures of the present study for their appearance, and may readily be identified as higher members of the 721–742 cm^{-1} sequence, 12^2-03^3,** 13^3-04^4, and 14^4-05^5.

Figure 9 presents the region from 845–1160 cm^{-1} (11.8–8.6μ), obtained with the NaCl prism spectrometer. In this region the room-temperature air spectrum (tracing C) is essentially blank, the apparent dips being due to source instability and instrument noise. A few weak H_2O lines appear in tracing B, for which the air was heated to 480°C. There is, however, considerable absorption in tracing A, cell filled with steam at 511°C, throughout this region. There is overlapping between the pure rotation spectrum and that of the wing of the 6-μ band, absorption due to which increases rapidly beyond 9μ reaching near-opacity at 8μ. The resolution here is not comparable to that attained in the grating studies, but confirmation of those assignments and new information concerning the highest energy levels may be obtained.

Tracing D, taken with the cell nearly filled with CO_2 at 509°C, shows two weak Q branches at 859 and 864 cm^{-1}. These are the highest frequency members of the ν_2 sequence that were recorded and are assigned to the transitions 13^3-04^2 and 20^0-03^1. The CO_2 absorption between 880–1120 cm^{-1} is due to the doublet-type bands, with Q branches, which are transitions from the $\begin{Bmatrix}02^00\\10\ 0\end{Bmatrix}$ resonance pair to the ν_3 fundamental, and higher transitions of the same type. In addition to the well-known principal "difference bands" at 961 and 1064 cm^{-1}, there is definite indication of the band 01^11-11^10 whose origin is calculated to lie at 927.0 cm^{-1}. The origin of the other member is calculated to lie at 1071.6 cm^{-1} and undoubtedly contributes to the strengthened R branch of the 1064 cm^{-1} band.

The absorption resulting from the weak CO_2 bands near 5μ, as observed with the LiF prism, is shown in Fig. 10. Tracings A and B were both taken with the cell nearly full of CO_2 at 42°C, tracing B being at higher amplification. In tracing C the cell was heated to 511°C. At the low temperature the 2077 cm^{-1} band, with its strong Q branch, partially resolved P branch, and anomalously weak R branch,[9] appears, together with two satellite Q branches, as observed previously[10]

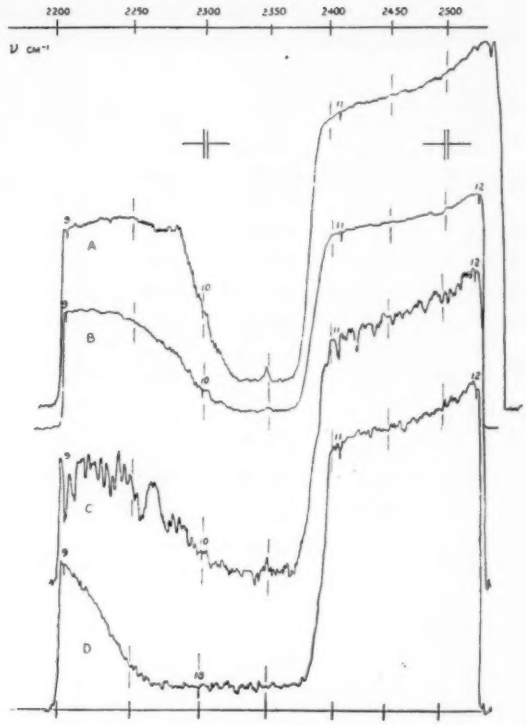

FIG. 11. LiF prism spectra, 2210–2540 cm^{-1} (4.52–3.94 microns). A; ten meters of air at room temperature. B; cell heated to 507°C. C; cell partially filled with additional water vapor at 517°C. D; cell partially filled with dry CO_2 at 518°C.

which belong to bands originating on the first excited level of ν_2. The long-wave member of the $\begin{Bmatrix}11^1\\ -00\\03^1\end{Bmatrix}$ resonance doublet, at 1933 cm^{-1}, can barely be seen above the noise level and H_2O background. At the elevated temperature six additional Q branches, as denoted by arrows whose lengths are indicative of the temperature-sensitivity, appear. The frequencies and suggested assignments of these bands, together with those of the long-wave region, are given in Table II. With the amount of hot CO_2 used for tracing C, the ν_3 fundamental and its upper-state satellites give opacity beyond 2180 cm^{-1} and contribute to the background absorption beyond 2125 cm^{-1}.

The region of the ν_3 fundamental is shown in Fig. 11. Tracing A shows the room-temperature absorption, resulting from the 10-meter path of laboratory air. The resolution is barely sufficient to show a few lines of the rotational structure in the P branch from 2296–2313 cm^{-1}, and in the P branch of the $C^{13}O_2$ isotope band, from 2251–2275 cm^{-1}. With the cell at 507°C, tracing B, the absorption in the region 2240–2320 cm^{-1} is very much increased, and the rotational structure is no longer resolved. This is due to the greater relative contribution of the high-J lines of (001–000), and even more to the greatly increased strength of the upper state bands ($0\ 1^1\ 1-0\ 1^1\ 0$), ($0\ 2^2\ 1-0\ 2^2\ 0$), etc. The increased number of lines also results in increased ab-

[8] Shaw, Oxholm, and Claassen, "The Solar Spectrum from 7μ to 13μ," Scientific Report No. 1A–4, Ohio State University Research Foundation, (August 30, 1951).

** A number of lines of the R branch of this band may be identified in the high-resolution solar spectra[8] (8). These data fix the band origin at 756.75 cm^{-1}.

[9] D. F. Eggers and B. L. Crawford, J. Chem. Phys. **19**, 1554 (1951).

[10] E. F. Barker and T. Y. Wu, Phys. Rev. **45**, 1 (1934).

TABLE I. Strongly temperature dependent lines in H_2O, 407–768 cm^{-1}.

ν_{obs} cm^{-1}	J_τ'	J_τ''	ν_{calc} cm^{-1}	E'' cm^{-1}	A_{calc}	A_{obs}
407.4	? 18_{-9}	17_{-9}	407	4025	0.11	0.19
	a 12_{-3}	11_{-3}	407.66	3532.9	0.12	
408.8	? 22_{-21}	21_{-21}	?408.5	4440	0.15	0.17
	21_{-19}	20_{-17}	?409.0	4413	0.14	
410.8	a 9_{-3}	8_{-5}	409.53	2495	0.11	0.11
414.4	a 8_{-4}	7_{-6}	414.63	2181.3	0.05	0.28
427.8	? 23_{-23}	22_{-21}, etc.	426–428	~4800	~0.07	0.14
429.0	10_1	10_{-5}	428.87	1446.4	0.07	0.03
434.9	12_{-1}	11_{-1}	434.84	1999.3	0.58	0.65
	a 11_{-1}	10_{-3}	435.40	3224.8	0.15	
436.5	9_9	8_7	436.47	1789.4	1.08	0.65
443.8	10_5	8_5	443.79	1810.8	1.00	0.60
446.8	a 9_7	9_5	446.00	3306.6	0.25	0.70
	11_2	10_2	446.48	1875.7	0.43	
	11_3	10_1	447.01	1875.2	0.73	
449.8	a 10_3	9_3	449.9	3321.0	0.22	0.40
	a 11_1	10_{-1}	450.2	3383.7	0.18	
452.0	12_0	11_{-2}	451.78	1986.1	0.32	0.35
455.7	14_{-3}	13_{-3}	455.50	2629.6	0.33	0.32
463.5	a 9_9	8_7	463.34	3531	0.22	0.46
	a 12_{-1}	11_{-1}	463.53	3660	0.13	
	? 16_{-5}	15_{-5}	464	3366	0.15	
467.9	11_5	10_3	467.91	2054.6	0.80	0.76
	12_1	11_1	468.80	2144.5	0.60	
470.8	12_2	11_0	470.49	2143.0	0.35	0.56
	a 10_5	9_5	471.0	3526.8	0.21	
476.7	10_9	9_9	476.53	2225.9	0.34	0.49
481.0	a 9_{-5}	8_{-7}	480.56	2337.8	0.09	0.41
	13_{-1}	12_{-3}	480.96	2275.5	0.47	
486.2	11_7	10_5	486.18	2254.6	0.93	0.52
488.4	a 10_7	9_7	488.42	3752.6	0.24	0.29
489.6	13_0	12_0	489.54	2437.8	0.34	0.34
491.7	12_3	11_3	491.69	2322.2	0.77	0.65
	9_0	8_{-4}	491.95	983.1	0.20	
494.0	13_1	12_{-1}	494.31	2434.2	0.56	0.46
495.2	a 11_5	10_3	495.10	3771	0.21	0.26
496.2	a 12_1	11_1	495.97	3833.9	0.15	0.22
501.8	11_9	10_7	501.48	2471.6	0.83	0.67
	10_{-3}	9_{-7}	502.37	1079.2	0.47	
	a 10_9	9_9	502.8	3994.4	0.20	
504.7	13_{-3}	12_{-5}	504.70	2124.8	0.36	0.43
507.5	14_{-1}	13_{-1}	507.6	2756.7	0.42	0.41
510.6	12_{-4}	11_{-6}	510.71	1694.9	0.25	0.50
	12_5	11_5	510.71	2522.5	0.73	
514.5	a 11_7	10_5	513.5	3997.8	0.18	0.70
	11_{11}	10_9	514.51	2702.6	0.71	
	13_2	12_2	514.76	2613.5	0.31	
	13_3	12_1	514.99	2613.2	0.54	
	14_{-2}	13_{-4}	515.15	2587	0.21	
519.7	14_0	13_{-2}	518.0	2748	0.25	0.52
	a 12_3	11_3	519.2	4039	0.17	
	11_{-5}	10_{-7}	519.67	1293.8	0.41	
	a 13_1	12_{-1}	520.3	4124	0.15	
523.2	15_{-2}	14_{-2}	523.1	3101.7	0.17	0.18
526.3	10_{-5}	9_{-9}	526.03	920.2	0.33	0.58
	12_7	11_7	526.5	2740.7	0.64	
528.5	a 11_9	10_7	528.4	4241	0.15	0.15
534.3	13_5	12_3	534.26	2814.2	0.56	0.41
537.0	6_5	5_1	536.36	508.8	0.05	0.48
	a 11_{-5}	10_{-7}	536.54	2904.7	0.09	
	14_1	13_1	536.73	2928.4	0.39	
	14_2	13_0	538.02	2927.4	0.23	
539.8	12_9	11_9	539.7	2973.1	0.55	0.40
544.7	15_{-1}	14_{-3}	543.7	3085.0	0.29	0.29
550.5	11_{-4}	10_{-8}	550.10	1293.2	0.21	0.53
	12_{11}	11_{11}	550.5	3216.6	0.45	
	13_7	12_5	550.8	3033.2	0.48	
554.0	a 12_7	11_7	554.5	4511	0.11	0.15
555.0	15_{-3}	14_{-5}	555.5	2917.5	0.21	0.23
557.7	14_3	13_3	557.4	3128.2	0.39	0.41
	14_{-4}	13_{-6}	557.6	2426.0	0.15	
	15_0	14_0	558.4	3266.4	0.16	
561.9	15_1	14_{-1}	562.1	3264.2	0.27	0.22
565.3	13_9	12_7	564.8	3267.2	0.39	0.32
571.7	13_{-5}	12_{-7}	571.54	1962.7	0.28	0.24
575.8	14_5	13_5	575.2	3348	0.34	0.39
	13_{11}	12_9	575.4	3514	0.32	
	11_{-7}	10_{-9}	576.28	1114.7	0.25	
580.5	? 16_{-1}	15_{-1}	580	3629	0.19	0.45
	15_3	14_1	580.32	3465	0.27	
	11_{-6}	10_{-10}	580.65	1114.7	0.13	
	12_{-6}	11_{-8}	581.4	1525.3	0.15	
584.7	13_{13}	12_{11}	584.7	3767.1	0.39	0.35
	12_{-3}	11_{-7}	584.80	1690.9	0.45	
589.0	14_7	13_7	588.9	3584.0	0.43	0.18
600.2	12_{-5}	11_{-9}	599.82	1525.0	0.39	0.35
	15_5	14_3	600.2	3685.6	0.34	
	14_9	13_9	600.5	3832.0	0.32	
601.8	16_1	15_1	602.2	3826.1	0.23	0.20
604.0	11_0	10_{-4}	604.7	1538.3	0.095	0.08
606.2	? 17_{-1}	16_{-3}	606	4010	0.11	0.20
	? 17_{-3}	16_{-5}	607.0	3830	0.10	
609.7	14_{11}	13_{11}	609.5	4088	0.19	0.14
614.0	15_7	14_5	613.6	3923	0.19	0.17
617.5	14_{13}	13_{13}	617.5	4351	0.14	0.35[a]
620.5	15_{-5}	14_{-7}	620.5	2745	0.16	0.22
	12_{-1}	11_{-5}	620.7	1813.5	0.17	
624.8	16_3	15_3	?623.5	4046	0.15	0.37
	17_1	16_{-1}	?625	4209	0.097	
	13_{-4}	12_{-1}	625.1	1961.0	0.12	
	9_3	8_{-3}	625.25	1006.2	0.093	
	15_9	14_7	?625.3	4173	0.15	
633.5	12_{-8}	11_{-10}	633.7	1327.3	0.094	0.12
	15_{11}	14_9	634.2	4432	0.12	
635.2	12_{-7}	11_{-11}	635.3	1327.3	0.17	0.25
	14_{-6}	13_{-8}	635.3	2248.2	0.092	
	16_5	15_5	?636.5	4285	0.12	
640.5	13_{-7}	12_{-9}	641.1	1774.9	0.17	0.10[a]
642.0	13_{-2}	12_{-6}	641.7	2106.7	0.10	0.15[a]
	15_{13}	14_{11}	?642.5	4697	0.09	
648	17_3	16_1	?648.5	4430	0.095	0.15[a]
	15_{15}	14_{13}	?648.8	4969	0.059	
651.2	16_7	15_7	?650.5	4537	0.10	0.14[a]
	13_{-6}	12_{-10}	651.3	1774.8	0.093	

TABLE I.—*Continued.*

ν_{obs} cm^{-1}	J_T'	J_T''	ν_{calc} cm^{-1}	E'' cm^{-1}	A_{calc}	A_{obs}
659	16_9	15_9	?658.5	4798	0.077	0.20[a]
	10_2	9_{-4}	658.8	1216.4	0.050	
	17_{-5}	16_{-7}	?659	3640	0.068	
	17_5	16_3	?661	4669	0.075	
?670	14_{-3}	13_{-7}	669.6	2416.0	0.13	0.20[a]
	14_{-5}	13_{-9}	670.5	2247.0	0.14	
678.8	? 16_{-6}	15_{-8}	679	3084	0.057	0.03[a]
688.8	13_{-9}	12_{-11}	688.9	1558.1	0.16	0.22[a]
693.2	9_5	8_{-1}	694.0	1122.8	0.085	0.10
697.0	11_1	10_{-5}	696.6	1446.4	0.105	0.14
	15_{-7}	14_{-9}	697	2551.7	0.122	
	14_{-8}	13_{-10}	698.0	2042.5	0.093	
703.2	14_{-7}	13_{-11}	703.0	2042.5	0.156	0.18
705.5	15_{-4}	14_{-8}	705.5	2740.5	0.049	0.02
713.0	12_1	11_{-3}	713.0	1900.2	0.083	0.06
721	15_{-6}	14_{-10}	719.5	2551.0	0.068	0.07[a]
	13_0	12_{-4}	721.5	2206.0	0.048	
729.9	14_{-1}	13_{-5}	730.1	2534.1	0.102	0.07
735.2	? 18_{-6}	17_{-8}	735.2	4028	0.029	0.04
741.5	11_3	10_{-3}	740.7	1581.5	0.064	0.20
	15_{-2}	14_{-6}	741.9	2883.5	0.046	
	? 17_{-7}	16_{-9}	742	3440	0.064	
744.1	14_{-10}	13_{-12}	744.0	1806.9	0.052	0.18
	14_{-9}	13_{-13}	744.5	1806.9	0.090	
752.3	15_{-9}	14_{-11}	752.3	2328.2	0.090	0.12
755.6	15_{-8}	14_{-12}	755.3	2328.2	0.052	0.08
	16_{-5}	15_{-9}	755.6	3081	0.078	
761.6	? 16_{-8}	15_{-10}	760	2872.9	0.039	0.06
	16_{-3}	15_{-7}	761.6	3248.5	0.054	
767.4	16_{-7}	15_{-11}	767.4	2872.6	0.067	0.10

[a] The H_2O absorption is superposed on strong CO_2 absorption and hence is quantitatively very uncertain.

sorption at the position of the band origin, 2349.3 cm^{-1}. The R branch is, however, only very slightly broadened. With additional CO_2 in the hot cell, tracing D, the convergence of the R branch to its head at 2497 cm^{-1} may be noted,[11] while the long-wave region broadens greatly. With even more CO_2, as in tracing C of Fig. 10, the ν_3 region is opaque to 2180 cm^{-1}, and extends to 2125 cm^{-1}. It is noteworthy that under these conditions there is little, if any, detectable absorption at frequencies above 2400 cm^{-1}, indicating that such transitions as (1 0 1 − 0 2^0 0), with $\nu_0 = 2429.0$ cm^{-1}, have much lower transition probabilities than such as (0 2^0 1 − 1 0 0) with $\nu_0 = 2224.6$ cm^{-1}.

Tracing C, taken with the cell partially filled with H_2O at 517°C, is of interest in that it shows the H_2O absorption lines of the ν_2 R branch extending well beyond the CO_2 absorption region, nearly to 2500 cm^{-1}. Some of the stronger lines may be fitted to the R-branch series of ν_2. The H_2O absorption in this region, as was revealed by the high resolution work, is also due to the difference band $\nu_3 - \nu_1$.

DISCUSSION

H_2O

The absorption due to water vapor at room temperature, and to several meters of steam at 110°C, has been observed under varying degrees of resolving power[5,6,12] from 150–4.5μ. The present observations are the first in which superheated steam has been studied with fairly high resolving power.

In the pioneer work of Randall, Dennison, Ginsburg, and Weber, all the levels of $J \leqslant 11$ were located, as well as a few of higher J, extending to about 2200 cm^{-1}. Ginsburg[13] later made tentative assignments up to $J = 15$. While his assignments appeared highly reasonable in that regular series relationships were obeyed, intensity calculations make it extremely unlikely that lines originating on levels above 3000 cm^{-1} could have been observed in previous studies. The energy levels proposed to account for the recent high resolution studies[5] above 765 cm^{-1} differ with only a few exceptions by only fractions of a wave number from those of Randall, Dennison, Ginsburg, and Weber for $J \leqslant 11$, and are based on a comprehensive study of the entire vibration-rotation spectrum. They extend to about 3800 cm^{-1}, and include levels of J up to 18. The present results confirm most of the assignments of that work and permit an extension to still higher energies.

In making rotational assignments, one is guided by two factors; the energy levels and the line frequencies given by the difference in energy between two levels must fall in regular series; and the intensities must agree with those calculated. Since the intensities of lines originating from high energy levels are very sensitive functions of temperature, our studies provide additional information of great utility in making assignments, even though the spectral resolution is not equal to that achieved in some of the previous work.

S, the integrated intensity, of any line in the pure rotation spectrum, is given by the expression

$$S = \frac{8\pi^3 N\mu^2}{3hcQ}\nu(1-e^{-hc\nu/kT})gLe^{-E''/kT} = C\cdot f(\nu)\cdot I_T.$$

This may be lumped into a term which is approximately constant for all lines (containing the universal constants, the dipole moment μ, the number of molecules N in the absorbing path, etc.); a frequency-dependent term, $f(\nu) = \nu(1-e^{-h\nu/kT})$, and two terms which characterize each line, the *Line Strength*, L, and the (temperature dependent) *Boltzmann Factor* $ge^{-E''/kT}$ (g, the statistical

[11] Benedict, Herman, and Silverman, J. Chem. Phys. **19**, 1325 (1951).
[12] G. Hettner, Ann. Physik **55**, 476 (1918).
[13] N. Ginsburg, Phys. Rev. **74**, 1052 (1948).

TABLE II. Q branches of CO_2 bands in the regions of 15μ and 5μ.

v_1'	v_2'	l'	v_1''	v_2''	l''	E'' cm^{-1}	$gR^{v'v''}$	$I_{773}°$	ν_{calc} cm^{-1}	ν_{obs} cm^{-1}
0	1	1	0	0	0	0.00	1	100	667.3	[667.3]
0	2	0	0	1	1	667.3	0.5	14.5	618.3	[618.3]
1	0	0	0	1	1	667.3	0.5	14.5	721.0	[721.0]
0	2	2	0	1	1	667.3	4	116	668.1	[667.3]
0	3	1	0	2	0	1285.6	0.75	6.90	647.6	648.2
1	1	1	0	2	0	1285.6	0.75	6.90	791.4	791.8
0	3	1	0	2	2	1335.4	1	8.44	597.8	596.5
1	1	1	0	2	2	1335.4	1	8.44	741.6	741.8
0	3	1	1	0	0	1388.3	0.75	5.66	544.9	545.5
1	1	1	1	0	0	1388.3	0.75	5.66	688.7	688.8
0	3	3	0	2	2	1335.4	6	50.6	668.3	[667.3]
0	4	4	0	3	3	2003.7	8	19.2	669.1	[667.3]
0	4	2	0	3	3	2003.7	1	2.40	581.2	581.2
1	2	2	0	3	3	2003.7	1	2.40	756.7	757.2
0	4	2	0	3	1	1933.2	2.5	6.82	653.4	?
1	2	2	0	3	1	1933.2	2.5	6.82	827.2	829.5
0	4	2	1	1	1	2077.0	2.5	5.30	507.9	···
1	2	2	1	1	1	2077.0	2.5	5.30	683.4	···
0	4	0	0	3	1	1933.2	0.5	1.36	617.8	[618.3]
0	4	0	1	1	1	2077.0	0.5	1.06	474.1	···
1	2	0	0	3	1	1933.2	0.5	1.36	739.8	[741.8]
1	2	0	1	1	1	2077.0	0.5	1.06	596.0	[596.5]
2	0	0	0	3	1	1933.2	0.5	1.36	863.3	864
2	0	0	1	1	1	2077.0	0.5	1.06	719.5	[721.0]
0	5	3	0	4	4	2672.4	1.0	0.70	568.7	568.7
1	3	3	0	4	4	2672.4	1.0	0.70	769.5	769.5
0	5	3	0	4	2	2584.9	3.5	2.86	656.0	···
1	3	3	0	4	2	2584.9	3.5	2.86	857.4	859
0	5	3	1	2	2	2760.4	3.5	2.06	480.9	···
1	3	3	1	2	2	2760.4	3.5	2.06	681.9	···
1	4	4	0	5	5	3341.8	1.0	0.20	780.9	780.9
1	1	1	0	0	0	0	1	100	2077.0	2077.6
1	2	2	0	1	1	667.3	4	116	2093.1	2093.6
2	0	0	0	1	1	667.3	0.9?	26.5?	2128.2	2129.0
1	2	0	0	1	1	667.3	0.1?	2.9?	2005.7	?
1	3	3	0	2	2	1335.4	6	50.6	2106.9	2106.9
1	4	4	0	3	3	2003.7	8	19.2	2119.0	2119.0
2	1	1	0	2	2	1335.4	0.9?	7.60	2166.6	2167.6
2	1	1	1	0	0	1388.3	1.8?	13.6	2113.7	2112.7
3	0	0	1	1	1	2077.0	0.9?	1.9?	2147.1	2147.1
0	3	1	0	0	0	0			1933.2	1933.6
0	4	2	0	1	1	667.3			1917.6	?
0	4	0	0	1	1	667.3			1883.7	?
0	5	3	0	2	2	1335.4			1905.9	?

Note: Observed values in light brackets [ ] were used as calibration points; those in heavy brackets **[ ]** fall in regions of stronger absorption.

weight, is 1 for levels with τ even, and 3 for τ odd). The line strength, which is the quantity tabulated by Cross, Hainer, and King,[14] varies over a wide range for asymmetric-top molecules; for the water-vapor lines in the frequency range of interest, it ranges from the order of magnitude of J(1–20) for lines of certain *allowed branches*, down to 0.0001 and even lower for lines of *partially-forbidden* or *highly-forbidden* branches.

With our air path of 10 meters at 20°C and 25 percent relative humidity,

$$S=1.25f(\nu)I_{287}\ (\text{cm}^{-1}),$$

where

$$f(\nu)=\nu(\text{cm}^{-1})(1-e^{-\nu/200})$$

and

$$I_{287}=gLe^{-E''/200}.$$

[14] Cross, Hainer, and King, J. Chem. Phys. **12**, 210 (1944).

The observed absorption A is related to the values of S, depending on the resolving power of the spectrometer, the number of lines of different S lying with the effective slit width, $\Delta\nu$, and the line shape, here assumed to have the Lorentz form

$$K_\nu=\frac{S}{\pi}\frac{\alpha}{(\nu-\nu_0)^2+\alpha^2}.$$

If there is a single line with $S/\pi\alpha\gg1$ and $\alpha/\Delta\nu\ll1$ within the interval $\Delta\nu$, conditions which obtain for most of the lines, there results for the maximum absorption $A_{max}=(2(S\alpha)^{\frac{1}{2}})/\Delta\nu$. When several lines fall within the interval $\Delta\nu$ some uncertainty is introduced; if the difference between the line positions is small compared to α, $A\cong(\Sigma S)^{\frac{1}{2}}$ whereas, if the difference is large compared to α but small compared to $\Delta\nu$, $A\cong\Sigma(S)^{\frac{1}{2}}$.

The value of α for atmospheric H_2O is uncertain to about 50 percent. It has been determined with some precision as 0.09 cm^{-1} for one line in the microwave spectrum,[15] $6_{-5}-5_{-1}$, $\nu=0.74$ cm^{-1}; and as 0.11–0.12 cm^{-1} for two lines[16] in the region we are discussing, 6_5-5_1, $\nu=536.3$ cm^{-1} and 9_3-8_{-3}, $\nu=625.3$ cm^{-1}. Recent studies by W. H. Cloud[17] indicate, however, that for a number of lines between 490–590 cm^{-1} α is lower than the previous results, $\sim$0.05 cm^{-1}. In any event, one might expect α to vary somewhat from line to line.[18] For purposes of calculation, we will assume $\alpha=0.08$ cm^{-1} at room temperature. Using the empirical values for $\Delta\nu$

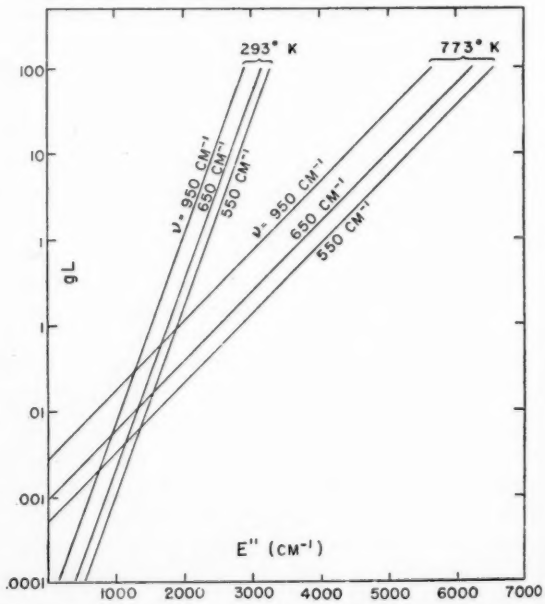

FIG. 12. A plot of the values of E'' and gL that yield $A=0.10$ at two temperatures (293°K and 773°K) and at three frequencies (550, 650, and 950 cm^{-1}).

[15] G. E. Becker and S. H. Autler, Phys. Rev. **70**, 300 (1946).
[16] A. Adel, Phys. Rev. **71**, 806 (1947).
[17] W. H. Cloud, "Pressure broadening of pure rotation lines of the water vapor spectrum from 490 to 590 wave numbers" ONR-Johns Hopkins Report (May 15, 1952).
[18] P. W. Anderson, Phys. Rev. **76**, 647 (1949); etc.

(Fig. 6), it is then possible to calculate the absorption of each line. Good agreement with the observed relative absorption is found. The calculated absolute absorption is about 100 percent greater than the observed, which probably is the result of optical imperfections causing the actual effective slits to be ~50 percent greater than assumed. Accordingly for the high temperature calculations $\Delta\nu$ was increased by this amount.

For calculation of the absorption at elevated temperatures, the uncertainties of the assumed parameters become greater, since the water content was poorly controlled in the experiments. If the fractional H_2O content of the air in the three-meter hot path was the same as in the laboratory air, at 500°C, $S=0.0501f'(\nu)I_{773}$, where $f'(\nu)=\nu(1-e^{-\nu/537.4})$ and $I_{773}=gLe^{-E''/537.4}$. The temperature dependence of α should lie somewhere between T^{-1}, as it would be at constant pressure if the collision diameter is inversely proportional to the collision velocity (dipole-dipole forces), and $T^{-0.5}$ if the diameter is velocity independent (hard-spheres). It is believed that dipole-quadrupole forces may be the main mechanism of broadening of H_2O lines by N_2 molecules: for these $\alpha\sim T^{-0.7}$, which dependence was assumed.

With these parameters it is possible to graph the values of E'' and gL that yield a given A at both temperatures and at several frequencies. Such curves are presented, for $A=0.10$, in Fig. 12. It will be seen that the lower limit of detectability varies greatly with the increase of temperature. At room temperature, one may expect, and does observe, lines with gL as low as 0.0001, coming from $E''<600$ cm^{-1}, while lines of $gL\cong 50$, the most strongly allowed doublets in the series with $\Delta K_{-1}=+1$, $\Delta K_1=\pm 1$, $K_{-1}=J, J-1$, etc., will fade out of observation for $E''>3000$ cm^{-1}. At 500°C, on the other hand, no lines with $gL<0.01$ will make an appreciable contribution relative to the air outside of the cell, while the $gL\cong 50$ lines up to $E''\sim 6000$ cm^{-1} should appear. All lines with $E''>2000$ cm^{-1} will be so enhanced at 500°C as to appear to be essentially new lines.

In addition to the pure rotation lines in the ground vibration level, lines of high L, from transitions within the lowest excited vibrational level, ν_2, will also appear at high temperature, since they come from states ~1700 cm^{-1} above the corresponding E'' in the ground state. Inasmuch as the rotational constant A is much greater in (010) than in (000), the lines will lie at higher frequencies than their ground-state analogs.

By comparing the results at room temperature and at 500°C, together with some runs at intermediate temperature (~280°C), and with the higher resolution studies previously reported in the regions <555 cm^{-1} [6] and >762 cm^{-1},[5] it is possible to obtain a satisfactory assignment for all the strongly temperature-dependent lines, from 405–768 cm^{-1}. The results were presented in Table I. The table includes most of the stronger lines of high E'' that should be observed at 500°C, and contains the following entries. ν_{obs} is the observed frequency (which very often results from the superposition of several overlapping lines, because of our relatively limited resolving power). J_τ' and J_τ'' are the quantum numbers of the upper and lower states; the letter "a" is prefixed to J_τ' when both levels are in the excited vibrational state ν_2; and, in order to conserve space, only the strong component (τ odd) is listed when pairs of lines and levels lie within 0.3 cm^{-1}. Line assignments that are speculative in that they are based on series and intensity relationships, with no confirmation from other transitions involving the levels, are prefixed by "?." ν_{calc} is the frequency difference between the energy levels of J_τ' and J_τ'' as listed in Table II of reference (5), which is extended, from the present results, as Table III. For some of the lines the agreement between ν_{obs} and ν_{calc} is meaningless, as the energy levels are based on the spectra, but there are many internal checks, when levels give rise to several lines. A_{calc}, is the calculated maximum absorption for the 500°C atmospheric path, obtained as described in the preceding paragraphs.

The results of Table I show that most of the new absorption in the longer-wavelength pure rotation region

TABLE III. Newly identified energy levels of H_2O.

000 Level				010 Level	
J_τ	E, cm^{-1}	J_τ	E	J_τ	E
$13_{2,9}$	3831.5	17_{-9}	4025	$10_{9,10}$	4497.2
$13_{10,11}$	4087.9	17_{-8}	4028		
$13_{12,13}$	4351.7	17_{-7}	4182	$11_{6,7}$	4511.6
		17_{-5}	4299	$11_{8,9}$	4768.7
14_{-5}	2917.5	17_{-4}	4418		
$14_{5,6}$	3923.1	17_{-3}	4437	12_{-8}	3587.8
$14_{7,8}$	4172.7	17_{-1}	4616	12_{-6}	3744
$14_{9,10}$	4432	17_{1}	4834	$12_{5,6}$	4809
$14_{11,12}$	4697	17_{3}	5076	$12_{7,8}$	5065
$14_{13,14}$	4969	17_{5}	5330	$12_{9,10}$	5336
				$12_{11,12}$	5614
15_{-7}	3248.5	18_{-10}	4431		
15_{-6}	3270	18_{-9}	4432	13_{-7}	4052.7
15_{-5}	3366	18_{-8}	4614	13_{-6}	4073
15_{-4}	3446	18_{-7}	4644	13_{-5}	4190
15_{-3}	3473.0	18_{-6}	4763	13_{-4}	4253
15_{-2}	3625.1	18_{-5}	4841	$13_{2,3}$	4872
15_{-1}	3628.7			$13_{4,5}$	5121
15_{0}	3824.8	19_{-17}	4023	$13_{10,11}$	5935
15_{1}	3826.3	19_{-15}	4328	$13_{12,13}$	6222
$15_{2,3}$	4045.1	19_{-13}	4609		
$15_{4,5}$	4285	19_{-11}	4853	14_{-10}	4183.5
$15_{6,7}$	4536	19_{-9}	5063	14_{-9}	4184.9
$15_{8,9}$	4798	19_{-8}	5075	14_{-7}	4395.4
$15_{10,11}$	5066			14_{-5}	4585.6
$15_{12,13}$	5340	20_{-13}	5034	14_{-3}	4778
$15_{14,15}$	5616	20_{-11}	5286	14_{-2}	4785
		20_{-9}	5540	14_{-1}	4980
16_{-8}	3633			14_{1}	5210
16_{-7}	3639.9			$14_{7,8}$	5998
16_{-6}	3763			$14_{11,12}$	6569
16_{-5}	3830				
16_{-4}	3871			$15_{-13,-12}$	4243
16_{-3}	4010			$15_{6,7}$	6362
16_{-2}	4017				
16_{-1}	4209			$16_{-14,-13}$	4565
16_{0}	4213			$16_{-12,-11}$	4842.6
$16_{1,2}$	4428			$16_{3,4}$	6468
$16_{3,4}$	4669			$16_{5,6}$	6748
$16_{5,6}$	4922				
$16_{7,8}$	5185				
$16_{9,10}$	5456				
$16_{11,12}$	5731				

can be accounted for in position and intensity. No precise quantitative significance should, however, be ascribed to the results on the intensity; to verify the assumptions that were made concerning the line strengths and widths of the high J transitions would require somewhat higher resolution, more accurate control of the water content, and more precise determination of the absorption as a function of slit width.

The newly identified lines listed in Table I and the resulting new energy levels in Table III fall into fairly regular series and are believed reliable to within 2 cm^{-1}. Confirmation by studies with higher resolution, either in the present region or by analyses of vibration rotation bands at elevated temperatures—or in flames—would be desirable. Work of the latter kind is currently in progress.[19]

An assignment, similar to that of Table I, may be made for the remainder of the pure-rotation absorption between 768–1100 cm^{-1}. This is not presented here, since it essentially duplicates the assignment made from the higher resolution data. There are indications of additional higher energy lines; the energy levels to which they lead are included in Table III. The corresponding lines may readily be deduced from the energy levels. In this region, the strongest lines at 500°C belong to the partially forbidden series, e.g., those with $\Delta K_{-1}=+1$, $\Delta K_1=-3$. For example, the strongest components of the strong series of incompletely resolved lines at 911, 961, 1012, 1062 cm^{-1} are believed to be the transitions $18_{-11}-17_{-15}$, $19_{-13}-18_{-15}$, $20_{-13}-19_{-17}$, $21_{-15}-20_{-17}$, $\cdots$. These lines have strengths of the order of 0.2, and should be strong, as observed, since $E''\cong 4000$ cm^{-1}. It would appear that transitions of this nature might readily lead to complete opacity in the spectral region around 10μ, with only moderate increase in temperature and optical density above those used in the present studies. This fact must be considered in making calculations of the emissivity of H_2O at elevated temperatures.

The poorly resolved absorption in the long-wavelength wings of the 6μ vibration rotation band, which overlaps the pure rotation from 900–1100 cm^{-1}; and the slightly better-resolved absorption in the short-wavelength wing, from 1900–2500 cm^{-1}, may also be recognized as agreeing with the expected absorption at 500°C, as calculated from the assignments made from the higher-resolution 110°C studies. Tentative assignments of some of the higher energy levels of ν_2 may also be made, by extending the series to higher J values. The resulting energy levels are included in Table III.

The high temperature studies also appear to confirm the fact that there are anomalies in the line-strengths of this vibration-rotation band. If the line-strengths were those characteristic of a rigid rotator with equal asymmetry in the upper and lower vibrational states, calculation shows that, in a given frequency interval at a given difference from the band origin, the R branch intensity should be greater than the P branch intensity. The observed absorption is, however, greater on the low-frequency side; for example, the region 1250–1350 cm^{-1} shows more nearly complete absorption than the region 1850–1950 cm^{-1}. This confirms observations made on the basis of individual resolved lines, and indicates that the assumption that the transition probabilities are those of a rigid asymmetric rotor is not fulfilled in this vibration-rotation band. Such anomalous intensities appear to be common in water-type molecules, and are probably due principally to the failure of the assumption that the transition probability can be factored into purely rotational and purely vibrational portions.[20]

The anomalous intensities appear most prominently in the "partially forbidden" branches. For example, lines of the series with $\Delta J=-1$, $\Delta K_{-1}=-1$, $\Delta K_1=+3$: $8_{-6}-9_{-2}$, $9_{-7}-10_{-3}$, and $10_{-8}-11_{-4}$ at 1149.5, 1106.7, and 1060.1 cm^{-1} are strong ($\sim$50 percent absorption for the high-steam-content path at 511°C) whereas, with comparable amounts of H_2O and comparable slits, the corresponding lines of the series with $\Delta J=+1$: $9_{-2}-8_{-6}$, $10_{-3}-9_{-7}$, and $11_{-4}-10_{-8}$ at 2100.5, 2145.4, and 2194.5 cm^{-1} are barely observable ($\sim$20 percent absorption). Since the Boltzmann factors and terms involving ν in the intensity formula favor the R branch lines, it would appear that the line strengths differ by factors of from 5–10. They should be, in the first approximation, equal. Similar behavior may be observed in a number of the other lines, particularly at high J. A more quantitative study of this phenomenon is desirable, and will be undertaken in the near future.

CO_2

The absorption spectra of CO_2 at 500°C showed a number of Q branches in the regions 545–860 cm^{-1} and 2077–2160 cm^{-1}. The transitions responsible for these bands are all of the type in which the bending vibration, ν_2, changes by an odd number of quanta. Because of the resonance between ν_1 and $2\nu_2$, the energy levels when $V_2\geqslant 2$ are split. The result is that the single-quantum changes in the 15μ region cover a wide frequency range, as observed. A further result is that the expected intensity of a transition in ν_2, as for example $0\,4^2-0\,3^1$, is distributed among a number of the resonating levels: in the above example there would be four bands, $0\,4^2-0\,3^1$, $1\,2^2-0\,3^1$, $0\,4^2-1\,1^1$, and $1\,2^2-1\,1^1$.

The transitions in the 4.7μ region correspond to 3-quantum changes, of the type $\left\{\begin{matrix}1\,1^1\\ \\ 0\,3^1\end{matrix}\right.\!\!-0\,0\,0\!\left.\right\}$, etc. It is a poorly understood empirical fact that despite the close resonance in energy between the $1\,1^1$ and $0\,3^1$ levels, the intensity of the former band is much the greater.

[19] See Bass, Benedict, and Plyler, Paper H-4, "Symposium on Molecular Structure and Spectroscopy," Ohio State University, (1951).

[20] H. H. Nielsen, Phys. Rev. 83, 838 (1951).

All of the expected transitions in the long-wave region, involving levels up to $V_2'=4$, together with a few of the higher transitions, were listed in Table II. The table gives the position of the Q branch, both as observed and as calculated from levels obtained in a manner to be described presently, the calculated relative transition probability, $gR^{v'v''}$, and the calculated intensity at 773°K, obtained from the formula $I=gR^{v'v''}e^{-E''/kT}$, relative to 100 for the fundamental. The transition probabilities are only approximate, being based on the harmonic-oscillator approximation, together with the oversimplified assumption that the resonance between $2\nu_2$ and ν_1 is exact. (The correct value for the two lowest resonating pairs is in the neighborhood of 0.56:0.44 instead of 0.5:0.5 as assumed here.)

Inspection of Table II, and comparison with the figures, shows that nearly all of the transitions to levels up to $V'=4$ have been observed. Those that are still missing are either those that are of low intrinsic probability, being components of $l=0$ resonating groups in which there are many transitions, or which fall in the regions of strong absorption. The observed intensities do not agree in detail with those calculated, but follow the correct general trend. The lack of detailed agreement is to be expected, since the calculation is a grossly oversimplified first approximation.

The observed bands in the 5μ region, together with a few of the expected unobserved bands from the lower excited levels, are also presented in Table II. The calculated intensities are based on the much oversimplified assumption, which, however, is empirically true for the ground-state doublet, that all the intensity of the resonating pairs is concentrated in the highest frequency member. The assignment of the strongest bands is quite unambiguous, and together with the long-wave observations provides values for the energy of a number of the higher levels that had previously been unobserved or in doubt. Our band at 2129.0 cm^{-1}, which is observable at room temperature, was reported previously[10] to be at 2137 cm^{-1}. Inspection of the authors' published curve shows, however, that their wavelength reduction must have been in error.

By combining the observations in the 15μ and 5μ regions, together with high-resolution results, it is possible to derive empirical values for the vibrational energy levels of CO_2. The "calculated" band origins of Table II are the appropriate differences of these levels. In Table IV, the empirical values are collected and compared with values calculated from newly derived molecular constants. These differ slightly from previous constants, inasmuch as the observation of levels of high l such as the resonance pairs ($0\,4^2-1\,2^2$) and ($0\,5^3-1\,3^3$), and $0\,3^3$, $0\,4^4$ and $0\,5^5$ yielded data which could not be obtained by observation at room temperature since such levels do not combine with the ground state. It has previously been attempted[11,21] to fit all the accurately known levels to a formula of the usual type,

$$G=\nu_1V_1+\nu_2V_2+\nu_3V_3+x_{11}(V_1^2-V_1)+x_{22}(V_2^2-V_2)+x_{ll}(l^2-V_2)+x_{33}(V_3^2-V_3)+x_{12}V_1V_2+x_{13}V_1V_3+x_{23}V_2V_3$$

together with the usual perturbation treatment in which all levels with V_1-1, V_2, l, $V_3=V_1$, V_2-2, l, V_3 mutually interact, with the perturbation parameter $\beta[(V_2^2-l^2)V_1]^{\frac{1}{2}}$. It was found that the known levels could not be fitted with perfect accuracy, presumably because of the necessity for higher terms in the formula. Moreover, it appeared that a single value of the constant, β, could not fit all the resonance pairs and triplets, but that better agreement with experiment could be obtained if β decreased with increasing quantum number, as it would be expected to do in higher approximation. The new additional data confirm this latter finding and are in rather good agreement otherwise with the previously suggested constants. To demonstrate the necessity for the variation of β with V, note that the separation of the levels $\Delta G_1=100-02^00$, $\Delta G_2=11^10-03^10$, $\Delta G_3=12^20-04^20$, $\Delta G_4=1\,3^3\,0-0\,5^3\,0$

TABLE IV. Low vibrational energy levels of CO_2.

V_1	V_2	l	ν_{calc} cm^{-1}	ν_{obs} cm^{-1}
0	0	0	0.00	0.00
0	1	1	667.30	667.30
0	2	0	1285.60	1285.6
1	0	0	1388.30	1388.3
0	2	2	1335.16	1335.4
0	3	1	1932.64	1933.2
1	1	1	2076.62	2077.0
0	3	3	2003.58	2003.7
0	4	0	2549.63	2551.1?
1	2	0	2672.91	2673. ?
2	0	0	2796.28	2796.5
0	4	2	2584.98	2584.9
1	2	2	2760.25	2760.4
0	4	4	2672.56	2672.8
0	5	1	3183.75	...
1	3	1	3340.52	...
2	1	1	3498.73	3502.0
0	5	3	3240.95	3241.3
1	3	3	3442.39	3442.3
0	5	5	3342.10	3341.8
0	6	0	3798.02	...
1	4	0	3946.43	...
2	2	0	4066.75	...
3	0	0	4220.68	4224.1
0	6	2	3841.33	...
1	4	2	4016.68	...
2	2	2	4170.85	...
0	6	4	3898.96	...
1	4	4	4123.24	4122.7
0	6	6	4012.20	...

[21] D. M. Dennison, Revs. Modern Phys. 12, 175 (1940).

should be given by the formulas

$$(\Delta G_1)^2 = 4\beta^2 + \delta_1^2,$$
$$(\Delta G_2)^2 = 8\beta^2 + (\delta_1 + x_{12} - 4x_{22})^2,$$
$$(\Delta G_3)^2 = 12\beta^2 + (\delta_1 + 2x_{12} - 8x_{22})^2,$$
$$(\Delta G_4)^2 = 16\beta^2 + (\delta_1 + 3x_{12} - 12x_{22})^2,$$

where $\delta_1 = \nu_1 - 2\nu_2 - 2x_{22} + 2x_{ll}$ and the other constants are as defined above. δ_1 cannot be observed directly, but from the relative rotational constants of the resonating levels, it must be small, so that the second term in the above equations must be very small compared to the β^2 terms. (Our analysis leads to $\delta_1 = 11.82$ cm^{-1}, Dennison's constants to $\delta_1 = 16.7$ cm^{-1}; the difference is negligible for the present argument.) The observed values of the $(\Delta G_i)^2$ are, respectively, 10547, 20678, 30800, and 40401 cm^{-2}; hence there are no possible real values of δ_1, x_{12} or x_{22} that can fit these with a constant β. The exact form of the dependence of β on the quantum numbers has not been worked out, but a much improved empirical fit of all the data is obtained if one assumes the reasonable form,

$$\beta_{\text{eff}}^2 = \beta^2[1 - \beta_2\{[(V_2^2 - l^2)V_1]^{\frac{1}{2}} - 2\} - \beta_3 V_3].$$

The following values of the constants, which differ only slightly from previously proposed sets,[11,21] have been used: $\nu_1 = 1342.86$, $\nu_2 = 667.30$, $\nu_3 = 2349.30$, $x_{11} = -2.20$, $x_{22} = -0.75$, $x_{ll} = 1.03$, $x_{33} = -12.50$, $x_{12} = 3.76$, $x_{13} = -21.84$, $x_{23} = -11.58$, $\beta = 72.14$, $\beta_2 = 0.0250$, $\beta_3 = 0.0095$. These yield values of the energy levels which are compared with observed values in Table IV. The agreement is satisfactory. Many additional higher levels, involving ν_3, have been observed, and were considered in deriving the constants; since they do not fall in the region studied here, except in so far as unresolved upper-state satellites of ν_3 contribute to the absorption near 4.5μ, they are not included at this time.

It may be pointed out that the upper-state bands in the 15μ region, as listed in Table II, will make appreciable contributions to the absorption of long columns of CO_2 gas at room temperature. A number of them have indeed been identified in the absorption of solar radiation by the entire atmosphere[8,22]; others undoubtedly will be noticeable, when high-resolution studies can be made in the region of 700–750 and 450–620 cm^{-1}. They must also contribute importantly to the absorption in the wings of the 15μ region, recently studied by Cloud in this laboratory.[23] Although the total intensity of upper-state bands is low compared to that of the 667.3 cm^{-1} band, at room temperature, their origins lie so far from the central band that at frequencies more than 100 cm^{-1} from 667 cm^{-1}, the absorption caused by the upper-state transitions is much more important than that caused by high-J rotational lines of the fundamental, or to the absorption in the distant wings of the strong low J lines. Moreover, since there are a number of these bands of comparable intensity, and since R and P branch lines of both odd and even J occur in transitions between levels in which l for both the upper and lower states is not zero, the average spacing between lines, in regions such as 540–580 and 740–780 cm^{-1}, will be very much less than 1.6 cm^{-1}. These facts must be borne in mind in applying treatments such as those of Elsasser[24] or Kaplan[25] to the calculation of the total band absorption and the exchange of radiant energy in the atmosphere.

[22] A. Adel, Astrophys. J. **94**, 375, 379, 451 (1941).
[23] W. H. Cloud, "The 15-micron band of CO_2 broadened by nitrogen and helium," ONR-Johns Hopkins Report, (January 1, 1952).
[24] W. M. Elsasser, Phys. Rev. **54**, 126 (1938).
[25] L. Kaplan, J. Chem. Phys. **18**, 186 (1950).

Energy Transfer by Collisions in *Cis*- and *Trans*-Dichloroethylene Vapors*

D. SETTE,† A. BUSALA, AND J. C. HUBBARD
Department of Physics, The Catholic University of America, Washington, D. C.

(Received June 12, 1952)

Some recent measurements by Sette of ultrasonic absorption in liquid halogenated hydrocarbons have indicated strong structural differences upon which, it was hoped, further light would be given by a study of some of these compounds in the vapor state. Ultrasonic velocity and absorption in *cis*- and *trans*-dichloroethylene have been measured at 34.7°C, at frequencies of 0.425, 1.985, and 2.982 Mc sec^{-1} and at pressures from 12 to 250 mm Hg, giving a range of f/p of 1.27 to 125 Mc/sec atmos. The results show that energy equilibrium in the molecule is more quickly attained in the *trans*- than in the *cis*-form. Without consideration of departure from the ideal gas law, the results may be explained by the assumption of two regions of f/p in which relaxation occurs, one relaxation frequency of 3.5 Mc/sec atmos being common to both, there being also one of 30 for the *cis* and 90 for the *trans*. The molecular absorption per wavelength computed from dispersion data are in good qualitative agreement with those measured. The values of C_v/R for both forms fall from 7.5 at one Mc/sec atmos to about 3.5 at 100 Mc/sec atmos. The results indicate the pre-eminent importance of short-range forces in determining the energy transfer by collisions.

INTRODUCTION

UNTIL the present, no clear-cut connection has been established between the ultrasonic behavior of a liquid and its vapor. It is to be expected that the vapors of normal liquids will not show associative effects and therefore that the corrections for "idealization" of ultrasonic velocity are small at moderately low pressure. Otherwise, as consequence of a progressive departure from the ideal gas law at increasing pressure, a noticeable dispersion of velocity will occur as well as a possible relaxation effect due to the Einstein effect, besides the thermal dispersion of Herzfeld and Rice.

Experiments with the two liquids, *cis*- and *trans*-dichloroethylene show similar linearly rising values of α/ν^2 between -20°C and 50°C.[1] Both liquids show a large excess of experimental over classical values of the absorption coefficient. The coefficient for the *cis*-compound in the liquid state is generally about 50 percent larger than that for the *trans*; the *cis*-form has a dipole moment of 1.9*d*, while the *trans*-form has none. This large difference in the behavior of the two similar compounds in the liquid state makes it desirable to examine them in the gaseous state. For this reason measurements of sound velocity and absorption have been made in their vapors. It is found that the two forms in the gaseous state also show well-differentiated behavior.

The interpretation of results in the vapors has been considered only in terms of relaxation times based upon transfer by collisions of energy between translational and vibrational modes. Some indication in fact was obtained that under the experimental conditions no large deviation from the ideal gas law was present in the behavior of the two vapors.

TABLE I. *Cis*-dichloroethylene. $t=34.7$°C. All absorptions here are computed from asymptotic data (reference 2, E. E. Swomley).

f, Mc/sec	p, mm Hg	f/p, Mc atmos^{-1}	V, m sec^{-1}	α, cm^{-1}
0.4250	195.6	1.65	173.0	1.2
0.4283	118.8	2.74	174.0	2.5
	79.2	4.11	174.2	3.0
	49.5	6.57	175.7	3.6
	29.5	11.03	176.8	1.6
2.9827	182.0	12.46	176.0	
1.9868	93.1	16.22	177.5	21
2.9827	122.1	18.57	178.2	
	75.9	29.86	179.4	43
	57.4	39.49	180.9	
1.9868	30.4	49.67	182.0	34
2.9827	36.6	61.82	180.7	
1.9868	21.2	71.24	181.5	26
2.9827	25.9	87.52	182.5	
1.9868	14.9	101.36	182.6	39
	12.2	123.76	183.1	34

METHOD AND APPARATUS

Ultrasonic velocity and absorption in the two vapors have been measured by the acoustic resonator interferom-

TABLE II. *Trans*-dichloroethylene. $t=34.7$°C.

f, Mc/sec	p, mm Hg	f/p, Mc atmos^{-1}	V, m sec^{-1}	α, cm^{-1}
0.4251	253.5	1.27	172.4	
	181.9	1.77	173.0	1.9
	110.2	2.93	173.6	1.3
	61.1	5.28	174.3	2.5
1.9847	249.2	6.05	172.5	5.9[a]
	231.0	6.53	173.1	4.4[a]
	190.0	7.94	174.1	6.0[a]
0.4251	40.5	7.97	174.5	3.3
1.9847	132.8	11.36	174.4	5.7
	97.0	15.55	175.7	12[a]
	69.6	21.67	175.5	
	48.7	30.97	175.3	20
1.9867	48.8	30.94	175.1	36
	35.4	42.65	177.3	35
1.9847	27.9	54.06	178.7	
1.9867	20.4	74.02	179.4	38
1.9847	16.4	91.97	182.5	
	13.9	108.51	181.3	46
1.9866	12.1	124.79	183.4	72

[a] By peak-width method. Other absorptions by asymptotic data (see reference 2).

* This work was supported by the ONR.

† Istituto di Ultracustica, Rome, Italy. At present at the Catholic University of America.

[1] D. Sette, J. Chem. Phys. 19, 1337–1341 (1951).

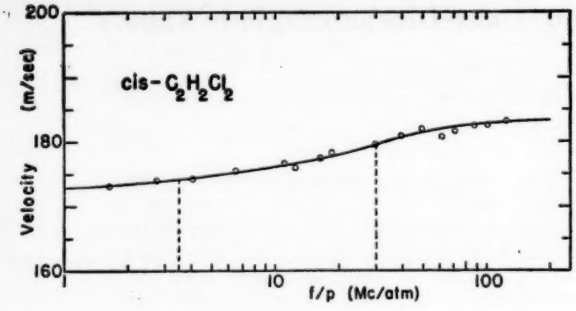

FIG. 1.

eter. The interferometer chamber is of the tubular form with the quartz crystal plate and moving piston, presenting plane surfaces perpendicular to the axis of the tube and covering the tube cross section. The crystal of the interferometer is connected across the terminals of the variable capacitor of a simple resonant circuit, loosely coupled to the output of a tuned rf amplifier driven by an electron-coupled oscillator. Oscillator and amplifier are powered by batteries.

Currents in the resonant circuit, with and without connection with the crystal, are measured by a vacuum thermocouple and a highly sensitive Leeds and Northrup galvanometer. Adjustments necessary and treatment of results have been well covered in several publications.[2]

EXPERIMENTAL RESULTS

The principal data, including frequency, f, Mc/sec; pressure, p, mm Hg; ultrasonic velocity, V, m/sec; and amplitude absorption coefficients, α, cm^{-1}; are shown in Tables I and II for *cis*- and *trans*-dichloroethylene, respectively.

The results for the two vapors cannot be represented within the experimental error by the assumption of one relaxation frequency for either. The assumption of two is, however, sufficient in each case. For this purpose, when the relaxation frequencies, f_{w1} and f_{w2}, are well separated as in this case, the following relation can be used:

$$V^2=V_0^2+a(f/f_{w1})^2/[1+(f/f_{w1})^2]+b(f/f_{w2})^2/[1+(f/f_{w2})^2], \quad (1)$$

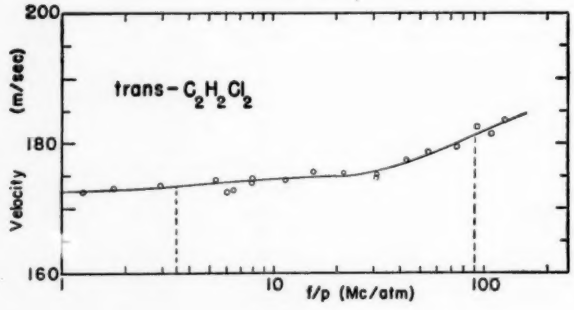

FIG. 2.

[2] See for example R. S. Alleman, Phys. Rev. **55**, 87 (1939); J. L. Stewart, Rev. Sci. Instr. **17**, 59 (1946); E. E. Swomley, Phys. Rev. **69**, 632 (1946).

in which f now stands for f/p and

$$a=V_1^2-V_0^2; \quad b=V_2^2-V_1^2, \quad (2)$$

where V_0 is the low frequency limit of the acoustic velocity, V_1 is at the same time the upper limit of velocity for the low frequency relaxation and the lower limit for the higher frequency relaxation, and V_2 is the upper limit for the high frequency relaxation.

We may put

$$V_{w1}^2=V_0^2+a/2; \quad V_{w2}^2=V_0^2+a+b/2. \quad (3)$$

The results for velocity as a function of f/p are well represented for the two vapors using the constants given in Table III.

The velocity data for the *cis*- and the *trans*-vapors are shown in Figs. 1 and 2, circles representing experimental values, and smooth curves those calculated from Eq. (1), using the constants of Table III.

In considering the results, the approximation has been made that the vapors of those unassociated liquids follow the ideal gas law. This really is not true, but idealization could not be done for the lack of data on the virial coefficients of the vapors. At the pressures used (12–200 Hg mm), however, it is not to be expected that their behavior deviate from that of ideal gases so strongly as to influence seriously the preceding calculations.

TABLE III. Relaxation constants.

Cis-dichloroethylene		*Trans*-dichloroethylene	
Mc/sec atmos	V, m/sec	Mc/sec atmos	V, m/sec
$f=0$	$V_0=172.6$	0	172.4
$f_{w1}=3.5$	$V_{w1}=174.1$	3.5	173.4
$f_{w2}=30$	$V_{w2}=179.5$	90	181.1
$f=\infty$	$V_2=183.5$	∞	187.6

Specific Heat

The values of C_v/R are shown for the two vapors in Figs. 3 and 4. They have been calculated using the equation

$$C_v/R=1/[(V^2M/RT)-1]. \quad (4)$$

The values range from 7 at 3 Mc/sec atmos to about 3.5 at 120 Mc/sec atmos for both vapors. In each case there is an indication of a plateau of C_v/R values of about 6, corresponding to f/p values of about 7 and 9 Mc/atmos, respectively, for the *cis*- and *trans*-vapors, or to respective V_1 values of 175.5 and 174.4 m/sec.

The values of C_v obtained from the low frequency velocity (Table III) are:

Cis-dichloroethylene, $V_0=172.6$ m/sec, $C_v=7.84$ R,
Trans-dichloroethylene, $V_0=172.4$ m/sec, $C_v=7.96$ R.

They can be compared with those calculated from spec-

troscopic data. The twelve vibration frequencies[3] and their contribution to the specific heat at constant volume at 34°C are given in Table IV. Adding 3 R for the translational and rotational contributions, the following figures are obtained:

Cis-dichloroethylene, $C_v=6.98$ R,
Trans-dichloroethylene, $C_v=7.16$ R.

The specific heats calculated in both ways for the *trans*-form are slightly higher than those for the *cis*. A difference exists, however, between the specific heats of the same compound calculated in the two ways. This difference may be accounted for by the fact that the ideal gas law has been assumed in using Eq. 4, so that in the evaluation of C_v from sound velocity data no account has been taken of deviation from the ideality of gases. The value of sound velocity in each vapor calculated using the C_v obtained from spectroscopic data, and the ideal gas law differs from the experimental value by about one meter/sec.

TABLE IV.

Cis-dichloroethylene $\bar{\nu}$, cm^{-1}	C_v/R	*Trans*-dichloroethylene $\bar{\nu}$, cm^{-1}	C_v/R
3077	0.0001	3071	0.0001
1587	0.0329	1576	0.0342
1179	0.1232	1270	0.0931
711	0.4269	844	0.3124
173	0.9471	349	0.8073
876	0.2961	895	0.2732
406	0.7467	192	0.9214
3072	0.0001	758	0.3838
1294	0.0867	3080	0.0001
848	0.3089	1200	0.1154
571	0.5698	817	0.3347
697	0.4413	265	0.8813
$\Sigma C_v/R=3.98$		$\Sigma C_v/R=4.16$	

The experimental data do not allow the determination of the vibrations involved in each relaxation because several vibrations have close frequency values. The difference of about 4 R between the low and the high frequency values of the specific heat seems to indicate that all the vibrations are relaxed in the two relaxation ranges.

Absorption

Absorptions per cm shown in Tables I and II have been reduced to absorptions per wavelength for convenient comparison of results of measurement with quartz plates of different frequency. We have computed the absorption per wavelength, using the dispersion formula of Kneser,

$$\alpha\lambda=\frac{\pi(Q_1^2-1)f/f_{w1}}{1+Q_1^2(f/f_{w1})^2}+\frac{\pi(Q_2^2-1)f/f_{w2}}{1+Q_2^2(f/f_{w2})^2}, \qquad (5)$$

[3] H. J. Bernstein and D. A. Ramsey, J. Chem. Phys. **17**, 556 (1949).

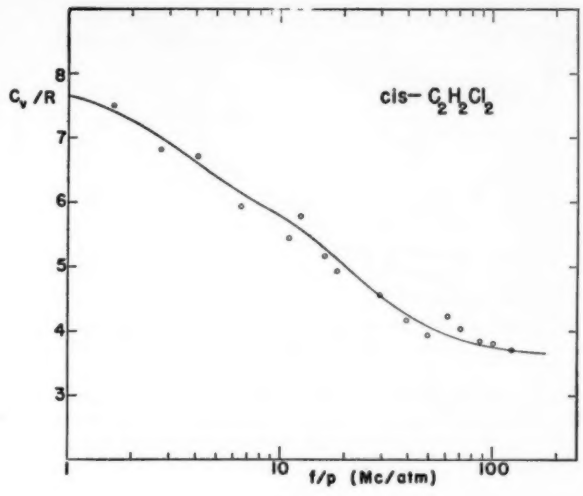

FIG. 3.

where

$$Q_1=V_1/V_0; \quad Q_2=V_2/V_1. \qquad (6)$$

The frequency f_m of maximum absorption is related to the relaxation frequency by

$$f_m=(V_0/V_1)f_w, \qquad (7)$$

or in the case of two relaxation frequencies by

$$f_{m1}=(V_0/V_1)f_{w1}; \quad f_{m2}=(V_1/V_2)f_{w2}. \qquad (8)$$

By using values of f and V in Table III, we have for maximum absorption frequencies and for the Q's of Eq. (5) the values given in Table V.

The values of $\alpha\lambda$ obtained from the experimental data (circles) and from Eq. (5) (dashed curves) are shown in Figs. 5 and 6. It is to be observed that for the experimental points the values of α of Tables I and II were used, without attempting to separate the classical absorption. The absence of data of viscosity and heat

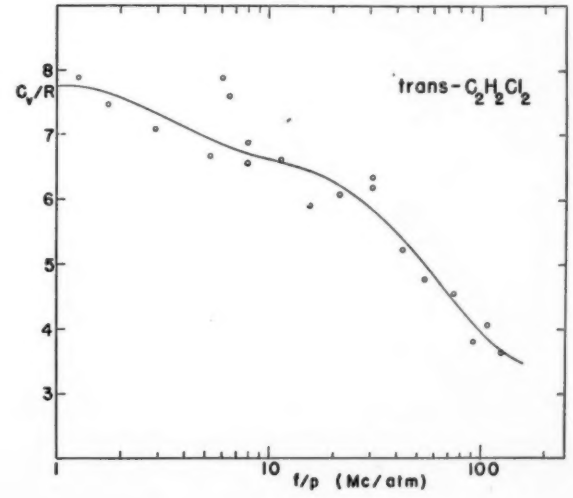

FIG. 4.

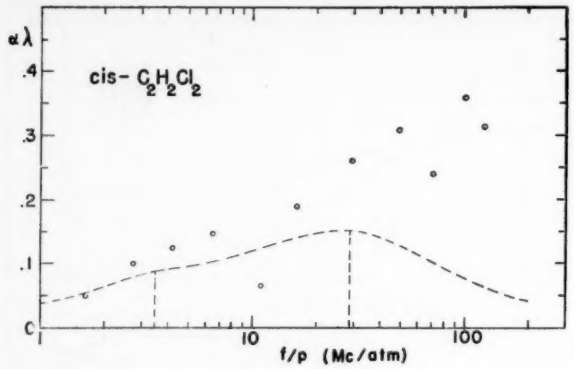

FIG. 5. Circles give experimental values of amplitude absorption multiplied by acoustic wavelength. The dashed curve shows acoustic molecular absorption per wavelength computed from the dispersion results.

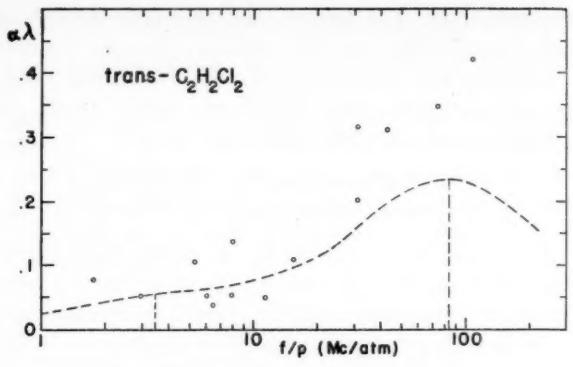

FIG. 6. See caption of Fig. 5.

conduction for the two vapors did not allow this calculation.

In the comparison between experimental and theoretical values of $\alpha\lambda$, it is also to be considered that the precision of absorption coefficients obtained with these kinds of measurements is not high. A quantitative comparison is therefore not possible, while a rough qualitative agreement is apparent.

CONCLUSION

Velocity of propagation of sound waves and their absorption have been studied in the two isomers, *cis*- and *trans*-dichloroethylene in the f/p range between 1.27 and 125 Mc/atmos.

Relaxation phenomena have been found which have to be ascribed to the energy exchange between translational and vibrational degrees of freedom. Practically all the vibrations of the molecules are involved in the phenomena observed, although large differences in the relative relaxation times are present. The experimental results seem satisfactorily described by the assumption of only two relaxation times in each case.

The equilibrium distribution of energy between external and internal degrees of freedom is attained more quickly in the *trans*-form which has no dipole moment than in the *cis*-dichloroethylene with a considerable one. This seems to prove that the long range forces do not change the order of magnitude of the probability of transitions between translational and vibrational energy states. The efficiency of collisions seems, therefore, essentially determined by short-range forces, at least in the temperature range studied.

TABLE V.

	Cis-dichloroethylene	*Trans*-dichloroethylene
f_{m_1}	3.44 Mc/atmos	3.46 Mc/atmos
f_{m_2}	28.69 Mc/atmos	83.7 Mc/atmos
Q_1	1.0171	1.0115
Q_2	1.0455	1.0758

The Near Ultraviolet Absorption Spectra of 1,4 Bis-(Trifluoromethyl)Benzene and 1,3,5 Tris-(Trifluoromethyl)Benzene

C. D. Cooper and F. W. Noegel
Department of Physics, University of Georgia, Athens, Georgia

(Received June 27, 1952)

The vapor absorption spectra of 1,4 $C_6H_4(CF_3)_2$ and 1,3,5 $C_6H_3(CF_3)_3$ have been obtained with a Bausch and Lomb Littrow spectrograph. Corresponding solution spectra were obtained with a Beckman DU spectrophotometer. Oscillator strengths f were found to be 12.0×10^{-3} and 2.1×10^{-3} for the *para* di- and tri-substituted compounds, respectively. Both of the vapor spectra are diffuse with the bands of the 1,3,5 compound showing extreme diffuseness. The 0,0 band of the 1,4 bis-(trifluoromethyl)benzene is located at 37460 cm^{-1}. Progressions and combinations involving the upper state frequencies of 210, 770, and 1020 cm^{-1} are observed. The 210 and 1020 values are correlated with the observed ground state values of 240 and 1070 cm^{-1}, and these are associated with totally symmetric vibrations. The 1,3,5 tris-(trifluoromethyl)benzene spectrum is interpreted as a "forbidden" one and the bands at 38670 and 38070 cm^{-1} are assigned as 0,1 and 1,0 bands, respectively. Rough calculations show the 0,0 band to be shifted about 300 cm^{-1} toward the violet relative to the benzene spectrum.

INTRODUCTION

IN extending the research on substituted benzenes it was decided to investigate the near ultraviolet spectra of *para* bis-(trifluoromethyl)benzene, 1,4 $C_6H_4(CF_3)_2$, and symmetrical tris-(trifluoromethyl)-benzene, 1,3,5 $C_6H_3(CF_3)_3$. These spectra should provide us with more information concerning the spectral shift produced by different substituents attached to the benzene ring, as well as some interesting comparisons with the spectra of *para*-xylene,[1] *para*-fluorobenzotrifluoride,[2] and mesitylene.[3] A search of the literature reveals that no spectral data have been reported for either 1,4 bis-(trifluoromethyl)benzene or 1,3,5 tris-(trifluoromethyl)benzene.

EXPERIMENTAL PROCEDURE

A Bausch and Lomb Littrow spectrograph was used to photograph the absorption vapor spectra. The continuum of ultraviolet light was supplied by a Beckman hydrogen lamp, and an iron spectrum was used as a comparison spectrum. Light from the hydrogen lamp was made approximately parallel by a quartz condensing lens and then allowed to pass through a 75-cm quartz absorption cell to a cylindrical lens which focused the light on the 15-micron spectrographic slit. The iron arc and a second condensing lens were set up at right angles to the above optical path, and a removable right angle prism was used to direct the light through the cylindrical lens to the slit.

The samples used in this research were given to us by the Chemistry Department of Duke University.* The 1,3,5 tris-(trifluoromethyl)benzene has a boiling point of 120°C and the 1,4 bis-(trifluoromethyl)benzene has a boiling point of 116°C. A study of the ultraviolet spectra shows no obvious traces of any impurities in the samples. In each case samples were loaded into the absorption cells in the following manner. An ampoule of the sample and an absorption cell were sealed to a vacuum system. The sample was outgassed and then by

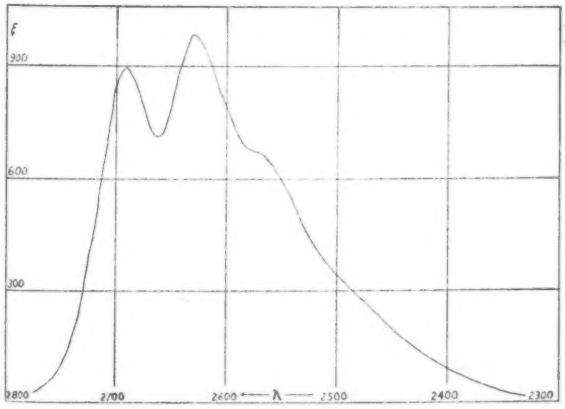

FIG. 1. Solution spectrum of *para* bis-(trifluoromethyl)benzene.

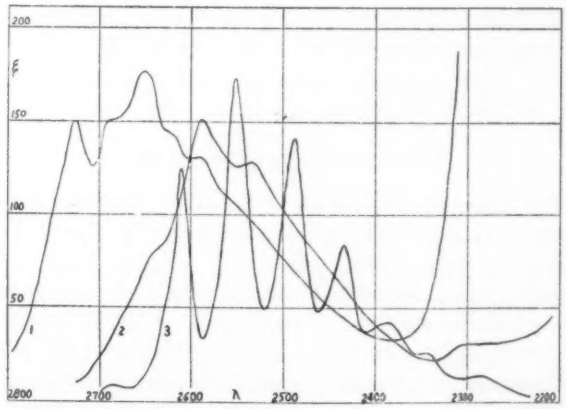

FIG. 2. Comparison of solution spectra of (1) mesitylene, (2) symmetrical tris-(trifluoromethyl)benzene, and (3) benzene.

[1] C. D. Cooper and M. L. N. Sastri, J. Chem. Phys. **20**, 607 (1952).
[2] W. T. Cave and H. W. Thompson, Disc. Faraday Soc. **9**, 35 (1950).
[3] H. Sponer and M. J. Stallcup, paper in V. Henri Memorial Vol., *Contributions à l'Étude de la Structure Moléculaire* (Desoer, Liège, 1948), p. 222.

* We are grateful to Dr. L. Bigelow for this gift.

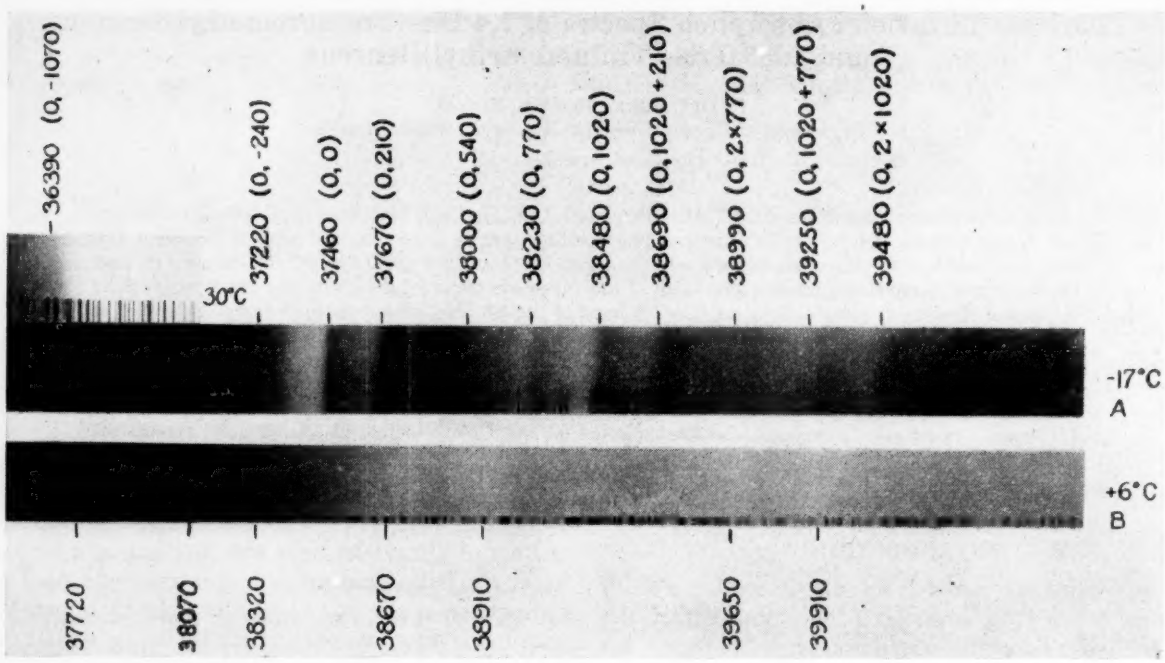

FIG. 3. A. Vapor absorption spectrum of 1,4 bis-(trifluoromethyl)benzene. B. Vapor absorption spectrum of 1,3,5 tris-(trifluoromethyl)benzene.

vacuum distillation the middle fraction was collected in the sidearm of the absorption cell. Following the distillation the sidearm containing the sample was immersed in a dry ice and acetone bath, and the cell was evacuated to a pressure of 10^{-6} mm of Hg. The cell was then sealed and removed from the system. After the cell was placed in the light path, the vapor pressure of the substance was controlled by a Dewar flask filled with suitable freezing mixture which enclosed the sidearm containing the liquid sample.

Eastman Kodak II-0 spectroscopic plates were utilized to record the spectra, and exposure times varied between 30 and 60 minutes. The plates were developed in D-19 for 3 minutes at 20°C. A Bausch and Lomb hand magnifier was used to measure the bands. The diffuseness of the band heads involved prevents measurements that are more accurate than the nearest angstrom.

The solution spectra were obtained with a Beckman DU spectrophotometer.

EXPERIMENTAL RESULTS

The absorption spectrum of 1,4 bis-(trifluoromethyl)-benzene in iso-octane solvent is shown in Fig. 1. The molecular extinction coefficient is plotted here as a function of wavelength. From the area under the curve the oscillator strength f was found to be 12.0×10^{-3}. Figure 2 shows the solution absorption of 1,3,5 tris-(trifluoromethyl)benzene, mesitylene, and benzene as a function of wavelength. Iso-octane was the solvent for all three compounds. Figure 2 shows that the spectral position of mesitylene is shifted to the red relative to the benzene spectrum, but the 1,3,5 tris-(trifluoromethyl)benzene spectrum is shifted toward the violet. An oscillator strength of 2.1×10^{-3} was found for 1,3,5 tris-(trifluoromethyl)benzene.

The vapor absorption spectrum of 1,4 bis-(trifluoromethyl)benzene lies between 2775A and 2450A. With a 75-cm absorption path the first evidence of absorption was obtained with the reservoir temperature at −40°C. For this temperature five broad bands at 2669A (37460 cm^{-1}), 2654A (37670 cm^{-1}), 2615A (38230 cm^{-1}), 2598A (38480 cm^{-1}), and 2584A (38680 cm^{-1}) are first detectable. As the temperature is increased other bands appear, as may be seen in Fig. 3. The bands show no fine structure and are broad and diffuse.

All of the measured bands are included in Table I. The first column contains the wavelengths, the second contains the corresponding wave numbers, and the next three columns show intensity estimates obtained by visual means at different temperatures. The scale used here as follows: ew—extremely weak, vw—very weak, w—weak, mw—medium weak, m—medium, ms—medium strong, s—strong, and vs—very strong. All bands reported here are diffuse, but to indicate very diffuse and extremely diffuse bands the designations vd and ed, respectively, are used in the intensity column. Bands not labeled with ed or vd are accurate to within 10 wave numbers. Those labeled with ed or vd are accurate to within 50 wave numbers. The sixth column gives the frequency difference between each band and the 0,0 band. Assignments are given in the last column.

The vapor absorption spectrum of 1,3,5 tris-(trifluoromethyl)benzene consists of about ten very broad, diffuse bands in the 2650 to 2400A region. Using a 75-

TABLE I. Vapor absorption bands of 1,4 bis-(trifluoromethyl)benzene.

Wavelength in A	Wave numbers in cm^{-1}	Intensity −30°C	Intensity −25°C	Intensity 12°C	Separation from 0,0 band	Assignments
2768	36,120			ew–ed	−1340	−1070−240?
47	390			vw	−1070	−1070
34	570			ew–ed	−890	−890?
03	980			ew–ed	−480	−2×240
				−20°C		
2686	37,220		vw	w	−240	−240
73	400			w–ed	−60	−60
69	460	m	ms	s	0	0,0
54	670	mw	m	ms	210	210
40	870	ew	vw	vw	410	2×210
31	38,000	ew	ew	vw–vd	540	540; 770–240
24	100	ew	ew	vw–vd	640	640; 3×210
15	230	w	m	ms	770	770
00	450		ms	s	990	770+210
2598	480	mw	m	ms	1020	1020
84	690	vw	m	m	1230	1020+210
79	760	ew	ew	ew	1300	2×640; 2×770−240
70	900	ew	ew	ew	1440	1020+2×210
64	990	ew	ew	ew	1530	2×770
55	39,130	ew	ew	ew	1670	1020+640; 1020+3×210
50	200	ew	ew	ew	1740	2×770+210
47	250	ew	ew	ew	1790	1020+770
		−19°C	−17°C	−20°C		
34	450	vw–ed	ew–ed		1990	1020+770+210
32	480	ew–ed	ew–ed	ew	2020	2×1020
19	690	vw–ed	ew–ed		2230	2×1020+210
16	730	ew–ed	ew–ed	ew	2270	3×770?
2499	40,000	ew–ed	ew–ed	ew	2540	2×770+1020
83	260	ew–ed	ew–ed		2800	2×1020+770

cm absorption cell, bands were first detected at a reservoir temperature of −12°C and complete absorption is observed in the above spectral region for temperatures above 8°C. Spectrograms exhibiting the most distinct bands were obtained for reservoir temperatures between −3 and 6°C. The bands do not form heads and most of them are from 150 to 200 cm^{-1} in width. Table II contains the experimental data relative to the vapor absorption spectrum. Here the centers of the bands in angstroms are recorded in the first column, with the corresponding wave numbers in the second column. The individual band widths in cm^{-1} are given in column three, visually estimated intensities in column four, and tentative assignments in the last column.

DISCUSSION

(A) 1,4 Bis-(trifluoromethyl)benzene

1, 4 Bis-(trifluoromethyl)benzene has D_{2h} symmetry if we treat each CF_3 group as one large atom. This is the same approximation made by Sponer and Lowe[4] in their interpretation of the benzotrifluoride spectrum. For this discussion the z axis has been chosen perpendicular to plane of the benzene ring and the y axis through the two CF_3 groups. Then the allowed electronic transition $^1A_{1g}-{}^1B_{3u}$ involved here has its transition moment in the x direction. As may be seen in Table I the 0,0 band of this transition is chosen to be 37460 cm^{-1} (2669A). This choice is validated by the apparent intensities of the bands and the appearance of certain progressions. On the violet side of the 37,460 cm^{-1} band, three members of a 210 cm^{-1} progression are observed at 37,670, 37,870, and 38,100 cm^{-1}, and on the red side of this 0,0 band two weak members of a 240-cm^{-1} progression appear at 37,220 and 36,980 cm^{-1}. The 210-cm^{-1} and 240-cm^{-1} frequencies are to be correlated with the excited and ground-state values, respectively, of a totally symmetric vibration. This vibration is not expected to be a pure substituent vibration since a check of the Raman values reported[5] for HCF_3 reveals that no fundamental frequency is found with values below 500 cm^{-1}. Raman data for 1,4 $C_6H_4(CF_3)_2$ has not been published, but for dibromobenzene Kohlrausch[6] has assigned a

TABLE II. Vapor absorption bands of 1,3,5 tris-(trifluoromethyl)benzene.

Centers of bands in A	Wave numbers	Width of band in cm^{-1}	Intensity at 6°C	Tentative assignments
2650	37,720	190	ew	$B-350$
26	38,070	180	vw	$B(1,0)$?
09	320	160	vw	$B+250$; $A-350$
2585	670	210	vs	$A(0,1)$?
69	910	250	vs	$A+250$
48	39,230	190	ms	$A+550$
21	650	130	s	$A+980$
05	910	190	s	$A+980+250$
2490	40,150	200	mw	$A+980+550$

[4] H. Sponer and D. S. Lowe, J. Opt. Soc. Am. **39**, 840 (1949).

[5] G. Glockler and W. F. Edgell, J. Chem. Phys. **9**, 224 (1941).

[6] K. W. F. Kohlrausch and O. Paulsen, Monatsh. Chem. **72**, 268 (1939).

strong Raman line of 215 cm^{-1} to the α_{1g} component of the ϵ_g^+(606 cm^{-1}) benzene vibration. Also if we compare the values assigned to this vibration in toluene[7] and benzotrifluoride,[4] and make the same comparison for *para*-xylene[1] and *para* bis-(trifluoromethyl)benzene, we find that the value expected in the latter compound is about 300 cm^{-1}. Then it appears that the 240 cm^{-1} and 210 cm^{-1} values are the respective ground- and excited state frequencies of the α_{1g}(606 ϵ_g^+ benzene vibration). An unambiguous assignment of the nontotally symmetric component of this vibration cannot be made at this time. The excited state frequency of this β_{1g} vibration may be represented by either of two very weak bands located at 38,000 and 38,100 cm^{-1}. These bands are separated by 540 and 640 cm^{-1} from the 0,0 band; however, both bands may easily be explained by a different assignment. Already the 640 cm^{-1} band has been assigned to 3×210 cm^{-1}, and the intensity of the 540 cm^{-1} band allows it to be assigned to a transition from a 240 cm^{-1} vibrational level in the ground state to a 770 cm^{-1} vibrational level in the excited state. Weak, temperature dependent bands on the red side of the 0,0 band that could be associated with the 540 and 640 cm^{-1} upper state values were not found. It is possible that such bands were unobservable because of the increasing diffuseness of the spectral bands with temperature.

Progressions and combinations involving the upper state frequencies of both 770 and 1020 cm^{-1} are observed Three members of the 770 cm^{-1} progression are located at 38230, 38990, and 39730 cm^{-1}. The only observed ground-state frequency that can be correlated with the excited state is 890 cm^{-1} as represented by the extremely diffuse band at 36570 cm^{-1}. The diffuseness prevents an accurate measurement of this band. Members of the 1020 progression are found at 38480 and 39480 cm^{-1}. A band at 36,390 is 1070 cm^{-1} toward the red from the 0,0 band and is taken as the ground-state value corresponding to the 1020 cm^{-1} upper-state frequency. Both the 770 and 1020 frequencies are to be associated with totally symmetric vibrations, but the particular mode of vibration is not certain. No doubt, one of them is to be correlated with the carbon breathing vibration, but previous assignments of such frequencies reported for other *para* di-substituted benzenes are in disagreement on this point.[6,8–10]

A comparison of the *para* bis-(trifluoromethyl)-benzene specturm (hereafter designated by *I*) with the *para*-fluorobenzotrifluoride spectrum (hereafter designed by *II*) is particularly interesting. The excited state frequencies of *II* have been reported[2] to be 283, 416, 538, 792, 1030, and 1231 cm^{-1}, while for *I* the values found are 210, 540?, 770, and 1020 cm^{-1}. There is close correspondence between these values except for the 416 and 1231 cm^{-1} frequencies in *II*; and bands corresponding to these in *I* could easily be masked by the broad diffuse bands assigned to the combinations $2\times$ 210 cm^{-1} and 1020+210 cm^{-1}. The two spectra differ widely whenever intensity and spectral position are considered. The 0,0 band in *I* is shifted about 630 cm^{-1} to the red from the 0,0 band of benzene. This shift is approximately twice that reported for benzotrifluoride and compares with spectra of the corresponding methylbenzenes. According to Thompson and Cave, the shift of the 0,0 band in *II* is less than in benzotrifluoride. A wide difference in intensity of absorption between *I* and *II* was expected[11] since both substituent CF_3 groups in *I* are *meta* directing while in *II* one group is *meta* directing and the other *ortho-para* directing.

(B) 1,3,5 Tris-(trifluoromethyl)benzene

Symmetrical tris-(trifluoromethyl)benzene has D_{3h} symmetry if the CF_3 groups are treated as single atoms. The expected electronic transition is the forbidden $A_1'-A_2'$ which is made allowed by an interaction with a ϵ' vibration. The transition moment involved lies in the molecular (x,y) plane. Spectra resulting from such forbidden transitions are expected to be weak, and the 0,0 band should be absent. The oscillator strength of 2.1×10^{-3} for 1,3,5 $C_6H_3(CF_3)_3$ is only slightly different from that reported for benzene.[4,11] This, plus the fact that both benzotrifluoride and 1,4 bis-(trifluoromethyl)-benzene absorb much more strongly than 1,3,5 $C_6H_3(CF_3)_3$, indicates that the spectrum discussed here is "forbidden."

The diffuseness of the vapor absorption spectrum introduces considerable uncertainty in any attempted interpretation. Measurements recorded in Table II represent the centers of bands that are from 150 to 200 cm^{-1} in width. Keeping this in mind, tentative assignments will be made. In the vapor spectrum the very strong band at 2585A (38,670 cm^{-1}) and the very weak band at 2626A (38,070 cm^{-1}) are chosen as 0,1 and 1,0 bands, respectively. Their separation of 600 cm^{-1} should represent the sum of the excited and ground-state values of the ϵ' vibration (ϵ_g^+ 606 benzene vibration). Then the ϵ' vibration involved here is expected to have a ground-state frequency between 300 and 350 cm^{-1}. Raman data should give us the correct frequency of this vibration, but such data have not been published. However, a comparison of the corresponding ϵ' frequencies in mesitylene and trichlorobenzene indicates that the above values are in the expected range. Using the average of the above values for the ϵ' vibration then the 0,0 band in symmetrical tris-(trifluoromethyl)benzene is calculated to be about 38,400 cm^{-1}.

There is apparently no serious argument against the above assignment of the 2585A and 2626A bands from intensity considerations. The intensity ratio of the

[7] Ginsburg, Robertson, and Matsen, J. Chem. Phys. **14**, 511 (1946).
[8] K. S. Pitzer and D. W. Scott, J. Am. Chem. Soc. **65**, 803 (1943).
[9] C. A. Beck, J. Chem. Phys. **18**, 1135 (1950).
[10] G. Nordheim and H. Sponer, J. Chem. Phys. **11**, 253 (1943).
[11] A. L. Sklar, J. Chem. Phys. **10**, 135 (1942).

corresponding bands in the solution spectrum at 2590A and 2640A is at least 4:1, taking into account the fact that the second band is partly overlapped by the first one. A calculation of the Boltzmann factors indicates that it should be 4 or 5:1, and visual observation of the vapor spectrum shows that the intensity ratio is in this range.

Labeling the 0,1 band A and 1,0 band B, the other bands in the vapor spectrum are assigned as in Table II. The upper-state frequencies are found to be roughly 250, 550, and 980 cm^{-1}, while a 350 cm^{-1} frequency is correlated with a vibration in the ground state. No attempt is made to assign these values to modes of vibration since the Raman spectrum is not known, but undoubtedly the 980 cm^{-1} is associated with a totally symmetric carbon vibration.

A comparison of the calculated 0,0 band in this spectrum with the calculated 0,0 band in benzene shows that the spectrum of 1,3,5 tris-(trifluoromethyl)benzene is shifted about 300 cm^{-1} toward the violet relative to the benzene spectrum. This shift is probably connected with the strong inductive effect of the CF_3 groups and is a subject for further theoretical considerations,[12] since present theories[13] assume that the shifts of the substituted spectra should always be toward the red relative to the benzene spectrum.

From a study of the two spectra reported here it is predicted that the spectra of 1,3 bis-(trifluoromethyl)-benzene will be diffuse and will show a violet shift relative to the benzotrifluoride spectrum.

[12] H. Sponer, Phys. Rev. **87**, 213 (1952).
[13] See for example, F. A. Matsen, J. Am. Chem. Soc. **72**, 5243 (1950).

THE JOURNAL OF CHEMICAL PHYSICS VOLUME 20, NUMBER 12 DECEMBER, 1952

The Cut-Off Phenomena of Protein Crystallography

ANDREW D. BOOTH
Birkbeck College Research Laboratory, University of London, London, England
(Received June 5, 1952)

The well-known paucity of experimentally observed reflections obtained from x-ray studies of protein single crystals, and their tendency to occur in well-marked spherical shells of reciprocal space, are examined quantitatively.

It is shown that, in the case of one protein for which data is available, a simple model with no assumed internal structure gives adequate agreement with experiment.

The addition of simple detail, such as nearest neighbor minimum approach distances, leads to further relations which could be used to produce improved agreement if required.

TWO noticeable features of x-ray single crystal photographs of biological substances are, firstly the generally low intensity of all reflections, and secondly the presence of annular regions in reciprocal space within which all reflections are so weak as to be unobservable.

For example, in the particularly simple protein ribonuclease Carlisle and Scouloudi[1] have observed minima at spacings of: 10.20A, 5.81A, 4.11A, 3.01A, 2.35A, 1.98A, 1.73A, 1.55A, 1.41A, etc.

In the case of normal and relatively simple organic compounds the data often extend, without obviously regular lacunae, to spacings of 0.8A or less, and it has been conjectured that the cut-off phenomena in proteins must be due to some cause other than the obvious one of thermal motion. In any case the latter could at the most account for only a single cut-off region embracing what may be called the first maximum of the whole effect.

It is the purpose of this paper to suggest an explanation of the simple phenomenon of generally low intensity which also accounts for the annular regions of low intensity which are so often a feature of the x-ray photographs of complex materials.

For the purposes of future reference Fig. 1 shows a radial intensity analysis of the (h, o, l) reflections of ribonuclease. This is derived by a smoothing process from data supplied by Dr. Carlisle and shows, at $A-I$, minima of the type described above.

Before entering into the quantitative aspects of the discussion it is necessary to examine the sources giving rise to the impressions recorded on an x-ray photograph. The most important are (a) Bragg reflection from the crystal, (b) air scatter from the primary and diffracted x-ray beams, (c) Compton scattering from the crystal, and (d) scatter from the film and its wrapping. Scatter from the film wrapping is often regarded as unimportant, but recent work by Reed[2] has shown that the black paper in common use gives a particularly strong background.

The common feature of all the above mentioned sources is their linear dependence on the intensity of

[1] Carlisle and Scouloudi, Proc. Roy. Soc. (London) **A207**, 496 (1951).

[2] Reed, Chicago College of Medicine (private communication).

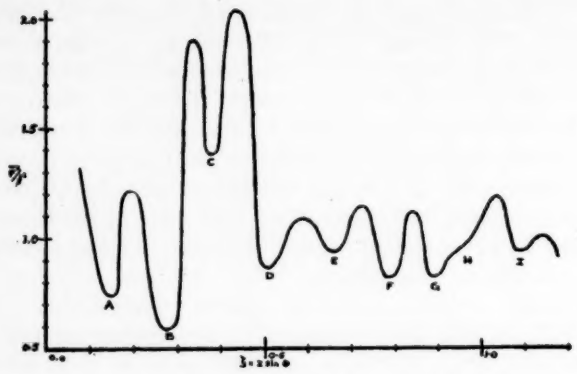

FIG. 1. Ribonuclease radial intensity analysis (h, o, l) zone.

the incident x-radiation. It can be stated that a Bragg reflection will be visible on a film if the ratio of its intensity to that of the background is greater than some threshold value. This phenomenon is well known in electronics, where a certain minimum "signal/noise" ratio is necessary for detection to be possible.

A first result of this analysis is, that for any given crystal, a long exposure using a moderately strong x-ray beam will yield all the information obtainable with a higher powered apparatus, although, of course, in the case of biological materials, a short exposure may be necessary on account of their instability.

To obtain further information it is necessary to consider in detail the factors governing the intensity of the x-ray reflection from a given crystal. Absorption can be neglected for small crystals of the type under consideration. The intensity of reflected radiation, I, is given by

$$I=k\cdot I_0\cdot L(\theta)\cdot N^2\cdot F^2\cdot dv, \tag{1}$$

where I_0 is the intensity of the incident radiation, k is a constant for any wavelength of radiation, $L(\theta)$ is the Lorentz and polarization factor, θ is the Bragg angle of the reflection, N is the number of unit cells per unit volume, and F is the structure factor of the reflecting plane.

Now $N=1$ volume of unit cell of crystal = const/total atomic number per unit cell = const/$\sum_1^n N_r$. The structure factor F is given by the expression

$$F^2(h,k,l)=(\sum_{r=1}^{n} f_r\cdot\cos\varphi_r)^2+(\sum_{r=1}^{n} f_r\cdot\sin\varphi_r)^2, \tag{2}$$

where

$$\varphi_r=2\pi\left(h\cdot\frac{x_r}{a}+k\cdot\frac{y_r}{b}+l\cdot\frac{z_r}{c}\right),$$

$(x_r\cdot y_r\cdot z_r)$ being the coordinates of the rth atom. On expansion and simplification (2) becomes

$$F^2=\sum_{r=1}^{n} f_r^2+2\sum_{r>s}^{n} f_r\cdot f_s\cdot\cos(\varphi_r-\varphi_s).$$

If the coordinates of the atomic centers are randomly distributed in space, the trigonometric terms in the last expression will tend to cancel out so that on the average[3]:

$$\bar{F}^2=\sum_{r=1}^{n} f_r^2. \tag{3}$$

This is not to be taken as implying that individual values of F^2 are given by Eq. (3) but only that statistically this relation holds. The chief source of error will be the fact that the atoms are not distributed in a truly random manner but have, for example a certain minimum distance of approach. This will be considered in detail later and for the present (3) will be assumed to hold. Equation (3) can be simplified further when the atoms composing the structure are of nearly equal atomic number since[4]

$$f_r=N_r\cdot f(\theta),$$

where $f(\theta)$ is a characteristic function, common to all related atoms, and N_r is the atomic number of the particular atom under consideration. With this simplification (3) may be written

$$\bar{F}^2=f^2(\theta)\cdot\sum_{r=1}^{n} N_r^2, \tag{4}$$

and Eq. (1) becomes

$$I=k'\cdot I_0\cdot L(\theta)\cdot f^2(\theta)\cdot\sum_{r=1}^{n} N_r^2\cdot dv/(\sum_{r=1}^{n} N_r)^2,$$

or if, as in biomolecular compounds, the values of N_r are nearly equal

$$I\simeq k'\cdot I_0\cdot L(\theta)\cdot f^2(\theta)\cdot dv/n. \tag{5}$$

Thus I/I_0, for crystal specimens of equal volumes reflecting at the same Bragg angles, decreases inversely as the number of atoms in the unit cell. Here again a slight change is necessary for complicated space groups, and more detailed analysis shows that the number "n" is then to be taken as the number of atoms in the independent scattering unit.

The previously enumerated causes of background radiation are independent of this molecular complexity factor, so that the "signal/noise" ratio decreases with increasing molecular weight, and thus causes a progressive diminution in the number of visible reflections. It is not possible to give a quantitative evaluation of the precise cut-off point in any particular case, firstly because the threshold ratio is unknown, and secondly on account of the analytical intractability of the functions $L(\theta)$ and $f(\theta)$.

As a corollary to the above it would appear that a promising line of experimental work would be to eliminate factors (b) and (d) by using light tight vacuum cameras and unwrapped film. The limiting

[3] Wilson, Nature **150**, 152 (1942).
[4] Booth, Nature **156**, 51 (1945).

factor would then be the Compton scattering from the crystal itself. Further improvement might result from cooling the crystal to liquid air temperature and thus increasing $f(\theta)$. This would effect a differential increase of Bragg/Compton intensity.

The next phenomenon to be considered is the presence of the low intensity areas previously mentioned. To obtain an explanation of these, it is necessary to make more detailed assumptions regarding the disposition of matter in the unit cell of the crystal than was hitherto the case. In the absence of exact knowledge of the atomic coordinates, it is impossible to hope for fully quantitative information, but it is hoped that the following treatment will be considered at least a plausible explanation.

Suppose first that the atoms in a particular structure are uniformly distributed throughout a spherical volume, centered on the origin of coordinates, and of radius r. Then Eq. (2) gives, on account of the implied center of symmetry

$$F(h,k,l)=\sum_{r=1}^{n} f_r \cos 2\pi\left(h\cdot\frac{x_r}{a}+k\cdot\frac{y_r}{b}+l\cdot\frac{z_r}{c}\right). \quad (6)$$

If it is assumed that the atoms are identical, and have a constant distribution density D per unit volume, Eq. (6) may be written

$$F(h,k,l)=D\cdot f(h,k,l)\int_V \times\cos 2\pi\left(h\cdot\frac{x}{a}+k\cdot\frac{y}{b}+l\cdot\frac{z}{c}\right)\cdot dV, \quad (7)$$

the integration extending over the spherical volume V, and $f(h,k,l)$ being the common atomic scattering factor. Transforming to axes parallel and normal to the plane (h,k,l), Eq. (7) reduces to

$$F(h,k,l)=D\cdot f(h,k,l)\int_{-r}^{+r}\pi(r^2-w^2)\cdot\cos 2\pi w/d(h,k,l)\cdot dw, \quad (8)$$

where $d(h,k,l)$ is the spacing of the plane (h,k,l). The integration is now readily performed and gives

$$F(h,k,l)=4\pi r^3\cdot D\cdot f(h,k,l)\cdot T(h,k,l), \quad (9)$$

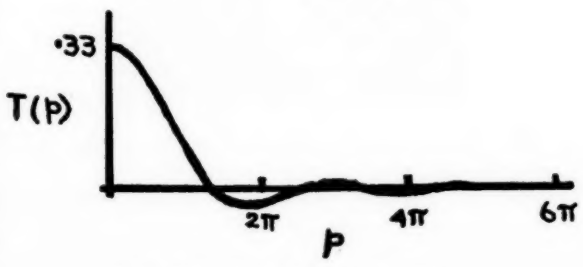

FIG. 2. Transform of spherical volume.

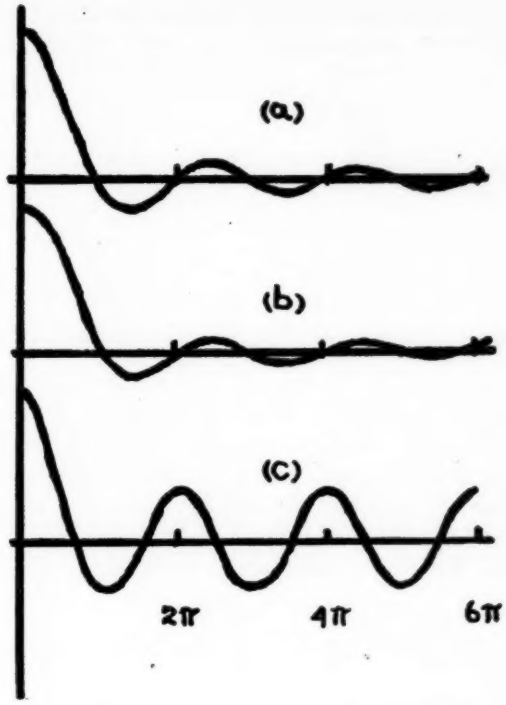

FIG. 3. Transforms, to common amplitude, of (a) spherical surface or cube volume, (b) octahedral volume, and (c) cube surface.

where

$$T(h,k,l)=(\sin p-p\cdot\cos p)/p^3, \quad (10)$$
$$p=2\pi r/d(h,k,l).$$

A graph of the function T is given in Fig. 2. It shows, first, that $T(h,k,l)$, and consequently $F(h,k,l)$, is a rapidly decaying function, and second, that the functions will be small in the region of the roots of the equation

$$\tan p=p, \quad (11)$$

these conclusions being true without any reference to the behavior of the atomic scattering factor.

This behavior is not confined to the spherical distribution which has been chosen. In Fig. 3 are drawn the transforms[5] of a number of quite varied shapes, and it is seen that the general features of the curves are the same.

It is suggested that some of the regions of low intensity in protein photographs occur in the neighborhood of these zeros of the transform of the protein molecule.

A second source of periodicity must also be considered. In obtaining Eq. (3) the distribution of atomic centers was assumed to be random, this, as was pointed out is not the case and there exists, in fact, a distribution function:

$$g(l,m,n), \quad (12)$$

[5] Wrinch, "Fourier transforms and structure factors," Am. Soc. X-Ray and Electron Diffraction (1946).

TABLE I. Observed and calculated minima.

Observed	Calculated
10.20	10.20
5.81	5.81
4.11	4.14
3.01	3.23
2.65	2.64
...	2.24
1.98	1.94
1.73	1.71
1.55	1.52
1.41	1.38

such that $g(l, m, n)dl \cdot dm \cdot dn$ gives the probability of finding an interatomic vector of coordinates (l, m, n).

It is clear, that the function g is not generally spherically symmetric but for its first period it can be assumed to be approximately so in the case of a unit cell which does not deviate too much from a cubic shape. With this assumption (3) is replaced by

$$F^2=\sum_{r=1}^{n} f_r^2+2\sum_{r>s} f_r \cdot f_s \int_V g(t)\cos(\varphi_r-\varphi_s)dv, \quad (13)$$

where

$$t^2=(x_r-x_s)^2+(y_r-y_s)^2+(z_r-z_s)^2 \quad (14)$$

and the integration extends over the whole vector space.

To evaluate the integral it can be assumed that

$$g(t)=\sum_i \delta(t-b_i)G(b_i), \quad (15)$$

where δ is the Dirac delta-function defined by

$$\delta(x-x_0)=0 \quad x\neq x_0$$

$$\int_{-\infty}^{\infty}\delta(x-x_0)dx=1.$$

Thus the distribution postulated assumes that atoms occur at discrete distances b_i.

The density of distribution $G(b_i)$ will, of course, be peculiar to the structure under consideration.

Inserting (15) in (13) and performing the integration leads to

$$F^2=\sum_{r=1}^{n} f_r^2+2\sum_{r>s} f_r \cdot f_s\left[\sum_i 4\pi b_i^2 G(b_i)\frac{\sin p_i}{p_i}\right], \quad (16)$$

where

$$p_i=2\pi b_i/d_{hkl}. \quad (17)$$

It thus follows, without need for greater particularization, that minima of F^2 may occur at or near planes whose spacings $d(hkl)$ are the roots of $p_i=(4n+3)\pi/2$ —that is,

$$d_{hkl}=4b_i/4n+3. \quad (18)$$

Two equations, (11) and (18), are thus available for comparison with experiment. In the case of ribonuclease, minima occur at spacings of 10.20, 5.81, 4.11, 3.01, 2.35, 1.98, 1.73, 1.55, and 1.41A. Taking first Eq. (11), its solutions occur at

$$p\sim 1.42\pi, \quad p\sim(2n+3)\pi/2 \quad (n=1.2\cdots);$$

thus $r=.71d(hkl)$, which, for ribonuclease, would predict a molecular "radius"

$$r=7.26 \text{ A.U.}$$

for the 10.20A minimum.

Assuming this basic "radius" the other zeros can be calculated. They are compared with the observed values in Table I. These agree in a surprising fashion with the observed values considering the extremely general character of the assumptions made in their derivation.

In the case of Eq. (18) insertion of various probable bond lengths, from the 2.52A of hydrogen bonding to the 1.5–1.3A of C−C, C−O and C−N bonds leads to minima at spacings of 3.36, 2.00, 1.89, 1.70, 1.44, 0.92, 0.86, 0.81A. These, again find their counterparts in the observed data (although not perhaps so accurately) and it appears that the physical bases expressed in (11) and (18) are adequate to explain the macroscopic features of a typical protein intensity map. It remains to remark that, taking account of the continuity properties of the analytic function $F(hkl)$, phase changes in any centrosymmetric level may at least be suggested by the transition of the complex $F(hkl)$ of other levels through the minima which have been the subject of this discussion.

The author wishes to express his thanks to Professor J. D. Bernal for the several stimulating discussions which suggested the subject of this paper.

Application of Eller's Optical Machine to the Determination of the Molecular Structure of Gases by Electron Diffraction. II. Nonrigid Molecules

L. Bru, M. Perez Rodriguez, and M. Cubero
University of Seville, Seville, Spain

(Received June 13, 1952)

In this work we shall demonstrate the possibility of applying Eller's optical machine, as an auxiliary method of making calculations, to the study of the determination of the structure of gaseous molecules (nonrigid molecules) by means of the diffraction of electrons. The particular case of the $CF_3-C\equiv CH$ will be used as an illustration.

IN a previous work,[1] we showed how Eller's machine,[2] properly applied, is capable of replacing, with undoubted advantage, other auxiliary methods of making calculations in the study of the determination of the structure of gaseous molecules by electron diffraction.

The method was applied to the case of rigid molecules only. In the present work we apply it to the case of nonrigid molecules.

As is known, the intensity of the electron radiation diffracted by gaseous molecules in which the atoms vibrate appreciably around the position of equilibrium in a manner such that the interatomic distances r_{ij} vary simple harmonically with the time can be expressed by the simplified equation[3]:

$$I'(q)=q\cdot I(q)=\sum_i\sum_j Z_iZ_j\frac{\exp(-b_{ij}q^2)}{r_{ij}}\sin r_{ij}q, \quad (1)$$

in which the factor b_{ij} is a temperature dependent factor.

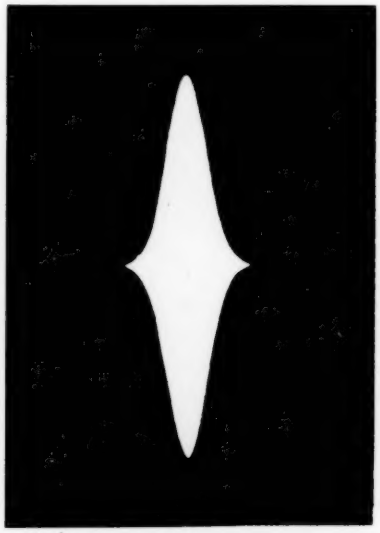

FIG. 1. Screen A [function $y_A=\exp(-kx^2)$].

We have thus to modify the machine to make it capable of summarizing photographically the terms of the second member of Eq. (1). To achieve this, two new screens have to be introduced which delimit the light, and which we shall call A and B (Figs. 1 and 2). Both are parallel to the sinusoidal grating. The light incident on the photographic plate is modulated by the screen A by the function:

$$y_A=t_1\exp(-kr^2q^2),$$

where r is the distance which separates it from the luminous slit.

The screen B reproduces the function

$$y_B=t_1(1-\exp(-kr^2q^2))$$

on the photographic plate, and its purpose is to correct the alteration which the intensities registered on the photographic plate suffer by the introduction of the screen A.

If we make

$$kr^2=b_{ij},$$

there remains

$$y_A=t_1\exp(-b_{ij}q^2).$$

As we know, the sinusoidal grating, which we shall call P, modulates light incident on the photographic

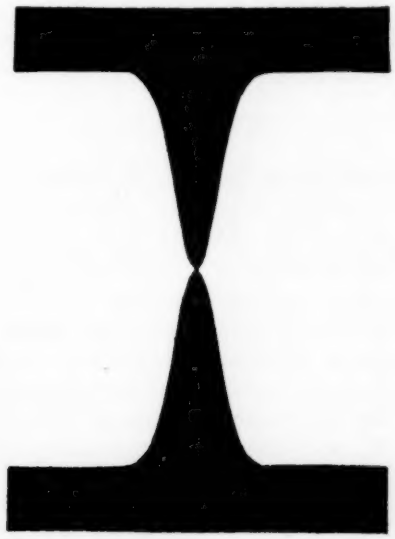

FIG. 2. Screen B [function $y_B=1-\exp(-kx^2)$].

[1] Bru, Perez Rodriguez, and Cubero, J. Chem. Phys. **20**, 1069 (1952).
[2] G. Eller, Compt. rend. **232**, 1122 (1951); **233**, 2333 (1951).
[3] Shaffer, Shomaker, and Pauling, J. Chem. Phys. **14**, 659 (1946).

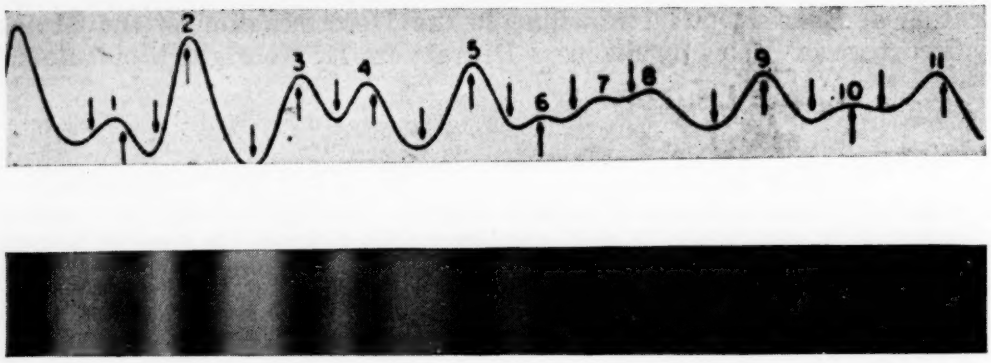

FIG. 3. Comparison of intensities (visual) of the electron diffraction pattern and the intensities of the diagrams obtained with the Eller's optical machine (molecule $CF_3-C\equiv CH$).

plate by the function

$$y_P=k(1+\sin Rq).$$

Thus, using simultaneously screens A and P, by means of successive impressions we can succeed in representing the function

$$I_1(q)=\sum_i t_1 \exp(-b_{ij}q^2)(1+\sin Rq). \qquad (2)$$

If each exposure time is equal to

$$t_i=Z_iZ_j/r_{ij}$$

and

$$R=r_{ij},$$

Eqs. (1) and (2) will be different in the variable factor.

$$\sum \frac{Z_iZ_j}{r_{ij}} \exp(-b_{ij}q^2).$$

Now, if we only use screen B placed for each impression exactly in the same position previously occupied by screen A and each time using identical times of exposure, the function obtained on the photographic plate will differ from Eq. (1) only in the constant

$$\sum(Z_iZ_j/r_{ij}).$$

Really, as can be easily seen, the times of exposure should be taken proportional to

$$\frac{Z_iZ_j}{r_{ij}} \Big/ \left[1-\left(\frac{b_{ij}}{k}\right)^{\frac{1}{2}}\right].$$

The problem likewise offers no difficulties when the equation utilized for the diffracted intensity is

$$I(q)=\sum_i \sum_j Z_iZ_j \exp(-b_{ij}q^2)\frac{\sin r_{ij}q}{r_{ij}q},$$

which frequently utilized for several authors.[4]

We give now an experimental proof of this method by applying it to the determination of the structure of the $CF_3-C\equiv CH$.

The theoretical curves, calculated for the different values of the interatomic distances, as well as for the

TABLE I.

Z_i-Z_j	r_{ij}	b_{ij}
$F-F$	2.152	0.000689
$F-C$	1.335	152
$F-C'$	2.315	913
$F-C''$	3.39	2586
$F-H$	4.39	7352
$C-C'$	1.464	101
$C-C''$	2.665	466
$C-H$	3.721	3086
$C'-C''$	1.201	0000
$C'-H$	2.257	2616
$C''-H$	1.056	2251

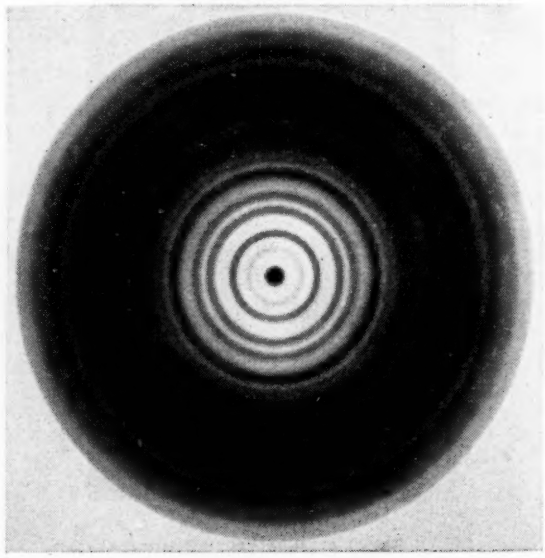

FIG. 4. Diagram obtaining by rotating the original plate 3 during the printing of a diapositive.

[4] I. Karle and J. Karle, J. Chem. Phys. 17, 1056 (1949).

various temperature factors, are taken from a recent publication.[5]

We have used the values which seem best for this combination in Table I.

In Fig. 3 we show the relative theoretical curve, and the diagram obtained with Eller's machine. As can be seen, the concordance between the positions and intensities of the respective maxima is excellent.

[5] Shooley, Chulman, Scheehan, Shomaker, and Yost, J. Chem. Phys. **19**, 1364 (1951).

The time of each exposure were such that the whole time required to obtain our diagrams was 30 seconds. That is to say, this method supplies the information with the utmost rapidity and sufficiently accurately to be used with confidence.

In order to learn the distances which separate the maxima and minima with greater precision, a diagram was prepared by gyrating the pattern shown in Fig. 3 thus obtained the pattern shown in Fig. 4, which is very convenient for comparison with the original diagram of the diffraction of electrons.

THE JOURNAL OF CHEMICAL PHYSICS VOLUME 20, NUMBER 12 DECEMBER, 1952

Infrared Studies of Mixed Crystals: Naphthalene-d_8 in Naphthalene

WILLIS B. PERSON AND GEORGE C. PIMENTEL
Department of Chemistry and Chemical Engineering, University of California, Berkeley, California

(Received May 26, 1952)

Polarized infrared studies in the region 615 to 645 cm^{-1} have been made using dilute solid solutions of naphthalene-d_8 in naphthalene. The *ab* plane at normal incidence was studied with light polarized either parallel or perpendicular to the *b* axis. The mole fraction of $C_{10}D_8$ was varied from 0.10 to 0.30. The dichroic splitting of the 632-cm^{-1} band observed in pure $C_{10}D_8$ decreases with concentration. This is the splitting predicted in the factor group analysis and is attributed to intermolecular coupling. This is a further indication that the magnitude of this splitting in molecular crystals such as $C_{10}H_8$ is only a few cm^{-1}, and that the "oriented gas" model is applicable. Using this model, the 632-cm^{-1} band of $C_{10}D_8$ is assigned as a single fundamental of the B_{1u} or B_{3u} class.

RECENTLY, attempts have been made to interpret the spectra of molecular crystals on the basis of an "oriented gas" model.[1,2] However, the use of this model can be justified only if it can be shown that lattice perturbations are small. It has been noted[3] that infrared studies of dilute solid solutions permit a study of the effect of coupling among the several molecules of the unit cell. Such a study has been made of dilute solutions of naphthalene in anthracene.[4] Another study of this type has been reported for the system DCl in HCl by Hiebert and Hornig.[5]

In the spectrum of a single crystal of naphthalene, observed in the *ab* cleavage plane at normal incidence, a large dichroic effect is observed around 787 cm^{-1}. This effect has been interpreted[1] to be the dichroic splitting predicted by the factor group analysis[6,7] for $C_{10}H_8$ crystals. This explanation has been substantiated by the results of the study of naphthalene in anthracene.[4]

Naphthalene and anthracene have identical lattice symmetries, but the unit cell dimensions are quite different. For any such mixed crystal system, it is possible to attribute concentration-dependent spectra changes to distortions of the host lattice by the solute molecules, as well as to reduced coupling with the lattice. This situation does not exist for mixed crystals in which the solute molecules differ from the host lattice molecules only in isotopic substitution. For this reason, it seemed desirable to study mixed crystals such as deuterated naphthalene in naphthalene. In this system the dilute component, $C_{10}D_8$, is in an undistorted $C_{10}H_8$ lattice, and there is no question about the orientation of the $C_{10}D_8$ molecules. In addition, this system eliminates some of the possible sources of other difficulties of the $C_{10}H_8$ in $C_{14}H_{10}$ study, such as small crystals and a weak absorption by $C_{14}H_{10}$ at 779 cm^{-1}.

Naphthalene-d_8 has a strong absorption band in the gas phase at 633 cm^{-1}. Studies in this region of a single crystal of $C_{10}D_8$ (*ab* plane, normal incidence) showed that light polarized parallel to the *b* axis has an absorption maximum at 634 cm^{-1} and light polarized perpendicular to the *b* axis has an absorption maximum at 631 cm^{-1}. Pure naphthalene crystals of thicknesses comparable to those used in the present study are perfectly transparent in this region, so mixed crystals of $C_{10}D_8$ in $C_{10}H_8$ meet the criteria suggested[4] for the study of factor group splitting with mixed crystals.

EXPERIMENTAL

Single crystals of $C_{10}D_8$ as large as 1.0×0.2 cm and about 20–100 microns thick may be grown fairly readily

[1] G. C. Pimentel and A. L. McClellan, J. Chem. Phys. **20**, 270 (1952).
[2] Ambrose, Elliott, and Temple, Proc. Roy. Soc. (London) **A206**, 192 (1951).
[3] H. J. Hrostowski and G. C. Pimentel, J. Chem. Phys. **19**, 661 (1951).
[4] G. C. Pimentel, J. Chem. Phys. **19**, 1536 (1951).
[5] G. L. Hiebert and D. F. Hornig, J. Chem. Phys. **20**, 918 (1952).
[6] H. Winston and R. S. Halford, J. Chem. Phys. **17**, 607 (1949).
[7] D. F. Hornig, J. Chem. Phys. **16**, 1063 (1948).

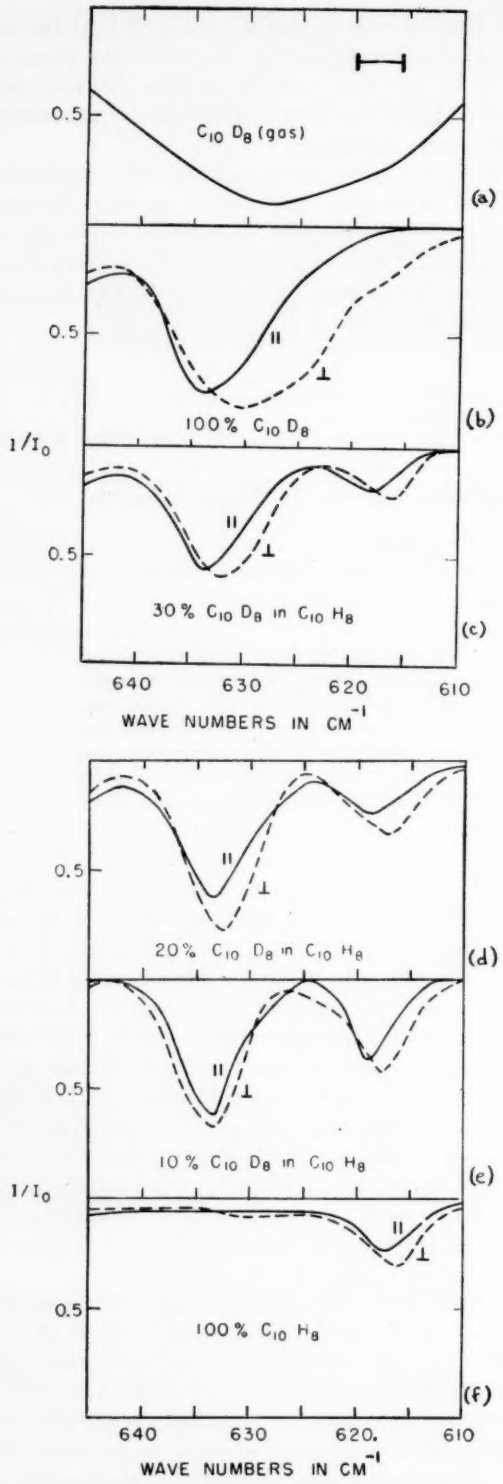

FIG. 1. Spectra of $C_{10}D_8$ and $C_{10}H_8$. (a) $C_{10}D_8$, gas, $p \cong 120$ mm, 7-cm cell. (b) $C_{10}D_8$ solid. (c)–(e) mixed crystals of $C_{10}D_8$ in $C_{10}H_8$. Concentrations given in mole percent $C_{10}D_8$. (f) $C_{10}H_8$ solid. ——— light polarized parallel to the *b* axis; *ab* plane, normal incidence. – – – – light polarized perpendicular to the *b* axis; *ab* plane, normal incidence.

by sublimation. These crystals grow in sheets whose surfaces are the *ab* cleavage plane, and they were found to grow with the *b* axis in the long dimension. The *b* axis was located by observing the isogyre pattern with a petrographic microscope. Completeness of extinction under crossed Nicol prisms in the petrographic microscope was used as a criterion in selecting perfect single crystals.

Baker's resublimed naphthalene was used in these experiments. The deuterated naphthalene was prepared by exchange with D_2SO_4 and was estimated spectroscopically to have about two percent hydrogen remaining.[8] This is enough to give about 15 mole percent of $C_{10}D_7H$ which will influence the band contours. However, the impurities do not affect the present study, for the presence of two bands in the crystal spectrum and only one band in the gas spectrum still implies factor group splitting.

The mixed crystals were prepared by placing weighed amounts of $C_{10}H_8$ and $C_{10}D_8$ in a weighing bottle and subliming the crystals to the top of the bottle. This procedure gave crystals large enough and thin enough for the present studies. It was assumed that the $C_{10}H_8$ and $C_{10}D_8$ sublimed in a random manner so that the sublimed crystals were true solid solutions. The concentrations given refer to the measured concentration in the stock used for sublimation.

The spectra were taken on a Perkin-Elmer Model 12*C* spectrometer, with NaCl optics. A conventional transmission polarizer with ten AgCl sheets was used. The slit width is shown in Fig. 1(a). Each spectrum included the 667 cm^{-1} CO_2 band and usually also the 618 cm^{-1} band of $C_{10}H_8$ as calibration points to ensure absence of calibration shifts. Frequencies should be accurate to ± 3 cm^{-1}, but frequency differences between two successive spectra, as observed here, should be accurate to ± 0.3 cm^{-1}. Each of the spectra given here was repeated several times, and each concentration was studied with two separately prepared crystals. These crystals were estimated to be about 30 microns in thickness.

The crystals were mounted either just in front of the entrance slit, or just in front of the thermocouple. The latter technique was used with some of the early crystals, which were too small to mount in front of the slit. In this case, the crystals were mounted with the *b* axis vertical or horizontal and the polarizer fixed to pass light polarized vertically. Thus, the polarization effects of the instrument enhanced the polarization of the light. It was possible to mount the crystals so that they were aligned to about $\pm 10°$. When the crystals were mounted in front of the slit, the polarizer was turned to polarize light parallel and perpendicular to the vertical *b* axis. The polarization of the optics in the monochromator causes an intensity change on rotation of the polarizer. A correction has been made for this effect. The false energy has been estimated and a correction applied. No

[8] Further details on the preparation of the $C_{10}D_8$, as well as complete details of its spectrum, will be published soon. We should like to thank Mr. Nelson Alley and Mr. Henry Rodeen for their work in the preparation of the $C_{10}D_8$.

differences due to other optical effects, such as change in angle of convergence of the incident light, were detected when the crystal was mounted in the two ways.

RESULTS

Figures 1(a) and 1(b) show the spectra of $C_{10}D_8$ vapor and solid, respectively, in the region 610–645 cm^{-1}. Figures 1(c), 1(d), 1(e), and 1(f) show the spectra of 30, 20, 10, and 0 mole percent $C_{10}D_8$ in $C_{10}H_8$. The observed dichroic splittings are 3.5, 1.5, 1.0, and 0.0 cm^{-1} for 100, 30, 20, and 10 mole percent $C_{10}D_8$ in $C_{10}H_8$, respectively. It is interesting to note that the naphthalene band at 618 cm^{-1} shows no such concentration dependence. The dichroism of this band is unchanged within experimental error.

Approximate dichroic ratios $I_\perp/I_\parallel$ were estimated for the 632 cm^{-1} band for each mixed crystal and these values were about 1.2. The ratio for pure $C_{10}D_8$ was not substantially different (about 1.3), but the band contour indicates that this ratio may not be considered to be well defined. These dichroic ratios do not have quantitative significance, but they allow qualitative comparisons.

DISCUSSION

The factor group analysis for naphthalene single crystals[1] predicts that each infrared band in the gas phase will split into two infrared bands in the solid, one polarized parallel to the *b* axis and one polarized perpendicular to the *b* axis. The study of naphthalene crystals[1] indicates that this splitting is less than 10 cm^{-1}, and by the argument presented in reference 3, this splitting is expected to decrease in a mixed crystal as the concentration of the absorbing species is decreased. This is observed as may be seen in Figs. 1(c), 1(d), and 1(e). The band studied here had about the largest dichroic splitting recognized in the spectrum of $C_{10}D_8$ crystals, as was true for the band studied in $C_{10}H_8$. The results of this study and of the earlier studies[1,4] indicate that the factor group splitting of vibrational energy levels for naphthalene crystals may be considered to be only a small perturbation of the corresponding molecular energy levels.

The small perturbations of the molecular energy levels constitute one necessary condition for the applicability of the "oriented gas" model. Its applicability is not assured since the perturbations of the intensity must also be small. However, the general qualitative agreement in these and the earlier studies[1,4] between the spectra and the predictions of the model do indicate that the main features of the spectra of solid naphthalene may be interpreted with the aid of the predictions of the "oriented gas" model together with the predictions of the site group analysis.[9]

The dichroic ratio was observed to be roughly constant for the mixed crystal concentrations studied. This is in agreement with the prediction of the "oriented gas" model that this ratio should be independent of concentration. Neither the site group analysis nor the factor group analysis provides information concerning this ratio. The "oriented gas" model further predicts that this ratio should have a value corresponding to the molecular symmetry representation of the vibration of interest. These are calculated by the method indicated in references 4 and 1 to be B_{1u}, 3.6; B_{2u}, 0.14; and B_{3u}, 4.2. Since the dichroic ratios were found to be near 1.2, the 632-cm^{-1} band is assigned to a B_{1u} or B_{3u} motion.

CONCLUSION

The polarized spectra of mixed crystals of $C_{10}D_8$ in $C_{10}H_8$ indicate that the splitting of the 632-cm^{-1} band of $C_{10}D_8$ decreases as the concentration of $C_{10}D_8$ decreases. It seems likely that the dichroic splitting observed in this band in the spectrum of a single crystal of $C_{10}D_8$ is the result of intermolecular coupling and is the splitting predicted in the factor group analysis. This study eliminates certain inherent difficulties in earlier mixed crystal work involving naphthalene and anthracene, and provides further verification that the dichroic splitting of vibrational energy levels is small for molecular crystals such as $C_{10}H_8$. Application of the "oriented gas" model in interpreting the observed dichroic ratio of this band leads to its assignment to the B_{1u} or B_{3u} class.

---

[9] R. S. Halford, J. Chem. Phys. 14, 8 (1946).

Infrared and Raman Spectra of Fluorinated Ethylenes. V. Hexafluoropropene*

J. RUD NIELSEN AND H. H. CLAASSEN, *Department of Physics, University of Oklahoma, Norman, Oklahoma*

AND

D. C. SMITH,† *Naval Research Laboratory, Washington, D. C.*

(Received July 14, 1952)

The infrared absorption spectrum of gaseous $CF_2{:}CF-CF_3$ has been obtained in the region from 2 to 38μ, with the aid of LiF, NaCl, KBr, and KRS-5 prisms. The Raman spectrum of both the gaseous and the liquid phase has been photographed with a three-prism glass spectrograph of linear dispersion 15 A/mm at 4358A, and depolarization ratios have been measured for the stronger bands. A complete assignment of fundamental vibrational frequencies is given, although four of the twenty-one fundamentals must be regarded as uncertain. The spectra are interpreted in detail.

INTRODUCTION

WHEN tetrafluoroethylene polymer is subjected to pyrolysis, a compound of composition C_3F_6 is formed. It was first believed to be cyclic but was later shown to be $CF_2{:}CF-CF_3$.[1-3] Edgell[2] investigated the Raman spectrum of this compound in the liquid state and made a tentative assignment of all but one of the twenty-one fundamentals. Young and Murray,[1] Edgell,[2] and also Lacher, McKinley, Walden, Lea, and Park,[4] have obtained the infrared absorption spectrum with low resolution. In the present paper, new infrared and Raman data and a revised assignment of fundamentals are presented.

EXPERIMENTAL RESULTS

The infrared absorption of gaseous $CF_2{:}CF-CF_3$ from 2 to 23μ is shown in Fig. 1. This sample (Ser. No. 327) contained a small amount of C_3F_8 as impurity, as evidenced by the bands at 731 and 1263 cm^{-1}. Another sample (Ser. No. 358) showed no absorption at 731 cm^{-1} but had other impurity bands in the region from 870 to 980 cm^{-1} and around 2950 cm^{-1}. The infrared spectrum of the first sample was obtained in the KRS-5 region in the manner previously described.[5] The Raman spectrum of this sample (Ser. No. 327) was obtained in the vapor state at a pressure of about five atmospheres and a few degrees above room temperature. The first attempts to obtain the Raman spectrum of the compound in the liquid state failed because of polymerization caused by the irradiation. However, such a spectrum was obtained at room temperature, and polarization measurements were made, on a third sample (Ser. No. 374) contained in a sealed Raman tube.

The observed infrared absorption maxima are listed in the first column of Table I. The Raman shifts of gaseous and liquid hexafluoropropene, and the observed depolarization ratios, are listed in Table II. For comparison, Edgell's data for liquid $CF_2{:}CF-CF_3$ at an unspecified low temperature also are given.

The deviations between Edgell's and the present data, which should be the more accurate, are in some cases as high as 10 cm^{-1}. The Raman shifts reported by Edgell at 213 and 306 cm^{-1} were not observed in the present investigation. The former is probably spurious. The second may be the 361 cm^{-1} shift from the 4348 A mercury line. Corresponding to Edgell's band at 714 cm^{-1}, a very sharp faint Raman band was observed having a shift of 710 cm^{-1} from the 4358 Hg line. It was interpreted as 767 cm^{-1} excited by the 4348 Hg line. Five very faint Raman bands not observed by Edgell were found in the present work.

INTERPRETATION

1. Assignment of Fundamentals

The hexafluoropropene molecule has at most a single symmetry element, the plane through the three carbon atoms. If this symmetry C_s is assumed, the 21 normal vibrations divide themselves into 14 of species A' (symmetrical with respect to the plane) and 7 of species A'' (antisymmetrical with respect to the plane). Fundamentals of both species, and all combinations, are allowed both in infrared absorption and in the Raman effect. Infrared bands of species A'' should have type C contours. Raman bands of species A'' are depolarized.

On the basis of the intensities with which they occur in one or both of the two spectra, seventeen frequencies can with almost complete certainty be picked out as fundamentals. The remaining four fundamentals cannot be assigned with certainty. One of these should lie above 1000 cm^{-1}. It has been tentatively identified with the fairly strong infrared band at 1122 cm^{-1}, the counterpart of which has not been observed in the Raman spectrum. This assignment provides an interpretation of the weak infrared band at 2907 cm^{-1}, which cannot otherwise be interpreted as a binary combination

* This work has been supported in part by the ONR and the AEC.

† Present address: Phillips Petroleum Company, Bartlesville, Oklahoma.

[1] E. G. Young and W. S. Murray, J. Am. Chem. Soc. **70**, 2814 (1948).

[2] W. F. Edgell, J. Am. Chem. Soc. **70**, 2816 (1948).

[3] F. A. M. Buck and R. L. Livingston, J. Am. Chem. Soc. **70**, 2817 (1948).

[4] Lacher, McKinley, Walden, Lea, and Park, J. Am. Chem. Soc. **71**, 1334 (1949).

[5] Nielsen, Liang, and Smith, J. Chem. Phys. **20**, 1090 (1952).

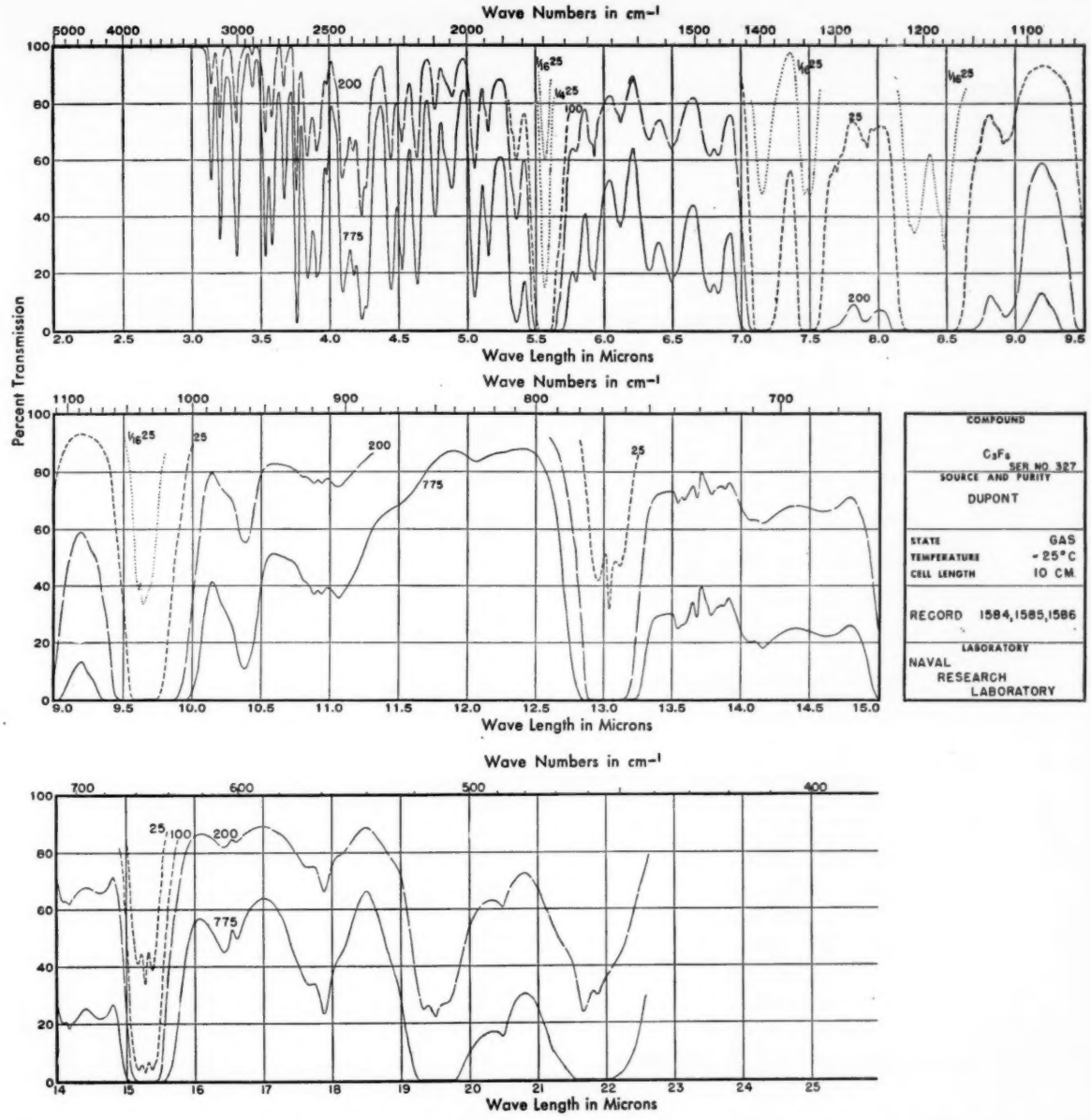

FIG. 1. Infrared spectrum of hexafluoropropene (gas). KRS-5 region not shown.

band, as well as alternative interpretations of several other infrared bands. However, the infrared band at 1122 cm^{-1} could readily be interpreted as a combination band, $360+767=1127$ or $462+655=1117$, or as an overtone, $2\times559=1118$, and it could be assumed that two of the fundamentals above 1000 cm^{-1} overlap.

From the spectra of related compounds, in particular CF_2:CFCl and C_3F_8, it may be concluded with reasonable certainty that two of the remaining fundamentals lie between 500 and 700 cm^{-1}. It is assumed tentatively that one of these is represented by the weak infrared band at 609 cm^{-1} and the faint Raman band at 603 cm^{-1} (in the liquid), although these bands could also be interpreted as binary combination bands. There is no real basis for assigning the other fundamental expected in this region. However, since the infrared absorption at 559 cm^{-1} appears to have a somewhat irregular contour and since this frequency is about what is to be expected for a motion involving largely CF_3 asymmetrical deformation, it has been assumed to represent two fundamentals of different species.

The last fundamental may be expected to lie below 300 cm^{-1}. It has been assumed, somewhat arbitrarily, to coincide with another fundamental at 250 cm^{-1}.

The symmetry species of nearly half of the fundamentals are determined with certainty by the observed depolarization ratios. The Raman band at 1164 cm^{-1} has been assigned as an A'' fundamental in spite of its somewhat low depolarization ratio, since there must be one A'' fundamental above 1000 cm^{-1}, and since the

TABLE I. Infrared spectrum of hexafluoropropene (gas).

Wave number	Description	Interpretation[a]
364[b] cm^{-1}	s	$A'+A''$ fundamentals
~457	s	(94)+359=453A''; (94)+369=463A'
462	s	A'' fundamental
488	w	(134)+359=493A'
~508		
513	s	A' fundamental
~517		
~552		
559	m	$A'+A''$ fundamentals
~566		
602	w	(94)+511=605A''; (250)+359=609
609	w	A' fundamental
651		
655	vs	A' fundamental
659		
684	m	(171)+511=682A'; (134)+559=693
706	m	(94)+609=703A''
711	m	(250)+462=712
720	vw	2×359=718A'
726	w	
731	w	C_3F_8 impurity
736	w	
739	w	2×369=738A'; (134)+609=743A'
762		
767	vs	A' fundamental
772		
829	vvw	369+462=831A'; (171)+655=826A''
~868	vvw	359+511=870A'
~904	w	(250)+655=905; (134)+767=901A'
914	w	359+560=919
919	w	2×462=924A'
963	m	359+609=968A'
~978	vw	369+609=978A''
1037	vs	A' fundamental
1041	s	
1122	s	A' fundamental
1179	vs	A'' fundamental
1255	w	609+655=1264A'
1263	m	C_3F_8 impurity
1299	w	(171)+1122=1293A''; (94)+1213=1307A''; 2×655=1310A'
1333	vs	A' fundamental
1340	vs	(134)+1213=1347A'?
1399	vs	A' fundamental
1464	m	(250)+1213=1463
1477	m	359+1122=1481A'
1541	m	359+1180=1539A''; 369+1180=1549A'
1580	m	369+1213=1582A''; (250)+1333=1583
1635	w	462+1180=1642A'
1687	w	511+1180=1691A''; 655+1037=1692A'; 359+1333=1692A'
1727	w	511+1213=1724A'
1797	vs	A' fundamental
1868	m	655+1213=1868A'; 462+1398=1860A''
1941	w	609+1333=1942A'; 767+1180=1947A''
1980	m	767+1213=1980A'; 655+1333=1988A'
~2047	w	(250)+1796=2046; 655+1398=2053A'
2099	w	767+1333=2100A'
2157	m	359+1796=2155A'; 369+1796=2165A''; 767+1398=2165A'
2210	m	1037+1180=2217A''
2250	m	1037+1213=2250A'; 462+1796=2258A''
2345	m	560+1796=2356
2364	s	2×1180=2360A'; 1037+1333=2370A'
2398	w	1180+1213=2393A''; 609+1796=2405A'
2444	m	655+1796=2451A'
2512	vw	1180+1333=2513A''
2560	m	767+1796=2563A'
2606	m	1213+1398=2611A'
2661	s	2×1333=2666A'
2723	w	1333+1398=2731A'
2792	m	2×1398=2796A'
2829	m	1037+1796=2833A'
2907	vw	1122+1796=2918A'
3008	m	1213+1796=3009A'
3122	m	1333+1796=3129A'
3185	w	1398+1796=3194A'

[a] Wave numbers enclosed in parentheses are for the liquid state.
[b] Observed with KRS-5 prism.

corresponding infrared band evidently has type C contour. Its low depolarization ratio may be a result of overlapping with the combination 511+652=1163 of species A'.

The species of the fundamentals that are too weak in the Raman effect to permit measurement of their depolarization ratios have been assigned on the basis of the appearance of the bands and the expected spectral distribution of the seven A'' fundamentals.

The assignment of fundamentals is given under the heading "Interpretation" in Tables I and II, and the assigned fundamentals are collected in Table III. The highest fundamental, at 1797 cm^{-1}, must be associated with a stretching of the carbon-carbon double bond. The other six fundamentals lying above 1000 cm^{-1} must involve largely C−F stretching. The highest of these, at 1398 cm^{-1}, and those at 1179 and 1211 cm^{-1}, undoubtedly correspond to motions in which the CF_3 group participates strongly, while the fundamental at 1336 cm^{-1} is associated with asymmetric stretching of the $=CF_2$ group. The fundamental at 767 cm^{-1} must involve largely C−C stretching, that at 655 cm^{-1} CF_2 deformation, those at 561 and 609 asymmetrical and symmetrical CF_3 deformation, those at 513 and 462 cm^{-1} CF_2 rocking and wagging, and that at 370 cm^{-1} largely CF wagging. The remaining low fundamentals correspond to motions involving deformation of the C:C−C angle, C−F rocking, CF_2 and CF_3 twisting, and CF_3 rocking and wagging.

2. Interpretation of the Spectra

On the basis of the fundamental frequencies listed in Table III it has been possible to interpret all of the observed infrared and Raman bands, except for a few

TABLE II. Raman spectrum of hexafluoropropene.

Gas[a]		Liquid[b] (~30°C)			Liquid[c] (low temp.)		
Wave number	Description	Wave number	Description	Depolarization	Wave number	Description	Interpretation
		94 cm^{-1}	m		84 cm^{-1}	w	A'' fundamental
		134	s		140	w	A' fundamental
		171	m, d		173		A'' fundamental
					213	w	
		250	m	~0.8	248	w	$A'+A''$ fundamentals
					306	vw	361 excited by 4348A
359 cm^{-1}	w	361.0	vs, sh	~0.3	360	s	A' fundamental
369	w	370	m				A'' fundamental
		462	vw, d		453	vw	A'' fundamental
509	w	511	w	0.5	511	m	A' fundamental
561	m	561.7	s, d	0.87	560	s	$A'+A''$ fundamentals
		603	vw		607	m	A' fundamental
655	m, d	652	s	0.49	648	s	A' fundamental
					714	w	767 excited by 4348A
		742	vvw, sh				$2\times370=740A'$
767.2	vs, sh	767.3	vs, sh	0.10	764	s	A' fundamental
777	vw						C_3F_8 impurity
		875	vvw				$361+511=872A'$;
							$370+511=881A''$
		1030	vw	~0.3	1020	w	A' fundamental
1081	w	1164	w	~0.7	1156	m	A'' fundamental
1215	w	1217	w	0.43	1208	m	A' fundamental
		1269	vvw				$134+1030=1264A'$
1333	m	1331.5	m	0.23	1330	m	A' fundamental
		1369	vvw				C_3F_8 impurity
1397	m	1395.3	m	0.23	1386	m	A' fundamental
1795	vs	1792.3	vs, sh	0.32	1790	s	A' fundamental

[a] Sample Ser. No. 327.
[b] Sample Ser. No. 374.
[c] Data from W. F. Edgell (reference 2).

TABLE III. Fundamental vibration frequencies of hexafluoropropene.

Symmetry species	Infrared (gas)		Raman (gas)		Raman (liquid)		
	Wave number	Description	Wave number	Description	Wave number	Description	Depolarization
A''					94[c]	m	
A'					134[c]	s	
A''					171[c]	m, d	
$A'+A''$					250[b]	m	~0.8
A'	364	s	359	w	361.0	vs, sh	~0.3
A''			369	w	370	m	
A''	462	s			462	vw, d	
A'	513	s	509	w	511	w	0.5
$A'+A''$	559[b]	m	561	m	561.7	s, d	0.87
A'	609[a]	w			603	vw	
A'	655	vs	655	m	652	s	0.49
A'	767	vs	767.2	vs, sh	767.3	vs, sh	0.10
A'	1037	vs			1030	vw	~0.3
A'	1122[a]	s					
A''	1179	vs	1181	w	1164	w	~0.7
A'	1211	vs	1215	w	1217	w	0.43
A'	1333	vs	1333	m	1331.5	m	0.23
A'	1399	vs	1397	m	1395.3	m	0.23
A'	1797	vs	1795	vs	1792.3	vs, sh	0.32

[a] Fundamental uncertain.
[b] Overlapping of two fundamentals uncertain.
[c] Symmetry species uncertain.

bands that are ascribed to C_3F_8 impurity. The interpretations are given in the third column of Table I and the eighth column of Table II. For most of the infrared bands, especially those lying between 1500 and 2500 cm^{-1}, it is possible to give more than one interpretation. This fact, which is a result of the large number of fundamentals and the low symmetry of the $CF_2{:}CF-CF_3$ molecule, makes the observation of overtone and combination bands of little value for checking the doubtful fundamentals.

ACKNOWLEDGMENT

The writers wish to express their indebtedness to E. I. du Pont de Nemours and Company, Inc., for the gift of the samples.

Absorption Spectra of SH and SD Produced by Flash Photolysis of H_2S and D_2S

D. A. RAMSAY
Division of Physics, National Research Council, Ottawa, Canada
(Received April 2, 1952)

H_2S and D_2S were irradiated in a flash photolysis apparatus, and the absorption spectra of the products were photographed within 1 millisecond of the photolysis flash using the second order of a 21 ft grating spectrograph. The (0, 0) and (1, 0) bands of SH and SD were observed and analyzed. The following molecular constants for SH were obtained: $^2\Sigma^+$ state: $B_e' = 8.538_1$ cm^{-1}, $\alpha_e' = 0.509_1$ cm^{-1}, $r_e' = 1.421_5$A, $\nu_{00} = 30{,}662.4_2$ cm^{-1}, $\Delta G_{\frac{1}{2}}' = 1784.6_3$ cm^{-1}, $\gamma_0 = 0.313$ cm^{-1}. $^2\Pi$ state: $B_0'' = 9.461_1$ cm^{-1}, $r_0'' = 1.350_3$A, $A = -376.9_6$ cm^{-1}. The rotational lines of the (1, 0) SH band were observed to be diffuse, indicating a predissociation in the first vibrational level of the $^2\Sigma^+$ state. This establishes an upper limit of 92.7 kcal and a lower limit of 66.3 kcal for the ground state dissociation energy of SH.

INTRODUCTION

THE $^2\Sigma \leftarrow {}^2\Pi$ band system of SH with band heads at 3236.6A and 3279.1A was first observed by Lewis and White[1] in absorption in a pulsed radio-frequency discharge through H_2S, after several unsuccessful attempts by earlier workers to obtain this band system in emission. A rotational analysis of the $^2\Sigma \leftarrow {}^2\Pi_{\frac{1}{2}}$ sub-band was carried out and the $^2\Pi$ state was shown to be inverted. Gaydon and Whittingham[2] obtained band heads of the same band in emission in the spectra of coal gas flames to which H_2S had been added, and Dyne and Style[3] obtained similar band heads in fluorescence by irradiating H_2S with vacuum ultraviolet radiation. Leach[4] observed about 50 lines of this band in emission using a Schüler-type discharge tube containing H_2S and evaluated constants for the $^2\Sigma$ and $^2\Pi$ states. More recently he has reported[5] three new bands for SD in emission. Porter[6] obtained the band at 3236.6A in absorption by the flash photolysis of H_2S and observed another similar band at 3060A. By obtaining the corresponding bands for SD he was able to show that the 3236.6A band was the (0, 0) and the 3060 band the (1, 0) band for SH. At the same time we[7] were engaged on an independent investigation of the flash photolysis of H_2S and D_2S using higher resolving power than Porter and have carried out analyses of the (0, 0) and (1, 0) bands of SH and SD. The values for the molecular constants obtained are more accurate than those determined in earlier investigations.[1,4] The rotational lines of the (1, 0) band of SH were observed to be *diffuse* while those of the (0, 0) band were sharp, establishing with certainty a predissociation in the first vibrational level of the $^2\Sigma$ state.

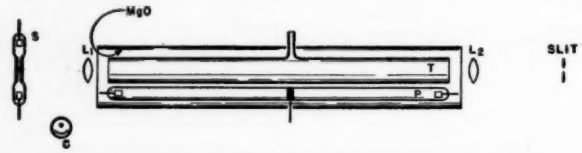

FIG. 1. Flash photolysis apparatus.

EXPERIMENTAL

1. Description of Apparatus

The flash photolysis apparatus was similar in many aspects to the one described earlier by Porter.[8] A quartz absorption tube T was mounted parallel to a quartz flash tube P known as the photolysis flash tube (see Fig. 1). The gas to be photolyzed was introduced into T and subjected to a light flash of high intensity and short duration ($\sim 10^{-3}$ sec) by discharging a bank of large condensers through P. To increase the amount of photodecomposition both tubes were surrounded by two hemicylinders coated with magnesium oxide.[9,10]

The absorption spectrum of the photolysis products was observed by mounting a second quartz flash tube S—known as the "source" tube—on the axis of T, and focusing it by means of quartz lenses L_1 and L_2 on to the slit of a 21 ft concave grating spectrograph. The source tube contained a central 3-mm quartz capillary and under suitable conditions (see below) emitted an almost pure continuum. The photolysis and source flashes were initiated by means of high voltage pulses from two spark coils applied to external trigger electrodes wrapped round the middle of the flash tubes, the time delay between the flashes being controlled by means of a thyratron circuit (see Fig. 2). The details of the apparatus were as follows:

Quartz absorption tube: 1-meter long, 5-cm diameter, fitted with quartz windows.

Photolysis flash tube: 1-meter long, 1-cm diameter, $\frac{3}{8}$-in. diameter tungsten electrodes, filled with xenon to 70-mm pressure, dissipates 4800 joules (600 μf at 4000 v) per flash, duration of flash 1.5×10^{-3} sec.

[1] M. N. Lewis and J. U. White, Phys. Rev. **55**, 894 (1939).
[2] A. G. Gaydon and G. Whittingham, Proc. Roy. Soc. (London) **A189**, 313 (1947).
[3] P. J. Dyne and D. W. G. Style, Nature **167**, 899 (1951).
[4] S. Leach, Compt. rend. **230**, 2181 (1950).
[5] S. Leach, Disc. Faraday Soc. No. 9, p. 81 (1950).
[6] G. Porter, Disc. Faraday Soc. No. 9, p. 60 (1950).
[7] G. Herzberg and D. A. Ramsay, Disc. Faraday Soc. No. 9, p. 80 (1950).
[8] G. Porter, Proc. Roy. Soc. (London) **A200**, 284 (1950).
[9] A. C. Menzies and J. Skinner, J. Sci. Instr. **26**, 299 (1949).
[10] The diffuse reflectance of magnesium oxide has been recently measured by W. E. K. Middleton and C. L. Sanders, J. Opt. Soc. Am. **41**, 419 (1951) and found to be between 95 percent and 98 percent for the spectral region 2400A to 8000A.

Source flash tube: Approximately 5-in. long with a central quartz capillary 2-in. long and 3-mm internal diameter, tungsten electrodes, filled with xenon to 150-mm pressure, dissipates 80 joules (10 μf at 4000 v) per flash, duration of flash 3×10^{-4} secs.

Details of the charging circuits and timing mechanism are given in Fig. 2. The condensers C_1, C_2, C_3, and C_4 were charged, and the firing sequence started by closing the control switch S_3. The condenser C_4 discharged through the primary of the spark coil SC_1 and triggered the photolysis flash. As the condenser C_1 discharged through the photolysis flash tube P, the negative potential on the grid of the thyratron M_3 decreased until at a certain potential the thyratron fired. This discharged the condenser C_3 through the spark coil SC_2 and triggered the source flash. The time delay between the photolysis and source flashes was determined by the constants of the circuits and could be varied from 0–5 milliseconds by means of the variable condenser C_5. The time delay was measured by means of a photocell coupled to the vertical plates of a cathode-ray oscilloscope and was found to be reproducible to better than 0.1 millisecond.

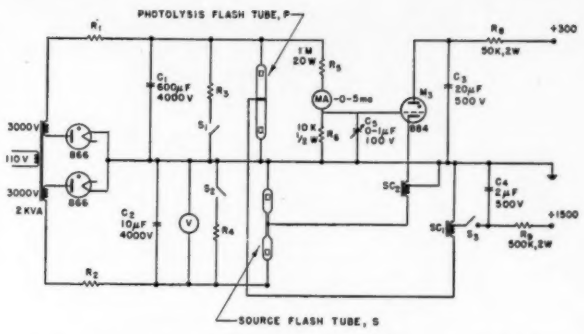

FIG. 2. R_1, R_2 charging resistors, R_3, R_4 discharging resistors. Electrical circuit diagram.

2. Flash Tube Performance[11]

It was found that if sufficient care was taken in outgassing the walls of the tube and the electrodes before filling with xenon, the photolysis flash tube could be flashed repeatedly at intervals of approximately 10 sec and had a lifetime of a few thousand flashes. The radiation emitted consisted mainly of xenon lines with very little continuum.

The radiation from the source tube consisted mainly of continuum with a few emission and absorption lines. The ratio of continuum to line emission could be increased by (a) increasing the capacity of the condensers, (b) increasing the voltage applied, (c) reducing the diameter of the quartz capillary. With the source tube used and a dissipation of 80 joules per flash, an almost pure continuum was obtained extending from 9000 to 2000A with virtually no emission lines and only a few silicon absorption lines. The quality of the continuum was found to be very sensitive to the internal diameter of the quartz capillary and deteriorated slowly with repeated flashing due to the gradual enlargement of the quartz capillary. After several thousand flashes when the internal diameter had increased with approximately 3 to 5 mm it became necessary to renew the quartz capillary.

3. Absorption Spectra of SH and SD

The H_2S was obtained from commercial cylinders while the D_2S was prepared by dropping 99.6 percent D_2O on to Al_2S_3 which had previously been heated to red heat to remove any H_2S. Both gases were purified by distilling twice from a dry ice trap to one at liquid air temperature.

Initial experiments were carried out varying (a) the pressure of H_2S or D_2S, and (b) the time interval between the photolysis and the source flashes to determine the conditions for the optimum concentration of SH and SD radicals. Eastman Kodak 103a0 plates were used with a wide slit (0.1 mm) so that exposures could be obtained with the 21-ft grating in a single flash. With pressures of H_2S from 1 to 10-mm Hg the (0, 0) SH band was obtained together with the $^3\Sigma-{}^3\Sigma$ absorption system of S_2 extending from 3300A to the H_2S absorption limit near 2450A. The S_2 bands were not very troublesome in the region of the (0, 0) SH band but were sufficiently intense to obscure most of the (1, 0) SH band. With higher pressures of H_2S (100–500-mm Hg) the S_2 bands were considerably reduced in intensity and the (1, 0) SH band was clearly visible. Under these conditions however the (0, 0) SH band appeared to be less intense. Similar results were obtained by adding an excess inert gas. Thus when H_2S at 10-mm pressure was photolyzed in the presence of 200-mm helium, the S_2 bands were again reduced in intensity and the (1, 0) SH band was readily observed. The (0, 0) SH band also was somewhat reduced in intensity. Variation of the time interval between the photolysis and source flashes indicated that the optimum concentration of SH radicals occurred, as might be expected, when the source flash immediately followed the photolysis flash, though weak spectra could be observed even 5 milliseconds after the photolysis flash.

Final plates were taken with a resolving power of $\sim$100,000. Five flashes were required using Eastman Kodak 103a0 plates. For the (0, 0) SH and SD bands, 10-mm pressure of H_2S or D_2S was used while for the (1, 0) bands 200-mm helium was added. The H_2S or D_2S was renewed between flashes, and the quartz absorption tube was flamed at the end of each exposure to remove the thin deposit of sulfur. A spectrogram of the (0, 0) SH band is shown in Fig. 3.

The rotational lines of the SD bands and the (0, 0) SH band were observed to be sharp while those of the

[11] Further discussions of flash tubes and their characteristics have been given by P. M. Murphy and H. E. Edgerton, J. Appl. Phys. **12**, 848 (1941); G. Porter (see references 6 and 8); G. D. Hoyt and W. W. MacCormick, J. Opt. Soc. Am. **40**, 658 (1950).

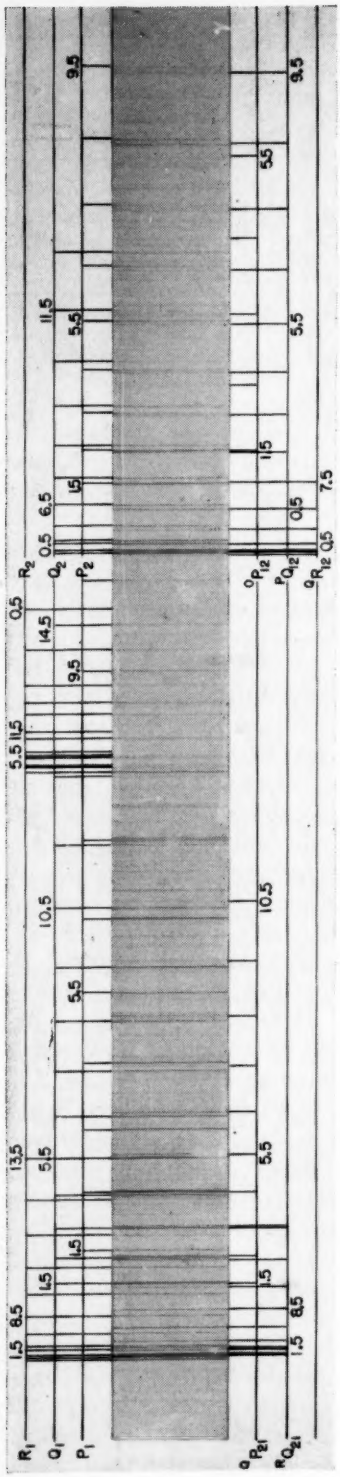

FIG. 3. The (0, 0) band of SH in absorption. The R_2 head is at 3236.6A and the Q_2 head is at 3279.3A.

(1, 0) SH band were found to be distinctly *diffuse*. Vacuum wave numbers were obtained in the usual manner[12] and are listed in Tables I–IV. The wave numbers are accurate to about 0.03 cm^{-1} for the sharp lines and 0.15 cm^{-1} for the diffuse lines.

[12] M. I. T. wavelength tables were used for the Fe lines, and Kayser's *Schwingungszahlen* were used for the vacuum corrections.

ROTATIONAL ANALYSIS

For a $^2\Sigma-^2\Pi_i$ (a) transition[13] a total of twelve branches is predicted by theory and are designated P_1, Q_1, R_1, ${}^QP_{21}$, ${}^RQ_{21}$, ${}^SR_{21}$ for the $^2\Sigma-^2\Pi_{\frac{3}{2}}$ sub-band and P_2, Q_2, R_2, ${}^OP_{12}$, ${}^PQ_{12}$, ${}^QR_{12}$ for the $^2\Sigma-^2\Pi_{\frac{1}{2}}$ sub-band. In the present investigation all twelve branches have been identified for the (0, 0) bands of SH and SD while only the stronger branches have been identified for the (1, 0) bands (Tables I–IV). The principal branches were picked out by inspection and the other branches identified by means of combination relations.[14]

1. Determination of Accurate Molecular Constants

A. The $^2\Sigma$ State

The rotational term values for a $^2\Sigma$ state are given by[15]

$$F_1(K)=B_vK(K+1)-D_vK^2(K+1)^2-\tfrac{1}{2}\gamma K, \quad (1)$$

$$F_2(K)=B_vK(K+1)-D_vK^2(K+1)^2-\tfrac{1}{2}\gamma(K+1), \quad (2)$$

where $F_1(K)$ refers to components with $J=K+\frac{1}{2}$ and $F_2(K)$ refers to those with $J=K-\frac{1}{2}$. B_v and D_v are effective rotational constants and γ is the spin doubling constant. When the initial and final states are in the relation of pure precession[16]

$$B_v=B_{v_{\text{true}}}-\frac{2B^2v_{\text{true}}l(l+1)}{\nu(\Pi,\Sigma)}, \quad (3)$$

where $B_{v_{\text{true}}}$ is the true rotational constant; $\nu(\Pi,\Sigma)$ is the separation of the Π from the Σ state, and $l=1$ for a Π state.

(*a*) *Determination of* γ.—The spin doubling in the $^2\Sigma$ state was determined from the combination relations[14]

$$R_1(J)-{}^RQ_{21}(J)=Q_1(J+1)-{}^QP_{21}(J+1)={}^QR_{12}(J)$$
$$-Q_2(J)={}^PQ_{12}(J+1)-P_2(J+1)=\gamma(J+1) \quad (4)$$

and found to be a linear function of J (see Fig. 4). The best values of γ obtained are given in Table V.

(*b*) *Determination of* B_v' *and* D_v'.—It is readily shown from Eqs. (1) and (2) that

$$\Delta_2F_1'(J)=(4B_v'-6D_v')J-8D_v'J^3+\gamma, \quad (5)$$

$$\Delta_2F_2'(J)=(4B_v'-6D_v')(J+1)-8D_v'(J+1)^3-\gamma. \quad (6)$$

The quantities $\Delta_2F_1'(J)$ and $\Delta_2F_2'(J)$ were obtained from the combination relations[14]

$$\Delta_2F_1'(J)=R_1(J)-P_1(J)={}^QR_{12}(J)-{}^OP_{12}(J), \quad (7)$$

$$\Delta_2F_2'(J)=R_2(J)-P_2(J)={}^SR_{21}(J)-{}^QP_{21}(J). \quad (8)$$

[13] G. Herzberg, Spectra of Diatomic Molecules (D. Van Nostrand Company Inc., New York, 1950), p. 258.

[14] See W. Jevons, "Report on the Band-Spectra of Diatomic Molecules" (The Physical Society, London, 1932), p. 164, for an energy level diagram of a $^2\Sigma-^2\Pi_i$ transition and pps. 172–3 for combination relations in a $^2\Sigma-^2\Pi_i$ band.

[15] See reference 13, p. 222.

[16] J. H. Van Vleck, Phys. Rev. **33**, 467 (1929).

TABLE I. Vacuum wave numbers and assignments of the rotational lines of the (0, 0) SH band.

J	P_1	Q_1	R_1	$^QP_{21}$	$^RQ_{21}$	$^SR_{21}$	P_2	Q_2	R_2	$^OP_{12}$	$^PQ_{12}$	$^QR_{12}$
0.5								30,480.88	30,513.57		30,464.38	30,481.38[a]
1.5	30,832.68	30,849.42	30,882.71	30,848.95	30,881.95	30,931.39	30,451.39	30,484.89	30,533.87	30,435.75[a]	30,451.88[a]	30,485.94[a]
2.5	30,803.45[a]	30,836.54	30,886.57[a]	30,835.76	30,885.30[a]	30,951.16	30,435.75[a]	30,485.94[a]	30,551.17	30,404.14	30,436.60	30,487.22
3.5	30,771.96	30,821.67[a]	30,888.01[a]	30,820.62	30,886.57[a]	30,968.89	30,417.44	30,484.50	30,565.76	30,369.84	30,418.55	30,485.94[a]
4.5	30,738.84	30,805.00	30,887.61[a]	30,803.45[a]	30,886.12[a]	30,984.57	30,396.30	30,479.92	30,577.34	30,332.80	30,397.69	30,481.75[a]
5.5	30,703.79	30,786.26[a]	30,885.30[a]	30,784.53	30,883.39	30,998.13	30,372.38	30,472.61	30,585.97	30,293.04	30,374.10	30,474.67
6.5	30,666.87	30,765.58	30,881.06	30,763.54	30,878.67	30,009.43	30,345.73	30,462.34	30,591.62	30,250.52	30,347.76	30,464.66
7.5	30,627.88	30,742.79	30,874.47	30,740.42	30,871.93[a]	31,018.50	30,316.25	30,449.25	30,594.27	30,205.40	30,318.63	30,451.88[a]
8.5	30,586.99	30,717.94	30,865.69	30,715.16[a]	30,862.69	31,025.09[a]	30,284.09	30,433.15	30,593.96	30,157.53	30,286.72	30,436.10
9.5	30,544.17	30,690.96	30,854.66	30,687.94	30,851.38	31,029.37	30,249.14	30,414.17	30,590.45	30,106.86	30,252.17	
10.5	30,499.22	30,661.69	30,841.27	30,658.21[a]	30,837.68	31,031.08	30,211.39	30,392.23	30,583.93		30,214.62	
11.5	30,452.03[a]	30,630.14	30,825.37		30,821.67[a]	31,030.03	30,170.83	30,367.30	30,574.30		30,174.42	
12.5	30,403.05	30,596.27	30,807.05		30,803.45[a]		30,127.48				30,131.35	
13.5		30,559.92	30,786.26[a]									
14.5		30,521.19										

[a] Denotes blended line.

The rotational constants were obtained by plotting

$$\frac{\Delta_2F_2'(J)-\gamma}{J} \quad \text{and} \quad \frac{\Delta_2F_2'(J-1)+\gamma}{J}$$

against J^2. The best straight line was determined by the method of least squares, each point being given a weight of J^2. The values of B_v' and D_v' obtained are given in Table V.

(*c*) *Determination of* $\Delta G_{\frac{1}{2}}'$ *and* α'.—The quantities $\Delta G_{\frac{1}{2}}'$ and α' were obtained from combination relations between corresponding lines of the (0, 0) and (1, 0) bands.[17] It is readily shown that

$$Q_1^{1,0}(J)-Q_1^{0,0}(J)=\Delta G_{\frac{1}{2}}'-(B_0'-B_1')(J-\tfrac{1}{2})(J+\tfrac{1}{2}), \quad (9)$$

neglecting terms involving $(D_0'-D_1')$ and $(\gamma_0-\gamma_1)$. Similar relations may be obtained for the other branches of the (0, 0) and (1, 0) bands. By plotting all these combination differences against $(J-\frac{1}{2})$ $(J+\frac{1}{2})$ the best values of $\Delta G_{\frac{1}{2}}'$ and $(B_0'-B_1')=\alpha'$ were obtained (see Table V).

(*d*) *Determination of* B_e', I_e' *and* r_e'.—From the B_0' and α' values obtained above, values of B_e', I_e', and r_e' were calculated[18] (see Table V). The r_e' values agree to 0.001_0A which is the order of agreement found for hydrides and deuterides.[19] It should be noted however that these r_e' values are still effective values, and the agreement is slightly improved if true values are calculated using Eq. (3). The values obtained are

$$\text{for SH } r_{e_{\text{true}}}=1.422_2\text{A}, \quad \text{for SD } r_{e_{\text{true}}}=1.422_9\text{A}.$$

B. The $^2\Pi$ *State*

Two general expressions have been derived for the rotational term values of the components of a $^2\Pi$ state. In the first, due to Hill and Van Vleck[20,21] the centrifugal distortion term has been assumed to be the same as for Hund's case (b). The term values are given by

$$F_1(J)=B_v[(J+\tfrac{1}{2})^2-\Lambda^2-\tfrac{1}{2}\{4(J+\tfrac{1}{2})^2+Y(Y-4)\Lambda^2\}^{\frac{1}{2}}] -D_vJ^4\pm\varphi_1(J),$$

$$F_2(J)=B_v[(J+\tfrac{1}{2})^2-\Lambda^2+\tfrac{1}{2}\{4(J+\tfrac{1}{2})^2+Y(Y-4)\Lambda^2\}^{\frac{1}{2}}] -D_v(J+1)^4\pm\varphi_2(J), \quad (10)$$

where $Y=A/B_v$, A is the spin-coupling constant and $\varphi_i(J)$ denotes the expressions for the Λ-doubling. Terms for which $\varphi_i(J)$ are positive are denoted F_{1d}, F_{2d} while those for which $\varphi_i(J)$ are negative are denoted F_{1c}, F_{2c}.

TABLE II. Vacuum wave numbers and assignments of the rotational lines of the (1, 0) SH band.

J	P_1	Q_1	R_1	$^RQ_{21}$	Q_2	P_2
0.5					32,264.54[a]	
1.5	32,617.72[a]	32,633.04	32,664.18[a]	32,663.53[a]	32,266.50[a]	32,234.95
2.5	32,586.98	32,617.72[a]	32,664.18[a]	32,663.53[a]	32,264.54[a]	
3.5	32,553.73	32,599.69[a]	32,662.80[a]	32,660.83[a]	32,258.90	
4.5	32,517.16	32,579.34	32,657.25		32,249.42	
5.5	32,478.37	32,555.73	32,648.73		32,235.88	
6.5	32,436.09	32,528.85			32,218.50	
7.5	32,390.93	32,498.98				
8.5		32,465.76				

[a] Denotes blended line.

[17] See G. Herzberg, reference 13, p. 188.

[18] The formula $B_e=\frac{27.98_{30}\times10^{-40}}{I_e}$ (G. Herzberg, reference 13, p. 106) was employed. Reduced masses were calculated from the isotopic data given by J. Mattauch and A. Flammersfeld, Z. Naturforsch. (Tübingen) (1949), and the following values obtained: $\mu_{SH}=0.97732_{24}$ at. wt units, $\mu_{SD}=1.895323_{01}$ at. wt units.

[19] G. Herzberg, reference 13, pp. 501–581.

[20] E. L. Hill and J. H. Van Vleck, Phys. Rev. **32**, 250 (1928).

[21] See also R. S. Mulliken and A. Christy, Phys. Rev. **38**, 87 (1931).

TABLE III. Vacuum wave numbers for the (0, 0) SD band.

J	P_1	Q_1	R_1	$^QP_{21}$	$^RQ_{21}$	$^SR_{21}$	P_2	Q_2	R_2	$^OP_{12}$	$^PQ_{12}$	$^QR_{12}$
0.5								30,584.73[a]	30,601.15		30,576.14	30,584.73[a]
1.5	30,948.24[a]	30,957.19[a]	30,974.27[a]	30,956.80[a]	30,973.92[a]	30,999.47	30,569.80[a]	30,586.98[a]	30,612.15		30,569.80[a]	30,587.66[a]
2.5	30,932.78	30,950.10	30,976.00[a]	30,949.66[a]	30,975.33[a]	31,009.73	30,562.25[a]	30,588.03[a]	30,621.90[a]	30,545.37	30,562.25[a]	30,588.46[a]
3.5	30,916.24	30,942.12	30,976.63	30,941.58[a]	30,976.00[a]	31,018.80	30,552.87	30,587.66[a]	30,630.02	30,528.20	30,553.31	30,588.46[a]
4.5	30,898.64	30,933.06	30,976.00[a]	30,932.33	30,975.33[a]	31,026.66	30,542.40	30,586.04	30,636.69	30,509.44	30,543.15	30,586.98
5.5	30,880.00	30,923.01	30,974.63	30,922.08	30,973.62	31,033.45[a]	30,530.77	30,583.05	30,642.08	30,489.19[a]	30,531.61	30,584.07
6.5	30,860.30	30,911.85	30,971.97	30,910.78	30,970.69	31,039.15[a]	30,517.72	30,578.66	30,646.13	30,468.31	30,518.78	30,579.89
7.5	30,839.46[a]	30,899.56	30,968.22	30,898.39	30,966.80	31,043.80	30,503.44	30,572.96	30,648.72	30,445.76	30,504.61	30,574.37
8.5	30,817.68	30,886.19	30,963.33	30,884.85	30,961.77	31,046.98	30,487.79	30,565.93	30,649.73[a]		30,489.19[a]	30,567.39[a]
9.5	30,794.77	30,871.73	30,957.19	30,870.22	30,955.55	31,049.20	30,470.85	30,557.52	30,649.73[a]		30,472.38	30,559.47[a]
10.5	30,770.79	30,856.12	30,949.66[a]	30,854.43	30,948.24[a]	31,050.07	30,452.46	30,547.71			30,454.21	
11.5	30,745.75	30,839.46[a]	30,941.58[a]	30,837.56	30,939.69		30,432.88	30,536.52			30,434.83	
12.5	30,719.48	30,821.54		30,819.45			30,411.81[a]	30,523.92			30,413.93	
13.5	30,692.13	30,802.51										
14.5		30,782.25										
15.5		30,760.83										

[a] Denotes blended line.

In the second expression, due to Almy and Horsfall,[22] a more detailed treatment of the centrifugal distortion term has been considered. The formulas developed are considerably more complicated than the Hill and Van Vleck expressions, but give a somewhat better representation of the term values and slight modifications in the molecular constants (see below).

(*a*) *Determination of B_v'' and D_v''.*—It may be shown from (10) that

$$\frac{\Delta_2F_1''(J)+\Delta_2F_2''(J)}{4J+2} = (2B_v''-7D_v'')-4D_v''(J+\tfrac{1}{2})^2. \quad (11)$$

The LHS involves the mean of the four second differences Δ_2F_{1c}'', Δ_2F_{1d}'', Δ_2F_{2c}'', Δ_2F_{2d}''. Since it was not possible in general to derive all these quantities for a given value of J from the usual combination relations[14] without using blended lines, it was decided to calculate the term values of the $^2\Pi$ state from those of the $^2\Sigma$ state and the wave numbers of the unblended lines. When more than one value for a given term value was obtained, the mean was taken. The rotational constants B_v'' and D_v'' were determined by plotting $[\Delta_2F_1''(J)+\Delta_2F_2''(J)]/[4J+2]$ against $(J+\frac{1}{2})^2$ and determining the best straight line by the method of least squares, each point being given a weight of $(J+\frac{1}{2})^2$. The values obtained are given in Table V.

The formulas of Almy and Horsfall[22] give a similar expression to Eq. (11) except that the intercept is $(2B_v''-2D_v'')$. The slopes are identical. There is thus a discrepancy of $2\frac{1}{2}$ D_v'' between the B_v'' values calculated by the two methods although the D_v'' values are identical. It should be remembered that the B_v'' and D_v'' values obtained by these methods are effective rotational constants and to obtain true B_v'' values a small correction term must be applied.[22]

(*b*) *Determination of the Λ-Doubling.*—The doublet separations $\Delta\nu_{dc}$ for the Λ-doubling in a $^2\Pi$ state are given by[16,21]

$$\Delta\nu_{dc}(J)=[(\tfrac{1}{2}p+q)(\pm1+2X^{-1}-YX^{-1}) +2qX^{-1}(J-\tfrac{1}{2})(J+\tfrac{3}{2})](J+\tfrac{1}{2}), \quad (12)$$

where the + sign in ±1 refers to F_2 levels and the − sign to F_1 levels and $X=+[Y(Y-4)+(J+\frac{1}{2})^2]^{\frac{1}{2}}$, $Y=A/B_v$,

$$p=p_0\Big/\left[1+\frac{D_v}{B_v}J(J+1)\right], \quad q=q_0\Big/\left[1+\frac{D_v}{B_v}J(J+1)\right]^2.$$

For the case of "pure precession"

$$p_0=\frac{2AB_vl(l+1)}{\nu(\Pi,\Sigma)}, \quad q_0=\frac{2B_v^2l(l+1)}{\nu(\Pi,\Sigma)}. \quad (13)$$

The doublet separations were calculated directly from the energy levels of the $^2\Pi$ state and were checked by means of combination relations.[14,21] The doublet separations are shown in Fig. 5. The Λ-doubling curves for SH are remarkably similar to those for the isoelectronic molecule HCl^+ both in form and magnitude.[21] The values of p_0 and q_0 in Eq. (12) required to give the best fit with the experimental data were found by trial and error and were compared with the theoretical values calculated from Eq. (13) assuming pure precession. The values obtained were found to be in reasonable agreement, *viz.*,

	Experimental		Theoretical	
	p_0	q_0	p_0	q_0
SH	0.304	−0.012	0.465	−0.012
SD	0.160	−0.0031	0.238	−0.0031

TABLE IV. Vacuum wave numbers for the (1, 0) SD band.

J	P_1	Q_1	R_1	$^QP_{21}$	$^RQ_{21}$
1.5	32,267.67	32,275.79[a]	32,292.49[a]	32,275.79[a]	32,291.99[a]
2.5	32,251.73	32,268.28	32,292.49[a]	32,267.97[a]	32,292.49[a]
3.5	32,234.48	32,259.19	32,291.99[a]	32,258.62	32,291.57[a]
4.5	32,215.76	32,248.68	32,289.95	32,248.00	32,289.09
5.5	21,195.61	32,236.84	32,286.25	32,235.89	32,285.18
6.5	32,174.06[a]	32,223.43	32,280.89	32,222.39	32,279.74
7.5	32,151.13	32,208.54	32,274.26	32,207.26	32,272.95
8.5	32,126.70	32,192.32	32,266.08	32,190.88	32,264.56
9.5	32,100.98	32,174.46	32,256.49	32,172.97	32,254.67
10.5	32,073.64	32,155.29		32,153.61	32,243.27
11.5	32,044.85	32,134.26		32,132.52	
12.5		32,112.09			

[a] Denotes blended line.

[22] G. M. Almy and R. B. Horsfall, Phys. Rev. **51**, 491 (1937).

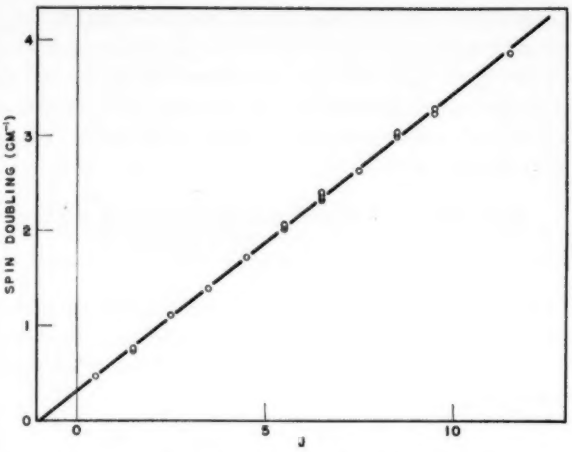

FIG. 4. Spin doubling in the (0, 0) SH band as a function of J.

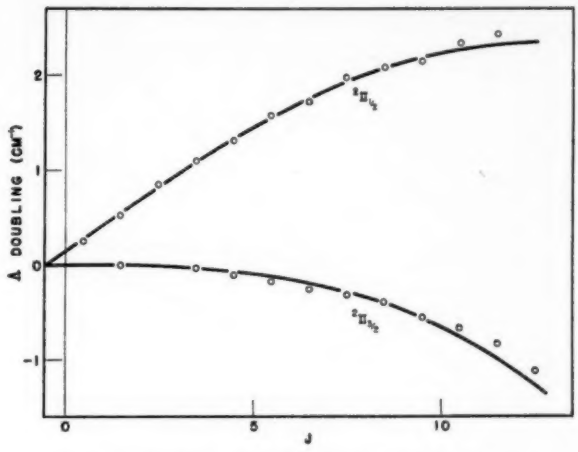

FIG. 5. Λ-doubling in the $^2\Pi_{\frac{3}{2}}$ and $^2\Pi_{\frac{1}{2}}$ states of SH.

(*c*) *Determination of the spin-coupling constant A.*—It is readily seen from (10) that

$$\left\{\frac{F_1''(J)-F_2''(J)-D_v''[(J+1)^4-J^4]}{B_v''}\right\}^2 -4(J+\tfrac{1}{2})^2=Y(Y-4). \quad (14)$$

Values of Y and A were calculated for different J using the $F_1''(J)$, $F_2''(J)$, B_v'' and D_v'' values obtained above. The values of A obtained were not constant but depended slightly on J. By plotting A against $(J-\frac{1}{2})^2$ a linear relationship was obtained (see Fig. 6). The values of A given in Table V were obtained by extrapolating to $(J-\frac{1}{2})^2=0$.

Further values of A were calculated using the Almy and Horsfall formulas and were found to be linearly dependent on $(J-\frac{1}{2})^2$ (see Fig. 6). The slope of the graph using the Almy and Horsfall values was somewhat less than with the Hill and Van Vleck values, though the intercepts in the two cases were the same to within 0.10 cm^{-1}.

(*d*) *Determination of* ν_{00}.—The quantity ν_{00} was obtained from the wavenumbers of the Q_1 and Q_2 lines by means of the equation

$$Q_1(J)+Q_2(J)+D_v'[(J-\tfrac{1}{2})^2(J+\tfrac{1}{2})^2 +(J+\tfrac{1}{2})^2(J+\tfrac{3}{2})^2]-D_v''[J^4+(J+1)^4] +\varphi_1(J)-\varphi_2(J)=2\nu_{00}+2(B_v'-B_v'')J(J+1) +\tfrac{1}{2}B_v'+\tfrac{3}{2}B_v''-\gamma. \quad (15)$$

The LHS was plotted against $J(J+1)$ and the best straight line determined by the method of least squares. The values obtained for ν_{00} for SH and SD are given in Table V. Identical values of ν_{00} were obtained using the formulas of Almy and Horsfall.

(*e*) *Comparison of the* HVV *and* AH *formulas.*—Term values for the $^2\Pi$ state were calculated using the formulas of Hill and Van Vleck and Almy and Horsfall using the molecular constants determined above. The values obtained by the AH formulas were found to be in better agreement with the experimental term values than those calculated by the HVV formulas, the discrepancies for term values of 1000 cm^{-1} being ~0.3 cm^{-1} for the AH formulas and ~0.8 cm^{-1} for the HVV formulas (see Fig. 7).

TABLE V. Molecular constants of SH and SD.

	SH	SD	Units
A. The $^2\Sigma$ state			
γ_0	0.313	0.163	cm^{-1}
B_0'	8.283_6	4.304_5	cm^{-1}
D_0'	0.00066_6	0.00018_1	cm^{-1}
$\Delta G_{\frac{1}{2}}'$	1784.6_3	1319.3_0	cm^{-1}
α'	0.509_1	0.183_6	cm^{-1}
B_e'	8.538_1	4.396_3	cm^{-1}
I_e'	3.277_4	6.365_1	$\times 10^{-40}$ g cm^2
r_e'	1.421_5	1.422_5	A
ν_{00}	$30{,}662.4_2$	$30{,}769.4_9$	cm^{-1}
B. The $^2\Pi$ state			
B_0''	9.461_1	4.900_3	cm^{-1}
D_0''	0.00048_0	0.00013_5	cm^{-1}
r_0	1.350_3	1.347_3	A
A_0	-376.9_6	-376.7_5	cm^{-1}

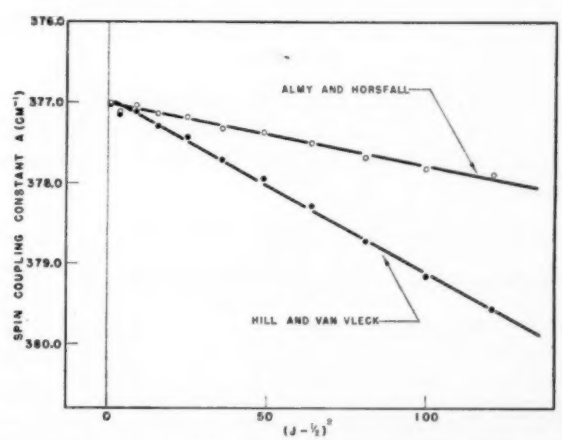

FIG. 6. The spin-coupling constant A as a function of $(J-\frac{1}{2})^2$.

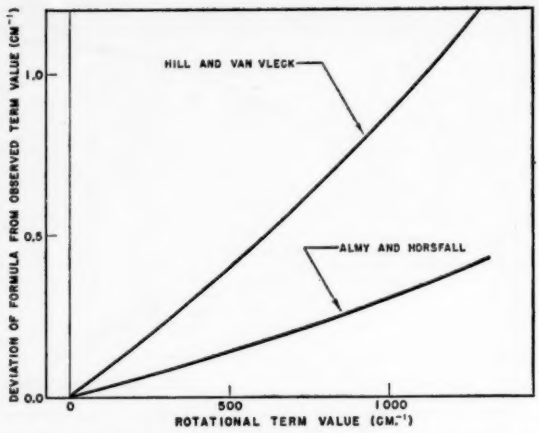

FIG. 7. The differences between the observed rotational term values for the $^2\Pi$ state and those calculated using the energy formulas of Hill and Van Vleck and Almy and Horsfall, plotted as a function of the rotational term value.

2. Molecular Constants Derived from Isotopic Relations

The molecular constants above have been determined with a high degree of precision. Further molecular constants may be calculated with a moderate degree of accuracy using certain isotopic relations.

A. The $^2\Sigma$ State

(*a*) *Estimation of ω_e' and $\omega_e'x_e'$.*—The quantities ω_e' and $\omega_e'x_e'$ were determined by means of the isotopic relations.[23]

$$\Delta G_{\frac{1}{2}}' = \omega_e' - 2\omega_e'x_e', \tag{16}$$

$$\Delta G_{\frac{1}{2}}{}^{i\prime} = \rho\omega' - \rho^2\omega_e'x_e', \tag{17}$$

where $\rho=(\mu/\mu^i)^{\frac{1}{2}}$. The values obtained are given in Table VI.

B. The $^2\Pi$ State

(*a*) *Estimation of B_e'', I_e'', and r_e''.*—Although only B_0'' values have been determined accurately for SH and SD, fairly reliable estimates for the B_e'' values (see Table VI) may be obtained using the conditions[24]

$$\begin{aligned} r_e{}^i &= r_e, \\ \alpha_e{}^i &= \rho^3\alpha_e. \end{aligned} \tag{18}$$

Values of I_e'' and r_e'' are then easily deduced.

(*b*) *Estimation of ω_e'', $\omega_e''x_e''$, and ν_e.*—The quantities ω_e'', $\omega_e''x_e''$, and ν_e were estimated from the relations[25]

$$\nu_{00} = \nu_e + \tfrac{1}{2}\omega_e' - \tfrac{1}{4}\omega_e'x_e' - \tfrac{1}{2}\omega_e'' + \tfrac{1}{4}\omega_e''x_e'', \tag{20}$$

$$\nu_{00}{}^i = \nu_e + \tfrac{1}{2}\rho\omega_e' - \tfrac{1}{4}\rho^2\omega_e'x_e' - \tfrac{1}{2}\rho\omega_e'' + \tfrac{1}{4}\rho^2\omega_e''x_e'', \tag{21}$$

$$\alpha_e = \frac{6(\omega_e x_e B_e{}^3)^{\frac{1}{2}}}{\omega_e} - \frac{6B_e{}^2}{\omega_e}. \tag{22}$$

[23] G. Herzberg, reference 13, p. 142.
[24] G. Herzberg, reference 13, p. 144.
[25] Reference 13, pp. 162. 108.

Equation (22) is based on a Morse potential function and is accurate to 2 percent for the $^2\Sigma$ states of SH and SD. By using the values of α estimated above and the accurate values determined for ν_{00} and $\nu_{00}{}^i$, values for ω_e'', $\omega_e''x_e''$, and ν_e were calculated with the accuracies indicated in Table VI.

NATURE OF THE PREDISSOCIATION AND DISCUSSION OF DISSOCIATION ENERGIES

The possible electronic states of SH formed from the low lying electronic states of sulfur and hydrogen may be determined by means of the Wigner-Witmer correlation rules[26] as follows:

$$\begin{aligned} &H(^2S_g)+S(^3P_g)\rightarrow{}^2\Sigma^-,\ ^2\Pi,\ ^4\Sigma^-,\ ^4\Pi, \\ &H(^2S_g)+S(^1D_g)\rightarrow{}^2\Sigma^+,\ ^2\Pi,\ ^2\Delta, \\ &H(^2S_g)+S(^1S_g)\rightarrow{}^2\Sigma^+. \end{aligned}$$

The only low-lying electronic state of the united atom Cl is the ^2P_u ground state which splits[27] into the observed $^2\Sigma^+$ and $^2\Pi$ states for SH. All the other possible electronic states of SH given above have to be correlated with excited states[28] of the united Cl atom at $\sim$70,000−80,000 cm^{-1} above the ground state. It seems probable, therefore, that these other states are either repulsive or have shallow potential minima.

The existence of only two low lying electronic states for SH is consistent with predictions based on electron configuration,[29] *viz.*,

$$\begin{aligned} &(3s\sigma)^2(3p\sigma)^2(3p\pi)^3\rightarrow{}^2\Pi_i \\ &(2s\sigma^2)(3p\sigma)(3p\pi)^4\rightarrow{}^2\Sigma^+. \end{aligned}$$

For all these reasons it seems highly probable that the $^2\Pi_i$ ground state of SH dissociates into normal atoms while the $^2\Sigma^+$ state dissociates into $S(^1D_g)+H(^2S_g)$ (see Fig. 8).

The diffuseness of the rotational lines of the (1, 0) band of SH indicates a predissociation into normal atoms and immediately establishes both an upper and a

TABLE VI. Molecular constants of SH and SD derived from isotope relationships.

	SH	SD	Units
A. The $^2\Sigma$ state			
ω_e'	1971	1415	cm^{-1}
$\omega_e'x_e'$	93	48	cm^{-1}
ν_e	31,036	31,036	cm^{-1}
B. The $^2\Pi$ state			
B_e''	9.61_1	4.95_6	cm^{-1}
α_e''	0.30_0	0.11_1	cm^{-1}
I_e''	2.91_2	5.64_6	$\times10^{-40}$ g cm^2
r_e''	1.34_0	1.34_0	A
ω_e''	2702	1940	cm^{-1}
$\omega_e''x_e''$	60	31	cm^{-1}

[26] Reference 13, p. 318.
[27] Reference 13, p. 322.
[28] Charlotte E. Moore, *Atomic Energy Levels*, Vol. 1, National Bureau of Standards, Circular No. 467, (1949).
[29] Reference 13, p. 336.

lower limit for the dissociation energy of SH in the ground state. Since for the SH (1, 0) band, $\nu_{10}=32{,}477\cdot05$ cm^{-1}, the upper limit is given by $D_0''<32{,}477$ cm^{-1} ($=92.7$ kcal$=4.02$ ev), while the lower limit is obtained by subtracting the energy of excitation of a sulfur atom from the ^3P to the ^1D state, *viz.*, $D_0''>23{,}208$ cm^{-1} ($=66.3$ kcal$=2.88$ ev).

A further rough estimate of the dissociation energy of SH may be obtained using the Birge-Sponer relation[30]

$$D_0=(\omega_e^2/4\omega_e x_e)-G(0). \tag{23}$$

For the $^2\Sigma^+$ state this gives a value of $D_0'=9450$ cm^{-1}. It should be remembered however that the values of ω_e and $\omega_e x_e$ were obtained using isotope relationships. If it is assumed that a linear Birge-Sponer extrapolation gives a value which is about 20 percent too high[31] as has been found for many molecules with non-ionic binding, then $D_0'=7560$ cm^{-1}. The dissociation energy of the ground state of SH may now be obtained by adding ν_{00} and subtracting the energy of excitation of a sulfur atom from a ^3P to a ^1D state, giving $D_0''=28{,}980$ cm^{-1} ($=82.8$ kcal$=3.59$ ev). Fortunately, the $^2\Sigma^+$ state is a shallow state, so that even if the dissociation energy for this state is in error by as much as 50 percent, the ground state dissociation energy will still be accurate to ~4000 cm^{-1} (~11 kcal ~0.5 ev). These figures are in good agreement with the results of Porter[32] and Darwent and Sehon,[33] but are at variance with the dissociation energy quoted by Franklin and Lumpkin.[34]

Since the widths of the rotational lines of the (1, 0) SH band are ~0.1 cm^{-1}, the lifetime of the SH radical in this state is $\sim10^{-10}$ sec compared with the normal radiation lifetime $\sim10^{-8}$ sec. This indicates a fairly strong predissociation which is somewhat surprising

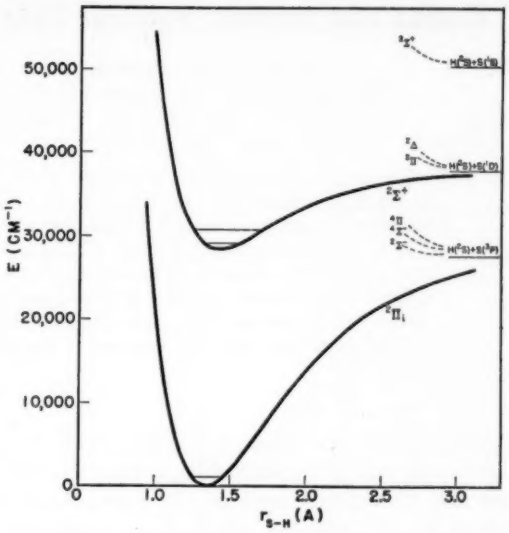

FIG. 8. Approximate potential curves for SH.

since the only states which could produce the predissociation are the $^2\Sigma^-$, $^4\Sigma^-$, and $^4\Pi$ states, and predissociation by these states is forbidden by the selection rules[35] $\Delta S=0$ and $\Sigma^+\leftrightarrow\Sigma^-$. It is well known, however, that these selection rules hold less rigorously for molecules containing heavy atoms. A similar predissociation in the $^2\Sigma^+$ state of OH has been found by Gaydon and Wolfhard[36] and attributed by them to predissociation by the $^2\Sigma^-$ state.

The author is indebted to Dr. G. Herzberg for his continued interest in this work and for many helpful discussions. The author wishes to express his thanks to Dr. A. E. Douglas for many helpful experimental suggestions. The author is indebted to Mr. G. Ensell for his skill and patience in the construction and repair of the flash tubes. Finally, the author wishes to express his thanks to Mr. F. Doren for valuable assistance in the construction of the apparatus and to Miss R. H. Craig for much help with the numerical computations.

[30] G. Herzberg, reference 13, p. 100.
[31] A. G. Gaydon, Proc. Phys. Soc. (London), **58**, 525 (1946).
[32] G. Porter, Disc. Faraday Soc. No. 9, p. 60 (1950).
[33] A. H. Sehon and B. deB. Darwent, J. Chem. Phys. (to be published); see also A. H. Sehon, J. Chem. Phys. (to be published).
[34] J. L. Franklin and H. E. Lumpkin, J. Am. Chem. Soc. **74**, 1023 (1952).
[35] G. Herzberg, reference 13, p. 416.
[36] A. G. Gaydon and H. G. Wolfhard, Proc. Roy. Soc. (London), **A208**, 63 (1951).

Raman and Infrared Spectral Data and Assignments for Dimethyldiacetylene*

SALVADOR M. FERIGLE,† FORREST F. CLEVELAND, AND ARNOLD G. MEISTER
Spectroscopy Laboratory, Department of Physics, Illinois Institute of Technology, Chicago 16, Illinois
(Received May 24, 1952)

Raman displacements and quantitative depolarization factors, and wave numbers for the infrared bands in the KBr region have been obtained for dimethyldiacetylene in CCl_4 and benzene solutions. Since the results of the present work are inconsistent with some of the previous assignments, these have been changed. In particular, the line at 475 cm^{-1}, which was previously considered an A_1-type fundamental vibration, is now proved to be depolarized and is assigned as an E-type fundamental. Consistently with this change, the assignment of the 644 cm^{-1} line of diacetylene as a bending mode is considered. The previous assignments of both of these lines were the cause of the conflicting data existing in the literature between the bond length and the stretching potential constant of the central bond in the structure $-C\equiv C-C\equiv C-$.

THREE papers have been published on the molecular spectra of dimethyldiacetylene (DMDA). Meister and Cleveland[1] reported Raman spectral data of DMDA in CCl_4 solution and made an assignment of the Raman frequencies. Later,[2] they published the normal coordinate treatment of the nondegenerate vibrations of this molecule and modified some of the assignments. Finally, Cleveland, Greenlee, and Bell[3] reported infrared absorption data for DMDA in the region 700 to 6000 cm^{-1} and gave a tentative list of fundamental frequencies.

The experimental data of previous investigations were incomplete. On the one hand, the depolarization factors given before[1] were obtained by a double-exposure method[4] which later was found to be inaccurate, especially in the case of compounds like DMDA which decompose under exposure to the exciting light. More recently, a single-exposure method has been developed in this laboratory.[5] For this reason and because some lines of the compound could be overlapped by CCl_4 bands, it seemed desirable to obtain the Raman spectrum in more than one solvent and to obtain precise polarization data. On the other hand, the study of the infrared absorption in the region below 700 cm^{-1} was also necessary since several of the fundamental frequencies lie in this region. Furthermore, as a consequence of the lack of experimental data the normal coordinate treatment of the degenerate vibrations was not carried out in the earlier investigations. The object of the present work was to add new Raman and infrared data to those previously reported for DMDA with the aim of completing the assignments. The normal coordinate treatment and the thermodynamic properties will be published later.

The sample of DMDA used in this research was furnished by Dr. K. W. Greenlee and was reported to be 99.9 percent pure. The method of preparation as well as the method used to determine the purity of the sample have been described by Cleveland, Greenlee, and Bell.[3]

RAMAN SPECTRUM

The Raman spectrum has been obtained in both CCl_4 and benzene solutions. The spectrograms were obtained on Eastman 103-J plates with a Hilger *E*-518 spectrograph having a dispersion of 320 cm^{-1}/mm at 4500A and with a two-prism spectrograph having a dispersion of 144 cm^{-1}/mm at 4500A, with Hg 4358A as the exciting line, by the experimental methods previously described.[6] The depolarization factors have been obtained by the single-exposure method given by Cleveland[5] and measured with a Leeds and Northrup microphotometer equipped with a Speedomax pen recorder, as described in a previous paper.[7] The present results and those of the previous investigation[1] are given in Table I.

INFRARED SPECTRUM

Infrared absorption data have been obtained with a Beckman *IR*-2 spectrometer equipped with KBr optics. A continuous slit drive was used to maintain the incident energy as constant as possible. The results of the present and the previous investigation[3] are given in Table I. A sample of the compound was sent to Dr. E. K. Plyler of the National Bureau of Standards who kindly obtained the spectrum in the region of low wave numbers (below 400 cm^{-1}) for which no instrument is available in our laboratory; his results are incorporated in Table I.

* Partly presented at the Chicago meeting of the American Physical Society, November 1950; abstract in Phys. Rev. **81**, 302 (1951), and at the Symposium on Molecular Structure and Spectroscopy, Ohio State University, June 1951. This work has been supported in part by a grant from the Research Corporation and by contract DA-11-022-ORD-464 with the Office of Ordnance Research.

† One of the investigations carried out in partial fulfillment of the requirements for the Ph.D. degree.

[1] A. G. Meister and F. F. Cleveland, J. Chem. Phys. **12**, 393 (1944).

[2] A. G. Meister and F. F. Cleveland, J. Chem. Phys. **15**, 349 (1947).

[3] Cleveland, Greenlee, and Bell, J. Chem. Phys. **18**, 355 (1950).

[4] F. F. Cleveland and M. J. Murray, J. Chem. Phys. **7**, 396 (1939).

[5] F. F. Cleveland, J. Chem. Phys. **13**, 101 (1945). This new method has been erroneously referred to in a recent paper (P. Bender and P. A. Lyons, J. Chem. Phys. **18**, 438 (1950)) as a double-exposure method.

[6] F. F. Cleveland, J. Chem. Phys. **11**, 1, 227 (1943).

[7] Ferigle, Cleveland, Boyer, and Bernstein, J. Chem. Phys. **18**, 1073 (1950).

TABLE I. Raman and infrared spectral data and assignments for dimethyldiacetylene (2,4-hexadiyne, $H_3C-C\equiv C-C\equiv C-CH_3$).[a]

Raman $\Delta\nu$			Raman ρ		Infrared ν_a	I_a	Infrared ν_a	I_a	Infrared ν_a	I_a			
MC	*PR*	I[e]	*MC*	*PR*	*CGB* Gas		*CGB* Solution		*PR*		Assignment[b]	Calc.	Type
247	246	8	0.64	0.83							$\nu_{20}{}^{sk}$		$\bar{E}$
											$\nu_{15}+\nu_{20}$	(347)	$\bar{A}_1+\bar{A}_2+\bar{E}$
	345	*vw*									$(\nu_{14}+\nu_{20})-\nu_{20}$	346	$\bar{A}_1+\bar{A}_2+2E+\bar{E}$
	357	*vw*							353[d]	*s*	$\nu_{14}{}^{sk}$		E
									472[d]	*m*	$(\nu_{19}+\nu_{20})-\nu_{20}$	474	$\bar{A}_1+\bar{A}_2+3\bar{E}$
475	475	22	0.64	0.84							$\nu_{19}{}^{sk}$		$\bar{E}$
	494	*vw*									$2\nu_{20}$	494	A_1+E
	554	*vw*									$\nu_5{}^{C-C}$		A_1
									593	*m*	$\nu_{14}+\nu_{20}$	600	$\bar{A}_1+\bar{A}_2+\bar{E}$
686		*vw*									$2\nu_{14}$	706	A_1+E
					721	*vw*					$\nu_{19}+\nu_{20}$	722	A_1+A_2+E
					941	*m*	940	*m*	941	*m*	$\nu_{10}{}^{C-C}$		$\bar{A}_2$
957		*vw*									$2\nu_{19}$	950	A_1+E
1020	1027	*vw*									$\nu_{18}{}^{CH_3}$		$\bar{E}$
					1030	*vw*	1016	*m*	1020	*m*	$\nu_{13}{}^{CH_3}$		E
1151		*vw*									$2\nu_{14}+\nu_{19}$	1161	$\bar{A}_1+\bar{A}_2+2\bar{E}$
1185		*vw*									$\nu_{10}+\nu_{20}$	1188	E
1228		*vw*									$\nu_4{}^{C-C}$		A_1
1253	1255	2			1254	*m*	1253	*w*			$\nu_{18}+\nu_{20}$	1271	A_1+A_2+E
											$\nu_{13}+\nu_{20}$	1277	$\bar{A}_1+\bar{A}_2+\bar{E}$
					1379	*s*	1369	*s*			$\nu_9{}^{CH_2}$		$\bar{A}_2$
1381	1381	12	0.62	0.54							$\nu_3{}^{CH_3}$		A_1
1426	1428	1									$\nu_{17}{}^{CH_3}$		$\bar{E}$
1458		*vw*			(1472)	*m*	1433	*s*			$\nu_{12}{}^{CH_3}$		E
											$2\nu_{18}$	2048	A_1+E
					2050	*m*	2037	*w*			$\nu_{13}+\nu_{18}$	2054	$\bar{A}_1+\bar{A}_2+\bar{E}$
											$2\nu_{13}$	2060	A_1+E
					2163	*w*	2157	*m*			$\nu_8{}^{C\equiv C}$		$\bar{A}_2$
2225		*vw*			2234	*m*	2223	*m*			$\nu_4+\nu_{18}$	2252	$\bar{E}$
											$\nu_4+\nu_{13}$	2262	E
2264	2265	100	0.40	Pol.[e]							$\nu_2{}^{C\equiv C}$		A_1
2309	2309	1									$\nu_9+\nu_{10}$	2320	A_1
2502	2507	*vw*									$\nu_2+\nu_{20}$	2512	$\bar{E}$
					2667	*vw*					$\nu_4+\nu_{12}$	2686	E
					2782	*m*	2758	*w*			$\nu_3+\nu_9$	2760	$\bar{A}_2$
2821		*vw*									$\nu_9+\nu_{12}$	2837	$\bar{E}$
											$\nu_3+\nu_{12}$	2839	E
2848	2849	2									$2\nu_{17}$	2852	A_1+E
							2867	*m*			$\nu_{12}+\nu_{17}$	2884	$\bar{A}_1+\bar{A}_2+\bar{E}$
2914	2914	40	0.17	0.10							$\nu_1{}^{CH}$		A_1
					2947	*s*	2920	*s*			$\nu_7{}^{CH}$, $\nu_{11}{}^{CH}$		$\bar{A}_2$, E
2954	2953	4									$\nu_{16}{}^{CH}$		$\bar{E}$
					3277	*s*	3262	*vw*			$\nu_{14}+\nu_{16}$	3268	$\bar{A}_1+\bar{A}_2+\bar{E}$
					4435	*m*	4352	*w*			$\nu_{16}+\nu_{17}$	4380	A_1+A_2+E
					5845	*w*					$\nu_1+\nu_7$	5861	$\bar{A}_2$

[a] $\Delta\nu$ is the Raman displacement in cm^{-1}; I is the semiquantitative relative intensity; ρ is the depolarization factor of the Raman line; ν_a is the wave number of the infrared absorption band in cm^{-1}; and I_a is the qualitative relative absorption. In the intensities, *s* = strong, *m* = medium, *w* = weak, and *v* = very. *MC* = Meister and Cleveland, reference 1; *CGB* = Cleveland, Greenlee, and Bell, reference 3; *PR* = Present Results.

[b] The numbering of the fundamentals follows that of reference 3; in addition, the approximate nature of the fundamental vibrations is indicated by descriptive superscripts; *sk* = skeletal deformation.

[c] The relative intensities are those given in reference 1, except for the very weak bands not reported there.

[d] Measured by E. K. Plyler.

[e] The depolarization factor of this line has not been measured because in all the plates of the present investigation the strong component was too intense for accurate measurement.

ASSIGNMENTS

Since the results of the present work are inconsistent with some of the previous assignments, it is necessary to make some changes. The molecule is assumed, as in previous assignments, to belong to the D_{3h}' group which presupposes free rotation about the central carbon-carbon bond. For this symmetry, DMDA has the following fundamental vibrations: $5A_1$, $1\bar{A}_1$, $4\bar{A}_2$, $5E$, and $5\bar{E}$. The selection rules for the fundamentals as well as for the overtones and combinations were given previously.[3]

An assignment of the observed Raman and infrared frequencies, consistent with the selection rules, is given at the right in Table I. The C≡C stretching frequencies ν_2 and ν_8; the methyl group fundamentals ν_1, ν_7, ν_{16}, (C−H stretching); ν_3, ν_9, ν_{12}, ν_{17} (deformation); ν_{13}, and

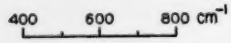

		REFERENCE
613 731	$HC\equiv CH$	12
606	$HC\equiv C-Cl$	13
642	$HC\equiv C-CH_3$	14,15
642	$HC\equiv C-CH_2-CH_3$	16
632	$HC\equiv C-(CH_2)_2-CH_3$	16
632	$HC\equiv C-(CH_2)_3-CH_3$	16
633	$HC\equiv C-C(CH_3)_3$	20,21
615, 629	$HC\equiv C-C=CH_2$	17,18,19
627, 630	$HC\equiv C-C\equiv CH$	9

FIG. 1. Bending modes of the $-C\equiv C-H$ group for several molecules.

ν_{18} (rocking); and the $\bar{A}_2$ end C—C stretching ν_{10}, were definitely assigned in previous papers.[1-3]

The central carbon-carbon bond stretching frequency requires reexamination. The 475 cm^{-1} line was first assigned by Meister and Cleveland[1] as an E or $\bar{E}$ fundamental, but the former normal coordinate treatment[2] indicated that it should be the A_1 fundamental corresponding to the central carbon-carbon bond stretching. However, the present value of the depolarization factor (0.84) rules out this assignment. It has to be taken into account that the previous value of the depolarization factor[1] (0.64) was obtained by the double-exposure method, as stated above, and besides this, in CCl_4 solution where the line is very close to the highly polarized 460 cm^{-1} line of the solvent. Also, the calculations[2] were based on the potential constant for the central bond obtained from the assignment of the 644 cm^{-1} band of diacetylene (DA) as an A_{1g} fundamental. It seems that this assignment was based upon the fact that 644 cm^{-1} was the highest observed Raman displacement, with the exception of the 2183 cm^{-1} line which obviously corresponds to the triple bond stretching fundamental. Recently, A. V. Jones[8,9] has obtained new Raman and infrared spectral data for DA, has assigned the central carbon-carbon stretching fundamental to a polarized Raman line at 874 cm^{-1} which had not been observed in previous investigations, and has ascribed the line at 642 cm^{-1} to a hydrogen bending vibration. The same assignment for the 642 cm^{-1} band had been made[10,11] in this laboratory by comparison of the vibrational data of a number of molecules containing the $-C\equiv C-H$ group for which frequencies close to 644 cm^{-1} have been assigned to bending modes.

The bending frequency of the acetylenic hydrogen in acetylene itself has the values 613.3 and 730.74 cm^{-1}, respectively.[12] A band at 606 cm^{-1} in chloroacetylene is assigned[13] as the $H-C\equiv C-$ bending, which assignment is substantiated by the large isotopic shift in the deuteroderivative. The line at 642 cm^{-1} observed in the Raman spectrum of methylacetylene was assigned to the $-C\equiv C-H$ bending by Crawford.[14,15] Cleveland *et al.*[16] found a rather strong line near 642 cm^{-1} in several monosubstituted acetylenes and identified it with the bending of the $-C\equiv C-H$ group. The bending frequencies of the same group in vinylacetylene correspond, according to Sheppard,[17] to the values 615 and 629 cm^{-1} observed in the infrared and in the Raman, respectively, by Bartholome and Karweil[18] and by Glockler and Davis.[19] The 633 cm^{-1} band observed in the Raman spectrum of 2,2-dimethylbutyne by Cleveland and Murray[20] was assigned to the $-C\equiv C-H$ wagging by Sheppard[21] in a correlation study of the vibrational spectra of 2,2-dimethylbutane, 2,2-dimethylbutene and 2,2-dimethylbutyne. Figure 1 shows this consistent behavior of all the molecules with the $-C\equiv C-H$ group. Jones' values[8,9] for the bending modes of this group in DA have been incorporated in the figure.

The consistency shown in Fig. 1 and, more directly, the new experimental data of Jones[8,9] rule out the previous assignment of the 644 cm^{-1} line of DA. Consistently, the present value of the depolarization factor of the 475 cm^{-1} line of DMDA rules out its assignment as an A_1 fundamental vibration. This is then an E or $\bar{E}$ vibration as originally proposed by Meister and Cleveland.[1] It is considered to be the ν_{19} analog of the 482 cm^{-1} line of DA, belonging therefore to the $\bar{E}$ type, which is in line with the reasoning used by Crawford in the assignment of the degenerate vibrations of dimethylacetylene,[22] according to which we should expect the E vibrations of this molecule to be more weakly Raman active than the $\bar{E}$ vibrations. The other skeletal $\bar{E}$ deformation ν_{20} corresponds to 247 cm^{-1}, the only strong Raman line in the region of small wave numbers. As for the E-type skeletal vibrations, an approximate calculation made before the study of the infrared spectrum in the region of low wave numbers, gave the values of 357 and about 100 cm^{-1}. The infrared work of Dr. Plyler confirmed very nicely the first value, but the second remains as yet unobserved. The weak

[8] A. V. Jones, Paper at the Symposium on Molecular Structure and Spectroscopy, Ohio State University (June, 1951).
[9] A. V. Jones, Proc. Roy. Soc. (London) **A211**, 285 (1952).
[10] Ferigle, Cleveland, and Meister, Phys. Rev. **81**, 302 (1951).
[11] Ferigle, Cleveland, and Meister, Paper at the Symposium on Molecular Structure and Spectroscopy, Ohio State University, June, 1951.
[12] E. E. Bell and H. H. Nielsen, J. Chem. Phys. **18**, 1382 (1950).
[13] W. S. Richardson and J. H. Goldstein, J. Chem. Phys. **18**, 1314 (1950).
[14] B. L. Crawford, Jr., J. Chem. Phys. **7**, 140 (1939).
[15] B. L. Crawford, Jr., J. Chem. Phys. **8**, 526 (1940).
[16] Cleveland, Murray, and Taufen, J. Chem. Phys. **10**, 172 (1942).
[17] N. Sheppard, J. Chem. Phys. **17**, 74 (1949).
[18] E. Bartholome and J. Karweil, Z. Physik. Chem. **B35**, 442 (1937).
[19] G. Glockler and H. M. Davis, J. Chem. Phys. **2**, 881 (1934).
[20] F. F. Cleveland and M. J. Murray, J. Chem. Phys. **11**, 450 (1943).
[21] N. Sheppard, J. Chem. Phys. **17**, 455 (1949).
[22] B. L. Crawford, Jr., J. Chem. Phys. **7**, 555 (1939).

Raman lines at 554 and 1228 cm^{-1} have been assigned as the two A_1-type single bond stretchings, the assignment being substantiated by the normal coordinate treatment.

Probably the most significant result of this work is the change in the assignment of the 475 cm^{-1} band. The previous assignment of this band and that of the 644 cm^{-1} band of DA, were the cause of the conflicting data existing in the literature between the bond length and the stretching potential constant of the central bond in the structure $-C\equiv C-C\equiv C-$, to which we made reference in a previous paper.[23] Jones[9] and Duchesne[24] have discussed this new assignment in connection with their work on DA and cyanogen, respectively. Torkington[25] has also considered recently the assignment of the 644 cm^{-1} band of DA as a bending mode.

The spectrographs used in the present work were obtained in part with grants from the Society of the Sigma Xi and from the American Academy of Arts and Sciences, and the work has been further aided by a second grant from the latter. The work was also supported in part by Office of Ordnance Research Contract DA-11-022-ORD-464. A Research Corporation fellowship enabled one of us (S. M. F.) to carry out his part of the research. The diagram used as Fig. 1 was prepared by Mr. Alfons Weber. The sample was furnished by Dr. Kenneth W. Greenlee of Ohio State University. Dr. Earle K. Plyler kindly obtained the infrared spectrum in the region below 400 cm^{-1}. The authors are grateful for all this assistance.

[23] Ferigle, Cleveland, and Meister, J. Chem. Phys. **20**, 526 (1952).

[24] J. Duchesne, Acad. Roy. Belg. **26**, 1 (1952).

[25] P. Torkington, Proc. Roy. Soc. (London) **A206**, 17 (1951).

THE JOURNAL OF CHEMICAL PHYSICS VOLUME 20, NUMBER 12 DECEMBER, 1952

Dielectric Constants of Solutions of Charged Particles

GEORGE K. FRAENKEL *
Department of Chemistry, Columbia University, New York 27, New York

(Received March 3, 1952)

Calculations are carried out to determine the relation between the dielectric constant of solutions of large charged particles and the charge distribution on the particles. It is shown that if the hydrodynamic forces cause the particles to rotate about a point fixed in each particle, the dielectric constant is determined by the dipole moment about this point.

FOR some years, interest has been shown in the relation between the dielectric constants of solutions of charged proteins and the charge distribution on the protein molecules. Oncley and Mysels[1] concluded in an unpublished work that the dipole moment, calculated in the usual way from measurements of the dielectric constant, should be interpreted as the dipole moment about the "center of symmetry" of the molecule. In the present paper, these results have been confirmed by a somewhat different method of reasoning which also predicts the nature of the dielectric dispersion.

For particles with a net charge, the difficulty of interpretation arises because the dipole moment of the charge distribution is not a unique property of the distribution. The ambiguity is evident from the definition of the dipole moment: for any charge distribution with charge density $\rho(\mathbf{r})$ at a vector distance $\mathbf{r}$ from an arbitrary origin, the dipole moment $\boldsymbol{\mu}$ is given by $\boldsymbol{\mu}=\int \rho(\mathbf{r})\mathbf{r}d\tau$. Thus, only if the net charge is zero is $\boldsymbol{\mu}$ independent of the choice of origin and therefore a unique property of the charge distribution. It will be shown, however, that if the particles are constrained to rotate about a definite point which is fixed in the body, the dielectric constant will be determined by a dipole moment calculated with this point as origin.

In the following, the relation of the dielectric constant to the current density due to all the charges on the particles is given, and it is shown how the current density is related to the velocity of the particles averaged over their Brownian motion. By the choice of coordinates appropriate to the hydrodynamic motion of the particles, the contribution of the average current to the in phase (real) part of the dielectric constant is found to be determined by the dipole moment referred to the center of rotation of each of the particles.

It will be assumed that the solvent is nonpolar and that the solution is sufficiently dilute to permit the neglect of corrections due to both the local electric fields acting on the solute particles and the interactions between the particles. Strictly, the neglect of local fields limits the validity of the following results to dilute gases. In sufficiently dilute solutions in nonpolar solvents, however, local field corrections for the solvent alone, such as the Clausius-Mossotti field, can be applied in the usual way. The requirement that the solution be sufficiently dilute to allow the neglect of interactions

* This work was initiated while the author was a National Research Council Predoctoral Fellow at Cornell University.

[1] J. L. Oncley and K. J. Mysels, quoted in E. J. Cohn and J. T. Edsall, *Proteins, Amino Acids and Peptides* (Reinhold Publishing Corporation, New York, 1943), p. 552.

between the charged particles automatically removes from consideration terms in the multipole expansion of the particle charge distribution higher than the dipole.[2] It is further supposed that the charge distribution on the particles is constant and the same for every particle.

We will initially describe the macroscopic electrical characteristics of the solution by accounting for all the charges and currents, not only the placed charge and the currents in metallic conductors, so that the appropriate electrical vector is $\mathbf{E}$ instead of $\mathbf{D}$, and the magnetic vector is $\mathbf{B}$ instead of $\mathbf{H}$. The current which gives rise to the curl of the magnetic field is then, by Maxwell's equations, $\mathbf{J}+(1/4\pi)(\partial\mathbf{E}/\partial t)$, where $\mathbf{J}$ is the current density due to the average of the translational and rotational motions of the charged particles. To bring out clearly the effects of the large charged molecules whose charge distribution is of interest, currents due to other charges in the solution will not be considered. In particular, the counter ions required to neutralize the large charged particles will give rise to a conductivity which will be assumed to contribute only to the real (in phase) part of the current. Any out of phase contribution to the currents caused by the small molecules will be assumed to be corrected for by blank experiments. By considering the relation between the admittance and the current density for a measuring circuit containing a condenser filled with the solution, it is possible to show that the dielectric constant ϵ is determined by $(\epsilon-1)(\partial\mathbf{E}/\partial t)=4\pi\mathbf{J}$.

The current density $\mathbf{J}$ is evaluated by calculating the product of the charge in a small element of volume by its velocity and averaging per unit volume over a macroscopic volume. In order to compute the velocity of a charge element, it will be assumed that the motion of the charge bearing particles brought about by hydrodynamic forces can be described as a rotation about a point fixed in the body, the center of rotation, and a translation of this point. It is important to note that this may not be true for arbitrarily shaped particles for which hydrodynamic forces would bring about sufficiently complicated motions. We locate a particular point on the jth particle by a vector $\mathbf{R}_j$ from an arbitrary origin to the center of rotation fixed in the particle and a vector $\mathbf{r}_j$ from this center to the specified point on the particle. For an element $d\tau_j$ of the jth particle at $\mathbf{R}_j+\mathbf{r}_j$ with charge $\rho(\mathbf{r}_j)d\tau_j$, there is a contribution to the current density, which must be averaged per unit volume, that may be written as

$$\int \rho_j \frac{d}{dt}[\mathbf{R}_j+\mathbf{r}_j]d\tau_j,$$

where the integral is extended over the volume of the jth particle. If there are n identical particles per unit volume, the current density is

$$\mathbf{J}=n\left\langle q\mathbf{v}+\frac{d}{dt}\int \rho\mathbf{r}d\tau\right\rangle_{Av},$$

where $q=\int\rho d\tau$ is the total charge on a particle, $\mathbf{v}=(d\mathbf{R}/dt)$ is the velocity of the center of rotation relative to a stationary origin, the integrals are extended over the volume of a single particle and the average is performed over the molecular motions of the particles.

Expressing the dielectric constant in terms of the current and introducing the dipole moment $\boldsymbol{\mu}$,

$$(\epsilon-1)(\partial\mathbf{E}/\partial t)=4\pi n\langle q\mathbf{v}+(d\boldsymbol{\mu}/dt)\rangle_{Av},$$

which, for sinusoidal fields of circular frequency ω, may be written as

$$(\epsilon-1)\mathbf{E}=4\pi n\{-iq\omega^{-1}\langle\mathbf{v}\rangle_{Av}+\langle\boldsymbol{\mu}\rangle_{Av}\}.$$

Thus, by the introduction of coordinates referred to the center of rotation, one part of the dielectric constant is seen to arise from the rotational motion and is expressible in terms of the average dipole moment about the center of rotation. The other contribution to the dielectric constant is determined by the average translational velocity.

The translational velocity is found from the equilibrium between the electrical and frictional forces: $\bar{f}\mathbf{v}=q\mathbf{E}$. Here $\bar{f}$ is the appropriate translational friction constant. It will be assumed that no concentration gradients are set up by the electric field, an assumption which is equivalent to having a measuring cell with a very long dimension in the direction of the electric field. The translational motion of the particles is thus in phase with the electric field and contributes only to the real part of the current. This assumption is tacitly made whenever charged particles are present in the solution, and there is no reason to expect that a charge on the large particles of interest should contribute effects appreciably larger than those of the small particles. The average translational velocity is then given by $\mathbf{v}=q\mathbf{E}/\bar{f}$, and the average of the dipole moment reduces to a determination of the average over only the rotational motion.

The average of the dipole moment over the rotatory Brownian motion is formally identical to the average value given for uncharged particles by Debye.[3] Debye's result for spheres, and Perrin's[4] for ellipsoids, may be expressed as

$$\langle\mu_E\rangle_{Av}=(E/3kT)\sum_j \mu_j^2(1+i\omega\tau_j)^{-1}$$

where μ_E, the component of the average dipole moment in the direction of the applied field E, is the only nonvanishing component of the moment, and τ_j is the relaxation time. The μ_j are the components of the moment along the principal axes of the body. For ellipsoids there

[2] J. H. Van Vleck, *The Theory of Electric and Magnetic Susceptibilities* (Oxford University Press, London, 1932), p. 12.

[3] P. Debye, *Polar Molecules* (Chemical Catalog Company, New York, 1929).

[4] F. Perrin, J. phys. VII, 5, 497 (1934).

can be three components of the moment and three relaxation times, but for spheres there is only one moment and one relaxation time. These results are applicable to the charged particles considered here because: (1) The center of rotation used in developing the present equations coincides with the center of symmetry used in making the Brownian motion calculations. (2) The torque about the center of rotation, which is required to evaluate the convection current in the Brownian motion (Fokker-Planck) diffusion equation, is $-\mu E \sin\theta$. Here θ is the angle between $\boldsymbol{\mu}$ and $\mathbf{E}$, and $\boldsymbol{\mu}$ is the dipole moment about the center of rotation. This torque is formally identical to that for particles with no net charge, although if the net charge vanishes, it is not necessary to define the center to which either the torque or the dipole moment is referred. (3) The diffusion equation governing the rotatory Brownian motion is independent of the translational motion.[5] The only modification of the usual formulas is in the interpretation of the μ_j which, for a charged body, must be calculated about the center of rotation.

If the dielectric constant is written in terms of its real and imaginary parts, $\epsilon=\epsilon'-i\epsilon''$,

$$\epsilon'=1+(4\pi n/3kT)\sum_j \mu_j^2(1+\omega^2\tau_j^2)^{-1},$$
$$\epsilon''=4\pi nq^2/\omega\bar{f}+(4\pi n/3kT)\sum_j \omega\tau_j\mu_j^2(1+\omega^2\tau_j^2)^{-1}.$$

It is to be recalled that these expressions do not include the effects of charged or polarizable particles other than a single species of large molecules. An additional term must be added in the usual way to account for the temperature independent optical polarizability.

The fact that the dipole moment which gives rise to the real part of the dielectric constant must be computed about the center of rotation is a direct result of the separation of the motion into a translation of a point fixed in the body and a rotation about this point. Oncley and Mysels[6] have also been interested in the case of bodies which do not rotate about a fixed center. No attempt to treat a problem of this nature by the foregoing approach has been made. The present method can, however, also be applied to less symmetric bodies than spheres or ellipsoids.

A simple illustration of an assymmetric body is provided by a rigid rod of infinitesimal thickness. The rod is assumed long enough to permit the neglect of hydrodynamic interactions between the two ends. If the friction constants of the two ends are designated by f_1 and f_2, and the distance between the centers of the spheres by a, the center of rotation can be shown to be a distance $af_2/(f_1+f_2)$ from the end designated by (1). As is customary, inertial effects are neglected. Following the usual procedure, it can be shown that the friction tensor is diagonalized by the choice of the center of rotation as origin. If different charges e_1 and e_2 are placed on the ends of the dumbbell designated by (1) and (2), respectively, the diople moment μ calculated about the center of rotation is given by

$$\mu=a\left(\frac{e_1}{f_1}-\frac{e_2}{f_2}\right)\left(\frac{f_1f_2}{f_1+f_2}\right).$$

If $e_2=-e_1$, this reduces properly to $\mu=ae_1$ and is independent of the location of the origin. The Brownian motion diffusion equation can be shown to be

$$\frac{\partial\Psi}{\partial t}=(kT/\bar{f})\frac{\partial}{\partial Z}\left[\frac{\partial\Psi}{\partial Z}-(qE/kT)\Psi\right]$$
$$+(kT/f_\theta)\left\{\frac{1}{\sin\theta}\frac{\partial}{\partial\theta}\left[\sin\theta\frac{\partial\Psi}{\partial\theta}+(\mu E/kT)\Psi\sin^2\theta\right]\right\},$$

where $\Psi(\theta,Z,t)$ is the Brownian motion distribution function, $\bar{f}=f_1+f_2$, $f_\theta=a^2f_1f_2/(f_1+f_2)$, $q=e_1+e_2$, and Z is the coordinate of the center of rotation in the direction of the field. The terms in the X and Y coordinates and in the azimuthal angle are not included because there are no electrical forces with components in these directions, and on the assumption that no appreciable concentration gradients are set up, the dependence of Ψ on Z can be neglected. By making the usual approximations[3,4] for small sinusoidal fields, the distribution function is found to be

$$\Psi(\theta,t)=A\left[1+\frac{\mu E_0\exp(i\omega t)}{kT(1+i\omega\tau)}\cos\theta\right],$$

where $\tau=f_\theta/2kT$. The average dipole moment can then be expressed in terms of this μ and τ by the general equation given above for $\langle\mu_E\rangle_{Av}$.

These calculations have required the averaging over the rotatory Brownian motion of the particles, a procedure which is not readily performed for bodies with more complicated shapes than ellipsoids. The much simpler equilibrium calculation which yields the well-known Langevin-Debye equation for electric and magnetic susceptibilities cannot be rigorously applied to a solution of charged particles because there is no unique way to separate the large polarization caused by the translational motion of the charges from the polarization due to the rotational motion. If, however, one considers an imaginary system in which Maxwell demons hold the centers of rotation at fixed positions in the solution, the system can be considered to be at equilibrium and the classical Debye calculation can be carried out. It is immediately evident that the dipole moment which determines the susceptibility is dependent, except for particles which have no net charge, on the choice of the point held fast by the Maxwell demons.

The writer would like to express his appreciation to Professor P. Debye for suggesting this problem and for valuable discussions in the initial course of the work.

[5] F. Perrin, J. phys. VII, 7, 1 (1936).
[6] Private communication.

A Modified Silberstein Model of Optical Anisotropy*

FRANK MATOSSI
U. S. Naval Ordnance Laboratory, White Oak, Maryland
(Received August 20, 1952)

The Silberstein model of optical anisotropy is modified by the introduction of screening factors for the fields of the interacting induced dipoles. Thus, it is possible to apply the model consistently to molecular refraction, Rayleigh scattering, Raman effect, dipole moment, infrared intensities, and Kerr effect. The numerical evaluation is carried out for O_2, N_2, Cl_2, CO_2, and CS_2.

INTRODUCTION

IN previous papers,[1] the Silberstein model of optical anisotropy was applied to Raman line depolarization factors and a related classical model for dipole moments, to infrared intensities. However, as pointed out already,[1] there is a serious defect in the Silberstein model. Although the model was originally intended to be applied to Rayleigh scattering and molecular refraction,[2] it describes these phenomena only if incorrect values for the interatomic distances are used. As long as the fruitfulness of the model seemed to be restricted to the data just mentioned, this defect need not be considered to be too serious. But after it could be shown that it may be applied more generally, we must look for some modification which brings all phenomena related to atomic polarizabilities (depolarization of Rayleigh and Raman lines, infrared intensities, dipole moments, molecular refraction, and Kerr effect) under one consistent cover.

THE MODIFIED MODEL

The modification proposed here is based on a remark by Mott and Gurney,[3] according to which the fields of the interacting induced dipoles may be modified, because of overlapping of the ions, by a factor β. This "screening factor" may assume quite small values and may be different in different directions. We distinguish β and γ for the directions parallel and perpendicular to the direction of the dipole moment ("end on" and "side on" positions), respectively. A similar screening factor σ was recently introduced[4] also for the ionic fields in the polarizability model of the dipole moment.

Utilizing these screening factors, we obtain for the components A and B of the molecular polarizability parallel and perpendicular to the symmetry axis, and for the dipole moment μ, the following expressions in terms of the atomic polarizabilities α_i and the interatomic distance r (for diatomic molecules):

$$A=\frac{\alpha_1+\alpha_2+4\beta\alpha_1\alpha_2/r^3}{1-4\beta^2\alpha_1\alpha_2/r^6}, \quad B=\frac{\alpha_1+\alpha_2-2\gamma\alpha_1\alpha_2/r^3}{1-\gamma^2\alpha_1\alpha_2/r^6},$$

$$\mu=e[r-\sigma(\alpha_1+\alpha_2)/r^2].$$

A similar modification applies to the equations for triatomic molecules. It may be that β is different for different atoms. Then β would have to be replaced by $\frac{1}{2}(\beta_1+\beta_2)$ and β^2, by $\beta_1\beta_2$.

The equations can be evaluated in the same manner as described earlier.[1] A and B can be obtained from Rayleigh scattering (or Kerr effect) and refraction data, which are essentially determined by $A-B$ and $A+2B$, respectively. Further data are furnished by Raman line depolarization factors and infrared intensities, involving $A'=dA/dr$, $B'=dB/dr$, and $\mu'=d\mu/dr$. The atomic distances are known from spectroscopic measurements. In order to compute σ for the YX_2 molecules, bond moments of the YX bond of about $0.6D$ have been assumed.[5]

In Table I some results for X_2 and linear XYX molecules are given. The details of the computation are omitted. As always, the evaluation is not unambiguous because there are more unknown parameters than independent data. Therefore, again some arbitrary assumptions were made, e.g., $\beta=\gamma$, or $\gamma=1$, or transferability of the α's from one molecule to another one.

TABLE I. Polarizabilities and screening factors.

Molecule	α(10-24 cm³)		α (10^{-1} cm²)		β	γ	
N_2	0.83		0.71		0.24	0.24	
	0.96		1.23		0.32	0.64	
O_2	0.72		0.66		0.49	0.49	
	0.90		0.49		0.24	1.0	
Cl_2	2.1		...		0.65	0.65	
	2.35		...		0.48	1.0 (no Raman data)	
	α_C	$\alpha_{O(S)}$	α'_C	$\alpha'_{O(S)}$	β	γ	σ
CO_2	1.0	1.0	1.3	3.0	0.10	1.0	0.70
CS_2	1.0	3.4	0.6	5.1	0.27	1.0	0.79

* Presented at the Washington meeting of the American Physical Society, May 2, 1952.

[1] F. Matossi, J. Chem. Phys. **19**, 1007 (1951); **20**, 819 (1952).

[2] See, for instance, J. Cabannes, *La diffusion moléculaire de la lumière* (Hermann et Cie., Paris, 1929).

[3] N. F. Mott and R. W. Gurney, *Electronic Processes in Ionic Crystals* (Clarendon Press, Oxford, 1948), second edition, p. 17.

[4] C. K. Møller, J. Chem. Phys. **20**, 203 (1952).

[5] D. Z. Robinson, Review papers from Symposium on Molecular Structure and Spectroscopy (ONR, June, 1951), p. 47.

DISCUSSION

The values obtained for the parameters from the experimental data are in the acceptable range. If β and γ are both equal to 1, no solution at all of the equations for A and B can be found, but only for A' and B', i.e., for Raman effect but not for Rayleigh scattering and refraction.

While the introduction of β and γ is essential for the applicability of the model, σ could have been disregarded for the molecules considered here. $\sigma=1$ would give a bond moment of zero with $\gamma=0.30$ and of $-0.6D$ with $\gamma=1$, for CO_2. This seems to indicate a preference for $\gamma=1$. But $\gamma=1$ is impossible for N_2.

The evaluation for XY molecules, as CO and NO, yields formally possible solutions of the equations, but they cannot be considered as final and therefore are not presented in detail. The main drawback of the solutions is too large a difference between α_1 and α_2 (about 1.5 and 0.3, respectively) than to be considered reasonable. Perhaps the introduction of $\beta_1 \neq \beta_2$ would give a better result, but the evaluation then requires too much guess work.

However, the results for the other molecules seem to be sufficient indication that the Silberstein model as modified by screening factors (and the previously discussed variable atomic polarizabilities $\alpha_i' = d\alpha_i/dr \neq 0$) is a workable concept for the quantitative description of several phenomena for which polarizability effects are responsible.

THE JOURNAL OF CHEMICAL PHYSICS VOLUME 20, NUMBER 12 DECEMBER, 1952

Infrared Spectroscopy and the Character of Chemical Binding

R. MECKE
Institute for Physical Chemistry, University of Freiburg, Germany
(Received May 20, 1952)

The importance of the study of the intensities of vibrational bands yielding information concerning the charge distribution in chemical bonds is stressed.

A method is developed for obtaining bond moments in the ground state by the extrapolation of the values calculated for the transition moments of the bond, these being obtained from intensity measurements on the fundamental and overtone bands.

An empirical attempt is made to explain the total moment as the sum of an ionic, a polar, and an inductive component. Agreement between experimental results and the empirical relations is good for OH and CH bonds in a large number of compounds.

IN spite of the very considerable technical developments in spectroscopic apparatus for the infrared region, the question of the intensities of the absorption bands in relation to certain aspects of the chemical bond has still received far less than the necessary attention. Spectroscopic work still shows a concentration of interest in the study of frequencies, i.e., it is limited to the determination of the proper frequencies and their interpretation in terms of atomic oscillations within the molecule. Apart from simple analytical problems and the control of purity, the intensities of the bands are invoked only in so far as they can establish which proper frequencies of the molecule are "active" or "inactive" in the infrared owing to definite symmetry properties of the molecular model.

However, in a number of publications,[1] the present author has repeatedly indicated that spectroscopic intensities are in no way less worthy of attention than spectroscopic frequencies, and that the former may well be of over-riding importance as soon as the assignment of the bands to the proper modes of the molecule being studied is completed.

As a considerable amount of experimental material which can be used for testing the theoretical relations has now been accumulated in the Freiburg Institute,[2] a new and more complete formulation of the method of evaluating intensity measurements in the infrared and its theoretical basis will be described here. It will be shown how, from careful intensity measurements of the overtones of a given valence vibration, conclusions can be obtained as to the bond character—i.e., concerning the charge distribution in a particular chemical bond. In these circumstances, it is the so-called bond moment (i.e., the dipole moment of the individual bond) which is studied, and this can be resolved into ionic, polar (dipole), and inductive (quadrupole) parts. Our results indicate that these components can be represented by a readily understood treatment of a simple model and, further, that in this way the relations between the electrical properties and the chemical reactivity of the bonds concerned can be obtained.

The classical basis of dispersion theory is assumed known: Electromagnetic radiation can be absorbed and causes a molecular vibration only when the following conditions are fulfilled:

[1] B. Timm and R. Mecke, Z. Physik **98**, 363 (1935). R. Mecke, Z. physik. Chem. **B33**, 156 (1936). R. Mecke, Z. Physik **107**, 595 (1937).

[2] K. Rumpf and R. Mecke, Z. physik. Chem. **B44**, 299 (1939). O. Vierling and R. Mecke, Z. Physik **99**, 204 (1936). H. Kempter and R. Mecke, Z. Naturforsch. **2a**, 549 (1947). F. Oswald, thesis, Freiburg i. Br. (1950). E. Lippert and R. Mecke, Z. f. Elektrochemie **55**, 366 (1951).

(a) The molecular vibration and the incident energy must have the same frequency (resonance condition);

(b) the molecular vibration must involve a change of the dipole moment of the molecule, i.e., it must involve in addition to a vibrating mass $\bar{M}$ a (coupled) vibrating electric charge $e_{v,v'}$ (selection rule).

From wave mechanics it is known that the intensity of an infrared absorption band is determined by the electric transition moment $P_{v,v'}$ for the corresponding quantum jump $v \rightarrow v'$. Now this transition moment can be evaluated on the one hand from direct experimental measurement of the total absorption $A_{v,v'}=\int \epsilon_\nu \cdot d\nu$ for the infrared absorption band concerned, on the basis of relation (1):

$$P_{v,v'}{}^2=(3hc/8\pi^3\nu)\int \epsilon_\nu d\nu. \tag{1}$$

The "intensity" of an absorption band is thus always defined by the area under the curve of the molar extinction coefficient (in cm^2/g mole) plotted against frequency (ν in cm^{-1}).

On the other hand, the electric transition moment can be calculated from the dependence of the bond moment μ upon the internuclear distance, provided the eigenfunction ψ_v and the normal coordinate r are known for the vibration which is assumed to be linear:

$$P_{v,v'}=\frac{1}{N_v N_{v'}}\int \mu \psi_v \bar{\psi}_{v'} dr. \tag{2}$$

The normalization factors are defined in the usual way by

$$N_v{}^2=\int \psi_v{}^2 dr. \tag{3}$$

In complete analogy to the *electrical* transition moment $P_{v,v'}$, one finds for the *mechanical* transition moment $Q_{v,v'}$ (i.e., the mean amplitude of vibration) for the quantized transition $v \rightarrow v'$:

$$Q_{v,v'}=(1/N_v N_{v'})\int r \psi_v \bar{\psi}_{v'} dr. \tag{4}$$

From consideration of dispersion theory, it also follows that the effective coupled vibrating charge $e_{v,v'}$, characteristic of the bond type and mentioned at (b) above, can be represented by the quotient

$$e_{v,v'}=(P_{v,v'}/Q_{v,v'})=\frac{\int \mu \psi_v \bar{\psi}_{v'} dr}{\int r \psi_v \bar{\psi}_{v'} dr}. \tag{5}$$

In simple cases (e.g., for the hydrogen atom, simple rotator, harmonic oscillator) such integrals can be fully calculated. In the case of the anharmonic oscillator which is relevant for us here, the integration in (5) can be carried out by the introduction of the Morse potential function.[3]

$$E_{\text{pot}}=D_0(1-y)^2-D_0, \tag{6}$$

where

$$D_0=h\nu_0 k/4, \quad y=e^{a(r-r_0)},$$

and

$$a^2 D_0=2\pi^2 \nu_0{}^2 M,$$

where these symbols have their usual significance. With this eigenfunctions ψ_v and eigenvalues E_v are obtained as

$$\psi_v=L_v z^{\frac{1}{2}(k-2v-1)} e^{-z/2}, \tag{7a}$$

where

$$L_v=\sum_{n=0}^{v}\binom{k-v-1}{v-n}(-z)^n/n!$$

and

$$E_v=h\nu_0(v+\tfrac{1}{2})(k-v-\tfrac{1}{2})/k. \tag{7b}$$

(L_v = Laguerre polynomial of the auxiliary variable $z=k\cdot y$.) The evaluation of the integrals (2), (4) and (5) always leads to gamma-functions. In particular for the normalization factors one finds

$$aN_v{}^2=a\int \psi_v{}^2 dr=\frac{1}{v!}\frac{\Gamma(k-v)}{k-2v-1}. \tag{8}$$

For the mechanical transition moment, only the transition starting from the ground state (i.e., $0 \rightarrow v$) is of immediate practical interest and this is

$$avQ_{0v}=\left[v!\left(\frac{k-2v-1}{k-v-1}\right)\frac{\Gamma(k-v-1)}{\Gamma(k-1)}\right]^{\frac{1}{2}}. \tag{9}$$

By combining Eqs. (1) and (9) a relation between the oscillating charge e_{0v} and the experimentally measureable quantity A_{0v} follows:

$$e_{0v}{}^2=\frac{1}{(v-1)!(k-2v-1)}\cdot\frac{\Gamma(k-1)}{\Gamma(k-v-1)}\cdot\frac{3c\bar{M}}{\pi}\cdot A_{0v}. \tag{10}$$

The factor e_{0v} is thus unequivocally determined by the integrated absorption A_{0v}, the vibrating mass $\bar{M}$, and an "anharmonicity term." Neglecting higher orders of the quantity $1/k(\sim 0.02)$, this factor has the value $\sim(k-v/2)^{v-1}/(v-1)!\cdot(k/k-1)$. If the molar extinction coefficient ϵ is given in decadic units ($\log_{10}$), the frequency in wave numbers (cm^{-1}), the vibrating mass $\bar{M}$ in gram moles and the vibrating charge in units of the electronic charge (e), then

$$\frac{e_{0v}}{e}\cong 1.54\cdot 10^{-4}\left[\frac{k^{v-1}}{(v-1)!}\left[1-\frac{(v-2)(v+1)}{2k}\right]\bar{M}A_{0v}\right]^{\frac{1}{2}}. \tag{11}$$

For the hydrides XH, the vibrating mass $\bar{M}=(M_H M_X/M_H+M_X)$ is essentially determined by the hydrogen

[3] P. M. Morse, Phys. Rev. **34**, 57 (1929).

atom so that these compounds are particularly simple to investigate. Our measurements show that in these cases the oscillating charge is of the order of magnitude 0.1 to 0.5e.

The integral (2) leads to a closed value, provided it is possible to represent the bond moment (μ) as a function of the distance (r) by a power-series formula $\sum c_p(r/r_0)^p \cdot y^m$. It has been noted earlier that the following expression is satisfactory:

$$\mu=\mu_0[c_0+c_1(r/r_0)+c_2(r/r_0)^2]y, \tag{12}$$

i.e., the values $m=1$, $p=0$, 1 and 2 are used in the general expression.

Equation (12) represents the following simple model; the total moment has two components, $\mu=\mu_1+\mu_2$, where μ_1 is a polar and μ_2 an inductive contribution.

The "polar" part of the bond moment should possess the property that on separation of the atoms (e.g., the H atom of the $X-H$ bond) a residual moment μ_0 remains, but that both for infinite separation ($r=\infty$) and fusion of the nuclei ($r=0$) the effective charge $d\mu/dr$ vanishes. In other words, no ionic component is present, as that can be defined by $d\mu/dr\neq 0$ for $r=\infty$. These conditions are satisfied by the general expression

$$\mu_1=\mu_{\text{pol}}(1-e^{-\text{mar}}-\text{mar}e^{-\text{mar}})e^{\text{mar}_0}, \tag{13}$$

where a is the Morse constant.

For the inductive (quadrupole) component (μ_2) both $d\mu/dr$ and μ should be zero for $r=0$ and $r=\infty$, while in the neighborhood of the equilibrium position $r=r_0$, as a result of the internal field, the induced moment should pass through a minimum. The general formula

$$\mu_2=-\mu_{\text{ind}}(\text{mar})^p \cdot e^{p-\text{mar}};\quad p\sim\text{mar}_0 \tag{14}$$

suffices for this case (Fig. 1). The measurements on $C-H$ bonds indicate that $p=2$ and $m=1$. In addition, the following limiting conditions can also be imposed:

(a) In the absence of any ionic bonding, the effective vibrating charge e_{0v} should become zero in addition to Q_{0v} and P_{0v}, when complete separation of the bonded atoms is attained: i.e., $Q_{0v}\to 0$; $P_{0v}\to 0$; $e_{0v}\to 0$ for $v\to(k-1)/2$;

(b) The transition moment μ_{00} extrapolated to $v=0$ must give the bond moment (i.e., the equilibrium $r=r_0$ value of that part of the dipole moment varying with distance r):

$$\mu_{00}=\mu_{\text{pol}}e^{\text{mar}_0}-\mu_1-\mu_2(v\to 0). \tag{15}$$

The integration of Eqs. (2) and (5), using Eqs. (13) and (14), which need not be detailed here, is based on the well-known properties of gamma-functions, some of which are detailed in the appendix.

For the practical integration of Eq. (2) the following change is helpful in smoothing out the great difference in intensities of the successive overtones: The transition moment P_{0v} given by Eq. (1) and the mean amplitude

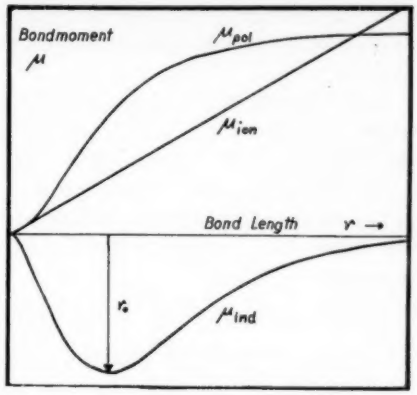

FIG. 1. Dependence of the ionic, polar, and inductive components of the bond moment on bond length.

Q_{0v} are first reduced by multiplication with the factor[2]

$$F_{0v}^{\frac{1}{2}}=akN_0N_v\Big/\int\psi_0\bar{\psi}_v dz$$

$$=\left[\frac{k^2}{(k-2v-1)}\frac{\Gamma(k-1)}{\Gamma(k-v)}\frac{1}{v!}\right]^{\frac{1}{2}}, \tag{16}$$

$$\mu_{0v}=\int(k\mu/z)\psi_0\bar{\psi}_v dz\Big/\int\psi_0\bar{\psi}_v dz.$$

The reduced moments obtained in this way are designated μ_{0v} and q_{0v}

$$\left.\begin{aligned}\mu_{0v}&=0.00198\cdot 10^{-18}\cdot[F_{0v}A_{0v}/\nu_{0v}]^{\frac{1}{2}}\\ q_{0v}&=Q_{0v}[F_{0v}]^{\frac{1}{2}}=\nu_0/a\nu_{0v}.\end{aligned}\right\}, \tag{17}$$

The effective vibrating charge is then very simply given by

$$e_{0v}=\mu_{0v}/q_{0v}=a\mu_{0v}(\nu_{0v}/\nu_0).$$

If Eq. (2) is now integrated with the substitution of (13) (with $m=1$), or (14) with $m=1$ and $p=2$, on using Stirling's formula [approximately Eq. (25)] there is obtained for μ_{0v}.

$$\mu_{0v}=\mu_{\text{pol}}[ar_0+1-\log(v+\gamma)(k-v-1+\gamma)/k\gamma], \tag{18a}$$

$$\mu_{0v}=\mu_{\text{ind}}\left[\{ar_0-\log(v+\gamma)(k-v-1+\gamma)/k\gamma_0\}^2-s_2+\frac{k}{(v+\gamma')(k-v-1+\gamma')}\right], \tag{18b}$$

where γ is the correction factor usually omitted in Stirling's formula,

$$s_\alpha=\sum_1^\infty\frac{1}{n^\alpha}(n=1, 2, 3\cdots\infty) \tag{19}$$

and $\log\gamma_{v=0}$ is Euler's constant. Both relations obey the limiting condition (b), i.e., they give for $v\to 0$, the bond

moments $\mu_{00}=\mu_{pol}(ar_0+1)$, or $\mu_{00}=\mu_{ind}(ar_0)^2$ if one neglects a small item $\sim 1/2k$ which arises from the zero-point vibration.

Further, both relations show a minimum for the limit of dissociation ($v_\infty=(k-1)/2$) and this, corresponding to the condition (a), must be set equal to zero. This restriction, of course, implies that ar_0 and k are not independent of one another, but, according as the polar or inductive bond components preponderate, must lie between the limits

$$1<(\log k/4+c-ar_0)<[s_2-4/k]^{\frac{1}{2}}\sim 1.25,$$

where $s_2=\pi^2/6$. For $X-H$ bonds with the average value $ar_0=2$, for instance, k can only assume the values between 45 and 57, a restriction which in actual fact is remarkably well fulfilled, but of which the fundamental meaning is still not clear.

Retaining this condition and taking $\gamma=\frac{1}{2}$ for all bonds—which is already a sufficiently good approximation for the fundamental vibration v_{01}—and inserting in our treatment the ionic component of the bond (with constant $e_{0v}=a\mu_{ion}$) the observed (reduced) transition moment can be represented additively from its three components as a function of the eigenvalues E_v (Eq. (7)) and $D_0=hv_0k/4$:

$$\left.\begin{aligned}&\text{(a) ionic component:}\\ &\mu_{0v}=\mu_{ion}\frac{hv_0}{E_v-E_0}\\ &\text{(b) polar component:}\\ &\mu_{0v}=\mu_{pol}\log D_0/E_v\\ &\text{(c) inductive component:}\\ &\mu_{0v}=\mu_{ind}\left[(s-\log D_0/E_v)^2-s^2+\left(\frac{hv_0}{E_v}-\frac{hv_0}{D_0}\right)\right]\end{aligned}\right\},\quad (20)$$

where $s\sim 1.25$. The behavior of these components of the transition moment with respect to v, the vibrational quantum number, is shown in Fig. 2.

While the ionic component varies in a hyperbolic fashion and the polar component steadily decreases logarithmically, the inductive contribution passes through an extreme value at $\ln v_{0v}/v_0=ar_0-c$. For $ar_0=2$, this occurs at about the third overtone ($v\sim 4$), with $\mu_{0v}=0.35\mu_{00}$. Thus, an extreme value is only observed provided μ_{pol} does not exceed certain limits: $(-2.8\mu_{ind}<\mu_{pol}<\mu_{ind})$. The associated vibrating charge e_{0v} for a covalent bond must always exhibit an extreme (maximum) value as in the limiting conditions, i.e., both for $v=0$, and for $v=(k-1)/2$, it becomes zero. This maximum value in the effective vibrating charge for $X-H$ bonds will probably occur between the overtones $v\sim 4(\mu_{ind}=0)$ and $v\sim 7(\mu_{pol}=0)$ (see Fig. 3).

The comparison with experimental data will be given later, as soon as a few final measurements have been made. Here, only the following need be mentioned in relation to Fig. 4: The measurements are very satisfactorily represented by Eq. (20). The OH bonds (phenols, alcohols, water) which with their replaceable hydrogen are more or less "acid" and which also exhibit association through hydrogen bridge, all show the steady decrease characteristic of polar or ionic bonds. By contrast, for the C—H bonds the nonpolar inductive component is clearly predominant, as the transition moments have a distinct minimum. Acetylene, for which measurements are at present in progress, appears to assume an intermediate position.

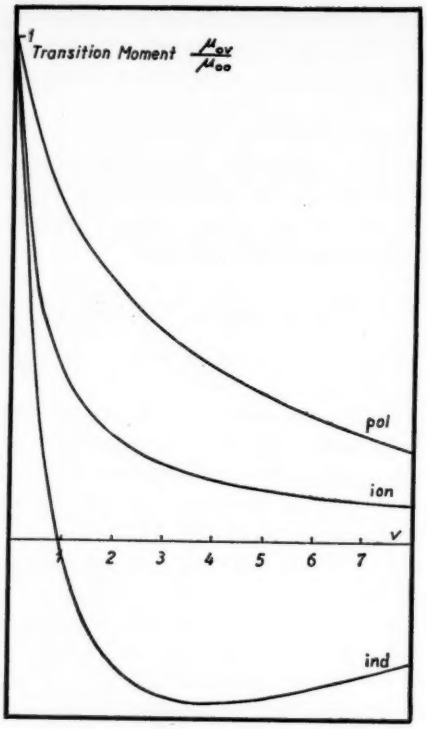

FIG. 2. The reduced transition moment as a function of the vibrational quantum number.

APPENDIX

The following properties of gamma-functions are useful for purposes of integration; It follows from the definition of Laguerre polynomials:

$$e^{-z}\cdot z^{k-2v-1}L_v(z)=\frac{d^v(e^{-z}\cdot z^{k-v-1})}{dz^v},$$

$$\phi(v,m,k)=\int z^{m+v-1}\frac{d^v(e^{-z}\cdot z^{k-v-1})}{dz^v}dz,$$

$$\phi(v,m,k)=\int_0^\infty z^{m-1}\psi_0\bar{\psi}_v dz$$

$$=\binom{m+v-1}{v}\Gamma(k-v-1+m)$$

$$=\frac{\Gamma(v+m)\Gamma(k-v-1+m)}{v!\Gamma(m)}.\quad (21)$$

Further one obtains

$$\frac{d^p\phi(m,v,k)}{dm^p}=\int(\log z)^p z^{m-1}\psi_0\bar{\psi}_v dz \qquad (22)$$

or the special cases

$$\frac{\int(\log z)z^{m-1}\psi_0\bar{\psi}_v dz}{\int z^{m-1}\psi_0\bar{\psi}_v dz}$$

$$=\left[\frac{\Gamma'(v+m)}{\Gamma(v+m)}+\frac{\Gamma'(k-v-1+m)}{\Gamma(k-v-1+m)}-\frac{\Gamma'(m)}{\Gamma(m)}\right], \qquad (23a)$$

$$\int(\log z)^2 z^{m-1}\psi_0\bar{\psi}_v dz=\phi''(m,v,k). \qquad (23b)$$

For integral values of $x(=v+m$, or $m)$ one can write

$$\varphi(1+x)=\frac{\Gamma'(1+x)}{\Gamma(1+x)}=-C+\sum_{n=1}^{x}\frac{1}{n},$$
$$\varphi'(1+x)=s_2-\sum_{n=1}^{x}\frac{1}{n^2}. \qquad (24)$$

$\log_e\gamma_{v=0}=-C=-0.5772=$ Euler's constant; $s_2=\pi^2/6=1.6447$, $\gamma_{v=0}=0.562$. Quite good approximation formulas (Stirling's formula) for $x\gtrsim 1$, are

$$\frac{\Gamma'(1+x)}{\Gamma(1+x)}=\log(x+\gamma)=\log(x+\tfrac{1}{2})+\frac{1}{24(x+\frac{1}{2})^2}, \qquad (25a)$$

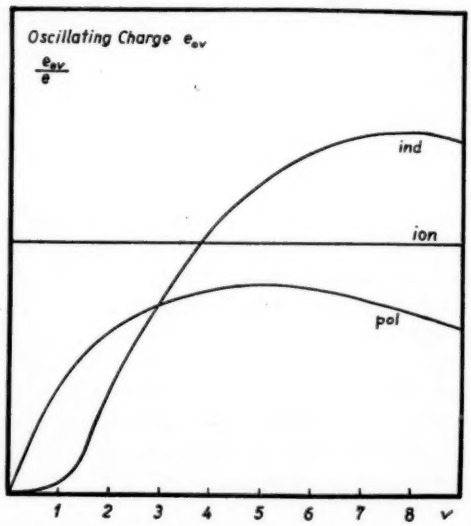

FIG. 3. The oscillating charge as a function of the vibrational quantum number.

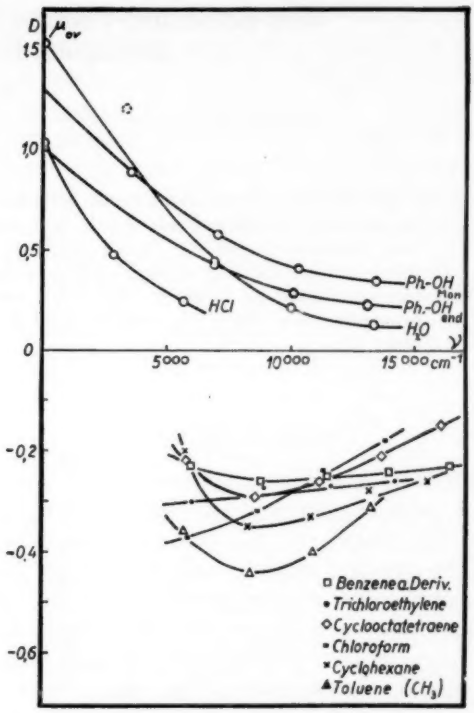

FIG. 4. Transition moments in chemical compounds.

$0.562>\gamma>0.5$ for $0<x<\infty$; $\log 0.562=-c$,

$$\varphi'(1+x)=\frac{\Gamma''(1+x)}{\Gamma'(1+x)}-\left(\frac{\Gamma''(1+x)}{\Gamma'(1+x)}\right)^2$$
$$=\frac{1}{x+\gamma}\simeq\frac{1}{(x+\frac{1}{2})}-\frac{1}{12(x+\frac{1}{2})^3}, \qquad (25b)$$

$0.608>\gamma>0.5$ for $0<x<\infty$:

$$\frac{\Gamma'(1+x)}{\Gamma(1+x)}=\frac{\Gamma'(x)}{\Gamma(x)}+\frac{1}{x}=-c+s_2x-s_3x^2+s_4x^3\cdots, \qquad (26)$$

$$s_\alpha=\sum_1^\infty\frac{1}{n^\alpha};\quad s_2=\frac{\pi^2}{6}=1.645;\quad s_3=1.201;\quad s_4=\frac{\pi^4}{90}=1.082.$$

ACKNOWLEDGMENTS

The author's thanks are due to Dr. Mansel Davies of the University College of Wales and Professor G. Glockler of the State University of Iowa for aid in the translating of this paper. Acknowledgment is also due to Dr. W. J. Orville Thomas of the University College of Wales for assistance in preparing the final draft.

The Excluded Volume Effect in Polymer Chains and the Analogous Random Walk Problem*

ROBERT J. RUBIN
Applied Physics Laboratory, The Johns Hopkins University, Silver Spring, Maryland
(Received June 23, 1952)

An excluded volume random walk is studied in an m-dimensional space. A general expression is obtained for the mean square length of a walk of N steps, $\langle R_N^2\rangle$. It is shown that the increase in $\langle R_N^2\rangle$, δ_s, resulting from the interaction of only the ith and $i+s$th steps in the walk is a constant independent of s in two dimensions. In three and four dimensions δ_s is of the order $s^{-\frac{1}{2}}$ and s^{-1}, respectively. Thus, the interaction of the steps is surprisingly large. An estimate is made of the upper bound on $\langle R_N^2\rangle$ caused by the simultaneous interaction of all steps. The result in three dimensions is that in the limit of large N, $\langle R_N^2\rangle/N$ is at most of order $N^{\frac{1}{2}}$.

INTRODUCTION

THEORETICAL investigations of the properties of polymer chains in solution are based on the average distribution of the monomer elements in a chain. The standard random walk models[1] for polymer chains average over all configurations and thus neglect the effect of the excluded volume. The excluded volume has its origin in the fact that those random walk configurations for the skeleton of the chain which correspond to overlapping of the atoms or monomer units must be excluded in any averaging procedure. Consequently, the standard polymer models should have mean square lengths that are shorter than those of real polymers.

Recently, in the various approximate treatments of the excluded volume effect,[2] conflicting results have been obtained. On the one hand, Hermans,[2] Hadwiger,[2] and Grimley[2] find that the excluded volume correction to the mean square length of a chain of N links, $\langle R_N^2\rangle$, goes to zero in the limit of large N. On the other hand, Flory[2] finds the correction larger and

$$\lim_{N\to\infty}\langle R_N^2\rangle/N\sim N^{1/5}.$$

The purpose of this paper is to investigate the behavior of $\langle R_N^2\rangle$ for large N. The value of $\langle R_N^2\rangle$ calculated by neglecting excluded volume is a lower limit to $\langle R_N^2\rangle$ for the excluded volume random walk; here we will be concerned with obtaining an upper bound to $\langle R_N^2\rangle$. To this end, an excluded volume random walk model is studied in an m-dimensional space. By considering the walk in this general fashion, the appropriate approximation for the problem in 2, 3, and 4 dimensions is indicated. As the number of dimensions increases, a trend appears in the dependence of $\langle R_N^2\rangle$ on N.

The calculations are based on a random walk in which each successive step in the walk has a Gaussian distribution, but with the additional restriction that no two steps in the walk can overlap, i.e., be closer than a fixed distance b. Such a model, while not considering the influence of fixed bond length and angles, should exhibit the essential features that result from the excluded volume effect in real polymers. An advantage of the present model is the ease with which an analytical expression for $\langle R_N^2\rangle$ can be formulated and the ease with which results can be obtained for a simple class of interactions of steps.

MODEL AND METHOD

Consider an m-dimensional vector space. Then, if the probability for a step whose vector displacement is $\mathbf{s}$ is proportional to $\exp[-\mathbf{s}\cdot\mathbf{s}/a^2]$, the unnormalized probability $P_N^{(0)}$ for a particular sequence of N steps is

$$P_N^{(0)}=\prod_{i=1}^{N}\exp[-\mathbf{s}_i\cdot\mathbf{s}_i/a^2].$$

To introduce the excluded volume, the procedure employed here is to multiply $P_N^{(0)}$ by a product of factors, Δ_{jk}, which are zero or relatively very small when the jth and kth steps are within a distance b of each other and are unity otherwise. Thus, the factors weight the distribution function in such a way as to include only those configurations of the N steps for which there is no overlapping. In the following sections, calculations will be made with two different representations of Δ_{jk}. The first and simplest representation is

$$\Delta_{jk}=1-\exp[-(\sum_{i=j+1}^{k}\mathbf{s}_i)^2/b^2], \tag{1}$$

which is effectively unity except when the jth and kth steps are within a distance b of each other, and then Δ_{jk} is small. The second representation, Δ_{jk}', corresponds to a hard sphere repulsion of the jth and kth steps. Δ_{jk}' can be expressed by two equivalent forms.

* The work described in this paper was supported by the Bureau of Ordnance, U. S. Navy, under Contract NOrd-7386.

[1] H. Eyring, Phys. Rev. **39**, 746 (1932); W. Kuhn, Kolloid-Z. **68**, 2 (1934); M. H. Benoit, J. chim. phys. **44**, 18 (1947); W. J. Taylor, J. Chem. Phys. **15**, 412 (1947).

[2] P. J. Flory, J. Chem. Phys. **17**, 303 (1949); J. J. Hermans, Rec. trav. chim. **69**, 220 (1950); E. W. Montroll, J. Chem. Phys. **18**, 734 (1950); H. Hadwiger, Makromolekulare Chemie **5**, 148 (1950); P. Debye and R. J. Rubin, Phys. Rev. **87**, 214 (1952); T. B. Grimley, Proc. Roy. Soc. (London) **212**, 339 (1952). Some related papers are: C. M. Tchen, J. Chem. Phys. **20**, 214 (1952); R. Simha, J. Polymer Sci. **3**, 227 (1948); K. Suzuki, J. Chem. Phys. **19**, 385 (1951); Frisch, Collins, and Friedman, J. Chem. Phys. **19**, 1402 (1951).

The form of the first is similar to (1),

$$\Delta_{jk}'=1-\frac{1}{\pi}\int_{-\infty}^{\infty}\frac{\sin z_{jk}}{z_{jk}}\exp[(\sum_{i=j+1}^{k}\mathbf{s}_i)^2 iz_{jk}/b^2]dz_{jk}; \quad (2)$$

and the second is[3]

$$\Delta_{jk}'=\frac{1}{2\pi i}\int_{-ic-\infty}^{-ic+\infty}\frac{\exp[(\sum_{i=j+1}^{k}\mathbf{s}_i)^2 iz_{jk}/a^2-ib^2z_{jk}/a^2]}{z_{jk}}dz_{jk}, \quad c>0. \quad (3)$$

In either case, the value of Δ_{jk}' is

$$\Delta_{jk}'=\begin{cases}1, & \text{if } (\sum_{i=j+1}^{k}\mathbf{s}_i)^2>b^2\\ 0, & \text{if } (\sum_{i=j+1}^{k}\mathbf{s}_i)^2<b^2,\end{cases}$$

so that Δ_{jk}' gives zero weight to any random walk configuration in which there is overlapping of the jth and kth steps. The advantage of (3) over (2) is purely one of ease of manipulation. As will be seen later, the excluded volume correction for the two interactions Δ_{jk} and Δ_{jk}' are essentially the same for ratios of b to a of the order of unity.

The unnormalized distribution function for a random walk with excluded volume is then

$$P_N(\mathbf{s}_1,\cdots,\mathbf{s}_N)=P_N^{(0)}\prod_{j=0}^{N-1}\prod_{k=j+1}^{N}\Delta_{jk}. \quad (4)$$

The quantity with which we are primarily concerned is the mean square distance moved in the walk:

$$\langle R_N^2\rangle=\frac{\int_{-\infty}^{\infty}\cdots\int(\sum_{i=1}^{N}\mathbf{s}_i)^2P_N(\mathbf{s}_1,\cdots,\mathbf{s}_N)d\mathbf{s}_1\cdots d\mathbf{s}_N}{\int_{-\infty}^{\infty}\cdots\int P_N(\mathbf{s}_1,\cdots,\mathbf{s}_N)d\mathbf{s}_1\cdots d\mathbf{s}_N}. \quad (5)$$

Formally, the right side of (5) can be rewritten

$$\langle R_N^2\rangle=-a^2\frac{d}{d\alpha}\log I(\alpha)\Big|_{\alpha=0} \quad (6)$$

where

$$I(\alpha)=\int_{-\infty}^{\infty}\cdots\int P_N(a\mathbf{s}_1,\cdots,a\mathbf{s}_N)\times\exp[-\alpha(\sum_{i=1}^{N}\mathbf{s}_i)^2]d\mathbf{s}_1\cdots d\mathbf{s}_N. \quad (7)$$

The higher moments of P_N are obtained by successive applications of the operator

$$-a^2\frac{d}{d\alpha}(\ )\Big|_{\alpha=0}.$$

[3] See E. C. Titschmarsh, *Theory of Functions* (Oxford University Press, London, 1949), p. 107.

GENERAL EXPRESSION FOR $\langle R_N^2\rangle$

The function $I(\alpha)$ is similar in form to the partition function for a system of interacting particles with an added degree of complexity in the ordering of the particles, introduced through $P_N^{(0)}$. Thus, all the difficulties met with in the theory of dense gases are present. This fact becomes evident on considering the expansion of $P_N(\mathbf{s}_1,\cdots,\mathbf{s}_N)$, using the first representation of Δ_{jk}:

$$P_N(\mathbf{s}_1,\cdots,\mathbf{s}_N)=P_N^{(0)}\{1-\sum_{j=0}^{N-1}\sum_{k>j}\times\exp[-(\sum_{i=j+1}^{k}\mathbf{s}_i)^2/b^2]+\sum_j\sum_k\sum_l\sum_n\times\exp[-(\sum_{i=j+1}^{k}\mathbf{s}_i)^2/b^2-(\sum_{i=l+1}^{n}\mathbf{s}_i)^2/b^2]-\cdots\}. \quad (8)$$

When Eq. (1) is substituted in (8), the subsequent term-by-term integration produces a set of integrals like the Mayer cluster integrals. Whereas with the Mayer cluster integrals, the integration cannot be performed explicitly, here the value of each cluster integral can be expressed in terms of the determinant of the quadratic form in the exponent of the integrand. It will be shown that higher order terms in the expansion of $\langle R_N^2\rangle$ become important in the case of interest, namely, $N\to\infty$ and b/a fixed. In the analogous case of the imperfect gas, the corresponding limit would be $N\to\infty$ and V, the total volume, fixed. We therefore conclude that for large N it is incorrect to neglect higher order interactions.

In the next two sections, expressions for $\langle R_N^2\rangle$ will be obtained for step interactions corresponding to Δ_{jk} and Δ_{jk}'. Results in closed form cannot be obtained in general. However, for a simple class of interactions of steps, explicit calculations can be made. The explicit results obtained are used to fix an upper bound on $\langle R_N^2\rangle$.

(A) Formal Solution Using Δ_{jk}

Substituting (8) in (7) and interchanging orders of summation and integration, one obtains

$$I(\alpha)=\int_{-\infty}^{\infty}\cdots\int\exp[-\sum_{i=1}^{N}\mathbf{s}_i\cdot\mathbf{s}_i-\alpha(\sum_{i=1}^{N}\mathbf{s}_i)^2]d\mathbf{s}_1\cdots d\mathbf{s}_N-\sum_{j=0}^{N-1}\sum_{k>j}\int_{-\infty}^{\infty}\cdots\int\exp[-\sum_{i=1}^{N}\mathbf{s}_i\cdot\mathbf{s}_i-\alpha(\sum_{i=1}^{N}\mathbf{s}_i)^2-\beta^{-2}(\sum_{i=j+1}^{k}\mathbf{s}_i)^2]d\mathbf{s}_1\cdots d\mathbf{s}_N+\sum_j\sum_k\sum_l\sum_n\int_{-\infty}^{\infty}\cdots\int\exp[-\sum_{i=1}^{N}\mathbf{s}_i\cdot\mathbf{s}_i-\alpha(\sum_{i=1}^{N}\mathbf{s}_i)^2-\beta^{-2}(\sum_{i=j+1}^{k}\mathbf{s}_i)^2-\beta^{-2}(\sum_{i=l+1}^{n}\mathbf{s}_i)^2d\mathbf{s}_1\cdots d\mathbf{s}_N-\cdots], \quad (9)$$

where β^{-2} is a^2/b^2. The general type of integral in (9) is

$$I(j,k;l,n;\cdots;\alpha)=\int_{-\infty}^{\infty}\cdots\int\exp\{-[\sum_{i=1}^{N}\mathbf{s}_i\cdot\mathbf{s}_i+\alpha(\sum_{i=1}^{N}\mathbf{s}_i)^2+\beta^{-2}(\sum_{i=j+1}^{k}\mathbf{s}_i)^2+\beta^{-2}(\sum_{i=l+1}^{n}\mathbf{s}_i)^2+\cdots]\}d\mathbf{s}_1\cdots d\mathbf{s}_N$$

$$=\left[\int_{-\infty}^{\infty}\cdots\int\exp\{-[\sum_{i=1}^{N}x_i^2+\alpha(\sum_{i=1}^{N}x_i)^2+\beta^{-2}(\sum_{i=j+1}^{k}x_i)^2+\beta^{-2}(\sum_{i=l+1}^{n}x_i)^2+\cdots]\}dx_1\cdots dx_N\right]^m. \quad (10)$$

Since the quadratic form in the exponent of the integrand is positive definite, the value of the integral is[4]

$$I(j,k;l,n;\cdots;\alpha)=\pi^{mN/2}D^{-m/2}(j,k;l,n;\cdots;\alpha), \quad (11)$$

where $D(j,k,l,n,\cdots,\alpha)$ is the determinant of the matrix of the coefficients of the quadratic form in the exponent in (10). The matrix of the quadratic form in (10), $\mathbf{M}$, is the sum of matrices

$$\mathbf{M}=\mathbf{M}_0+\mathbf{M}_\alpha+\beta^{-2}\mathbf{M}_{jk}+\beta^{-2}\mathbf{M}_{lm}+\cdots,$$

where $\mathbf{M}_0$ is the matrix of the coefficients of $\sum_{i=1}^{N}x_i^2$, $\mathbf{M}_\alpha$ is the matrix of the coefficients of $\alpha(\sum_{i=1}^{N}x_i)^2$, and $\mathbf{M}_{jk}$ is the matrix of the coefficients of $(\sum_{i=j+1}^{k}x_i)^2$. The value of $\langle R_N^2\rangle$ upon simplification is

$$\langle R_N^2\rangle=\frac{ma^2}{2}\,\frac{N-\sum_{j=0}^{N-1}\sum_{k>j}[\sum_{i=1}^{N}D_i^{(1)}(j,k)]D^{-m/2-1}(j,k)+\sum_j\sum_k\sum_l\sum_n[\sum_{i=1}^{N}D_i^{(1)}(j,k;l,n)]D^{-m/2-1}(j,k;l,n)-\cdots}{1-\sum_{j=0}^{N-1}\sum_{k>j}D^{-m/2}(j,k)+\sum_j\sum_k\sum_l\sum_n D^{-m/2}(j,k;l,n)-\cdots}, \quad (12)$$

where $D(j,k;l,n;\cdots)$ is $D(j,k;l,n;\cdots;0)$ and $D_i^{(1)}(j,k;l,n;\cdots)$ is $D(j,k;l,n;\cdots)$ with the elements of the ith column replaced by unity. The values of the determinants in the first few terms of (12) are[5]

$$D(j,k)=1+s\beta^{-2};\quad s=k-j,\ k>j, \quad (13)$$

$$\sum_{i=1}^{N}D_i^{(1)}(j,k)=(N-s)(1+s\beta^{-2})+s;\quad s=k-j,\ k>j, \quad (14)$$

$$D(j,k;l,n)=(1+s\beta^{-2})(1+t\beta^{-2});\quad s=k-j,\ t=n-l,\ j<k<l<n, \quad (15)$$

$$\sum_{i=1}^{N}D_i^{(1)}(j,k;l,n)=(N-s-t)D(j,k;l,n)+s(1+t\beta^{-2})[\sum_{i=1}^{N}D_i^{(1)}(j,k)]+t(1+s\beta^{-2})[\sum_{i=1}^{N}D_i^{(1)}(l,n)];\quad s=k-j,\ t=n-l,\ j<k<l<n, \quad (16)$$

$$D(j,k;l,n)=1+(s+t)\beta^{-2}+t(s-t)\beta^{-4};\quad s=k-j,\ t=n-l,\ j\leqslant l,\ k\geqslant n,\ s>t, \quad (17)$$

$$\sum_{i=1}^{N}D_i^{(1)}(j,k;l,n)=ND(j,k;l,n)-(s^2+t^2)\beta^{-2}-2t(s-t)\beta^{-4};\quad s=k-j,\ t=n-l,\ j\leqslant l,\ k\geqslant n,\ s>t. \quad (18)$$

The general determinant $D(j,k;l,n;\cdots)$ is a complicated polynomial in β^{-2}. For small excluded volume, i.e., $\beta^2\ll 1$, and large N, the order of magnitude of the first few terms in the numerator and denominator of (12) can be estimated using Eqs. (13)–(18). The orders of magnitude are

$$\sum_j\sum_k[\sum_i D_i^{(1)}(j,k)]D^{-m/2-1}(j,k)\sim c_1N^3\beta^m, \quad (19)$$

$$\sum_j\sum_k D^{-m/2}(j,k)\sim c_1'N^2\beta^m, \quad (20)$$

$$\sum_j\sum_k\sum_l\sum_n[\sum_i D_i^{(1)}(j,k;l,n)]\times D^{-m/2-1}(j,k;l,n)\sim c_2N^5\beta^m, \quad (21)$$

$$\sum_j\sum_k\sum_l\sum_n D^{-m/2}(j,k;l,n)\sim c_2'N^4\beta^{2m}, \quad (22)$$

where the c's are constants. Inserting Eqs. (19)–(22) in (12), one obtains

$$\langle R_N^2\rangle\sim\frac{ma^2}{2}\,\frac{N-c_1N^3\beta^m+c_2N^5\beta^{2m}-\cdots}{1-c_1'N^2\beta^m+c_2'N^4\beta^{2m}-\cdots}. \quad (23)$$

[4] S. S. Wilks, *Mathematical Statistics* (Princeton University Press, Princeton, 1947), p. 63.

[5] The most appropriate expansion of determinants like $D(j,k;l,n;\cdots)$ and $D_i^{(1)}(j,k;l,n;\cdots)$ is an expansion by diagonal elements. When a matrix $\mathbf{M}$ is the sum of the unit matrix $\mathbf{M}_0$ and another matrix $\mathbf{M}_1$, the determinant of $\mathbf{M}$ is unity plus all principal minors of $\mathbf{M}_1$ (minors of the principal diagonal). See A. C. Aitken, *Determinants and Matrices* (Oliver and Boyd, Edinburgh, 1949), p. 87.

Thus in the limit, β fixed and $N\to\infty$, higher and higher order terms in (12) become important.

If one does not include the interaction of every pair of steps in the product $\prod_{j=0}^{N-1}\prod_{k=j+1}^{N}\Delta_{jk}$, there is a simple class of interactions of steps for which $\langle R_N^2\rangle$ may be easily calculated. The characteristic of this class is that the nonzero elements of the matrices $\mathbf{M}_{jk}$, $\mathbf{M}_{lm}$, $\cdots$ do not overlap. In such a case the determinants $D(j,k;\cdots)$ factor into products of determinants of the matrices $\mathbf{M}_0+\mathbf{M}_{jk}$. There is a similar simplification for $D_i^{(1)}(j,k;\cdots)$. The physical reason for the simplification is that the interference of the pairs of steps are independent of each other. One can therefore calculate separately the increase in $\langle R_N^2\rangle$, δ_s, caused by the interaction of the jth and $j+s$th steps and sum up the increments δ_s to obtain the total increase. δ_s is a useful quantity since it is an upper bound on the increase in size caused by the interaction of the jth and $j+s$th steps when intermediate steps interact. The reason for this fact is that the interaction of intermediate steps increases the average distance between the jth and $j+s$th steps and therefore decreases the contribution of their interaction to $\langle R_N^2\rangle$. Using the expression for δ_s, one can obtain an upper bound on $\langle R_N^2\rangle$ in (12). Such a procedure avoids the difficulties involved in estimating the ratio of two series whose partial sums oscillate.

We now obtain $\langle R_N^2\rangle$ for the interaction of only the jth and $j+s$th steps. Equation (12) reduces simply to

$$\langle R_N^2\rangle=\frac{ma^2}{2}\frac{N-[\sum_i D_i^{(1)}(j,j+s)]D^{-m/2-1}(j,j+s)}{1-D^{-m/2}(j,j+s)}. \quad (24)$$

Substituting the values of $D(j,j+s)$ and

$$\sum_{i=1}^{N} D_i^{(1)}(j,j+s)$$

given in (13) and (14) into (24), one obtains

$$\langle R_N^2\rangle=\frac{ma^2}{2}\left[N+\frac{s^2\beta^{-2}(1+s\beta^{-2})^{-m/2-1}}{1-(1+s\beta^{-2})^{-m/2}}\right]. \quad (25)$$

A very interesting and significant result can be deduced from (25). When the step separation is large, the increase, δ_s, in $\langle R_N^2\rangle$ is approximately

$$\delta_s\cong\frac{ma^2}{2}s^{-m/2+1}\beta^m. \quad (26)$$

Therefore, in two dimensions, δ_s is a constant for large s. Thus, there is a very strong long-range interaction of steps in two dimensions. In three and four dimensions the step interaction for large s is still large. δ_s in three and four dimensions is proportional to $s^{-\frac{1}{2}}$ and s^{-1}, respectively. The above result is consistent with the heuristic idea that as the number of dimensions increases, the interaction of the steps should decrease because there is more room for the steps to avoid each other. On the other hand, the magnitude of the interaction in two, three, and four dimensions is surprisingly large.

(B) Formal Solution for Hard Sphere Interaction of Steps

Substituting (3) in (7), one obtains

$$I(\alpha)=\int_{-\infty}^{\infty}\cdots\int\exp\Big[-\sum_{i=1}^{N}\mathbf{s}_i\cdot\mathbf{s}_i - \alpha\Big(\sum_{i=1}^{N}\mathbf{s}_i\Big)^2\Big]\prod_{j=0}^{N-1}\prod_{k>j}\left\{\frac{1}{2\pi i}\int_{-ic-\infty}^{-ic+\infty}\frac{\exp[(\sum_{i=j+1}^{k}\mathbf{s}_i)^2 iz_{jk}-i\beta^2 z_{jk}]}{z_{jk}}dz_{jk}\right\}d\mathbf{s}_1\cdots d\mathbf{s}_N. \quad (27)$$

Interchanging orders of integration in (27), $I(\alpha)$ is

$$I(\alpha)=\int_{-ic-\infty}^{-ic+\infty}\cdots\int\left[\int_{-\infty}^{\infty}\cdots\int\exp\Big\{-\Big[\sum_{i=1}^{N}x_i^2+\alpha\Big(\sum_{i=1}^{N}x_i\Big)^2-\beta^2\sum_{j=0}^{N-1}\sum_{k>j}iz_{jk}\Big(\sum_{i=j+1}^{k}x_i\Big)^2\Big]\Big\}\right]^m \times\prod_{j=0}^{N-1}\prod_{k>j}\left\{\frac{\exp(-i\beta^2 z_{jk})}{2\pi i z_{jk}}dz_{jk}\right\}. \quad (28)$$

It is shown in the appendix that for c less than $(N^2+N)^{-1}$, the eigenvalues of the matrix of the coefficients of the quadratic form in (28) have positive real parts. Thus it is possible to perform the integration over the space coordinates in (28) using (11):

$$I(\alpha)=\pi^{mN/2}\int_{-ic-\infty}^{-ic+\infty}\cdots\int D^{-m/2}(z_{01},\cdots,z_{jk},\cdots;\alpha)\times\prod_{j=0}^{N-1}\prod_{k=j+1}^{N}\left\{\frac{\exp(-i\beta^2 z_{jk})}{2\pi i z_{jk}}dz_{jk}\right\}, \quad (29)$$

where $D(z_{01},\cdots,z_{jk},\cdots;\alpha)$ is the determinant of the matrix of the quadratic form in (28).

The value of $\langle R_N^2\rangle$ is

$$\langle R_N^2\rangle = \frac{ma^2}{2}\frac{\int_{-ic-\infty}^{-ic+\infty}\cdots\int[\sum_{i=1}^{N}D_i^{(1)}(z_{01},\cdots)]D^{-m/2-1}(z_{01},\cdots)\prod_{j=0}^{N-1}\prod_{k>j}\left\{\frac{\exp(-i\beta^2 z_{jk})}{2\pi i z_{jk}}dz_{jk}\right\}}{\int_{-ic-\infty}^{-ic+\infty}\cdots\int D^{-m/2}(z_{01},\cdots)\prod_{j=0}^{N-1}\prod_{k>j}\left\{\frac{\exp(-i\beta^2 z_{jk})}{2\pi i z_{jk}}dz_{jk}\right\}}, \tag{30}$$

where $D(z_{01},\cdots)=D(z_{01},\cdots;0)$ and $D_i^{(1)}(z_{01},\cdots)$ is $D(z_{01},\cdots)$ with the ith column replaced by unity.

Although one may transform (30) by integration by parts with respect to z_{0N} or by use of a multiple convolution transformation, no real progress can be made in integrating (30). However, for the same simple class of interactions defined in the last section, results similar to (26) are obtained.

For the hard sphere interaction of steps j and $j+s$, Eq. (30) reduces to

$$\langle R_N^2\rangle = \frac{ma^2}{2}\frac{\frac{1}{2\pi i}\int_{-ic-\infty}^{-ic+\infty}\frac{\exp[-i\beta^2 z_{j,\,j+s}]}{z_{j,\,j+s}}[\sum_{i=1}^{N}D_i^{(1)}(z_{j,\,j+s})]D^{-m/2-1}(z_{j,\,j+s})dz_{j,\,j+s}}{\frac{1}{2\pi i}\int_{-ic-\infty}^{-ic+\infty}\frac{\exp[-i\beta^2 z_{j,\,j+s}]}{z_{j,\,j+s}}D^{-m/2}(z_{j,\,j+s})dz_{j,\,j+s}}. \tag{31}$$

Substituting the values of $D(z_{j,\,j+s})$ and $\sum_{i=1}^{N}D_i^{(1)}(z_{j,\,j+s})$ given in (13) and (14) into (31), one obtains

$$\langle R_N^2\rangle = \frac{ma^2}{2}\left[N-s+s\frac{\frac{1}{2\pi i}\int_{-ic-\infty}^{-ic+\infty}\frac{\exp(-i\beta^2 z)}{z}\frac{dz}{(1-isz)^{m/2+1}}}{\frac{1}{2\pi i}\int_{-ic-\infty}^{-ic+\infty}\frac{\exp(-i\beta^2 z)}{z}\frac{dz}{(1-isz)^{m/2}}}\right]. \tag{32}$$

The integrals in (32) can be evaluated by contour integration, closing the contour around the pole at $z=-i/s$.[6]

The value of $\langle R_N^2\rangle$ for even m is[7]

$$\langle R_N^2\rangle = \frac{ma^2}{2}\left[N-s+\frac{2i}{m}\frac{\frac{d^{m/2}}{dz^{m/2}}\left[\frac{\exp(-i\beta^2 z)}{z}\right]\Big|_{z=-i/s}}{\frac{d^{m/2-1}}{dz^{m/2-1}}\left[\frac{\exp(-i\beta^2 z)}{z}\right]\Big|_{z=-i/s}}\right]. \tag{33}$$

In two dimensions the value of $\langle R_N^2\rangle$ is

$$\begin{aligned}\langle R_N^2\rangle &= Na^2+a^2\beta^2\\ &= Na^2+b^2.\end{aligned} \tag{34}$$

Thus the increase in size δ_s is the constant b^2. In four dimensions, the value of $\langle R_N^2\rangle$ is

$$\langle R_N^2\rangle = 2Na^2+\frac{a^2\beta^4}{\beta^2+s}. \tag{35}$$

In (34) and (35) the dependence of δ_s on s is the same as for Gaussian repulsion of steps.

[6] The restriction that c be less than $(N^2+N)^{-1}$ in (29) reduces in the present case to $c<1/s$.

[7] It was not possible to obtain a simple expression for m odd.

AN UPPER BOUND ON $\langle R_N^2\rangle$

As already indicated, an upper bound for the mean square length is

$$\langle R_N^2\rangle < \frac{ma^2}{2}[N+\sum_{s=1}^{N}(N-s+1)\delta_s], \tag{36}$$

where the form of the sum in (36) results from the fact that there are $N-s+1$ pairs of steps separated by s steps.

Substituting (26) in (36), one obtains the inequality

$$\langle R_N^2\rangle < \frac{ma^2}{2}[N+C\sum_{s=1}^{N}(N-s+1)s^{-m/2+1}\beta^m], \tag{37}$$

where C is a constant.

According to (37), $\langle R_N^2\rangle$ is at most of order N for $m\geqslant 5$. In four, three, and two dimensions, $\langle R_N^2\rangle$ is at most of order $N\log N$, $N^{\frac{3}{2}}$, and N^2, respectively. The above estimates in four, three, and two dimensions are not sharp. For if step interactions are large, the interaction of a pair of steps should be appreciably decreased by interactions involving intermediate steps. An indication of this decrease can be obtained by calculating the increase in $\langle R_N^2\rangle$ when the jth and $j+s$th steps interact and the intermediate steps k and $k+t$ also

interact. Using Gaussian step interaction, the value of $\langle R_N^2\rangle$ is

$$\langle R_N^2\rangle=\frac{ma^2}{2}\left[\frac{N-[\sum_{i=1}^{N}D_i^{(1)}(j,j+s)]D^{-m/2-1}(j,j+s)-[\sum_{i=1}^{N}D_i^{(1)}(k,k+t)]D^{-m/2-1}(k,k+t)+[\sum_{i=1}^{N}D_i^{(1)}(j,j+s;k,k+t)]D^{-m/2-1}(j,j+s;k,k+t)}{1-D^{-m/2}(j,j+s)-D^{-m/2}(k,k+t)+D^{-m/2}(j,j+s;k,k+t)}\right]. \quad (38)$$

Substituting the values of the determinants given in Eqs. (13), (14), (17), and (18), $\langle R_N^2\rangle$ simplifies to

$$\langle R_N^2\rangle=\frac{ma^2}{2}\left[N+\frac{\dfrac{s^2\beta^{-2}}{(1+s\beta^{-2})^{m/2+1}}+\dfrac{t^2\beta^{-2}}{(1+t\beta^{-2})^{m/2+1}}-\dfrac{(s^2+t^2)\beta^{-2}+2t(s-t)\beta^{-4}}{[1+(s+t)\beta^{-2}+t(s-t)\beta^{-4}]^{m/2+1}}}{1-(1+s\beta^{-2})^{-m/2}-(1+t\beta^{-2})^{-m/2}+[1+(s+t)\beta^{-2}+t(s-t)\beta^{-4}]^{-m/2}}\right]. \quad (39)$$

For the case $\beta=1$, $s=2$, $t=1$, Eq. (39) is

$$\langle R_N^2\rangle=\frac{ma^2}{2}\left[N+\frac{4(3)^{-m/2-1}+2^{-m/2-1}-7(5)^{-m/2-1}}{1-3^{-m/2}-2^{-m/2}+5^{-m/2}}.\right] \quad (40)$$

In two, three, and four dimensions, the increases in $\langle R_N^2\rangle$ from (40) are $1.129a^2$, $0.850a^2$ and $0.639a^2$, respectively. These values should be compared with $1.167a^2$, $0.888a^2$, and $0.667a^2$, which are the increases in $\langle R_N^2\rangle$ in two, three, and four dimensions resulting from the independent interaction of the two pairs of steps.

While it has not as yet been possible to improve the upper bound on $\langle R_N^2\rangle$ in three dimensions,[8] one can still make the following two statements about the asymptotic behavior of $\langle R_N^2\rangle/Na^2$ for large N:

(1) From the foregoing discussion, it is clear that

$$\lim_{N\to\infty}\langle R_N^2\rangle/Na^2$$

is certainly greater than one, contrary to the conclusions of Hermans,[2] Hadwiger,[2] and Grimley.[2]

(2) The value of

$$\lim_{N\to\infty}\langle R_N^2\rangle/Na^2$$

depends on a power of N which is probably intermediate between 0 and $\frac{1}{2}$.

ACKNOWLEDGMENTS

The author wishes to thank his wife for her patience and encouragement and Miss Agnes Fogelgren for typing the manuscript.

APPENDIX

Proof that the eigenvalues of the matrix of the quadratic form in the integrand in (28) have positive real parts.—The matrix $\mathbf{M}$ of the quadratic form in the exponent in (28) is

$$\mathbf{M}=\mathbf{M}_0+\mathbf{M}_\alpha-\sum_{j=0}^{N-1}\sum_{k=j+1}^{N}iz_{jk}\mathbf{M}_{jk}.$$

Consider the sum of the interaction matrices

$$\mathbf{M}_I=\sum_{j=0}^{N-1}\sum_{k=j+1}^{N}iz_{jk}\mathbf{M}_{jk}.$$

On the path of integration in (28), the quantity iz_{jk} can be replaced by $c+ix_{jk}$. The matrix sum $\sum_{j=0}^{N-1}\sum_{k>j}\mathbf{M}_{jk}$ is positive. Therefore, $\mathbf{M}_I$ has eigenvalues λ_i whose real parts a_i are greater than or equal to zero. The eigenvalues of the combination of matrices $\mathbf{M}_0-\mathbf{M}_I$ have real parts equal to $1-a_i$. In order that $1-a_i$ be positive, c must be restricted to small positive values. The limit on c can be set as follows. The maximum a_i, $a_{\max}$ is bounded by the real part of the trace of $\mathbf{M}_I$:

$$a_{\max}\leqslant\sum_{j=0}^{N-1}\sum_{k=j+1}^{N}c$$

$$\leqslant c(N^2+N)/2.$$

So if c is less than $(N^2+N)^{-1}$, all the eigenvalues of $\mathbf{M}_0+\mathbf{M}_I$ have positive real parts. The matrix $\mathbf{M}$ will also have eigenvalues with positive real parts, since the effect of $\mathbf{M}_\alpha$ on the eigenvalues can be made as small as necessary by making α small.

Note added in proof:—In a recent paper, J. J. Hermans, M. S. Klamkin, and R. Ullman, J. Chem. Phys. **20**, 1360 (1952), (HKU), a result was obtained which was similar to that obtained by Debye and Rubin (reference 2) (DR). Although the results of HKU and DR are consistent with the conclusions arrived at in this paper, their assumption concerning low bead density, at the very least, is open to question. This point will be discussed in a subsequent letter.

[8] The possibility of improving the bound on $\langle R_N^2\rangle$ is being investigated.

The Thermodynamic Properties of Sodium Vapor*

A. BENTON AND T. H. INATOMI
Atomic Energy Research Department, North American Aviation, Inc., Downey, California
(Received June 13, 1952)

The free energy, enthalpy, entropy, and specific heat for both monatomic and diatomic sodium vapor have been calculated from spectroscopic data by the well-known methods of statistical mechanics. Also, the equilibrium constant K_p for the gaseous reaction $Na+Na=Na_2$, as well as the entropies and enthalpies for the equilibrium mixture of these two species, were obtained. These calculations were made for the vapors as ideal gases at a pressure of 1 atmosphere, and for the temperature range 100°K to 2600°K. The results are presented in tables.

INTRODUCTION

THE formulation of Mayer and Mayer,[1] including their high temperature anharmonicity corrections to the rigid rotator-harmonic oscillator model, was employed to calculate several of the thermodynamic properties of sodium vapor from spectroscopic data for the temperature range 100°K to 2600°K. In all cases, the vapors were assumed to be ideal gases at a pressure of one atmosphere. The free energy, $(F^0-E_0^0/T)$, enthalpy, $(H^0-E_0^0/T)$, entropy, S^0, and specific heat, C_p^0, for both the monatomic and diatomic species are given in Table I along with the equilibrium constant K_p for the reaction $2Na \rightleftarrows Na_2$. The composition, molecular weight, entropy, and enthalpy for the equilibrium mixtures are given in Table II.

The physical constants which were used appear in Table III, and the spectroscopic data in Tables IV and V. The following two sections list the formulas which were used in the calculations and contain a few explanatory comments to facilitate understanding how the results were obtained. The notation, except where otherwise noted, is that of Mayer and Mayer.

INDIVIDUAL SPECIES

The equations from which the properties of the individual species were calculated are:

$$\left(\frac{F^0-E_0^0}{T}\right)=R\left[\frac{3}{2}\ln\left(\frac{h^2N_0}{2\pi k}\right)-\frac{3}{2}\ln M-\frac{5}{2}\ln T+\ln\frac{N_0}{R}\right]+\left(\frac{F^0-E_0^0}{T}\right)_v+R\left[\ln B_0+\ln\left(\frac{hc}{k}\right)-\ln T-\frac{\sigma}{3}\right]+(R\ln 2)-R\left[\frac{A}{\theta}-B+C\theta-D\theta^2-E\theta^3\right],$$

$$\left(\frac{H^0-E_0^0}{T}\right)=\left(\frac{7}{2}\right)R+\left(\frac{H^0-E_0^0}{T}\right)_v-\frac{R\sigma}{3}+R\left[\frac{A}{\theta}-C\theta+2D\theta^2+3E\theta^3\right],$$

$$C_p^0=\frac{7}{2}R+(C_p)_v+R\left[2\frac{A}{\theta}-2D\theta^2-6E\theta^3\right],$$

$$S^0=\left(\frac{H^0-E_0^0}{T}\right)-\left(\frac{F^0-E_0^0}{T}\right).$$

All symbols are those of Mayer and Mayer except the following (see Table V):

$$A=\frac{8B_e}{\omega_e}+\frac{\alpha_e}{B_e}+\frac{2\omega_e x_e}{\omega_e},$$

$$B=\frac{\alpha_e}{2B_e}+\frac{2\omega_e x_e}{\omega_e},$$

$$C=\frac{\alpha_e}{12B_e}+\frac{5}{6}\frac{\omega_e x_e}{\omega_e},$$

$$D=\frac{1}{6}\frac{\omega_e x_e}{\omega_e},$$

$$E=\frac{\alpha_e}{720B_e}-\frac{\omega_e x_e}{120\omega_e},$$

$$\theta=\frac{hc\omega}{kT};\quad \text{where}\quad \omega=\omega_e-2\omega_e x_e.$$

For the convenience of the reader, one additional symbol is given here:

$$\sigma=\frac{B_0 hc}{kT},\quad \text{where}\quad B_0=B_e-\frac{\alpha_e}{2}.$$

The vibrational contributions to the free energy, enthalpy, and specific heat were evaluated from the

* This report was based upon studies conducted for the Atomic Energy Commission under Contract AT-40-1-Gen-1064.
[1] J. E. Mayer and M. G. Mayer, *Statistical Mechanics* (John Wiley and Sons, Inc., New York, 1948).

TABLE I. Thermodynamic functions for monatomic and diatomic sodium vapor as perfect gases, in their standard state of one atmosphere pressure.[a]

T, °K	$-\left(\frac{F^0-E_0^0}{T}\right)_1$ cal/mole °K	$-\left(\frac{F^0-E_0^0}{T}\right)_2$ cal/mole °K	K_p	$\left(\frac{H^0-E_0^0}{T}\right)_1$ cal/mole °K	$\left(\frac{H^0-E_0^0}{T}\right)_2$ cal/mole °K	S_1^0 cal/mole °K	S_2^0 cal/mole °K	C_{p1}^0 cal/mole °K	C_{p2}^0 cal/mole °K
100	26.318	37.996	3.9362×10^{33}	4.9680	7.4871	31.286	45.483	4.9680	8.2982
298.1	31.744	46.659	4.6236×10^{8}	4.9680	8.3331	36.712	54.992	4.9680	8.9623
371	32.831	48.496	1.4664×10^{6}	4.9680	8.4630	37.799	56.959	4.9680	9.0233
500	34.313	51.045	3.2853×10^{3}	4.9680	8.6181	39.281	59.663	4.9680	9.1005
800	36.648	55.146	4.2905	4.9680	8.8255	41.616	63.971	4.9680	9.2369
1000	37.757	57.125	0.45780	4.9680	8.9160	42.7250	66.041	4.9680	9.3188
1155	38.473	58.414	0.13688	4.9680	8.9742	43.441	67.389	4.9680	9.3807
1200	38.663	58.758	0.10193	4.9680	8.9898	43.631	67.748	4.9680	9.3985
1400	39.429	60.148	0.034630	4.9680	9.0538	44.397	69.202	4.9680	9.4771
1600	40.092	61.361	0.015346	4.9680	9.1116	45.060	70.473	4.9680	9.5552
1800	40.677	62.438	0.0081268	4.9680	9.1652	45.645	71.603	4.9680	9.6329
2000	41.201	63.406	0.0048796	4.9680	9.2159	46.169	72.622	4.9680	9.7104
2200	41.674	64.287	0.0032108	4.9680	9.2643	46.642	73.551	4.9680	9.7879
2273	41.836	64.589	0.0028065	4.9680	9.2816	46.804	73.871	4.9680	9.8161
2400	42.106	65.095	0.0022641	4.9680	9.3112	47.074	74.406	4.9680	9.8652
2600	42.504	65.842	0.0016844	4.9680	9.3568	47.472	75.199	4.9680	9.9424

[a] Subscript 1 refers to monatomic sodium vapor. Subscript 2 refers to diatomic sodium vapor. K_p = Equilibrium constant for reaction $2Na \rightleftarrows Na_2$.

Rand tables;[2] hence, the explicit expressions for them are not given in the above formulas.

MIXTURES

The properties of the mixtures were obtained from the formulas:

$$S_M^0=\sum_{i=1}^{2} x_i S_i^0 - R\sum_{i=1}^{2} x_i \ln x_i,$$

$$H_M^0=H_1^0x_1+H_2^0x_2,$$

$$W=M_1x_1+M_2x_2,$$

where the subscripts M, 1, 2 denote, respectively, the mixture, monatomic, and diatomic sodium; the x's are mole fractions; W is the molecular weight of the mixture, and M_1 and M_2 those of the individual species. In these equations, the entropies S^0 and the enthalpies H^0 are all molar, and those of the constituents are to be taken at the temperature and pressure of the mixture. The mol fractions were obtained from the equilibrium constant, K_p, of the reaction $2Na \rightleftarrows Na_2$, by means of the relationship

$$-R\ln K_p=\frac{\Delta E_0^0}{T}+\left(\frac{F^0-E_0^0}{T}\right)_{Na_2}-2\left(\frac{F^0-E_0^0}{T}\right)_{Na}.$$

To evaluate H_M^0, it is necessary to know H_1^0 and H_2^0. These were obtained from $(H^0-E_0^0/T)_{Na}$ and

TABLE II. The composition and molecular weight, entropy, and enthalpy of the equilibrium mixture of monatomic and diatomic sodium vapor (total pressure = 1 atmosphere).[a]

T, °K	X_1	X_2	W gm/mole	S_M^0 cal/mole °K	S_m^0 cal/(22.997 gm) °K	$(H^0)_1$ cal/mole	$(H^0)_2$ cal/mole	H_M^0 cal/mole	H_m^0 cal/(22.997 gm)
100	1.5939×10^{-17}	1.0000	45.994	45.483	22.742	26,547	36,009	36,009	18,004
298.1	4.6505×10^{-5}	0.99995	45.993	54.992	27.497	27,531	37,744	37,744	18,872
371	8.2546×10^{-4}	0.99917	45.975	56.957	28.490	27,893	38,400	38,391	19,204
500	0.017295	0.98271	45.596	59.484	30.002	28,534	39,569	39,378	19,861
800	0.38011	0.61990	37.253	56.794	35.060	30,024	42,320	37,647	23,240
1000	0.74554	0.25446	28.849	49.785	39.687	31,018	44,176	34,366	27,395
1155	0.89139	0.10861	25.495	46.725	42.147	31,788	45,625	33,291	30,029
1200	0.91471	0.085286	24.958	46.267	42.631	32,012	46,048	33,209	30,599
1400	0.96758	0.032421	23.743	45.485	44.057	33,005	47,935	33,489	32,438
1600	0.98511	0.014893	23.340	45.592	44.923	33,999	49,839	34,235	33,732
1800	0.99200	0.007997	23.181	45.945	45.581	34,992	51,757	35,126	34,848
2000	0.99517	0.004833	23.108	46.357	46.134	35,986	53,692	36,072	35,898
2200	0.99681	0.003190	23.070	46.771	46.622	36,980	55,642	37,039	36,921
2273	0.99721	0.002791	23.061	46.918	46.787	37,342	56,357	37,395	37,291
2400	0.99775	0.002254	23.049	47.168	47.062	37,973	57,607	38,017	37,932
2600	0.99832	0.001679	23.036	47.543	47.463	38,967	59,588	39,001	38,936

[a] Subscript 1 refers to monatomic sodium vapor. Subscript 2 refers to diatomic sodium vapor. X_1 = mole fraction Na in equilibrium mixture. X_2 = mole fraction Na_2 in equilibrium mixture. W = molecular weight of mixture.

[2] F. J. Krieger, *A Table of Vibrational Contributions of a Harmonic Oscillator to Thermodynamic Functions* (Project Rand Ra-15088, Douglas Aircraft Company, 1948).

TABLE III. Physical constants.[a]

h	Planck's constant	6.623773×10^{-27} erg sec
c	Velocity of light	2.9979022×10^{10} cm/sec
R	Gas constant	$1.98719\ \frac{\text{cal}}{\text{g mole °K}}$
	or	
		$82.0790\ \frac{\text{cm}^3\ \text{atm}}{\text{g mole °K}}$
N_0	Avogadro's number	$6.025438\times10^{23}\ \frac{\text{molec.}}{\text{mole}}$
k	Boltzmann constant	$1.3802565\times10^{-6}\ \frac{\text{ergs}}{\text{deg}}$
$\frac{hc}{k}$		1.438675 cm deg
Sodium atomic weight (physical scale)		22.99618

[a] J. W. M. DuMond and E. R. Cohen, A least-squares adjustment of the atomic constants as of December, 1950—A report to the national research council committee on constants and conversion factors of physics; J. W. M. DuMond and E. R. Cohen, Phys. Rev. **82**, 555 (1951).

TABLE IV. Spectroscopic data for sodium atom.[a]

	Energy level, cm^{-1}	Degeneracy
$^2S_{\frac{1}{2}}$	0	2
$^2P_{\frac{1}{2}}$	16956.183	2
$^2P_{\frac{3}{2}}$	16973.379	4
$^2S_{\frac{1}{2}}$	25739.86	2
$^2D_{\frac{3}{2}}$	29172.855	6
$^2D_{\frac{5}{2}}$	29172.904	4
	:	:

[a] C. E. Moore, *Atomic Energy Levels* (U. S. Department of Commerce, Bureau of Standards, June 15, 1949), Vol. I, Circular 467, p. 89.

$(H^0-E_0^0/T)_{Na_2}$ by evaluating $(E_0^0)_{Na}$ and $(E_0^0)_{Na_2}$ as follows. For the heat of formation of monatomic sodium gas at 0°K, the Bureau of Standards[3] gives the following value:

$$Na_{(solid)} \rightleftharpoons Na_{gas}, \quad (\Delta E_0^0)_f = 26{,}050 \text{ cal/mole}.$$

Since, for

$$2Na_{(gas)} \rightleftharpoons Na_{2(gas)}, \quad \Delta E_0^0 = -16{,}836 \text{ cal/mole},$$

we obtain from these two thermal relationships the heat of formation of the diatomic sodium gas:

$$2Na_{(solid)} \rightleftharpoons Na_{2(gas)}, \quad (\Delta E_0^0)_f = 35{,}260 \text{ cal/mole}.$$

The zero point energy values for the monatomic and diatomic sodium gas are then,

$$(E_0^0)_{Na} = 26{,}050 \text{ cal/mole}$$
$$(E_0^0)_{Na_2} = 35{,}260 \text{ cal/mole}$$

based on zero for the heat of formation of crystalline sodium.

There is some doubt about the energy of dissociation of diatomic sodium vapor. Gordon, in an earlier work,[4] used the value $\Delta E_0^0 = 0.76$ ev $= 17{,}515$ cal/mole. In these calculations, Herzberg's value of $\Delta E_0^0 = 16{,}836$ cal/mole was selected. For further details and references on this point, the reader is referred to Herzberg.[5]

[3] *Selected Values of Chemical Thermodynamic Properties* (National Bureau of Standards, June 30, 1949), Series 1, Vol. 1, Table 92–1.

TABLE V. Spectroscopic constants for sodium molecules.[a, b]

	Te, cm^{-1}	ω_e, cm^{-1}	$\omega_e x_e$, cm^{-1}	$\omega_e y_e$, cm^{-1}	B_e, cm^{-1}	α_e, cm^{-1}
$1\,\Sigma_g+$	0	159.23	0.726	−0.0027	0.15471	0.00079
$1\,\Sigma_u+$	14680.4	117.6	0.38	···	0.1107	0.00054
$1\,\Pi_u$	20320.2	123.79	0.6303	−0.00936	0.12588	0.00094

[a] G. Herzberg, *Molecular Spectra and Molecular Structure I. Spectra of Diatomic Molecules* (D. Van Nostrand Company, Inc., New York, 1950), second edition, p. 554.

[b] $2Na_{(gas)} \rightleftharpoons Na_{2(gas)}$; $\Delta E_0^0 = -0.73$ ev $= -16.836\ \frac{\text{cal}}{\text{mole}}$.

[4] A. R. Gordon, J. Chem. Phys. **4**, 100 (1936).

[5] G. Herzberg, *Molecular Spectra and Molecular Structure I. Spectra of Diatomic Molecules* (D. Van Nostrand Company, Inc., New York, 1950), second edition, p. 554.

Substituted Methanes. IX.* Raman and Infrared Spectra, Assignments, Potential Constants, and Calculated Thermodynamic Properties for $CHClBr_2$ and $CDClBr_2$†

DONALD A. PONTARELLI,‡ ARNOLD G. MEISTER, FORREST F. CLEVELAND, AND FRED L. VOELZ,
Spectroscopy Laboratory, Department of Physics

AND

RICHARD B. BERNSTEIN AND ROBERT H. SHERMAN, *Department of Chemistry,*
Illinois Institute of Technology, Chicago 16, Illinois

(Received July 25, 1952)

Raman displacements, semiquantitative relative intensities, and quantitative depolarization factors for liquid chlorodibromomethane and deuterochlorodibromomethane, and infrared wave numbers and percent transmission curves for both the liquid and gaseous states in the region 400–4300 cm^{-1} were obtained and compared with previous data. A normal coordinate treatment (Wilson *FG* matrix method) was carried out, and a consistent set of potential constants for both molecules was determined, using a potential energy function containing all possible 2nd degree terms. Assignments were made for all observed bands. The heat content, free energy, entropy, and heat capacity at constant pressure were calculated for 12 temperatures from 100° to 1000°K.

RAMAN displacements and visual estimates of the relative intensities of the Raman lines for $CHClBr_2$ have been obtained previously.[1] Also, predictions (theoretical, not experimental) of the polarization state of the lines have been made[2,3] but no qualitative or quantitative experimental values have been reported. Infrared spectral data also have been reported[4–6] for $CHClBr_2$. However, no previous spectral data could be found for $CDClBr_2$, and no calculated or experimental thermodynamic properties for either molecule were found in the literature.

In this investigation, Raman and infrared spectral data were obtained for $CHClBr_2$ and $CDClBr_2$, normal coordinate treatments were carried out, and thermodynamic properties for the ideal gaseous state were calculated to a rigid rotator, harmonic oscillator approximation.

EXPERIMENTAL DETAILS

Preparation of the Samples

The $CHClBr_2$ was purified by distillation at reduced pressure in a small packed column. The purified material was distilled in vacuum into the Raman tube and into several ampoules for subsequent infrared studies. The $CDClBr_2$ was prepared by the exchange reaction of the protium compound with deuterium oxide in the presence of deuteroxide ion.[7] The isotopic mixture, consisting of approximately $\frac{2}{3}$ $CDClBr_2$, was dried and purified as above.

Spectroscopic Technique

Raman displacement spectrograms were obtained with a 2-prism spectrograph, constructed in this laboratory, having a dispersion of 162 cm^{-1}/mm (33A/mm) at 4500A. The spectrograms were taken on Eastman 103-J plates, with Hg 4358A as the exciting line. Depolarization spectrograms were obtained with a Hilger E-518 spectrograph having a dispersion of 307 cm^{-1}/mm (63A/mm) at 4500A. The relative intensities[8] and depolarization factors[9] were determined by previously described methods, using a Gaertner microdensitometer. Infrared data were secured from records obtained with a Beckman IR-2 recording spectrophotometer equipped with KBr optics, and a Perkin-Elmer double-beam infrared spectrometer Model 21 having NaCl optics. Records of the atmospheric absorption were taken immediately preceding the sample record in order to make possible the elimination of spurious bands.

RESULTS

Chlorodibromomethane

The present and previous Raman and infrared spectral data for $CHClBr_2$ are summarized in Tables I, II, and III. The present Raman displacements are in good agreement with the only previously reported values of

* For previous papers of this series, see J. Chem. Phys. **18**, 346, 1073, 1076, 1081 (1950); **19**, 119, 784, 1561 (1951); **20**, 454 (1952).

† Presented in part at the Chicago meeting of the American Physical Society, November, 1950; see abstract in Phys. Rev. **81**, 301 (1951); and at the Columbus meeting of the Division of Chemical Physics of the American Physical Society, June 11–13, 1951.

‡ Based upon investigations carried out in partial fulfillment of the requirements for the degree of Master of Science, at Illinois Institute of Technology. Present address: Armour Research Foundation of Illinois Institute of Technology, Chicago 16, Illinois.

[1] G. Glockler and G. R. Leader, J. Chem. Phys. **7**, 553 (1939).
[2] G. Glockler and G. R. Leader, J. Chem. Phys. **8**, 699 (1940).
[3] M. L. Delwaulle and F. Francois, J. phys. et radium **7**, 15 (1946).
[4] G. Emschwiller and J. Lecomte, J. phys. et radium **8**, 130 (1937).
[5] E. K. Plyler, J. Chem. Phys. **17**, 218 (1949).
[6] E. K. Plyler and W. S. Benedict, J. Research Natl. Bur. Standards **47**, 202 (1951).
[7] R. H. Sherman and R. B. Bernstein, J. Am. Chem. Soc. **73**, 1376 (1951).
[8] F. F. Cleveland, J. Chem. Phys. **11**, 1, 227 (1943).
[9] F. F. Cleveland, J. Chem. Phys. **13**, 101 (1945).

TABLE I. Raman spectral data for liquid chlorodibromomethane ($CHClBr_2$).

Raman displacement (cm^{-1})			Relative intensity	Depolarization factor	
Present results	Glockler, Leader	Probable values	Present results	Present results	Polarization state
168	168.3	168	71	0.59	Polarized
201	201.1	201	33	0.83	Depolarized
279	279.4	279	100	0.21	Polarized
330	...	330	very weak	...	...
569	568.9	569	75	0.14	Polarized
659	658.7	659	11	0.86	Depolarized
729	...	729	very weak	...	...
750	749.5	750	3	(0.89)[a]	Polarized[b]
1111	...	1111	very weak	...	...
1146	1145.5	1146	2	0.85	Depolarized
1190	1193.8	1192	2	0.66	Polarized
1219	...	1219	very weak	...	...
1309	...	1309	0.5	...	...
1405	...	1405	very weak	...	...
2281	...	2281	very weak	...	...
2866	...	2866	very weak	...	...
3020	3022.6	3021	13	0.29	Polarized

[a] This value is somewhat uncertain.
[b] Despite the high observed value of the depolarization factor, this line is interpreted as a polarized line for reasons given in the text.

Glockler and Leader.[1,2] The present relative intensities are more reliable than the previous visual estimates. The theoretical predictions of GL[2] and of Delwaulle and Francois[3] agree with the polarization states deduced from the present experimental results, except for the 659, 750, 1146, and 1192 cm^{-1} lines. For the 659, 1146, and 1192 lines, the present results are in agreement with DF, but not with GL. For the 750 line, the present results indicate that it is a depolarized line, in agreement with the prediction of GL. However, the normal coordinate treatment shows that this line must be polarized, in agreement with the prediction of DF. The cause of this discrepancy probably lies partly in the experimental uncertainty in the depolarization factor, for this is a weak and diffuse line; but, besides this, the summation band $\nu_4+\nu_9$ (which should be depolarized) falls in this region and probably contributes to the observed depolarization factor, especially since long exposures were required to obtain this line.

Agreement between the present Raman displacements

TABLE II. Infrared spectral data for chlorodibromomethane ($CHClBr_2$).[a]

Liquid							Gas	
Emschwiller, Lecomte	Plyler, Benedict		Present results		Probable values		Present results	
cm^{-1}	cm^{-1}	Int.	cm^{-1}	Int.	cm^{-1}	Int.	cm^{-1}	Int.
...	[b]278	w	...	...	278	w	...	...
...	383	w	...	...	383	w	...	...
...	460	w	...	...	460	w	...	...
...	492	w	...	...	492	w	...	...
568	570	s	568	s	569	s	576	s
655	657	vs	659	vs	658	vs	669	s
737	733	m	...	...	733	m	...	...
	746	s	745	vs	746	s	756	s
...	796	m	...	...	796	m	...	...
...	821	w	839	vw	830	vw	...	...
856	844	w	864	vs	855	m	...	...
938	937	w	934	w	936	w	...	...
1010	1004	w	999	vw	100[c]	vw	...	...
...	1029	vw	...	...	1029	vw	...	...
...	1053	w	1048	vw	1050	vw	...	...
1169	1144	vs	1148	s	1146	s	1149	s
	1189	s	1193	s	1191	s	1191	s
...	1218	w	...	...	1218	w	...	...
...	1309	w	1307	w	1308	w	...	...
...	1340	vw	1342	w	1341	w	...	...
...	1410	w	1410	w	1410	w	...	...
...	1473	w	1468	m	1470	m	...	...
...	1488	w	...	...	1488	w	...	...
...	[c](1592)	w	1599	vw	1599	vw	...	...
...	2278	m	2285	m	2281	m	...	...
...	...	...	2369	w	2369	w	...	...
...	3034	s	3021	s	3021	s	...	...
...	...	...	(3556)	vw	(3556)	vw	...	...
...	4203	m	...	...	4203	m	...	...
...	4257	w	...	...	4257	w	...	...

[a] cm^{-1} = wave number in cm^{-1} at point of maximum absorption; Int. = intensity (w = weak, m = medium, s = strong, v = very).
[b] The infrared spectrum has not been investigated below 278 cm^{-1}.
[c] Uncertain values are enclosed in parentheses.

TABLE III. Probable values for the Raman and infrared spectral data, calculated wave numbers, and assignments for liquid $CHClBr_2$.[a]

Raman			Infrared		Calculated wave number	Assignment	Type
RD	Int.	PS	cm^{-1}	Int.			
168	71	P	[b]...	...	**168**	ν_6	A'
201	33	D	...	...	**200**	ν_9	A''
279	100	P	278	w	**273**	ν_5	A'
330	vw	...	...	...	*336*	$2\nu_6$	A'
...	...	...	383	w	*380*	$\nu_8-\nu_5$	A''
...	...	...	460	w	*458*	$\nu_8-\nu_9$	A'
...	...	...	492	w	*491*	$\nu_8-\nu_6$	A''
569	75	P	569	s	**576**	ν_4	A'
659	11	D	658	vs	659	ν_8	A''
729	vw	...	733	m	*737*	$\nu_4+\nu_6$	A'
750	3	(P)	746	s	**749**	ν_3	A'
...	...	...	796	m	*770*	$\nu_4+\nu_9$	A''
					803	[c]$(\nu_3+\nu_5)-\nu_9$	A''
...	...	...	830	vw	*848*	$\nu_4+\nu_5$	A'
...	...	...	855	m	*860*	$\nu_8+\nu_9$	A'
...	...	...	936	w	*945*	$\nu_7-\nu_9$	A'
...	...	...	1004	vw	*1029*	$\nu_3+\nu_5$	A'
...	...	...	1029	vw	*1024*	$\nu_2-\nu_6$	A'
...	...	...	1050	vw	*1059*	$2\nu_9+\nu_8$	A''
1111	vw	...	...	...	*1138*	$2\nu_4$	A'
1146	2	D	1146	s	**1151**	ν_7	A''
1192	2	P	1191	s	**1191**	ν_2	A'
1219	vw	...	1218	w	*1228*	$\nu_4+\nu_6$	A''
					1314	$\nu_6+\nu_7$	A''
1309	0.5	...	1308	w	*1318*	$2\nu_8$	A'
					1319	$\nu_3+\nu_4$	A'
...	...	...	1341	w	*1347*	$\nu_7+\nu_9$	A'
1405	vw	...	1410	w	*1409*	$\nu_3+\nu_8$	A''
...	...	...	1470	m	*1471*	$\nu_2+\nu_5$	A'
...	...	...	1488	w	*1500*	$2\nu_3$	A'
...	...	...	1599	vw	*1605*	$\nu_3+(\nu_8+\nu_9)$	A'
2281	vw	...	2281	m	*2292*	$2\nu_7$	A'
...	...	...	2369	w	*2384*	$2\nu_2$	A'
2866	vw	...	...	...	*2853*	$\nu_1-\nu_6$	A'
3021	13	P	3021	s	**3023**	ν_1	A'
...	...	...	(3556)	vw	*3590*	$\nu_1+\nu_4$	A'
...	...	...	4203	m	*4213*	$\nu_1+\nu_2$	A'
...	...	...	4257	w	*4306*	$(\nu_1+\nu_4)+\nu_3$	A'

[a] RD = Raman displacement in cm^{-1}; PS = polarization state (P = polarized, D = depolarized); other symbols have the same meaning as in Table II.
[b] The infrared spectrum has not been investigated below 278 cm^{-1}.
[c] In the ternary combinations, the *observed* value of the binary combination frequency, which is enclosed by the parentheses, was used in obtaining the calculated value.

TABLE IV. Raman and infrared spectral data, calculated wave numbers, and assignments for deuterochlorodibromomethane ($CDClBr_2$).[a]

Raman Liquid				Infrared Liquid		Infrared Gas		Calculated wave number	Assignment	Type
RD	Int.	D	PS	cm^{-1}	Int.	cm^{-1}	Int.			
168	68	0.59	P	[b]...	...	...	...	**168**	ν_6	A'
201	30	0.83	D	...	...	...	...	**200**	ν_9	A''
279	100	0.21	P	...	...	...	...	**272**	ν_5	A'
545	71	0.07	P	545	s	...	...	**547**	ν_4	A'
635	8	0.81	D	635	vs	648	s	**636**	ν_8	A''
725	2	...	P[c]	725	vs	...	...	**725**	ν_3	A'
...	...	...	...	797	w	...	...	*803*	$\nu_6+\nu_8$	A''
853	2	0.82	D	852	vs	858	s	**849**	ν_7	A''
888	2	0.55	P	886	vs	891	s	**888**	ν_2	A'
...	...	...	...	1003	vw	...	...	*1021*	$\nu_6+\nu_7$	A''
...	...	...	...	1048	w	...	...	*1054*	$\nu_7+\nu_9$	A'
...	...	...	...	1081	w	...	...	*1089*	$\nu_2+\nu_9$	A''
								1090	$2\nu_4$	A'
...	...	...	...	1258	vw	...	...	*1270*	$2\nu_8$	A'
								1270	$\nu_3+\nu_4$	A'
1357	vw	...	...	1353	vw	...	...	*1360*	$\nu_3+\nu_8$	A''
1441	vw	...	...	1428	w	...	...	*1433*	$\nu_2+\nu_4$	A'
								1450	$2\nu_3$	A'
1482	vw	...	...	...	...	...	...	*1488*	$\nu_7+\nu_8$	A'
...	...	...	...	1603	vw	...	...	*1613*	$\nu_3+\nu_3$	A'
1697	vw	...	...	1690	m	...	...	*1706*	$2\nu_7$	A'
...	...	...	...	1739	vw	...	...	*1741*	$\nu_2+\nu_7$	A''
...	...	...	...	1764	w	...	...	*1776*	$2\nu_2$	A'
2252	8	0.26	P	2248	m	...	...	**2253**	ν_1	A'
...	...	...	...	2779	vvw	...	...	*2797*	$\nu_1+\nu_4$	A'
...	...	...	...	(3142)	vvw	...	...	*3140*	$\nu_1+\nu_2$	A'

[a] D = depolarization factor; other symbols have same meaning as in Tables II and III.
[b] The infrared spectrum has not been investigated below 400 cm^{-1}.
[c] Normal coordinate treatment indicates that this line should be polarized.

and infrared wave numbers for the liquid is within experimental error, except for the 750 cm^{-1} band for which the infrared value is 5 cm^{-1} smaller.

Deuterochlorodibromomethane

The present Raman and infrared spectral data for $CDClBr_2$ (obtained in the presence of some $CHClBr_2$) are listed in Table IV. The 3 lowest bands, corresponding to the C—Br symmetrical and antisymmetrical deformation and the C—Cl symmetrical deformation frequencies, were unaffected by replacing H by D, with the dispersion used in the present work. However, for the other 6 fundamentals, in which the H and D atoms play a more active part, the wave numbers for the D isotope are lower. As expected, the relative intensities are similar for the 2 compounds. Also, corresponding displacements in the Raman spectra of the 2 compounds have similar polarization states. The depolarization factor for the 725 cm^{-1} line could not be obtained because of its low intensity and its proximity to the 750 cm^{-1} band of $CHClBr_2$. Because of the presence of both $CHClBr_2$ and $CDClBr_2$ in the sample, and the consequent masking of the $CDClBr_2$ bands by those of the $CHClBr_2$, only 3 bands were observed in the infrared for the gaseous state. It will be noticed that the wave numbers for the gas in both compounds are higher than the wave numbers for the liquid, the average difference being 8 cm^{-1} greater in each case.

The infrared percent transmission curves are shown in Figs. 1, 2, and 3.

SYMMETRY, SELECTION RULES, AND ASSIGNMENTS

The $CHClBr_2$ and $CDClBr_2$ molecules belong to the C_{1h} point group and each has 9 normal vibrations: 6 type A', symmetric and 3 type A'', antisymmetric with respect to the only plane of symmetry. All fundamentals, overtones, and combinations are allowed in both the Raman and infrared spectrum. The A' lines should be polarized, the A'' lines depolarized.

The assignments shown in Tables III and IV were made after consideration of the selection rules and the observed depolarization factors. Only binary combinations and 1st overtones were used, except for 3 weak bands observed only by Plyler and Benedict.[6]

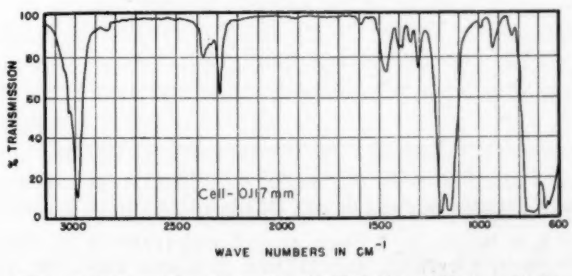

FIG. 1. Infrared bands for liquid $CHClBr_2$ (NaCl optics).

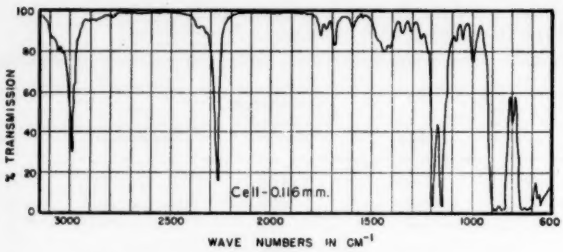

FIG. 2. Infrared bands for liquid $CHClBr_2$+$CDClBr_2$ (NaCl optics).

In Table V are given the probable values for the fundamentals of $CHClBr_2$ and $CDClBr_2$. These were determined by critical examination of both the present and previous spectral data (Tables I–IV).

NORMAL COORDINATE TREATMENT

As a test of the assignments and of the transferability of potential (force) constants, a normal coordinate treatment was carried out for both molecules, using the Wilson *FG* matrix method[10] and the most general quadratic potential function. The potential energy constants and equilibrium coordinates are expressed in the descriptive notation introduced in VIII.[11] The symbols used for the equilibrium values of the bond distances and interbond angles for $CHClBr_2$ are:

$$b_1=C-Br_1, \quad b_2=C-Br_2, \quad c=C-Cl,$$
$$h=C-H, \quad b_1c=Br_1-C-Cl, \quad b_2c=Br_2-C-Cl,$$
$$b_1h=Br_1-C-H, \quad b_2h=Br_2-C-H, \quad ch=Cl-C-H,$$

and

$$b_1b_2=Br_1-C-Br_2.$$

For $CDClBr_2$, the h and H are replaced throughout by d and D, respectively.

From the internal coordinates the following orthonormal symmetry coordinates were formed:

for the A' vibrations,

$$R_1=\Delta h,$$
$$R_2=6^{-\frac{1}{2}}(\Delta b_1+\Delta b_2-2\Delta c),$$
$$R_3=6^{-\frac{1}{2}}(\Delta b_1h+\Delta b_2h-2\Delta ch),$$
$$R_4=3^{-\frac{1}{2}}(\Delta b_1+\Delta b_2+\Delta c),$$
$$R_5=6^{-\frac{1}{2}}(\Delta b_1h+\Delta b_2h+\Delta ch-\Delta b_1c-\Delta b_2c-\Delta b_1b_2),$$
$$R_6=6^{-\frac{1}{2}}(\Delta b_1c+\Delta b_2c-2\Delta b_1b_2),$$

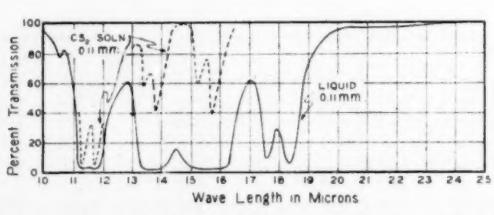

FIG. 3. Infrared bands for liquid $CHClBr_2$+$CDClBr_2$ (KBr optics).

[10] E. B. Wilson, Jr., J. Chem. Phys. **7**, 1047 (1939); **9**, 76 (1941).
[11] Davis, Cleveland, and Meister, J. Chem. Phys. **20**, 454 (1952).

and for the redundant coordinate,

$$R'=6^{-\frac{1}{2}}(\Delta b_1h+\Delta b_2h+\Delta b_1c+\Delta b_2c+\Delta b_1b_2+\Delta ch)$$

for the A'' vibrations,

$$R_7=2^{-\frac{1}{2}}(\Delta b_1h-\Delta b_2h),$$
$$R_8=2^{-\frac{1}{2}}(\Delta b_1-\Delta b_2), \text{ and}$$
$$R_9=2^{-\frac{1}{2}}(\Delta b_1c-\Delta b_2c).$$

The numbering of these coordinates corresponds to the numbering of the fundamentals in Table III.

From the f matrix (Table VI) and the U matrix, formed from the coefficients in the symmetry coordinates, one gets the following F matrix elements:

TABLE V. Observed wave numbers and degeneracies for the fundamentals of $CHClBr_2$ and $CDClBr_2$.

Designation	Degeneracy	Type	Wave number in cm⁻¹ $CHClBr_2$ Liquid	$CHClBr_2$ Gas	$CDClBr_2$ Liquid	$CDClBr_2$ Gas
ν_1	1	A'	3021		2252	
ν_2	1	A'	1192	1191	888	891
ν_3	1	A'	750	756	725	
ν_4	1	A'	569	576	545	
ν_5	1	A'	279		279	
ν_6	1	A'	168		168	
ν_7	1	A''	1146	1149	853	858
ν_8	1	A''	659	669	635	648
ν_9	1	A''	201		201	

for the A' vibrations,

$$F_{11}=f_h,$$
$$F_{12}=6^{-\frac{1}{2}}(2f_b{}^h-2f_c{}^h),$$
$$F_{13}=6^{-\frac{1}{2}}(2f_h{}^{bh}-2f_h{}^{ch}),$$
$$F_{14}=3^{-\frac{1}{2}}(f_c{}^h+2f_b{}^h),$$
$$F_{15}=6^{-\frac{1}{2}}(f_h{}^{ch}+2f_h{}^{bh}-f_h{}^{bb}-2f_h{}^{bc}),$$
$$F_{16}=6^{-\frac{1}{2}}(2f_h{}^{bc}-2f_h{}^{bb}),$$
$$F_{22}=(f_b+f_b{}^b-4f_b{}^c+2f_c)/3,$$
$$F_{23}=(f_b{}^{bh}+f_b{}^{b'h}-2f_b{}^{ch}-2f_c{}^{bh}+2f_c{}^{ch})/3,$$
$$F_{24}=2^{\frac{1}{2}}(f_b+f_b{}^b-f_b{}^c-f_c)/3,$$
$$F_{25}=(f_b{}^{bh}+f_b{}^{b'h}+f_b{}^{ch}-f_b{}^{bc}-f_b{}^{b'c}-f_b{}^{bb}-2f_c{}^{bh}+2f_c{}^{bc}-f_c{}^{ch}+f_c{}^{bb})/3,$$
$$F_{26}=(f_b{}^{bc}+f_b{}^{b'c}-2f_b{}^{bb}-2f_c{}^{bc}+2f_c{}^{bb})/3,$$
$$F_{33}=(f_{bh}+f_{bh}{}^{b'h}-4f_{bh}{}^{ch}+2f_{ch})/3,$$
$$F_{34}=2^{\frac{1}{2}}(f_b{}^{bh}+f_b{}^{b'h}-2f_b{}^{ch}+f_c{}^{bh}-f_c{}^{ch})/3,$$
$$F_{35}=(f_{bh}+f_{bh}{}^{bh'}-f_{bh}{}^{ch}-f_{bc}{}^{bh}-f_{bc}{}^{b'h}-f_{bb}{}^{bh}+2f_{bc}{}^{ch}-f_{ch}+f_{bb}{}^{ch})/3,$$
$$F_{36}=(f_{bc}{}^{bh}+f_{bc}{}^{b'h}-2f_{bb}{}^{bh}+2f_{bb}{}^{ch}-2f_{bc}{}^{ch})/3,$$
$$F_{44}=(2f_b+2f_b{}^b+4f_b{}^c+f_c)/3,$$
$$F_{45}=(2f_b{}^{bh}+2f_b{}^{b'h}+2f_c{}^{bh}+2f_b{}^{ch}-2f_b{}^{bc}-2f_b{}^{b'c}-2f_b{}^{bb}-2f_c{}^{bc}+f_c{}^{ch}-f_c{}^{bb})2^{\frac{1}{2}}/6,$$
$$F_{46}=(f_b{}^{bc}+f_b{}^{b'c}-2f_b{}^{bb}+f_c{}^{bc}-f_c{}^{bb})2^{\frac{1}{2}}/3,$$
$$F_{55}=(2f_{bh}+2f_{bc}+f_{ch}+f_{bb}+4f_{bh}{}^{ch}-4f_{bc}{}^{bh}-4f_{bc}{}^{ch}-4f_{bc}{}^{b'h}-4f_{bb}{}^{bh}-2f_{bb}{}^{ch}+2f_{bc}{}^{b'c}+4f_{bb}{}^{bc})/6,$$

$F_{56}=(f_{bc}{}^{bh}+f_{bc}{}^{b'h}+f_{bc}{}^{ch}-f_{bc}{}^{b'c}-f_{bc}+f_{bb}{}^{bc}-2f_{bb}{}^{bh}$
$-f_{bb}{}^{ch}+f_{bb})/3$, and
$F_{66}=(f_{bc}+f_{bc}{}^{b'c}-4f_{bb}{}^{bc}+2f_{bb})/3$;

and for the A'' vibrations,

$F_{77}=f_{bh}-f_{bh}{}^{b'h}$,
$F_{78}=f_b{}^{bh}-f_b{}^{b'h}$,
$F_{79}=f_{bc}{}^{bh}-f_{bc}{}^{b'h}$,
$F_{88}=f_b-f_b{}^b$,
$F_{89}=f_b{}^{bc}-f_b{}^{b'c}$, and
$F_{99}=f_{bc}-f_{bc}{}^{b'c}$.

The G matrix elements, obtained by use of the tables of Decius,[12] are as follows:

for the A' vibrations

$G_{11}=\mu_C+\mu_H$,
$G_{12}=0$,
$G_{13}=3^{\frac{1}{2}}(c^{-1}-b^{-1})4\mu_C/9$,
$G_{14}=-3^{-\frac{1}{2}}\mu_C$,
$G_{15}=-3^{\frac{1}{2}}(2b^{-1}+c^{-1})4\mu_C/9$,
$G_{16}=3^{\frac{1}{2}}(c^{-1}-b^{-1})2\mu_C/9$,
$G_{22}=(4\mu_C+\mu_{Br}+2\mu_{Cl})/3$,
$G_{23}=-2^{\frac{1}{2}}(b^{-1}+2c^{-1}+9h^{-1})\mu_C/9$,
$G_{24}=2^{\frac{1}{2}}(\mu_{Br}-\mu_{Cl})/3$,
$G_{25}=2^{\frac{1}{2}}(c^{-1}-b^{-1})?\mu_C/9$,
$G_{26}=2^{\frac{1}{2}}(13b^{-1}-c^{-1})\mu_C/9$,
$G_{33}=b^{-2}\mu_{Br}/3+2c^{-2}\mu_{Cl}/3+3h^{-2}\mu_H/2+(11b^{-2}+12c^{-2}$
$+27h^{-2}-20b^{-1}c^{-1}+6b^{-1}h^{-1}+12c^{-1}h^{-1})\mu_C/18$,
$G_{34}=4(b^{-1}-c^{-1})\mu_C/9$,
$G_{35}=2b^{-2}\mu_{Br}/3-2c^{-2}\mu_{Cl}/3+(11b^{-2}-6c^{-2}-5c^{-1}b^{-1}$
$+3b^{-1}h^{-1}-3h^{-1}c^{-1})\mu_C/9$,
$G_{36}=b^{-2}\mu_{Br}/6+c^{-2}\mu_{Cl}/3+(b^{-2}+6c^{-2}-19b^{-1}c^{-1}$
$-39b^{-1}h^{-1}+3c^{-1}h^{-1})\mu_C/18$,
$G_{44}=(\mu_C+\mu_{Cl}+2\mu_{Br})/3$,
$G_{45}=4(2b^{-1}+c^{-1})\mu_C/9$,

TABLE VI. The f matrix.[a]

	b_1	b_2	c	h	b_1c	b_2c	b_1h	b_2h	ch	b_1b_2
b_1	f_b	$f_b{}^b$	$f_b{}^c$	$f_b{}^h$	$f_b{}^{bc}$	$f_b{}^{b'c}$	$f_b{}^{bh}$	$f_b{}^{b'h}$	$f_b{}^{ch}$	$f_b{}^{bb}$
b_2		f_b	$f_b{}^c$	$f_b{}^h$	$f_b{}^{b'c}$	$f_b{}^{bc}$	$f_b{}^{b'h}$	$f_b{}^{bh}$	$f_b{}^{ch}$	$f_b{}^{bb}$
c			f_c	$f_c{}^h$	$f_c{}^{bc}$	$f_c{}^{bc}$	$f_c{}^{bh}$	$f_c{}^{bh}$	$f_c{}^{ch}$	$f_c{}^{bb}$
h				f_h	$f_h{}^{bc}$	$f_h{}^{bc}$	$f_h{}^{bh}$	$f_h{}^{bh}$	$f_h{}^{ch}$	$f_h{}^{bb}$
b_1c					f_{bc}	$f_{bc}{}^{b'c}$	$f_{bc}{}^{bh}$	$f_{bc}{}^{b'h}$	$f_{bc}{}^{ch}$	$f_{bb}{}^{bc}$
b_2c						f_{bc}	$f_{bc}{}^{b'h}$	$f_{bc}{}^{bh}$	$f_{bc}{}^{ch}$	$f_{bb}{}^{bc}$
b_1h							f_{bh}	$f_{bh}{}^{b'h}$	$f_{bh}{}^{ch}$	$f_{bb}{}^{bh}$
b_2h								f_{bh}	$f_{bh}{}^{ch}$	$f_{bb}{}^{bh}$
ch									f_{ch}	$f_{bb}{}^{ch}$
b_1b_2										f_{bb}

[a] Since the matrix is symmetric ($f_{ij}=f_{ji}$), the elements below the diagonal may easily be determined. The primed and unprimed symbols refer to different bonds of the same type.

[12] J. C. Decius, J. Chem. Phys. **16**, 1025 (1948).

TABLE VII. Potential constants for CHClBr$_2$ and CDClBr$_2$.[a]

Type	CHClBr$_2$	CBr$_2$Cl$_2$	CBr$_3$H	CCl$_3$H	CCl$_3$Br
f_b	2.8704[b]	2.7530	2.8976	···	2.8976
f_c	3.4204	3.3713	···	3.4580	3.4580
f_h	4.8642	···	4.8828	4.8002	···
$f_b{}^b$	0.27187	0.21296	0.29910	···	···
$f_b{}^c$	0.32037	0.32465	···	···	0.37782
$f_b{}^h$	0.058900	···	0.05890	···	···
$f_c{}^h$	0.088000	···	···	0.088000	···
$f_b{}^{bh}$	0.25970	···	0.25970	···	···
$f_b{}^{b'h}$	−0.15200	···	−0.15200	···	···
$f_b{}^{ch}$	−0.16400	···	···	···	···
$f_b{}^{bc}$	0.36345	0.35007	···	···	···
$f_b{}^{b'c}$	−0.18178	−0.17178	···	···	···
$f_b{}^{bb}$	0.30000	0.34088	0.33734	···	···
$f_c{}^{bc}$	0.30000	0.36022	···	···	0.42630
$f_c{}^{ch}$	0.18601	···	···	0.18601	···
$f_c{}^{bb}$	−0.22500	−0.20547	···	···	···
$f_c{}^{bh}$	−0.15200	···	···	···	···
f_{bb}	1.2458	1.2391	1.2136	···	···
f_{bc}	1.1798	1.1383	···	···	1.3038
f_{bh}	0.59044	···	0.59044	···	···
f_{ch}	0.82650	···	···	0.92126	···
$f_{bb}{}^{bc}$	0.23083	0.12944	···	···	···
$f_{bb}{}^{bh}$	0.03000	···	0.077810	···	···
$f_{bb}{}^{ch}$	0.01000	···	···	···	···
$f_{bc}{}^{bh}$	0.077810	···	···	···	···
$f_{bc}{}^{ch}$	0.01000	···	···	···	···
$f_{bc}{}^{b'h}$	0	···	···	···	···
$f_{bc}{}^{b'c}$	0.15793	0.087897	···	···	···
$f_{bh}{}^{ch}$	0.08350	···	···	···	···
$f_{bh}{}^{b'h}$	−0.00798	···	−0.00500	···	···
$f_h{}^{ch}-f_h{}^{bc}$	−0.52412	···	···	···	···
$f_h{}^{bh}-f_h{}^{bb}$	−0.52412	···	···	···	···

[a] Bond stretching and bond interaction constants are in units of md/A; angle-bond interaction constants are in md/rad; angle, and angle interaction, constants are in md A/rad^2.
[b] This number of significant figures is not really justified but is necessary to give the best reproduction of the observed wave numbers and to secure internal consistency in the calculations.

$G_{46}=2(b^{-1}-c^{-1})\mu_C/9$,
$G_{55}=4b^{-2}\mu_{Br}/3+2c^{-2}\mu_{Cl}/3+(11b^{-2}+3c^{-2}$
$+10b^{-1}c^{-1})2\mu_C/9$,
$G_{56}=b^{-2}\mu_{Br}/3-c^{-2}\mu_{Cl}/3-(3c^{-2}-b^{-2}-2b^{-1}c^{-1})\mu_C/9$,
$G_{66}=7b^{-2}\mu_{Br}/3+c^{-2}\mu_{Cl}/6+(59b^{-2}+3c^{-2}$
$-14b^{-1}c^{-1})\mu_C/18$;

and for the A'' vibrations,

$G_{77}=b^{-2}\mu_{Br}+3h^{-2}\mu_H/2+(b^{-1}+3h^{-1})^2\mu_C/6$,
$G_{78}=-2^{\frac{1}{2}}(b^{-1}+3h^{-1})\mu_C/3$,
$G_{79}=-b^{-2}\mu_{Br}/2+(b^{-1}+3c^{-1})(b^{-1}+3h^{-1})\mu_C/6$,
$G_{88}=4\mu_C/3+\mu_{Br}$,
$G_{89}=-2^{\frac{1}{2}}(b^{-1}+3c^{-1})\mu_C/3$, and
$G_{99}=b^{-2}\mu_{Br}+3c^{-2}\mu_{Cl}/2+(b^{-1}+3c^{-1})^2\mu_C/6$.

Here μ_C, μ_{Br}, μ_{Cl}, and μ_H are, respectively, the reciprocals of the masses of the C, Br, Cl, and H atoms, while $b(=1.91\text{A})$, $c(=1.76\text{A})$, and $h(=1.093\text{A})$ are the equilibrium values for the C−Br, C−Cl, and C−H bond lengths.

In order to get approximate potential constants, values were transferred from CCl_3X,[13] CBr_3X,[14] and

[13] Zietlow, Cleveland, and Meister, J. Chem. Phys. **18**, 1076 (1950).
[14] Meister, Rosser, and Cleveland, J. Chem. Phys. **18**, 346 (1950).

TABLE VIII. Heat content, free energy, entropy, and heat capacity of $CHClBr_2$ for the ideal gaseous state at 1 atmos pressure.[a]

T	$(H^0-E_0^0)/T$	$-(F^0-E_0^0)/T$	S^0	C_p^0
100	8.91	54.72	63.63	10.88
200	10.74	61.47	72.21	14.08
273.16	11.89	65.00	76.89	15.96
298.16	12.26	66.05	78.31	16.53
300	12.28	66.13	78.41	16.57
400	13.60	69.85	83.45	18.46
500	14.72	73.01	87.73	19.82
600	15.66	75.78	91.43	20.82
700	16.45	78.27	94.72	21.57
800	17.13	80.49	97.62	22.16
900	17.72	82.54	100.26	22.64
1000	18.23	84.44	102.67	23.03

[a] T is in °K and the other quantities are in cal deg^{-1} mole^{-1}.

TABLE IX. Heat content, free energy, entropy, and heat capacity of $CDClBr_2$ for the ideal gaseous state at 1 atmos pressure.[a]

T	$(H^0-E_0^0)/T$	$-(F^0-E_0^0)/T$	S^0	C_p^0
100	8.91	54.75	63.67	10.90
200	10.82	61.53	72.35	14.46
273.16	12.10	65.10	77.20	16.67
298.16	12.51	66.17	78.69	17.32
300	12.54	66.25	78.79	17.37
400	14.02	70.06	84.08	19.40
500	15.24	73.33	88.57	20.77
600	16.25	76.20	92.45	21.74
700	17.08	78.79	95.87	22.45
800	17.79	81.10	98.89	23.00
900	18.40	83.23	101.62	23.44
1000	18.92	85.20	104.11	23.78

[a] T is in °K and the other quantities are in cal deg^{-1} mole^{-1}.

CBr_2Cl_2.[11] After several modifications, the resulting potential constants yielded calculated fundamentals that were, in most cases, well within 2 percent of the observed values for the liquid. These constants are given in Table VII and, for comparison, values of corresponding constants determined previously for CBr_2Cl_2,[11] $CBrCl_3$,[13] CCl_3H,[13] and CBr_3H[14] also are given.

Since a large number of potential constants had to be determined for which no previous values were available the simplifying assumption was made that

$$f_h^{bh}=f_h^{ch}, \quad \text{and} \quad f_h^{bc}=f_h^{bb}.$$

Also, these constants had to be given as the linear combinations $f_h^{ch}-f_h^{bc}$ and $f_h^{bh}-f_h^{bb}$ because each combination occurred only once so that separate values of the constants could not be found.

THERMODYNAMIC PROPERTIES

The heat content, free energy, entropy, and heat capacity at constant pressure were calculated for 12 temperatures from 100° to 1000°K, using the wave numbers and degeneracies given in Table V. Values for the gaseous state were used when possible, a rigid rotator, harmonic oscillator model was assumed, and the values were calculated for the ideal gaseous state at 1 atmos pressure. The product of the principal moments of inertia was determined by the Hirschfelder[15] formulas, using tetrahedral angles and the previously given values of the internuclear distances. The values obtained were: for $CHClBr_2$,

$$I_AI_BI_C=45.98\cdot10^6 \text{ awu.}^3\text{A}^6,$$

and for $CDClBr_2$,

$$I_AI_BI_C=47.01\cdot10^6 \text{ awu.}^3\text{A}^6.$$

The symmetry number is 1. Birge's values[16] of the physical constants were used throughout.

The values obtained for the thermodynamic properties are given in Tables VIII and IX.

ACKNOWLEDGMENTS

The Hilger E-518 spectrograph used for the depolarization spectrograms was obtained in part with a grant from the American Academy of Arts and Sciences, and the work was further aided by a later grant from this society. The optical parts of the 2-prism spectrograph used for the Raman displacement spectrograms were secured with a grant from the Society of the Sigma Xi. The Perkin-Elmer Model 21 Infrared Spectrophotometer was made available through the auspicies of the Office of Naval Research. The work was supported in part by the Office of Ordnance Research (contract DA-11-022-ORD-464) and by the U. S. Atomic Energy Commission. The D_2O was obtained through the courtesy of the U. S. Atomic Energy Commission. The authors are grateful for this assistance.

[15] J. O. Hirschfelder, J. Chem. Phys. **8**, 431 (1940).

[16] R. T. Birge, Revs. Modern Phys. **13**, 233 (1941).

The Molecular Structure of Arsine*

HARALD H. NIELSEN
Department of Physics and Astronomy, The Ohio State University, Columbus, Ohio
(Received August 1, 1952)

The method discussed by Nielsen for determining the rotational term values for the vibration states ν_3 and ν_4 has been applied to the spectrum of AsH_3 and by this means the Coriolis factor $\zeta_4^{(z)}$ has been determined. The value of $\zeta_2^{(z)}$ was known from an earlier work as was the value $B^{(xx)}$. This permits the evaluation of $B^{(zz)}$ when use is made of the zeta sum rule for pyramidal XY_3 molecules, i.e., $\zeta_2^{(z)}+\zeta_4^{(z)}=(-1+(B^{(xx)}/2B^{(zz)})$. These constants lead to values for the AsH distance $r_0=1.523$A and for the H−As−H angle $\alpha=91°34'$.

I. INTRODUCTION

THE high frequency fundamental bands ν_1, in the spectra of AsH_3 and AsD_3, have been studied and analyzed,[1] and from this analysis values for the moments of inertia I_{xx} have been arrived at for the two isotopic molecules. These, in turn, are sufficient to fix the size and shape of the molecule. The values obtained for the H−As−H angle α and the As−H distance r_0 are the following: $\alpha=91°38'$ and $r_0=1.522$A.[2] These values are in reasonably good agreement with the values obtained from microwave spectra.[3] It has been pointed out by Nielsen[4] that the value of α depends very critically upon the accuracy with which the moments of inertia I_{xx} and I_{zz}* can be evaluated for the two molecules. It seems important, therefore, to redetermine these constants from the AsH_3 data alone (or the AsD_3 alone) making use, this time, of the information to be derived from all of the four fundamental bands. The values of both of the moments of inertia I_{xx} and I_{zz} can be determined from the information available from these bands if the lines can be properly identified. A knowledge of I_{xx} and I_{zz} for pyramidal XH_3 molecules is sufficient to fix its size and shape.

TABLE I. Line positions and identifications in the band ν_4.

^RR (2,2)	1030.4 cm^{-1}	^RR (7,6)	1079.9 cm^{-1}
^RR (3,2)	1038.9	^RR (7,7)	1080.8
^RR (3,3)	1040.8	^RR (8,7)	1090.0
^RR (4,3)	1049.0	^RR (8,8)	1090.8
^RR (4,4)	1050.6	^RR (9,8)	1100.0
^RR (5,4)	1059.7	^RR (9,9)	1100.5
^RR (5,5)	1061.0	^RR (10,9)	1109.5
^RR (6,5)	1069.9	^RR (10,10)	1110.2
^RR (6,6)	1071.5		

II. DISCUSSION OF THE SPECTROSCOPIC DATA ON ARSINE

An analysis of the frequency ν_1 in the infrared spectrum of arsine leads to a value $B^{(xx)''}$ of 3.723 cm^{-1}. The perpendicular band ν_3 is not completely resolved, but shows sufficient details so that the value $[(1-\zeta_2^{(z)})B^{(zz)}-B^{(xx)}]$ may be estimated to be 0.16 cm^{-1} with considerable accuracy.

Turning now to the low frequency fundamental band, ν_4, an effort has been made to identify the $^RR(J,J)$ and $^RR(J,J-1)$ lines. The identification we have made is given in Table I. From these we may determine the intervals between the lines $^RR(J+1,K+1=J+1)$ and $^RR(J,K=J)$ and the intervals between the lines $^RR(J+1,K+1=J)$ and $^RR(J,K=J-1)$. These are known to be $2[(1-\zeta_4^{(z)})B^{(zz)}+2(\zeta_{2,4}^{(x)}B^{(xx)})^2/\delta]$ and $2[(1-\zeta_4^{(z)})B^{(zz)}+4(\zeta_{2,4}^{(x)}B^{(xx)})^2/\delta]$,[4] respectively, where $\zeta_{2,4}^{(x)}$ is the Coriolis coupling factor between ω_2 and ω_4 and $\delta=\omega_4-\omega_2$. Setting δ equal to 100 cm^{-1} we obtain for these, respectively, 4.94 cm^{-1} and 5.093 cm^{-1}. This gives a value of $2(\zeta_{2,4}^{(x)}B^{(xx)})^2/\delta=0.15$ and for $(1-\zeta_4)B^{(zz)}=4.80$ cm^{-1}.

Similarly in the band ν_2 an identification of the lines $P(J,K)$ has been made, in particular the $P(J,0)$ lines. Our identification of these is given in Table II. An independent evaluation of the perturbing term $2(\zeta_{2,4}^{(x)}B^{(xx)})^2/\delta$ may be made with the aid of Eq. (8) of reference 4. The value obtained is $2(\zeta_{2,4}^{(x)}B^{(xx)})^2/\delta=0.13$, which is in satisfactory agreement with the value obtained above.

III. DETERMINATION OF THE STRUCTURE OF THE MOLECULE

One may now evaluate the constant $B^{(zz)}$ also from the information given in Sec. II, particularly when one takes account of the fact that $\zeta_2^{(z)}+\zeta_4^{(z)}=-1+B^{(xx)}/2B^{(zz)}$. We obtain the value $B^{(zz)}=3.514$ cm^{-1}. The values $B^{(xx)}$ and $B^{(zz)}$ lead to magnitudes for the

TABLE II. Line positions and identifications in the band ν_2.

P (2,0)	883.6 cm^{-1}
P (3,0)	875.1
P (4,0)	866.3
P (5,0)	857.5

* This work was assisted by the ONR under Contract No. N6 onr-22526, NR019-123 with The Ohio State University.

[1] V. M. McConaghie and H. H. Nielsen, Phys. Rev. **75**, 633 (1949).

[2] The values α and r_0 given here are slightly different from those given in reference 1. The values stated here were arrived at when the calculations were made with some greater accuracy and when more recent values for certain of the atomic constants were used.

[3] C. C. Loomis and M. W. P. Strandberg, Phys. Rev. **81**, 798 (1951).

[4] H. H. Nielsen, J. Chem. Phys. **20**, 759 (1952).

two principal moments of inertia I_{xx} and I_{zz} as follows: $I_{xx}=7.516\times10^{-40}$ g cm^2 and $I_{zz}=7.963\times10^{-40}$ g cm^2. These are, in terms of the constants of the molecule, respectively equal to $I_{xx}=\frac{1}{2}I^{(zz)}+[3mM/(3m+M)]h^2$ and $I_{zz}=3mh^2\tan^2\beta$ where m and M are respectively the masses of the hydrogen and the arsenic atoms and where h is the altitude of the pyramid and β is the angle between h and one of the AsH distances. These may now be evaluated and are found to be $h=0.8562$A and $\beta=55°48'$. The values r_0 and α are quickly evaluated ($\sin\beta=2/\sqrt{3}\sin\alpha/2$) and for these we obtain $r_0=1.523$A and $\alpha=91°34'$. These values are in reasonably good agreement with the values for r_0 and α obtained by the method of reference 1, and are in excellent agreement with the values $r_0=1.523$A and $\alpha=92°$ given for arsine by Loomis and Strandberg,[3] as determined by them from the microwave data taken on the hybrid molecules of arsine.

THE JOURNAL OF CHEMICAL PHYSICS VOLUME 20, NUMBER 12 DECEMBER, 1952

The Measurement of Self-Diffusion in Solid Polymers*

F. Bueche,† W. M. Cashin,‡ and P. Debye
Department of Chemistry, Cornell University, Ithaca, New York

(Received July 3, 1952)

The self-diffusion constant of the macromolecules in plasticized polystyrene and pure poly-*n*-butyl acrylate has been measured over a wide variety of conditions by a radioactive tracer technique. Well-characterized polymer fractions were used throughout. Simultaneous measurements of the bulk viscosity were also made. From the data obtained one is able to show that within experimental error the product of the self-diffusion constant and the bulk viscosity is equal to a constant. This constant has been predicted by theory, and the agreement with the experimental value is good. Therefore, it appears possible to obtain diffusion constants directly from bulk viscosity data.

INTRODUCTION

NEARLY every physical property of solid polymers is influenced by the rate of diffusion of the polymer molecules through the solid. In particular, phenomena associated with viscous flow, elasticity, and hysteresis must be intimately related to the molecular diffusion constant D. In spite of its importance for these properties, there appear to have been no attempts to measure D for bulk polymers. It is the purpose of this paper to present the experimental data we have obtained concerning the self-diffusion coefficient and bulk viscosity of two polymer systems. A theoretical treatment of the problem is given in a companion paper.

METHOD OF MEASUREMENT

The measurement of the diffusion constant was carried out by use of a radioactive tracer method. Since it was originally planned to use polystyrene for these studies a sample of radioactive styrene was obtained which was tagged with C_{14} in the side chain on the second carbon position. Small amounts of this material were then polymerized with varying large amounts of nonradioactive material in benzene solution. Two general types of radioactive polymer were prepared, pure polystyrene and an *n*-butyl acrylate styrene copolymer. The copolymer was always less than one percent styrene unless otherwise stated.

The radioactive polymer was precipitated in methanol (styrene) or pentane (acrylate). After drying and redissolving in benzene the materials were fractionated from a one percent solution by the addition of the above precipitants. Similar samples of nonradioactive material were also obtained and fractionated. The weight average molecular weights of the fractions were obtained from their intrinsic viscosity in benzene in the case of polystyrene[1] and by light scattering for the acrylates.

The diffusion measurements were made by the method of Raynor, Thomassen, and Rouse.[2] When using this method one lays down a thin layer of radioactive material upon a flat base block of similar but nonradioactive material. As the radioactive material diffuses into the base material the intensity of emitted radiation (in this case β-particles) observed by a counter placed above the block will decrease due to absorption of the radiation by the material of the block. Using equations derived for this process one is able to plot theoretical curves for $\log(\mu^2Dt)$ *vs* $\log I$ for any initial thickness of the radioactive layer. The quantity μ is the absorption coefficient of the material of the block

* The work discussed herein was performed as a part of a research project sponsored by the Reconstruction Finance Corporation, Synthetic Rubber Division, in connection with the United States Government Synthetic Rubber Program.

† Present address: Department of Physics, University of Wyoming, Laramie, Wyoming.
‡ Present address: Department of Chemistry, University of Vermont, Burlington, Vermont.

[1] A. M. Bueche, J. Am. Chem. Soc. **71**, 1452 (1949). The molecular weight values have been multiplied by a factor 3.50/2.79 to correct for a better determination of the turbidity standard.

[2] Raynor, Thomassen, and Rouse, Trans. Am. Soc. Metals **30**, 313 (1942).

(in this case $\mu = 302\ \text{cm}^{-1}$), t is the time the material has been diffusing, and I is the intensity of radiation emitted from the block at time t.

If one plots $\log t$ *vs* $\log I$ the quantity $\mu^2 D$ is given by the fact that, when the theoretical and experimental curves are superposed by shifting along the t axis, the point $\log t = 0$ on the experimental plot will coincide with the point $\log(\mu^2 D)$ on the theoretical plot.

In these experiments standard methods for measuring the radioactivity were used. For the most part the intensity readings were about 20 to 100 times background, and the statistical error was negligible compared to other sources of error. The polymer sample itself was held in a brass cup below a thin mica window Geiger tube. The sample was so shielded that no radiation from material near the walls of the cup was received by the counter tube. The base material was placed in the cup and heated under vacuum or nitrogen until it formed a flat solid block of polymer without bubbles. Care was taken to keep the samples level at all times.

In order to apply a thin film of radioactive polymer to the base, the radioactive material (having the same molecular weight as the base) was dissolved in benzene

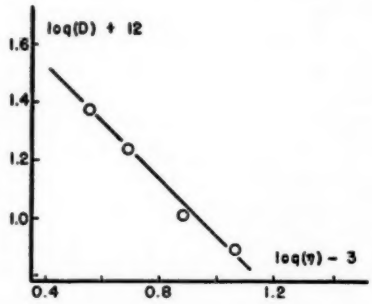

FIG. 1. Diffusion and viscosity data for poly-*n*-butyl acrylate at temperatures from 30 to 47°C. $M = 180{,}000$.

and a known amount of solution was placed on the block. The benzene was evaporated at once under vacuum. The thickness of the radioactive layers varied from 0.5×10^{-3} to 2.5×10^{-3} cm.

RESULTS

Preliminary data on pure polystyrene of molecular weight = 100,000 showed that even at temperatures of 150°C the diffusion rate was so slow that it was impossible to obtain significant diffusion over a period of a few weeks. Since even at this temperature some degradation probably took place, it was decided that higher temperatures could not safely be tolerated.

Because of this our attention was shifted toward plasticized polystyrene and poly-*n*-butyl acrylate. The latter polymer seemed most promising since it is easily prepared and has a transition temperature far below room temperature. Unfortunately, this polymer was found to cross link slowly at temperatures above 90°C, and so it could be used only at lower temperatures. However, it was found that this polymer was sufficiently fluid to give measurable diffusion rates at the lower

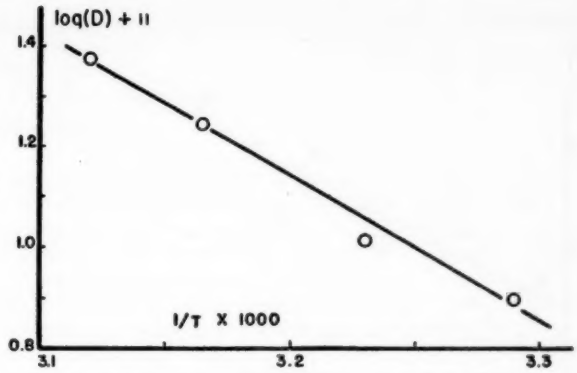

FIG. 2. Variation of D with $1/T$ for poly-*n*-butyl acrylate.

temperatures provided the molecular weight was kept below about 300,000.

The data taken with the acrylate polymers are illustrated in Fig. 1. This shows the variation of $\log D$ with $\log\eta$, where η is the bulk viscosity. The polymer had a molecular weight of 180,000. The points represent data taken at various temperatures. It will be noticed that the slope of the line fitting the data is -1.0, which indicates that $D \sim 1/\eta$. The bulk viscosity was measured by a method described by Fox and Flory.[3] It consists of measuring the rate of rise of the polymer in a capillary under a fixed pressure differential. The fact that the flow of such material is known to be non-Newtonian need not concern us here, since the rates of shear used were very small.

The temperature variation of both $\ln D$ and $\ln\eta$ with $1/T$ was approximately linear and it is possible to represent the data by straight lines. This would probably not be possible over a wider temperature range as has been pointed out for other systems by Fox and Flory.[3] The slopes of these lines may be used to obtain apparent energies of activation. A typical set of temperature data on poly-*n*-butyl acrylate is shown in Fig. 2. In this case the activation energy for diffusion is 13.2 kcal/mole while the activation energy for viscous flow is 13.8 kcal/mole. Since the diffusion data is not too precise, the difference in these values is well within the experimental error.

Similar data were taken on other samples of poly-*n*-butyl acrylate; and the activation energy for both processes, diffusion and viscosity, were found to be the same as above, within experimental error. Also, a polymer containing 16 percent styrene was measured, and although the apparent activation energy for viscous flow had increased to 18.0 kcal/mole, it was found that the activation energy for diffusion had increased to 19 kcal/mole which was the same within the rather large experimental error present for this run. We may therefore say with some certainty that the apparent energy of activation for the diffusion and viscous flow processes is the same.

[3] T. G. Fox and P. J. Flory, J. Phys. Colloid Chem. **55**, 221 (1950).

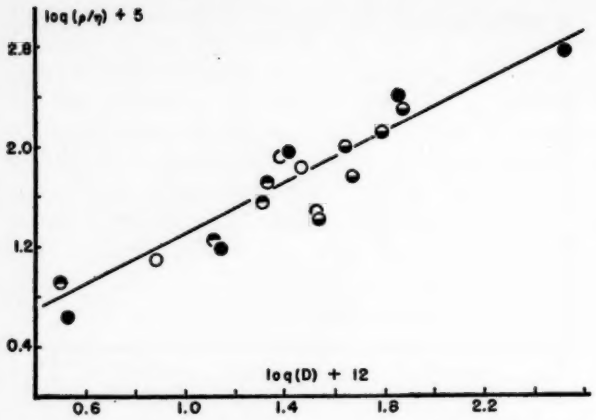

FIG. 3. Compendium of diffusion and viscosity data for polystyrene. The variable is as follows: ● molecular weight; ○ plasticizer concentration, $T=92°C$; ◓ plasticizer concentration, $T=80°C$; ◒ plasticizer concentration, $T=84°C$.

One might expect that factors other than temperature which influence the bulk viscosity of polymers may also show an intimate relationship with the diffusion constant. The most obvious approaches that suggest themselves are the determination of the effects of changing molecular weight and plasticizer content. Both of these quantities have been varied through rather large ranges and their effect has been evaluated.

Some difficulty was experienced with each of these variables. In particular, it was difficult to obtain data over a wide range of molecular weight and plasticizer concentration because of the inflexibility of the diffusion measuring process over widely varying times. Nevertheless, considerable data were obtained, although its accuracy is not all that could be desired.

A valid estimate of the probable error in D is obtained from the data of Fig. 3 where the experimental relation between D and ρ/η is shown. ρ is the density (g/cc) of the polymer in the particular sample used. This shows a compendium of the data obtained for polystyrene plasticized with diethyl phthalate at varied temperatures, plasticizer concentration (30–60 percent polymer), and molecular weight (30,000 to 200,000). The scatter of the experimental points is due mainly to uncertainty in the diffusion data. In spite of this scatter, the points strongly indicate that the product of $D\eta/\rho$ is a constant. This would be true for the straight line of the figure. Although the data cover a hundredfold change of D, the widest deviation from the line is less than a factor 2.5 in either D or η. Therefore, even though it may not be precisely true, the product of D and η/ρ must be essentially constant.

DISCUSSION

It is shown in the theoretical treatment of diffusion given in the companion paper that the following relation should be expected to hold:

$$D\eta/\rho=(AkT/36)(R^2/M),$$

where A is Avagodro's number, k is Boltzmann's constant, T is the absolute temperature, M is the molecular weight, and R^2 is the average square end to end distance of a single polymer chain.

To check this relation one need only know R^2/M which has been determined by many authors from light scattering data. Although R^2/M will change from solvent to solvent, it is expected that its value at this concentration should be near to that found for a dilute solution in a poor solvent.[4] Making use of the experimental data of Outer, Carr, and Zimm[5] one finds that $R^2/M=0.50\times10^{-16}$. Using this value one finds the theoretical value for $D\eta/\rho$ to be 4.2×10^{-8}, where an average temperature has been used for the calculation. The line drawn in the figure corresponds to a value of 4.7×10^{-8}. Considering the experimental error, the agreement between experiment and theory is rather good.

It is also possible to check the theory using the data of Fig. 1 on poly-*n*-butyl acrylate. Although an exact value (for R^2/M) for this polymer is not known, measurements made in this laboratory have indicated that in 2-butanone, a rather poor solvent for this polymer, $R^2/M=0.98\times10^{-16}$. If this value is accepted, one finds $D\eta/\rho=8.4\times10^{-8}$. This is to be compared with the experimental value of 8.0×10^{-8}. Again the agreement is as good as can be expected.

From the above considerations it appears that to the accuracy ordinarily obtainable in diffusion measurements, the diffusion constant of a polymer molecule is related to the bulk viscosity by the simple relation given here. Since bulk viscosity is far easier to measure than the diffusion constant, the above relation leads to a much more simple means of evaluating molecular motion in solid polymers than has been available previously.

ACKNOWLEDGMENT

The authors are indebted to Mrs. Gloria Potter for assisting with many of the measurements reported here. We are also grateful to Dr. A. M. Bueche for his many helpful suggestions during the course of this work.

[4] P. J. Flory, J. Chem. Phys. **17**, 303 (1949).
[5] Outer, Carr, and Zimm, J. Chem. Phys. **18**, 830 (1950); see also T. Fox and P. J. Flory, J. Am. Chem. Soc. **73**, 1909 (1951).

THE JOURNAL OF CHEMICAL PHYSICS VOLUME 20, NUMBER 12 DECEMBER, 1952

Viscosity, Self-Diffusion, and Allied Effects in Solid Polymers*

F. Bueche†
Department of Chemistry, Cornell University, Ithaca, New York
(Received July 3, 1952)

An attempt has been made to explain the observed viscous behavior of bulk polymers. It is found that the viscosity and diffusion may be represented by a theory which takes into account the coupling together of the molecules. Two equivalent treatments are given. One makes use of a segmental friction factor in the same manner as the common formulation of dilute solution viscosity of polymers. The second method uses the concept of segmental jumping. Since both are equivalent, an expression for the friction factor is found in terms of the segmental jumping frequency. Using this fact it is possible to calculate the segmental jumping frequency from bulk viscosity data. A simple application leads to the result that the jumping frequency is about 0.3 sec^{-1} at the transition temperature in polystyrene.

In addition a simple relation is found to hold between bulk viscosity and diffusion constant. The proportionality constant is easily evaluated and so one is now able to obtain self-diffusion constants directly from viscosity data.

INTRODUCTION

MANY data are now at hand concerning the basic flow properties of polymers over a wide range of temperature, molecular weight, and plasticizer concentration. Until now there has been no quantitative molecular theory to explain the observed behavior.[1] The purpose of this paper is to show how it is possible to obtain at least a semiquantitative theory for the bulk viscosity and self-diffusion of polymers.

In order to illustrate the simplicity of the concepts involved, no effort is made in this paper to maintain exceptional mathematical rigor. Physically reasonable approximations are made with the understanding that a more precise treatment is possible. It is to be expected that a more exact derivation of the relations found here will not alter the results to any great extent.

I. RELATION BETWEEN VISCOSITY AND DIFFUSION

The essential difference between the viscosity mechanism in a solid polymer and in a dilute solution of a polymer is that in the former case the solvent is composed of polymer molecules. Since most theories of dilute solution viscosity of polymers make no assumptions as to the character of the solvent, it is possible to apply them almost directly to the case of bulk polymers. One must only keep in mind that in this case the polymer and solvent are identical.

There are essentially two types of calculations for the viscosity of dilute polymer solutions. The first of these assumes that the polymer molecule does not distort the flow lines in the solvent.[2] This is often referred to as the "free draining" approximation since it is the case which would apply if the solvent flowed freely through the polymer molecule. Unfortunately, the term "free draining" does not tell the whole story. (It is possible to imagine instances where the molecules are far from free draining, and still the flow lines of the solvent are not distorted appreciably by the presence of the polymer molecule. For this reason, it would be preferable to refer to the calculations of that type as "zero-distortion" calculations of viscosity.) The second type of calculation[3] of dilute solution viscosity recognizes that the flow lines of the solvent may be distorted by the presence of the polymer molecule. In the extreme limit, such a calculation leads to the viscosity of hard spheres in a low molecular weight solvent.

It is apparent that if the solvent itself is a polymer, one has the case of a bulk polymer. Moreover, since all points in the bulk are equivalent, the flow lines in such a "solution" will be essentially undistorted about any single molecule in the "solution." For this reason the "zero-distortion" calculation of dilute solution viscosity may be applied providing one recognizes that the solvent is itself the polymer.

The theory for dilute solutions amounts essentially to a calculation of the frictional energy loss between polymer and solvent. One therefore needs to calculate the product of the velocity of each segment of a molecule with respect to the solvent and the frictional force resisting this motion. The sum of all such products for all segments of the molecule times the number of molecules per cc gives the energy loss per cc which is due to the presence of the polymer molecules. This quantity is equal to the polymeric contribution to the solution viscosity provided the velocity gradient in the solution is taken as unity.

In a low molecular weight solvent, the frictional force on a segment of a polymer molecule is due to the fact that it is sliding past the solvent molecules. In addition

* The work discussed herein was performed as a part of a research project sponsored by the Reconstruction Finance Corporation, Synthetic Rubber Division, in connection with the U. S. Government's Synthetic Rubber Program.

† Present address: Department of Physics, University of Wyoming.

[1] R. E. Powell and H. Eyring have presented an interpretation of some low molecular weight data on polyesters in *Advances in Colloid Science* (Interscience Publishers, Inc., New York, 1947), Vol. I, p. 199.

[2] M. L. Huggins, J. Phys. Chem. **43**, 439 (1939); W. and H. Kuhn, Helv. Chim. Acta **26**, 1394 (1943); P. Debye, J. Chem. Phys. **14**, 636 (1946).

[3] W. Kuhn, Kolloid-Z. **68**, 2 (1934); J. Kirkwood and J. Riseman, J. Chem. Phys. **16**, 565 (1948); P. Debye and A. M. Bueche, J. Chem. Phys. **16**, 573 (1948).

to this effect, one also has another effect if the solvent is polymeric. This second type of friction force is due to the fact that polymer molecules may be intertwined to such an extent that in order for one polymer molecule to move it must drag others with it.

The sliding friction force may be represented as usual as a constant times the velocity of the segment. This may also be done for the second force just mentioned. However, if the molecule is undergoing rotation as well as translation, this second friction constant may depend upon the position of the segment in the molecule as well as upon its velocity. Whether this positional dependence is important or not is intimately related with the manner of coupling between molecules. It may be shown that if the coupling is not extremely rigid this variation will not cause very serious trouble. For the present purposes we shall assume that the friction constant per chain segment is the same for all segments of the chain.

If this is done, one may follow through Debye's free draining calculation of viscosity to give the following expression for the bulk viscosity:

$$\eta=\frac{R^2}{M}\frac{N\rho A}{36}f, \tag{1}$$

where R^2 is the average square end-to-end chain distance, N is the number of chain segments per molecule, A is Avogadro's number, ρ is the density of polymer, M is the molecular weight, and f is the friction constant, which is evaluated more critically in Sec. II.

Since N and R^2 are both proportional to M, one might at first thought assume that the bulk viscosity should vary proportionally to the first power of M. This is not found to be true experimentally. The reason for this is that f, the friction factor, is also a function of the molecular weight. This functionality will be derived in a later section.

Fortunately, it is possible to obtain a relation between the diffusion constant D and the bulk viscosity, which does not contain f. This is done most simply by remembering the classical Einstein relation, which says

$$D=kT/\text{molecular friction constant}.$$

The molecular friction constant is defined as the force needed to pull a single molecule through the solvent with unit velocity. From the definition of f one sees that this will be just Nf. Therefore,

$$D=kT/Nf. \tag{2}$$

Taking the product between D and η one obtains

$$D\eta=(A\rho kT/36)(R^2/M). \tag{3}$$

Since R^2/M is essentially a constant for any bulk polymer and since its value is readily found from light scattering or dilute solution viscosity measurements *near the precipitation point*,[4] it is possible to predict D if η is known. This is of considerable interest since, although D is the more easily interpreted physical quantity, η is far easier to measure.

The diffusion constant D has been measured along with η over a wide variety of conditions. These data are given in the preceding paper. They confirm the above relation within the experimental error of the measurements. Incidentally, this also shows that the assumption made concerning the friction factor f is really not too bad.

II. THE FRICTION FACTOR

If one considers a particular molecule of the solid, it is possible to imagine that a sedimenting force F could be applied to that molecule alone. As a result of this force the molecule will move with a velocity v just such that the viscous force will equal the sedimenting force, i.e.,

$$F=Nfv. \tag{4}$$

The above relation gives the same meaning to f which was used above. In order to find out what the physical basis for f really is, it will be necessary to calculate the viscous force by a more detailed method.

When the sedimenting molecule moves, it is restrained by two types of forces. The first of these is the ordinary friction experienced by each chain segment as it slides past the other surrounding segments. This force per segment may be represented by the product of a sliding friction constant f_0 and the velocity of the segment.

A second restraining force must be considered when the "solvent" is polymeric. It arises as a result of the fact that from time to time a "solvent" molecule will be hooked into the moving molecule in such a way that the two molecules must move more or less together. Mathematically, this may be described by assuming that a chain of molecular weight M will have KM molecules coupled to it. One would expect the coupling constant K to vary from polymer to polymer but to be independent of molecular weight. For polystyrene one would have K equal to 0.0001 if there were one coupled chain for every 200 chain atoms.

It would be wrong to think that each coupled chain moves with the same velocity v as the sedimenting chain. In fact, it may be shown from a consideration of the simple problem of ropes sliding over each other in a viscous medium that the coupled chain will move with an average velocity equal to $(4/9)v$. If the chains may not be considered smooth, this factor may be somewhat larger. It is possible to express this behavior by a slippage factor s, defined by the fact that on the average a coupled molecule will move with a velocity sv. It is expected that s will be a constant for any one polymer and should have a value of about 0.1 to 0.5.

[4] P. J. Flory, J. Chem. Phys. **17**, 303 (1949).

With the above definitions in mind it is possible to calculate F, the force needed to pull a molecule through the polymeric solvent with a velocity v. It will be

$$F=vNf_0+C_1Nf_0sv+C_2Nf_0s^2v+\cdots,$$

where C_1 is the number of first-order coupled chains (i.e., number of chains coupled to the primary molecule), C_2 is the number of second-order coupled chains, etc.

A crude approximation would be to set $C_1=KM$, $C_2=(KM)^2$, etc. This cannot be correct since it would predict that at a value of M such that $KMs=1$, the force will become infinite. The reason that such is not actually the case is that not all couples can be effective. There are two reasons why a coupling may be ineffective. The coupling may be made to a chain which has been previously coupled and so would be moving with a velocity larger than the required velocity; or two couplings of the same order may be made to the same molecule, in which case each would exert only one-half its normal force.

Therefore,

$$F=vNf_0\{1+C_1s+C_2s^2+\cdots\}. \qquad (5)$$

It is apparent that the only remaining obstacle to the calculation of F is the evaluation of the C_n.

Qualitatively it is possible to see quite readily what the values of the C_n will be. One would expect the first-order couplings to be nearly all effective and so C_1 will be KM. However, if we represent the sedimenting molecule as a sphere, the number of effective second-order couplings will be decreased within that sphere, because there is a possibility that some of the couplings will be made to chains already coupled as first-order chains. From this, C_2 should be less than $(KM)^2$ and similarly for $C_3\cdots C_m$. In fact, it will eventually be true at some critical coupling order, say the mth order, that essentially no uncoupled molecules will exist inside the sphere available for couplings. At this value of $m=g$, the C_n will decrease fairly rapidly since effective couplings may only be made at the surface of the coupling sphere.

The calculation of the C_n may be carried out reasonably rigorously, as is shown in the appendix. When this is done, one arrives at the result that

$$F=vf_0N^* \quad \text{or} \quad Nf=N^*f_0, \qquad (6)$$

where N^* is an effective number of chain links. The behavior of N^* is shown in Fig. 1 where $\log N^*\sim\log\eta$ is plotted against $\log N\sim\log M$. It will be seen that N is proportional to N^* for small values of N. However, when N becomes large enough so that on the average one chain is coupled to one other chain, i.e., $KM\cong 1$, the effective number of segments N^* varies as some higher power of N. The exact power is chiefly dependent upon the value of the slippage factor s, as shown in Fig. 1. At very large values of N, the quantity $N^*\sim N^{2.5}$.

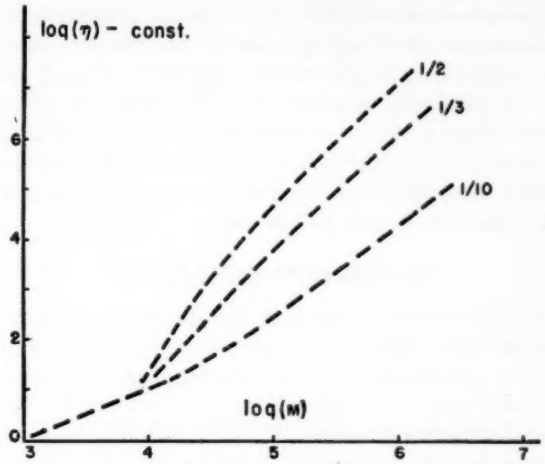

FIG. 1. The variation of viscosity with molecular weight for polystyrene according to theory. For these curves the coupling constant K was taken as 10^{-4}. The slippage factor s has the values indicated on the curves.

In order to compare this theoretical viscosity with that found by experiment, the values for R^2 and ρ have been chosen to approximate those known for polystyrene.

The value used is that for a very poor solvent ($R^2/M=0.50\times10^{-16}$) since Flory[4] has shown this to be the proper value to use in concentrated polymer systems.[5] Using this value, the family of curves plotted in Fig. 1 were obtained. The quantity K was chosen as 10^{-4}. Choice of other values of K merely shifts the break in the curve along the axis since the break always occurs at the place where $KM\cong 1$.

Since Fox and Flory[6] have found experimentally that the data exhibit a break much like the one shown by theory at $M=50{,}000$, one would estimate that K must have a value of about 2×10^{-5}. This would mean that a couple exists for each 500 chain units, which is not at all unreasonable.

Also, since experiment shows that the high molecular weight portion has a slope of about 1.5 units higher than the low molecular weight region, it is apparent that s must be about 0.3. This again is about the expected value. However, this value is uncertain due to the following fact.

The agreement between experiment and theory is not very good below $M=50{,}000$. Whereas it is found here that the slope should be unity, experiment leads to a rather complex curve with slope near two. Such a discrepancy is to be expected since we have not considered the important fact that the presence of chain ends acts to "loosen" the structure. This is treated a little more fully in a later section where it is shown that the discrepancy is most likely due to a change in segmental jumping frequency when the number of chain ends becomes large. Unfortunately, this fact ceases to become

[5] Outer, Carr, and Zimm, J. Chem. Phys. 18, 830 (1950).
[6] T. G. Fox and P. J. Flory, J. Phys. Colloid Chem. 55, 221 (1950).

important at $M=50{,}000$ (as shown by transition temperature and density data), and so a decrease in slope is superposed due to this effect. Therefore, a good value for s is not easily obtained until the chain end effect is better known. It is reasonable to assume that this chain end effect is largely responsible for the molecular weight dependence of Flory's data[7] on the viscosity of low molecular weight polyesters.

III. SEGMENTAL MOBILITY

It is possible to calculate the diffusion constant in another way which gives us direct information concerning segmental mobility. In addition, this second method leads to a more easily visualized picture of the actual diffusion process.

As a first approximation, consider the polymer molecule to be composed of N freely jointed segments. Further, suppose each chain link to have a probability P of jumping in either the positive or negative x direction in unit time. Call the average length of each jump a. One then knows that the number of links of a given chain jumping in the x direction in time Δt is $NP\Delta t$.

Now if Δt is taken short enough so that the number of jumps is small compared to N, each of these will be essentially independent, and so one has $n=NP\Delta t$ steps in a random walk.

From the theory of the random walk one may obtain a distribution function for the excess number of steps taken in the positive x direction. Call it $D(pa)$ where p is the number of excess steps and a is the length of each step. For a particular p the center of mass of the molecule will move a distance $pa/N=X$. To get $\langle X^2\rangle_{Av}$ one must evaluate

$$\int_0^n X^2 D(pa)dp.$$

This then gives

$$\langle X^2\rangle = na^2/N^2.$$

Now if the value of $\langle X^2\rangle$ in the next instant Δt is independent of its previous value, one may show that[8]

$$D=\langle X^2\rangle/2\Delta t. \tag{7}$$

The required independence of $\langle X^2\rangle$ may be shown to be approximately true for particular types of chains, and if one assumes it to hold closely enough for present purposes in all practical cases, one obtains

$$D=a^2P/2N. \tag{8}$$

But it was found above that

$$D=kT/f_0N^*.$$

To bring these two relations into agreement one must replace N by the effective number of chain segments N^*. After that is done one obtains the interesting result

$$f_0=2kT/a^2P. \tag{9}$$

This equation relates the friction coefficient to the easily estimated quantities P, the jumping frequency, and a, the average x component length of each jump. Using this fact it is now possible to express the previous equations for D and η in terms of either f_0 or Pa^2.

Before leaving this section it should be pointed out that it is easy to derive the above equations without recourse to Einstein's relation. This is accomplished by calculating the sedimentation velocity for both ways of considering the process—a viscous drag and a directed walk—and comparing results.[9]

Since it is now possible to relate the bulk viscosity of a polymer directly to the segmental jumping frequency, it would be of interest to calculate the jumping frequency at the volume expansion transition temperature. Fortunately, Fox and Flory[10] list the approximate values of the bulk viscosity which one would find experimentally at the transition temperature in the case of polystyrene. They list the values of η at T_g for several molecular weights between 3000 and 300,000. To avoid the errors involved in the estimation of N we shall use the data for $M=30{,}000$ where $N^*\cong N$. There one has $\eta=10^{11}$.

Upon combining Eqs. (1), (6), and (9) it is found that

$$\eta=\frac{R^2}{M}\frac{\rho A}{16}\frac{kT}{a^2P}N^*. \tag{10}$$

Taking $R^2/M=0.50\times10^{-16}$, $a^2=10^{-15}$, and $N^*=300$, one finds that P should be about 0.3 sec^{-1}.

According to this, if a sample of polystyrene of molecular weight $=30{,}000$ is held at its transition temperature, each chain segment makes one jump every 3 seconds on the average. Such a frequency is about what one would expect if the transition temperature represents the temperature at which the chain segments are just able to adjust to the most favored position in a reasonable length of time.

Fortunately, another check is available on this point. The volume expansion and 3000-cycle dielectric properties of a single sample of polyvinyl chloride have been measured in this laboratory. The volume expansion transition temperature was found to be 83°C. The dielectric properties were essentially the same as for a sample studied extensively by Fuoss,[11] so his much more complete data were used. By extrapolation of his data one is able to show that the dielectric resonance frequency for this polymer is about 0.05 cycle when the sample is held at 83°C.

Since the dipoles of polyvinyl chloride are attached

[7] P. J. Flory, J. Am. Chem. Soc. **62**, 3036 (1940).
[8] G. Joos, *Theoretical Physics* (Hafner Publishing Company, Inc., New York, 1934), p. 565.
[9] Originally the calculation was made in just that way. I am indebted to Professor P. Debye for pointing out this simpler approach.
[10] T. Fox and P. J. Flory, J. Appl. Phys. **21**, 581 (1950).
[11] R. M. Fuoss, J. Am. Chem. Soc. **63**, 378, 369, 2410 (1941).

directly to the chain, the average rotation frequency of the dipoles should be about equal to P, the jumping frequency. Moreover, the dielectric resonance frequency should be approximately equal to the average dipole rotation frequency. From dielectric measurements one would conclude that P should be about 0.05 at the transition temperature for polyvinyl chloride. This is to be compared with the value of 0.3 found for polystyrene at its transition temperature. Considering the inaccuracies of the extrapolations, the leeway in assuming values for the calculations, and the fact that the two polymers are much different, the agreement is quite acceptable. In fact, if one remembers that N is the number of freely orienting chain segments instead of actual segments as assumed here, the agreement can be made perfect. However, the author feels that the actual uncertainty in P is too large to justify perfect agreement.

It is also interesting to notice that the data for the molecular-weight dependence of Tg as given by Fox and Flory[10] seems to support the statement made previously concerning the molecular-weight dependence of η at low molecular weights. For if one calculates P for each molecular weight they have used, one finds that P is essentially constant at the transition temperature. Therefore, it would seem that the transition temperature represents a state of constant segmental jumping frequency. This, of course, fits in very well with Fox and Flory's[10] supposition that Tg is an iso free volume state.

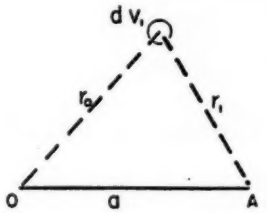

FIG. 2. Diagram illustrating the quantities used in the text.

APPENDIX

It is shown in the text that in order to calculate the force needed to pull a molecule through the solid with a given velocity one must know the value of C_n. This quantity is defined as the number of the nth-order couples which are effective. In order to calculate it, one must know the spatial distribution of coupling points for any coupling order. This may be found as follows.

The distribution of segments of a molecule may be taken as[4]

$$\sim\exp[-\beta_0 r_0^2]r_0^2 dr_0,$$

where β_0 is $9/R^2$ and r_0 is measured from the center of mass of the molecule.

Since this is also the distribution function for the coupling points, the probability that a second molecule having its center at a distance a from the first will have a couple in the volume element dV_1 (see Fig. 2) is given by

$$\sim\exp[-\beta_0 r_0^2-\beta_1 r_1^2]dV_1.$$

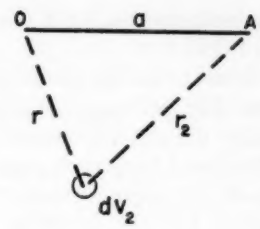

FIG. 3. Diagram illustrating the quantities used in the text.

Integrating this over all elements of volume gives the probability that a molecule with center at A is coupled to the original molecule:

$$(\text{constant})\exp(-a^2[\beta_0\beta_1/(\beta_0+\beta_1)]).$$

Since the molecule with center at A has the probability given above of being first-order coupled, the above expression may be used to represent the density of centers of first-order coupled molecules as a function of a.

The density of segments from first-order coupled molecules in a volume dV_2 is found by summing the contributions of all such molecules as A.

The density of segments in dV_2 due to first-order coupled molecules at A will be proportional to (see Fig. 3)

$$\exp\left[-a^2\left(\frac{\beta_0\beta_1}{\beta_0+\beta_1}\right)-\beta r_2^2\right].$$

Integrating over all positions of A one obtains for the distribution of segments of first-order coupled molecules and therefore of second-order coupling points

$$D\sim\exp\left\{\frac{\beta[(\beta_0\beta_1/\beta_0+\beta_1)]}{\beta+(\beta_0\beta_1/\beta_0+\beta_1)}\right\}r^2.$$

But $\beta_1=\beta_0=\beta_n=\alpha$, and so the distribution of nth-order coupling points is

$$D_n=(\text{constant})\exp[-r^2\alpha\gamma_n]$$

where $\gamma_1=1$, $\gamma_2=\frac{1}{3}$, $\cdots$, $\gamma_n=1/(2n-1)$.

But one also knows that

$$\int D_n dV=1.$$

This gives the normalization constant, and one then knows that the distribution of nth-order coupling points is given by

$$D_n=\left(\frac{\gamma_n\alpha}{\pi}\right)^{\frac{3}{2}}\exp[-r^2\alpha\gamma_n],$$

where $\alpha=9/R^2$, $\gamma_n=1/(2n-1)$, and r is the distance from the center of mass of the original molecule. A similar expression applies for the distribution of centers of nth-order coupled molecules. It is obtained

by replacing γ_n by a new constant λ_n, which is equal to $1/2n$.

Now from the definition of K, each primary chain has KM primary (or first-order) couples. This essentially divides the chain into KM coupling segments. There will be Q such segments per cc. Such a definition does not appear reasonable at KM values less than unity, but this is of no consequence for the present purposes.

It is necessary now to consider what happens as M becomes very large. In that event only a small number of coupling segments of the secondary molecule will be effectively pulled along by the primary couple. Call this number ξ_0. For $KM<\xi_0$ we shall have $\xi=KM$.

Therefore the density of nth-order couples will be approximately

$$\rho_n=3\alpha_n KM\xi^{n-1}\exp[-\alpha_n r^3]r^2dr,$$

where $\alpha_n=12.6\gamma_n^{\frac{1}{3}}/R^3$. In writing this expression the Gaussian previously used has been replaced by an exponential to r^3 having the same average of r^2. This is done to facilitate later computation and is probably not a serious limitation.

The effective number of couples may be obtained to good approximation by multiplying ρ by $e^{-\rho/Q}$ and integrating. One then finds

$$C_n=\frac{KM\xi^{n-1}}{A_n}(1-e^{-A_n}),$$

where

$$A_n=(3\alpha_n KM\xi^{n-1})/(4\pi Q).$$

Now the total force is given by

$$F=vNf_0\{1+C_1s+C_2s^2+\cdots\}$$

or

$$F=vNf_0\left\{1+KM\sum_1^\infty\frac{s^n\xi^{n-1}}{A_n}(1-e^{-A_n})\right\}.$$

This may be simplified in special cases. But in general one has $F=vf_0N^*$ where N^* is defined as $N\{\ \}$.

For the calculations of the text, $\xi_0=5$ and $K=10^{-4}$. The function is not very sensitive to ξ_0, and a change to a value of $\xi_0=10$ does nothing but increase N^* slightly above the break.

THE JOURNAL OF CHEMICAL PHYSICS VOLUME 20, NUMBER 12 DECEMBER, 1952

The Complete Symmetry Group for Internal Rotation in CH_3CF_3 and Like Molecules

HENRY T. MINDEN
Princeton, New Jersey

(Received August 29, 1952)

The symmetry for the wave functions of molecules like CH_3CF_3 is analyzed, and a new group, C_9 is proposed. The irreducible representations in C_9 are derived in the general case for the nuclear spin and internal rotation factors of the wave function. The procedure is described for determining the symmetry and statistical weight of any given internal rotation, vibration energy level.

PAST treatments of the symmetry for internal rotation in molecules like CH_3CF_3 have utilized the group of threefold rotations of one top alone.[1,2] This has led to the introduction of an artificial asymmetry into the problem, which gives rise to certain problems in assigning symmetry characteristics to the various wave functions, and statistical weights to the corresponding energy levels.[2] Actually the combined rotations of both tops comprise a group, called here C_9, which must be used in considering the symmetry of the wave functions.

If R_1 is a rotation of the CH_3 top by 120° and R_2 the corresponding rotation of the CF_3 top, the complete set of operations is

E; R_1; R_1^2; R_2; R_2^2; R_1R_2; $R_1R_2^2$; $R_1^2R_2$; $R_1^2R_2^2$, where E is the identity element. The subgroup E; R_1R_2; $R_1^2R_2^2$ is the well-known three-fold external rotation group of the molecule, while E; R_1; R_1^2 and E; R_2; R_2^2 are the rotational subgroups for the CH_3 and the CF_3 tops, respectively. Each of the latter has the representations

	E	R	R^2
A	1	1	1
E	1	ω	ω^2
	1	ω^2	ω

where $\omega=\exp(2\pi i/3)$.

In constructing the representation of the total group, one can assign the characters to the rotations as follows:

$$E_1\begin{cases}R_1\sim\omega & R_2\sim1\\ R_1\sim\omega^2 & R_2\sim1\end{cases}\qquad E_2\begin{cases}R_1\sim1 & R_2\sim\omega\\ R_1\sim1 & R_2\sim\omega^2\end{cases}$$

$$E_3\begin{cases}R_1\sim\omega & R_2\sim\omega\\ R_1\sim\omega^2 & R_2\sim\omega\end{cases}\qquad E_4\begin{cases}R_1\sim\omega & R_2\sim\omega^2\\ R_1\sim\omega^2 & R_2\sim\omega^2.\end{cases}$$

[1] J. S. Koehler and D. M. Dennison, Phys. Rev. **57**, 1006 (1940).
[2] J. O. Halford, J. Chem. Phys. **18**, 444 (1950).

The character table which results from these assignments is

	E	R_1	R_1^2	R_2	R_2^2	R_1R_2	$R_1R_2^2$	$R_1^2R_2$	$R_1^2R_2^2$
A	1	1	1	1	1	1	1	1	1
E_1	1	ω	ω^2	1	1	ω	ω	ω^2	ω^2
	1	ω^2	ω	1	1	ω^2	ω^2	ω	ω
E_2	1	1	1	ω	ω^2	ω	ω^2	ω	ω^2
	1	1	1	ω^2	ω	ω^2	ω	ω^2	ω
E_3	1	ω	ω^2	ω	ω^2	ω^2	1	1	ω
	1	ω^2	ω	ω^2	ω	ω	1	1	ω^2
E_4	1	ω	ω^2	ω^2	ω	1	ω^2	ω	1
	1	ω^2	ω	ω	ω^2	1	ω	ω^2	1

The direct products are $A\cdot A=A$; $A\cdot E_i=E_i$; $E_i^2=2A+E_i$ and $E_1\cdot E_2=E_3+E_4$ plus all permutations of the subscripts.

The rotations of the group permute cyclically the hydrogen nuclei and the fluorine nuclei. For generality let

I_1=nuclear spin of the atoms on top 1 (hydrogen)

I_2=nuclear spin of the atoms on top 2 (fluorine).

The total number of spin functions are $(2I_1+1)^3\times(2I_2+1)^3$. For the rotation of top 1 there are $(2I_1+1)\times(2I_2+1)^3$ functions which remain invariant; similarly for the rotation of top 2 there are $(2I_1+1)^3(2I_2+1)$ such functions. For the simultaneous rotation of both tops there are only $(2I_1+1)(2I_2+1)$ invariant functions. Therefore the characters for the reducible representation of the nuclear spin functions are

E	$R_1;\ R_1^2$
$(2I_1+1)^3(2I_2+1)^3$	$(2I_1+1)(2I_2+1)^3$
$R_2;\ R_2^2$	$R_1R_2;\ R_1R_2^2;\ R_1^2R_2;\ R_1^2R_2^2$
$(2I_1+1)^3(2I_2+1)$	$(2I_1+1)(2I_2+1)$.

When this is broken down into its irreducible representations, there are

$$(1/9)(2I_1+1)(2I_2+1)\times[(2I_1+1)^2(2I_2+1)^2+2(2I_1+1)^2+2(2I_2+1)^2+4]$$

functions in A,

$$(1/9)(2I_1+1)(2I_2+1)\times[(2I_1+1)^2(2I_2+1)^2-2(2I_2+1)^2+2(2I_1+1)^2-2]$$

in E_1,

$$(1/9)(2I_1+1)(2I_2+1)\times[(2I_1+1)^2(2I_2+1)^2+2(2I_2+1)^2-(2I_1+1)^2-2]$$

in E_2, and

$$(1/9)(2I_1+1)(2I_2+1)\times[(2I_1+1)^2(2I_2+1)^2-(2I_2+1)^2-(2I_1+1)^2+1]$$

each in E_3 and in E_4.

For CH_3CF_3 $I_1=I_2=\frac{1}{2}$; the representations are $16A+8E_1+8E_2+4E_3+4E_4$.

Discussion of the wave functions for internal rotation is best begun by considering the case in which the hindering barrier is zero.[1] The coordinates for the rotation of the two tops about the figure axis are then ignorable variables, and the solutions are

$$\Phi_j=(1/2\pi)^{\frac{1}{2}}\exp(iK_j\varphi_j)\quad j=1,\ 2.$$

The total angular momentum about the figure axis is $\hbar K=\hbar(K_1+K_2)$ and the energy $[\hbar^2(C_1+C_2)/2C_1C_2]K^2$, where C_1 and C_2 are the top moments of inertia about the figure axis.

Consider the effect of a rotation of α_1 on top 1 and of α_2 on top 2

$$\exp(iK_1\varphi_1)\exp(iK_2\varphi_2)\rightarrow \exp i(K_1\alpha_1+K_2\alpha_2)\exp(iK_1\varphi_1)\exp(iK_2\varphi_2).$$

For the rotations of C_9, R_1 means $\alpha_1=2\pi/3$, $\alpha_2=0$; R_1^2 means $\alpha_1=4\pi/3$, $\alpha_2=0$, etc. The characters for the representation of the internal rotation functions are then

E	R_1	R_1^2	R_2	R_2^2	R_1R_2	$R_1R_2^2$	$R_1^2R_2$	$R_1^2R_2^2$
1	ω^{K_1}	ω^{2K_1}	ω^{K_2}	ω^{2K_2}	$\omega^{K_1+K_2}$	$\omega^{K_1+2K_2}$	$\omega^{2K_1+K_2}$	$\omega^{2(K_1+K_2)}$

The five following cases may be distinguished.

1. K_1 and $K_2=3q$; the product function is in A
2. $K_1=3q$, $K_2\neq 3q$; the product function is in E_2
3. $K_1\neq 3q$, $K_2=3q$; the product function is in E_1
4. K_1 and $K_2\neq 3q$ (a) $K_1+K_2=3q$; the function is in E_4,
   (b) $K_1+2K_2=3q$; the function is in E_3,

where q=an integer.

In case the barrier is not zero, K_1 and K_2 are no longer good quantum numbers for the energy, although their sum K is still good. Nevertheless, each level in the bound case can be identified with the level it approaches in the free case, and what is more, the representation in C_9 of the wave function for the level does not change in going from the free to the bound case, since the hindering potential has the symmetry of the group. Finally, the order of the energy levels will remain the same because the "no crossing rule" applies in this problem.

To treat the vibrations of the molecule as a whole, one must revert to the subgroup $C_3(E,\ R_1R_2,\ R_1^2R_2^2)$. The representations A and E_4 of C_9 pass over into A of C_3 while the representations E_1, E_2, and E_3 pass over into E. The internal coordinate $\chi=\varphi_1-\varphi_2$ is symmetrical with respect to C_3 so it will not be involved in any functions of the vibrational coordinates. Furthermore, the statistical weight of a given combined internal and external vibrational level will simply be the weight found by consideration on the internal wave functions as above, multiplied by the weight calculated by consideration of the symmetry in C_3 of the rotational and external vibrational wave functions. This latter calculation has been described by E. B. Wilson, Jr.[3]

[3] E. B. Wilson, Jr., J. Chem. Phys. **3**, 276 (1935).

Enhancement of X-Ray Induced Absorption Bands in Alkaline Earth Compounds

JAMES H. SCHULMAN, ROBERT J. GINTHER, AND RUSSELL D. KIRK
Crystal Branch, Metallurgy Division, Naval Research Laboratory, Washington, D. C.
(Received September 2, 1952)

It is deduced that the incorporation of monovalent positive ion impurities in alkaline earth salts should increase the discoloration of these compounds by ionizing radiations. This deduction is confirmed experimentally with alkaline earth fluorides and strontium sulfate "sensitized" with alkali-ion impurities. As predicted, M^{+3}-ion and X^{-}-ion impurities poison the sensitizing effect of the M^{+1}-ion impurities.

THE small amount of information that has been published concerning x-ray induced absorption bands in alkaline earth salts indicates that the efficiency of production of color centers in these materials by x-rays is much lower than that observed in the alkali halides.[1,2] Thus, Barile[2] finds absorption coefficients of the order of 2 cm^{-1} in heavily x-rayed CaF_2, corresponding to about 10^{16} color centers per cm^3, while Estermann, Leivo, and Stern[3] observed F-center concentrations of the order of $5 \cdot (10)^{17}$ per cm^3 in well-annealed KCl which had been subjected to similar x-ray exposure. We have been able to effect a considerable increase in the sensitivity of alkaline earth fluorides, strontium chloride, and strontium sulfate to discoloration by x-rays, by making use of the following simple considerations.

From the generally accepted model of the F-center and similar trapped electron centers in the alkali halides,[4] it follows that an increase in the concentration of negative ion vacancies in the crystal should lead to an increased x-ray yield of such color centers. This conclusion applies to salts of divalent cations as well, if the x-ray induced absorption bands in these materials are assumed to be the result of trapped electron centers. The substitutional solution of a monovalent cation in a divalent cation salt suggests itself as a simple method of increasing the negative ion vacancy concentration of such a salt. For, in order to preserve electrical neutrality as a result of this substitution, the crystal must either dissolve interstitially one M^{+}-ion for each M^{+}-ion entering substitutionally, or form the requisite number of negative ion vacancies. If charge compensation is effected by the latter mechanism, and if the impurity-induced anion vacancies are spatially dissociated from the M^{+} impurity ions, the concentration of anion vacancies available for electron trapping will be higher than that present in the pure crystal. X-raying should then result in the same species of trapped electron centers in the "impurity-sensitized" crystal as in the pure crystal, but with a greater yield of color centers in the former. Even if the impurity-induced vacancies are closely associated spatially with the impurity ion to form what may be called "complexes,"[5] they may, nevertheless, constitute electron traps. Such traps, however, will be in general of different depth (shallower) from those consisting of "free" vacancies, and should give rise to different absorption bands upon x-irradiation from those produced in the pure crystal. If the first method of charge compensation is the one adopted by the crystal, the interstitial M^{+}-ions may also act as additional electron traps, which again may be of different depth from those that result from anion vacancies in the pure crystal.

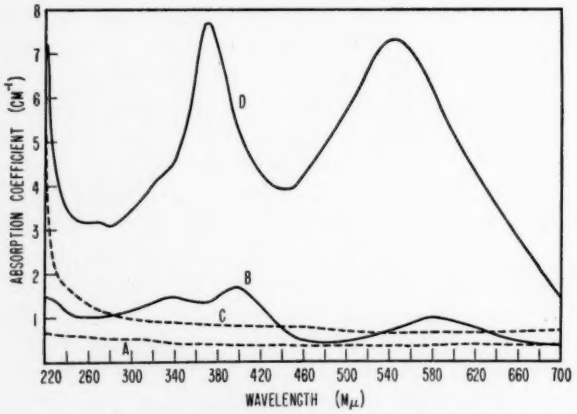

FIG. 1. Absorption spectra of CaF_2. A, crystal before x-ray; B, crystal after x-ray; C, crystal heated to 1200°C in He, before x-ray; D, crystal heated to 1200°C in He, after x-ray.

From arguments similar to those involved in predicting "sensitization" of divalent cation salts by M^{+}-ions, deductions may be made concerning the "desensitizing" or "poisoning" effect of various kinds of additional impurities. Trivalent and higher valent cation impurities in any M^{+2} salt, and monovalent anion impurities in M^{+2} salts of the type $M^{+2}X^{-2}$ should both provide the necessary charge compensation required by the substitutional solid solution of M^{+}-ions in these compounds, and should therefore poison the sensitizing effect of the M^{+}-ions. On the other hand, divalent cation impurities should obviously have no poisoning effect on this sensitization, although large concentrations of such impurities may shift the position of the x-ray induced absorption bands.

Although the foregoing discussion deals entirely with trapped electron centers in divalent cation salts, these considerations may be applied in an obvious manner to such centers in compounds of higher valency cations and

[1] A. Smakula, Phys. Rev. **77**, 408 (1950).
[2] S. Barile, J. Chem. Phys. **20**, 297 (1952).
[3] Estermann, Leivo, and Stern, Phys. Rev. **75**, 627 (1949).
[4] F. Seitz, Revs. Modern Phys. **18**, 384 (1946).
[5] H. W. Etzel, and R. J. Maurer, J. Chem. Phys. **18**, 1003 (1950).

to trapped hole centers in compounds of multivalent anions.

The above-postulated enhancement of discoloration by x-rays was observed experimentally upon the introduction of any alkali ion impurity in CaF_2, SrF_2, and BaF_2; of Na^+-ion in $SrCl_2$; and of Na^+ or K^+ ions in $SrSO_4$. Incorporation of the alkali ion was performed in all cases by firing intimate powder mixtures of the alkaline earth salt and the alkali salt of the same anion. Information concerning the absorption bands in the resulting powders, both before and after x-irradiation, was derived from measurements of the diffuse reflection spectra, minima in these spectra corresponding to absorption peaks. The x-ray treatment consisted of a one-hour exposure of powder plaques at a distance of 6 cm from the Be window of a Machlett tube operated at 40 KVP and 15 ma.

In the experiments with CaF_2, Harshaw single crystal material or clear optical quality natural fluorite were ground for use as raw material. Firing with the alkali fluorides was done in vacuum or in an atmosphere of dry

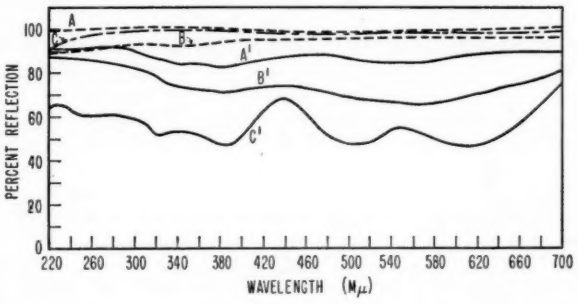

FIG. 2. Reflection spectra of CaF_2. *A*, ground crystal, before x-ray; *A'*, ground crystal, after x-ray; *B*, ground crystal heated to 1200°C before x-ray; *B'*, ground crystal heated to 1200°C, after x-ray; *C*, ground crystal heated to 1200°C with 0.1 mole percent NaF, before x-ray; *C'*, ground crystal heated to 1200°C with 0.1 mole percent NaF, after x-ray.

helium at 1200°C for 30 minutes. The absorption spectra of the pure CaF_2 starting material, before and after heating at 1200°C, were measured directly on single crystal plates. The results of these measurements are shown in Fig. 1. The absorption spectra of pure, unheated CaF_2, before and after x-raying, agree very well with the results of Smakula[1] and Barile.[2] Firing of the pure CaF_2 under the above-specified conditions produces noticeable changes in the absorption spectra of both the un-x-rayed and x-rayed material. The absorption of the un-x-rayed CaF_2, particularly in the ultraviolet, is increased by the heat treatment, and major changes in the positions, magnitudes, and relative intensities of the x-ray induced absorption bands are produced. Figure 2 shows the reflection spectra of corresponding powdered samples of pure CaF_2, as well as those of CaF_2 sensitized with 0.1 mole percent of NaF. The weak absorption bands produced by x-raying the pure material are not well resolved by the reflection technique. It appears that grinding the pure CaF_2 causes shifts in the positions of the x-ray induced absorption bands similar to that produced by heat treat-

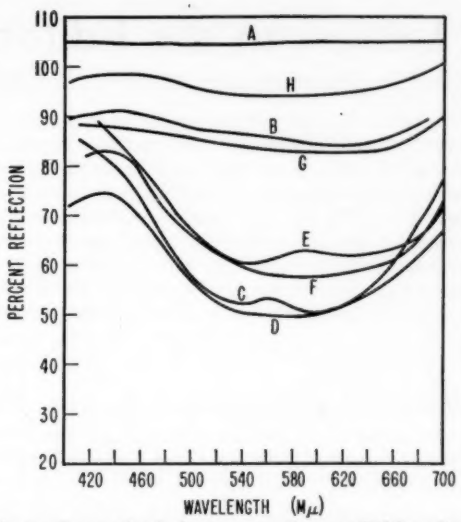

FIG. 3. *A*, all samples before x-ray; *B*, pure $SrSO_4$, after x-ray; *C*, $SrSO_4$: 1–2 mole percent K_2SO_4, after x-ray; *D*, $SrSO_4$: 2 mole percent Na_2SO_4, after x-ray; *E*, $SrSO_4$: 1 mole percent Na_2SO_4+20 mole percent $CaSO_4$, after x-ray; *F*, $SrSO_4$: 1 mole percent Na_2SO_4+20 mole percent $BaSO_4$, after x-ray; *G*, $SrSO_4$: 1 mole percent Na_2SO_4+1 mole percent $SrCl_2$, after x-ray; *H*, $SrSO_4$: 1 mole percent Na_2SO_4+1 mole percent $La_2(SO_4)_3$, after x-ray.

ment of a single crystal of this material. The addition of NaF produced a noteworthy increase of the x-ray induced absorption. At least two of these absorption bands, e.g., those peaking at about 3300A and 3800A, appear identical with the bands produced in pure CaF_2. A determination of the magnitude of the increase in x-ray sensitivity caused by the M^+ impurity awaits the growth of single crystals of CaF_2 sensitized with NaF, on which it will be possible to make absorption measurements comparable to those in Fig. 1.

Even the purest commercially obtainable $SrSO_4$ was sensitive to x-rays after firing at 1050°C, irradiation producing a purple color. Spectrographic analysis showed, as suspected, that sodium was a contaminant. Special alkali-free preparations made in our laboratory and fired at 1050°C were practically insensitive to x-rays; while firing of this material with 0.01 to 1.0 mole percent Na_2SO_4 or K_2SO_4 gave products discolored by x-rays approximately in proportion to their alkali content. The effect of trivalent cations and monovalent anions on the sensitization by alkali ions was investigated with $SrSO_4$. The sensitizing effect of Na^+-ion was found to be strongly poisoned by small additions of La^{+3}, Ce^{+3}, and Sm^{+3} as sulfates, or by Cl^- or F^- either as Na^+ or Sr^{+2} salts. Substitution of large amounts of Ca^{+2} or Ba^{+2} for Sr^{+2} had no major effect on the sensitizing ability of Na^+-ion. The results, illustrated by the reflection spectra of Fig. 3, constitute a gratifying confirmation of the predictions.

Further studies now being pursued along these lines include investigations of the effects of various monovalent cation impurities and their concentration on the sensitization of alkaline earth salts, and of the thermal and optical bleaching of the x-ray induced absorption bands in these materials. The results will be reported in greater detail in a later paper.

Letters to the Editor

THIS section will accept reports of new work, provided these are terse and contain few figures, and especially few half-tone cuts. The Editorial Board will not hold itself responsible for opinions expressed by the correspondents. Contributions to this section should not exceed 600 words in length and must reach the office of the Editor not later than the 15th of the second month preceding that of the issue in which the Letter is to appear. No proof will be sent to the authors. A publication charge of $10.00 per Letter is made which, when honored, will entitle the Institution to 100 free reprints.

Vibration Potential Function of the ClO_2 Molecule

JULES DUCHESNE AND ALVIN H. NIELSEN*
Institut d'Astrophysique, University of Liège, Cointe-Sclessin, Belgium
(Received May 19, 1952)

THE most general quadratic potential function controlling the fundamental vibrations of triatomic molecules of C_{2v} symmetry may be written[1]

$$2V = f_1(\overline{\Delta l_1}^2+\overline{\Delta l_2}^2)+l_1l_2f_\theta\overline{\Delta\theta}^2+2f_{12}\Delta l_1\Delta l_2+2l_1g_e(\Delta l_1+\Delta l_2)\Delta\theta.$$

In the case considered here, l_i are the Cl—O bond lengths and θ is the O—Cl—O bond angle at the equilibrium position. Their values, as obtained from the recent electron diffraction work of Dunitz and Hedberg[2] are $1.4_{\prime 1}\pm0.01_4$A and 116.5°±2.5°, respectively. From their infrared spectroscopic work, Nielsen and Woltz[3] show that the Cl—O bond length and bond angle are consistent with the above values within the limits of the accuracy given by Dunitz and Hedberg. The present authors have adopted as the values of these constants 1.49A and 118.5°† which result from a combination of the electron diffraction and infrared data. The three observed fundamental frequencies are, however, not sufficient to fix the exact values of the four force constants f_1, f_θ, f_{12}, and g_e which appear in the potential function. To obviate this difficulty as method was introduced by Duchesne[1,4] and extended by others[5] which consists in calculating ranges of solution and in selecting the most reliable ones. This method was first used by Duchesne[1] and later by Hedberg[6] for discussing the potential function of ClO_2.—The former author adopted molecular dimensions given by Pauling[7] l_i(Cl—O)=1.53±0.03A and θ=125°, which differ somewhat from the present ones, while the latter author did not give a detailed discussion of the potential function. Duchesne[1] used the frequencies as given by Coon,[8] whereas Hedberg[6] used his own values for ν_1 and ν_3 and Coon's[8] value for ν_2. However, from new electronic band spectra data, and by utilizing all the previously available infrared data, Coon and Ortiz[9] have computed values of the harmonic frequencies, and of the anharmonic constants. Band centers computed from these constants agree fairly well with the infrared band centers observed by Nielsen and Woltz.[3] It, therefore, appeared to be of interest to recalculate the force constants in terms of the new data.

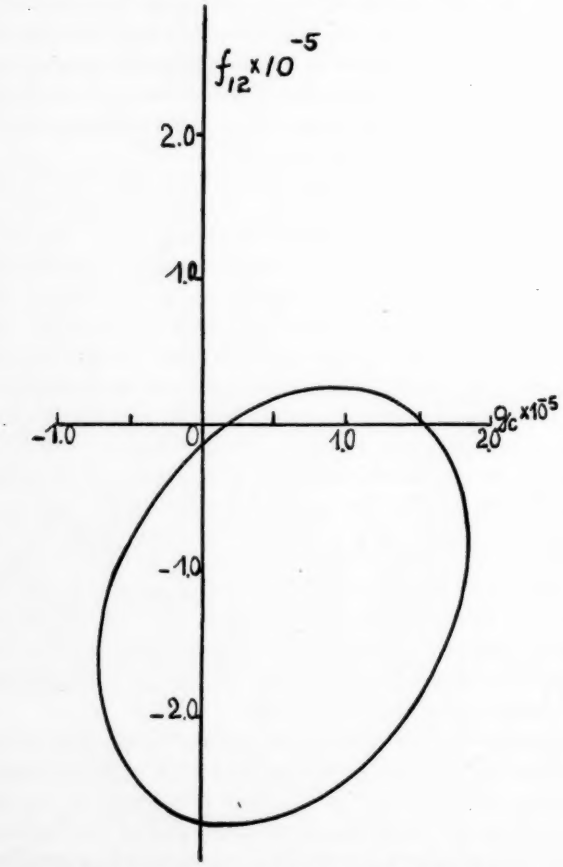

FIG. 1. Ellipse representing the variation of f_{12} with g.

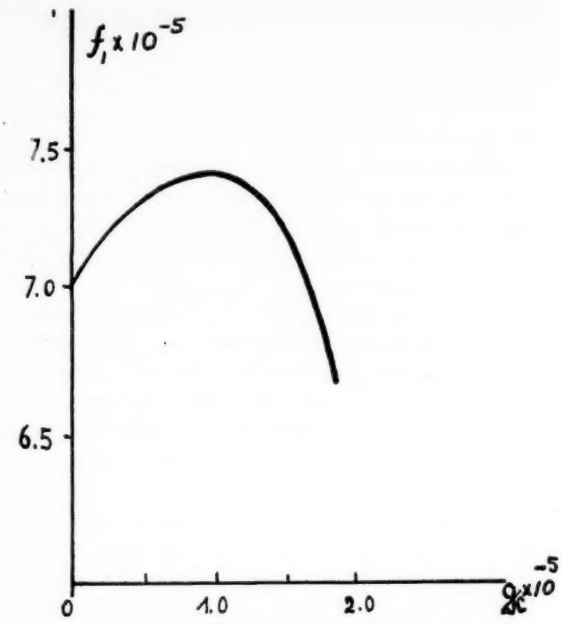

FIG. 2. Curve representing the variation of f_1 with g_e.

The zeroth-order frequencies are[9] ω_1=964.8 cm^{-1}, ω_2=451.8 cm^{-1}, and ω_3=1127.3 cm^{-1}, and the bond-angle is 118.5°. From these data it is possible to calculate f_{12} in terms of g_e along the lines of the method reported.[1,4,5] The curve obtained is an ellipse and is shown in Fig. 1. If it is assumed that g_e must be positive and at least as large as 0.2×10^5 dynes/cm (this is strongly suggested by its behavior in many other molecules), it will be seen from an inspection of the ellipse that the bond-bond interaction f_{12} is positive and cannot be larger than 0.258×10^5 dynes/cm. These narrow limits are made possible because the negative values of f_{12} corresponding to reasonable ones of g_e ($0.2<g_e<1$) are much greater than would be expected, and therefore must be discarded. From the antisymmetric vibration ω_3 it is then found that $f_1=7.14\times10^5+f_{12}$. Consequently, a lower limit for f_1 is established because of the positive sign of f_{12}. The upper limit of f_1, which depends upon the maximum value 0.258×10^5 dynes/cm for f_{12}, is, therefore, 7.4×10^5 dynes/cm. It is now practically certain that the Cl—O valency bond f_1 is strong and that values such as 7.4×10^5 dynes/cm for it and 0.258×10^5 dynes/cm for f_{12} are fairly close to the true values. According to Fig. 1 it appears

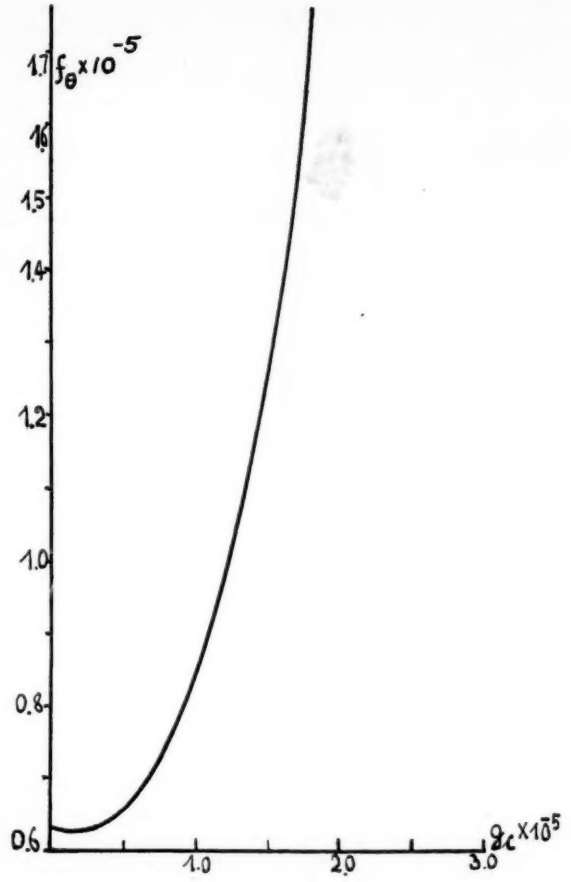

FIG. 3. Curve representing the variation of f_θ with g_e.

that g_e, which is very sensitive to f_{12}, cannot be very accurately determined. The value of g_e computed from the previously given f_1 and f_{12} is 0.8×10^5 dynes/cm. According to Fig. 3, which is a plot of f_θ *versus* g_e, f_θ equals 0.74×10^5 dynes/cm. Figures 1–3 show how the force constants depend upon one another.

* The University of Tennessee, Knoxville, Tennessee. Fulbright research scholar, Institut d'Astrophysique, University of Liège, Belgium, 1951–1952.

[1] J. Duchesne, Mém. Soc. Roy. Sci. Liège **II**, 429 (1943).

[2] J. D. Dunitz and K. Hedberg, J. Am. Chem. Soc. **72**, 3108 (1950).

[3] A. H. Nielsen and P. J. Woltz, J. Chem. Phys. **20**, 1878 (1952).

† A paper was recently given by J. B. Coon, Phys. Rev. **85**, 746 (1952), in which he has calculated the l(Cl−O) = 1.484A and $\theta = 114.4°$ for the ground electronic state from analysis of the rotational structure of electronic bands. His values differ somewhat from the ones used in this calculation, being near the lower limit of the error given by Dunitz and Hedberg, while the present ones are near the higher limit. It is believed that the two sets of values are equally good and show that the internuclear distance and angle are indeed in the vicinity of 1.49A and 116.5°, respectively. The use of Coon's values would hardly alter the values of the force constants.

[4] J. Duchesne, Physica, **9**, 249 (1942).

[5] G. Glockler and J. Y. Tung, J. Chem. Phys. **13**, 388 (1945); P. Torkington, *ibid.* **17**, 357 (1949); J. Duchesne and L. Burnelle, *ibid.* **19**, 1191 (1951).

[6] K. Hedberg, J. Chem. Phys. **19**, 509 (1951).

[7] L. Pauling, *The Nature of the Chemical Bond* (Cornell University Press, Ithaca, New York, 1939), p. 255.

[8] J. B. Coon, Phys. Rev. **58**, 926 (1940).

[9] J. B. Coon and E. Ortiz, Phys. Rev. **82**, 766 (1951).

Absorption Coefficients of Gases in the Vacuum Ultraviolet

K. WATANABE, EDWARD C. Y. INN, AND MURRAY ZELIKOFF
Geophysics Research Directorate, Air Research and Development Command, Air Force Cambridge Research Center, Cambridge, Massachusetts
(Received October 13, 1952)

ABSORPTION cross sections of several gases were measured in the region 1050–2500A, by a method somewhat different from that used by previous investigators, to obtain additional data and, wherever possible, more precise values. The uncertainties inherent in photographic photometry were avoided by employing a 1P21 photomultiplier tube coated with sodium salicylate as a detector, with a Baird one-meter vacuum monochromator. This arrangement allowed the absorption cell with LiF windows to be placed between the exit slit (0.05 mm) and the detector. The cell was in communication with a gas-filled system which facilitated frequent evacuations, changes of pressure, and sampling of gas for mass-spectrometric analyses. Repeated measurements, with the cell empty and filled, minimized errors due to drifts (±5 percent) in the light intensity of the H_2 discharge tube.

Our results disagree considerably with some of the reported data obtained by photographic photometry. For example, the maximum coefficient of the Schumann-Runge continuum of O_2 was found to be 380 cm^{-1} (base e) at 1420A, in contrast to the accepted value of about 490 cm^{-1} at 1450A obtained by Ladenburg and van Voorhis.[1] Furthermore, the intensity distribution of the continuum was found to be rather asymmetric as compared to their results (curve L–V in Fig. 1). Three narrow continua or

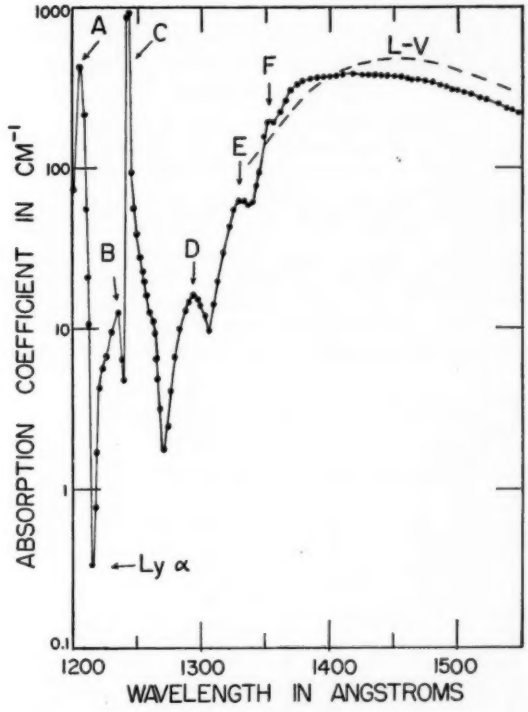

FIG. 1. Absorption coefficient of O_2.

diffuse bands (D, E, F in Fig. 1), which were recently reported by Tanaka,[2] were found on the short-wavelength slope of the $S-R$ continuum at about 1352, 1330, and 1293A. In the region below 1270A, there are several very diffuse bands of which three (A, B, and C) are shown in Fig. 1. In a photograph taken by Tanaka[2] with a three-meter grazing incidence spectrograph, these bands show apparently no structure, probably due to strong predissociation. Thus, the absorption coefficients shown in Fig. 1 should be quite reliable, although the band width of our monochromator was 0.85A. At Lyman alpha, the absorption coefficient was 0.33 cm^{-1}, which is in good agreement with the value 0.315 cm^{-1} found by Preston[3] for a corresponding pressure (7.5 cm Hg). Our result (2.0 cm^{-1}) for CO_2 at Lyman alpha also agrees with his carefully determined value (2.01 cm^{-1}). This is believed to be significant since he used for a detector an argon-filled platinum photocell with a LiF window, while other investigators employed photographic plates.

For CO_2, our measured coefficients are as much as a factor two

greater than those found by Wilkinson and Johnston[4] for the "continuum" in the region 1450–1700A. They reported bands at 1662, 1673, and 1690A; however, in addition to these bands, we were able to observe nearly forty diffuse bands superposed on the continuum which extends down to about 1200A. Nearly all of these diffuse bands seem to appear on the reproduction by Price and Simpson[5] who, however, did not report their wavelengths. The continuum itself has at least two maxima of about 14 cm^{-1} and 18.5 cm^{-1} at 1475A and 1335A, respectively.

The method of scanning the spectrum with a phosphor-coated photomultiplier responds well to small variations in the absorption intensity as a function of wavelength. It is capable of detecting weak bands superposed on a strong continuum or a weak continuum underlying a number of strong bands. A more detailed description of our results for several gases will be submitted.

[1] R. Ladenburg and C. C. van Voorhis, Phys. Rev. **43**, 315 (1932).
[2] Yoshio Tanaka, J. Chem. Phys. **20**, 1728 (1952).
[3] W. M. Preston, Phys. Rev. **57**, 887 (1940).
[4] P. G. Wilkinson and H. L. Johnston, J. Chem. Phys. **18**, 190 (1950).
[5] W. C. Price and D. M. Simpson, Proc. Roy. Soc. (London) **A169**, 501 (1938).

The New Method of Studying Lattice Defects in Solids by Debye Absorption: Case of Semiconductors

MARIE FREYMANN AND RENÉ FREYMANN
Faculté des Sciences, Rennes, France
(Received October 7, 1952)

THE study of lattice defects up to the present day has included several conventional processes: conductibility, diffusion, etc. In this summary, we intend to lay a stress upon a new method: the study of Debye absorption, from kilometer to centimeter waves, and the application of the $\log\nu_c - 1/T$ representation. This method is based on the idea that we should distinguish two different types of dipoles: (1) the dipoles connected with the orientation of molecules or atom groups,[1] and (2) the dipoles connected with crystalline lattice defects.

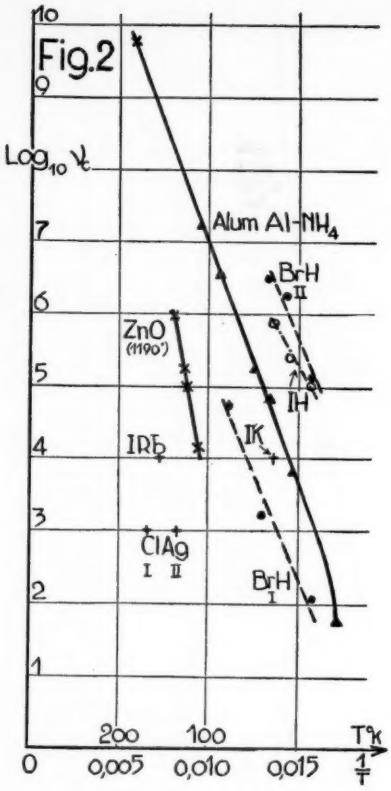

FIG. 2. (see Fig. 1 for explanation of symbols).

I. The $\log\nu_c - 1/T$ representation.—We have already emphasized[2] that, in agreement with Debye theory, it is convenient to connect the frequency of the maximum of Debye absorption with the corresponding temperature T. Figures 1 and 2 (corresponding to two different scales of temperature) gather, in this way, the results of the following studies: (1) studies on ionic crystals (type ClNa) which had been examined, for one frequency only, by Breckenridge;[3] (2) studies on semiconductors (uranium oxides, for example) that we began in collaboration with the French "Commissariat à l'Energie Atomique;"[4] (3) studies on ammonium salts by one of us;[5] (4) studies on adsorbed water on silica gel that we had developed in Rennes;[6] studies on ice by Smyth and collaborators; and (5) studies on halogen acids by Smyth, Powles, and Philips.

II. The two types of dipoles.—It was admitted, until now, that

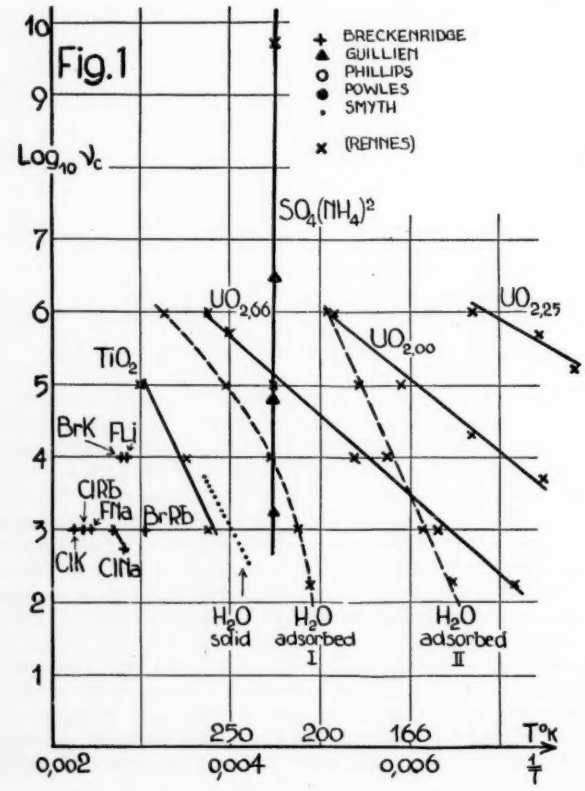

FIG. 1.

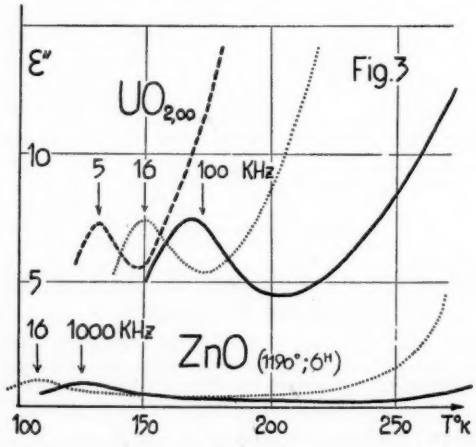

FIG. 3.

the Debye absorption was connected with the orientation of groups of molecules or atoms. Yet, we noticed in 1949[4] the existence of a strong absorption of uranium oxides; however, their structure forbids any interpretation of this absorption by the orientation of atomic groups. It was therefore necessary to put side by side our results and those of Breckenridge[3] concerning ionic crystals of the ClNa type. Enlarging the hypothesis of the latter, we should admit that, in the case of oxides as in the case of halides, there is a new type of dipole: the dipoles depending on the lattice defects. From $\nu_c = A \exp -U/kT$ and the $\log \nu_c - 1/T$ representation (which suppresses the arbitrary choice of the frequency ν_0 of the lattice vibrations[2]), we can infer the activation energy U for the diffusion of the defect through the crystal, the coefficient A (connected with ν_0), and the number n of lattice defects.

III. Extension of the method.—We have recently observed[7] phenomena similar to those which we have already pointed out for uranium oxides. For instance (Figs. 1, 2, 3), TiO_2, ZnO, etc., treated properly, offer characteristic Debye absorptions. They must also be explained as produced by lattice defects. Finally, we may wonder, cautiously, if ammonium salts and halogen acids do not offer the two types of Debye absorption: molecular orientation and lattice defects.

[1] Frohlich, *Theory of Dielectrics* (Clarendon Press, Oxford, England).
[2] M. Freymann and R. Freymann, Compt. rend. **232**, 2312 (1951).
[3] R. G. Breckenridge, J. Chem. Phys. **16**, 959 (1948); **18**, 913 (1950).
[4] M. Freymann and R. Freymann, Compt. rend. **229**, 1013 (1949); **230**, 2094 (1950); **232**, 2312 (1951).
[5] M. Freymann and R. Freymann, Compt. rend. **232**, 2312 (1951); **233**, 1449 (1951).
[6] M. Freymann and R. Freymann, Compt. rend. **232**, 401, 1096, 1098, 2312 (1951); **233**, 862, 864, 951 (1951).
[7] M. Freymann and R. Freymann (to be published).

Direct Evidence for the $n \rightarrow \pi$ Electronic Transition of the Nitroso-Absorption

KAZUO NAKAMOTO AND KEISUKE SUZUKI
Department of Chemistry, Faculty of Science, Osaka University
Nakanoshima, Kita, Osaka, Japan
(Received October 6, 1952)

RECENTLY McConnell[1] has shown by the measurement of solvent effects that the band at 13.3×10^3 cm^{-1} in nitrosobenzene is ascribed to the $n \rightarrow \pi$ transition.[2] A direct evidence for the above interpretation, however, may be deduced from the following discussion on the dichroism of *m*-nitronitrosobenzene monomer in crystalline state, which was measured already by one of the present authors.[3]

As schematically shown in Fig. 1, the planar molecules* of *m*-nitronitrosobenzene in the crystal used† are piled up along the *c* axis, making their molecular planes almost parallel to the *a* axis and inclined by about 20° referred to the *b* axis. Absorption spectra by linearly polarized lights, with the electric vectors vibrating parallel to the *b* and *c* axes, respectively, are shown in Fig. 1.

As is shown in the figure, there exist two absorption bands at 760 mμ (visible region) and 360∼350 mμ (ultraviolet region). In the former weak band, the ⊥ absorption is hyperchromic to the || absorption. However, in the latter intense band, the || absorption is bathochromic and hyperchromic to the ⊥ absorption.

These experimental results may be explained fully by group theoretical consideration. Since the molecule *m*-nitronitrosobenzene belongs to the symmetry point group C_{1h}, we can divide its 56 valence electrons into three classes, i.e., 30σ bonded electrons ($\subset A'$), 14σ lone pair electrons ($\subset A'$) and 12π electrons ($\subset A''$).

Then, the approximate wave functions (and irreducible representations to which they belong) for the ground state and some of the lower excited states are as follows:

$$\Psi_g = \mathfrak{A}(2S_O)^2(2S_N)^2(\sigma_1)^2 \cdots (\sigma_{15})^2(\pi_1)^2 \cdots (\pi_6)^2(l_0)^2(l_0')^4 \cdot \text{spin functions } (\subset A'),$$

$$\Psi_{e1} = \mathfrak{A}(2S_O)^2(2S_N)^2(\sigma_1)^2 \cdots (\sigma_{15})^2(\pi_1)^2 \cdots (\pi_6)^2(l_0')^4(l_0)^2(\pi_7) \cdot \text{spin functions } (\subset A''),$$

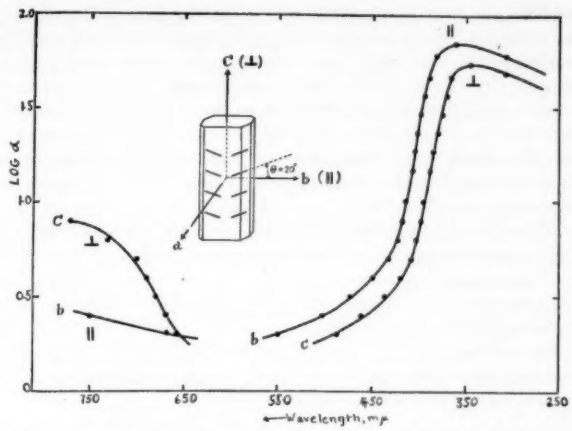

FIG. 1. The dichroism of *m*-nitronitrosobenzene in crystalline state. The ordinate α denotes the absorption coefficient per mm of the crystal. The symbols || or ⊥ mean the spectrum by the light with the electric vector nearly parallel or perpendicular to the molecular plane.

$$\Psi_{e2} = \mathfrak{A}(2S_O)^2(2S_N)^2(\sigma_1)^2 \cdots (\sigma_{15})^2(\pi_1)^2 \cdots (\pi_6)^2(l_0)^2(l_0')^3(\pi_7) \cdot \text{spin functions } (\subset A''),$$

$$\Psi_{e3} = \mathfrak{A}(2S_O)^2(2S_N)^2(\sigma_1)^2 \cdots (\sigma_{15})^2(\pi_1)^2 \cdots (\pi_5)^2(l_0')^4(l_0)^2(\pi_6)(\pi_7) \cdot \text{spin functions } (\subset A'),$$

where Ψ_g, Ψ_{e1}, Ψ_{e2}, and Ψ_{e3} are the wave functions for the ground and excited states; $(2S_N)$ and $(2S_O)$, the 2*S* A.O. of the N and O atoms; σ_i and π_i the *i*th σ and π M.O.; l_0 and l_0' the $2p\sigma$ lone pair orbitals of the NO and NO_2 groups, respectively, and $\mathfrak{A}$ the antisymmetrizer.

The three components of the dipole moment P_x, P_y, and P_z (see Fig. 2) evidently have the symmetry P_x, $P_y \subset A'$, $P_z \subset A''$,

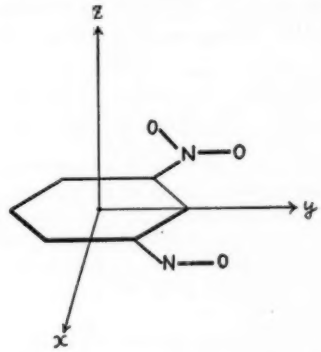

FIG. 2.

respectively. Hence, the features of the dipole strengths are given as shown in Table I.

As a result, three kinds of transitions are possible, i.e., two $n \rightarrow \pi$ (nitro- and nitroso-) and one $\pi \rightarrow \pi$ transitions. In the $\Psi_g \rightarrow \Psi_{e1}$ or Ψ_{e2} $(n \rightarrow \pi)$ transitions, the ⊥ absorption is allowed, whereas the || absorption is forbidden. On the other hand, in the $\Psi_g \rightarrow \Psi_{e3}(\pi \rightarrow \pi)$ transition, the || absorption is allowed, whereas the ⊥ absorption is forbidden.

The above theoretical conclusions are in fair agreement with the foregoing spectroscopic observation. From the standpoint of dichroic property, the band at 360∼350 mμ is interpreted as the absorption due to the $\pi \rightarrow \pi$ transition. In other words, it is the absorption due to the π-electron of the benzene ring perturbed by

TABLE I.

Transitions	$\int \Psi_g P_x \Psi_e d\tau$,	$\int \Psi_g P_y \Psi_e d\tau$	$\int \Psi_g P_z \Psi_e d\tau$
$\Psi_g \rightarrow \Psi_{e1}(n \rightarrow \pi)$	zero (forbidden)		nonzero (allowed)
$\Psi_g \rightarrow \Psi_{e2}(n \rightarrow \pi)$	zero (forbidden)		nonzero (allowed)
$\Psi_g \rightarrow \Psi_{e3}(\pi \rightarrow \pi)$	nonzero (allowed)		zero (forbidden)

the NO and NO_2 groups. As required by the above theory, the || absorption is hyperchromic to the ⊥ absorption in this band. This result suggests that the general rule regarding the dichroism of the benzene ring[4] holds also for the present band.

The band at 760 mμ is attributed to one of the $n\rightarrow\pi$ transitions, since the ⊥ absorption is hyperchromic to the || absorption. As the nitro-band does not appear at such a long wavelength,‡ it must be the absorption resulting from the nitroso $n\rightarrow\pi$ transition. The weak nitro-band which should appear in the region between *ca* 400∼390 mμ would be covered by the intense $\pi\rightarrow\pi$ absorption.

As a conclusion, a direct evidence for a real existence of the $n\rightarrow\pi$ transition has been offered by the present theoretical consideration on the measurement of the dichroism of *m*-nitronitrosobenzene in crystalline state.

The authors wish to express their sincere thanks to Professor R. Tsuchida and Assistant Professor S. Seki for their kind advice and encouragement throughout this work.

[1] H. McConnell, J. Chem. Phys. **20**, 700 (1952).
[2] R. S. Mulliken, J. Chem. Phys. **3**, 564 (1933); **7**, 121 (1939); H. L. McMurry, J. Chem. Phys. **9**, 231 (1941).
[3] K. Nakamoto, Bull. Chem. Soc. Japan **25**, 255 (1952).
* Here, the C−N−O bond of the nitroso group is assumed to be coplanar with the benzene plane. However, a recent study of the x-ray analysis of *p*-bromonitrosobenzene dimer by C. Darwin and D. C. Hodgkin (Nature **166**, 827 (1950)) suggests the validity for the above assumption. Moreover, the fact that the identity period along the *c* axis in *m*-dinitrobenzene crystal does not change when it forms solid solution with *m*-nitronitrosobenzene may also support this assumption.
† The dichroism of *m*-nitronitrosobenzene monomer in Fig. 1 has been calculated from the measurement of dichroism of the solid solution of *m*-dinitrobenzene with *m*-nitronitrosobenzene. As for the detailed experimental facts, see the original article (reference 3).
[4] Nakamoto, Kobayashi, and Tsuchida, J. Chem. Soc. Japan **70**, 14 (1949); K. Nakamoto, J. Am. Chem. Soc. **74**, 392 (1952).
‡ The nitro- and nitroso-bands in the spectrum of an alcoholic solution of *m*-nitronitrosobenzene occur at 390 and 750 mμ, respectively (see reference 3).

The Molecular Spectra of Condensed Oxygen and the O_4 Molecule*

A. Lee Smith and Herrick L. Johnston
The Cryogenic Laboratory and Department of Chemistry, The Ohio State University, Columbus, Ohio
(Received October 17, 1952)

WHILE the infrared[1] and Raman[2,3] spectra of liquid oxygen have hitherto failed to reveal any molecular vibrations which might be ascribed to O_4, it is the purpose of this letter to point out certain unusual features of the molecular spectra of condensed oxygen which, although they cannot be interpreted unambiguously as arising from O_4, are at least consistent with the concept.

Infrared and Raman spectra of liquid and solid oxygen and liquid oxygen-nitrogen mixtures were taken in this laboratory using apparatus previously described.[4,5] The infrared spectrum of pure liquid oxygen in layers up to 16 mm thick was examined from 400 to 4000 cm^{-1}, and, besides the absorption at 1557 cm^{-1}, only an overtone band with its center at 3102 cm^{-1} was found. The Raman spectrum of liquid oxygen was studied, using very long exposures. Exposures up to 56 hours showed 1551 cm^{-1} shifts from the relatively weak 4347 and 4339A mercury lines, but no other Raman lines. No indication was found of the 3049 cm^{-1} line reported by McLennan and McLeod[6] and attributed by them to the $v=0$ to $v=2$ jump (compare the infrared value of 3102 cm^{-1} for this transition). They did not observe this line with 4047A excitation, and it seems probable that the line at 3049 cm^{-1} or 5026.5A (using Hg 4358A) is actually Hg 5025.6A. We have also observed the Raman spectrum of solid γ-oxygen, and find a single shift of 1552 cm^{-1}.

Since, in the infrared spectrum, the absorption coefficient for the fundamental vibration of liquid oxygen is roughly twice that for liquid nitrogen,[7] it was first thought that the O_4 molecule might be contributing to the absorption intensity. Therefore, a series of spectra of liquid oxygen-nitrogen solutions were studied to see if Beer's law held. Oxygen showed an apparent decrease in absorption coefficient with decreasing concentration, but the variation was within the experimental error and the results were inconclusive.

It was also noted that the calculated rotational band envelopes for liquid and solid oxygen did not agree with those observed

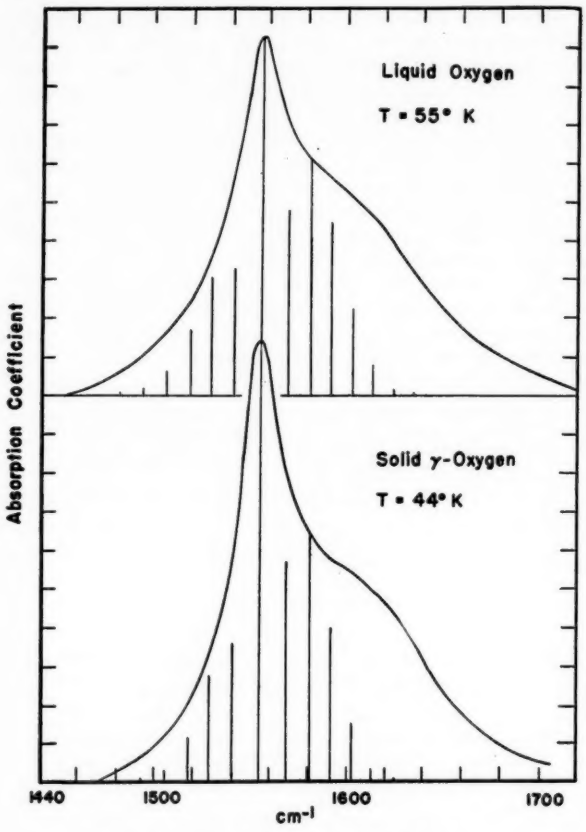

FIG. 1. Infrared spectra of condensed oxygen.

(Fig. 1). This is to be expected for a condensed phase, but the unexpected result is that the observed envelope covers a considerably greater frequency range then the calculated structure for both liquid and solid γ-oxygen would indicate. Furthermore, the same strong shoulder appears in both phases[7] at 1610 cm^{-1}, and γ-oxygen is supposed to consist entirely of O_4 molecules.[8] Thus, one might suspect that this shoulder is connected with the

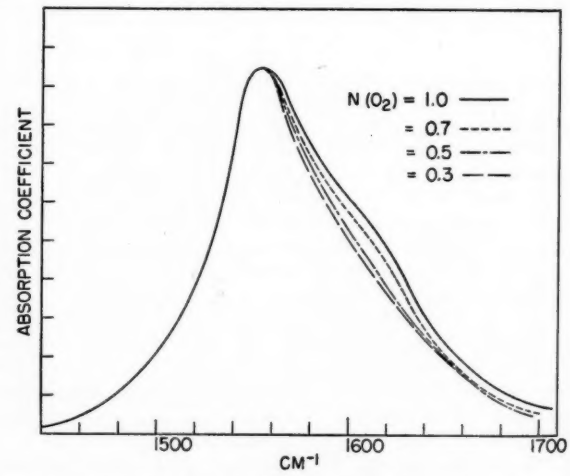

FIG. 2. Variation of absorption coefficient with concentration.

vibrations of the oxygen dimer. Plots of the absorption coefficient for oxygen in nitrogen solutions show that the shoulder apparently disappears with decreasing oxygen concentration (Fig. 2 shows the absorption coefficient as a function of the mole fraction of oxygen at a temperature of 78°K). Exactly this behavior would result if the shoulder were due to O_4, whose concentrations depend on the square of the oxygen concentration. In so far as could be determined, the nitrogen fundamental showed no such change in character with decreasing nitrogen concentration.

The fact that the band appears on the high frequency side of the unchanged fundamental frequency may be more readily visualized by the rather crude analogy of two weakly coupled oscillators, each of reduced mass μ and coupled by a potential of the form $V=\frac{1}{2}k(x_1-x_2)^2$ (where x_1 and x_2 are the displacements). Two frequencies arise: one, the same as the original ω_0 and a higher one, $\omega_0+(k/\mu)\omega_0$. It is possible, however, that the anomalous shoulder may arise from other sources, and further work is necessary before definite conclusions can be drawn.

In view of the small heat of dissociation of the O_4 molecule (about 130 cal per mole[1]), it is not surprising that the spectrum does not show discrete vibrational lines due to O_4.

We are indebted to Professor W. H. Shaffer for suggesting the coupled oscillator analogy.

* This work was supported in part by the ONR under contract with the Ohio State University Research Foundation.

[1] Crawford, Welsh, and Locke, Phys. Rev. **75**, 1607 (1949).
[2] B. Saha, Indian J. Phys. **14**, 123 (1940).
[3] Crawford, Welsh, and Harrold, Can. J. Phys. **30**, 81 (1952).
[4] Holden, Taylor, and Johnston, J. Opt. Soc. Am. **40**, 757 (1950).
[5] Taylor, Smith, and Johnston, J. Opt. Soc. Am. **41**, 91 (1951).
[6] J. C. McLennan and J. H. McLeod, Nature **123**, 160 (1929).
[7] Smith, Keller, and Johnston, Phys. Rev. **79**, 728 (1950).
[8] L. Vegard, Nature **136**, 720 (1935).

The Third Virial Coefficient of Ethane

H. G. David, S. D. Hamann, and R. G. H. Prince
C.S.I.R.O. Division of Industrial Chemistry, High Pressure Laboratory, Sydney University, Sydney, Australia

(Received October 15, 1952)

THE product pV/RT for a gas is frequently expressed by the power series

$$pV/RT=1+B(T)/V+C(T)/V^2+\cdots, \quad (1)$$

$$pV/RT=1+B'(T)p+C'(T)p^2+\cdots. \quad (2)$$

$B(T)$, $C(T)$, $\cdots$ are customarily called the second, third, $\cdots$ virial coefficients, and they are related to $B'(T)$, $C'(T)$, $\cdots$ by the formulas

$$B(T)=B'(T)RT, \quad C(T)=[B'(T)^2+C'(T)]R^2T^2, \cdots. \quad (3)$$

Bird, Spotz, and Hirschfelder[1] have calculated the third virial coefficient $C(T)$ for gases whose molecules interact according to a Lennard-Jones 12, 6 potential, and they have compared their theoretical figures with the experimental third virial coefficients for a number of gases. Among these experimental data were some values of $C(T)$ for ethane which Bird, Spotz, and Hirschfelder derived from the compressibility measurements of Michels and Nederbragt.[2] They were $C(273.16)=-37{,}300$, $C(298.16)=-72{,}100$, $C(323.16)=-30{,}900$ cm^6 mole^{-2}. Both in their negative sign and in their large magnitude, these figures are in contrast to all the other experimental data and are in conflict with the theory of $C(T)$. We believe that they were based on a faulty analysis of the experimental results.

It would appear that, for ethane, Bird, Spotz, and Hirschfelder fitted pV/RT, by the method of least squares, with Eq. (2) (ending the series at $C'(T)p^2$) and then used the conversion (3) to find $C(T)$. We have applied this procedure to the same experimental data and found that it gives $C(T)$ in good agreement with the figures quoted above. But at the same time we observed that the quadratic in p is a very bad fit of the experimental results when there are more than three points. The disagreement is much greater than the experimental inaccuracy and means that insufficient terms have been used and that the coefficients are therefore highly suspect. Fitting a limited pressure series for pV/RT is, in general, an unreliable way of calculating the virial coefficients unless the reduced temperature is high.

On the other hand, we have found that the expansion of pV/RT in powers of density [Eq. (1)] gives an excellent fit of Michels and Nederbragt's data, even when it stops at the term $C(T)/V^2$. The two expansions are compared in Table I. The coefficients in the

TABLE I. Experimental and fitted values of $1-pV/RT$ for ethane at 25°C.

p (atmos)	0	10	20	30	40
Experimental $(1-pV/RT)$	0	0.0809	0.1737	0.2882	0.4695
Quadratic in p $(1-pV/RT)$	0	0.0705	0.1712	0.3020	0.4630
Quadratic in $1/V$ $(1-pV/RT)$	0	0.0807	0.1736	0.2884	0.4695

density formula are $B(273.16)=-223$, $B(298.16)=-187$, $B(323.16)=-157$ cm^3 mole^{-1}; $C(273.16)=+11{,}710$, $C(298.16)=+11{,}070$, $C(323.16)=+9660$ cm^6 mole^{-2}. Both the second and third virial coefficients differ markedly from the values listed by Bird, Spotz, and Hirschfelder and both are in much better agreement with theory.

Further information on $C(T)$ for ethane is found in the measurements of Reamer, Olds, Sage, and Lacey.[3] From an analysis of their compressibility factors as functions of the density we have derived the values given in Table II.

TABLE II. $C(T)$ for ethane from the measurements of Reamer, Olds, Sage, and Lacey.

T°K	310.94	344.27	377.60	410.94	444.27	477.60	510.94
$C(T)$ (cm^6 mole^{-2})	+9100	+8300	+7400	+6600	+6000	+5400	+4700

Finally, it is interesting to compare thet wo new sets of $C(T)$ with the theoretical third virial coefficients of Bird, Spotz, and Hirschfelder. This is done in the reduced plot of Fig. 1. The

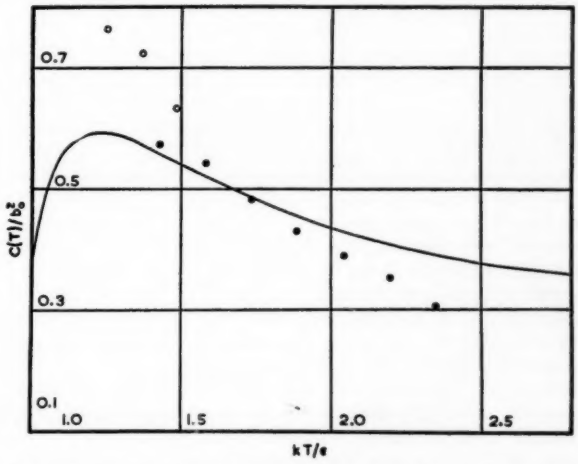

FIG. 1. The reduced third virial coefficient of ethane. The circles represent the data of Michels and Nederbragt; the dots are calculated from the results of Reamer, Olds, Sage, and Lacey. The curve is the theoretical one derived by Bird, Spotz, and Hirschfelder.

parameters b_0 and ϵ, associated with the intermolecular potential, were derived from some second virial coefficients which we had previously calculated[4] from the results of Reamer, Olds, Sage, and Lacey. They are $b_0=123.8$ cm^3 mole^{-1}, $\epsilon/k=217.5$°K. It is seen that ethane shows as good agreement as most gases with the theoretical plot and that the trend in the experimental points parallels the trend in the third virial coefficient of ethylene.[1]

[1] Bird, Spotz, and Hirschfelder, J. Chem. Phys. **18**, 1395 (1950).
[2] A. Michels and G. W. Nederbragt, Physica **6**, 656 (1939).
[3] Reamer, Olds, Sage, and Lacey, Ind. Eng. Chem. **36**, 956 (1944).
[4] S. D. Hamann and W. J. McManamey (to be published).

Luminescence Behavior in Tritium Oxide

W. M. JONES
Los Alamos Scientific Laboratory, University of California, Los Alamos, New Mexico
(Received October 14, 1952)

THIS note describes preliminary observations on solid T_2O luminescence which is due to the tritium radioactivity. Grossweiner and Matheson[1] have observed photographic plate blackening by light from 0.3 percent T tritium oxide at liquid nitrogen temperature and have made observations on x-irradiated ice. In this laboratory the visible luminescence of a T_2O ice crystal was noted by R. M. Potter and E. S. Robinson ($P-R$ sample).

Two 0.07-cc T_2O samples were prepared from CuO and ~99 percent T_2 (as was the $P-R$ sample) and condensed in 4 mm i.d. quartz tubes (method A). The samples were placed in a liquid nitrogen Dewar, with an unsilvered port placed against the slit of a quartz spectrograph or Gaertner monochromator. In the latter case, the photomultiplier output was amplified and recorded, and the prism was driven automatically between 3900–8000A.

When water or ice is placed in a Dewar at 76°K, the intensity at each wavelength rises rapidly to a maximum and decays to a limit.[2] Figure 1 shows total intensity decay. Behavior is repeatable

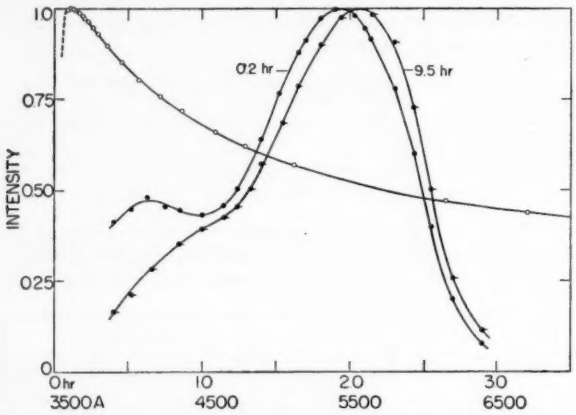

FIG. 1. Luminescence spectra of T_2O ice at 0.2 and 9.5 hr after cooling to 76°K. Total intensity (method B preparation and location) at 76°K *vs* time. Additional intensities at longer times are 0.391 (4.60 hr), 0.350 (5.89 hr), 0.338 (8.29 hr), 0.326 (11.62 hr), 0.327 (13.81 hr). Curves normalized to unit maximum.

after first allowing the ice to warm (melting unnecessary). Similar behavior occurs at 88°K. At 190°K the steady intensity is very rapidly attained and is about 90 percent of peak intensity.

Correction for dispersion and typical photomultiplier response gives spectra at various times, examples of which are shown. Standard lamp calibration of the monochromator-photomultiplier has not yet been made, but the small peak at early times is not removed even by using available abnormal response curves. Spectra from Eastman 103-F and 1-L plates using slit widths down to 0.125 mm are in approximate agreement with the more precise monochromator data and suggest a continuous spectrum. The plates show some intensity down to about 3000A, and the 1-L spectrum gave some intensity to about 8000A.

A tan coloration which fades on warming, develops in the solid at 76°K, e.g., instantly disappears to the eye on plunging into a 190°K bath. Work is in progress on the growth and absorption spectrum in connection with the decay, spectral changes, and their quantitative explanation.

No glow phenomenon was observed in total intensity when a sample was allowed to warm up from 76 to 250°K at rates varying from 4 to 0.7 deg min^{-1}.

Glass luminescence and impurities (e.g., mercury and copper) were suspect, and a different method of sample preparation and mounting was used as follows (method B). A preparation system utilizing break-off seals was doubly trapped with liquid nitrogen before exposure to pumps. No Hg lines were observed with the monochromator during end-on view of a tritium discharge. Oxygen, unexposed to Hg, reacted at the Pd tube through which tritium was diffusing. The ice was freed from gases and condensed into the observation cell. The ice was located at the bottom of a Pt cup which had been hard soldered into a Kovar tube. A Kovar-glass seal allowed filling and observation with 3 cm ice-window separation. A spectrum has not yet been measured, but visual appearance and total intensity as a function of time at 76°K, shown in Fig. 1, are of the same nature as observed with method A. The B viewing method, or a modification, will be needed to eliminate the effect of quartz on spectral details, but the principal luminescence is not due to quartz, since (a) the $P-R$ crystal, formed between two wires in a Ni-wire-filled trap at 76°K, was 3 cm from the nearest glass and definitely self-luminesced; (b) method A ice luminesced in the same way whether viewed from above or directly through quartz; (c) in method B, luminescence intensity depended on ice temperature and not on window temperature; (d) measurements of intensity and spectrum at 76°K on the weak light from packed (silica) and unpacked silica tubes filled with T_2 gas indicate that quartz exerts no large effect on the ice measurements. Tritium decay causes formation of He^3, O_2, and T_2 at 76°K,[3] but the ice showed the same general behavior two days after gas purging as when undisturbed (except for melting and freezing) for several months. Tentatively, we are unable to ascribe any effects to a chemical impurity. No study has yet been made regarding the influence of the physical state of the ice.

It is a pleasure to acknowledge the cooperation of R. T. Phelps and O. R. Simi with the photographic exposures.

[1] L. I. Grossweiner and M. S. Matheson, Argonne National Laboratory, private communication; J. Chem. Phys. **20**, 1654 (1952).
[2] See L. E. Smith, Phys. Rev. **28**, 431 (1926), for similar behavior in $BaBr_2$ and for other references.
[3] In connection with triple point temperature and vapor pressure measurements, T_2O at 76°K was found to give O_2:He:T_2 roughly as 1:0.17:0.0043 by mass spectrometer analysis.

On the Anisotropic Dissolution and the Orientation of the Phosphorescent Dye, Trypaflavin, in the Crystal of Citric Acid

DAIJIRO YAMAMOTO
Department of Chemistry, Tokyo University of Education, Otsuka, Tokyo, Japan
(Received October 6, 1952)

OF many phosphorescent dyes, such as trypaflavin, acridine yellow, fluorescein, rhodamine-B, etc., trypaflavin dissolved best in crystalline citric acid, while others hardly did. The crystal, grown in the supersaturated water solution containing both citric acid and trypaflavin, was rhombic as shown in Fig. 1.

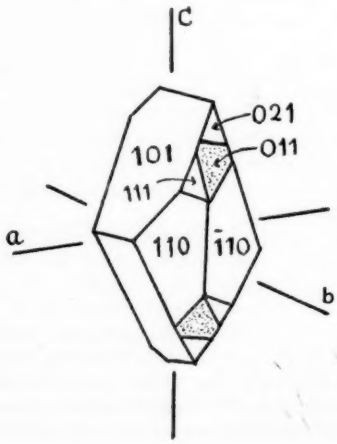

FIG. 1. Citric acid crystal with dissolved trypaflavin. Rhombic. Axial ratio; 0.583:1:0.812. Dotted faces are not colored.

FIG. 2. Phosphorescence emitted from a sheet of citric acid crystal with dissolved dye. Each bright part left and right corresponds to the direction of (110) and ($\bar{1}$10).

There appeared, however, a striking growth of (101) and (110) faces in the crystal instead of (111) face as in a common crystal of citric acid. The quantity of the dye dissolved in one gram of the crystal was about $1.0\sim1.5\times10^{-6}$ mole, as determined by a colorimetric method. The dissolution of the dye was always anisotropic, and the (011), (0$\bar{1}$1), (01$\bar{1}$), and, (0$\bar{1}\bar{1}$) faces were not colored.

TABLE I. Intensities of phosphorescence excited by polarized light.

Vibrational direction of polarized light	No. 1	No. 2	No. 3
$c\parallel$	5.9	10.0	9.0
$c\perp$	1.0	1.0	1.0

This anisotropic dissolution was further determined by means of the examination of phosphorescence emitted by the crystal. Figure 2 is a photograph of the phosphorescence emitted by a sheet, set in a cylindrical phosphorscope of 1800 rpm, and cut about 0.5 mm thick in parallel with the c and b axes and perpendicular to the a axis. There was no phosphorescence in the direction of (011) and (01$\bar{1}$), and the phosphorescence of the sand-clock type appeared just as shown by Rupp[1] in the case of fluorescence emitted by fluorescein-lead acetate crystal.

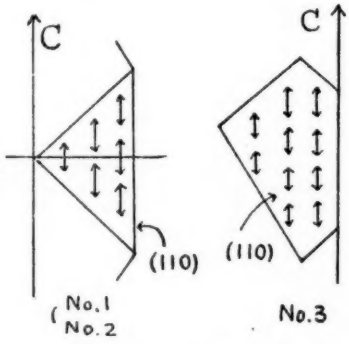

FIG. 3. Direction of the oscillator of the dye molecule in the crystal.

The orientation of the dye molecules in the crystal was examined by means of the excitation by polarized light. The results obtained about (110) face of three different samples are shown in Table I. In the table, the samples No. 1 and No. 2 were cut parallel to the c axis and with the direction of (110), and No. 3 parallel to the (110) plane. Based on the experimental results, the author may suggest that the direction of the oscillator of the dye molecule runs parallel to the c axis as shown in Fig. 3.

[1] H. Rupp, *Die Leuchtmassen und ihre Verwendung* (Berlin, 1937), p. 100.

Ionic Mobility at Grain Boundaries

P. E. GODDARD AND F. URBACH
Kodak Research Laboratories, Rochester, New York
(Received September 26, 1952)

IN view of the significance for a variety of problems of the mobility of ions or atoms at grain boundaries, the experimental result shown in Fig. 1 may be of some interest.

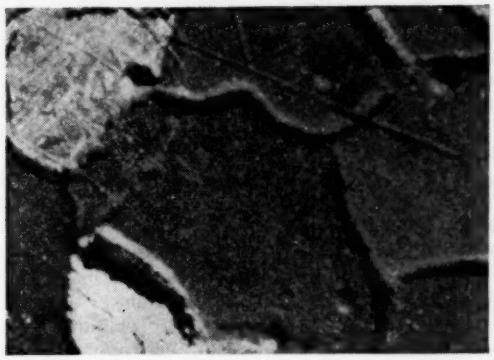

FIG. 1. Ridges along grain boundaries of polycrystalline silver bromide slab formed during electrolysis, approximately four times natural size, light incident under approximately 45 degrees from top.

A cast slab of silver bromide consisting of individual crystals of a few millimeters in linear dimensions was placed between silver nitrate and potassium bromide solutions, each containing a platinum electrode. A potential difference was applied to the electrodes with the positive pole in the silver nitrate solution. Using a slab of a few millimeters thickness and potentials of the order of 100 volts, a constant current could be obtained, sufficient to deposit in several hours a few milligrams of silver bromide on the potassium bromide side of the slab, while no appreciable change took place on the silver nitrate side. This corresponds to the well-known fact that the mobility of the silver ion is far preponderant in the ionic conductivity of silver bromide. The weight increase of the silver bromide slab corresponded closely, as it should, to the current integral.

In all of the experiments, inspection of the added silver bromide layer disclosed an appearance like that shown in Fig. 1. Ridges of silver bromide appeared at the boundaries of the variously oriented crystals of the slab, which were also distinguishable before electrolysis by differences in light reflection. (The latter are emphasized in the photograph by suitable illumination.) It is clearly seen that the transport of silver ions through the slab occurs preferentially at the grain boundaries.[1] The ridges are at least twice as high as the halide deposit between them. Whether the latter is due to conduction through nearly perfect crystals or whether it is supplied from the ridges cannot be conclusively answered by the present experiments. Some indications favor the first alternative. The pits visible in Fig. 1 are a result of the casting procedure, and the nearly straight lines are slight scratches on the slab surface; both were present before the electrolysis.

These experiments were undertaken about two years ago, and several undesirable complications caused us to discontinue them. The preferential mobility of the silver ions at grain boundaries, however, appears clearly illustrated.

[1] I. Shapiro, and I. M. Kolthoff, J. Chem. Phys. **15**, 41 (1947).

Some Methods of Determining Molecular Constants

D. H. RANK
The Pennsylvania State College, State College, Pennsylvania
(Received September 22, 1952)

THE rotational energy levels of a diatomic or linear polyatomic molecule may be represented by the well-known expression[1]

$$F_v(J)=B_vJ(J+1)-D_vJ^2(J+1)^2+\cdots, \quad (1)$$

where the molecular constants B_v and D_v have their usual significance.

The general practice has been to determine the molecular constants by means of graphical methods which have the advantag

of being rapid, moderately precise, and capable of showing gross perturbations which may be present. Herzberg[2,3] has given very complete treatment with examples of the various graphical methods available for determining molecular constants. Birge[4] and Birge and Shea[5] have given general and approximate least mean squares methods of deriving molecular constants by analytical methods. Rank, Ruth, and Vander Sluis[6] have recently demonstrated the statistical procedures necessary to obtain extremely accurate molecular constants for parallel type bands using least mean squares methods.

The advent of microwave spectroscopy, with the fantastic precision obtained for the rotational constants of the ground state of many molecules, allows the determination of molecular constants in many cases for excited states by analytical least mean squares methods without an inordinate amount of labor and with correspondingly improved precision.

In this discussion we shall limit ourselves to two cases which are of very common occurrence: (1) fragmentary bands where the J numbering can be decided but, owing to a large number of missing or blended lines, only a small number of Δ_2F's can be obtained; (2) cases where the microwave B'' value for the ground state has been accurately determined.

The general expression representing the P and R branches of the type of band here under discussion is given by the following well-known equation:

$$\nu(m)=\nu_0+(B'+B'')m+(B'-B''-D'+D'')m^2 -2(D'+D'')m^3-(D'-D'')m^4+\cdots, \quad (2)$$

where $R(J)=\nu(m-1)$, $P(J)=\nu(-m)$, and B and D have their usual significance (the primes and double primes referring to the upper and lower states, respectively). ν_0 is the band origin and $\nu(m)$ the frequencies of the particular band lines. In many cases of infrared rotation, vibration bands D' and D'' are practically indistinguishable. Thus, we can make the approximation, especially if m is not very large so that $D'=D''=D$ and Eq. (2) becomes

$$\nu(m)=\nu_0+(B'+B'')m+(B'-B'')m^2-4Dm^3. \quad (3)$$

Case I. Fragmentary bands.—Once the numbering of the lines of the band has been established, the molecular constants can be determined by fitting the data to the following set of least mean squares equations:

$$\begin{aligned} an+b\Sigma m+c\Sigma m^2+d\Sigma m^3&=\Sigma y,\\ a\Sigma m+b\Sigma m^2+c\Sigma m^3+d\Sigma m^4&=\Sigma ym,\\ a\Sigma m^2+b\Sigma m^3+c\Sigma m^4+d\Sigma m^5&=\Sigma ym^2,\\ a\Sigma m^3+b\Sigma m^4+c\Sigma m^5+d\Sigma m^6&=\Sigma ym^3, \end{aligned} \quad (3a)$$

where $a=\nu_0$, $b=B'+B''$, $c=B'-B''$, $d=-4D$, the y's are the frequencies of the band lines, and n the number of band lines.

It should be pointed out that Eq. (3a) applies to complete as well as fragmentary bands but is particularly useful for the latter bands since, in general, one is able to make use of much more experimental data than can be done with Δ_2F methods of determining the constants.

Case II. Microwave B'' known.—Using the same degree of approximation as in Case I, we can write

$$f(B')=y-\nu_0-B''(m-m^2)+4Dm^3=B'(m+m^2). \quad (4)$$

Using B'' microwave, and D and ν_0' determined from Eq. (3a) above, one can calculate a value of B' from each band line, i.e., for each value of m. If the value of ν_0 is not quite correct as obtained in the approximation (3a), these approximate values of B', which we shall call B_a', will show a variation across the band. The correct value of B' we shall call B_c' (i.e., constancy of B_a' values across the band). It is easy to show that

$$B_a'=B_c'-\Delta\nu_0/(m+m^2), \quad (5)$$

where $\Delta\nu_0$ is the shift of the band origin necessary to produce constancy of the B_a' values. If B_a' *vs* $1/(m+m^2)$ is plotted, it can be seen that the intercept yields $B_c'\equiv B'$ and the slope is the necessary correction to the band origin found from Eq. (3a).

[1] For detailed discussion see G. Herzberg, *Spectra of Diatomic Molecules* (D. Van Nostrand Company, Inc., New York, 1950), Chapters III and IV.
[2] G. Herzberg, *Spectra of Diatomic Molecules* (D. Van Nostrand Company, Inc., New York, 1950).
[3] G. Herzberg, *Infrared and Raman Spectra* (D. Van Nostrand Company, Inc., New York, 1951).
[4] R. T. Birge, Revs. Modern Phys. **19**, 298 (1947).
[5] R. T. Birge and J. D. Shea, Univ. Calif. Pubs. Math. **2**, 67 (1927).
[6] Rank, Ruth, and Vander Sluis, J. Opt. Soc. Am. **42**, 693 (1952).

Internal Rotation in Dichlorobutine

YONEZO MORINO, ICHIRO MIYAGAWA AND AKIYOSHI WADA
Department of Chemistry, Faculty of Science, Tokyo University, Bunkyo-ku, Tokyo, Japan
(Received October 13, 1952)

DICHLOROBUTINE $ClH_2C-C\equiv C-CH_2Cl$ will provide an interesting case for internal rotation, because the two C−Cl dipoles are situated at far more distant positions (5.37A in the *cis* position) than 1,2-dichloroethane, and the axis $C-C\equiv C-C$ puts no restriction on the rotation.[1] For the purpose of evaluating the hindering potential in this molecule, the dipole moment was measured in carbon tetrachloride and benzene solutions in the temperature range from −20 to +60°C. The sample was kindly prepared by Professor O. Shimamura of this institute, its boiling point being 34.5–35.0°/4.8 mm. The result is given in Table I, which clearly shows that the dipole moment increases with temperature, so that the rotation is evidently hindered in this molecule.

TABLE I. The molecular polarization and dipole moment of dichlorobutine.[a]

Carbon tetrachloride solution			Benzene solution		
temp. (°C)	$P_{2\infty}$(cc)	$\mu(D)$	temp. (°C)	$P_{2\infty}$(cc)	$\mu(D)$
−18.5	116.0	1.88	...	...	...
+1.5	113.4	1.92	+10	108.8	1.90
+25	108.5	1.95	+30	106.4	1.93
+55	103.8	1.97	+50	102.9	1.95

[a] Atomic polarization is assumed to be 5 percent of the electronic polarization, i.e., $P_E+P_A=29.8$ cc.

Since the two CH_2Cl groups in this molecule are situated far apart, the steric repulsions between the chlorine and hydrogen atoms must be so small that the hindering potential may be mainly due to the electrostatic forces. Accordingly, the hindering potential may be the form used by Smyth[2]: $V=(\bar{V}_0/2)(1-\cos\theta)$, where θ denotes the angle of internal rotation, $\theta=0$ corresponding to the *trans*-position. Assuming this potential the observed values in Table I give the potential barrier $V_0=0.75\pm0.20$ kcal and the moment perpendicular to the rotational axis $\mu_\perp=1.64\pm0.20$D for carbon tetrachloride solution. Almost the same values were obtained also for benzene solution, though not so accurately as the former because of the smaller temperature range of the measurement in the latter solution. Of course, the hindering potential of a free molecule should be obtained from the measurement in the gaseous state. However, in such a case as dichlorobutine, the value of the hindering potential obtained in solutions may not be far from that of the free molecule. The reason is that the change of the hindering potential by solvents was found to be due to the Onsager's reaction field,[3] while in dichlorobutine which has two dipoles in the extreme ends of a long straight molecule, each dipole reacts by itself with the surrounding media, so that the contribution of the reaction field to the hindering potential is considered to be small.

The hindering potential barrier due to the electrostatic force between the dipoles is estimated to be $V_0=0.5$ kcal, assuming the bond moments of C−Cl and C−H to be 1.5D and 0.4D, respectively, each dipole locating at the point 0.77A, the radius of carbon atom, from the center of each carbon atom. Almost the same values

are obtained by other reasonable assumptions. If we take into consideration the fact that the C—Cl bond of this molecule has the possibility of larger ionic character, as evidenced by the abnormally larger C—Cl distance in propargyl chloride,[4] the electrostatic potential may be larger than that calculated above and come nearer to the observed value. Thus, we can safely conclude the hindering potential of this molecule is mainly due to the electrostatic interaction of the dipoles in the rotating groups.

It should be mphasized that the moments obtained in benzene solution are almost the same as those in carbon tetrachloride, and, in particular, they show an increase with temperature. This result stands out in sharp contrast to that of dichloroethane,[5] which indicated an abnormally larger dipole moment in benzene solution. This "benzene effect" was interpreted by the assumption[6] that their molecules associate in benzene solution with the solvent molecules. As stated above, in dichlorobutine the distance between the two chlorine atoms is larger than the diameter of benzene molecule, so that the special association such as found in dichloroethane may not take place in this case.

The details will be published elsewhere in the near future. We are grateful to Professor O. Shimamura for his kindness in preparing the sample of dichlorobutine.

[1] B. L. Crawford, Jr., and W. W. Rice, J. Chem. Phys. **7**, 435 (1939); G. B. Kistiakowsky and W. W. Rice, J. Chem. Phys. **8**, 618 (1940); Osborne, Garner, and Yost, J. Chem. Phys. **8**, 131 (1940).
[2] R. A. Oriani and C. P. Smyth, J. Chem. Phys. **17**, 1174 (1949).
[3] Watanabe, Mizushima, Masiko, Sci. Pap. Inst. Phys. Chem. Research (Tokyo) **40**, 425 (1943); J. Powling and H. J. Bernstein, J. Am. Chem. Soc. **73**, 1815 (1951).
[4] Pauling, Gordy, and Saylor, J. Am. Chem. Soc. **64**, 1753 (1942).
[5] Mizushima, Morino, and Higashi, Sci. Pap. Inst. Phys. Chem. Research (Tokyo) **25**, 159 (1934).

The Effect of Hydrogen Bonding on the Hindered Rotation of the Hydroxyl Group in Alcohols

A. V. Stuart and G. B. B. M. Sutherland
Physics Department, University of Michigan, Ann Arbor, Michigan
(Received September 26, 1952)

It has been shown by Dennison and his co-workers[1,2] that in gaseous methyl alcohol, the OH group executes a hindered rotation (or libration) about the CO axis and that the height of the potential barrier hindered free rotation is about 380 cm^{-1} (1.1 kcal/mole). If one regards this motion as a libration, then the value of the corresponding normal frequency is approximately 225 cm^{-1}. However, the motion is far from simple harmonic, and the infrared absorption due to this libration extends from about 700 cm^{-1} to below 50 cm^{-1} for isolated CH_3OH molecules in the gaseous state. When methyl alcohol is in the liquid state, where it is known that hydrogen bonding exists between the OH groups of neighboring molecules, it is to be expected that the hindred rotation will be completely inhibited and this motion will now more closely resemble the usual type of fundamental vibration. One would also anticipate that the value of the fundamental frequency would be very much greater than 225 cm^{-1}, since the restoring forces will have increased considerably.

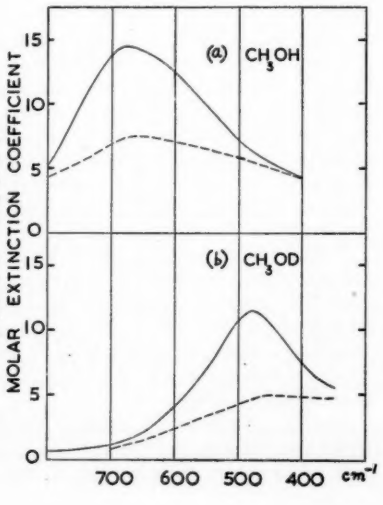

FIG. 1. (a) Infrared absorption of CH_3OH in CS_2 and CCl_4 solution at concentration of 1.50 moles/liter (——) and 0.15 moles/liter (– – –). (b) Infrared absorption of CH_3OD solution in CS_2 and CCl_4 at concentrations of 1.50 moles/liter (——) and 0.15 moles/liter (– – –). The CS_2 was used from 800 to 650 cm^{-1} and CCl_4 from 650 to 350 cm^{-1}.

Investigation of the infrared spectra of a series of alcohols reveals a broad absorption band starting about 800 cm^{-1}, reaching a maximum near 670 cm^{-1} and extending to beyond 500 cm^{-1}. If, by deuteration, the OH group is converted into an OD group, this band is found to shift to lower frequencies, the maximum now being found close to 475 cm^{-1} in the case of methyl alcohol (Fig. 1). Since the ratio of the frequencies of maximum absorption is almost exactly $\sqrt{2}$, the 670 cm^{-1} band must be due to a pure deformation vibration of the OH group. It seems most probable that it is the deformation vibration in which the hydrogen moves at right angles to the COH plane, i.e., the motion which in this gaseous state becomes the hindered rotation of the OH group.

If the hydrogen bonds are now broken up by diluting the alcohol to a low concentration in carbon disulfide or carbon tetrachloride, one would expect the 670 cm^{-1} band to disappear and be replaced by a band at lower frequencies. The effect of dilution on this band in CH_3OH and CH_3OD is also illustrated in Fig. 1. This dilution effect has been checked for a large number of alcohols. It will be seen that the intensity of this band does decrease enormously when the molar concentration is lowered to a point where the degree of hydrogen bonding is known to be low from studies on the OH stretching frequency near 3250 cm^{-1}. It has not yet been possible to determine where this band moves to on dilution, but studies are being continued in the low frequency region. It is interesting and significant that this 670 cm^{-1} band has a broad diffuse shape, very similar in extent to the well-known hydrogen-bonded OH stretching frequency near 3250 cm^{-1}.

The effect of hydrogen bonding on the in-plane OH deformation vibration has also been studied. The results here are not so straightforward and will be presented in a subsequent publication.

[1] J. S. Koehler and D. M. Dennison, Phys. Rev. **57**, 1006 (1940).
[2] D. C. Burkhard and D. M. Dennison, Phys. Rev. **86**, 108 (1951).

Note on the Free Volume Equation of State for Hard Spheres

Louis H. Lund
Missouri School of Mines and Metallurgy, Rolla, Missouri
(Received October 14, 1952)

In a recent Letter to the Editor, Wood[1] has given an exact solution for a system composed of rigid spheres to the following integral equation derived by Kirkwood[2] in his critique of the free volume theory of the liquid state

$$\varphi(\mathbf{r}) = \exp\beta[\alpha - \psi(\mathbf{r})],$$

$$\psi(\mathbf{r}) = \sum_1 \int_{cell} V_{11}(\mathbf{R}_{11} + \mathbf{r} - \mathbf{r}') \exp[\beta(\alpha - \psi(\mathbf{r}'))]dv', \quad (1)$$

$$\exp -\beta\alpha = \int_{cell} \exp -\beta\psi(\mathbf{r})dv = v_f,$$

where $\varphi(\mathbf{r})$ is the configurational distribution function for a molecule in its cell, and the terms in $\bar{E}$, the energy with all molecules at their cell centers, are omitted since it is here zero.

Wood has considered a face-centered cubic lattice and chosen as the cell the dodecahedron Δ of Buehler *et al.*[3] The nearest neighbor distance a and volume per molecule v are related by $a^3 = \sqrt{2}(v)$, and the minimum volume per molecules is $v_0 = r_0^3/\sqrt{2}$, where r_0 denotes the diameter of the sphere. His solution for the system of Eq. (1) is

$$\psi(\mathbf{r}) = \begin{cases} 0 & \text{if } r \text{ is in } \Delta' \\ \infty & \text{if } r \text{ not in } \Delta', \end{cases} \quad (2)$$

where Δ' is the free volume $(v^{\frac{1}{3}} - v_0^{\frac{1}{3}})^3$ per molecule and is a dodeca-

hedron similar to Δ but with altitude $(a-r_0)/2$ instead of $a/2$. The equation of state may also be obtained.

It would appear that the solution (2) will hold for other types of molecular packing where it is possible to define and estimate a free volume; that is, in those cases where the potential within the cell is uniform and is effectively infinite at the boundary. In the case of cubic packing where one molecule may be considered oscillating at the origin, with the six nearest neighbors regarded as fixed in their mean positions along three axes, the free volume per molecule may easily be shown to be

$$v_f = 8(v^{\frac{1}{3}} - r_0)^3, \tag{3}$$

where v is the mean volume per molecule and r_0 the diameter of the molecule. It is reasonable that Eq. (3) will hold approximately for other kinds of molecular packing with the "8" replaced by a different constant.

Thus, one might conclude that the solution (2) would hold for many molecular packings of rigid spheres where it is feasible to define a free volume and where one may have

$$\varphi(r) = \begin{cases} 1/v_f & \text{if } r \text{ inside } v_f \\ 0 & \text{if } r \text{ outside } v_f. \end{cases}$$

[1] William W. Wood, J. Chem. Phys. **20**, 1334 (1952).
[2] J. G. Kirkwood, J. Chem. Phys. **18**, 380 (1950).
[3] Buehler, Wentorf, Hirschfelder, and Curtis, J. Chem. Phys. **19**, 61 (1951).

Effect of Opposed Disubstitution on Intensities of Even-Even Electronic Transitions

HARDEN MCCONNELL
Shell Development Company, Emeryville, California
(Received October 7, 1952)

THE theory of spectroscopic moments devised by Platt[1] has been used by him for the experimental determination of the *even-odd* $(g-u)$ character of electronic wave functions of excited singlet states of centrally symmetric molecules.[2,3] One feature of this theory is the prediction that the absorption intensities of "forbidden" even-even $(g\rightarrow g)$ electronic transitions in centrally symmetric molecules are not affected by opposed disubstitutions, such as, for example, 2,6-dimethyl substitution in naphthalene. The purpose of this letter is to point out that (a) the above prediction is strictly valid only to within the limits of the Born-Oppenheimer approximation (neglect of perturbations of electronic wave functions by nuclear vibrations) and (b) by inclusion of corrections to this approximation in the spectroscopic moment theory, it is possible to obtain an improved prediction of intensity changes of $g\rightarrow g$ transitions produced by opposed disubstitution in centrally symmetric molecules. Failure of a transition of unknown symmetry to conform at least qualitatively to this new prediction for $g\rightarrow g$ transitions can be taken as evidence that the transition is not $g\rightarrow g$ but $g\rightarrow u$.

The absorption intensity which a $g\rightarrow g$ transition "steals" from a strongly allowed $g\rightarrow u$ transition can be approximated by first-order perturbation theory. This stolen intensity depends in part on the difference in energy of the g and u excited states. Disubstitution can change this energy difference and thereby change the $g\rightarrow g$ transition intensity. A simplified calculation shows that the equation,

$$\epsilon = \epsilon_0[1-(\Delta\nu/\nu)]^2, \tag{1}$$

relates the intensity (ϵ_0) of the $g\rightarrow g$ transition in the unsubstituted molecule to the intensity (ϵ) of this transition in the disubstituted molecule. In Eq. (1), ν is the frequency separating the g and u electronic states, and $\Delta\nu$ is the change of this frequency produced by opposed disubstitution. More detailed expressions relating ϵ and ϵ_0 can be derived, but for many molecular spectra it appears reasonable that ν can be taken as the frequency separating a 0, 1 vibrational state of the weak transition (whose excited state symmetry is to be determined) and a 0, 0 vibrational state of a strong allowed $g\rightarrow u$ transition; ϵ and ϵ_0 in Eq. (1) then apply the intensities of the 0, 1 band of the $g\rightarrow g$ transition.

Equation (1) predicts that on opposed disubstitution the intensity of a $g\rightarrow g$ transition will (a) decrease if $\Delta\nu$ is positive, (b) increase if $\Delta\nu$ is negative, or (c) remain practically unaltered if $(\Delta\nu/\nu)\ll 1$. Sufficient experimental data are not available for an adequate test of these predictions. It is noteworthy, however, that the effect of opposed dimethyl substitutions in naphthalene on the intensity of the $^1A-{}^1L_b$ transition cannot be accounted for by Eq. (1); this result is consistent with the previously assigned u symmetry of this ^1L_b excited state.[1,3,4] Also, 9, 10-dimethyl substitution in anthracene decreases the intensity of the $^1A-{}^1C_b$ transition to an extent compatible with Eq. (1); this result is consistent with the previously assigned g symmetry of the ^1C_b state of anthracene at 45,000 cm^{-1} and the assumption that the ^1C_b state steals intensity from the nearby strongly allowed ^1B_b (u) state at 39,500 cm^{-1}.[3,4] Further discussion of these predictions will be deferred until more data are available.

[1] J. R. Platt, J. Chem. Phys. **19**, 263 (1951).
[2] J. R. Platt, J. Am. Chem. Soc. **74**, 2376 (1952).
[3] J. R. Platt, J. Chem. Phys. **19**, 1418 (1951).
[4] R. A. Friedel and M. Orchin, *Ultraviolet Spectra of Aromatic Compounds* (John Wiley and Sons, Inc., New York), Spectrograms 195, 202, 207 and 388, 390.

Molecular Weight of Potato Amylopectin as Determined by Light Scattering*

L. P. WITNAUER AND F. R. SENTI†
Eastern Regional Research Laboratory, United States Department of Agriculture, Philadelphia, Pennsylvania
AND
M. D. STERN
Department of Chemistry, Temple University, Philadelphia, Pennsylvania
(Received September 22, 1952)

MOLECULAR weights reported for amylopectin range from less than 200,000, as determined by end-group methods,[1] to 230 million by the light-scattering method.[2] We report here the results of light scattering measurements on potato amylopectin in water solutions and on acetylated amylopectin in several organic solvents.

Potato starch (potassium form[3]) was dispersed with vigorous stirring in water at 90°. The amylose was precipitated with pentanol. Amylopectin recovery was 90 percent. Scattering was measured[4,5] at angles with 135 to 22°. Reliable extrapolation to 0° could be made, proving the absence of large particles of dirt or microgel in the solutions. Concentrations ranged from 10^{-4} to 10^{-3} g/ml. Solutions were centrifuged at 40,000 rpm and then passed through ultrafine sintered glass filters. Three molecular weight determinations averaged 36 million$\pm$10 percent. Values at 546 and 436 mu for a series of solutions of varying concentration agreed to $\pm$5 percent. The 90° scattering was unaffected by temperature in the range 25 to 75°. An amylopectin solution 0.5 *N* in sodium hydroxide was heated two hours at 90°. It showed less than 10 percent decrease in turbidity if oxygen was absent. An amylopectin solution was heated one hour at 120° in a sealed tube free from oxygen without appreciable change in turbidity. These results indicate that if the light-scattering particles are aggregates they are not broken up by temperature or alkali. In acetone solution the acetate of this amylopectin had a molecular weight (corrected for 40 percent acetyl content) of 38 million.

Nine fractions were obtained by adding ethanol to a water solution of this amylopectin containing 0.1 percent sodium chloride. The molecular weight of the fractions, which represented 93 percent of the amylopectin, ranged from 52 to 7 million. One-third had a molecular weight 48 to 52 million. The weight average for the nine fractions was 36 million. The particle diameter ranged from 4300A to 2200A.

Another potato starch (calcium form[3]) was dispersed by autoclaving at *p*H 6.0, and the amylose was removed by complexing with nitrobenzene and adsorbing on cotton. The molecular weight

of the amylopectin was 14 million. The average particle diameter was 2900A. Again there was no effect of temperature on the 90° scattering. The difference in the molecular weight of the two amylopectin preparations is attributed to differences in the original starches or in the fractionation treatments.

Since completely acetylated potato amylopectin is apparently not entirely soluble in any single solvent, a partial acetate (40 percent acetyl) was prepared.[6] Turbidity of the acetate dissolved in acetone, chloroform, dioxane, nitromethane, and acetonitrile was measured. Because of less favorable dn/dc, the concentrations were higher than in water solution, and were, in general, 10^{-4} to 3×10^{-3} g/ml. In all these solvents the molecular weight, corrected for acetyl, was approximately 10 million. On deacetylation the molecular weight in water solution was also 10 million. There was no abnormality in the scattering at low concentrations to suggest dissociation of molecular aggregates, as has been suggested on the basis of osmotic pressure measurements.[7]

We believe our results mean that potato amylopectin has a weight average molecular weight of 10 million or more and that molecules of this magnitude probably exist in the starch granules and are not artifacts of preparation.

* This work will form part of a thesis in chemistry to be submitted by L. P. Witnauer to Temple University in partial fulfillment of the requirements for the Ph.D. degree.

† Present address: Northern Regional Research Laboratory, Peoria, Illinois.

[1] Meyer, Bernfeld, Boissonnas, Gürtler, and Noelting, J. Phys. and Colloid Chem. **53**, 319 (1949).
[2] B. H. Zimm and C. D. Thurmond, J. Am. Chem. Soc. **74**, 1111 (1952).
[3] G. C. Nutting, J. Colloid Sci. **7**, 128 (1952).
[4] Brice, Halwer, and Speiser, J. Opt. Soc. Am. **40** 768 (1950).
[5] L. P. Witnauer and H. J. Scherr, Rev. Sci. Instr. **23**, 99 (1952).
[6] J. F. Carson and W. D. Maclay, J. Am. Chem. Soc. **68**, 1015 (1946).
[7] Kerr, Cleveland, and Katzbeck, J. Am. Chem. Soc. **73**, 111 (1951).

Substituted Methanes. XII. Infrared Spectral Data for Deuterotrichloromethane*

RICHARD B. BERNSTEIN AND ADON A. GORDUS
Department of Chemistry
AND
FORREST F. CLEVELAND
Spectroscopy Laboratory, Department of Physics, Illinois Institute of Technology, Chicago 16, Illinois
(Received October 15, 1952)

THE vibrational spectra of deuterotrichloromethane have been analyzed by Madigan *et al.*[1] The first infrared spectra data for CCl_3D, presented in this paper, were obtained with single-beam spectrometers (NaCl and KBr optics) with an isotopic mixture containing some 10 percent CCl_3H. Subsequent single-beam work by Earing and Cloke[2] (NaCl region) with a mixture containing *ca* 5 percent CCl_3H indicated the presence of three additional combination bands.

The present report summarizes recent data on a sample of CCl_3D containing approximately 1 percent CCl_3H. A Perkin-Elmer Model 21 Double-Beam Spectrophotometer with NaCl optics was used, making possible the detection of weak bands in the spectral regions normally obscured by atmospheric absorption. A 10-cm gas cell and a 0.12-mm liquid cell were employed. Gas pressures ranged from 0.001 to 0.26 atmosphere. Both pure liquid and solutions in CS_2 and CCl_3H were studied. Listed in Table I are the observed wave numbers and intensities of the bands for both liquid and gaseous states. The calculated values for combinations and overtones are based on the fundamentals *observed* for the compound in the appropriate state (liquid or gaseous). The values for ν_3 and ν_6 were necessarily taken from Raman data for the liquid, however. Twelve new bands are reported for the vapor, and nine new frequencies are listed for the liquid, of which three have been observed previously in the Raman spectrum.

Anharmonicity increments, $\nu_{calc}-\nu_{obs}$, are seen to be small for combinations and overtones in both the gaseous and liquid states, with the exception of combinations involving ν_1, the C–D stretching mode. For the gas these increments are always positive; however, for the liquid the anharmonicity difference appears occasionally with reversed sign. It may be noted that, if one were to attempt to use *liquid* values of the fundamentals in calculating the combinations and overtones for the *gas*, one would obtain very large discrepancies, with anharmonic increments of reversed sign throughout. Thus, it appears desirable to consider the liquid and gaseous states as two distinct species, each with a reasonably self-consistent spectrum of fundamentals, overtones, and combinations.

It is of interest to note the rather large frequency shifts between the liquid and gaseous states for CCl_3D. Gas frequencies range from 3–18 cm^{-1} greater than liquid values. For CCl_3H[3] the data are less extensive, but the shifts are of comparable magnitude.

TABLE I. Infrared spectral data for deuterotrichloromethane (CCl_3D).

Liquid (0.11 mm) ν (cm^{-1}) Obs	Calc	I[a]	Vapor (10 cm) ν (cm^{-1}) Obs	Calc	I[b]	Assignment	Type
3155	*3164*	m	*(3171)*[c]	*3179*	vw	$\nu_1+\nu_4$	E
2978	*2993*	w	*(2993)*[c]	*3012*	vw	$\nu_1+\nu_5$	E
2899	*2910*	vw	...	...	...	$\nu_1+\nu_2$	A_1
2259	**2259**	s	**(2266)**[c]	**2266**	vw	ν_1	a_1
1819	*1835*[d]	m	...	...	...	$\nu_3+2\nu_5$	A_1+E
1796	*1810*	m	*1823*	*1826*	w	$2\nu_4$	A_1+E
644	*639*	w	*1658*	*1659*	w	$\nu_4+\nu_5$	A_1+A_2+E
1560	*1556*	w	*1568*	*1568*	w	$\nu_3+\nu_4$	E
1470	*1468*	m	*1488*	*1492*	m	$2\nu_5$	A_1+E
1384	*1385*	s	*1399*	*1401*	m	$\nu_3+\nu_5$	E
1295	*1302*	w	...	...	...	$2\nu_2$	A_1
1166	*1167*	w	*1169*	*1175*	vw	$\nu_4+\nu_6$	A_1+A_2+E
1097	*1099*	m	*1106*	*1111*	m	$\nu_3+\nu_5$	E
988	*996*	m	*1002*	*1008*	w	$\nu_5+\nu_6$	A_1+A_2+E
905	**905**	vvs	**913**	**913**	vvs	ν_4	e
734	**734**	vvs	**746**[e]	**746**	vvs	ν_5	e
651	**651**	vvs	**655**	**655**	vs	ν_2	a_1
...	**365**[f]	...	...	**365**[f]	...	ν_3	a_1
...	**262**[f]	...	...	**262**[f]	...	ν_6	e

[a] Relative intensity symbols determined by percent transmission as follows: vw, 95–100; w, 90–95; m, 60–90; s, 20–60; vs, 5–20; vvs, 0–5.
[b] For gas at 0.26 atmos.
[c] Very weak bands. Frequencies uncertain.
[d] Alternatively: $(\nu_4+\nu_6)+\nu_2=1817$ or $(\nu_2+\nu_4)+\nu_6=1822$ cm^{-1}.
[e] Resolved into doublet: 749, 743 cm^{-1}.
[f] Raman data (reference 1) for liquid.

* The authors appreciate the assistance of the AEC, the ONR, and the OOR for support of this research program.

[1] Madigan, Cleveland, Boyer, and Bernstein, J. Chem. Phys. **18**, 1081 (1950).
[2] M. Earing and J. Cloke, J. Am. Chem. Soc. **73**, 769 (1951).
[3] J. R. Madigan and F. F. Cleveland, J. Chem. Phys. **19**, 119 (1951).

The Mercury Photosensitized Oxidation of Paraffins

B. DEB. DARWENT
Olin Industries, Inc., New Haven, Connecticut
(Received October 6, 1952)

THE mercury ($^3P_1$) photosensitized oxidation of paraffins has been studied by Nalbandyan[1] and, more recently, by Gray.[2] They both assume that the reaction occurs by virtue of the photosensitized decomposition of the paraffin. However, an inspection of the quenching cross sections of methane,[3] ethane,[4] and oxygen[5] for λ2537 shows clearly that, with those paraffins, by far the greater proportion of the collisions in which $Hg(^3P_1)$ are deactivated occurs with oxygen and not with the paraffin. If we consider the reactions of $Hg(^3P_1)$ with O_2 and C_2H_6:

$$Hg(^3P_1)+O_2\rightarrow HgO+O \quad (1)$$

$$Hg(^3P_1)+C_2H_6\rightarrow C_2H_5+H+Hg(^1So), \quad (2)$$

the ratio of the rates is given by the ratios of the concentrations of the reactants, the quenching cross sections, and the reduced masses of the reactants and mercury. Since the molecular weights of ethane and oxygen are approximately equal, we may put $R_1/R_2=(\sigma^2_{Q_1}/\sigma^2_{Q_2})([O_2]/[C_2H_6])$.

Using the values $\sigma^2 Q_1 = 13$ and $\sigma^2 Q_2 = 0.1$, we find that, when $[O_2]/[C_2H_6] = 1/9$, as in Gray's experiments, $R_1/R_2 = 13$, i.e., reaction (1) will account for about 93 percent of the total quenching, and reaction (2) for only 7 percent. Also results have recently been obtained[6] which indicate that ethane quenches $Hg(^3P_1)$, at least in part, to the metastable (^3Po) state, whereas oxygen effects the transfer directly to ground (^1So) state. This suggests that an even greater fraction of the total quenching will be done by oxygen. It is certain that with methane, because of its very small σ_Q^2, even less of the initial quenching reaction will involve the paraffin and, therefore, the reaction will proceed almost entirely by process (1).

This, of course, does not affect Gray's reasoning with respect to the subsequent reactions since methyl and ethyl radicals are probably formed by reactions between the oxygen atoms produced in (1) and the substrate.

[1] A. B. Nalbandyan, Compt. rend. U.R.S.S. **66**, 413 (1949).
[2] J. A. Gray, J. Chem. Soc. 3150 (1952).
[3] J. R. Bates, J. Am. Chem. Soc. **52**, 3825 (1930).
[4] B. deB. Darwent, J. Chem. Phys. **18**, 1532 (1950).
[5] M. W. Zemansky, Phys. Rev. **36**, 919 (1930).
[6] B. deB. Darwent and F. G. Hurtubise, J. Chem. Phys. (to be published).

Erratum: Temperature Dependence of Viscosity of Associated Liquids

[J. Chem. Phys. **20**, 1088 (1952)]

THEODORE A. LITOVITZ
Physics Department, Catholic University of America, Washington, D. C.

IN the above-mentioned paper it was stated that the $1/T^2$ dependence on temperature for the activation energy of associated liquids extends to the simple alcohols, (e.g., ethyl, methyl, and propyl alcohol). Actually, this dependence does not hold over a large range of temperature for these alcohols, although it fits well the data for the water and the two higher alcohols mentioned (glycerol, ethylene glycol). Thus, it appears that only certain associated liquids have an activation energy which can be described in this manner.

The Transformation Properties of Internal Coordinates under Covering Operations

MARVIN C. TOBIN
Arthur D. Little, Inc., Cambridge, Massachusetts
(Received October 13, 1952)

AS a prerequisite to setting up molecular symmetry coordinates, it is necessary to have the multiplication table for the transformations of the internal coordinates under the covering operations of the molecular group. This table is a tabulation of equations of the type $R(\Delta a_1) \rightarrow (\Delta a_2)$, where R is a covering operation, and a_1 and a_2 are members of an equivalent set of internal coordinates.

It is the purpose of this note to point out that in certain cases, $R(\Delta a_1) \rightarrow -(\Delta a_2)$; that is to say, the covering operation sends the change in one internal coordinate into the negative of the change in an equivalent coordinate.

Failure to notice this where it occurs may result in a symmetry coordinate being assigned to the wrong symmetry class.

The rules given below were derived from a consideration of the s vectors[1-3] (which have the direction which represents the displacement of the atoms which produces the maximal change in the internal coordinates) for various internal coordinates in suitable model molecules.

1. *Bond stretchings and angle bendings.* $R(\Delta_1) \rightarrow +(\Delta a_2)$ for all R.

2. *Out-of-plane bendings in planar molecules consisting of several bonds terminating in a central atom.*[4] This coordinate is represented by the out-of-plane bendings in BF_3 or $AuCl_4^-$. $\sigma_h(\Delta a_1) \rightarrow -(\Delta a_2)$, C_2 in-plane $(\Delta a_1) \rightarrow -(\Delta a_2)$, $R(\Delta a_1) \rightarrow +(\Delta a_2)$ for all other covering operations.

3. *Torsions.* Torsional coordinates are formed by three consecutive noncolinear bonds, $i-k$, $j-k$, and $k-l$. If $j-k$ is parallel to a plane of symmetry or is bisected by a plane of symmetry perpendicular to it, $\sigma(\Delta a_1) \rightarrow -(\Delta a_2)$, $R(\Delta a_1) \rightarrow +(\Delta a_2)$ for all other R.

If $j-k$ has any other orientation with respect to the symmetry planes (as in the S_8 molecule), $R(\Delta a_1) \rightarrow +(\Delta a_2)$ for all R.

4. *Bendings in linear submolecules of planar molecules.* This type of coordinate is represented by the C=C=O bendings in ketene. If the bending lies in the plane of the molecule, $\sigma_h(\Delta a_1) \rightarrow +(\Delta a_1)$, $\sigma_v(\Delta a_1) \rightarrow -(\Delta a_1)$, $C_2(\Delta a_1) \rightarrow -(\Delta a_1)$. If the coordinate is taken perpendicular to the plane of the molecule, $\sigma_h(\Delta a_2) \rightarrow -(\Delta a_2)$, $\sigma_v(\Delta a_2) \rightarrow +(\Delta a_2)$, $C_2(\Delta a_2) \rightarrow -(\Delta a_2)$. In both cases, $R(\Delta a) \rightarrow +(\Delta a)$ for all other covering operations. a_1 and a_2 are not equivalent coordinates.

5. *Bendings of linear molecules or linear submolecules lying on a greater-than-two fold symmetry axis.* No general rules can be given for these coordinates, since they represent degenerate modes of vibration, and do not transform in any simple manner. In general, they occur in pairs a_{1A} and a_{1B}, such that $\sigma_v(\Delta a_A) \rightarrow X\Delta a_A + Y\Delta a_B$, where X and Y are matrix elements of the irreducible representation of the group.

In linear molecules of symmetry $D_{\infty h}$, $\sigma_h(\Delta a_{1A}) \rightarrow +(\Delta a_{2A})$, if the s vectors for a_{1A} and a_{2A} are coplanar.

As an example illustrating the preceding remarks, we take the torsional symmetry coordinates for the C_2 model of hydrazine. These are $R_1 = (\Delta T_1 + \Delta T_2)/\sqrt{2}$ and $R_2 = (\Delta T_1 - \Delta T_2)/\sqrt{2}$. It is easily seen that R_2 belongs to species A_1, and R_1 belongs to species A_2.

If care had not been taken in ascertaining the transformation properties of the torsional coordinates, R_1 would have been erroneously assigned to A_1, and R_2 to A_2.

[1] E. B. Wilson, J. Chem. Phys. **9**, 76 (1941).
[2] J. Decius, J. Chem. Phys. **16**, 1025 (1948).
[3] S. Ferigle and A. Meister, J. Chem. Phys. **19**, 982 (1951).
[4] J. Decius, private communication, gives s vectors for this coordinate.

The Swelling and Aggregation of Colloid Particles During the Sol-Gel Transition

P. K. KATTI
Department of Applied Science, Delhi Polytechnic, Delhi, India
(Received October 6, 1952)

IN spite of earlier attempts by Arisz,[1] Dexter and Kraemer,[2] Mardles,[3] and Krishnamurthi,[4] the light scattering technique has only recently been perfected by Krishnan,[5] and Doty and Kaufman[6] who have rendered it suitable for the determination of the changes in the size and shape of the colloid particles. These workers have shown that the depolarizations P_v and P_h of the transversly scattered light with the incident vertically and horizontally polarized light, respectively, are measures of the anisotropy and the size of the scattering particles. $P_v = 0$ for spherically symmetrical particles and increases with the deviation from spherical symmetry. $P_h = 100$ percent for particles small in comparison with the wavelength of light and decreases as the size increases. If the intensity I_z of the transversly scattered light with incident vertically polarized light and the corresponding P_v is known, then the density scattering I_d can be calculated by the relation $I_d = I_z \cdot (3 - 4P_v/3 + 3P_v)$. It is easy to show that during the process of coagulation considered by Smoluchowski,[7] I_δ increases with time during the earlier stages, reaches a maximum, and later on tends to decrease when the total number of scattering centers decrease rapidly. The existence of a point of maxima is thus an indication of the increase in size by aggregation. During the last few years the author has made an extensive study under different conditions of temperature, concentration, electrolyte content etc., of the variations in the depolarizations and the density scattering during the sol-gel transition of agar, gelatine,

and cellulose acetate and a few lyophobic gels with a view to get a clearer picture of the main processes leading to the growth of the colloid particles in these gels. This note is intended to give a brief summary of the main results. Some preliminary results have been published earlier.[8]

During the sol-gel transition of the lyophilic gels, we have only the coagulation of the sol particles forming large anisotropic aggregates, the I_d-time curves for these transitions showing distinct points of maxima. If the viscosity increases early enough to prevent coagulation before they grow too large, the sol sets to a gel. The sol-gel transition of lyophilic gels takes place in three distinct stages:

(1) In the earlier stages there is an appreciable increase in viscosity without any change in the size or shape of the particles. During this stage the particle tends to develope a cloud of water molecules which, however, does not enter its structure.

(2) The particles grow larger and become more symmetrical. During this stage I_d increases continuously without showing any tendency to reach a maximum.

(3) The particles grow still further but become more unsymmetrical.

The final size of the gel particles and its other physical properties evidently depend upon the relative predominence, during the transition of the above three stages, which itself depends on the temperature, concentration etc., of the gel. Normally, the last stage overshadows the first two. Gels in which the second stage is predominent till it sets can be realized under carefully controlled conditions, while the last stage can be introduced at any instant by slightly altering the concentration, temperature, etc., or even by stirring or shaking the sol during the earlier stages. Gels in which the second stage persists till they set completely showing P_h as low as 80 percent have been obtained. The $I_\delta - t$ curves for these transitions show no points of maxima. Instead, the density scattering increases rapidly with time till the gel sets. However, if the third stage is introduced during the earlier stages of the above gel, a distinct point of maxima appears even before P_h decreases to 80 percent.

It, therefore, seems possible that the growth of the particles during the second stage results from the swelling of the individual particles by some of the surrounding liquid entering its structure—a process in which the total number of the particles does not decrease. The growth of the particles in the third stage is obviously the result of aggregation. The swelling of the particles was apparent in an observation made by Krishnamurthi[9] on the desiccation of some gelatine gels. His[10] own arguments against swelling were probably due to the fact that his later experimental techniques were incapable of separating swelling from the predominent aggregation.

Detailed observations shall be discussed elsewhere.

[1] Arisz, Kolloidchem. Beihefte **7**, 22 (1915).
[2] Dexter and Kraemer, J. Phys. Chem. **31**, 764 (1927).
[3] Mardles, Trans. Faraday Soc. **18**, 318 (1923).
[4] Krishnamurthi, Proc. Roy. Soc. (London) **122A**, 76 (1929).
[5] R. S. Krishnan, Proc. Indian Acad. Sci. **1A**, 782 (1935).
[6] Doty and Kaufman, Colloid. Sci. by Alexander and Johnson. Vol. 1 (1949).
[7] Smoluchowski, Phil. Mag. **44**, 305 (1922).
[8] P. K. Katti, Proc. Indian Acad. Sci. **28**, 216 (1948); **30**, 30 (1949).
[9] Krishnamurthi, Nature **123**, 143 (1929).
[10] Krishnamurthi, Proc. Roy. Soc. (London) **129A**, 490 (1930).

The Microwave Spectrum of Vinylacetylene

H. W. Morgan and J. H. Goldstein
Stable Isotope Research and Production Division Oak Ridge National Laboratory, Y-12 Area, Oak Ridge, Tennessee*
(Received October 7, 1952)

THE pure rotational spectrum of vinylacetylene has been investigated in a Stark effect microwave spectrograph in the region about 27,000 Mc. Five weak lines, comprising the $J=2\rightarrow3$ grouping, were found and identified on the basis of estimated rotational constants and qualitative Stark effect. Table I lists these lines and the observed frequencies.

TABLE I. Observed spectrum of vinylacetylene.

	Transition	Frequency
ν_1	$2_{02}\rightarrow3_{03}$	27212.71 ±0.05 Mc
ν_2	$2_{11}\rightarrow3_{12}$	27845.35 ±0.05 Mc
ν_3	$2_{12}\rightarrow3_{13}$	26600.00 ±0.05 Mc
ν_4	$2_{20}\rightarrow3_{21}$	27237.09 ±0.05 Mc
ν_5	$2_{21}\rightarrow3_{22}$	27226.03 ±0.05 Mc

Since it appears from the above data that appreciable centrifugal distortion exists in the vinylacetylene molecule, the calculation of rotational constants was designed to minimize this factor. Thus, $(b-c)$ was determined from $(\nu_2-\nu_3)$, δ from $(\nu_4-\nu_5)$ and $(b+c)$ from the relation $3(b+c)=(\nu_1+\nu_4-\nu_5)$. The values obtained are listed in Table II.

TABLE II. Rotational constants for vinylacetylene.

$(b+c)$	=9074.59 Mc
$(b-c)$	= 415.12 Mc
δ	= 0.008842

Further work on centrifugal distortion and on the Stark effect in this molecule is in progress and will be reported at a later date.

* This paper is based on work performed for the AEC by Carbide and Carbon Chemicals Company, a Division of Union Carbide and Carbon Corporation, at the Oak Ridge National Laboratory.

Constants in the Equation of State of a Gas*

Leo F. Epstein
General Electric Company, Knolls Atomic Power Laboratory, Schenectady, New York
(Received October 17, 1952)

GIVEN an equation of state of a gas in the virial form

$$V=(RT/p)[1+(B_v/V)+(C_v/V^2)+(D_v/V^3)+(E_v/V^4)+\cdots], \quad (1)$$

it is often desirable to express the volume in a form explicit in the pressure

$$V=(RT/p)[1+B_pp+C_pp^2+D_pp^3+E_pp^4+\cdots]. \quad (2)$$

The relations between the coefficients of (2) and those of (1) are often derived by assuming the ideal gas value $V=RT/p$ to be sufficiently accurate for the computation of the correction terms on the right-hand side of (1). It is the purpose of this note to point out that this is an unnecessary procedure and that the exact expression for the relation between the coefficients can readily be obtained. The computation involves only straightforward algebra but it is somewhat tedious, and so it is considered worthwhile to present a general method for going from (1) to (2), and results of these calculations here.

In terms of the molal density $\rho=1/V$, Eq. (1) can be written as

$$p/RT=\rho+B_v\rho^2+C_v\rho^3+D_v\rho^4+E_v\rho^5+\cdots. \quad (3)$$

This series may now be reverted, using a method due to Van Orstrand.[1] Consider the series

$$\rho=\sum_{k=1} A_{k-1}(p/RT)^k. \quad (4)$$

Differentiating with respect to ρ and dividing both sides of the equation through by $(p/RT)^n$,

$$(RT/p)^n=\left[\frac{d}{d\rho}(p/RT)\right]\sum_{k=1} kA_{k-1}(p/RT)^{k-n-1}. \quad (5)$$

It can be shown that the only term on the right which contains ρ^{-1} is $nA_{n-1}(RT/p)[(d/d\rho)(p/RT)]$, by substitution of (3) or otherwise. *Thus nA_{n-1} is the coefficient of ρ^{-1} in the expansion of* $(p/RT)^{-n}$. By substituting (3) in this expression and applying the multinomial theorem to find $(p/RT)^{-n}$, the A_n values can be

determined. The process has been carried out for the general case; the coefficients of terms up to $(p/RT)^7$ are given in the *Smithsonian Tables*, and Van Orstrand[1] gives the coefficients up to the $(p/RT)^{13}$ term. The result is

$$\begin{aligned}\rho=1/V=(p/RT)[1&-B_v(p/RT)\\&+(+2B_v^2-C_v)(p/RT)^2\\&+(-5B_v^3+5B_vC_v-D_v)(p/RT)^3\\&+(+14B_v^4-21B_v^2C_v+6B_vD_v+3C_v^2-E_v)(p/RT)^4\\&+(-42B_v^5+84B_v^3C_v-28B_v^2D_v\\&-28B_vC_v^2+7B_vE_v+7C_vD_v-F_v)(p/RT)^5+\cdots] \qquad (6)\end{aligned}$$

as long as $(p/RT)<1$, which is always true for cases of physical interest.

The reciprocal of this series may be taken by algebraic division, or more simply, by using a theorem given in the *Smithsonian Tables*,[2] i.e., if

$$1/\sum_{i=0} a_ix^i=(1/a_0)\sum_{i=0} c_ix^i, \qquad (7)$$

the relation between the c_i and a_i constants is given by

$$c_0=1, \qquad (8a)$$

$$c_i=(-1/a_0)\sum_{k=1}^{i} c_{i-k}a_k. \qquad (8b)$$

With these formulas, the final equation for V has the form of (2) with

$$\begin{aligned}B_p&=B_v/(RT),\\C_p&=(C_v-B_v^2)/(RT)^2,\\D_p&=(D_v-3B_vC_v+2B_v^3)/(RT)^3,\\E_p&=(E_v-2C_v^2-4B_vD_v+10B_vC_v^4)/(RT)^4, \qquad (9)\\&\cdot\\&\cdot\\&\cdot\end{aligned}$$

These relations may also be inverted to give

$$\begin{aligned}B_v&=(RT)B_p,\\C_v&=(RT)^2(C_p+B_p^2),\\D_v&=(RT)^3(D_p+3C_pB_p+B_p^3),\\E_v&=(RT)^4(E_p+4D_pB_p+6C_pB_p^2+2C_p^2+B_p^4), \qquad (10)\\&\cdot\\&\cdot\\&\cdot\end{aligned}$$

The technique can, in general, be extended to any number of terms and should eliminate the necessity for the approximation of assuming V to have the ideal gas value RT/p in the higher terms[3] of Eq. (1); this assumption gives only the leading terms of Eqs. (9) as written.

The first three terms given in Eq. (9) are in exact agreement with the results given by Scatchard.[4] These were obtained by (a) substituting the ideal gas expression for V in the correction terms of Eq. (1) and (b) substituting the resulting expression for V in terms of p in Eq. (1) again, and carrying through the algebra retaining the proper number of terms. The extension of this method to higher terms in the series is likely to be somewhat painful. Some years ago, Hicks[5] outlined an alternative process for going from Eq. (1) to Eq. (2). The complete details of the process have not been published, however, and Dr. Hicks has advised[6] that they probably will not be.

It should be mentioned in passing that, as Scatchard[4] has pointed out, while an equation of state of the form (2) is more convenient for many purposes, the virial expansion (1), in powers of $1/V$, appears to give a better fit to the experimental data.

* The Knolls Atomic Power Laboratory is operated by the General Electric Company for the AEC. The work reported here was carried out under contract No. W-31-109 Eng-52.

[1] C. E. Van Orstrand, Phil. Mag. **19**, 366 (1910); also *Smithsonian Mathematical Formula and Tables of Elliptic Functions*, E. A. Adams, editor. (Smithsonian Institution, Washington, 1922), p. 116.

[2] See reference 1, *Smithsonian Mathematical Formula and Tables of Elliptic Functions*, 1, p. 119.

[3] J. A. Beattie, Proc. Natl. Acad. Sci. **16**, 14 (1930).

[4] G. Scatchard, Proc. Natl. Acad. Sci. **16**, 811 (1930).

[5] Bruce L. Hicks, Phys. Rev. **58**, 209 (1940).

[6] Bruce L. Hicks, private communication (March 31, 1952).

Born Repulsion and Restricted Free Rotation

JOHAN VAN DRANEN
Laboratory for Analytical Chemistry, University of Amsterdam, Amsterdam, Netherlands

(Received September 26, 1952)

FROM measurements of thermochemical quantities Kemp and Pitzer[1] deduced the fact that the rotation about the single C−C bond in ethane is not completely free but restricted by a potential barrier of about 2750 cal/mole.

Spectroscopic data lead to the conclusion that the staggered position (D_{3d}) is the stable one.[2]

Several suggestions have been made in an effort to clarify the reasons for the existence of this potential barrier, e.g., the influence of *d* and *f* orbitals (Eyring), repulsive forces (Aston *et al.*, Lenard-Jones), interaction of charge distributions (Lassettre and Dean, Oosterhoff). In a recent discussion Pitzer[3] stated that more than one phenomenon contributes to the total barrier. According to Pitzer, distortions of the sp^2 orbitals on the carbon atoms may have a very appreciable effect.

The trouble is, of course, that such a small energy difference is very difficult to evaluate with the aid of our crude quantum mechanical methods. To obtain, however, some further insight in this problem, we have applied a somewhat unusual procedure.

We restrict our attention on the two valence electrons forming the C−H bond, and we shall try to estimate (the order of magnitude) the difference of the Born repulsions between these systems of valence electrons in the staggered and eclipsed (D_{3h}) position, respectively. A theoretical calculation of the interaction of two systems of valence electrons cannot be given. Therefore, we replace these two valence electrons (moving in the field of a proton and a C^+-ion) by another system, having two electrons. For this system we choose a helium atom and a hydrogen molecule. Comparing now the charge distributions of the helium atom, the C−H bond, and the hydrogen molecule, we come to the conclusion that in the helium atom the electrons are more and in the hydrogen molecule less concentrated than in the C−H bond. We have deduced from the very thorough calculations of Oosterhoff[4] for the experimental dipole moment of the C−H bond (−0.4 *D*) the following charge distribution: −1.15 electron in the sp^3 orbital of the C-atom, distance of the charge center to the carbon nucleus 0.370A; −0.60 electron in the overlap charge of the sp^3 and 1*s* orbital of the H-atom, distance 0.794A; −0.25 electron in the 1*s* orbital, distance (C−H) 1.093A. The exponential parts of the Slater functions for H, C, and He are: $\exp-1.17\ r/a_0$, $\exp-1.63\ r/a_0$ and $\exp-1.70\ r/a_0$, respectively. (The charge distribution for the C−H bond has been calculated using an effective nuclear charge 1.10 for the 1*s* orbital.) We assume now that there has to exist some correlation between this charge distribution and the Born repulsion.

Replacing then the two valence electrons by a helium atom or a hydrogen molecule, we obtain a lower or a higher value, respectively, for the potential barrier.

For the interaction energy V of the particles we take the Lenard-Jones potential

$$V(r)=-4\epsilon\{(\sigma/r)^6-(\sigma/r)^{12}\},$$

where ϵ is the energy of the equilibrium-state ($r_{eq}=2^{1/6}\sigma$), and σ the characteristic diameter.

ϵ and σ can be calculated from the second virial coefficient. For helium[5]

$\epsilon=20.31$ cal/mole hydrogen molecule $\epsilon=73.5$ cal/mole
$\sigma=2.56$A $\sigma=2.93$A.

From the values for the methane molecule ($\epsilon=297$ and $\sigma=3.74$), there is some (admittedly not very strong) evidence too that the C−H bond, with respect to Born repulsion, lies between He and H_2. To obtain the values for a virtual C−H bond, ϵ has to be divided by a factor between 4 and 16, but very probably for this Born repulsion the factor is much nearer to 4; $\sigma\approx 3.74\text{A}\times 0.75 \approx 2.81\text{A}$.

Locating now the helium atom midway between the C- and the H-atom, we obtain that the staggered configuration is the stable one; the potential barrier is equal to 700 cal/mole. In the case of the hydrogen molecule this value is equal to 11,000 cal/mole[6] ($r_{cc}=1.54$A).

If we take as our basis the experimental dipole moment $-0.4D$, then without making further assumptions, the calculations of Lassettre and Dean[7] as well as of Oosterhoff give for the charge distribution a contribution to the potential barrier of about 1200 cal/mole.[8]

In view of the values given for the Born repulsion, we think that there is some, of course not convincing but on the other hand not wholly unfounded, reason to attribute to the Born repulsion the major part of the contribution to the potential barrier, namely about 1600 cal/mole.

We have given here this treatment because in this stage of practical quantum-mechanical calculations for a complicated system as the ethane molecule such a small effect (the potential barrier corresponds to the energy difference of two electrons on the distances of 1.60A and 1.62A) cannot be exactly calculated using the one-electron wave functions and thus neglecting the correlation effect. Anyhow, applying this procedure of closing in this effect between two limits, it is perhaps possible to detect the physical explanation for the restricted free rotation.

In the future we hope to publish an account on the influence of the Born repulsion energies on the additivity of bond energies.

[1] D. Kemp and K. S. Pitzer, J. Chem. Phys. **4**, 749 (1936).
[2] L. G. Smith, J. Chem. Phys. **17**, 139 (1949).
[3] K. S. Pitzer, Disc. Faraday Soc. No. 10, Hydrocarbons (1951), p. 124.
[4] L. I. Oosterhoff, "Restricted free rotation and cyclic molecules," thesis, Leiden (1949); and reference 3, page 79.
[5] R. I. Lunbeck, "The principle of corresponding states in quantum-mechanics," thesis (written in Dutch), Amsterdam (1951).
[6] As there are no theoretical calculations of comparable accuracy for helium and hydrogen, we use the best experimental values. The use of other potential fields, e.g., a Morse curve, does not alter the conclusion of this note.
[7] E. N. Lassettre and L. B. Dean, J. Chem. Phys. **16**, 151, 553 (1948); J. Chem. Phys. **17**, 317 (1949).
[8] J. van Dranen, "Contribution to the theory of quantummechanical methods in chemistry," thesis (Amsterdam, 1951), p. 23.

On the Exchange Terms in the HLSP Theory of an n-Electron Molecule

K. NUKASAWA
Research Institute of Applied Electricity, Hokkaido University, Sapporo, Japan
(Received August 20, 1952)

THE electronic energy W of an n-electron molecule, when calculated by the HLSP theory, is usually approximated by the sum of the Coulomb term Q and simple exchange terms $\alpha_2(pq, qp)$ as

$$W=Q+\Sigma x(pq, qp)\alpha_2(pq, qp), \tag{1}$$

where $x(pq, qp)$ is the quantity depending upon the spin orientation. It should be remembered that in Eq. (1) $\alpha_2(pq, qp)$ has been considered as characteristic for a pair of orbitals p and q, thus the influence of the remaining orbitals being ignored. However, the terms required to be neglected in this procedure are so numerous for large molecules, that the individual smallness cannot be considered as sufficient reason to justify Eq. (1). It is desirable to be more careful in the way of neglection of the higher order terms.

If all of the terms are included, the expression of the energy of a nondegenerating system becomes,

$$W=[Q_n+\Sigma_m\Sigma_{P,Q}x(P, Q; m)J_n(P, Q; m)]/\Delta, \tag{2}$$

where

$$\Delta=1+\Sigma_m\Sigma_{P,Q}x(P, Q; m)S(P, Q; m). \tag{3}$$

The notation $(P, Q; m)$ is the abbreviation for $(p'p''\cdots p^m, q'q''\cdots q^m)$, which indicates the quantity arising from the electronic state, where the first electron lies in orbitals p' and q', the second in p'' and q'', and so on, while the remaining $n-m$ electrons do not share their orbitals. Therefore, the overlap term $S(P, Q; m)$ equals to $S_{p'q'}\cdot S_{p''q''}\cdots S_{p^m q^m}$ where S_{pq} has its usual meaning. Either P- or Q-system can be derived from the one another's exchange. The suffix n in Eq. (2) indicates that the integral concerns to the n-electron system. As Mulliken[1] pointed out, Eq. (2) can be recast to

$$W=Q_n+[\Sigma_m\Sigma_{P,Q}x(P, Q; m)\alpha_n(P, Q; m)]/\Delta, \tag{4}$$

where

$$\alpha_n(P, Q; m)=J_n(P, Q; m)-S(P, Q; m)Q_n. \tag{5}$$

It should be remarked that the α's are invariant for the origin, the fact that gives the α's more significance than the J's.

The α's in Eq. (4) which are connected with the n-electron system can be approximated by the terms for 2-electron systems as

$$\alpha_n(P, Q; m)\sim S(P, Q; m)\sum_{i=1}^{m}\alpha_2(p^iq^i, q^ip^i)/2S^2{}_{p^iq^i}, \tag{6}$$

where

$$\alpha_2(p^iq^i, q^ip^i)=J_2(p^iq^i, q^ip^i)-S^2{}_{p^iq^i}Q_2(p^iq^i). \tag{7}$$

$J_2(pq, qp)$ and $Q_2(pq)$ are the exchange and Coulomb integral, respectively, of the system which consists of the atom cores of the orbitals p and q, and the two electrons lying in p and q. The necessary conditions for Eq. (6) is to assume the approximations first introduced by Mulliken[2]

$$2\int x_p{}^*U_ix_qd\tau\sim\left[\int x_p{}^*U_ix_pd\tau+\int x_q{}^*U_ix_qd\tau\right]S_{pq} \tag{8}$$

$$2(pq|jj)\sim[(pp|jj)+(qq|jj)]S_{pq}, \tag{9}$$

where $i\neq p, q$ and the notations have the same meanings as given by Parr and Mulliken.[3] By Eq. (6), the simple n-electron exchange term $\alpha_n(pq, qp)$ can be approximated to $\alpha_2(pq, qp)$, justifying the usual representation of Eq. (1). The meaning of $\alpha_2(pq, qp)$, however, should be applied to Eq. (7), the usual interpretation

$$\alpha_2(pq, qp)\sim J_2(pq, qp) \tag{10}$$

being incorrect.

We have calculated the energy of four π-electrons of 1,3-butadiene for twelve resonance structures, accurately by Eq. (2) and approximately by Eqs. (1) and (7). The errors due to this approximation were ± 0.3 ev at most, which are rather satisfactory, compared with the errors of about 3 ev which were found when Eq. (1) was employed instead of (7). Detailed discussion, including the proof of Eqs. (6) and (7), and the method of the approximate calculation of nondiagonal elements of Hamiltonian operator which appear when the interaction between the resonance structures exists, will be published elsewhere.

[1] R. S. Mulliken, J. Phys. Chem. **56**, 295 (1952).
[2] R. S. Mulliken, J. phys. chim. **46**, 497 (1949).
[3] R. G. Parr and R. S. Mulliken, J. Chem. Phys. **18**, 1338 (1950).

Transport Phenomena (continued)
On the energetic treatment of non-isothermal processes, Hans Holtan, Jr.—539(L). Erratum to **19**, 519 (1951)
On the principle of thermal interaction, Hans Holtan, Jr. —526. Erratum to above—1644(L)
On the scattering of H_2^+ by H_2, Vernon Myers—195(L)
Theory of ion exchange for polyelectrolytes undergoing electrolytic transference, Frederick T. Wall and Philip F. Grieger—1200
Thermal conductivity of fluid argon and nitrogen, Arthur Uhlir, Jr.—463
Thermal conductivity of solids and fluids from studies of aggregate matter, H. S. Strickler—1333(L)
Ultrasonic absorption in the critical temperature region, W. G. Schneider—759(L). Erratum to **18**, 1300 (1950)
Ultrasonic propagation in binary liquid systems near their critical solution temperature, A. G. Chynoweth and W. G. Schneider—760(L). Erratum to **19**, 1566 (1951)

Ultrasonics
Calculation of vibrational relaxation times in gases, R. N. Schwartz, Z. I. Slawsky, and K. F. Herzfeld—1591
Chemical effects of ultrasonics, Virginia Griffing—939
Energy transfer by collisions in *cis*- and *trans*-dichloroethylene vapors, D. Sette, A. Busala, and J. C. Hubbard —1899
On the relaxation time of equilibrium systems as related to ultrasonic absorption and reaction kinetics, Milton Manes—1658(L)
Origin of the ultrasonic absorption in liquids. II, Karl F. Herzfeld—288
Reaction sites in a field of stationary ultrasonic waves, Olle Lindström—917(L). Erratum to **19**, 1613 (1951)
Ultrasonic absorption in the critical temperature region, W. G. Schneider—759(L). Erratum to **18**, 1300 (1950)
Ultrasonic propagation in binary liquid systems near their critical solution temperature, A. G. Chynoweth and W. G. Schneider—760(L). Erratum to **19**, 1566 (1951)
Ultrasonic propagation in xenon in the region of its critical temperature, A. G. Chynoweth and W. G. Schneider—1777
Ultrasonic velocity in liquids and liquid mixtures, Bertil Jacobson—927(L)
Velocity of sound in electrolytic solutions, Sidney Barnartt —278

Valence (see **Mechanics, Quantum**)
Viscosity
Frictional coefficient for flexible chain molecules in dilute solutions, Leo Mandelkern and Paul J. Flory—212
Lennard-Jones 12:6 potential and the viscosity of gases, E. Whalley and W. G. Schneider—657
On the frequency dependence of the viscosity of high polymer solutions, Roger Cerf—395
Temperature dependence of the viscosity of associated liquids, Theodore A. Litovitz—1088. Erratum to above —1980(L)
Visco-elastic effect in solutions of simple particles, George K. Fraenkel—642
Viscosities of some lower aliphatic alcohols at constant volume, A. Jobling and A. S. C. Lawrence—1296
Viscosity of concentrated suspensions and solutions, H. C. Brinkman—571
Viscosity self-diffusion and allied effects in solid polymers, B. Bueche—1959

X-Ray Diffraction
Crystallography of nickel kieselguhr, Raymond B. Roof, Jr.—1181(L)
Crystal structure of formic acid, F. Holtzberg, B. Post, and I. Fankuchen—198(L)
Cut-off phenomena of protein crystallography, Andrew D. Booth—1907
Diffraction of x-rays by liquid alloys of sodium and potassium, N. S. Gingrich and R. E. Henderson—1117
New effect of cold work on powder x-ray patterns, Shoichi Annaka—1662(L)
On the vector map of crystalline horse hemoglobin, Dorothy Wrinch—1051(L)
Structure of $Na_xPt_3O_4$, Jürg Waser and Edwin D. McClanahan, Jr.—199(L)
Structure of platinum oxides, Ernesto E. Galloni and Rodolfo H. Busch—198(L)
X-ray diffraction of heat-treated carbon blacks, H. T. Pinnick—756(L)
X-ray diffraction study of crystalline neopentane (tetramethylmethane), Arthur H. Mones and Benjamin Post —755(L)
X-ray investigation of $Co(NH_3)_6PbCl_6$ and $Co(NH_3)_6BiCl_6$, Masao Atoji and Tokunosuke Watanabe—1045(L)

UNIVERSITY OF MICHIGAN
JAN 15 1953
PHYSICS LIBRARY

THE JOURNAL OF CHEMICAL PHYSICS

VOLUME 20 NUMBER 12

DECEMBER, 1952

Published by the
AMERICAN INSTITUTE OF PHYSICS
Incorporated
Lancaster, Pa. and New York, N. Y.

CHEMICAL PHYSICS

EDITORS

Editor

Term ending December 31, 1953

Term ending December 31, 1954

THEODORE R. BERLIN
B. P. DAILEY
A. W. LAWSON
HAROLD H. NIELSEN
HARRISON SHULL
CHARLES P. SMYTH
FRANK H. WESTHEIMER

Tables may be typewritten on sheets separate from the running text. Each table must have a caption which will make the data in the table intelligible without reference to the text. Avoid complicated column headings.

Wherever possible figures should be planned for the width of a column (3 in.). A convenient reduction ratio is about 2:1 or 3:1. Lettering should be large enough on the original that when reduced it shall not be less than about 1/16 in. (~1.5 mm). Line drawings must be in *india ink* on white paper or tracing cloth. Coordinate paper is not desirable but if used must be blue lined and the coordinate lines which are to show must be inked over. Photographs should have maximum black and white contrast. Identify each original drawing or photograph on the back with the author's name and the figure number. Figures should be numbered consecutively. Captions should be typed on a separate sheet of paper.

A limited number of alterations in proof are unavoidable, but the cost of making extensive alterations after the article has been set in type will be charged to the author.

Proof and all correspondence concerning papers in the process of publication should be addressed to the Publication Manager, American Institute of Physics, 57 East 55 Street, New York 22, New York.

Subscription Price

	U. S. and Canada	Elsewhere
To members of the American Institute of Physics and Affiliated Societies	$12.00	$13.00
To all others	15.00	16.00

Back Number Prices

Yearly rate when complete year is available: $17.00.
Single copies: $1.50 each.

Subscriptions, renewals, and orders for single copies should be addressed to the American Institute of Physics, 57 East 55 Street, New York 22, New York.

Changes of address should be sent to the American Institute of Physics.

Printed monthly at Prince and Lemon Streets, Lancaster, Pennsylvania.

Entered as second-class matter December 1, 1922, at the Post Office at Lancaster, Pa., under the Act of August 24, 1912, as amended by the Act of March 3, 1933. Acceptance for mailing at special rate of postage provided for in paragraph (d-2), section 34.40, P. L. & R. of 1948, authorized February 3, 1933.